Engineering Biomaterials for Regenerative Medicine

Sujata K. Bhatia
Editor

Engineering Biomaterials for Regenerative Medicine

Novel Technologies for Clinical Applications

Springer

Editor
Sujata K. Bhatia
Harvard University
School of Engineering and Applied Sciences
29 Oxford Street
Cambridge, MA 02138, USA
sbhatia@seas.harvard.edu

ISBN 978-1-4614-1079-9 e-ISBN 978-1-4614-1080-5
DOI 10.1007/978-1-4614-1080-5
Springer New York Dordrecht Heidelberg London

Library of Congress Control Number: 2011938461

Preface: The Clinical Imperative for Regenerative Medicine

A critical need exists in clinical medicine for effective methods to regenerate tissues. Many of the world's leading killers, including coronary artery disease, stroke, emphysema, diabetes, cancer, and traumatic injuries, could be alleviated by regenerative medicine. For example, novel methods for pancreatic islet regeneration can address diabetes; autologous cells for heart muscle regeneration can address coronary artery disease; and nerve regeneration technologies can be utilized to treat stroke. Effective materials for tissue regeneration will, therefore, find applications in practically every clinical discipline. Regenerative medicine has the potential to improve patient outcomes, lower the incidence of complications, and reduce hospital stays. Such technologies will enable cost-effective treatments, and lessen morbidity and mortality.

The ultimate goal of tissue engineering is to regenerate tissues that restore normal physiological function. A general strategy of tissue engineering is to replace lost tissues or organs with polymeric scaffolds that contain specialized populations of viable cells. Within a tissue engineered construct, a three-dimensional polymer scaffold provides support and structure, while living cells contribute biological functionality. The scaffold may take the form of a mesh, patch, or foam, and it may incorporate mechanical or chemical cellular signals to stimulate the expansion of desirable cell populations. Once implanted, the tissue-engineered construct guides the growth and development of new tissue; the polymer scaffold degrades away to be replaced by healthy functioning tissue. An optimal biomaterial for tissue regeneration enhances cell attachment, proliferation, and differentiation. To initiate tissue renewal, the biomaterial must integrate with the host tissue and promote in vivo revascularization to ensure adequate oxygen supply. The biomaterial must also exhibit mechanical properties that are compatible with native tissue. At the same time, the implanted biomaterial must safely degrade at a rate similar to that of the new tissue formation, such that the biomaterial is eventually removed from the body by natural metabolic processes. Ultimately, any biomaterial platform for regenerative medicine must provide clinical benefit for patients.

This book will describe the latest methods for regulating the biological and chemical composition of engineered biomaterials, as well as techniques for

modulating mechanical properties of engineered constructs. The book will delineate methods for guiding the host response to implantable materials, and explain the use of biologically inspired materials for optimal biological functionality and compatibility. The book will culminate in a discussion of the clinical applications of regenerative medicine.

The first section of this book details methods for optimizing cellular populations and cellular behavior. Michael King and Srinivas Narasipura of Cornell University discuss biomaterial surfaces for capture and purification of hematopoietic stem cells and progenitor cells. Such methods can be utilized to provide cell sources for tissue engineering; these surfaces could also be incorporated into tissue-engineered scaffolds, to attract desirable native cell populations and promote engraftment. Cynthia Reinhart-King and colleagues of Cornell University then review cellular mechanics, specifically the role of the extracellular matrix in tuning cellular properties and tissue formation. These insights are useful for enhancing cellular migration and proliferation within engineered constructs and may be utilized to promote tissue integration of engineered matrices. The next section of this book covers another essential component of tissue engineering, the delivery of oxygen to nascent constructs. Susan Roberts and Whitney Stoppel of the University of Massachusetts-Amherst review methods for ensuring adequate oxygen transport within engrafted tissues.

The book then turns to the mechanical structure of the polymer scaffold, and discusses strategies for controlling the mechanical properties of biomaterials. Santanu Kundu of NIST and Edwin Chan of the University of Massachusetts-Amherst explain the adhesion behavior of soft materials, including elastomers and hydrogels. Incorporation of patterned surfaces and other topological features can enhance the adhesive performance of biomaterials. Proceeding on this theme, Gregory Tew and Surita Bhatia of the University of Massachusetts-Amherst summarize efforts to regulate structural and mechanical properties of novel hydrogels. The self-assembly, cross-linking, and stiffness of hydrogels are critical structural characteristics which can be modulated. This approach enables adaptation of biomaterials for a wide variety of implantation sites and a wide variety of applications in regenerative medicine.

The book continues with a detailed discussion of biocompatibility and host–biomaterial interactions. Anjelica Gonzalez-Simon of Yale University and Omolola Eniola-Adefeso of the University of Michigan delineate the host response to biomaterials. The host reaction is an essential consideration for any tissue-engineered construct. Thomas Dziubla and Paritosh Wattamwar build on this subject and describe a novel biomaterial platform which incorporates antioxidants to minimize inflammation and maximize wound healing. Such an antioxidant-conjugated scaffold may add therapeutic functionality to implantable biomaterials.

Because implanted biomaterials must be biocompatible with natural tissues, some of the most effective biomaterials are those inspired by natural structures. The book thus progresses with a section on biologically inspired materials for tissue engineering. Jeffrey Karp, Woo Kyung Cho, Robert Langer and colleagues at Harvard-MIT describe their invention of tape-based adhesives for regenerative medicine.

These biomaterials are nanotopographically patterned to mimic the adhesive footpad of the gecko. Kristi Kiick and Christopher McGann of the University of Delaware discuss their innovation of hydrogels functionalized with the natural polysaccharide heparin. Such hydrogels may assemble through protein–polysaccharide interactions, and the inclusion of heparin can impart anti-thrombogenic activity to scaffolds for tissue regeneration.

The real value of tissue-engineered scaffolds lies in their clinical utility. This book concludes with a significant section on the design of biomaterials for specific clinical applications. Xinqiao Jia and colleagues of the University of Delaware detail their efforts to create biomimetic matrices for vocal fold repair and regeneration. These matrices recapitulate the features of the vocal fold lamina propria; the scaffolds encourage the attachment and proliferation of vocal fold cells, as well as the production of an extracellular matrix that resembles native tissue. Millicent Sullivan and Kory Blocker of the University of Delaware review methods of nonviral gene delivery for tissue regeneration. This work enables spatial and temporal control of gene delivery and has specific applications for promoting angiogenesis. Finally, Yunzhi Yang and Sungwoo Kim of the University of Texas Health Science Center describe their progress in chitosan-based systems for applications in chemotherapy, wound healing, and regenerative medicine.

Together, the innovations of these investigators demonstrate the versatility and the potential of engineered biomaterials for regenerative medicine. Fundamental advances in cellular mechanics, intracellular and extracellular signaling, host–cell interactions, polymer chemistry, and materials science have been applied to create biomaterials with novel design and functionality. These visionary approaches to tissue engineering will, in turn, enable breakthroughs in clinical medicine, enhancing the human body's capability to regenerate and repair itself.

Cambridge, MA, USA Sujata K. Bhatia

Contents

Part I
Cellular Recruitment and Delivery

Chapter 1
Biomaterial Surfaces for the Isolation of Hematopoietic Stem and Progenitor Cells

Srinivas D. Narasipura and Michael R. King

Abstract Enrichment and purification of hematopoietic stem and progenitor cells (HSPCs) is important in basic research as well as in clinical transplantation of HSPCs. Currently, fluorescent-activated cell sorting (FACS) and immunomagnetic separation techniques are widely used for HSPC isolation. Although both methods offer relatively pure subpopulations, FACS can introduce potential sources of contamination and flow cytometers with high-speed sorting ability are prohibitively expensive for smaller laboratories. Immunomagnetic separation requires large amounts of starting material, involves several steps, and furthermore, cell-surface antibodies may prohibit cell proliferation and differentiation. Hence, development of simpler methods for the capture and purification of HSPCs are warranted. By exploiting the differential rolling behavior of CD34+ HSPCs from mature blood cells on selectins, we have developed a flow-based, adhesion molecule-mediated capture method, which may be a viable alternative approach to the isolation of HSPCs.

Hematopoietic Stem and Progenitor Cells

Hematopoietic stem and progenitor cells (HSPCs) comprise a small portion of cells in the marrow (<1–5%) and an even smaller fraction of peripheral blood [1–6], and they are usually identified and isolated based on their expression, or lack of expression, of specific cell surface antigens. CD34 is a type I transmembrane

S.D. Narasipura
Department of Immunology and Microbiology, Rush University Medical Center,
1735 W Harrison Street, Chicago, IL 60612, USA

M.R. King (✉)
Department of Biomedical Engineering, Cornell University,
205 Weill Hall, Ithaca, NY 14853, USA
e-mail: mike.king@cornell.edu

S.K. Bhatia (ed.), *Engineering Biomaterials for Regenerative Medicine: Novel Technologies for Clinical Applications*, DOI 10.1007/978-1-4614-1080-5_1,

glycoprotein that is believed to be expressed by the majority of HSPCs, but is downregulated with maturation into terminally differentiated blood cells [4, 7–9]. Certain glycoforms of CD34 are ligands for L-selectin, but the CD34 expressed on HSPCs lacks essential fucosylation and sulfation to facilitate that interaction so its role in vivo is still unclear [9–11]. Since it is still the widely studied HSPC marker, most current clinical methods for identifying HSPCs use antibodies against CD34 [12, 13]. The majority of HSPCs are CD34+, but most of the primitive cells are limited to the CD34 + CD38− fraction. Most long-term culture initiating cells, those responsible for long-term engraftment, have been shown to be CD34 + CD38−, although the majority of cells within this subset do not divide in methylcellulose [14–16].

Hematopoietic stem cell transplantation (HSCT) refers to a medical procedure in which healthy HSPCs are transferred to a recipient following full or partial myeloablation by using chemotherapeutic agents or irradiation [17–23]. HSCT can be used to treat both hematologic and non-hematologic conditions [23, 24], and is usually employed when patients are no longer responsive to conventional treatments or for diseases where conventional treatments have repeatedly proven to be unsuccessful [23]. HSCT generally falls into two categories depending on the source of the HSPCs – *allogeneic* HSCT utilizes HSPCs collected from a suitable donor, while *autologous* HSCT uses HSPCs collected from the patient prior to preparative conditioning.

HSCT has been performed with nucleated cells ranging from 0.7×10^7 to 57.9×10^7 cells/kg body weight, and CD34+ cells ranging from $0.4 \times 10^5$to 39.1×10^5 CD34+ HSPCs/kg body weight [12, 25–28], and while the collected bone marrow and peripheral blood extracts can be used "as is," CD34+ HSPC enrichment prior to transplantation is common. CD34+ HSPC enrichment has been performed prior to allogeneic HSCT to reduce the T-cell load and hence, reduce the likelihood of *graft* vs. *host disease* (GVHD) [12, 25, 29–32]. CD34+ HSPC enrichment can also be employed to purge residual cancer cells from autologous transplants to reduce the likelihood of relapse [33–35]. During a transplant at least two million CD34+ cells per kg body weight is recommended as a minimum dose [28, 36, 37]. HSPCs have traditionally been harvested directly from the bone marrow, but the current trend is to induce the mobilization of HSPCs from the bone marrow environment to peripheral blood through the administration of granulocyte colony-stimulating factor (G-CSF) [38]. Mobilized peripheral blood tends to yield more HSPCs and the collection procedure is less taxing on the donor [25, 29].

Stem cell homing is the process in which HSPCs migrate from peripheral blood to the bone marrow microenvironment. HSPCs circulate regularly between the bone marrow and peripheral blood and while it is still unclear what the physiological role of this mechanism is, there is no doubt that the success of HSCT depends on the ability of the transplanted cells to complete this cycle. The migration from the blood to the bone marrow occurs via four distinct steps, similar to the inflammation cascade for leukocytes: (1) initial capture and tethering, (2) rolling mediated by P- and/or E-selectin, (3) activation by cytokines [usually stromal-derived factor-1 (SDF-1)] followed by integrin-dependent firm adhesion [mediated by very late

adhesion molecule-4 (VLA-4), vascular cell adhesion molecule-1 (VCAM-1), and intracellular adhesion molecule-1 (ICAM-1)], and (4) transendothelial migration in response to an SDF-1 gradient [39–44]. While selectins and cytokines are upregulated by most vascular endothelial cells during inflammation, P- and E-selectin, VLA-4, VCAM-1, and SDF-1 are all constitutively expressed on bone marrow endothelium [39]. Once HSPCs migrate into the bone marrow microenvironment, they must subsequently interact with the stroma within the stem cell niche to receive proliferation and differentiation signals to begin the process of engraftment.

Methods of Cell Enrichment

Cell enrichment techniques remain an important aspect of HSCT preparation as well as general clinical and biomedical research. There are three types of cell enrichment methods based on the attributes of the cell that they target – physical, immunological, and functional. Figure 1.1 depicts some techniques that are routinely employed for processing HSPCs.

Physical Cell Enrichment Methods

Physical cell enrichment methods utilize differences in physical attributes of the cells such as size, density, or pH and include such common techniques as filtration and centrifugation. They are usually bulk cell enrichment methods and in many cases, they serve as precursors for more sensitive enrichment techniques [45].

Immunological Cell Enrichment Methods

Immunological cell enrichment methods utilize antibodies targeted against specific cell surface antigens to select cells of interest. They can either be bulk methods, as is the case of current immunomagnetic technology, or individual methods, such as fluorescence-activated cell sorting (FACS). Since they are highly selective, immunological cell enrichment methods are better suited for rare cell enrichment [46].

FACS is generally not ideally suited for HSPC enrichment in a clinical setting, where large numbers of cells must be sorted to produce acceptably high purity and yield in a reasonable time. FACS will consistently give very high HSPC purities, usually upwards of 80%, but it is prohibitively slow and, even with high speed cell sorters, the process will still take 1.5 h to sort 2×10^8 cells which is 100–1,000 times slower than current immunomagnetic HSPC cell separation techniques [47, 48].

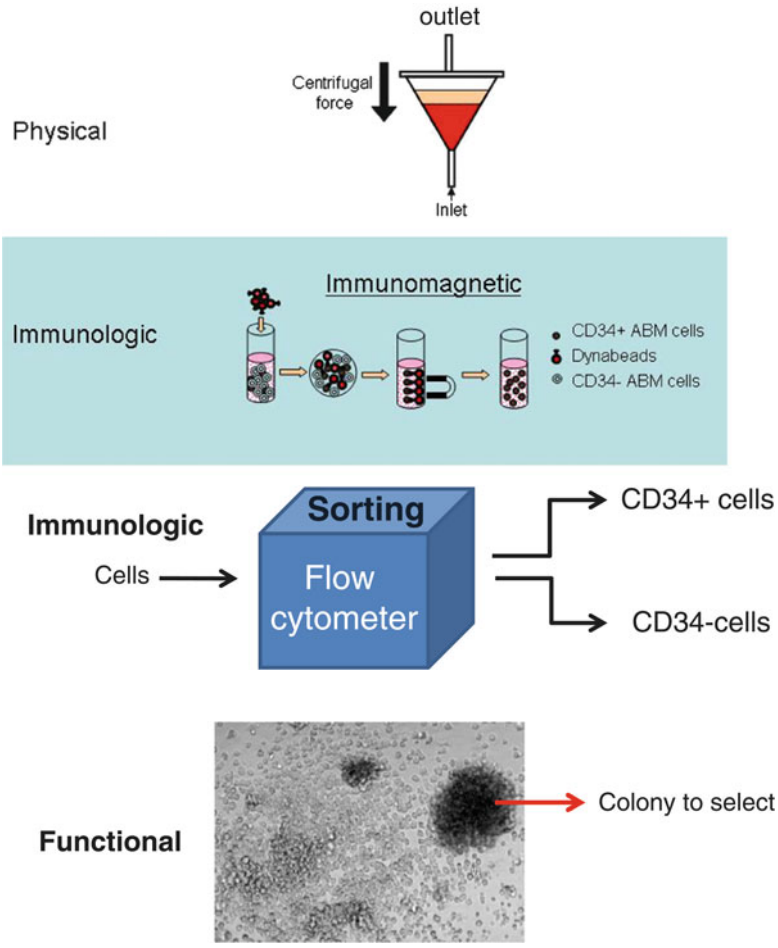

Fig. 1.1 Common methods of cell separation used to process hematopoietic cells in the clinic and laboratory. Cell separation methods can be based on physical, immunological, or functional characteristics of the cell. Physical: Apheresis of mobilized peripheral blood utilizes counter-flow centrifugation to fractionate blood into a dense red cell layer, a buffy coat (containing leukocytes and HSPC), and serum based on their size and density. Immunological: (**a**) Immunomagnetic cell enrichment targets CD34+ cells from mobilized peripheral blood, bone marrow, or cord blood. Antibodies conjugated to paramagnetic beads or ferrous nanoparticles interact with CD34+ cells and application of a magnetic field precipitates the CD34+ cells out of the suspension. (**b**) Fluorescence-activated cell sorting sorts CD34+ cells labeled with an anti-CD34 antibody tagged to a fluorescent dye from PBMCs obtained from mobilized peripheral blood, bone marrow, or cord blood. Functional: A common test for quantifying progenitor cells is to stimulate the cells to form colonies in methylcellulose and select such colonies and expand them

In clinical settings, immunomagnetic HSPC cell enrichment is preferred. Anti-CD34 antibodies conjugated to iron–dextran particles (CliniMACS®) or paramagnetic microspheres (Isolex®) are used to select and enrich CD34+ HSPCs from hematopoietic mononuclear cells (MNCs). These immunological bulk cell sorting

methods are simple to use and produce reasonably high HSPC purities and acceptable yields in relatively short time. MiniMACS® (or CliniMACS®) can generate purities 85–98% with yields ranging from 40 to 100%, while Dynabeads® (or Isolex®) can produce purities ranging from 27 to 99% and yields between 9% and 83% [2, 3, 49–54]. In all cases, the final yield and purity is always a function of the starting CD34+ HSPC concentration.

Shortcomings of Immunomagnetic Cell Enrichment

Although the majority of clinical HSPC enrichment procedures utilize immunomagnetic means to enrich CD34+ HSPCs, there is sufficient evidence to suggest that not all HSPCs are $CD34^{high}$ [55–59] – many $CD34^{low}$ and CD34− HSPCs are lost during the enrichment process [49]. CD133 is a heavily glycosylated transmembrane protein that has also been reported to be an HSPC marker [60], and cells expressing this surface antigen are thought to be more primitive and possess a higher engraftment potential than CD133− CD34+ HSPCs. Although many CD133+ HSPCs also express CD34, a small population remains CD34− while retaining many of the characteristics associated with stem cells [58, 61–63]. Expression of ATP binding cassette superfamily G member 2 (ABCG2) has also been associated with HSPC identification. ABCG2 is a transporter protein that is localized to the plasma membrane and is responsible for Hoescht dye efflux from many stem cell populations (referred to as side population or SP cells). Many SP cells are CD34−, but are capable of self-renewal and development into terminally differentiated blood cells [55, 57, 64].

In addition to the inability to select certain populations of HSPCs, immunological cell enrichment methods are also incapable of indicating whether the enriched cells are truly capable of homing to the marrow to reconstitute the blood supply after HSCT since there is no measure of cell functionality. Rather than utilizing antigen expression as the only tool for HPSC enrichment, an alternative approach is to select HSPCs that show a predisposition to initiate interactions with bone marrow endothelium and hence a greater likelihood of a successful HSCT procedure.

Functional Cell Enrichment Methods

Functional methods for cell enrichment isolate cells based on their response to stimuli. The signal might induce apoptosis, proliferation, or differentiation but only the cells that are able to generate the required response will be selected [45]. Colony-forming cell (CFC) and long-term culture-initiating cell (LTC-IC) assays are types of functional enrichment methods that are used to determine the number of primitive and progenitor cells in a sample [65, 66]. Many of the cells recovered at

the end of the experiments are differentiated and hence, very different from the parent material, and like immunological cell enrichment, these assays provide no measure of the homing potential of the cells.

Adhesion Molecule-Mediated Flow-Based Isolation of CD34+ HSPCs

Current HSPC isolation technologies rely solely on the CD34 surface marker and while they have proven to be invaluable, HSCT that utilizes very pure samples of CD34+ HSPCs are associated with higher incidences of failure and infection and delayed T-cell engraftment [67–73]. Since HSPCs must interact with selectins to successfully home to the marrow, a functional technique to isolate HSPCs based on their interaction with immobilized selectins might improve HSCT by simultaneously purifying the HSPCs and selecting only the cells with the highest probability of homing to the marrow [39–44].

Selectins

Hemodynamics influences the behavior of blood cells in bulk flow and near the vessel wall during adhesion events. The selectins are a group of membrane-bound, adhesion molecules responsible for mediating the initial interactions of leukocytes with the endothelium in response to inflammation or homing signals. Selectin expression is vital for HSPC homing and engraftment; and in experiments using P- and E-selectin double-null NOD/SCID mice show >90% reduction in the number of transplanted CD34+ cells that were retained within the bone marrow environment [74]. Selectins are characterized by an N terminus calcium-dependent lectin domain, an epidermal growth factor (EGF)-like domain, two to nine consensus repeats and a short cytoplasmic tail [75, 76]. P-selectin was originally identified on platelets and is the largest of the selectins. It is stored in α-granules of platelets and Weibel-Palade bodies of endothelial cells and is expressed by activated platelets and endothelial cells in response to inflammation or trauma [77, 78]. E-selectin is produced by endothelial cells only after stimulation with inflammatory cytokines, while L-selectin, the smallest member of the family, is constitutively expressed on the surface of all leukocytes. The binding of selectins to their ligands requires the presence of Ca^{2+} and most selectin ligands found in humans are sialylated and fucosylated glycoproteins [76, 79–82]. Due to the transient nature of the bonds formed, cells involved in selectin-mediated adhesion are found to slowly roll when subjected to a flow field. Tethering requires a relatively high rate of bond formation between the selectin and their ligands to form many bonds that together are capable of balancing the large hydrodynamic forces and torques

exerted by the flowing blood [77]. The rapid rate of bond dissociation coupled with high tensile strength of the bond cause cells to roll in the direction of flow while remaining bound to the surface [77]. The rolling behavior is highly influenced by the surface density of selectin and ligands available to bind. Thus, for cells with a higher number of functional ligands on their surface, the forward reaction (bond formation) is favored leading to a higher rate of bond formation and lower rate of bond dissociation. The overall result is lower-rolling velocities, more cell recruitment, and more resistance to detachment. The bond kinetics for cells rolling on immobilized selectins are such that, generally, rolling velocity on E-selectin < P-selectin < L-selectin for the same surface density of protein.

Previous research has indicated that there exists an inherent difference in rolling behavior between CD34+ and CD34− mononuclear cells – the CD34+ cells rolled slower than CD34− cells on P, E, and L-selectin [83–85]. We have exploited this differential rolling characteristic of CD34+ HSPCs on selectins, to capture and enrich them in flow both an in vitro and an in vivo rat model. Commonalities for both sets of studies included the development of functionalized microtubes that were internally coated with adhesion molecules consisting of a recombinant human P-selectin/Fc chimera (rhP/Fc; Fig. 1.2a). Efficacy of rhP/Fc binding on the interior surface of the microtube is approximately 40–70% across the range of incubation concentrations. A typical concentration of 40 mg/L exhibits ~55% adhesion efficiency [86]. After perfusion, tubes are mounted on the stage of an IX-81 microscope coupled to a CCD camera for direct visualization of the adherent cells in the tube lumen (Fig. 1.2b). The tube lumen is washed with Ca^{2+}-containing PBS or HBSS buffer for 20 min to remove non-adherent cells and erythrocytes, and adherent cells are eluted by using a combination of high shear (flow rate 40 μL/min), calcium-free PBS, and air embolism or simply by perfusing with PBS-containing 0.1 mM EDTA [86, 87].

In vitro capture studies using bone marrow MNCs from healthy donors have yielded 16–20% pure CD34+ HSPCs with an overall enrichment of ~8-fold in P-selectin-coated microtubes. Moreover, enriched HSPCs were viable and functional [86]. For the in vivo capture studies, rats were mobilized with GCSF, anesthetized and P-selectin-coated microtubes were inserted into the left femoral artery for blood perfusion. Analysis of the captured cells exhibited a sevenfold enrichment of CD34 + HSPCs over levels found after ficoll density gradient separation of whole blood, with an average purity of 28% somewhat similar to that of in vitro studies [87]. Robust cell capture and HSPC enrichment were also demonstrated in devices that were implanted in a closed-loop arteriovenous shunt conformation. Moreover, adherent cells were viable in culture and able to differentiate into burst-forming units [87]. Taken together, these studies demonstrated that P-selectin can be successfully used in a compact flow device to capture and enrich HSPCs and that flow-based, adhesion molecule-mediated capture may be a viable alternative approach to the capture and purification of HSPCs.

In addition to the isolation of HSPCs, adhesion molecule-coated tubes can also be employed for the purification of CD45+ MNCs from bone marrow MNCs, PBMCs, or directly from plasma-depleted peripheral blood as these cells

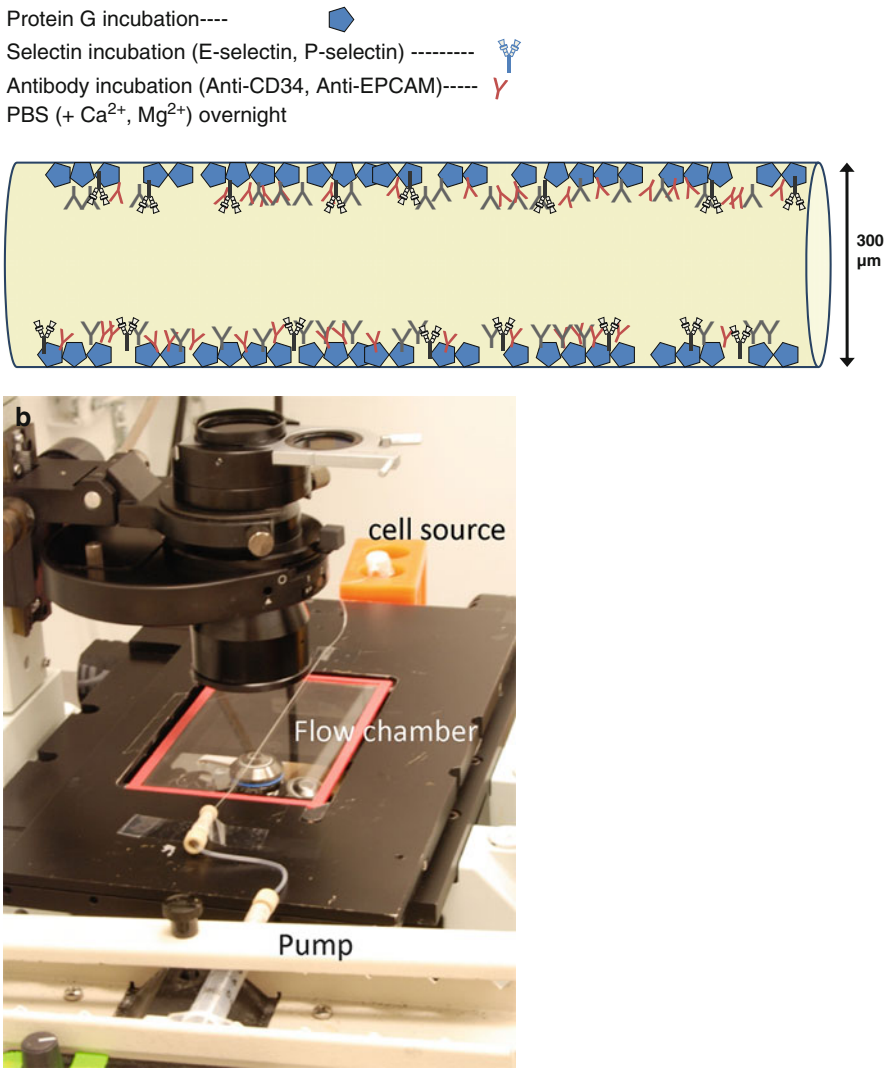

Fig. 1.2 (**a**) Diagram showing the microtube attachment chemistry for immobilizing functional selectin and antibody protein. Protein G is randomly physisorbed onto the microtube surface. Next, a mixture of chimeric selectin/Fc protein and IgG antibody is incubated, resulting in attachment of selectin and antibody in the proper orientation. (**b**) Setup of P-selectin-coated microtube set on the stage of an IX-81 microscope attached to a CCD camera. The tubing is attached to a syringe through special connectors, and syringes are mounted on a syringe pump. The other end of the tubing is immersed in a microfuge tube filled with buffer-containing PBMCs

ubiquitously express PSGL-1, a ligand for P-selectin. Our attempts to perform CD45+ cell purification using selectin-coated microtubes were highly successful, achieving purities of >90% [88, 89]. Furthermore, our lab has demonstrated that apoptotic signals can be delivered specifically to flowing cancer cells without harming normal cells by capturing and rolling them on TNF-related apoptosis-inducing ligand (TRAIL) and E-selectin-coated surfaces [90].

Functionalized Nanoparticle Coatings

We have also shown that thin coatings of immobilized nanoparticles, functionalized with adhesive selectin protein, can further enhance the capture of flowing cells [91, 92]. In one study, colloidal silica nanoparticles were stably immobilized on the interior surface of polymeric microtubing using either inorganic titanate resin or poly-L-lysine [91]. Adding nanoscale roughness to the device surface was found to significantly: (1) increase the amount of immobilized protein; (2) increase the number of captured cells; and (3) decrease the average rolling velocity of captured cells. Naturally occurring halloysite nanotubes can also be immobilized and functionalized with adhesion receptors to enhance cell capture under flow to a similar degree [92]. Halloysite nanotubes are also hollow, raising the possibility of the delivery of slowly eluting drugs to cells rolling across the surface. Nanoparticle coatings were found to not alter the macroscopic fluid mechanics, while bridging the lubrication layer that resists the final micron of cell sedimentation toward the surface, thereby capturing cells closer to the flow device inlet and to a larger degree. Similarly, utilizing the same cell rolling and capture strategy and a novel surface coated with siRNA-encapsulated P-selectin, PEGylated, nanoscale liposomes, our lab demonstrated efficient knockdown of targeted genes in circulating cells [93].

Future Directions

The main debate behind stem cell enrichment stems from the dual roles of T cells after HSCT. T cells are the major contributor to the development of GVHD, a potentially fatal condition that affects many patients receiving allogenic transplants [12, 25, 29–32]. However, the presence of some T cells in the transplants reduces the incidences of relapse, opportunistic infections, and graft failure [94–96]. It would be interesting to investigate how T-cell depletion is influenced by selectin-mediated enrichment to assess whether selectin-mediated enrichment might be superior to immunomagnetic or no enrichment.

Part of the motivation for exploring selectin-mediated enrichment was the fact that cell selection is not based on immunological properties. Since immunological methods of selection favor the $CD34^{hi}$ cells [49], many other cells with stem-like properties are discarded. With selectin-mediated enrichment, all identified and

unidentified cells with stem-like properties have an equal likelihood of selection. If mononuclear cells enriched using immobilized selectin are found to retain more cells with stem-like properties, and this translates into improved homing and engraftment over immunological enrichment in vivo, then this technology could have a real clinical impact. The in vivo experiments must demonstrate that cells isolated with the proposed method are of better quality than cells isolated using immunomagnetic isolation by showing faster engraftment and less incidences of graft failure.

The enrichment potential can be further improved by exploiting the rolling velocity differences between cell subpopulations. One could also achieve higher purities by identifying better elution methods for captured cells specific to CD34+ HSPCs or CD34− MNCs. Multiple cycles of enrichment can also be employed to improve purity and yield. We believe that in future studies it will be possible to improve the purity of HSPCs by engineering selectin molecules so that they will have higher affinity toward HSPCs or lower affinity toward CD34-MNCs. It would also be advantageous to understand the mechanisms that govern the dependence of cell retention with time. The continuous loss of cells with increasing perfusion time suggests that either the passive adsorption of selectin is not an adequate immobilization technique or the cells are losing their functional ligands with time. If improper immobilization is the issue, covalent bonding can eliminate this concern [97].

References

1. Barnett, D., Janossy, G., Lubenko, A., et al.: Guideline for the flow cytometric enumeration of CD34+ haematopoietic stem cells. Prepared by the CD34+ haematopoietic stem cell working party. General Haematology Task Force of the British Committee for Standards in Haematology. Clin. Lab. Haematol. **21**, 301–308 (1999)
2. Servida, F., Soligo, D., Caneva, L., et al.: Functional and morphological characterization of immunomagnetically selected CD34+ hematopoietic progenitor cells. Stem Cells **14**, 430–438 (1996)
3. Cancelas, J.A., Querol, S., Martin-Henao, G., et al.: Isolation of hematopoietic progenitors. An appraoch to two different immunomagnetic methods at the lab scale. Pure Appl. Chem. **68**, 1897–1901 (1996)
4. Andrews, R.G., Singer, J.W., Bernstein, I.D.: Monoclonal antibody 12–8 recognizes a 115-kd molecule present on both unipotent and multipotent hematopoietic colony-forming cells and their precursors. Blood **67**, 842–845 (1986)
5. Barnett, D., Granger, V., Storie, I., et al.: Quality assessment of CD34+ stem cell enumeration: experience of the United Kingdom National External Quality Assessment Scheme (UK NEQAS) using a unique stable whole blood preparation. Br. J. Haematol. **102**, 553–565 (1998)
6. Baum, C.M., Weissman, I.L., Tsukamoto, A.S., et al.: Isolation of a candidate human hematopoietic stem-cell population. Proc. Natl. Acad. Sci. USA **89**, 2804–2808 (1992)
7. Civin, C., Banquerigo, M.L., Strauss, L.C., et al.: Antigenic analysis of hematopoiesis. VI. Flow cytometric characterization of My-10-positive progenitor cells in normal human bone marrow. Exp. Hematol. **15**, 10–17 (1987)

8. Kondo, M., Wagers, A.J., Manz, M.G., et al.: Biology of hematopoietic stem cells and progenitors: implications for clinical application. Annu. Rev. Immunol. **21**, 759–806 (2003)
9. Lanza, F., Healy, L., Sutherland, D.R.: Structural and functional features of the CD34 antigen: an update. J. Biol. Regul. Homeost. Agents **15**, 1–13 (2001)
10. Oxley, S.M., Sackstein, R.: Detection of an L-selectin ligand on a hematopoietic progenitor cell line. Blood **84**, 3299–3306 (1994)
11. Rosen, S.D.: Endothelial ligands for L-selectin: from lymphocyte recirculation to allograft rejection. Am. J. Pathol. **155**, 1013–1020 (1999)
12. Cornetta, K., Gharpure, V., Mills, B., et al.: Rapid engraftment after allogeneic transplantation using CD34-enriched marrow cells. Bone Marrow Transplant. **21**, 65–71 (1998)
13. Lang, P., Schumm, M., Taylor, G., et al.: Clinical scale isolation of highly purified peripheral CD34 + progenitors for autologous and allogeneic transplantation in children. Bone Marrow Transplant. **24**, 583–589 (1999)
14. Pflumio, F., Izac, B., Katz, A., et al.: Phenotype and function of human hematopoietic cells engrafting immune-deficient CB17-severe combined immunodeficiency mice and nonobese diabetic-severe combined immunodeficiency mice after transplantation of human cord blood mononuclear cells. Blood **88**, 3731–3740 (1996)
15. Manz, M.G., Miyamoto, T., Akashi, K., et al.: Prospective isolation of human clonogenic common myeloid progenitors. Proc. Natl. Acad. Sci. USA **99**, 11872–11877 (2002)
16. Bhatia, M., Bonnet, D., Murdoch, B., et al.: A newly discovered class of human hematopoietic cells with SCID-repopulating activity. Nat. Med. **4**, 1038–1045 (1998)
17. Benson Jr., D.M., Elder, P.J., Lin, T.S., et al.: High-dose melphalan versus busulfan, cyclophosphamide, and etoposide as preparative regimens for autologous stem cell transplantation in patients with multiple myeloma. Leuk. Res. **31**, 1069–1075 (2007)
18. Copelan, E.A.: Hematopoietic stem-cell transplantation. N. Engl. J. Med. **354**, 1813–1826 (2006)
19. Farag, S.S., Bolwell, B.J., Elder, P.J., et al.: High-dose busulfan, cyclophosphamide, and etoposide does not improve outcome of allogeneic stem cell transplantation compared to BuCy2 in patients with acute myeloid leukemia. Bone Marrow Transplant. **35**, 653–661 (2005)
20. Farag, S.S., Elder, P.J., Marcucci, G., et al.: Radiation-free regimens result in similar outcomes of allogeneic hematopoietic progenitor cell transplantation in patients aged $>$ or $=$ 50 years compared to younger adults with low-risk disease. Bone Marrow Transplant. **31**, 87–93 (2003)
21. Marks, D.I., Forman, S.J., Blume, K.G., et al.: A comparison of cyclophosphamide and total body irradiation with etoposide and total body irradiation as conditioning regimens for patients undergoing sibling allografting for acute lymphoblastic leukemia in first or second complete remission. Biol. Blood Marrow Transplant. **12**, 438–453 (2006)
22. Berenson, R.J., Andrews, R.G., Bensinger, W.I., et al.: Antigen CD34+ marrow cells engraft lethally irradiated baboons. J. Clin. Invest. **81**, 951–955 (1988)
23. Appelbaum, F.R.: The current status of hematopoietic cell transplantation. Annu. Rev. Med. **54**, 491–512 (2003)
24. Armitage, J.O.: Bone marrow transplantation. N. Engl. J. Med. **330**, 827–838 (1994)
25. Bertolini, F., de Vincentiis, A., Lanata, L., et al.: Allogeneic hematopoietic stem cells from sources other than bone marrow: biological and technical aspects. Haematologica **82**, 220–238 (1997)
26. Wagner, J.E., Barker, J.N., DeFor, T.E., et al.: Transplantation of unrelated donor umbilical cord blood in 102 patients with malignant and nonmalignant diseases: influence of CD34 cell dose and HLA disparity on treatment-related mortality and survival. Blood **100**, 1611–1618 (2002)
27. Barker, J.N., Davies, S.M., DeFor, T., et al.: Survival after transplantation of unrelated donor umbilical cord blood is comparable to that of human leukocyte antigen-matched unrelated donor bone marrow: results of a matched-pair analysis. Blood **97**, 2957–2961 (2001)
28. Bittencourt, H., Rocha, V., Chevret, S., et al.: Association of CD34 cell dose with hematopoietic recovery, infections, and other outcomes after HLA identical sibling bone marrow transplantation. Blood **99**, 2726–2733 (2002)

29. Guardiola, P., Pasquini, R., Dokal, I., et al.: Outcome of 69 allogeneic stem cell transplantations for Fanconi anemia using HLA-matched unrelated donors: a study on behalf of the European Group for Blood and Marrow Transplantation. Blood **95**, 422–429 (2000)
30. Elmaagacli, A.H., Peceny, R., Steckel, N., et al.: Outcome of transplantation of highly purified peripheral blood CD34+ cells with T-cell add-back compared with unmanipulated bone marrow or peripheral blood stem cells from HLA-identical sibling donors in patients with first chronic phase chronic myeloid leukemia. Blood **101**, 446–453 (2003)
31. Bunin, N., Aplenc, R., Leahey, A., et al.: Outcomes of transplantation with partial T-cell depletion of matched or mismatched unrelated or partially matched related donor bone marrow in children and adolescents with leukemias. Bone Marrow Transplant. **35**, 151–158 (2005)
32. Farag, S.S.: Chronic graft-versus-host disease: where do we go from here? Bone Marrow Transplant. **33**, 569–577 (2004)
33. Damiani, D., Sperotto, A., Geromin, A., et al.: Impact of CD34 cell dose on acute graft versus host disease after allogeneic bone marrow stem cell transplantation. Leuk. Lymphoma **43**, 2245–2247 (2002)
34. Lemoli, R.M., Cavo, M., Fortuna, A.: Concomitant mobilization of plasma cells and hematopoietic progenitors into peripheral blood of patients with multiple myeloma. J. Hematother. **5**, 339–349 (1996)
35. Lowdell, M.W., Theocharous, P.: "Less is More": The Role of Purging in Hematopoietic Stem Cell Transplantation. Oncologist **2**, 268–274 (1997)
36. Bensinger, W., Singer, J., Appelbaum, F., et al.: Autologous transplantation with peripheral blood mononuclear cells collected after administration of recombinant granulocyte stimulating factor. Blood **81**, 3158–3163 (1993)
37. Catley, L., Anderson, K.: Strategies to improve the outcome of stem cell transplantation in multiple myeloma. Hematol. J. **5**, 9–23 (2004)
38. Waller, C.F., Bertz, H., Wenger, M.K., et al.: Mobilization of peripheral blood progenitor cells for allogeneic transplantation: efficacy and toxicity of a high-dose rhG-CSF regimen. Bone Marrow Transplant. **18**, 279–283 (1996)
39. Sackstein, R.: The Bone Marrow Is Akin to Skin: HCELL and the Biology of Hematopoietic Stem Cell Homing. J. Inv. Derm. **122**, 1061–1069 (2004)
40. Whetton, A.D., Graham, G.J.: Homing and mobilization in the stem cell niche. Trends Cell Biol. **9**, 233–238 (1999)
41. Peled, A., Kollet, O., Ponomaryov, T., et al.: The chemokine SDF-1 activates the integrins LFA-1, VLA-4, and VLA-5 on immature human CD34(+) cells: role in transendothelial/stromal migration and engraftment of NOD/SCID mice. Blood **95**, 3289–3296 (2000)
42. Chavakis, E., Urbich, C., Dimmeler, S.: Homing and engraftment of progenitor cells: A prerequisite for cell therapy. J. Mol. Cell Cardiol. **45**, 514–522 (2008)
43. Frenette, P.S., Subbarao, S., Mazo, I.B., et al.: Endothelial selectins and vascular cell adhesion molecule-1 promote hematopoietic progenitor homing to bone marrow. Proc. Natl Acad. Sci. USA **95**, 14423–14428 (1998)
44. Nilsson, S.K., Simmons, P.J.: Transplantable stem cells: home to specific niches. Curr. Opin. Hematol. **11**, 102–106 (2004)
45. Orfao, A., Ruiz-Arguelles, A.: General Concepts About Cell Sorting Techniques. Clin. Biochem. **29**, 5–9 (1996)
46. Stella, C.C., Cazzola, M., De Fabritiis, P., et al.: CD34-positive cells: biology and clinical relevance. Haematologica **80**, 367–387 (1995)
47. Ibrahim, S.F., van den Engh, G.: High-speed cell sorting: fundamentals and recent advances. Curr. Opin. Biotechnol. **14**, 5–12 (2003)
48. Chalmers, J.J., Zborowski, M., Sun, L., et al.: Flow through, immunomagnetic cell separation. Biotechnol. Prog. **14**, 141–148 (1998)
49. Johnsen, H.E., Hutchings, M., Taaning, E., et al.: Selective loss of progenitor subsets following clinical CD34+ cell enrichment by magnetic field, magnetic beads or chromatography separation. Bone Marrow Transplant. **24**, 1329–1336 (1999)

50. Hildebrandt, M., Serke, S., Meyer, O., et al.: Immunomagnetic selection of CD34+ cells: factors influencing component purity and yield. Transfusion **40**, 507–512 (2000)
51. Martin-Henao, G.A., Picon, M., Amill, B., et al.: Isolation of CD34+ progenitor cells from peripheral blood by use of an automated immunomagnetic selection system: factors affecting the results. Transfusion **40**, 35–43 (2000)
52. de Wynter, E.A., Ryder, D., Lanza, F., et al.: Multicentre European study comparing selection techniques for the isolation of CD34+ cells. Bone Marrow Transplant. **23**, 1191–1196 (1999)
53. Firat, H., Giarratana, M.C., Kobari, L., et al.: Comparison of CD34+ bone marrow cells purified by immunomagnetic and immunoadsorption cell separation techniques. Bone Marrow Transplant. **21**, 933–938 (1998)
54. Miltenyi, S., Muller, W., Weichel, W., et al.: High gradient magnetic cell separation with MACS. Cytometry **11**, 231–238 (1990)
55. Storms, R.W., Goodell, M.A., Fisher, A., et al.: Hoechst dye efflux reveals a novel CD7(+) CD34(−) lymphoid progenitor in human umbilical cord blood. Blood **96**, 2125–2133 (2000)
56. Smith, C.: Hematopoietic stem cells and hematopoiesis. Cancer Control **10**, 9–16 (2003)
57. Goodell, M.A., Rosenzweig, M., Kim, H., et al.: Dye efflux studies suggest that hematopoietic stem cells expressing low or undetectable levels of CD34 antigen exist in multiple species. Nat. Med. **3**, 1337–1345 (1997)
58. Gallacher, L., Murdoch, B., Wu, D.M., et al.: Isolation and characterization of human CD34 (−)Lin(−) and CD34(+)Lin(−) hematopoietic stem cells using cell surface markers AC133 and CD7. Blood **95**, 2813–2820 (2000)
59. Kuci, S., Wessels, J.T., Buhring, H.J., et al.: Identification of a novel class of human adherent CD34- stem cells that give rise to SCID-repopulating cells. Blood **101**, 869–876 (2003)
60. Miraglia, S., Godfrey, W., Yin, A.H., et al.: A novel five-transmembrane hematopoietic stem cell antigen: isolation, characterization, and molecular cloning. Blood **90**, 5013–5021 (1997)
61. de Wynter, E.A., Buck, D., Hart, C., et al.: CD34 + AC133+ cells isolated from cord blood are highly enriched in long-term culture-initiating cells, NOD/SCID-repopulating cells and dendritic cell progenitors. Stem Cells **16**, 387–396 (1998)
62. Yin, A.H., Miraglia, S., Zanjani, E.D., et al.: AC133, a novel marker for human hematopoietic stem and progenitor cells. Blood **90**, 5002–5012 (1997)
63. Handgretinger, R., Gordon, P.R., Leimig, T., et al.: Biology and plasticity of CD133+ hematopoietic stem cells. Ann. NY Acad. Sci. **996**, 141–151 (2003)
64. Guo, Y., Lubbert, M., Engelhardt, M.: CD34- hematopoietic stem cells: current concepts and controversies. Stem Cells **21**, 15–20 (2003)
65. Andrews, R.G., Singer, J.W., Bernstein, I.D.: Human hematopoietic precursors in long-term culture: single CD34+ cells that lack detectable T cell, B cell, and myeloid cell antigens produce multiple colony forming cells when cultured with marrow stromal cells. J. Exp. Med. **172**, 355–358 (1990)
66. Leary, A.G., Ogawa, M., Strauss, L.C., et al.: Single cell origin of multilineage colonies in culture. Evidence that differentiation of multipotent progenitors and restriction of proliferative potential of monopotent progenitors are stochastic processes. J. Clin. Invest. **74**, 2193–2197 (1984)
67. Kernan, N.A., Bordignon, C., Heller, G., et al.: Graft failure after T-celldepleted human leukocyte antigen identical marrow transplants for leukemia: I. Analysis of risk factors and results of secondary transplants. Blood **74**, 2227–2236 (1989)
68. Keever, C.A., Small, T.N., Flomenberg, N., et al.: Immune reconstitution following bone marrow transplantation: comparison of recipients of Tcell depleted marrow with recipients of conventional marrow grafts. Blood **73**, 1340–1350 (1989)
69. Martinez, C., Urbano-Ispizua, A., Rozman, C., et al.: Immune reconstitution following allogeneic peripheral blood progenitor cell transplantation: comparison of recipients of positive CD34 + selected grafts with recipients of unmanipulated grafts. Exp. Hematol. **27**, 561–568 (1999)
70. Daley, J.P., Rozans, M.K., Smith, B.R., et al.: Retarded recovery of functional T cell frequencies in T cell-depleted bone marrow transplant recipients. Blood **70**, 960–964 (1987)

71. Martino, R., Rovira, M., Carreras, E., et al.: Severe infections after allogeneic peripheral blood stem cell transplantation: a matched-pair comparison of unmanipulated and CD34+ cell-selected transplantation. Haematologica **86**, 1075–1086 (2001)
72. Crippa, F., Holmberg, L., Carter, R.A., et al.: Infectious complications after autologous CD34-selected peripheral blood stem cell transplantation. Biol. Blood Marrow Transplant. **8**, 281–289 (2002)
73. Negrin, R.S., Atkinson, K., Leemhuis, T., et al.: Transplantation of highly purified CD34 + Thy-1+ hematopoietic stem cells in patients with metastatic breast cancer. Biol. Blood Marrow Transplant. **6**, 262–271 (2000)
74. Hidalgo, A., Weiss, L.A., Frenette, P.S.: Functional selectin ligands mediating human CD34 (+) cell interactions with bone marrow endothelium are enhanced postnatally. J. Clin. Invest. **110**, 559–569 (2002)
75. Geng, J.G., Chen, M., Chou, K.C.: P-selectin cell adhesion molecule in inflammation, thrombosis, cancer growth and metastasis. Curr. Med. Chem. **11**, 2153–2160 (2004)
76. McEver, R.P.: Selectins: lectins that initiate cell adhesion under flow. Curr. Opin. Cell Biol. **14**, 581–586 (2002)
77. Konstantopoulos, K., Kukreti, S., McIntire, L.V.: Biomechanics of cell interactions in shear fields. Adv. Drug Deliv. Rev. **33**, 141–164 (1998)
78. Kansas, G.S.: Selectins and their ligands: current concepts and controversies. Blood **88**, 3259–3287 (1996)
79. Alon, R., Feizi, T., Yuen, C.T., et al.: Glycolipid ligands for selectins support leukocyte tethering and rolling under physiologic flow conditions. J. Immunol. **154**, 5356–5366 (1995)
80. Geng, J.G., Heavner, G.A., McEver, R.P.: Lectin domain peptides from selectins interact with both cell surface ligands and Ca2+ ions. J. Biol. Chem. **267**, 19846–19853 (1992)
81. Hidalgo, A., Frenette, P.S.: Enforced fucosylation of neonatal CD34+ cells generates selectin ligands that enhance the initial interactions with microvessels but not homing to bone marrow. Blood **105**, 567–575 (2005)
82. Moore, K.L., Eaton, S.F., Lyons, D.E., et al.: The P-selectin glycoprotein ligand from human neutrophils displays sialylated, fucosylated, Olinked poly-N-acetyllactosamine. J. Biol. Chem. **269**, 23318–23327 (1994)
83. Greenberg, A.W., Kerr, W.G., Hammer, D.A.: Relationship between selectin mediated rolling of hematopoietic stem and progenitor cells and progression in hematopoietic development. Blood **95**, 478–486 (2000)
84. Greenberg, A.W., Hammer, D.A.: Cell separation mediated by differential rolling adhesion. Biotechnol. Bioeng. **73**, 111–124 (2001)
85. Charles, N., Liesveld, J.L., King, M.R.: Investigating the feasibility of stem cell enrichment mediated by immobilized selectins. Biotechnol. Prog. **23**, 1463–1472 (2007)
86. Narasipura, S.D., Wojciechowski, J.C., Charles, N., et al.: P-selectin-coated microtube for enrichment of CD341 hematopoietic stem and progenitor cells from human bone marrow. Clin. Chem. **54**, 77–85 (2008)
87. Wojciechowski, J.C., Narasipura, S.D., Charles, N., et al.: Capture and enrichment of CD34-positive haematopoietic stem and progenitor cells from blood circulation using P-selectin in an implantable device. Br. J. Haematol. **140**, 673–681 (2008)
88. Narasipura, S.D., Wojciechowski, J.C., Duffy, B.M., et al.: Purification of CD45+ hematopoietic cells directly from human bone marrow using a flow-based P-selectin-coated microtube. Am. J. Hematol. **83**, 627–629 (2008)
89. Narasipura, S.D., King, M.R.: P-selectin-coated microtube for the purification of CD45+ ematopoietic cells directly from human peripheral blood. Blood Cells Mol. Dis. **42**, 136–139 (2009)
90. Rana, K., Liesveld, J.L., King, M.R.: Delivery of apoptotic signal to rolling cancer cells: a novel biomimetic technique using immobilized TRAIL and E-selectin. Biotechnol. Bioeng. **102**, 1692–1702 (2009)

91. Han, W., Allio, B.A., Foster, D.G., et al.: Nanoparticle coatings for enhanced capture of flowing cells in microtubes. ACS Nano **4**, 174–180 (2010)
92. Hughes, A.D., King, M.R.: Use of naturally occurring halloysite nanotubes for enhanced capture of flowing cells. Langmuir **26**, 12155–12164 (2010)
93. Huang, Z., King, M.R.: An immobilized nanoparticle-based platform for efficient gene knockdown of targeted cells in the circulation. Gene Ther. **16**, 1271–1282 (2009)
94. Martin, P.J., Hansen, J.A., Buckner, C.D., et al.: Effects of in vitro depletion of T cells in HLA-identical allogeneic marrow grafts. Blood **66**, 664–672 (1985)
95. Horowitz, M.M., Gale, R.P., Sondel, P.M., et al.: Graft-versus-leukemia reactions after bone marrow transplantation. Blood **75**, 555–562 (1990)
96. Holmberg, L.A., Boeckh, M., Hooper, H., et al.: Increased incidence of cytomegalovirus disease after autologous CD34-selected peripheral blood stem cell transplantation. Blood **94**, 4029–4035 (1999)
97. Hong, S., Lee, D., Zhang, H., et al.: Covalent immobilization of p-selectin enhances cell rolling. Langmuir **23**, 12261–12268 (2007)

Chapter 2
Matrix Stiffness: A Regulator of Cellular Behavior and Tissue Formation

Brooke N. Mason, Joseph P. Califano, and Cynthia A. Reinhart-King

Abstract The extracellular environment is an essential mediator of cell health and provides both chemical and mechanical stimuli to influence single and collective cell behaviors. While historically there has been significant emphasis placed on chemical regulators within the extracellular matrix, the role of the mechanical environment is less well known. Here, we review the role of matrix mechanics on cell function and tissue integrity. Cellular responses to mechanical signals include differentiation, migration, proliferation, and alterations in cell–cell and cell–matrix adhesion. Interestingly, the mechanical properties of tissues are altered in many disease states, leading to cellular dysfunction and further disease progression. Successful regenerative medicine strategies must consider the native mechanical environment so that they are able to elicit a favorable cellular response and integrate into the native tissue structure.

Matrix Mechanics Are Essential Design Parameters for Regenerative Medicine

Tissue engineering (TE) was defined in the late 1980s as a field concerned with "the application of the principles and methods of engineering and life sciences toward. . .the development of biological substitutes to restore, maintain, or improve functions" [111]. Motivated by a clinical need to restore normal physiologic function to tissues and organs that malfunction due to injury and disease, TE approaches may provide an avenue of treatment for patients with organ and tissue failure additionally plagued by increasing costs of care and donor shortages [63].

Significant numbers of investigations into biomaterials have confirmed that surface chemistry is a critical parameter contributing to the clinical success of

B.N. Mason • J.P. Califano • C.A. Reinhart-King (✉)
Department of Biomedical Engineering, Cornell University, Ithaca, NY 14850, USA
e-mail: cak57@cornell.edu

S.K. Bhatia (ed.), *Engineering Biomaterials for Regenerative Medicine: Novel Technologies for Clinical Applications*, DOI 10.1007/978-1-4614-1080-5_2,

implanted devices or TE constructs [118]. Surgery and implantation of biomaterial or TE constructs induces biochemical cascades that mediate the normal wound healing and foreign body responses that ultimately result in the success (functional integration into the tissue) or failure (rejection from the tissue, mechanical failure) of the implant. While the need to tailor the surface chemistry of an implant has been given significant attention for decades, the need to also consider the mechanical properties of an implant and its effects on cells has only been gaining momentum in recent years. Similar to surface chemistry, the mechanical properties affect the local behaviors of tissues and cells and contribute to the success of biomaterial and tissue-engineered implants.

While TE and regenerative medicine have recently focused on the micromechanical properties of a construct and its effects on cells, the notion that mechanical forces act as critical regulators of physiological processes at the cell and tissue level is not a new paradigm. Physical forces were known to contribute to the development of brain morphology [46] and bone remodeling [103, 128] as early as the late nineteenth century. Since then, elucidating the relationship between force and biological responses has spanned a variety of mechanical settings and length scales from probing the role of weightlessness on the musculoskeletal system during spaceflight [56] to understanding how shear stress in the vascular tree specifies endothelial cell phenotype [22]. These studies drew attention to the role of the physical environment as an important regulator of biological responses in living systems.

This chapter describes the role of the mechanical properties of the extracellular matrix (ECM) as a mediator of cellular responses and tissue formation. An overview of the nature of the mechanical properties of the cellular microenvironment and how it affects cellular function and tissue formation are discussed. Lastly, the role of matrix mechanics in disease states is presented.

The Cellular Response to Matrix Mechanics: Cellular Function Is Modulated by Local Matrix Stiffness

The Mechanical Environment of Cells

Cells *in vivo* are organized into tissues and organs that reside in complex mechanical environments. At the cellular level, the mechanical environment consists of endogenous (generated *by* cells) and exogenous (applied *to* cells) forces. Endogenous forces generated by cells on their ECM and neighboring cells largely result from cytoskeletal contractility (discussed below; [13, 76]). Examples of exogenous forces include gravity and tissue-specific interactions; for example, endothelial cells in the vasculature are subjected to pulsatile shear forces from blood flow [6] as well as migratory traction forces during leukocyte transmigration [94].

In addition to these actively imposed forces, the local stiffness of the ECM that serves as a biological scaffold is an important mechanical effector of cell function.

Stiffness is a measure of the ability of a material to resist deformation. In the body, tissue stiffness ranges several orders of magnitude, from adipose tissue (Young's Modulus E ~ several kPa) [106] to bone (E ~ GPa) [99]. In addition, tissue stiffness is not static, but changes during physiological processes including embryonic development, tissue remodeling during wound healing, and in pathological responses like tumorigenesis. Since there is an intimate association between cells and the ECM within tissues, and cells function in a variety of mechanical environments, many studies have investigated the mechanisms that cells use to sense and respond to their mechanical environment.

Biological Force Transducers

Tissue cells have an ability to sense and probe the stiffness of their surroundings as they adhere to and interact with the local ECM [28]. Mechanotransduction, where cells convert mechanical stimuli into chemical signals that affect cellular responses, occurs through a variety of mechanisms. Well-described mechanotransducers include stretch-mediated ion channels [74], primary cilia [8], and integrins [36, 100]. Additional mechanosensors, including G-protein receptors [70], cell–cell adhesions [57, 86], and the cytoskeleton [126] have been suggested. While these transducers sense the mechanical environment through a variety of mechanisms, they all share the ability to convert mechanical input into complex intracellular signaling cascades that ultimately regulate cellular responses including adhesion, spreading, migration, and proliferation [54]. The number and variety of mechanosensors identified in cells suggests that cells have a robust capacity to interact with their mechanical environment. This robustness is particularly important when considering that in addition to regulating normal physiological responses, abnormal mechanotransduction at the cellular level has been implicated in mediating a wide variety of prominent disease states including asthma [127], osteoporosis [2, 19], and cancer [51, 52, 115].

While it is likely that no single cell feature is responsible for driving all mechanobiological responses, the integrin family of proteins has emerged as a prominent and well-studied force transducer. The concept of a mechanical linkage between the ECM and the intracellular cytoskeleton was postulated in the mid-1970s [49], and the structure of integrins was determined in the next decade [116]. Composed of α and β subunits (18α and 8β subunits combine to form over 20 distinct integrin heterodimers to-date), integrin receptors are a family of transmembrane glycoproteins that serve as mechanical linkages between the ECM and the cytoskeleton [50]. On the exterior of the cell, integrins bind ECM protein ligands including collagen, laminin, and fibronectin [93]. Within the cell, the β subunit of integrin heterodimers binds to the actin cytoskeleton through a variety of adaptor proteins [66]. Integrins cluster into focal adhesions that spatially localize and

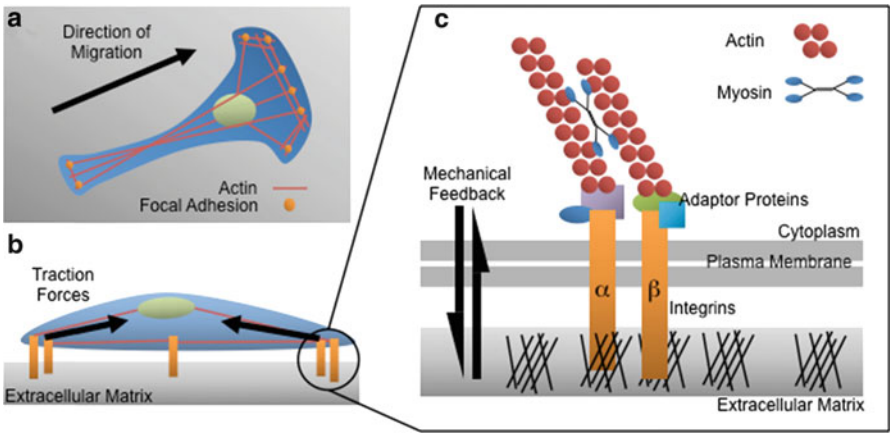

Fig. 2.1 (**a**) A typical cell migrating over a substrate utilizes actin stress fibers anchored to focal adhesions. (**b**) Together with the actin cytoskeleton, focal adhesions composed of integrins facilitate cell–substrate adhesion, contractility, and traction force generation. (**c**) A close-up depiction of a focal adhesion. Actin stress fibers are tensed by myosin motors and attach to integrin receptors via adaptor proteins within the cytoplasm. Integrin transmembrane receptors bind to the extracellular matrix outside the cell and participate in mechanosensing events

anchor actin stress fibers to the plasma membrane thus providing a mechanical linkage between the ECM and the cytoskeleton (Fig. 2.1a) [37]. Moreover, the integrin "adhesome" serves as a scaffold for a host of signaling proteins within the cell [132], suggesting that integrin receptors serve as prominent sensors and integrators of environmental signals.

Cells Sense Matrix Stiffness with Cellular Contractility and Traction Forces

"Stiffness sensing" means that cells have an ability to detect and respond to the mechanical resistivity of the extracellular environment. Stiffness sensing has been demonstrated in a variety of cell types including endothelial cells [17, 26, 96, 98], smooth muscle cells [31, 53], and transformed cells [67, 125]. The ability to sense stiffness is partly dependent on actomyosin-generated contractility that is transmitted to the extracellular environment through transmembrane integrin receptors that, with a number of intracellular signaling and scaffold proteins, organize into focal adhesions. Cells, in turn, respond to the stiffness of their substrate by altering cytoskeletal organization, cell–substrate adhesions, and other processes important for regulating cell behaviors.

Cellular contractility is generated in part by the actomyosin cytoskeleton. Actin stress fibers are tensed by myosin motors [61, 101], and cytoskeletal contractility is

transmitted to the ECM as traction forces (Fig. 2.1b, c) [65]. Cellular traction forces were first observed in landmark experiments as wrinkles or strains in flexible silicone rubber substrates [44]. Since then, methods have been developed to quantify traction forces generated by cells. Prominent techniques include traction force microscopy [25, 72] and the use of microfabricated post-array detectors [113, 117]. Other methods include the use of microfabricated cantilevers [35] and micropatterned silicone elastomeric substrates [4]. These techniques calculate traction forces based on strains created in the substrate by adherent cells. The ability of adherent cells to generate traction forces and cell–substrate adhesions facilitates sensing of the local extracellular environment and is involved in feedback mechanisms where matrix stiffness in turn modulates responses such as adhesion, spreading, and migration.

Matrix Stiffness Modulates Focal Adhesions, Cytoskeletal Assembly, and Traction Forces

The measurement of cell traction forces has helped to describe the role of force and focal adhesions as mediators of cell–substrate attachment and matrix stiffness. Experiments in real-time indicate that focal adhesion size is linearly dependent on the local force exerted by a cell [4]. Mature focal adhesions elongate and orient in the direction of actin stress fibers and applied force. However, the correlation of focal adhesion size with cell-generated forces may only hold for adhesions larger than 1 μm^2, as smaller adhesions are capable of exerting large traction forces that do not correlate with adhesion size [117]. Indeed, small nascent adhesions (focal complexes) at the leading edge of cells are capable of generating strong transient traction forces that drive cell migration [7]. Moreover, when cells on magnetic microposts are deflected by an external magnetic field, changes in traction force generation occur at sites of adhesion peripheral to the site of force application [112]. These data are indicative of a dynamic association between the actin cytoskeleton, cellular traction forces, and focal adhesions that mediates cell adhesion and migration.

Additional work has investigated focal adhesion organization with regard to matrix stiffness. Seminal experiments with fibroblasts and epithelial cells indicate that compliant ($E \sim 1$ kPa) substrates promote focal adhesions that are dynamic and irregular punctate structures [90]. In contrast, an increase in stiffness ($E \sim 30$–100 kPa) promotes the formation of stable arrays of elongated focal adhesions and an increase in tyrosine phosphorylation of focal adhesion kinase (FAK) and paxillin, suggesting that stiffness sensing involves intracellular signaling events. Such changes in focal adhesion organization suggest alterations in cell–substrate adhesivity. Accordingly, an increase in cell–substrate adhesion with increasing substrate stiffness has been demonstrated [32].

In general, stiff substrates increase both focal adhesion and cytoskeletal organization [31, 38, 41, 90, 130]. The formation of stable focal adhesions with increasing substrate stiffness is accompanied by changes in cell shape. For example, fibroblasts plated on compliant substrates are rounded with diffuse actin, while those plated on stiff substrates exhibit an increase in spread area and actin stress fiber organization [39, 130]. Similarly, endothelial cell spread area increases with increasing substrate stiffness [16, 97], where endothelial cells on compliant substrates adopt an elongated spindle-shaped morphology, while those on stiffer substrates exhibit more isotropic spreading [17]. Interestingly, endothelial cell stiffness is also modulated by matrix stiffness in 2D and 3D environments [15]. These data suggest an intimate association between substrate stiffness, cytoskeletal organization and cell shape, focal adhesions, and traction force generation.

The investigation of matrix stiffness as a mediator of cell shape has further elucidated the relationship between stiffness and force generation. It has been shown that matrix stiffness and cell shape help regulate the polarization and alignment of stress fibers within cells [134]. Indeed, matrix stiffness can alter cellular contractility [135]; traction force generation by fibroblasts and endothelial cells increases with increasing substrate stiffness [17, 41, 68]. Moreover, experiments with endothelial cells have demonstrated that both cell area and substrate stiffness are significant predictors of traction force generation [17]. In turn, the orientation and organization of the actin cytoskeleton helps determine cell shape; the ablation of a single stress fiber in a cell results in significant rearrangements in cell shape and cytoskeletal organization [61]. These data provide evidence for feedback mechanisms that relate matrix stiffness to cytoskeletal organization and traction force generation and provide a role for mechanotransduction as a contributor to cell shape.

The sensitivity of cellular traction force generation to matrix stiffness has implications for the organization of the local ECM. For example, the fibrillogenesis of the ECM protein fibronectin is mediated by endogenous cellular contractility [5]. Experiments with fibronectin-based native ECM scaffolds versus scaffolds stiffened by chemical crosslinking indicated differential scaffold remodeling by fibroblasts; native scaffolds were progressively remodeled over several days while cross-linked scaffolds were not [60]. These data indicate that there are feedback mechanisms that relate matrix stiffness to matrix remodeling and suggest that cellular responses to matrix stiffness may regulate ECM homeostasis.

Matrix Stiffness Modulates Cell–Cell Assembly, Migration, and Proliferation

In addition to modulating cellular contractility and force generation, matrix stiffness plays a role in mediating cell–cell interactions. Seminal work by Guo et al. established a relationship between matrix stiffness, cell–matrix, and cell–cell

interactions [43]. When heart tissue explants were plated on stiff matrices, cells from the tissue migrated out of the explant to cover the matrix. In contrast, cells in explants plated on compliant matrices did not migrate out of the explant. Separate studies with endothelial cells also indicate sensitivity of cell–cell interactions to matrix stiffness. On compliant substrates, endothelial cells prefer cell–cell interactions [98] and self-assemble into networks [16]. On stiffer substrates, ECs prefer cell–substrate interactions and fail to form network assemblies. In epithelial cells, cell–cell assembly is anisotropic along directions of stiff substrate and correlates with actin cytoskeletal organization and force generation [104]. These data suggest that matrix stiffness and traction forces modulate cell–cell organization.

Further work has investigated the role of matrix stiffness in mediating cell migration [55, 91]. For example, fibroblasts migrate toward substrates of increasing stiffness, a response termed durotaxis [68]. Smooth muscle cells also exhibit durotaxis with respect to the magnitude of substrate stiffness gradient [53]. These data indicate that substrate stiffness provides important cues that foster traction force organization responsible for cell migration. The sensitivity of cell migration to stiffness gradients may have important implications for disease states such as fibrosis or tumorigenesis that are accompanied in increases in ECM stiffness.

In addition to affecting migration, forces between contacting cells can also influence proliferation. Gray et al. found that the number of cell–cell contacts influences the proliferation of a cell in a bi-phasic manner [42]. Single cells are less proliferative than those with at least one cell–cell contact but increasing the number of neighbors inhibits proliferation. Interestingly, increasing the amount of cell–cell contacts may concurrently decrease the ability of cells to adhere to the ECM, thus decreasing proliferation. This response is essential for healthy tissue function where contractility, spreading, and proliferation are intricately regulated by cell–cell and cell–matrix adhesion and tension.

Collective Cell Responses to Matrix Mechanics: Implications for Tissue Development, Regeneration, and Repair

We have discussed the importance of matrix mechanics on individual cellular behavior and function. However, while single cell studies may be informative of cellular behavior, cells within tissues interact and respond collectively to stimuli. Similar to the influences on individual cells, mechanics are integral to overall tissue and organ physiology and mechanical alterations or disturbances can lead to disease and tissue malformation (discussed below). Interestingly, the earliest stages of embryonic development, tissue patterning, and organ formation are governed, in part, by mechanical interactions with the extracellular environment [21, 82, 110]. Studying these interactions can inform the design of tissue engineered and regenerative therapies.

Mechanical Stimuli Influence Embryonic Development

Throughout embryonic development, all tissues of the body are derived from a single-fertilized cell via a complex process of specification and differentiation. Cellular differentiation is the process whereby a cell with an unspecified fate is influenced by genetic, chemical, and mechanical [14] factors to become a specific cell type. A fully differentiated cell maintains its gene expression patterns through generations of proliferation and has a distinct role within an organized tissue. During embryogenesis, biochemical factors and pre-programmed genetic cues initially dictate the polarity of the embryo as well as the cell lineage specification of its progeny into the three germ layers: ectoderm, endoderm, and mesoderm [34, 92]. Concurrent with these chemical and genetic signals, mechanical stimuli reinforce and further specify cell fate and play a crucial role in the development of the unique tissues and organs of the body [34]. Specifically, mechanical signals such as pressure, fluid flow, shear stress, tension, and stiffness are important regulators of embryogenesis and have been shown to affect the development and tissue patterning of many major organs [71] including the eye [45, 82], heart [48, 89], vasculature [77], and neural tube [136].

Further investigations into developmental processes have indicated that matrix mechanics play a vital role in proper tissue development throughout the entire embryo. Recent work in *Xenopus* has confirmed a temporal and spatial distribution of mechanical stiffness within developing embryos due to the contraction of the actomyosin network [136]. This cytoskeletal contraction not only increases the stiffness of the surrounding tissue structures as much as 50-fold within 8 h, but may also drive the formation of the neural tube and allow for further cell patterning and differentiation [136]. Similarly, repeated and coordinated contractions of the actomyosin cortex in *Drosophila* embryos create tension between cells that facilitate cell invagination and formation of the ventral furrow [73]. These data indicate that intra- and inter-cellular contractility drive tissue morphogenesis.

In addition to the exogenous mechanical stimuli within developing tissues, differential adhesion and repulsion between cells and the surrounding matrix plays an integral role in embryonic tissue morphogenesis [114, 121]. It has been shown that the ectoderm–mesoderm boundary is not only maintained by self-sorting due to preferential adhesion of similar cells to each other, but is also a function of the active repulsion between unlike cells [102]. Interestingly, the development of structures within the retinal epithelium in *Drosophila* embryos mimics the formation of soap bubble aggregates, where the surface tension is minimized during aggregate formation [45]. This patterning occurs due to differential adhesion between cells with the most adhesive cells forming central aggregates surrounded by less-adhesive cells to minimize the "surface energies" of the cell contacts. Similarly, during a phase of embryogenesis known as epiboly, cell adhesion proteins are differentially expressed so that a group of cells can migrate toward the vegetal pole of the embryo and begin gastrulation [110]. These data indicate that tissue formation is influenced by the balance of cell–cell and cell–substrate adhesion.

The mechanical environment is intimately linked with collective cell behavior such as contractility, adhesion, and tissue patterning during embryogenesis. Importantly, matrix mechanics can regulate cellular specification and tissue formation. Regenerative strategies may exploit these responses to mechanical stimuli to produce organized cellular structures that mimic the original, healthy tissues.

Mechanical Control of Cellular Differentiation

In addition to embryogenesis, mechanical cues play an integral role in maintaining and influencing cell fate and tissue maintenance throughout life. While the process of differentiation is most obvious during embryonic development, some cells (e.g., stem cells) remain multipotent even in adult tissue [80]. These stem cells are essential for tissue maintenance and repair, may have important implications for disease progression, and have been the focus of many engineered tissue therapies. Importantly, each of these processes is influenced by the mechanical properties of the surrounding environment.

Although initial tissue engineering strategies were concerned primarily with maintaining the mechanical integrity of the implant, current therapies look to integrate mechanical cues to differentiate and pattern cells into complex tissues. Stem cells have been a popular choice for regenerative medicine research since they are capable of self-renewal and differentiating into multiple cell types [80]. The stem cell niche, the 3D microenvironment surrounding the cells, is a key factor in their maintenance and differentiation [9, 29, 124]. To further understand the factors that influence stem cell differentiation in 2D and 3D, synthetic and natural scaffolds have been used to probe the interactions of the cells with their extracellular environment [27]. Many groups have combined novel materials and chemical cues to encourage stem cell differentiation along a chosen lineage in the hopes of creating regenerative therapies [69].

Endogenous cellular stiffness is predominantly regulated by the actomyosin cytoskeleton and has been shown to change during differentiation [64]. Using AFM, Titushkin and Cho observed that mesenchymal stem cells stimulated with osteogenic medium became less stiff throughout their course of differentiation [119]. In contrast, cells differentiated from mouse embryonic stem cells are tenfold stiffer than their precursors [21]. Similarly, Pajerowski et al. found that the nucleus of human embryonic stem cells becomes sixfold stiffer when terminally differentiated (Fig. 2.2a) [87]. These results suggest that the mechanical properties of cells depend on both the origin and differentiation stage of the stem cells.

Matrix mechanics are also known to be independently capable of dictating stem cell differentiation into different lineages. In a seminal study, Engler and colleagues demonstrated that mesenchymal stem cells can be stimulated to differentiate into neurons and osteoblasts when plated on soft and stiff matrices, respectively, that were chemically similar (Fig. 2.2b) [33]. Recently, scientists have exploited the ability of stem cells to sense and respond to their mechanical environment to create

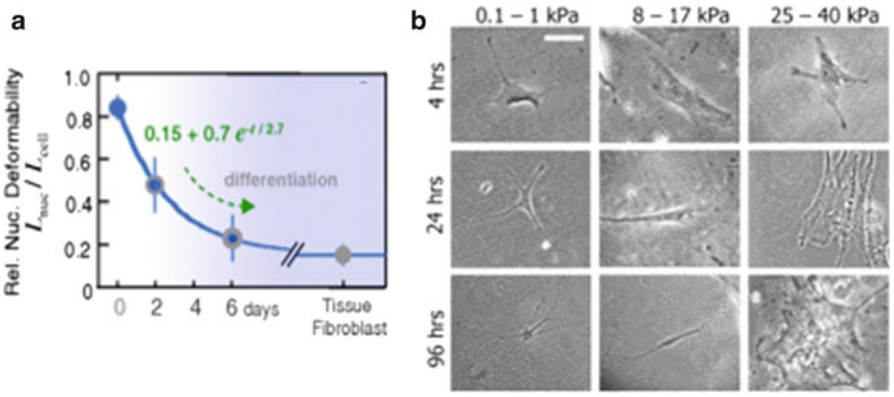

Fig. 2.2 (**a**) During differentiation, the nuclear compliance of human embryonic stem cells decreases (stiffness increases) relative to the cellular cytoplasm. Reprinted with permission from PNAS 104(40): Pajerowski et al.: Physical plasticity of the nucleus in stem cell differentiation, 15619–15624, Copyright 2007 National Academy of Sciences, U.S.A. [87]. (**b**) Mesenchymal stem cells sense and respond to substrate stiffness by changing differentiating to neural cells and myoblasts on soft and stiff substrates, respectively. Reprinted from Cell 126(4): Engler et al.: Matrix Elasticity Directs Stem Cell Lineage Specification, 677–689, Copyright 2006 [33], with permission from Elsevier

scaffolds that vary in stiffness spatially such that an entire tissue might be created by simply seeding the engineered matrix with stem cells [20, 59, 109, 123]. Very recent work indicates that mesenchymal stem cells plated on a stiffness gradient directionally migrate toward the stiffer portions of the substrate and subsequently differentiate [123]. Interestingly, the cells that migrate from soft to stiff regions of the substrate maintain neuronal markers similar to the cells that are plated on uniformly soft substrates [123]. Importantly, these results suggest that even though the cells in a specific lineage may become differentiated, they are able to retain a "memory" of the previous signals they have received. These data suggest that mechanical microenvironmental cues are essential to the promotion and preservation of stem cell lineage specification and, to produce a functional tissue replacement, will be required design parameters for regenerative therapeutics.

Matrix Mechanobiology Alterations in Disease and Injury

Altered tissue mechanics are a prominent feature of many injured diseased tissue states and are commonly a result of abnormal ECM deposition, matrix cross-linking and/or matrix degradation. Specifically, matrix stiffening accompanies aging [23], cardiovascular disease [105], wound healing [40], and tumor formation [85]. Native ECM mechanics can be modified by changes in protein deposition or cross-linking of preexisting matrix components. These changes in matrix mechanics can lead to aberrant cell behavior that can cause or exacerbate disease states [3, 62].

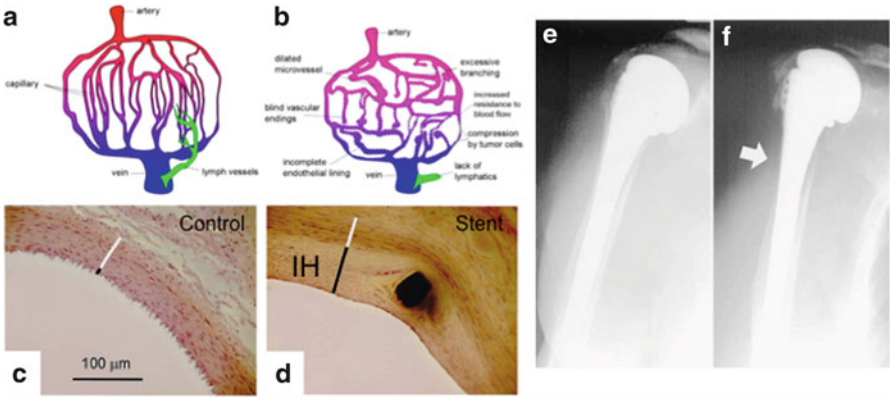

Fig. 2.3 (**a**, **b**) A cartoon depicting the vascular system in a normal tissue (**a**) and in a solid tumor (**b**). Reprinted with permission from Oxford University Press from Trédan et al.: Drug Resistance and the Solid Tumor Microenvironment. Journal of the National Cancer Institute 99(19):1441–54 [122]. (**c**, **d**) Measurements of intima (*black bars*) and media (*white bars*) in control (**c**) and stented (**d**) rabbit carotid arteries. *IH* intimal hyperplasia. Reprinted with permission from Oxford University Press from Alp et al.: Increased intimal hyperplasia in experimental vein graft stenting compared with arterial stenting: comparisons in a new rabbit model of stent injury. Cardiovascular Research 56(1):164–72, 2002 [1]. (**e**, **f**) Clinical radiograph taken immediately after shoulder prosthesis implantation (**e**) and after 7 years of follow-up (**f**). The arrow in (**f**) depicts a region of cortical bone resorption. Reprinted from the Journal of Shoulder and Elbow Surgery 12(1): Nagels et al.: Stress shielding and bone remodeling in shoulder arthroplasty, 35–39, 2003 [81], with permission from Elsevier

In general, tumor tissues have altered mechanical properties as compared to native, healthy tissue [83, 85, 108, 131]. In fact, breast cancer is often first detected by the patient or physician finding a palpable mass or lump that is stiffer than the surrounding tissue. Large tumors are associated with an increase in local ECM stiffness and angiogenesis, an in growth of newly sprouted blood vessels that facilitate increased tumor mass (Fig. 2.3a, b) [122]. The increase in ECM stiffness is primarily due to increased collagen deposition and cross-linking within the tumor stroma [85], but a disruption in the tensional homeostasis of the cells may also contribute [88]. As discussed previously, changes in the stiffness of the ECM can lead to phenotypic cellular changes such as increased proliferation and migration. Indeed, Paszek and colleagues found that increasing substrate stiffness correlated with changes in cytoskeletal tension, integrin expression, cellular proliferation, oncogene activity, and tissue formation in mammary epithelial cells [88]. Additionally, tumor cell migration was found to be modulated by the stiffness of the ECM [133]. These results indicate that the increased mechanical stiffness of the surrounding ECM that accompanies tumor progression may, in fact, drive malignancy.

ECM stiffening is also known to be a critical factor in the progression of cardiovascular disease. Vessel stiffening occurs through a number of mechanisms including glycation, the formation non-enzymatic cross-links (also known as

advanced glycation end products or AGEs) within the ECM [23]. These post-translational biochemical alterations cause tissue stiffening and prevent cellular remodeling of the existing tissue [79]. For example, the greater prevalence of reducing sugars such as glucose and ribose within the blood of diabetic patients leads to increased cross-link density of collagen and elastin, and consequently increased stiffness of the vasculature when compared with non-diabetics [12, 24]. These alterations in the mechanical environment cause changes in cellular behavior and result in an inability to maintain proper vascular tone and regulate blood pressure effectively [58]. Together, these changes contribute to the increased prevalence of cardiovascular disease in diabetic patients. These data indicate that changing the matrix mechanics of a tissue can lead to disease.

Tissue stiffening also accompanies wound healing. Unfortunately, most of the time the body is unable to perfectly replicate the native tissue structure and a scar is formed at the site of an injury. In some areas of the body, such as the skin, a small scar does not typically impair function. However, in other regions of the body such as the central nervous system, scar formation can cause the tissue to severely malfunction [75]. Specifically, within the brain and spinal cord, tissue injury leads to glial scar formation which acts as a mechanical barrier and inhibits signal transduction [47]. In a study that investigated the molecular changes that occur during glial scar maturation, Camand et al. found that fibronectin matrix deposition inhibits axonal growth and healing [18], but promotes astrocyte attachment as a mechanism of physically separating the injured site from the surrounding tissue [95]. To better understand how the mechanical cues from the glial scar affect cellular function, Georges and colleagues investigated the response of astrocytes and cortical neurons to matrix stiffness [40]. Interestingly, they found that while the cortical neurons were able to spread and extend neurites on both soft and stiff surfaces, the soft substrates were not conducive to astrocyte growth. These data suggest that the mechanical properties of the glial scar are promoting astrocyte recruitment and barrier formation, thus limiting axonal regeneration. These results suggest that matrix mechanics play a key role in wound healing and tissue regeneration.

Just as perturbations in native tissue mechanics can lead to disease states, regenerative tissue engineering therapies can also facilitate the formation and progression of disease when the mechanical properties of the native tissue are not recapitulated. One prominent example is intimal hyperplasia (IH), a response characterized by thickening of the blood vessel wall due in part to the proliferation and migration of smooth muscle cells from the medial layer of the vessel wall and increased ECM deposition (Fig. 2.3c, d) [84]. Notably, mechanical differences in the matrix have been shown to induce migration [129] and proliferation [11] of vascular smooth muscle cells, both hallmarks of IH. The causes of IH stem from mechanical damage to the endothelium due to compliance mismatch between synthetic vascular grafts and native vascular tissue at sites of anastomoses [105] and changes in blood flow characteristics or luminal diameter at the anastomosis [107]. IH is ultimately responsible for poor patency after bypass grafting [78, 120] that may require additional surgical intervention. Similarly, mechanical mismatch between implant and native tissue also occurs in orthopedic implants that reduce the

physical loading on nearby bone tissue. This phenomenon, known as stress shielding, results from the difference in stiffness between the orthopedic implant and the host tissue, and results in bone resorption and osteopenia (Fig. 2.3e, f) [30]. Such changes at the bone–implant interface may ultimately allow micromotion that facilitates implant loosening, osteolytic particle debris [10], and implant failure.

These examples demonstrate that matrix mechanobiology plays a significant role in promoting a diseased phenotype. Moreover, they illustrate that the mechanical properties of engineered regenerative therapies are a critical design consideration for implant success.

Conclusions

The mechanical properties of tissues are not only important for maintaining macroscale mechanical integrity but also essential regulators of cellular function. Cells sense stiffness using structures such as integrins to attach to the ECM and then respond and, oftentimes, remodel their environment by generating traction forces via actomyosin contractility. When alterations are made to the extracellular mechanical environment, cells can react to these mechanical stimuli by influencing tissue development, cellular differentiation, or disease progression. An understanding of how the mechanical properties of the ECM contribute to cell responses and tissue formation will ultimately further the understanding of disease states associated with aberrant mechanosensing and guide the design parameters of successful biomaterials and TE constructs. Future tissue engineering strategies should work to produce biomaterials and implants that are not only chemically favorable, but also integrate mechanical cues that dictate cellular behavior to aid in cellular differentiation and tissue regeneration.

References

1. Alp, N.J., West, N.E., et al.: Increased intimal hyperplasia in experimental vein graft stenting compared to arterial stenting: comparisons in a new rabbit model of stent injury. Cardiovasc. Res. **56**(1), 164–172 (2002)
2. Anderson, H.C.: An antagonist of osteoclast integrins prevents experimental osteoporosis. J. Clin. Invest. **99**(9), 2059 (1997)
3. Assoian, R.K., Klein, E.A.: Growth control by intracellular tension and extracellular stiffness. Trends Cell Biol. **18**(7), 347–352 (2008)
4. Balaban, N.Q., Schwarz, U.S., et al.: Force and focal adhesion assembly: a close relationship studied using elastic micropatterned substrates. Nat. Cell Biol. **3**(5), 466–472 (2001)
5. Baneyx, G., Baugh, L., et al.: Fibronectin extension and unfolding within cell matrix fibrils controlled by cytoskeletal tension. Proc. Natl Acad. Sci. USA **A99**(8), 5139–5143 (2002)
6. Barbee, K.A., Davies, P.F., et al.: Shear stress-induced reorganization of the surface topography of living endothelial cells imaged by atomic force microscopy. Circ. Res. **74**(1), 163–171 (1994)

7. Beningo, K.A., Dembo, M., et al.: Nascent focal adhesions are responsible for the generation of strong propulsive forces in migrating fibroblasts. J. Cell Biol. **153**(4), 881–888 (2001)
8. Berbari, N.F., O'Connor, A.K., et al.: The primary cilium as a complex signaling center. Curr. Biol. **19**(13), R526–R535 (2009)
9. Borovski, T., De Sousa, E.M.F., et al.: Cancer stem cell niche: the place to be. Cancer Res. **71** (3), 634–639 (2011)
10. Bougherara, H., Zdero, R., et al.: A preliminary biomechanical study of a novel carbon-fibre hip implant versus standard metallic hip implants. Med. Eng. Phys. **33**, 121–128 (2010)
11. Brown, X.Q., Bartolak-Suki, E., et al.: Effect of substrate stiffness and PDGF on the behavior of vascular smooth muscle cells: Implications for atherosclerosis. J. Cell. Physiol. **225**(1), 115–122 (2010)
12. Bruel, A., Oxlund, H.: Changes in biomechanical properties, composition of collagen and elastin, and advanced glycation endproducts of the rat aorta in relation to age. Atherosclerosis **127**(2), 155–165 (1996)
13. Burridge, K., Chrzanowska-Wodnicka, M.: Focal adhesions, contractility, and signaling. Annu. Rev. Cell Dev. Biol. **12**, 463–518 (1996)
14. Buxboim, A., Discher, D.E.: Stem cells feel the difference. Nat. Methods **7**(9), 695–697 (2010)
15. Byfield, F.J., Reen, R.K., et al.: Endothelial actin and cell stiffness is modulated by substrate stiffness in 2D and 3D. J. Biomech. **42**(8), 1114–1119 (2009)
16. Califano, J.P., Reinhart-King, C.A.: A Balance of Substrate Mechanics and Matrix Chemistry Regulates Endothelial Cell Network Assembly. Cell. Mol. Bioeng.. **1**(2–3), 122–132 (2008)
17. Califano, J.P., Reinhart-King, C.A.: Substrate stiffness and cell area drive cellular traction stresses in single cells and cells in contact. Cell. Mol. Bioeng. **3**(1), 68–75 (2010)
18. Camand, E., Morel, M.P., et al.: Long-term changes in the molecular composition of the glial scar and progressive increase of serotoninergic fibre sprouting after hemisection of the mouse spinal cord. Eur. J. Neurosci. **20**(5), 1161–1176 (2004)
19. Carmeliet, G., Vico, L., et al.: Space flight: a challenge for normal bone homeostasis. Crit. Rev. Eukaryot. Gene Expr. **11**(1–3), 131–144 (2001)
20. Chan, V., Zorlutuna, P., et al.: Three-dimensional photopatterning of hydrogels using stereolithography for long-term cell encapsulation. Lab Chip **10**(16), 2062–2070 (2010)
21. Chowdhury, F., Na, S., et al.: Material properties of the cell dictate stress-induced spreading and differentiation in embryonic stem cells. Nat. Mater. **9**(1), 82–88 (2010)
22. Davies, P.F., Barbee, K.A., et al.: Hemodynamics and atherogenesis. Endothelial surface dynamics in flow signal transduction. Ann. N. Y. Acad. Sci. **748**, 86–102 (1995). discussion 102–3
23. DeGroot, J.: The AGE of the matrix: chemistry, consequence and cure. Curr. Opin. Pharmacol. **4**(3), 301–305 (2004)
24. DeLoach, S.S., Townsend, R.R.: Vascular stiffness: its measurement and significance for epidemiologic and outcome studies. Clin. J. Am. Soc. Nephrol. **3**(1), 184–192 (2008)
25. Dembo, M., Oliver, T., et al.: Imaging the traction stresses exerted by locomoting cells with the elastic substratum method. Biophysics **J70**(4), 2008–2022 (1996)
26. Deroanne, C.F., Lapiere, C.M., et al.: In vitro tubulogenesis of endothelial cells by relaxation of the coupling extracellular matrix-cytoskeleton. Cardiovasc. Res. **49**(3), 647–658 (2001)
27. Dickinson, L.E., Kusuma, S., et al.: Reconstructing the differentiation niche of embryonic stem cells using biomaterials. Macromol. Biosci. **11**(1), 36–49 (2011)
28. Discher, D.E., Janmey, P., et al.: Tissue cells feel and respond to the stiffness of their substrate. Science **310**(5751), 1139–1143 (2005)
29. Discher, D.E., Mooney, D.J., et al.: Growth factors, matrices, and forces combine and control stem cells. Science **324**(5935), 1673–1677 (2009)
30. Engh, C.A., Bobyn, J.D., et al.: Porous-coated hip replacement. The factors governing bone ingrowth, stress shielding, and clinical results. J. Bone Joint Surg. Br. **69**(1), 45–55 (1987)

31. Engler, A., Bacakova, L., et al.: Substrate compliance versus ligand density in cell on gel responses. Biophys. J. **86**(1 Pt 1), 617–628 (2004)
32. Engler, A.J., Griffin, M.A., et al.: Myotubes differentiate optimally on substrates with tissue-like stiffness: pathological implications for soft or stiff microenvironments. J. Cell Biol. **166** (6), 877–887 (2004)
33. Engler, A.J., Sen, S., et al.: Matrix elasticity directs stem cell lineage specification. Cell **126** (4), 677–689 (2006)
34. Evans, N.D., Minelli, C., et al.: Substrate stiffness affects early differentiation events in embryonic stem cells. Eur. Cell. Mater. **18**, 1–13 (2009). discussion 13–4
35. Galbraith, C.G., Sheetz, M.P.: A micromachined device provides a new bend on fibroblast traction forces. Proc. Natl Acad. Sci. USA **A94**(17), 9114–9118 (1997)
36. Galbraith, C.G., Yamada, K.M., et al.: The relationship between force and focal complex development. J. Cell Biol. **159**(4), 695–705 (2002)
37. Geiger, B., Spatz, J.P., et al.: Environmental sensing through focal adhesions. Nat. Rev. Mol. Cell Biol. **10**(1), 21–33 (2009)
38. Genes, N.G., Rowley, J.A., et al.: Effect of substrate mechanics on chondrocyte adhesion to modified alginate surfaces. Arch. Biochem. Biophys. **422**(2), 161–167 (2004)
39. Georges, P.C., Janmey, P.A.: Cell type-specific response to growth on soft materials. J. Appl. Physiol. **98**(4), 1547–1553 (2005)
40. Georges, P.C., Miller, W.J., et al.: Matrices with compliance comparable to that of brain tissue select neuronal over glial growth in mixed cortical cultures. Biophysics **J90**(8), 3012–3018 (2006)
41. Ghibaudo, M., Saez, A., et al.: Traction forces and rigidity sensing regulate cell functions. Soft Matter **4**, 1836–1843 (2008)
42. Gray, D.S., Liu, W.F., et al.: Engineering amount of cell-cell contact demonstrates biphasic proliferative regulation through RhoA and the actin cytoskeleton. Exp. Cell Res. **314**(15), 2846–2854 (2008)
43. Guo, W.H., Frey, M.T., et al.: Substrate rigidity regulates the formation and maintenance of tissues. Biophys. J. **90**(6), 2213–2220 (2006)
44. Harris, A.K., Wild, P., et al.: Silicone rubber substrata: a new wrinkle in the study of cell locomotion. Science **208**(4440), 177–179 (1980)
45. Hayashi, T., Carthew, R.W.: Surface mechanics mediate pattern formation in the developing retina. Nature **431**(7009), 647–652 (2004)
46. His, W. (1874). Unsere Korperform und das physiologische Problem ihrer Enstehung; Briefe an einen Befreundeten Naturforscher. Leipzig, F.C.W. Vogel.
47. Horner, P.J., Gage, F.H.: Regenerating the damaged central nervous system. Nature **407** (6807), 963–970 (2000)
48. Hove, J.R., Koster, R.W., et al.: Intracardiac fluid forces are an essential epigenetic factor for embryonic cardiogenesis. Nature **421**(6919), 172–177 (2003)
49. Hynes, R.O.: Cell surface proteins and malignant transformation. Biochim. Biophys. Acta **458**(1), 73–107 (1976)
50. Hynes, R.O.: Integrins: bidirectional, allosteric signaling machines. Cell **110**(6), 673–687 (2002)
51. Ingber, D.E.: Cancer as a disease of epithelial-mesenchymal interactions and extracellular matrix regulation. Differentiation **70**(9–10), 547–560 (2002)
52. Ingber, D.E., Madri, J.A., et al.: Role of basal lamina in neoplastic disorganization of tissue architecture. Proc. Natl Acad. Sci. USA **A78**(6), 3901–3905 (1981)
53. Isenberg, B.C., Dimilla, P.A., et al.: Vascular smooth muscle cell durotaxis depends on substrate stiffness gradient strength. Biophysics **J97**(5), 1313–1322 (2009)
54. Jaalouk, D.E., Lammerding, J.: Mechanotransduction gone awry. Nat. Rev. Mol. Cell Biol. **10**(1), 63–73 (2009)
55. Jannat, R.A., Dembo, M., et al.: Neutrophil adhesion and chemotaxis depend on substrate mechanics. J. Phys. Condens. Matter **22**(19), 194117 (2010)

56. Johnston, R.S.; Dietlein, L.F.: The Proceedings of the Skylab Life Sciences Symposium, vol. 1 (1974).
57. Kaufman, D.A., Albelda, S.M., et al.: Role of lateral cell-cell border location and extracellular/transmembrane domains in PECAM/CD31 mechanosensation. Biochem. Biophys. Res. Commun. **320**(4), 1076–1081 (2004)
58. King, G.L., Brownlee, M.: The cellular and molecular mechanisms of diabetic complications. Endocrinol. Metab. Clin. North Am. **25**(2), 255–270 (1996)
59. Kloxin, A.M., Kasko, A.M., et al.: Photodegradable hydrogels for dynamic tuning of physical and chemical properties. Science **324**(5923), 59–63 (2009)
60. Kubow, K.E., Klotzsch, E., et al.: Crosslinking of cell-derived 3D scaffolds up-regulates the stretching and unfolding of new extracellular matrix assembled by reseeded cells. Integr. Biol. (Camb) **1**(11–12), 635–648 (2009)
61. Kumar, S., Maxwell, I.Z., et al.: Viscoelastic retraction of single living stress fibers and its impact on cell shape, cytoskeletal organization, and extracellular matrix mechanics. Biophysics **J90**(10), 3762–3773 (2006)
62. Kumar, S., Weaver, V.M.: Mechanics, malignancy, and metastasis: the force journey of a tumor cell. Cancer Metastasis Rev. **28**(1–2), 113–127 (2009)
63. Langer, R., Vacanti, J.P.: Tissue engineering. Science **260**(5110), 920–926 (1993)
64. Lee, D.A., Knight, M.M., et al.: Stem cell mechanobiology. J. Cell. Biochem. **112**(1), 1–9 (2010)
65. Lee, J., Leonard, M., et al.: Traction forces generated by locomoting keratocytes. J. Cell Biol. **127**(6 Pt 2), 1957–1964 (1994)
66. Legate, K.R., Fassler, R.: Mechanisms that regulate adaptor binding to beta-integrin cytoplasmic tails. J. Cell Sci. **122**(Pt 2), 187–198 (2009)
67. Levental, K.R., Yu, H., et al.: Matrix crosslinking forces tumor progression by enhancing integrin signaling. Cell **139**(5), 891–906 (2009)
68. Lo, C.M., Wang, H.B., et al.: Cell movement is guided by the rigidity of the substrate. Biophysics **J79**(1), 144–152 (2000)
69. Lutolf, M.P., Hubbell, J.A.: Synthetic biomaterials as instructive extracellular microenvironments for morphogenesis in tissue engineering. Nat. Biotechnol. **23**(1), 47–55 (2005)
70. Makino, A., Prossnitz, E.R., et al.: G protein-coupled receptors serve as mechanosensors for fluid shear stress in neutrophils. Am. J. Physiol. Cell Physiol. **290**(6), C1633–C1639 (2006)
71. Mammoto, T., Ingber, D.E.: Mechanical control of tissue and organ development. Development **137**(9), 1407–1420 (2010)
72. Marganski, W.A., Dembo, M., et al.: Measurements of cell-generated deformations on flexible substrata using correlation-based optical flow. Methods Enzymol. **361**, 197–211 (2003)
73. Martin, A.C., Wieschaus, E.F.: Tensions divide. Nat. Cell Biol. **12**(1), 5–7 (2010)
74. Martinac, B.: Mechanosensitive ion channels: molecules of mechanotransduction. J. Cell Sci. **117**(Pt 12), 2449–2460 (2004)
75. Maynard Jr., F.M., Bracken, M.B., et al.: International standards for neurological and functional classification of spinal cord injury. American Spinal Injury Association. Spinal Cord **35**(5), 266–274 (1997)
76. Mege, R.M., Gavard, J., et al.: Regulation of cell-cell junctions by the cytoskeleton. Curr. Opin. Cell Biol. **18**(5), 541–548 (2006)
77. Metallo, C.M., Vodyanik, M.A., et al.: The response of human embryonic stem cell-derived endothelial cells to shear stress. Biotechnol. Bioeng. **100**(4), 830–837 (2008)
78. Mitchell, R.N.: Graft vascular disease: immune response meets the vessel wall. Annu. Rev. Pathol. **4**, 19–47 (2009)
79. Monnier, V.M., Kohn, R.R., et al.: Accelerated age-related browning of human collagen in diabetes mellitus. Proc. Natl Acad. Sci. USA **A81**(2), 583–587 (1984)
80. Morrison, S.J., Shah, N.M., et al.: Regulatory mechanisms in stem cell biology. Cell **88**(3), 287–298 (1997)

81. Nagels, J., Stokdijk, M., et al.: Stress shielding and bone resorption in shoulder arthroplasty. J. Shoulder Elbow Surg. **12**(1), 35–39 (2003)
82. Neath, P., Roche, S.M., et al.: Intraocular pressure-dependent and -independent phases of growth of the embryonic chick eye and cornea. Invest. Ophthalmol. Vis. Sci. **32**(9), 2483–2491 (1991)
83. Nelson, C.M., Bissell, M.J.: Of extracellular matrix, scaffolds, and signaling: tissue architecture regulates development, homeostasis, and cancer. Annu. Rev. Cell Dev. Biol. **22**, 287–309 (2006)
84. Newby, A.C., Zaltsman, A.B.: Molecular mechanisms in intimal hyperplasia. J. Pathol. **190** (3), 300–309 (2000)
85. Ng, M.R., Brugge, J.S.: A stiff blow from the stroma: collagen crosslinking drives tumor progression. Cancer Cell **16**(6), 455–457 (2009)
86. Osawa, M., Masuda, M., et al.: Evidence for a role of platelet endothelial cell adhesion molecule-1 in endothelial cell mechanosignal transduction: is it a mechanoresponsive molecule? J. Cell Biol. **158**(4), 773–785 (2002)
87. Pajerowski, J.D., Dahl, K.N., et al.: Physical plasticity of the nucleus in stem cell differentiation. Proc. Natl Acad. Sci. USA **A104**(40), 15619–15624 (2007)
88. Paszek, M.J., Zahir, N., et al.: Tensional homeostasis and the malignant phenotype. Cancer Cell **8**(3), 241–254 (2005)
89. Patwari, P., Lee, R.T.: Mechanical control of tissue morphogenesis. Circ. Res. **103**(3), 234–243 (2008)
90. Pelham Jr., R.J., Wang, Y.: Cell locomotion and focal adhesions are regulated by substrate flexibility. Proc. Natl Acad. Sci. USA **A94**(25), 13661–13665 (1997)
91. Peyton, S.R., Putnam, A.J.: Extracellular matrix rigidity governs smooth muscle cell motility in a biphasic fashion. J. Cell. Physiol. **204**(1), 198–209 (2005)
92. Phillips, H.M., Davis, G.S.: Liquid-Tissue Mechanics in Amphibian Gastrulation – Germ-Layer Assembly in Rana-Pipiens. Am. Zool. **18**(1), 81–93 (1978)
93. Plow, E.F., Haas, T.A., et al.: Ligand binding to integrins. J. Biol. Chem. **275**(29), 21785–21788 (2000)
94. Rabodzey, A., Alcaide, P., et al.: Mechanical forces induced by the transendothelial migration of human neutrophils. Biophysics **J95**(3), 1428–1438 (2008)
95. Raivich, G., Bohatschek, M., et al.: Neuroglial activation repertoire in the injured brain: graded response, molecular mechanisms and cues to physiological function. Brain Res. Brain Res. Rev. **30**(1), 77–105 (1999)
96. Reinhart-King, C.A., Dembo, M., et al.: Endothelial cell traction forces on RGD-derivatized polyacrylamide substrata. Langmuir **19**(5), 1573–1579 (2003)
97. Reinhart-King, C.A., Dembo, M., et al.: The dynamics and mechanics of endothelial cell spreading. Biophys. J. **89**(1), 676–689 (2005)
98. Reinhart-King, C.A., Dembo, M., et al.: Cell-Cell Mechanical Communication through Compliant Substrates. Biophys. J. **95**(12), 6044–6051 (2008)
99. Rho, J.Y., Ashman, R.B., et al.: Young's modulus of trabecular and cortical bone material: ultrasonic and microtensile measurements. J. Biomech. **26**(2), 111–119 (1993)
100. Riveline, D., Zamir, E., et al.: Focal contacts as mechanosensors: externally applied local mechanical force induces growth of focal contacts by an mDia1-dependent and ROCK-independent mechanism. J. Cell Biol. **153**(6), 1175–1186 (2001)
101. Rodriguez, O.C., Schaefer, A.W., et al.: Conserved microtubule-actin interactions in cell movement and morphogenesis. Nat. Cell Biol. **5**(7), 599–609 (2003)
102. Rohani, N., Canty, L., et al.: EphrinB/EphB signaling controls embryonic germ layer separation by contact-induced cell detachment. PLoS Biol. **9**(3), e1000597 (2011)
103. Roux, W.: Der zuchtende Kampf der Teile, oder die Teilauslese im Organismus (Theorie der 'funktionellen Anpassung). Wilhelm Engelmann, Leipzig (1881)

104. Saez, A., Ghibaudo, M., et al.: Rigidity-driven growth and migration of epithelial cells on microstructured anisotropic substrates. Proc. Natl Acad. Sci. USA **A104**(20), 8281–8286 (2007)
105. Salacinski, H.J., Goldner, S., et al.: The mechanical behavior of vascular grafts: a review. J. Biomater. Appl. **15**(3), 241–278 (2001)
106. Samani, A., Plewes, D.: A method to measure the hyperelastic parameters of ex vivo breast tissue samples. Phys. Med. Biol. **49**(18), 4395–4405 (2004)
107. Sarkar, S., Salacinski, H.J., et al.: The mechanical properties of infrainguinal vascular bypass grafts: their role in influencing patency. Eur. J. Vasc. Endovasc. Surg. **31**(6), 627–636 (2006)
108. Schedin, P., Keely, P.J.: Mammary gland ECM remodeling, stiffness, and mechanosignaling in normal development and tumor progression. Cold Spring Harb. Perspect. Biol. **3**(1), a003228 (2010)
109. Sharma, R.I., Snedeker, J.G.: Biochemical and biomechanical gradients for directed bone marrow stromal cell differentiation toward tendon and bone. Biomaterials **31**(30), 7695–7704 (2010)
110. Shimizu, T., Yabe, T., et al.: E-cadherin is required for gastrulation cell movements in zebrafish. Mech. Dev. **122**(6), 747–763 (2005)
111. Skalak, R., Fox, C.F. (eds.): Tissue engineering. Alan R. Liss, New York (1988)
112. Sniadecki, N.J., Anguelouch, A., et al.: Magnetic microposts as an approach to apply forces to living cells. Proc. Natl Acad. Sci. USA **A104**(37), 14553–14558 (2007)
113. Sniadecki, N.J., Chen, C.S.: Microfabricated silicone elastomeric post arrays for measuring traction forces of adherent cells. Methods Cell Biol. **83**, 313–328 (2007)
114. Steinberg, M.S.: On the Mechanism of Tissue Reconstruction by Dissociated Cells, Iii. Free Energy Relations and the Reorganization of Fused, Heteronomic Tissue Fragments. Proc. Natl Acad. Sci. USA **A48**(10), 1769–1776 (1962)
115. Sternlicht, M.D., Bissell, M.J., et al.: The matrix metalloproteinase stromelysin-1 acts as a natural mammary tumor promoter. Oncogene **19**(8), 1102–1113 (2000)
116. Tamkun, J.W., DeSimone, D.W., et al.: Structure of integrin, a glycoprotein involved in the transmembrane linkage between fibronectin and actin. Cell **46**(2), 271–282 (1986)
117. Tan, J.L., Tien, J., et al.: Cells lying on a bed of microneedles: an approach to isolate mechanical force. Proc. Natl Acad. Sci. USA **A100**(4), 1484–1489 (2003)
118. Thevenot, P., Hu, W., et al.: Surface chemistry influences implant biocompatibility. Curr. Top. Med. Chem. **8**(4), 270–280 (2008)
119. Titushkin, I., Cho, M.: Modulation of cellular mechanics during osteogenic differentiation of human mesenchymal stem cells. Biophysics **J93**(10), 3693–3702 (2007)
120. Tiwari, A., Cheng, K.S., et al.: Improving the patency of vascular bypass grafts: the role of suture materials and surgical techniques on reducing anastomotic compliance mismatch. Eur. J. Vasc. Endovasc. Surg. **25**(4), 287–295 (2003)
121. Townes, P.L., Holtfreter, J.: Directed movements and selective adhesion of embryonic amphibian cells. J. Exp. Zool. **128**(1), 53–120 (1955)
122. Tredan, O., Galmarini, C.M., et al.: Drug resistance and the solid tumor microenvironment. J. Natl Cancer Inst. **99**(19), 1441–1454 (2007)
123. Tse, J.R., Engler, A.J.: Stiffness gradients mimicking in vivo tissue variation regulate mesenchymal stem cell fate. PLoS One **6**(1), e15978 (2011)
124. Votteler, M., Kluger, P.J., et al.: Stem cell microenvironments–unveiling the secret of how stem cell fate is defined. Macromol. Biosci. **10**(11), 1302–1315 (2010)
125. Wang, H.B., Dembo, M., et al.: Substrate flexibility regulates growth and apoptosis of normal but not transformed cells. Am. J. Physiol. Cell Physiol. **279**(5), C1345–C1350 (2000)
126. Wang, N., Butler, J.P., et al.: Mechanotransduction across the cell surface and through the cytoskeleton. Science **260**(5111), 1124–1127 (1993)
127. Waters, C.M., Sporn, P.H., et al.: Cellular biomechanics in the lung. Am. J. Physiol. Lung Cell. Mol. Physiol. **283**(3), L503–L509 (2002)
128. Wolff, J.: Das Gesetz der Transformation der Knochen. A. Hirschwald, Berlin (1892)

129. Wong, J.Y., Velasco, A., et al.: Directed movement of vascular smooth muscle cells on gradient-compliant hydrogels. Langmuir **19**(5), 1908–1913 (2003)
130. Yeung, T., Georges, P.C., et al.: Effects of substrate stiffness on cell morphology, cytoskeletal structure, and adhesion. Cell Motil. Cytoskeleton **60**(1), 24–34 (2005)
131. Yu, H., Mouw, J.K., et al.: Forcing form and function: biomechanical regulation of tumor evolution. Trends Cell Biol. **21**(1), 47–56 (2010)
132. Zaidel-Bar, R., Itzkovitz, S., et al.: Functional atlas of the integrin adhesome. Nat. Cell Biol. **9** (8), 858–867 (2007)
133. Zaman, M.H., Trapani, L.M., et al.: Migration of tumor cells in 3D matrices is governed by matrix stiffness along with cell-matrix adhesion and proteolysis. Proc. Natl Acad. Sci. USA **A103**(29), 10889–10894 (2006)
134. Zemel, A.; Rehfeld, H. et al.: Optimal matrix rigidity for stress-fibre polarization in stem cells. Nat. Phys. **6**, 468–473 (2010)
135. Zemel, A., Safran, S.A.: Active self-polarization of contractile cells in asymmetrically shaped domains. Phys. Rev. E Stat. Nonlin. Soft Matter Phys. **76**(2 Pt 1), 021905 (2007)
136. Zhou, J., Kim, H.Y., et al.: Actomyosin stiffens the vertebrate embryo during crucial stages of elongation and neural tube closure. Development **136**(4), 677–688 (2009)

Part II
Oxygen Delivery

Chapter 3
Oxygen Supply for Tissue Engineering

Whitney L. Stoppel and Susan C. Roberts

Abstract Adequate oxygen transport is vital to the success of a tissue-engineered construct. Modulating oxygen tension within tissue-engineered constructs is necessary for the creation of devices with optimal functionality. Oxygen tension significantly influences cellular behavior through mechanisms which promote both cell proliferation and apoptosis. Given the negative consequences of low oxygen tension for most grafted tissues, many investigators have worked to improve oxygen tension within tissue engineered scaffolds through the use of synthetic oxygen carriers, natural or artificial heme, and polymeric oxygen generating thin films, or by inducing blood vessel growth into the matrix. Cellular oxygen consumption and transport within a scaffold can be calculated and predicted using diffusion models to improve device design. This section explores the interplay between fundamental engineering and biological processes used to modulate oxygen tension for the creation of functional tissue-engineered devices.

Introduction

Adequate oxygen transport is vital to the success of a tissue-engineered construct. If sufficient oxygen tension is not maintained, grafted tissue will not survive and the device will fail. Given the negative consequences of low oxygen tensions for most grafted tissues, many investigators have worked to improve oxygen tensions within tissue engineering scaffolds through the use of synthetic oxygen carriers [1, 2], polymeric oxygen generating (POG) thin films [3, 4], or by inducing blood vessel growth into the matrix [5, 6] (see Fig. 3.1).

W.L. Stoppel • S.C. Roberts (✉)
Department of Chemical Engineering, University of Massachusetts Amherst,
159 Goessmann Lab, 686 N. Pleasant St., Amherst, MA 01003, USA
e-mail: wstoppel@ecs.umass.edu; sroberts@ecs.umass.edu

S.K. Bhatia (ed.), *Engineering Biomaterials for Regenerative Medicine: Novel Technologies for Clinical Applications*, DOI 10.1007/978-1-4614-1080-5_3,

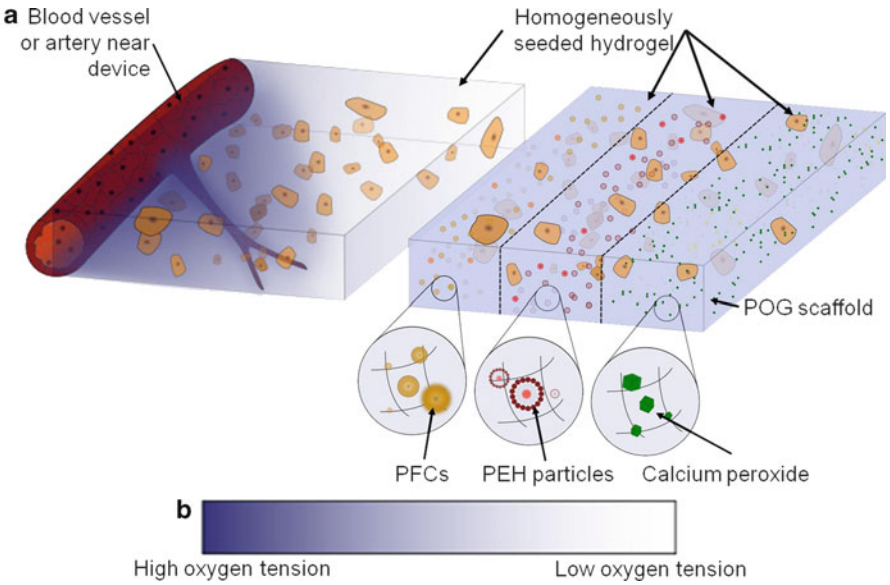

Fig. 3.1 Oxygen tension in a homogenously seeded hydrogel depends on the oxygen source. (**a**) Oxygen tension in a vascularized hydrogel or tissue decreases as the distance from the blood vessel increases. (**b**) Oxygen concentration in a hydrogel containing a synthetic oxygen carrier or oxygen-generating chemical is more homogenous throughout the device. Perfluorocarbon (PFC), polymersome encapsulated hemoglobin (PEH), polymeric oxygen-generating (POG)

Insufficient oxygen supply can cause a variety of intracellular changes. Most notably, metabolism switches from high energy-yielding aerobic metabolism to low energy-producing anaerobic metabolism, altering the cells' ability to efficiently process glucose and other nutrients [7]. Changes in gene expression are mediated by changes in metabolism through a variety of pathways, which often include stabilization of hypoxia-inducible factor-1 (HIF-1), a transcriptional activator [7–9]. Altered gene expression can also affect cell cycle progression, and oxygen radicals can induce DNA damage, leading to cell cycle arrest [10, 11].

For uniform cell seeding within a scaffold such as that shown in Fig. 3.1, it is well known that cells near an oxygen source consume oxygen and proliferate, while cells farther from the oxygen source die by apoptosis or necrosis due to the oxygen gradient within the material [12–15]. Therefore, cellular population density within the scaffold differs greatly based on spatial position, and a uniform tissue construct is generally not created [12, 13]. Cellular oxygen consumption and oxygen transport within a scaffold can be modeled using diffusion models and cellular oxygen consumption rates (OCRs) through external [12, 16, 17] or internal [4] oxygen sources and/or vascularization [18, 19]. These models can be useful in directing the design of devices to ensure adequate oxygen supply as discussed below in *Oxygen Delivery: Methods and Models* section.

Hypoxia and the Cellular Response

Sufficient oxygen transport within a construct is required for adequate cellular function and viability in a tissue engineering device [14, 20]. Cells sense and respond to extracellular and intracellular stimuli, such as oxygen, to maintain homeostasis. Consequently, the concentration of intracellular oxygen has a major effect on cell function, which is mediated by gene expression [7, 10]. Hypoxia occurs when cells do not receive adequate oxygen supply and the partial pressure of oxygen in the tissue or device (pO_2) is reduced from normal levels. There are many biological mechanisms involved in the regulation of cellular oxygen levels, which adjust protein production and cellular metabolism to account for changes in internal oxygen concentration, with results dependent upon the length of hypoxic exposure [7, 21]. Both cell proliferation (i.e., erthyropoiesis/proliferation of new red blood cells) and blood vessel growth (i.e., angiogenesis) are stimulated by hypoxia to enhance oxygenation of tissue, as shown in Fig. 3.2 [22]. Chronic hypoxia results in programmed cell death, or apoptosis, through multiple cellular cascades as shown in Fig. 3.2 and discussed further in *Hypoxia-Inducible Factor-1* and *Hypoxia-Induced Apoptosis* [7, 23, 24].

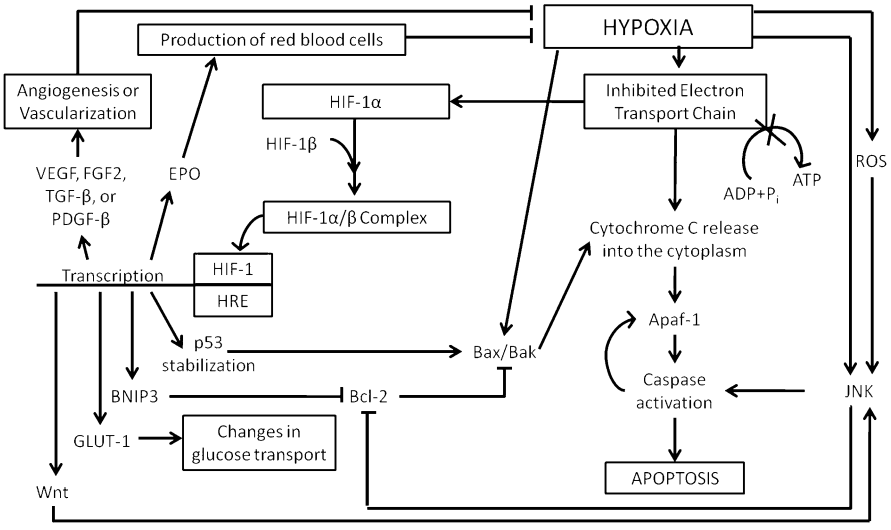

Fig. 3.2 Cellular pathways activated by hypoxia [7, 22, 23]. Hypoxia leads to a change in glucose metabolism, decreasing overall ATP yield, ultimately leading to apoptosis and HIF-1α stabilization. HIF-1α stabilization results in the upregulation of a number of genes including growth factors such as VEGF, which promote angiogenesis, and EPO, which stimulates production of red blood cells, in an attempt to relieve the local hypoxia

Hypoxia-Inducible Factor-1

HIF-1 is a prominent transcription factor that is tightly regulated by oxygen concentration. HIF-1 transcriptional activity increases exponentially as cellular oxygen decreases, and for 0–5% O_2, stabilization of HIF-1 transcripts is inversely proportional to oxygen concentration [7, 8]. HIF-1α (hypoxia-inducible factor-1α) and HIF-2α (endothelial PAS domain protein 1) are the subunits of HIF-1 and HIF-2, respectively, and are regulated by oxygen concentration [10, 25]. HIF-1α and HIF-1β (aryl hydrogen receptor nuclear translocator, ARNT) protein subunits are constitutively expressed during normoxia [26], but the alpha subunit is unstable and rapidly degraded by the ubiquitin proteosome pathway [23, 25]. Stabilization of HIF-1α requires oxygen concentration-dependent enzymatic hydroxylation, and therefore HIF-1α can only be hydroxylated during periods of hypoxia [27]. Once hydroxylated, it accumulates and is translocated to the nucleus where it binds to HIF-1β to form the active HIF-1 transcription factor, binding to hypoxia response elements (HREs) to initiate transcription [23]. HIF-2α behaves similar to HIF-1α, forming the HIF-2 complex with HIF-1β, which also binds HREs to initiate transcription, but the cellular response to stabilization and target genes activated may be different from those of HIF-1, depending on the cell type and signaling factors present [28–30].

HIF-1 can induce apoptosis [31, 32] or stimulate cell proliferation [33] through a variety of target genes, some of which are shown in Fig. 3.2. The HIF-1 expression pathway is not yet fully understood, but it is obvious that a delicate balance exists between HIF-1 expression inducing apoptotic or anti-apoptotic activity [7, 23]. The HIF-1 complex can bind HREs in the promoter region of several target genes to initiate transcription [34]. HIF-1 activates genes that encode for many proteins and enzymes including erythropoietin (EPO) [10, 35], glucose transporters (e.g., GLUT-1) and glycolytic enzymes [9], vascular endothelial growth factor (VEGF) [9, 31, 36], Wingless (Wnt) proteins [37, 38], and Hedgehog (Hh) proteins [39], while HIF-2 mediates expression of octamer-binding transcription factor 4 (Oct4), a gene upregulated in undifferentiated stem cells [40]. Gene products either increase the delivery of oxygen to cells or allow for changes in metabolism to mitigate the effect of decreased oxygen through protein expression [7].

HIF-1 can initiate angiogenesis through upregulation of VEGF and other angiogenic factors (e.g., FGF2, TGF-β, and PDGF-β) [9, 31, 41, 42], which leads to increased proliferation of endothelial cells in the matrix surrounding the tissue. Endothelial cell proliferation is a desired effect of hypoxia as it promotes angiogenesis in the construct (see *Vascularization of Bioengineered Tissue Constructs*) [43–45].

Hypoxia-Induced Apoptosis

Hypoxic conditions cause tissue engineering devices to fail by inducing apoptosis through multiple cellular mechanisms, primarily due to the reduction of mitochondrial adenosine triphosphate (ATP) production [7, 23]. Other mechanisms target

transcriptional activity of HIF-1, whose downstream effects may lead to proapoptotic activity [23, 31].

HIF-1 can initiate apoptosis by inducing high concentrations of proapoptotic proteins [23]. High levels of HIF-1 expression correlated with near anoxia may trigger apoptosis by induction and stabilization of p53, as shown in Fig. 3.2 [7, 23, 31, 46]. Stabilization of p53 induces programmed cell death by regulating Bax/Bak [23]. Increased concentrations of BNIP3 (Bcl-2 19 kDa interacting protein/adenovirus E1B 19 kDa interacting protein 3) are also correlated with hypoxia-induced apoptosis mediated by HIF-1 transcriptional activity [47]. BNIP3 blocks the activity of the Bcl-2 family of proteins which allows the activation of the Bax/Bak pathway [47].

Additionally, genetic instability and high hypoxia-induced mutation rates can lead to cell cycle arrest and ultimately result in apoptosis [23, 48]. Severe and chronic hypoxia will also cause a high mutation rate and genetic instability [48, 49]. Cells initiate cell cycle arrest which leads to apoptotic cell death to avoid the accumulation of cells with hypoxia-induced mutations [11, 23, 50].

In general, hypoxia can induce apoptosis through changes in glucose metabolism. In low oxygen environments, cells move from aerobic glycolysis/Krebs cycle to anaerobic glucose consumption and lactic acid production, thus decreasing the amount of mitochondria-derived ATP and affecting the electron transport chain [23]. Aerobic metabolism yields 36 ATPs, while the anaerobic pathway yields only 2 ATPs per glucose molecule, and therefore glucose consumption quickly increases, causing a drop in local glucose concentration [18, 51]. The drop in local glucose concentration increases the need for glucose transport into the scaffold material, which may not be attainable. As shown in Fig. 3.2, HIF-1α stabilization leads to the production of more glucose transporters to increase glucose transport during hypoxia. Ultimately, hypoxia results in a decrease in ATP production (2 instead of 36 per glucose), mitochondrial stress, and activation of Bax/Bak pathway, all leading to cytochrome C release into the cytosol which initiates the Apaf-1 pathway, inducing formation of the apoptosome, which ultimately leads to programmed cell death (Fig. 3.2) [51, 52]. Insufficient nutrient supply and lactic acid build-up will also lead to necrosis, another form of cell death [53].

Alternatively, the accumulation of radical oxygen species (ROS) upon hypoxia contributes to hypoxia-induced apoptosis through the activation of caspases via cleavage or activation of the JNK (Jun N-terminal kinase) pathway without the involvement of cytochrome C as shown in Fig. 3.2 [23, 54]. Following caspase activation, mitochondrial permeability increases resulting in the activation of Apaf-1 and the enhancement of caspase-mediated apoptosis [55]. Another mechanism for hypoxia-induced apoptosis involves the activation of the JNK pathway, which is also mediated by the Wnt family of proteins, which is a downstream product of HIF-1 transcriptional activation [38, 56, 57]. Chronic hypoxia may also lead to the activation of the JNK pathway through multiple cellular mechanisms, leading to decreased Bcl-2 activity and induction of apoptosis mediated by Bax/Bak, similar to the BNIP3 mechanism as shown in Fig. 3.2 [56].

Overall, it is clear that hypoxic conditions activate a variety of cellular pathways that lead to multiple outcomes, some of which result in cell death. In the design of a tissue engineering device, it is important to modulate these actions to improve the success of a tissue-engineered construct in vivo. Understanding the transport limitations of a tissue-engineered construct can aid in device design, reducing areas of low oxygen tension, and promoting cell viability and functionality.

Oxygen Delivery: Methods and Models

Sufficient oxygen and nutrient transport within a biomaterial is necessary to limit hypoxia-induced apoptosis and enhance the success rate for a tissue engineering device. High cellular consumption and low oxygen solubility and diffusivity limit the size and design of scaffolds. Without proper oxygen and nutrient supply, cell proliferation and viability decrease, leading to device failure. Recent computational analyses and in vitro studies have shown that the central regions of tissue-engineered constructs are most prone to hypoxia or anoxia, thereby creating a cell density gradient within the device [12, 13, 58]. Oxygen consuming cells on the outside edges of the device obstruct oxygen penetration, even when oxygen concentrations in the surrounding media are sufficient.

Large tissue engineering devices are necessary for a variety of applications, yet recent work has focused on encapsulation techniques [59, 60] and other methods to reduce device size [61–63] and ultimately limit diffusion distance within the device [17, 59, 64–69]. Consequently, recent studies have also focused on novel ways to improve, measure, and predict oxygen and nutrient transport within tissue engineering constructs [1, 4, 17, 18, 70–80]. Therefore, adequately reducing the risk of hypoxia within a construct relies on the physical constraints of the material itself, namely the geometric dimensions. Reducing the distance through which oxygen must diffuse eliminates the need to improve the transport properties of the material. Geometric constraints limit the design of materials to thin constructs or small capsules (20–250 μm diffusion distance [5, 13, 20]), which do not satisfy all of the possible applications for tissue-engineered devices, such as the device requirements needed to treat spinal cord injuries [81]. Understanding which mechanical properties and/or chemical additives facilitate greater oxygen transport could enhance device design and function. Methods for enhancing oxygen transport, such as the use of synthetic oxygen carriers or oxygen-generating biomaterials are discussed further in *Enhancing Oxygen Delivery to Tissue-Engineered Constructs*.

Determining and modeling oxygen transport within a cell-seeded construct requires knowledge of the cellular parameters of the system (i.e., effective diffusion coefficients (D_{eff}), OCRs, and cell growth rates) as well as the effect of scaffold design and size on the overall transport properties. Defining appropriate assumptions for each situation allows for the best estimation of the D_{eff}. The section on *Cellular Oxygen Consumption* outlines methods for determining the cellular demand and OCRs for different tissues. Using this information, D_{eff} can be calculated.

The limiting factor for oxygen availability is the low solubility of oxygen in water or cell culture medium ($S_{O_2 \text{ in } H_2O} = 2.2\text{mmol/L}$) [82]. The major shortcoming in most tissue engineering constructs is the low oxygen availability within the construct compared with the cellular demand or consumption, relative to the size of the construct or the diffusion distance in the material. Similar issues are seen with poor oxygen transport in vivo due to ischemia, where tissue will not receive the necessary oxygen concentration due to a drop in the pO_2 in circulating blood at the ischemic site.

Oxygen Transport

Oxygen diffusion within a tissue engineering construct is dependent upon the initial oxygen solubility in the matrix and cellular OCRs, as well as proximity to an oxygen source, such as vasculature. Transport limitations can be determined through mathematical modeling of oxygen transport.

A typical modeling strategy requires the use of a consumption equation. Assuming that mass is conserved, everything that is put into a system (In) and leaves the system (Out) as shown in (3.1).

$$0 = \text{In} - \text{Out}. \tag{3.1}$$

If complete removal of a substance is not achieved, then mass accumulates, as shown in (3.2). For example, in the case of a biomaterial for drug delivery, incomplete release of the encapsulated drug is accounted for using an accumulation term.

$$\text{Accumulation} = \text{In} - \text{Out}. \tag{3.2}$$

For the discussion of gasses, such as oxygen and carbon dioxide, oxygen could be supplied to a cell-seeded device and consumed by the cells, which subsequently release carbon dioxide. In this case, oxygen is consumed (consumption) and carbon dioxide is generated (generation), as shown in (3.3).

$$\text{Accumulation} = \text{In} - \text{Out} + \text{Generation} - \text{Consumption}. \tag{3.3}$$

In most cases, it is advantageous to look at how these variables change over time. For example, under steady-state conditions there is no accumulation over time and hence this term is zero (3.4). Once a system reaches steady state, the change in system inputs (In + Generation) are equal to the change in system outputs (Out + Consumption), as shown in (3.4).

$$0 = \Delta\text{In} - \Delta\text{Out} + \Delta\text{Generation} - \Delta\text{Consumption}. \tag{3.4}$$

Generation and consumption together are often referred to as a reaction term, R, shown in (3.5). R represents a differential in mass over time due to generation or

consumption of a specific substrate, such as cell mass or oxygen. In the case of oxygen concentration (C_{O_2}), the change in cellular oxygen consumption within a scaffold would decrease over time as the cells grow and divide, as more cells would be present within the scaffold (i.e., reaction vessel), hence consuming more oxygen.

$$R = \Delta\text{Generation} - \Delta\text{Consumption}. \tag{3.5}$$

Often, the reaction term can be depicted in terms of the change in oxygen mass per volume or cell mass over time. Mathematically, this describes the OCR when generation is assumed to equal 0, as shown in (3.6) for a spherical or cylindrical geometry.

$$-R_{O_2} = \text{OCR} = S(r,t) = \frac{\text{Consumption/volume or cell mass}}{\text{Time}}. \tag{3.6}$$

Diffusion Coefficients and Other Parameters Affecting Biomaterial Design

Appropriately calculating or estimating the OCR can be quite difficult as there are many parameters to consider. (1) Cell type. The type of cell seeded within the material will affect the OCR of a material because different cell types require different metabolic oxygen levels as discussed below (see *Oxygen Consumption Rates*). For example, hepatocytes are highly respiring while chondrocytes are not. (2) Biomaterial type. Most biomaterials (e.g., hydrogels) are composed primarily of water and therefore the scaffold material does not negatively affect the OCR. However, recent work on oxygen generating biomaterials has added complexity to estimating OCRs. For these materials, oxygen is generated, so the OCR can be modeled using (3.7).

$$\text{OCR}_{+\text{gen}} = \frac{\text{Consumption}_{\text{cellular}}/\text{volume}}{\text{Time}} - \frac{\text{Generation}_{\text{biomaterial}}/\text{volume}}{\text{Time}}. \tag{3.7}$$

The consumption and generation terms are not the only important variables to determine oxygen availability within a tissue engineering device. In some cases, such as a contact lens, the permeability, or ability to transport oxygen through a device, is critical to device performance. The permeability is often described using a diffusion coefficient D_{eff} (m^2/s) in terms of area per unit time. The D_{eff} is not dependent upon device geometry, but rather on the material and chemical properties of the scaffold. The solubility of oxygen in the material components greatly affects the oxygen diffusion coefficient, $D_{\text{eff};O_2}$ by altering the passive diffusion potential of the material.

The $D_{\text{eff};O_2}$ is dependent upon the material or medium through which the oxygen diffuses. Use of a silicone membrane, for example, would provide a high $D_{\text{eff};O_2}$

compared with an alginate hydrogel since silicone membranes have relatively high oxygen solubility when compared with alginate hydrogels [83]. In both of these cases, the pore size of the membrane or hydrogel does not affect oxygen transport; however, pore size plays a major role in the diffusion of larger particles, such as multi-domain proteins [84].

The $D_{\text{eff;O}_2}$ can be estimated in vitro by assuming that the culture medium is a Newtonian fluid and therefore, the scaffold does not hinder or enhance oxygen diffusion. For example, the $D_{\text{eff;O}_2}$ can be estimated simply as the diffusivity of oxygen in either water or cell culture media, measured as $D_{\text{eff,O}_2,\text{media}} = 2 \times 10^{-9}$ m^2/s, based on the viscosity of the solution [71]. This estimation applies to materials where pore size does not restrict the passive diffusion potential of gases.

A range of models with varying levels of complexity have been developed to model oxygen transport in a scaffold and are discussed below. In these models, the accumulation of oxygen in the device is represented by $(\partial C_{\text{O2}}(r,t)/\partial t)$, where the differential calculates the change in oxygen concentration (C_{O_2}) with respect to time. C_{O_2} varies with both time and position within a device. For example, at the start of an experiment where a spherical device (e.g., hydrogel capsule) is placed into a hyperbaric oxygen chamber, the center of the device will have a lower oxygen concentration than the surface of the device. Gradually, a gradient will develop, where higher oxygen concentrations exist near the surface with a linear decrease in the radial direction until a concentration equal to the initial value is reached at the center of the device. Once steady state is achieved, the concentration of oxygen throughout the device will no longer change with time. Depending upon the device size, the amount of time required to reach steady state varies. The gradient in oxygen concentration is mathematically depicted as $\nabla \cdot \left(D_{\text{eff,O}_2} \nabla C_{\text{O2}}(r,t)\right)$, where ∇ is the mathematical operator shown in (3.8), (3.9), and (3.10) for rectangular, cylindrical, and spherical coordinates, respectively, operating on the generic variable, F.

$$\nabla F(x,y,z) = \frac{\partial F}{\partial x}\hat{x} + \frac{\partial F}{\partial y}\hat{y} + \frac{\partial F}{\partial z}\hat{z}, \tag{3.8}$$

$$\nabla F(r,\theta,z) = \frac{\partial F}{\partial r}\hat{r} + \frac{1}{r}\frac{\partial F}{\partial \theta}\hat{\theta} + \frac{\partial F}{\partial z}\hat{z}, \tag{3.9}$$

$$\nabla F(r,\theta,\varphi) = \frac{\partial F}{\partial r}\hat{r} + \frac{1}{r\sin\varphi}\frac{\partial F}{\partial \theta}\hat{\theta} + \frac{1}{r}\frac{\partial F}{\partial \varphi}\hat{\varphi}. \tag{3.10}$$

It is often advantageous to use either cylindrical or spherical geometries to understand diffusion within a system because the dimensional complexity of the transport equations can be simplified. In both cylindrical and spherical coordinates, only the $\hat{r}$ is important. For a cylinder, this assumption assumes that diffusion is most prevalent in the $\hat{r}$ direction and that the transport in the z direction is minimal in comparison. In both cases, the angular directions are not important, if the system is homogeneous and the bulk solution is well mixed. Therefore, transport equations

can be solved in terms of one physical dimension $(\hat{r})$ rather than the two that are necessary in the rectangular system (x, y).

Equations (3.11)–(3.13) are shown such that C_{O2} is dependent only upon the radial direction, r, and the time, t. Equation (3.11) represents the simplest model, assuming that oxygen consumption is equal to a constant, R. Equation (3.12) represents a slightly more complex model, where oxygen consumption is dependent upon spatio-temporal parameters. The functional form of $S(r,t)$ can vary based on the assumptions made and the kinetic model chosen to represent the OCR. The possible functional forms of $S(r,t)$ are discussed below in *Oxygen Consumption Rates*.

$$\frac{\partial C_{O2}(r,t)}{\partial t} = \nabla \cdot \left(D_{\text{eff},O_2} \nabla C_{O2}(r,t)\right) + R, \tag{3.11}$$

$$\frac{\partial C_{O2}(r,t)}{\partial t} = \nabla \cdot \left(D_{\text{eff},O_2} \nabla C_{O2}(r,t)\right) - S(r,t). \tag{3.12}$$

Equations (3.13) and (3.14) are a set of coupled partial differential equations, which account for changes in cell density $(C_{\text{cell}}(r,t))$ within a scaffold as a function of both position and time [84]. Changes in cell density over time are due to both cell proliferation $(g(r,t))$ and cell death $(d(r,t))$.

$$\frac{\partial C_{O2}(r,t)}{\partial t} = \nabla \cdot \left(D_{\text{eff},O_2} C_{O_2}(r,t)\right) - \left(S(r,t) C_{\text{cell}}(r,t)\right), \tag{3.13}$$

$$\frac{\partial C_{\text{cell}}(r,t)}{\partial t} = C_{\text{cell}}(r,t)(\mathrm{g}(r,t) - \mathrm{d}(r,t)). \tag{3.14}$$

Using this set of coupled equations, oxygen consumption as a function of cell density gradients can be modeled and predicted. In the design of tissue engineering devices, the maximum device size (corresponding to the value of r) to create a given steady-state oxygen concentration within a device can be estimated, or the effect of different cell seeding densities can be predicted to determine optimal device parameters necessary to avoid cell death.

For a cylindrical system, addition of a z component to these coupled equations would further elucidate the effects of position on oxygen gradients within a material. A z component was included to better fit experimental data for oxygen transport and cell density gradients within fibrin hydrogels [85].

Oxygen Diffusion Coefficients in Tissue-Engineered Constructs

The $D_{\text{eff};O_2}$ represents the propensity for a given molecule to move into or out of a medium or material, as shown above in (3.11)–(3.13). The $D_{\text{eff};O_2}$ can be a constant

Table 3.1 Diffusion coefficients for various biological matrices

Material	Diffusion coefficient ($\times 10^9$ m^2/s)	Source
Alginate (1.5%)	1.43 ± 0.24	Measured by [90]
Alginate (3%)	1.22 ± 0.23	Measured by [90]
Agarose (2%)	2.70 ± 0.11	Measured by [90]
Agarose (4%)	2.70 ± 0.21	Measured by [90]
Collagen (11%)	0.45	Measured by [90]
Collagen (34%)	0.17	Measured by [90]
Collagen (11%, photochemical crosslinking)	0.34	Measured by [91]
Dacron	4.67 ± 1.44	Measured by [75]
Fibrin	0.31 ± 0.13	Measured by [87]
SIS-L	0.24 ± 0.04	Measured by [75]
SIS-A	0.56 ± 0.16	Measured by [75]
UBM-L	0.46 ± 0.07	Measured by [75]
UBM-A	0.38 ± 0.05	Measured by [75]
UBS	0.66 ± 0.12	Measured by [75]
Cell culture medium	2.0	Reported by [73]

SIS porcine small intestinal submucosa, *UBM* porcine urinary bladder matrix, *UBS* porcine urinary bladder submucosa, L is the luminal side of the tissue, A is the abluminal side of the tissue

under a given set of conditions or parameters for mathematical simplification. For example, in a tissue engineering scaffold or thin film without cells with a stable matrix structure, the diffusion of a small solute, metabolite, or gas, such as oxygen, is a constant. Table 3.1 lists the oxygen diffusion coefficients for various cell-free materials $\left(D_{\mathrm{eff,O_2,M}}\right)$ as well as the oxygen diffusion coefficient for various tissues within the body. The addition of additives, such as synthetic oxygen carriers, or cells will alter these values based on concentration.

One method for estimating the effective oxygen diffusivity in a homogenously cell-seeded hydrogel $\left(D_{\mathrm{eff,O_2}}(r,t)\right)$ assumes that the cells act as small particles evenly spaced throughout the scaffold, which is mathematically similar to Maxwell's solution for porous media [86], as shown in (3.15). The volume fraction of cells within the material $(\varepsilon_\sigma(r,t))$ is related to the cell diameter (d_{cell}, μm) and cell density, $C_{\mathrm{cell}}(r,t)$ (3.16). For simplicity, the volume of a cell can be estimated as 850 μm^3 in (3.16) [85], assuming that the cell is spherical in shape with an approximate diameter of 2–2.5 μm.

$$D_{\mathrm{eff,O_2}}(r,t) = D_{\mathrm{eff,O_2,M}}\left(\frac{2(1-\varepsilon_\sigma(r,t))}{2+\varepsilon_\sigma(r,t)}\right), \tag{3.15}$$

$$\varepsilon_\sigma(r,t) = \left(\frac{1}{6}\pi d_{\mathrm{cell}}^3\right) C_{\mathrm{cell}}(r,t). \tag{3.16}$$

Improvements to this model have been made to better predict oxygen diffusivity in a material with a high cell density gradient and a population of cells on the material

surface, by including $D_{\mathrm{eff,O_2,M}}$ for the specific material chosen and the diffusivity of oxygen in a cell ($D_{\mathrm{eff,O_2,cell}} = 3 \times 10^{-10}\mathrm{m}^2/\mathrm{s}$ [87]) as shown in (3.17) [85].

$$D_{\mathrm{eff,O_2}}(r,t) = D_{\mathrm{eff,O_2,M}}\left(\frac{(2/D_{\mathrm{eff,O_2,cell}}) + (1/D_{\mathrm{eff,O_2,M}}) - 2\varepsilon_\sigma(r,t)\left((1/D_{\mathrm{eff,O_2,cell}}) - (1/D_{\mathrm{eff,O_2,M}})\right)}{(2/D_{\mathrm{eff,O_2,cell}}) + (1/D_{\mathrm{eff,O_2,M}}) + \varepsilon_\sigma(r,t)\left((1/D_{\mathrm{eff,O_2,cell}}) - (1/D_{\mathrm{eff,O_2,M}})\right)}\right). \tag{3.17}$$

Oxygen Consumption Rates

Tissue engineering device design can be guided by the OCR of the incorporated cell type. OCRs can be measured using a ruthenium II dye such as that provided by the BD™ Oxygen Biosensor System (BD Biosciences) or the OxoPlate® system (Innovative Instruments, Inc.), which uses two dyes to create a calibration-free system [72]. Ruthenium is often used because when excited at 470 nm, it is sensitive to oxygen through a mechanism by which oxygen collides with the fluorescent molecule, transferring energy to the dye, increasing the "brightness" or fluorescent signal [72, 88]. OCRs can also be determined using a bioreactor set-up with an on-line oxygen meter such as those offered by New Brunswick Scientific (Edison, NJ), HEL (Lawrenceville, NJ), or Applikon Biotechnology, Inc. (Foster City, CA) [89–92].

OCRs $(S(r,t))$ can be modeled using simple first-order oxygen consumption [93] as shown in (3.18), where k_t is the first-order rate constant. Models with increasing complexity have been proposed. One of the most common models used to estimate Michaelis-Menten style consumption [18, 70] is shown in (3.19), where $V_{\max}$ is the maximum specific OCR and K_S is the half-rate constant.

$$S(r,t) = k_t C_{\mathrm{O_2}}(r,t), \tag{3.18}$$

$$S(r,t) = V_{\max}\left(\frac{C_{\mathrm{O_2}}(r,t)}{K_S + C_{\mathrm{O_2}}(r,t)}\right). \tag{3.19}$$

The Michaelis-Menten type model can be modified to incorporate cell growth kinetics, as shown in (3.20).

$$S(r,t) = V_{\max}\left(\frac{C_{\mathrm{O_2}}(r,t)}{K_S + C_{\mathrm{O_2}}(r,t)}\right)C_{\mathrm{cell}}(r,t). \tag{3.20}$$

The Monod model [18, 94] is shown in (3.21), where m_S is the cellular maintenance coefficient, the minimum substrate concentration required to maintain cell viability [18, 94]. The Monod model incorporates the maximum cell-specific growth rate $(\mu_{\max})$ and the cell yield coefficient (Y_{XS}), which are parameters that can be easily determined experimentally.

$$S(r,t) = \left(\frac{\mu_{\max}}{Y_{XS}} + m_S\right)\left(\frac{C_{O_2}(r,t)}{K_S + C_{O_2}(r,t)}\right)C_{\text{cell}}(r,t). \tag{3.21}$$

The rate of cell growth $(\mu(r,t))$ can be calculated based on Y_{XS} at a given time and position [95] and OCR, as shown in (3.22).

$$\mu(r,t) = Y_{XS}\left(\frac{S(r,t)}{C_{\text{cell}}(r,t)} - m_S\right). \tag{3.22}$$

Using a model such as the one shown in (3.12) can greatly improve the design of novel tissue engineering devices. By effective calculation, measurement, or estimation of either the OCR or D_{eff,O_2}, models can be developed which accurately predict cellular behavior and oxygen availability within a scaffold. The results of modeling exercises coupled with experimental results can effectively guide device design.

Oxygen Transport in Vascularized Tissue Constructs

A 1-D spherical diffusion model was used to model oxygen limitations in a biomaterial as angiogenesis occurred within the matrix [18] based on an in vivo arteriovenous loop chamber used to measure pO_2 in the blood [96]. Modeling results determined that the length of time cells experience hypoxia is the most important factor leading to the failure of a scaffold [18]. Results suggest that homogeneous methods for seeding scaffolds, such as the use of a bioreactor to enhance cell penetration into the scaffold through mixing [97], may only be beneficial for small scaffolds (i.e., few hundred micrometers) [18, 19]. These predictions agree with data regarding the growth of seeded cells in scaffolds, where only cells near the surface of the scaffold proliferate and function as desired, creating an inhomogeneous scaffold over time, as shown in Fig. 3.3 [12, 15]. A moving vascularization front (penetrating vascular network) was used to experimentally determine that the "speed of the vascularization front" (λ), or rate of vascular growth necessary to maintain viable tissue, is dependent upon δ, the rate of cell diffusion relative to the rate of cell proliferation, such that $\lambda > 2\sqrt{\delta}$. Results from these studies suggest that heterogeneous seeding of scaffolds through directed cell placement near the edge of the scaffold is necessary to reduce hypoxic exposure to the initial cells incorporated within the device, with the goal of inducing cell motility along the vascularization front [18, 19].

While mathematical models of oxygen transport assist in scaffold design, inducing directed vascularization is challenging. Preferentially seeding scaffolds with cells near the outer edge of the device is also difficult to achieve and maintain and requires an understanding of cell motility within the scaffold. Directing stem cell differentiation and motility using growth factor and/or nutrient gradients may

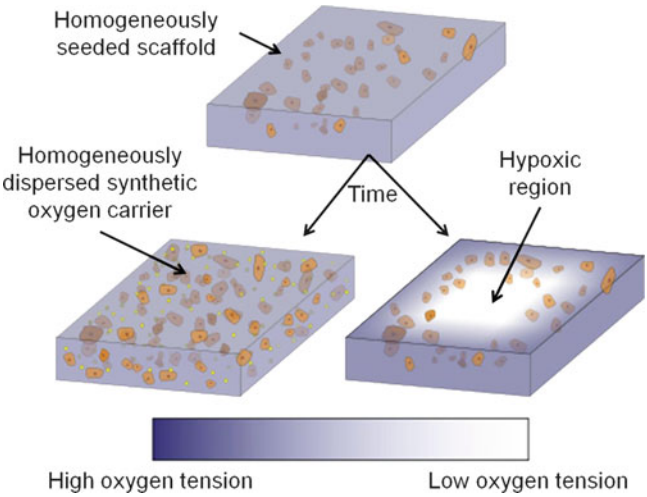

Fig. 3.3 Oxygen gradients form within traditional scaffolds over time limiting the growth and motility of cells. Homogeneously seeding a scaffold containing a synthetic oxygen carrier may lead to decreased hypoxia-mediated apoptosis and enhance growth and functionality of the seeded cells (*left*). Scaffolds kept in an oxygenated environment may benefit from higher levels of oxygen near the edge of the scaffold, while transport limitations may lead to hypoxia-mediated apoptosis in the center of the device (*right*)

provide a method for the creation of heterogeneously seeded scaffolds. Directed stem cell differentiation has been achieved using growth factor gradients within a scaffold, showing the feasibility of directing differentiation and cell motility [98].

Measuring Dissolved Oxygen Concentration In Vitro

Measuring the dissolved oxygen concentration within a scaffold material has proven difficult due to the inability to monitor changes or gradients within a biomaterial. General methods for determining dissolved oxygen in solution utilize fiber-optic and Clark-type [99] oxygen probes. Fiber-optic oxygen probes generate fluorescence at the tip, which is collected by the probe and carried by the optical fiber to a high-sensitivity spectrometer. When oxygen diffuses into the thin-film coating the fluorescence is quenched. The degree of quenching is related to the frequency of collisions, and therefore, to the concentration, pressure, and temperature of the oxygen-containing sample. Clark-type oxygen probes measure changes in the surrounding solution electrochemically. Use of these probes requires strict temperature control, as changes in temperature greater than 1°C will result in measurement shifts.

Both probe types measure the oxygen concentration in the bulk solution surrounding a material or device. Therefore, typical experiments measure the transport of oxygen across a membrane or thin hydrogel from a donor solution (saturated

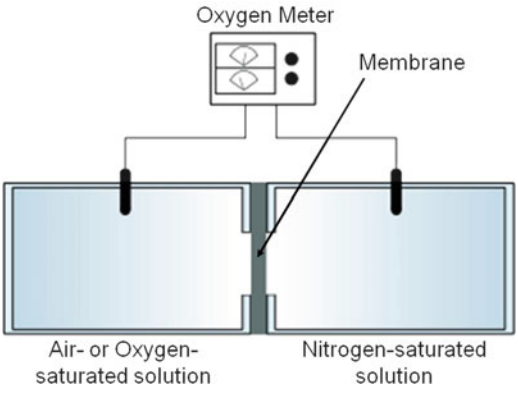

Fig. 3.4 Oxygen diffusion cell apparatus. Oxygen transport can be monitored by measuring the change in oxygen concentration in each chamber over time

with air or oxygen) to a receiving solution (saturated with nitrogen) [73], as shown in Fig. 3.4.

The D_{eff,O_2} for a membrane used in this apparatus accounts for both tortuosity and diffusion and is expressed by (3.23) [73], where z is the thickness of the membrane, A is the area through which diffusion occurs, t is time, V_R is the volume of the receiving chamber, C_D is the oxygen concentration in the donor chamber at time t, C_R is the oxygen concentration in the receiving chamber at time t, and C_{R0} is the oxygen concentration in the receiving chamber at time 0 (see Ref. 73 for derivation).

$$D_{\text{eff},O_2} = -\frac{zV_R}{tA}\ln\left(\frac{C_D - C_R}{C_D - C_{R0}}\right). \tag{3.23}$$

Difficulties with these measurements include accurate determination of initial conditions and accounting for system artifacts, such as the tendency for probes to drift over time [100]. Initial conditions can be determined using a Winkler test, which is commonly used to measure oxygen concentrations in lake or river water [101]. Alternatively, errors resulting from probe drift can be accounted for by modification of the model used to determine D_{eff,O_2} [100].

Recent advances in measuring dissolved oxygen concentrations include the use of fluorescent microparticles to sense the local oxygen environment [75]. Fluorescent particles made of silica gel containing the oxygen sensitive luminophore tris (4,7-diphenyl-1,10-phenanthroline) ruthenium (II) dichloride, or $Ru(Ph_2phen_3)Cl_2$, were created and added to the biomaterial formulation [75]. Advantages of this system include the ability to determine percent change in oxygen tension over time within a material [75]. Based on initial cytotoxicity studies [75], these systems may be useful for cell-seeded hydrogels as a method for visually detecting oxygen gradients within a construct.

Optical PEBBLE (probes encapsulated by biologically localized embedding) nanosensors measure dissolved oxygen using silicate nanoparticles modified with an oxygen-sensitive platinum porphyrin dye [102]. Nanoparticles can be injected into cells using particle bombardment (i.e., gene gun) technologies in vitro to

monitor intracellular dissolved oxygen [102]. Use of these nanosensors in multiple cell types yielded high sensitivity, making these particles functional for real-time measurements of dissolved oxygen concentration [102].

A fiber-optic-based system to measure local oxygen concentration within a hydrogel was developed using an oxygen microsensor (PreSens Co., Regensburg, Germany), which uses fiber-optic technology in the form of a needle with a 3 mm naked sensing tip connected to an oxygen meter (Microx TX3, PreSens Co.) [77]. Using this set-up, oxygen concentration at the top surface of a collagen-based biomaterial exposed to cell culture medium was measured to be 11 times that at the bottom surface, showing limitations for oxygen diffusion deeper within the gel over a 3-week period [77]. Advantages of this technique include the ability to look at the microenvironment within a biomaterial, enabling the possibility of probing oxygen concentration at the biomaterial-cell surface interface.

Enhancing Oxygen Delivery to Tissue-Engineered Constructs

Many investigators have devoted time to determine methods to enhance oxygen transport in tissue engineering constructs both in vitro and in vivo. Enhancements include addition of a synthetic component to the system to improve oxygen diffusion as well as addition of growth factors or other cell types to encourage growth of new blood vessels (i.e., vasculogenesis) or recruitment of existing vasculature (i.e., angiogenesis). Use of improved cell culture methods, such as microfluidic devices or perfused bioreactors, has also been explored.

For example, a method to embed a microfluidic network into a cell-seeded alginate scaffold was developed [103]. With this device, control over distribution of soluble signals was achieved through controlling mass transfer at the microenvironment level. Spatial and temporal control over metabolite delivery was demonstrated using fluorescently labeled calcein in a chondrocyte-seeded microfluidic scaffold [103]. Utilizing this method to regulate oxygen concentration and metabolite delivery within a cell-seeded scaffold might provide even greater control over cell growth and function [104].

Perfused Constructs for Tissue Growth

One common method for engineering tissue constructs for in vitro studies or later transplantation is to seed cells in a 3-D scaffold and maintain the construct in a bioreactor. Bone [92, 105–108], cartilage [97, 109, 110], skeletal muscle [111], smooth muscle [112], cardiac muscle [113, 114], and liver tissue [79, 115–117] have been extensively investigated in vitro to study tissue development and tissue response to exogenous stimuli. The use of perfusion bioreactors has been shown to

prevent cell death associated with hypoxia in 3-D tissue engineering scaffolds by maintaining higher oxygen concentrations at the scaffold core. Failure of 3-D constructs in vitro is associated with oxygen gradients which cause inhomogeneous tissue quality and functionality [14, 92]. The use of a perfusion bioreactor has been shown to prevent some hypoxia-related cell death of preosteoblasts by maintaining oxygen concentrations throughout the construct at 4%, equivalent to that on the periphery of the scaffold in a static culture [92].

For stem cell propagation and expansion using a perfused bioreactor, the effects of flow rate-induced shear stress on culture expansion and differentiation should be considered [118–120]. For example, bone marrow-derived human mesenchymal stem cells (BM-hMSCs) show greater osteoblast differentiation following longer periods of shear stress through an increase in alkaline phosphatase (ALP) activity and calcium deposition (osteoblast differentiation markers) in a 3-D poly(ethylene terephthalate) (PET) matrix [118].

Synthetic Oxygen Carriers

Synthetic oxygen carriers, such as hemoglobin-based oxygen carriers (HBOCs) and perfluorocarbons (PFCs), have been explored for their use as blood substitutes or in blood replacement therapy, and have been shown to increase oxygen solubility and availability in blood [82, 121, 122]. In the development of bioartificial liver assist devices (BLADs), the synergistic effect of both HBOC and PFC incorporation has been shown to aid in the oxygenation of the extra capillary space of a hepatic hollow fiber bioreactor [79].

Hemoglobin-Based Oxygen Carriers

HBOCs were originally designed as artificial blood substitutes to enhance oxygen transport in vivo for patient treatment following general surgery, emergency trauma, hemorrhagic shock, and for exchange transfusions [122]. Recent work has investigated the addition of HBOCs to liquid-culture bioreactors to enhance oxygen delivery to tissue engineering scaffolds [79, 117]. In vitro growth of tissues that demand high oxygen concentrations, such as liver [117] or cardiac muscle [113], may benefit from the use of blood substitutes in culture conditions prior to device implantation [14].

Hemoglobin (Hb) can be encapsulated in liposomes [123] and synthetic amphipathic copolymers [2] to enhance both stability in solution and delivery of oxygen once injected into the blood stream following a traumatic event [122]. Success of HBOCs relies on maintaining the functional state of the encapsulated Hb so that adequate oxygen delivery is achieved. Maintaining the oxygen carrying capacity of the native Hb and preventing conversion to methemoglobin (metHb, Fe^{3+} state of Hb) when in storage or once introduced into the body is a major goal of HBOC

design [123]. The ability of HBOCs to carry oxygen in vivo can be determined using a variety of radioisotope methods, such as the use of oxygen-15 (^{15}O) to quantify oxygen delivery to specific tissues (reviewed elsewhere [123]).

Initial studies with liposome-encapsulated hemoglobin (LEH) dispersions showed promise, but issues such as shelf-life, aggregation, encapsulation efficiency, and large scale manufacturing led to the need for improved formulations [122]. LEH dispersions have been modified to enhance circulation half-life and reduce aggregation through surface modification using poly(ethylene glycol) (PEG) [122–125]. PEG conjugation provides a steric barrier which can prevent aggregation of PEG-LEH particles in solution [126] as well as improve biocompatibility, hemodynamic properties, and structural properties of LEH dispersions [122, 125, 126]. *Neo Red Cells* commercially developed by Terumo (Kanagawa, Japan) are PEG-LEH dispersions formed by coating liposomes of hydrogenated soy phoshatidylcholines, cholesterol, myristic acid, and α-tocopherol with PEG-phosphatidylethanolamine [122, 127, 128]. To enhance the oxygen carrying capacity of LEH dispersions, liposome-encapsulated actin hemoglobin (LEAcHb) dispersions were formulated by incorporating actin and hemoglobin to create a dispersion that is mechanically stable and ellipsoidal in solution, to provide similar shape of a red blood cell for ease of flow in the blood [129].

Polymersome-encapsulated hemoglobin (PEH) particles are made from amphipathic di-block copolymers dissolved in water and are used to form vesicles with thicker, more robust membranes [130, 131] when compared with PEG-LEH particles [2]. Engineering polymersome structure and geometry to enhance mechanical properties and ability to escape the host immune system can be easily achieved by varying the preparation method, type of amphipathic copolymer, and PEG chain length [2, 131–133].

Perfluorocarbons

PFCs are able to dissolve high amounts of oxygen and carbon dioxide than that of water (see Table 3.2) [82, 134] due to low intermolecular interactions based on fluorine's low polarizability, and therefore low van der Waals forces [82, 121]. PFCs are both lipophobic and hydrophobic, adding to their biologically inert properties [134, 135]. PFCs can increase the ability of erythrocytes to transport and transfer oxygen to tissues when injected intravenously [136].

Gas dissolution by PFCs occurs through loose, non-directional van der Waals interactions rather than the strong coordination chemistry seen between oxygen and iron in Heme [121]. Weak cohesive forces and limitless saturation cause loose associations between gases and PFCs, allowing oxygen to be readily available to tissues [121]. Thus, oxygen uptake and release curves are linear in form, i.e., no concentration dependence, shown in Fig. 3.5 [121]. PFC emulsions are able to dissolve larger volumes of non-polar gases, and preference for a particular gas is related to the molecular volume of the gas (preference for PFCs is $CO_2 \gg O_2 >$

Table 3.2 Solubility of oxygen in various liquids (mmol/L at standard temperature and pressure)

Liquid	Oxygen	Carbon dioxide
Water	2.2	57
Perfluorotributylamine	35.2	123
Perfluorodecalin	35.5	125
Bis(perfluorohexyl)ethane	37.9	159
Perfluorotripropylamine	39.6	146
Perfluoroocytyl bromide	44.0	185
Bis(perfluorobuytl)ethene	44.0	203

Adapted from [84]

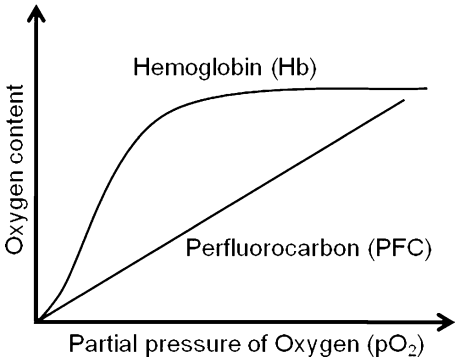

Fig. 3.5 Relationship between oxygen content (or oxygen associated with the PFC) and oxygen partial pressure [pO_2 for hemoglobin (Hb) and perfluorocarbons (PFCs)]. The linear relationship for PFCs is based on the weak van der Waals interactions between oxygen and PFC molecules when compared with the binding of oxygen to iron in Heme

$CO > N_2$) [82]. These characteristics improve the ability of PFCs to transport oxygen into (or carbon dioxide out of) tissue engineering constructs.

The stability of PFCs due to the strong C-F bonds within the molecule renders PFCs relatively inert. Due to their lipophobic and hydrophobic properties, PFC emulsions tend to phase separate quickly in aqueous medium [137]. Perfluorooctyl bromide (F-*octyl* bromide, PFOB) has been approved by the FDA for use as an MRI contrast agent [138] and liquid PFC has been used to fill the lungs of hypoxic patients as a form of liquid ventilation [138, 139].

PFC colloidal systems are under investigation for use in a variety of biomedical applications [134, 138], including islet preservation and encapsulation for diabetes treatment [78, 140, 141], bone regeneration [81], and creation of tissue-engineered trachea [142]. By increasing the dissolved oxygen concentration in a solution or biomaterial construct, oxygen diffusion limitations to the cells or tissues can be mediated by increasing oxygen solubility in oxygen-limited areas. In recent years, the biocompatibility and efficacy of PFCs have been investigated using a variety of cell types, including hepatocytes [1, 72, 79, 115], endothelial cells [143], stem cells [81], β-cells [141, 144], and fibroblasts [145].

PFCs have also been investigated for their use in guiding stem cell differentiation by controlling the native oxygen microenvironment. The use of perfluorotributylamine (PFTBA) in fibrin hydrogels improved the in vivo survival of modified mesenchymal stem cells (Tet-off BMP2 MSCs), increasing the overall bone volume by 1.4-fold and yielding better bone quality in bone-repair and spinal fusion models [81]. Our lab is interested in the addition of PFCs to alginate microcapsules and hydrogels to enhance cell viability and oxygen diffusion for a variety of applications, and recent work has focused on the effect of PFC incorporation on protein transport and cell viability within the matrix [1, 72].

Difficulty arises in evaluating the use of PFCs due to their hydrophobicity. To incorporate PFCs into cell culture media or a water-based biomaterial, such as a hydrogel, a surfactant must be used [1, 72]. Structure and concentration of surfactant used to create the PFC emulsion is a major part of the system design. Pluronics®, such as Pluronic® F-68 or F-127[1, 72], and natural surfactants, such as egg yolk phospholipids [145], have been investigated in PFC emulsion formulations.

Oxygen Generating Biomaterials

Novel poly(D-L-lactide-*co*-glycolide) (PLGA)-based biomaterials were developed, which utilize the decomposition of an oxygen-rich compound, sodium percarbonate (SPO) [3], or calcium peroxide [4], to generate oxygen in situ. POG films made with SPO were capable of steady oxygen release over a 24-h period, with complete decomposition of the incorporated SPO after 70 h. In vivo studies with rats confirmed delayed onset of necrosis, showing significantly decreased necrosis of dorsal skin flaps after 2 days, but with comparable necrosis (to the PLGS control) after 7 days [3]. POG 3-D scaffolds made with encapsulated calcium peroxide were designed to release oxygen over a 10-day period [4]. Results showed continually elevated oxygen levels in the scaffold core under hypoxic bulk conditions, and scaffolds were able to extend growth of NIH-3 T3 fibroblasts under hypoxic conditions to similar levels found in vivo after implantation [4]. The use of oxygen generating biomaterials may improve survival rates of implanted tissue prior to the establishment of a vascular network within the tissue-engineered construct without suppressing angiogenesis [146].

Vascularization of Bioengineered Tissue Constructs

One of the major issues with successful transplantation of tissues or constructs is the lack of functional vasculature to facilitate oxygen transport [44], which increases the likelihood of hypoxia-induced apoptosis [14]. Recruitment of vasculature into biomaterial constructs via angiogenesis or the induction of vasculogenesis improves tissue survival through increased oxygen transport [14, 147]. Vasculogenesis is the formation of new blood vessels from endothelial progenitor

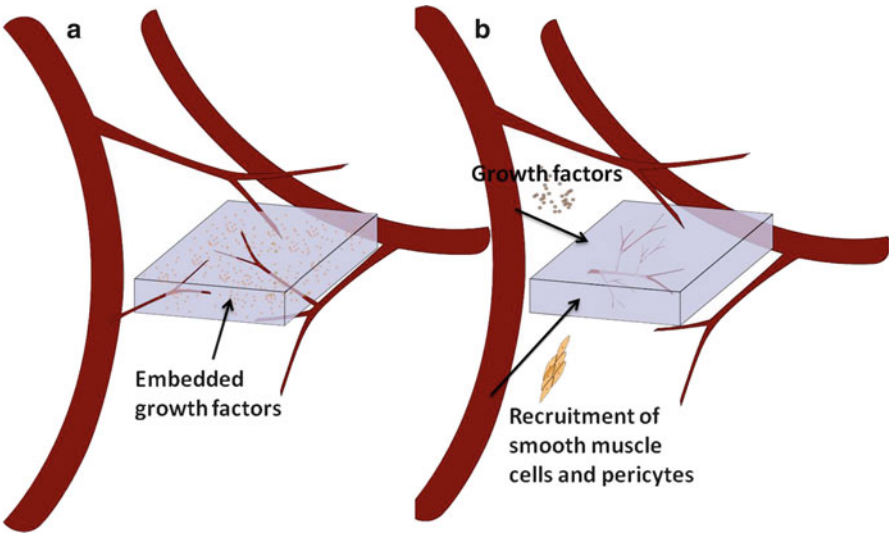

Fig. 3.6 Angiogenesis and Vasculogenesis – Methods for forming vasculature within a tissue-engineered scaffold. (**a**) Angiogenesis is the process of inducing the growth of an existing capillary network into the scaffold through signaling molecules such as VEGF (represented by orange dots). (**b**) Vasculogenesis requires seeding of vasculature progenitor cells into the scaffold, followed by differentiation of these cells to form mature vasculature. Mature vasculature requires recruitment of smooth muscle cells and pericytes to create a support structure in a process called arteriogenesis

cells, while angiogenesis is defined by the sprouting of new vessels from existing capillary networks, also referred to as recruitment of vasculature (Fig. 3.6).

In embryonic development and wound healing, vasculogenesis begins with differentiation of multipotent mesodermal progenitor cells into endothelial cell progenitors, which then differentiate into mature endothelial cells [148, 149]. New endothelial cells must organize into a primary capillary plexus, which involves recruitment of pericytes and smooth muscle cells to form a mature blood vessel through a combination of cell–cell and cell–matrix interactions in a process known as arteriogenesis [148, 150]. A variety of growth factors and soluble proteins are required at different stages in the process, including fibroblast growth factor-2 (FGF-2), VEGF, platelet-derived growth factor-B (PDGF-B), and tumor growth factor-β (TGF-β) (reviewed elsewhere [148]). For tissue engineering applications, the use of stem or progenitor cells has been investigated as a method for vasculogenesis within a scaffold. The role of biomaterials in stem cell differentiation for vasculogenesis has received attention over the last decade. Differentiation, growth, and functionality of stem cells have been controlled in vitro using spatial organization of growth factors and ECM domains to guide vasculogenesis (reviewed elsewhere [151]).

Instead of using stem or progenitor cells to grow new vasculature to enhance oxygen transport to tissue engineering scaffolds, the process of angiogenesis recruits existing capillary networks into the material. Angiogenesis is initiated by mature endothelial cells which experience certain biological stresses, such as inflammation, ischemia, hypoxia, change in pH, gradients in soluble signals, or

other changes to the microenvironment [152]. Endothelial cells control basement membrane and ECM degradation to extend vasculature using a variety of proteases, such as matrix metalloproteinases (MMPs) [147, 152]. The first ECM-mimicking biomaterial developed to induce angiogenesis consisted of protease-sensitive peptides grafted onto a PEG backbone [153]. A biointeractive PEG network exhibits key functionalities of natural ECM, including degradability by MMPs, which are critically important in the remodeling of tissue during angiogenesis [153, 154]. Angiogenesis and therefore vascularization of the synthetic scaffold was achieved by varying local concentrations of VEGF both in vitro and in vivo using a biointeractive, functionalized PEG hydrogel network [154, 155].

Growth factors and chemotaxis are important for proper growth and extension of blood vessels, which requires that endothelial tip cells at the beginning of new capillaries extend long filapodia in response to chemotactic factors which guide growth of the vessel by promoting proliferation of the tip cells closest to the chemotactic factors (i.e., VEGF, TGF-β, and PDGF). The lumen inside the sprout forms from vacuoles inside the endothelial tube cells which coalesce over time [156]. Mechanically, endothelial and mural cells need to be able to rearrange their microenvironment to allow for expansion and maturation of the growing capillary network [147, 153, 155, 157]. A biomimetic, yet purely synthetic scaffold, capable of promoting blood vessel formation in vitro and in vivo was developed [157], which contains an MMP-sensitive sequence from α1(I) collagen grafted to a PEG backbone with acrylate terminal groups with incorporated VEGF to promote angiogenesis and grafted RGDS (Arg-Gly-Asp-Ser) to enhance integrin binding [155, 157, 158]. Using this functionalized PEG hydrogel, it was shown that covalent immobilization of soluble factors, such as VEGF or an RGDS peptide, was able to control the angiogenic process and accelerate endothelial tubulogenesis within the scaffold [159].

Understanding and modulating the activity of endothelial cells for angiogenesis (or endothelial progenitor cells in vasculogenesis) are key requirements for successful therapeutic applications in tissue engineering [45] as well as in vascular regenerative engineering. Consequently, investigators are interested in creating materials which release multiple chemotactic factors over time to enhance the angiogenic potential of a construct [41, 160–163]. Recent successes indicate that soluble proteins and signaling molecules (i.e., VEGF or FGF-2), when incorporated into a biomaterial design, may lead to new biomaterial formulations that modulate blood vessel growth within the material. Mature blood vessel formation requires cooperation of not only endothelial cells but also pericytes and smooth muscle cells, which form the outer support structure of the vessel [152] through the process of arteriogenesis [164]. Many therapeutic delivery systems under investigation take advantage of these mechanisms through the dual delivery of growth factors and signaling molecules to optimize device design and modulate activity of a variety of angiogenic cell types, including endothelial progenitors and smooth muscle cells. Numerous signaling molecules and soluble factors have been identified in playing a role in blood vessel growth and formation, including VEGF, FGFs, TGFs, PDGFs, angiopoietins, ephrins, placental growth factors, and a variety of chemokines and oxygen sensors, such as HIF-1 [31, 163, 165]. For example, subcutaneous delivery of VEGF and MCP-1 (monocyte

chemotactic protein-1) loaded alginate microcapsules enhanced survival and engraftment of transplanted endothelial cells and promoted smooth muscle cell recruitment and final vessel maturation in an in vivo murine model. VEGF alone did not induce the formation of mature neovasculature because mural cells were not recruited and arteriogenesis was not promoted [149, 166].

While the growth factors present at all stages of blood vessel development are similar, their presence at different stages of vessel maturity and at different concentrations or density gradients can create a variety of responses within tissue engineering constructs [164, 167, 168]. For example, HIF-1 can initiate angiogenesis through upregulation of VEGF and other angiogenic factors, such as TGF-β, FGF2, and PDGF-β, as shown in Fig. 3.2 [31, 42]. VEGF is a widely studied angiogenic protein, which binds to the VEGF cognate receptor on endothelial cells (VEGF-R2). VEGF promotes growth of mature endothelial cells. FGF-2 enhances proliferation of endothelial cells in the presence of fibrin, an ECM protein [169]. Increasing concentrations of FGF-2 cause smooth muscle cell migration and proliferation, demonstrating the chemotactic potential of FGF-2 in arteriogenesis [170]. Also, PDGF-β and angiopoietin-1 (ang-1) have been shown to recruit mural cells around endothelial tube cells, leading to vessel maturity and proper functionality [163]. Overall, the development of tissue engineering scaffolds with spatio-temporal release of growth factors enhances control over cell growth, functionality, and differentiation to enhance oxygen delivery to target cells seeded within a 3-D scaffold through blood vessel formation.

Hypoxia and the Clinical Realization of Tissue-Engineered Constructs

While research continues to focus on mediating hypoxia in tissue constructs, many specific fields have made great strides in understanding the role of oxygen transport in device success. For example, contact lens design emphasizes maintaining optical properties while enhancing oxygen permeability within hydrogels to improve patient comfort, and encapsulation of islets for the treatment of type 1 diabetes focuses on creating small, yet immuno-isolative, hydrogel capsules which can protect islets from the host and maintain functionality and viability. In addition, the application of oxygen gradients in the maintenance of stem cell lines as well as promotion of differentiation has led to improved culture conditions and expansion procedures. This section highlights specific advancements in key clinical areas with respect to optimizing device performance through mediating oxygen supply.

Contact Lenses

Contact lens materials must have the required optical properties, chemical stability, reasonable production costs, wettability, resistance to deposits from tear film, and

high oxygen transmissibility (OT). High OT is necessary to meet the metabolic requirements of the cornea [171]. OT is based on diffusivity, D_{eff,O_2} (cm^2/s), Henry's solubility coefficient, k ($\text{cm}^3[O_2\ \text{STP}])/(\text{cm}^3(\text{polymer})\text{mmHg})$, and average lens thickness, L, as shown in (3.24) [172]. The numerator of (3.24), $D_{\text{eff},O_2}k$, is also known as the oxygen permeability coefficient, P [171].

$$\text{OT} = \frac{D_{\text{eff},O_2}k}{L} = \frac{P}{L}. \tag{3.24}$$

Many contact lens formulations have been developed to maximize oxygen permeability based on the use of polysiloxanes. Soft hydrogel contact lenses were originally made of single phase hydrogels, with the goal of creating a lens which provides more comfort, when compared with traditional rigid lenses [173, 174]. Contact lenses made with high water content have relatively high OT compared with dryer lenses or rigid contacts, but they have a tendency to dry out the eye [174]. The introduction of two phase hydrogels (e.g., lotrafilcon) composed of a hydrophobic siloxane phase dispersed within a standard hydrophilic hydrogel [e.g., PEG, *N*,*N*-dimethylacrylamide (DMA), poly(2-hydroxyethyl methacrylate) (PHEMA)] showed enhanced OT compared with the standard hydrogel alone [175, 176], by further increasing the oxygen permeability of the hydrogel in the siloxane regions, due to increased solubility of oxygen in the dispersed phase [175, 177, 178] .

The development of fluorine-containing, rigid, gas-permeable (RGP) contact lenses exposed the promise of fluoro-derivatives (e.g., fluorinated siloxanes) for increasing oxygen permeability in biomaterials [171]. Advancements in contact lens design over the past 50 years show the promise for clinical realization of enhanced oxygen supply through biomaterials for use both in vitro and in vivo. Contact lens formulation does not suffer from significant diffusion limitations because of the thin film design. Use of fluoro-derivatives in tissue engineering devices is more complicated because of the increased diffusion limitations, and therefore research advancements have been more challenging.

Islets of Langerhans and the Treatment of Diabetes

In an effort to eliminate the necessity for life-long treatment with immunosuppressants and improve the quality of life for diabetic patients, researchers have explored the idea of transplantation with islets enclosed in a semipermeable membrane (i.e., bioartificial pancreas) [65]. Various types of bioartificial pancreases have been proposed, and islet microencapsulation has been studied as a possible superior islet transplantation therapy for patients with type 1 diabetes (T1D) [179]. Encapsulation technology offers the possibility of providing feedback-controlled insulin delivery and normoglycemia without continuous patient intervention. Encapsulation also allows for the use of cells or tissue of non-human origin (i.e., xenografts), which may increase the amount of available donor tissue [68]. However, many parameters

and procedures still need to be optimized in order for islet encapsulation to reach full clinical realization [61, 179–187], namely the ability to maintain viability and functionality by reducing hypoxia and hypoxia-related apoptosis.

Hypoxia is a major factor affecting the use of islet encapsulation as a treatment for T1D [188–190]. When islets are isolated from the pancreas, the vascular network supplying the tissue with oxygen is destroyed. The necessity of immunoisolation for adequate treatment [191] requires microcapsules to protect islets from the host immune system, including macrophages and cytokines. Recruitment of endothelial cells for angiogenesis or revascularization of the material may be detrimental to graft survival or cause rejection. Therefore, encapsulated islets, both in vitro and in vivo, suffer from chronic hypoxia [188, 189].

After isolation, contact with the pancreatic capillary system disappears and islets must rely on diffusion into and out of the surrounding medium or matrix for all oxygen and nutrient supply as well as metabolic waste removal. In encapsulation systems, diffusion is even more limited by the semipermeable nature of the matrix. In addition, most islet-containing capsules are implanted in the peritoneal cavity, where partial oxygen tension is reduced compared with that of arterial blood [188]. These constraints, especially the hypoxic conditions, often put islets in a position where they are unable to function and survive for extended periods of time [192]. Hypoxia reduces islet viability and functionality, and unlike in other cell types, such as hepatocytes or endothelial cells, hypoxic conditions do not induce proliferation and growth [189].

Islet preservation post-explantation is a contributing factor to islet survival. If tissues cannot be adequately maintained prior to implantation, the transplanted islets have no chance of survival. Addition of PFCs [78, 140, 144, 193, 194], induction of angiogenesis [195–198], and hyperbaric oxygen chambers [199] have been studied as possible tools for preserving islets and maintaining their functionality in vitro (prior to transplantation) and in vivo (after transplantation). Typically, no more than two-thirds of the islets transplanted are functional within the patient [200], possibly due to trauma experienced during explantation and storage prior to transplantation [194]. Disruption of the blood supply, and therefore oxygen supply, alter the secretory functions (i.e., insulin) of the β-cells which ultimately reduces their functionality in vitro and in vivo [192, 194]. The use of perfluorooctyl bromide (PFOB) dispersed in egg yolk phospholipid and added to cell culture medium preserved islet viability and functionality in culture [194].

Encapsulated islets respond to hypoxia through the upregulation of MCP-1 mRNA expression [189], which promotes angiogenesis [201]. This response may actually contribute to graft rejection, since it is essential for graft tissue to remain immuno-isolated from the host blood stream [202]. The use of a prevascularized implantation device or scaffold may reduce the chemotactic response by the host immune system caused by the upregulation of MCP-1 and reduce the attraction of macrophages to the graft site [189, 203].

One method for increasing the supply of β-cells available for transplantation focuses on differentiating β-cells from pancreatic endocrine tissue. Higher levels of β-cell differentiation were achieved by growing β-cell progenitors on a novel PFC/

silicone membrane which provided greater oxygen concentrations to the differentiating cells in vitro [141]. Results point to the importance of providing the necessary physiological environment as well as providing the appropriate molecular environment to promote differentiation [141]. Enhancing oxygen transport in vitro may allow for better control over the microenvironment around progenitor cells, improving the success of directed stem cell differentiation, and improving the clinical feasibility of islet encapsulation and subsequent transplantation as a treatment for T1D [17].

Wound Healing

Modulating the pO_2 at the site of a wound is critical for all stages of disease prevention, detection, and treatment to improve patient prognosis [204, 205]. Optimizing the local concentration of oxygen can prevent amputation, decrease healing time and reduce the risk of infection in postoperative patients [206]. Overall success of tissue engineering devices and tissue grafts (e.g., encapsulated islets and artificial cartilage) is directly dependent on the ability of the patient to heal without infection or complication postoperation.

Extreme hypoxic or near-anoxic conditions are commonly found in chronic ischemic wounds and prevent adequate tissue repair and/or wound healing. Ischemia, or restricted blood flow in chronic wounds, is often induced by vascular complications and lack of perfusion, and results in decreased nutrient flow and ultimately low-oxygenated tissue. Wounded ischemic tissue suffers from longer healing times and a higher risk of infection and wound-associated pain [204, 207]. In a wound, hypoxia is caused by poor circulation and vascular transport, increased demand for oxygen by the healing tissue, and the generation of ROS as shown in Fig. 3.2 [204, 205]. In a chronic wound, areas of extreme hypoxia often contain many pro-angiogenic factors such as VEGF, yet functional vasculature will not form due to insufficient levels of oxygen and nutrients necessary to promote proper healing and growth of new tissue [208].

Tissue oxygenation and wound therapy are common treatments for chronic wounds, such leg ulcers caused by complications with type 2 diabetes (T2D) or peripheral vascular disease (PVD). Diabetic ulcers heal slowly, and often incompletely, due to underlying physiological conditions, such as T2D-induced neuropathy [209–211]. T2D is the leading cause for non-traumatic lower-limb amputation and in 2006, over 65,700 non-traumatic lower-limb amputations were performed due to poor healing of chronic wounds [212]. Peripheral arterial disease (PAD) is the most prevalent form of PVD and it is estimated that over eight million Americans are affected [204, 213]. Comprehensive wound care improves patient prognosis and reduces the number of amputated limbs and includes increasing arterial oxygen tension, managing fluids, maintaining proper temperature, minimizing pain, creating a sterile environment, and preventing infection through antibiotics [214, 215].

Current oxygenation methods focus on two routes of oxygen delivery: through oxygenated blood using hyperbaric oxygen (HBO) treatment or through topical application. HBO is not a successful treatment method for all patients and distinct treatment regiments and patient-specific dosing strategies need to be employed to obtain the greatest success rates [204]. Often lower-limb wounds are not affected by HBO treatment due to poor circulation in the patients, and therefore a better method for delivering oxygen to the wound bed is desired [204, 205, 216]. Topical oxygen treatments represent a relatively new field and include applying either oxygen gas [216–218] or PFC emulsion to the wound surface [219]. The use of a topical oxygen emulsion significantly enhanced the rate of epithelialization in a partial thickness wound and a second degree burn model in pigs [219]. The incorporation of a saturated PFC emulsion into a hydrogel may provide an adequate method for topically delivering oxygen while providing wound debridement and fluid management using a novel PFC composite wound dressing and these concepts are ongoing investigations in our laboratory [1, 72, 84].

Stem Cell Self-Renewal and Differentiation

Oxygen plays a critical role in the determination of stem cell fate. In mouse embryogenesis, the role of oxygen has been elucidated using genetic manipulation of the HIF family of proteins. Knock-out mice have shown that the loss of HIF-1β/ARNT and/or HIF-1α or HIF-2α expression hinders the proper development of organs and vasculature architecture within the developing mouse, leading to fatal consequences. As previously discussed, upregulation of HIF downstream products can affect cell growth and function (i.e., VEGF, FGF2, TGF-β, and PDGF-β lead to angiogenesis). Understanding the connection between hypoxia and gene expression in stem cells could lead to greater success in the development of stem cell-based therapies.

Thus far, the majority of research has focused on delivery of growth factors or other signaling molecules to stem cells in culture or determining the appropriate structure and matrix properties (e.g., stiffness, ECM composition, and peptide presentation) that are ideal for either maintenance of stemness (i.e., ability to differentiate into all three germ layers: ectoderm, mesoderm, and endoderm) or promotion of differentiation (reviewed elsewhere [98, 220–222]). The stem cell niche is composed of tissue and ECM, which provides molecular and physiological cues as well as the appropriate atmosphere to maintain stemness and regulate stem cell behavior [220, 221].

Recently, variations in oxygen tension have been shown to affect the maintenance of stemness or initiation of differentiation in both embryonic and adult stem cell lineages [36, 221, 223–230]. Results reviewed or presented in these studies suggest that oxygen tension plays key roles in stem cell behavior in vivo and therefore careful experimentation in vitro may suggest strategies to apply in tissue engineering and drug discovery applications. This section discusses the role of

oxygen in the maintenance of stemness as well as the role of matrix properties and oxygen concentrations in the differentiation of both adult and embryonic stem cells.

Role of HIF and Gene Expression in the Maintenance of Stemness

The belief that ambient air supplemented with CO_2 (20% O_2, 5% CO_2) is adequate for in vitro stem cell growth and renewal has recently been refuted by evidence that many stem cells exist in the body at much lower oxygen concentrations [221, 231–234]. For example, hematopoietic stem cells (HSCs) exist within the most hypoxic niches of the bone marrow, while proliferating progenitor cells exist at higher oxygen tensions [231, 234], while fully differentiated cells often exist in the areas of highest oxygen concentrations [221, 223, 225, 231, 235–237]. The discovery and creation of induced pluripotent stem cells (i.e., cells with the ability to differentiate into most primary cell types) from adult human fibroblasts (iPSCs) [238, 239] was the first study using human cells to definitively confirm the important role of oxygen tension in the maintenance of stemness, confirming previous results found in mice [36, 240–244]. Together, extensive results in both human and murine stem cells suggest a connection between hypoxia-induced mechanisms driven by HIF signaling and changes in gene expression [10, 227, 244].

iPSCs are formed from cells (e.g., fibroblasts), which are dedifferentiated into cells that have stemcell-like qualities, such as pluripotency and the appropriate gene expression profile (e.g., Oct4, Sox2, Nanog, and no differentiation markers). iPSCs were first created from murine adult fibroblasts by retrovirally transforming four transcription factors: Oct4, Sox2, c-Myc, and Klf4 [245]. The role of hypoxia in the differentiation or maintenance of stemness is not completely clear, but recent work suggests the role of HIF-mediated gene expression in stem cell differentiation or self-renewal. For example, HIF-2α activation has been shown to upregulate the Oct4 gene in murine ESCs [40], and loss of Oct4 expression causes differentiation in both mouse and human ESCs [243, 246, 247], suggesting a potential pathway for stem cell response to hypoxia through a HIF-2α-mediated response [221, 247]. Furthermore, results indicate that other genes associated with stemness, which provide the basic proteins necessary for survival and reproduction, such as Oct4 [40], Wnt [38], and Hh [39], are regulated by oxygen availability. Wnt signaling can be mediated by HIF-1 transcriptional activity in the maintenance of self-renewal in both adult and embryonic stem cells (reviewed elsewhere [38]). Hypoxia may also mediate the expression of Hh proteins through HIF-1α stabilization in mouse ischemic tissue models [39]. Combined, these results indicate the importance of oxygen and gene regulation in stem cell self-renewal.

Another important pathway involved in determining stem cell fate, Notch signaling, has recently been shown to be regulated by the presence of oxygen. Notch allows for cell–cell communication through expression of Notch receptors and Notch ligands, and members of this protein family inhibit progenitor cell differentiation [227, 248–251]. Oxygen can mediate Notch signaling through the interaction of the transactivation domain of HIF-1α with the Notch intracellular

domain. Definitive proof of the interaction between oxygen tension and Notch activation confirmed the critical importance of the Notch signaling pathway and its regulation by oxygen tension in the maintenance of self-renewable and undifferentiated populations of progenitor cells [248, 252]. Further investigation of HIF-1 and Notch signaling cascades in mouse ESCs identified genes which were coregulated by the upregulation of these two pathways [250]; further investigation of the role of these two pathways is necessary to determine the transcriptional level of interaction and the complete role of HIF-1-mediated Notch signaling in controlling stem cell fate.

The Roles of Tissue Engineering Scaffolds in Determining Stem Cell Fate

One of the major hurdles for the use of stem cells in tissue engineering constructs and disease models is the culture and maintenance of large quantities of stem cells and differentiated tissue [235, 253–256], such as in the case of islet encapsulation for the treatment of T1D [141, 257]. In the field of tissue engineering, it is well known that the mechanical properties of a 3-D scaffold can influence stem cell fate [222, 224, 258] and decrease the need for a feeder cell layer [typically mouse embryonic fibroblasts (MEFs)] [255, 259]; therefore growth and differentiation of stem cells in hydrogels and tissue engineering scaffolds have become major areas of exploration [260–264].

Differentiating between the effects of variations in structural, mechanical, and physiological properties of 3-D culture can be difficult. Initial studies with 3-D culture suggested a connection between oxygen concentration and stem cell fate, but direct evidence was only recently discovered [224, 227, 265]. For example, culture of human ESCs in a perfused bioreactor resulted in stem cell expansion at 30% air saturation [266], and also initiated differentiation at 4% oxygen tension [91] through control of dissolved oxygen concentration.

The osteogenic potential of PFC-enriched hydrogels using a well-studied bone marrow-derived MSC line (Tet-off BMP2 MSCs) [81] showed that the addition of 10% perfluorotributylamine (PFTBA, a PFC) to a fibrin hydrogel seeded with MSCs and implanted subcutaneously in mice resulted in robust bone formation, increased cell viability, and increased expression of osteocalcin when compared with the control [81]. However, only bone quantity and not bone quality, as determined by bone density analysis, was significantly improved by PFC addition [81]. During normal bone formation, cartilaginous tissue is formed first, becomes hypertrophic, and finally is replaced by bone tissue. More cartilage tissue after a given time point is expected in samples where bone tissue is faster developing. However, after 1 week, no significant difference in vessel formation or sulfated glycosaminoglycan production, indicative of a cartilage phenotype, was detected, suggesting that the mechanism for improving cell viability and bone formation may not be due to enhanced osteogenic potential for this subcutaneous model. Hence, the method of action for PFTBA addition in this subcutaneous model is unclear [81]. In a murine posterior spinal fusion model, improved bone quality

was achieved through significant increases in trabecular thickness and bone density in samples with 10% PFTBA incorporation after both 2 and 3 weeks in vivo [81]. After 6 weeks post-implantation, bone volume was significantly higher with 10% PFTBA addition [81]. In a separate experiment using 10% PFTBA with Tet-off BMP2 MSCs, results suggest that the presence of PFCs in a stem cell-seeded fibrin hydrogel achieves higher bone quality faster, and addition of PFCs also has long-term effects on bone volume produced from differentiated stem cells [81].

In another study, a collagen scaffold containing porous silk tubes was used to create a perfusion system to enhance oxygen transport by minimizing nutrient and mass transfer limitations throughout the scaffold [267]. By varying the oxygen tension within the reactor (5 and 20%), improved human MSC differentiation was observed for both chondrogenic and adipogenic cell lineages [267].

Stem cells can be readily isolated and expanded, therefore their use in cell-based therapies has become a major topic of investigation. Eventually, tighter control over the physiological culture environment in vitro may lead to directed differentiation of both adult and embryonic stem cells by simply varying the oxygen tension in a given scaffold [141]. Tissue engineering constructs are capable of providing very low oxygen tensions while maintaining adequate nutrient diffusion and matrix properties, and therefore current scaffold design may allow for maintenance of undifferentiated stem cells in vitro. In addition, culture in biomaterials may promote expansion or differentiation by providing the appropriate mechanical and physiological environments.

Cartilage Tissue Engineering

Engineering of cartilage tissue requires the creation of non-vascularized constructs with high cell densities for implantation for the repair of defects in joints, treatment of osteoarthritis, repair of cosmetic defects, and use in reconstructive surgery following a traumatic event (i.e., causalities of war and automobile accidents) [97, 268–270]. Nutrient and gaseous transport are limited in large, high cell-density constructs and therefore device failure is often attributed to the oxygen-sensitive nature of the chondrocyte phenotype and oxygen gradients within a device [12, 224, 271–273].

Cartilage tissue is avascular and composed of chondrocytes and progenitor cells surrounded by ECM, which predominantly consists of type II collagen and proteoglycans [274]. Tissue engineering and cell culture of chondrocytes requires a 3-D environment to prevent dedifferentiation into a fibroblast-like phenotype [275]. Unlike most tissues, cartilage is avascular and therefore receives nutrients and oxygen by passive diffusion from the synovial fluid [268, 271]. Oxygen tension in avascular cartilage ranges from 1 to 7%, and adaptation to this environment is influenced by HIF [28]. HIF-1α mediates growth arrest and chondrocyte survival, while HIF-2α is necessary for the maintenance of the human

articular chondrocyte phenotype as shown by increased expression of genes indicative of cartilage formation (i.e., SOX9, COL2A1, Aggrecan) [28, 276]. In vitro maintenance of ECM and regulation of growth, functionality, and differentiation of chondrogenic cells are mediated by low oxygen tension or hypoxia; chondrocytes have even been shown to dedifferentiate when in normoxic (i.e., 21% O_2) conditions [277, 278]. Consequently, low oxygen tensions are required for preservation of the chondrocyte phenotype [272] and prevention of cell swelling and bone formation [279]. However, the temporal strategies (i.e., altering the time exposed to hypoxia) employed to enhance chondrogenesis can lead to various results. Prolonged low oxygen tension in vitro has been shown to impair differentiation of murine adipose-derived adult stromal cells (ADASs) down the chondrogenic pathway [280], and low oxygen tensions (5%) were shown to enhance osteogenesis of human MSCs on silk scaffolds [264]. Enhanced differentiation into a chondrogenic phenotype was seen for ovine MSCs on a type I collagen surface [281] and for human dermal fibroblasts grown in a demineralized bone matrix [282] cultured at 5% O_2, while at 2% O_2, ADASs showed enhanced early chondrogenesis [273]. These variations in results indicate that temporal changes in the concentration of soluble factors [283] and in oxygen tension greatly affect the quality of tissue formed from stem or progenitor cells.

Hyperoxia, or chronically high oxygen tension, is not typically considered in the design of tissue engineering constructs because oxygen tensions do not reach sustained levels, which are high enough to warrant concern. However, for chondrocytes, hyperoxia can affect metabolism and viability [268], or even cause dedifferentiation into a more fibroblast-like phenotype [277, 278]. Autologous chondrocyte implantation may expose cells to hyperoxic shock [284], which can be caused by the generation of free radicals or reactive oxygen species (ROS) [268]. In the same way that hypoxia will induce apoptosis, increased levels of ROS will cause damage to DNA, lipids, and proteins, resulting in cell death [54, 285]. In cartilage tissue, free radicals degrade type II collagen and proteoglycans, alter metabolism, and destabilize DNA [54]. ROS also play a key role in intracellular signaling [54], which can lead to upregulation of the JNK pathway, leading to apoptosis, as shown in Fig. 3.2. The role of antioxidants in preventing JNK-related transcriptional activity for joint therapy is still under investigation [54]. While tissue-engineered constructs do not often suffer from hyperoxia, understanding the cellular oxygen limits of various tissue types can suggest superior strategies for improving the success of a device.

Conclusions

Oxygen status significantly influences cellular behavior through mechanisms which promote both cell proliferation and apoptosis. Understanding the delicate balance between pro- and anti-apoptotic signals will enhance the knowledge needed for successful design and creation of tissue engineering constructs. Reducing apoptotic

cues while promoting angiogenesis will ultimately lead to better device incorporation in vivo and enhanced tissue survival rates. Modulating hypoxia within tissue engineering constructs is necessary to create a device with optimal functionality. Recognizing the interconnected cellular mechanisms by which hypoxia is mediated can enhance device design and ultimate device success. Research goals have not changed considerably over the past 20 years, but the pathway to successful tissue engineering device design has significantly evolved. Improving cell growth and viability for extended periods of time still remains the ultimate goal and investigators have come to realize the importance of fundamental biology. Better understanding of the intracellular response (e.g., up- or downregulation of gene expression, pathway manipulation, signaling cascades, etc.) to a given external stimuli (i.e., matrix stiffness, oxygen tension, adhesive forces, and ECM composition) will ultimately lead to improved device performance.

Acknowledgments W.L.S. acknowledges support from a National Research Service Award T32 GM08515 from the National Institutes of Health. The authors would also like to acknowledge Joseph C. White for assistance in figure design and creation.

References

1. Khattak, S.F., Chin, K.S., Bhatia, S.R., Roberts, S.C.: Enhancing oxygen tension and cellular function in alginate cell encapsulation devices through the use of perfluorocarbons. Biotechnol. Bioeng. **96**(1), 156–166 (2007)
2. Arifin, D.R., Palmer, A.F.: Polymersome encapsulated hemoglobin: a novel type of oxygen carrier. Biomacromolecules **6**(4), 2172–2181 (2005)
3. Harrison, B.S., Eberli, D., Lee, S.J., Atala, A., Yoo, J.J.: Oxygen producing biomaterials for tissue regeneration. Biomaterials **28**(31), 4628–4634 (2007)
4. Oh, S.H., Ward, C.L., Atala, A., Yoo, J.J., Harrison, B.S.: Oxygen generating scaffolds for enhancing engineered tissue survival. Biomaterials **30**(5), 757–762 (2009)
5. Laschke, M.W., Harder, Y., Amon, M., Martin, I., Farhadi, J., Ring, A., et al.: Angiogenesis in tissue engineering: Breathing life into constructed tissue substitutes. Tissue Eng. **12**(8), 2093–2104 (2006)
6. Santos, M.I., Reis, R.L.: Vascularization in bone tissue engineering: physiology, current strategies, major hurdles and future challenges. Macromol. Biosci. **10**(1), 12–27 (2010)
7. Semenza, G.L.: Regulation of mamalian O_2 homeostasis by hypoxia-inducible factor 1. Annu. Rev. Cell Dev. Biol. **15**(1), 551–578 (1999)
8. Jiang, B.H., Semenza, G.L., Bauer, C., Marti, H.H.: Hypoxia-inducible factor 1 levels vary exponentially over a physiologically relevant range of O_2 tension. AJP - Cell Physiol. **271**(4), C1172–C1180 (1996)
9. Iyer, N.V., Kotch, L.E., Agani, F., Leung, S.W., Laughner, E., Wenger, R.H., et al.: Cellular and developmental control of O_2 homeostasis by hypoxia-inducible factor 1α. Genes Dev. **12**(2), 149–162 (1998)
10. Wang, G.L., Semenza, G.L.: General involvement of hypoxia-inducible factor 1 in transcriptional response to hypoxia. Proc. Natl. Acad. Sci. USA **90**(9), 4304–4308 (1993)
11. Reynolds, T.Y., Rockwell, S., Glazer, P.M.: Genetic instability induced by the tumor microenvironment. Cancer Res. **56**(24), 5754–5757 (1996)

12. Malda, J., Rouwkema, J., Martens, D.E., le Comte, E.P., Kooy, F.K., Tramper, J., et al.: Oxygen gradients in tissue-engineered PEGT/PBT cartilaginous constructs: Measurement and modeling. Biotechnol. Bioeng. **86**(1), 9–18 (2004)
13. Radisic, M., Malda, J., Epping, E., Geng, W., Langer, R., Vunjak-Novakovic, G.: Oxygen gradients correlate with cell density and cell viability in engineered cardiac tissue. Biotechnol. Bioeng. **93**(2), 332–343 (2006)
14. Malda, J., Klein, T.J., Upton, Z.: The roles of hypoxia in the in vitro engineering of tissues. Tissue Eng. **13**(9), 2153–2162 (2007)
15. Kellner, K., Liebsch, G., Klimant, I., Wolfbeis, O.S., Blunk, T., Schulz, M.B., et al.: Determination of oxygen gradients in engineered tissue using a fluorescent sensor. Biotechnol. Bioeng. **80**(1), 73–83 (2002)
16. Galban, C.J., Locke, B.R.: Effects of spatial variation of cells and nutrient and product concentrations coupled with product inhibition on cell growth in a polymer scaffold. Biotechnol. Bioeng. **64**(6), 633–643 (1999)
17. Johnson, A.S., Fisher, R.J., Weir, G.C., Colton, C.K.: Oxygen consumption and diffusion in assemblages of respiring spheres: Performance enhancement of a bioartificial pancreas. Chem. Eng. Sci. **64**(22), 4470–4487 (2009)
18. Croll, T.I., Gentz, S., Mueller, K., Davidson, M., O'Connor, A.J., Stevens, G.W., et al.: Modelling oxygen diffusion and cell growth in a porous, vascularising scaffold for soft tissue engineering applications. Chem. Eng. Sci. **60**(17), 4924–4934 (2005)
19. Landman, K., Cai, A.: Cell proliferation and oxygen diffusion in a vascularising scaffold. Bull. Math. Biol. **69**(7), 2405–2428 (2007)
20. Griffith, L.G., Naughton, G.: Tissue engineering – Current challenges and expanding opportunities. Science **295**(5557), 1009–1014 (2002)
21. Taylor, C., Pouyssegur, J.: Oxygen, hypoxia, and stress. Ann. N. Y. Acad. Sci. **1113**(1), 87–94 (2007)
22. Semenza, G.L.: Targeting HIF-1 for cancer therapy. Nat. Rev. Cancer **3**(10), 721–732 (2003)
23. Greijer, A., Van der Wall, E.: The role of hypoxia inducible factor 1 (HIF-1) in hypoxia induced apoptosis. J. Clin. Pathol. **57**(10), 1009–1014 (2004)
24. Bunn, H.F., Poyton, R.O.: Oxygen sensing and molecular adaptation to hypoxia. Physiol. Rev. **76**(3), 839–885 (1996)
25. Huang, L.E., Gu, J., Schau, M., Bunn, H.F.: Regulation of hypoxia-inducible factor 1α is mediated by an O_2-dependent degradation domain via the ubiquitin–proteasome pathway. Proc. Natl Acad. Sci. USA **95**(14), 7987–7992 (1998)
26. Krieg, M., Haas, R., Brauch, H., Acker, T., Flamme, I., Plate, K.: Up-regulation of hypoxia-inducible factors HIF-1 and HIF-2 under normoxic conditions in renal carcinoma cells by von Hippel-Lindau tumor suppressor gene loss of function. Oncogene **19**(48), 5435–5443 (2000)
27. Bruick, R.K., McKnight, S.L.: A conserved family of prolyl-4-hydroxylases that modify HIF. Science **294**(5545), 1337–1340 (2001)
28. Schipani, E., Ryan, H.E., Didrickson, S., Kobayashi, T., Knight, M., Johnson, R.S.: Hypoxia in cartilage: HIF-1α is essential for chondrocyte growth arrest and survival. Genes Dev. **15**(21), 2865–2876 (2001)
29. Guillemin, K., Krasnow, M.A.: The hypoxic response: Huffing and HIFing. Cell **89**(1), 9–12 (1997)
30. Raval, R.R., Lau, K.W., Tran, M.G.B., Sowter, H.M., Mandriota, S.J., Li, J.-L., et al.: Contrasting properties of hypoxia-inducible factor 1 (HIF-1) and HIF-2 in von Hippel-Lindau-associated renal cell carcinoma. Mol. Cell. Biol. **25**(13), 5675–5686 (2005)
31. Carmeliet, P., Dor, Y., Herbert, J.-M., Fukumura, D., Brusselmans, K., Dewerchin, M., et al.: Role of HIF-1α in hypoxia-mediated apoptosis, cell proliferation and tumour angiogenesis. Nature **394**(6692), 485–490 (1998)
32. Moritz, W., Meier, F., Stroka, D., Giuliani, M., Kugelmeier, P., Nett, P.C., et al.: Apoptosis in hypoxic human pancreatic islets correlates with HIF-1α expression. FASEB J. **16**, 745–747 (2002). doi:01-0403fje

33. Chen, J., Zhao, S., Nakada, K., Kuge, Y., Tamaki, N., Okada, F., et al.: Dominant-negative hypoxia-inducible factor-1α reduces tumorigenicity of pancreatic cancer cells through the suppression of glucose metabolism. Am. J. Pathol. **162**(4), 1283–1291 (2003)
34. Kvietikova, I., Wenger, R.H., Marti, H.H., Gassmann, M.: The transcription factors ATF-1 and CREB-1 bind constitutively to the hypoxia-inducible factor-1 (HIF-1) DNA recognition site. Nucleic Acids Res. **23**(22), 4542–4550 (1995)
35. Wang, G.L., Semenza, G.L.: Characterization of hypoxia-inducible factor 1 and regulation of DNA binding activity by hypoxia. J. Biol. Chem. **268**(29), 21513–21518 (1993)
36. Gassmann, M., Fandrey, J., Bichet, S., Wartenberg, M., Marti, H.H., Bauer, C., et al.: Oxygen supply and oxygen-dependent gene expression in differentiating embryonic stem cells. Proc. Natl Acad. Sci. USA **93**(7), 2867–2872 (1996)
37. Lim, J.-H., Chun, Y.-S., Park, J.-W.: Hypoxia-inducible factor-1α obstructs a Wnt signaling pathway by inhibiting the hARD1-mediated activation of β-catenin. Cancer Res. **68**(13), 5177–5184 (2008)
38. Kaufman, D.S.: HIF hits Wnt in the stem cell niche. Nat. Cell Biol. **12**(10), 926–927 (2010)
39. Bijlsma, M.F., Groot, A.P., Oduro, J.P., Franken, R.J., Schoenmakers, S.H.H.F., Peppelenbosch, M.P., et al.: Hypoxia induces a hedgehog response mediated by HIF-1α. J. Cell. Mol. Med. **13**(8(b)), 2053–2060 (2009)
40. Covello, K.L., Kehler, J., Yu, H., Gordan, J.D., Arsham, A.M., Hu, C.-J., et al.: HIF-2α regulates Oct-4: effects of hypoxia on stem cell function, embryonic development, and tumor growth. Genes Dev. **20**(5), 557–570 (2006)
41. Chen, R., Silva, E., Yuen, W., Mooney, D.: Spatio-temporal VEGF and PDGF delivery patterns blood vessel formation and maturation. Pharm. Res. **24**(2), 258–264 (2007)
42. Pugh, C., Ratcliffe, P.: Regulation of angiogenesis by hypoxia: role of the HIF system. Nat. Med. **9**(6), 677–684 (2003)
43. Lee, K., Mooney, D.: Hydrogels for tissue engineering. Chem. Rev. **101**(7), 1869–1880 (2001)
44. Ennett, A.B., Mooney, D.J.: Tissue engineering strategies for in vivo neovascularisation. Expert Opin. Biol. Ther. **2**(8), 805–818 (2002)
45. Mieszawska, A., Kaplan, D.: Smart biomaterials – regulating cell behavior through signaling molecules. BMC Biol. **8**(1), 59 (2010)
46. Halterman, M.W., Miller, C.C., Federoff, H.J.: Hypoxia-inducible factor-1α mediates hypoxia-induced delayed neuronal death that involves p53. J. Neurosci. **19**(16), 6818–6824 (1999)
47. Kothari, S., Cizeau, J., McMillan-Ward, E., Israels, S.J., Bailes, M., Ens, K., et al.: BNIP3 plays a role in hypoxic cell death in human epithelial cells that is inhibited by growth factors EGF and IGF. Oncogene **22**(30), 4734–4744 (2000)
48. Young, S.D., Marshall, R.S., Hill, R.P.: Hypoxia induces DNA overreplication and enhances metastatic potential of murine tumor cells. Proc. Natl Acad. Sci. USA **85**(24), 9533–9537 (1988)
49. Coquelle, A., Toledo, F., Stern, S., Bieth, A., Debatisse, M.: A new role for hypoxia in tumor progression: induction of fragile site triggering genomic rearrangements and formation of complex DMs and HSRs. Mol. Cell **2**(2), 259–265 (1998)
50. Bencokova, Z., Kaufmann, M.R., Pires, I.M., Lecane, P.S., Giaccia, A.J., Hammond, E.M.: ATM activation and signaling under hypoxic conditions. Mol. Cell. Biol. **29**(2), 526–537 (2009)
51. Zhu, W., Chen, J., Cong, X., Hu, S., Chen, X.: Hypoxia and serum deprivation-induced apoptosis in mesenchymal stem cells. Stem Cells **24**(2), 416–425 (2006)
52. Saikumar, P., Dong, Z., Patel, Y., Hall, K., Hopfer, U., Weinberg, J., et al.: Role of hypoxia-induced Bax translocation and cytochrome c release in reoxygenation injury. Oncogene **17**(26), 3401–3415 (1998)
53. Boutilier, R.G., St-Pierre, J.: Surviving hypoxia without really dying. Comp. Biochem. Physiol. A Mol. Integr. Physiol. **126**(4), 481–490 (2000)

54. Henrotin, Y.E., Bruckner, P., Pujol, J.P.L.: The role of reactive oxygen species in homeostasis and degradation of cartilage. Osteoarthritis Cartilage **11**(10), 747–755 (2003)
55. Kim, J.-Y., Park, J.-H.: ROS-dependent caspase-9 activation in hypoxic cell death. FEBS Lett. **549**(1–3), 94–98 (2003)
56. Kunz, M., Ibrahim, S., Koczan, D., Thiesen, H., Köhler, H., Acker, T., et al.: Activation of c-Jun NH2-terminal kinase/stress-activated protein kinase (JNK/SAPK) is critical for hypoxia-induced apoptosis of human malignant melanoma. Cell Growth Differ. **12**(3), 137–145 (2001)
57. Tibbles, L.A., Woodgett, J.R.: The stress-activated protein kinase pathways. Cell. Mol. Life Sci. **55**(10), 1230–1254 (1999)
58. Lovett, M., Lee, K., Edwards, A., Kaplan, D.: Vascularization strategies for tissue engineering. Tissue Eng. Part B Rev. **15**(3), 353–370 (2009)
59. Goosen, M.F.A.: Fundamentals of Animal Cell Encapsulation and Immobilization. CRC, Boca Raton (1993)
60. Poncelet, D., Bugarski, B., Amsden, B.G., Zhu, J., Neufeld, R., Goosen, M.F.A.: A parallel-plate electrostatic droplet generator – parameters affecting microbead size. Appl. Microbiol. Biotechnol. **42**(2–3), 251–255 (1994)
61. Strand, B.L., Gaserod, O., Kulseng, B., Espevik, T., Skjak-Braek, G.: Alginate-polylysine-alginate microcapsules: effect of size reduction on capsule properties. J. Microencapsul. **19**(5), 615–630 (2002)
62. Klokk, T.I., Melvik, J.E.: Controlling the size of alginate gel beads by use of a high electrostatic potential. J. Microencapsul. **19**(4), 415–424 (2002)
63. Sakai, S., Hashimoto, I., Kawakami, K.: Development of alginate-agarose subsieve-size capsules for subsequent modification with a polyelectrolyte complex membrane. Biochem. Eng. J. **30**(1), 76–81 (2006)
64. Agrawal, C.M., Ray, R.B.: Biodegradable polymeric scaffolds for musculoskeletal tissue engineering. J. Biomed. Mater. Res. **55**(2), 141–150 (2001)
65. Lim, F., Sun, A.M.: Microencapsulated islets as bioartificial endocrine pancreas. Science **210**(4472), 908–910 (1980)
66. Fu, X.W., Sun, A.M.: Microencapsulated parathyroid cells as a bioartificial parathyroid-in vivo studies. Transplantation **47**(3), 432–435 (1989)
67. Cieslinski, D.A., Humes, H.D.: Tissue engineering of a bioartificial kidney. Biotechnol. Bioeng. **43**(7), 678–681 (1994)
68. de Vos, P., Bucko, M., Gemeiner, P., Navratil, M., Svitel, J., Faas, M., et al.: Multiscale requirements for bioencapsulation in medicine and biotechnology. Biomaterials **30**(13), 2559–2570 (2009)
69. Hernández, R.M., Orive, G., Murua, A., Pedraz, J.L.: Microcapsules and microcarriers for in situ cell delivery. Adv. Drug Deliv. Rev. **62**(7–8), 711–730 (2010)
70. Hay, P.D., Veitch, A.R., Smith, M.D., Cousins, R.B., Gaylor, J.D.S.: Oxygen transfer in a diffusion-limited hollow fiber bioartificialâ liver. Artif. Organs **24**(4), 278–288 (2000)
71. Yu, P., Zeng, Y., Lee, T.S., Low, H.T.: A numerical analysis of cell density effect on oxygen transport in a micro-bioreactor with a tissue engineering scaffold. Int. Commun. Heat Mass Transfer **36**(6), 569–573 (2009)
72. Chin, K., Khattak, S.F., Bhatia, S.R., Roberts, S.C.: Hydrogel-perfluorocarbon composite scaffold promotes oxygen transport to immobilized cells. Biotechnol. Prog. **24**(2), 358–366 (2008)
73. Valentin, J.E., Freytes, D.O., Grasman, J.M., Pesyna, C., Freund, J., Gilbert, T.W., et al.: Oxygen diffusivity of biologic and synthetic scaffold materials for tissue engineering. J. Biomed. Mater. Res. A **91A**(4), 1010–1017 (2009)
74. Radisic, M., Deen, W., Langer, R., Vunjak-Novakovic, G.: Mathematical model of oxygen distribution in engineered cardiac tissue with parallel channel array perfused with culture medium containing oxygen carriers. Am. J. Physiol. Heart Circ. Physiol. **288**(3), H1278–H1289 (2005)

75. Acosta, M.A., Ymele-Leki, P., Kostov, Y.V., Leach, J.B.: Fluorescent microparticles for sensing cell microenvironment oxygen levels within 3D scaffolds. Biomaterials **30**(17), 3068–3074 (2009)
76. Mishra, A., Starly, B.: Real time in vitro measurement of oxygen uptake rates for HEPG2 liver cells encapsulated in alginate matrices. Microfluid. Nanofluidics **6**(3), 373–381 (2009)
77. Kino-oka, M., Kagita, S., Nadzir, M.M., Inoue, H., Sugawara, K., Taya, M.: Direct measurement of oxygen concentration inside cultured cartilage for relating to spatial growth of rabbit chondrocytes. J. Biosci. Bioeng. **110**(3), 363–366 (2010)
78. Terai, S., Tsujimura, T., Li, S., Hori, Y., Toyama, H., Shinzeki, M., et al.: Effect of oxygenated perfluorocarbon on isolated islets during transportation. J. Surg. Res. **162**(2), 284–289 (2010)
79. Chen, G., Palmer, A.F.: Mixtures of hemoglobin-based oxygen carriers and perfluorocarbons exhibit a synergistic effect in oxygenating hepatic hollow fiber bioreactors. Biotechnol. Bioeng. **105**(3), 534–542 (2010)
80. Brown, D.A., MacLellan, W.R., Laks, H., Dunn, J.C.Y., Wu, B.M., Beygui, R.E.: Analysis of oxygen transport in a diffusion-limited model of engineered heart tissue. Biotechnol. Bioeng. **97**(4), 962–975 (2007)
81. Kimelman-Bleich, N., Pelled, G., Sheyn, D., Kallai, I., Zilberman, Y., Mizrahi, O., et al.: The use of a synthetic oxygen carrier-enriched hydrogel to enhance mesenchymal stem cell-based bone formation in vivo. Biomaterials [Article] **30**(27), 4639–4648 (2009)
82. Lowe, K.C., Davey, M.R., Power, J.B.: Perfluorochemicals: their applications and benefits to cell culture. Trends Biotechnol. **16**(6), 272–277 (1998)
83. Peng, C.C., Kim, J., Chauhan, A.: Extended delivery of hydrophilic drugs from silicone-hydrogel contact lenses containing Vitamin E diffusion barriers. Biomaterials **31**(14), 4032–4047 (2010)
84. Stoppel, W.L., White, J.C., Horava, S.D., Bhatia, S.R., Roberts, S.C.: Transport of biological molecules in surfactant-alginate composite hydrogels. Acta Biomaterialia. In Press, Accepted Manuscript
85. Demol, J., Lambrechts, D., Geris, L., Schrooten, J., Van Oosterwyck, H.: Towards a quantitative understanding of oxygen tension and cell density evolution in fibrin hydrogels. Biomaterials **32**(1), 107–118 (2011)
86. Wood, B.D., Quintard, M., Whitaker, S.: Calculation of effective diffusivities for biofilms and tissues. Biotechnol. Bioeng. **77**(5), 495–516 (2002)
87. Rumsey, W.L., Schlosser, C., Nuutinen, E.M., Robiolio, M., Wilson, D.F.: Cellular energetics and the oxygen dependence of respiration in cardiac myocytes isolated from adult rat. J. Biol. Chem. **265**(26), 15392–15402 (1990)
88. Xiong, Y., Xu, J., Zhu, D-q, Duan, C-f, Guan, Y-f: Fiber-optic fluorescence sensor for dissolved oxygen detection based on fluorinated xerogel immobilized with ruthenium (II) complex. J. Sol-Gel Sci. Technol. **53**(2), 441–447 (2010)
89. Bellucci, J.J., Hamaker, K.H.: Evaluation of oxygen transfer rates in stirred-tank bioreactors for clinical manufacturing. Biotechnol. Prog. **27**(2), 368–376 (2011)
90. Suresh, S., Srivastava, V.C., Mishra, I.M.: Techniques for oxygen transfer measurement in bioreactors: a review. J. Chem. Technol. Biotechnol. **84**(8), 1091–1103 (2009)
91. Niebruegge, S., Bauwens, C.L., Peerani, R., Thavandiran, N., Masse, S., Sevaptisidis, E., et al.: Generation of human embryonic stem cell-derived mesoderm and cardiac cells using size-specified aggregates in an oxygen-controlled bioreactor. Biotechnol. Bioeng. **102**(2), 493–507 (2009)
92. Volkmer, E., Drosse, I., Otto, S., Stangelmayer, A., Stengele, M., Kallukalam, B.C., et al.: Hypoxia in static and dynamic 3D culture systems for tissue engineering of bone. Tissue Eng. Part A **14**(8), 1331–1340 (2008)
93. Janssen, F.W., Oostra, J., Oorschot, Av, van Blitterswijk, C.A.: A perfusion bioreactor system capable of producing clinically relevant volumes of tissue-engineered bone: In vivo bone formation showing proof of concept. Biomaterials **27**(3), 315–323 (2006)

94. Picioreanu, C., van Loosdrecht, M.C.M., Heijnen, J.J.: A new combined differential-discrete cellular automaton approach for biofilm modeling: Application for growth in gel beads. Biotechnol. Bioeng. **57**(6), 718–731 (1998)
95. Shuler, M., Kargi, F.: Bioprocess Engineering. Prentice Hall Upper Saddle River, NJ (2002)
96. Cassell, O.C.S., Morrison, W.A., Messina, A., Penington, A.J., Thompson, E.W., Stevens, G. W., et al.: The influence of extracellular matrix on the generation of vascularized, engineered, transplantable tissue. Ann. N. Y. Acad. Sci. **944**(1), 429–442 (2001)
97. Vunjak-Novakovic, G., Obradovic, B., Martin, I., Bursac, P.M., Langer, R., Freed, L.E.: Dynamic cell seeding of polymer scaffolds for cartilage tissue engineering. Biotechnol. Prog. **14**(2), 193–202 (1998)
98. Discher, D.E., Mooney, D.J., Zandstra, P.W.: Growth factors, matrices, and forces combine and control stem cells. Science **324**(5935), 1673–1677 (2009)
99. Clark, L.C.J.R., Wolf, R., Granger, D., Taylor, Z.: Continuous recording of blood oxygen tensions by polarography. J. Appl. Physiol. **6**(3), 189–193 (1953)
100. Androjna, C., Gatica, J., Belovich, J., Derwin, K.: Oxygen diffusion through natural extracellular matrices: Implications for estimating critical thickness" values in tendon tissue engineering. Tissue Eng. Part A **14**(4), 559–569 (2008)
101. Strickland, J.D.H., Parsons, T.R., Fisheries Research Board of Canada: A Practical Handbook of Seawater Analysis, 2nd edn. Fisheries Research Board of Canada, Ottawa (1972)
102. Koo, Y.-E.L., Cao, Y., Kopelman, R., Koo, S.M., Brasuel, M., Philbert, M.A.: Real-time measurements of dissolved oxygen inside live cells by organically modified silicate fluorescent nanosensors. Anal. Chem. **76**(9), 2498–2505 (2004)
103. Choi, N.W., Cabodi, M., Held, B., Gleghorn, J.P., Bonassar, L.J., Stroock, A.D.: Microfluidic scaffolds for tissue engineering. Nat. Mater. **6**(11), 908–915 (2007)
104. Oppegard, S.C., Blake, A.J., Williams, J.C., Eddington, D.T.: Precise control over the oxygen conditions within the Boyden chamber using a microfabricated insert. Lab Chip **10**(18), 2366–2373 (2010)
105. Ishaug, S.L., Crane, G.M., Miller, M.J., Yasko, A.W., Yaszemski, M.J., Mikos, A.G.: Bone formation by three-dimensional stromal osteoblast culture in biodegradable polymer scaffolds. J. Biomed. Mater. Res. **36**(1), 17–28 (1997)
106. Laurencin, C.T., Attawia, M.A., Elgendy, H.E., Herbert, K.M.: Tissue engineered bone-regeneration using degradable polymers: The formation of mineralized matrices. Bone **19**(1 Suppl), S93–S99 (1996)
107. Burg, K.J.L., Porter, S., Kellam, J.F.: Biomaterial developments for bone tissue engineering. Biomaterials **21**(23), 2347–2359 (2000)
108. Ma, P.X., Zhang, R., Xiao, G., Franceschi, R.: Engineering new bone tissue in vitro on highly porous poly(α-hydroxyl acids)/hydroxyapatite composite scaffolds. J. Biomed. Mater. Res. **54**(2), 284–293 (2001)
109. Pisu, M., Lai, N., Cincotti, A., Concas, A., Cao, G.: Modeling of engineered cartilage growth in rotating bioreactors. Chem. Eng. Sci. **59**(22–23), 5035–5040 (2004)
110. Grande, D.A., Halberstadt, C., Naughton, G., Schwartz, R., Manji, R.: Evaluation of matrix scaffolds for tissue engineering of articular cartilage grafts. J. Biomed. Mater. Res. **34**(2), 211–220 (1997)
111. Chromiak, J., Shansky, J., Perrone, C., Vandenburgh, H.: Bioreactor perfusion system for the long-term maintenance of tissue-engineered skeletal muscle organoids. In Vitro Cell. Dev. Biol. Anim. **34**(9), 694–703 (1998)
112. Jeong, S.I., Kwon, J.H., Lim, J.I., Cho, S.-W., Jung, Y., Sung, W.J., et al.: Mechano-active tissue engineering of vascular smooth muscle using pulsatile perfusion bioreactors and elastic PLCL scaffolds. Biomaterials **26**(12), 1405–1411 (2005)
113. Carrier, R.L., Rupnick, M., Langer, R., Schoen, F.J., Freed, L.E., Vunjak-Novakovic, G.: Effects of oxygen on engineered cardiac muscle. Biotechnol. Bioeng. **78**(6), 617–625 (2002)

114. Brown, D.A., MacLellan, W.R., Dunn, J.C.Y., Wu, B.M., Beygui, R.E.: Hypoxic cell death is reduced by pH buffering in a model of engineered heart tissue. Artif. Cells Blood Substit. Immobil. Biotechnol. **36**(2), 94–113 (2008)
115. Nieuwoudt, M.J., Moolman, S.F., Van Wyk, K.J., Kreft, E., Olivier, B., Laurens, J.B., et al.: Hepatocyte function in a radial-flow bioreactor using a perfluorocarbon oxygen carrier. Artif. Organs **29**(11), 915–918 (2005)
116. Nieuwoudt, M., Wiggett, S., Malfeld, S., van der Merwe, S.: Imaging glucose metabolism in perfluorocarbon-perfused hepatocyte bioreactors using positron emission tomography. J. Artif. Organs **12**(4), 247–257 (2009)
117. Gordon, J.E., Dare, M.R., Palmer, A.F.: Engineering select physical properties of cross-linked red blood cells and a simple a priori estimation of their efficacy as an oxygen delivery vehicle within the context of a hepatic hollow fiber bioreactor. Biotechnol. Prog. **21**(6), 1700–1707 (2005)
118. Zhao, F., Chella, R., Ma, T.: Effects of shear stress on 3-D human mesenchymal stem cell construct development in a perfusion bioreactor system: Experiments and hydrodynamic modeling. Biotechnol. Bioeng. **96**(3), 584–595 (2007)
119. Datta, N., Pham, Q.P., Sharma, U., Sikavitsas, V.I., Jansen, J.A., Mikos, A.G.: In vitro generated extracellular matrix and fluid shear stress synergistically enhance 3D osteoblastic differentiation. Proc. Natl Acad. Sci. USA **103**(8), 2488–2493 (2006)
120. Holtorf, H.L., Jansen, J.A., Mikos, A.G.: Flow perfusion culture induces the osteoblastic differentiation of marrow stromal cell-scaffold constructs in the absence of dexamethasone. J. Biomed. Mater. Res. A **72A**(3), 326–334 (2005)
121. Riess, J.G.: Perfluorocarbon-based oxygen delivery. Artif. Cells Blood Substit. Immobil. Biotechnol. **34**(6), 567–580 (2006)
122. Riess, J.G.: Oxygen carriers ("blood substitutes") – Raison d'Etre, chemistry, and some physiology. Chem. Rev. **101**(9), 2797–2919 (2001)
123. Phillips, W.T., Goins, B., Klipper, R., Cook, B.G., Martin, C., Lemen, L., et al.: Tissue oxygen delivery and tissue distribution of liposome encapsulated hemoglobin. In: Eishun, T. (ed.) Blood Substitutes, Present and Future Perspectives, pp. 147–160. Elsevier Science, Lausanne (1998)
124. Sakai, H., Tomiyama, K-i, Sou, K., Takeoka, S., Tsuchida, E.: Poly(ethylene glycol)-conjugation and deoxygenation enable long-term preservation of hemoglobin-vesicles as oxygen carriers in a liquid state. Bioconjug. Chem. **11**(3), 425–432 (2000)
125. Phillips, W.T., Klipper, R.W., Awasthi, V.D., Rudolph, A.S., Cliff, R., Kwasiborski, V., et al.: Polyethylene glycol-modified liposome-encapsulated hemoglobin: A long circulating red cell substitute. J. Pharmacol. Exp. Ther. **288**(2), 665–670 (1999)
126. Sakai, H., Takeoka, S., Park, S.I., Kose, T., Nishide, H., Izumi, Y., et al.: Surface modification of hemoglobin vesicles with poly(ethylene glycol) and effects on aggregation, viscosity, and blood flow during 90 exchange transfusion in anesthetized rats. Bioconjug. Chem. **8**(1), 23–30 (1997)
127. Usuba, A., Osuka, F., Kimura, T., Sato, R., Ogata, Y., Gotoh, H., et al.: Effect of liposome-encapsulated hemoglobin, neo red cells, on hemorrhagic shock. Surg. Today **28**(10), 1027–1035 (1998)
128. Takahashi, A.: Characterization of neo red cells (NRCs), their function and safety in vivo tests. Artif. Cells Blood Substit. Immobil.Biotechnol. **23**(3), 347–354 (1995)
129. Li, S., Nickels, J., Palmer, A.F.: Liposome-encapsulated actin-hemoglobin (LEAcHb) artificial blood substitutes. Biomaterials **26**(17), 3759–3769 (2005)
130. Discher, B.M., Bermudez, H., Hammer, D.A., Discher, D.E., Won, Y.-Y., Bates, F.S.: Cross-linked polymersome membranes: vesicles with broadly adjustable properties. J. Phys. Chem. B **106**(11), 2848–2854 (2002)
131. Discher, B.M., Won, Y.-Y., Ege, D.S., Lee, J.C.M., Bates, F.S., Discher, D.E., et al.: Polymersomes: Tough vesicles made from diblock copolymers. Science **284**(5417), 1143–1146 (1999)
132. Discher, D.E., Ahmed, F.: Polymersomes. Annu. Rev. Biomed. Eng. **8**(1), 323–341 (2006)

133. Rameez, S., Alosta, H., Palmer, A.F.: Biocompatible and biodegradable polymersome encapsulated hemoglobin: A potential oxygen carrier. Bioconjug. Chem. **19**(5), 1025–1032 (2008)
134. Riess, J.G.: Understanding the fundamentals of perfluorocarbons and perfluorocarbon emulsions relevant to in vivo oxygen delivery. Artif. Cells Blood Substit. Immobil. Biotechnol. **33**(1), 47–63 (2005)
135. Krafft, M.P., Riess, J.G.: Highly fluorinated amphiphiles and colloidal systems, and their applications in the biomedical field. A contribution. Biochimie **80**(5–6), 489–514 (1998)
136. Kuznetsova, I.N.: Perfluorocarbon emulsions: Stability in vitro and in vivo (A Review). Pharm. Chem. J. **37**(8), 415–420 (2003)
137. Fijan, R., Sostar-Turk, S., Lapasin, R.: Rheological study of interactions between non-ionic surfactants and polysaccharide thickeners used in textile printing. Carbohydr. Polym. **68**(4), 708–717 (2007)
138. Krafft, M.P., Riess, J.G.: Perfluorocarbons: Life sciences and biomedical uses dedicated to the memory of Professor Guy Ourisson, a true Renaissance man. J. Polym. Sci. A: Polym. Chem. **45**(7), 1185–1198 (2007)
139. Gauger, P.G., Pranikoff, T., Schreiner, R.J., Moler, F.W., Hirschl, R.B.: Initial experience with partial liquid ventilation in pediatric patients with the acute respiratory distress syndrome. Crit. Care Med. **24**(1), 16–22 (1996)
140. Kin, T., Mirbolooki, M., Salehi, P., Tsukada, M., O'Gorman, D., Imes, S., et al.: Islet isolation and transplantation outcomes of pancreas preserved with University of Wisconsin solution versus two-layer method using preoxygenated perfluorocarbon. Transplantation **82**(10), 1286–1290 (2006)
141. Fraker, C.A., Alvarez, S., Papadopoulos, P., Giraldo, J., Gu, W.Y., Ricordi, C., et al.: Enhanced oxygenation promotes beta-cell differentiation in vitro. Stem Cells **25**(12), 3155–3164 (2007)
142. Tan, Q., El-Badry, A.M., Contaldo, C., Steiner, R., Hillinger, S., Welti, M., et al.: The effect of perfluorocarbon-based artificial oxygen carriers on tissue-engineered trachea. Tissue Eng. Part A **15**(9), 2471–2480 (2009)
143. MathyHartert, M., Krafft, M.P., Deby, C., DebyDupont, G., Meurisse, M., Lamy, M., et al.: Effects of perfluorocarbon emulsions on cultured human endothelial cells. Artif. Cells Blood Substit. Immobil. Biotechnol. **25**(6), 563–575 (1997)
144. Ricordi, C., Fraker, C., Szust, J., Al-Abdullah, I., Poggioli, R., Kirlew, T., et al.: Improved human islet isolation outcome from marginal donors following addition of oxygenated perfluorocarbon to the cold-storage solution. Transplantation **75**(9), 1524–1527 (2003)
145. Centis, V., Doillon, C.J., Vermette, P.: (eds). Perfluorocarbon emulsions cytotoxic effects on human fibroblasts and effect of aging on particle size distribution. 9th Vienna International Workshop on Functional Electrical Stimulation; pp. 19–22. Krems, Austria (2007)
146. Ward, C., Haines, N., Patel, R., Eisele, E., Harrison, B.: Assessing angiogenic activity of cells in the presence of oxygen generating biomaterials. FASEB J. **23**((1_MeetingAbstracts)), 9518 (2009)
147. West, J., Moon, J.: Vascularization of engineered tissues: approaches to promote angiogenesis in biomaterials. Curr. Top. Med. Chem. **8**(4), 300–310 (2008)
148. Hirschi, K., Skalak, T., Peirce, S., Little, C.: Vascular assembly in natural and engineered tissues. Ann. N. Y. Acad. Sci. **961**(Reparative medicine: Growing tissues and organs), 223–242 (2002)
149. Jay, S., Shepherd, B., Andrejecsk, J., Kyriakides, T., Pober, J., Saltzman, W.: Dual delivery of VEGF and MCP-1 to support endothelial cell transplantation for therapeutic vascularization. Biomaterials **31**(11), 3054–3062 (2010)
150. Carmeliet, P.: Mechanisms of angiogenesis and arteriogenesis. Nat. Med. **6**(4), 389–395 (2000)

151. Sun, G., Kusuma, S., Gerecht, S.: The integrated role of biomaterials and stem cells in vascular regeneration. In: Roy, K. (ed.) Biomaterials as Stem Cell Niche, pp. 195–223. Springer, Berlin, Heidelberg (2010)
152. Jain, R.: Molecular regulation of vessel maturation. Nat. Med. **9**(6), 685–693 (2003)
153. West, J.L., Hubbell, J.A.: Polymeric biomaterials with degradation sites for proteases involved in cell migration. Macromolecules **32**(1), 241–244 (1998)
154. Lutolf, M.P., Hubbell, J.A.: Synthesis and physicochemical characterization of end-linked poly(ethylene glycol)-co-peptide hydrogels formed by Michael-type addition. Biomacromolecules **4**(3), 713–722 (2003)
155. Zisch, A.H., Lutolf, M.P., Ehrbar, M., Raeber, G.P., Rizzi, S.C., Davies, N., et al.: Cell-demanded release of VEGF from synthetic, biointeractive cell-ingrowth matrices for vascularized tissue growth. FASEB J. **17**(13), 2260–2262 (2003)
156. Kamei, M., Saunders, W.B., Bayless, K.J., Dye, L., Davis, G.E., Weinstein, B.M.: Endothelial tubes assemble from intracellular vacuoles in vivo. Nature **442**(7101), 453–456 (2006)
157. Moon, J.J., Saik, J.E., Poche, R.A., Leslie-Barbick, J.E., Lee, S.H., Smith, A.A., et al.: Biomimetic hydrogels with pro-angiogenic properties. Biomaterials **31**(14), 3840–3847 (2010)
158. Leslie-Barbick, J., Moon, J., West, J.: Covalently-immobilized vascular endothelial growth factor promotes endothelial cell tubulogenesis in poly (ethylene glycol) diacrylate hydrogels. J. Biomater. Sci. Polym. Ed. **20**(12), 1763–1779 (2009)
159. Leslie-Barbick, J.E., Shen, C., Chen, C., West, J.L.: Micron-scale spatially patterned, covalently immobilized vascular endothelial growth factor on hydrogels accelerates endothelial tubulogenesis and increases cellular angiogenic responses. Tissue Eng. Part A **17**(1–2), 221–229 (2011)
160. Richardson, T.P., Peters, M.C., Ennett, A.B., Mooney, D.J.: Polymeric system for dual growth factor delivery. Nat. Biotechnol. **19**(11), 1029–1034 (2001)
161. Pike, D.B., Cai, S., Pomraning, K.R., Firpo, M.A., Fisher, R.J., Shu, X.Z., et al.: Heparin-regulated release of growth factors in vitro and angiogenic response in vivo to implanted hyaluronan hydrogels containing VEGF and bFGF. Biomaterials **27**(30), 5242–5251 (2006)
162. Freeman, I., Cohen, S.: The influence of the sequential delivery of angiogenic factors from affinity-binding alginate scaffolds on vascularization. Biomaterials **30**(11), 2122–2131 (2009)
163. Carmeliet, P.: Angiogenesis in life, disease and medicine. Nature **438**(7070), 932–936 (2005)
164. Lutolf, M.P., Hubbell, J.A.: Synthetic biomaterials as instructive extracellular microenvironments for morphogenesis in tissue engineering. Nat. Biotechnol. **23**(1), 47–55 (2005)
165. Carmeliet, P.: Angiogenesis in health and disease. Nat. Med. **9**(6), 653–660 (2003)
166. Jay, S.M., Shepherd, B.R., Bertram, J.P., Pober, J.S., Saltzman, W.M.: Engineering of multifunctional gels integrating highly efficient growth factor delivery with endothelial cell transplantation. FASEB J. **22**(8), 2949–2956 (2008)
167. Ozawa, C.R., Banfi, A., Glazer, N.L., Thurston, G., Springer, M.L., Kraft, P.E., et al.: Microenvironmental VEGF concentration, not total dose, determines a threshold between normal and aberrant angiogenesis. J. Clin. Invest. **113**(4), 516–527 (2004)
168. Wei, G., Jin, Q., Giannobile, W.V., Ma, P.X.: Nano-fibrous scaffold for controlled delivery of recombinant human PDGF-BB. J. Control. Release **112**(1), 103–110 (2006)
169. Sahni, A., Sporn, L.A., Francis, C.W.: Potentiation of endothelial cell proliferation by fibrin (ogen)-bound fibroblast growth factor-2. J. Biol. Chem. **274**(21), 14936–14941 (1999)
170. DeLong, S.A., Moon, J.J., West, J.L.: Covalently immobilized gradients of bFGF on hydrogel scaffolds for directed cell migration. Biomaterials **26**(16), 3227–3234 (2005)
171. Refojo, M.F.: Ophthalmological Applications. In: Rattner, B.D., Hoffman, A.S., Schoen, F.J., Lemons, J.E. (eds.) Biomaterials science: An introduction to materials in medicine, 2nd edn, pp. 583–591. Elsevier Academic, San Diego (2004)

172. Holden, B.A., Newton-Howes, J., Winterton, L., Fatt, I., Hamano, H., Hood, D.L., et al.: The Dk project: An interlaboratory comparison of DK/L measurements. Optom. Vis. Sci. **67**(6), 476–481 (1990)
173. Peppas, N.A., Yang, W.-H.M.: Properties-based optimization of the structure of polymers for contact lens applications. Eye Contact Lens **7**(4), 300–314 (1981)
174. Hong, X.I.N., Himebaugh, N., Thibos, L.N.: On-eye evaluation of optical performance of rigid and soft contact lenses. Optom. Vis. Sci. **78**(12), 872–880 (2001)
175. Alvord, L., Court, J., Davis, T., Morgan, C.F., Schindhelm, K., Vogt, J., et al.: Oxygen permeability of a new type of high Dk soft contact lens material. Optom. Vis. Sci. **75**(1), 30–36 (1998)
176. Wichterle, O., Lim, D.: Hydrophilic gels for biological use. Nature **185**(4706), 117–118 (1960)
177. Ehlers, W., Donshik, P.C.: Update on lotrafilcon A contact lenses. Expert Rev. Ophthalmol. **5**, 19–25 (2010)
178. Dillehay, S.M., Miller, M.B.: Performance of lotrafilcon B silicone hydrogel contact lenses in experienced low-Dk/t daily lens wearers. Eye Contact Lens **33**(6, Part 1 of 2), 272–277 (2007)
179. Teramura, Y., Iwata, H.: Islet encapsulation with living cells for improvement of biocompatibility. Biomaterials **30**(12), 2270–2275 (2009)
180. Schneider, S., Feilen, P.J., Slotty, V., Kampfner, D., Preuss, S., Berger, S., et al.: Multilayer capsules: a promising microencapsulation system for transplantation of pancreatic islets. Biomaterials **22**(14), 1961–1970 (2001)
181. de Vos, P., Marchetti, P.: Encapsulation of pancreatic islets for transplantation in diabetes: the untouchable islets. Trends Mol. Med. **8**(8), 363–366 (2002)
182. Zimmermann, H., Hillgartner, M., Manz, B., Feilen, P., Brunnenmeier, F., Leinfelder, U., et al.: Fabrication of homogeneously cross-linked, functional alginate microcapsules validated by NMR-, CLSM- and AFM-imaging. Biomaterials **24**(12), 2083–2096 (2003)
183. Cheung, C.Y., Anseth, K.S.: Synthesis of immunoisolation barriers that provide localized immunosuppression for encapsulated pancreatic islets. Bioconjug. Chem. **17**(4), 1036–1042 (2006)
184. Weber, L.M., Cheung, C.Y., Anseth, K.S.: Multifunctional pancreatic islet encapsulation barriers achieved via multilayer PEG hydrogels. Cell Transplant. **16**(10), 1049–1057 (2007)
185. Abalovich, A.G., Bacque, M.C., Grana, D., Milei, J. (eds). Pig pancreatic islet transplantation into spontaneously diabetic dogs. 22nd International Congress of the Transplantation-Society, Sydney, Australia, 10–14 Aug 2008
186. Koo, S.K., Kim, S.C., Wee, Y.M., Kim, Y.H., Jung, E.J., Choi, M.Y., et al.: Experimental microencapsulation of porcine and rat pancreatic islet cells with air-driven droplet generator and alginate. Transplant. Proc. **40**(8), 2578–2580 (2008)
187. Qi, M., Strand, B.L., Morch, Y., Lacik, I., Wang, Y., Salehi, P., et al.: Encapsulation of human islets in novel inhomogeneous alginate-Ca^{2+}/Ba^{2+} microbeads: In vitro and in vivo function. Artif. Cells Blood Substit.Immobil. Biotechnol. **36**(5), 403–420 (2008)
188. de Groot, M., Schuurs, T.A., van Schilfgaarde, R.: Causes of limited survival of microencapsulated pancreatic islet grafts. J. Surg. Res. **121**(1), 141–150 (2004)
189. de Groot, M., Schuurs, T., Keizer, P., Fekken, S., Leuvenink, H., van Schilfgaarde, R.: Response of encapsulated rat pancreatic islets to hypoxia. Cell Transplant. **12**(8), 867–875 (2003)
190. Zimmermann, H., Shirley, S., Zimmermann, U.: Alginate-based encapsulation of cells: Past, present, and future. Curr. Diab. Rep. **7**(4), 314–320 (2007)
191. Strand, B.L., Ryan, L., Veld, P.I., Kulseng, B., Rokstad, A.M., Skjak-Braek, G., et al.: Poly-L-lysine induces fibrosis on alginate microcapsules via the induction of cytokines. Cell Transplant. **10**(3), 263–275 (2001)
192. Dionne, K.E., Colton, C.K., Yarmush, M.L.: Effect of hypoxia on insulin-secretion by isolated rate and canine islets of Langerhans. Diabetes **42**(1), 12–21 (1993)

193. Matsumoto, S., Qualley, S.A., Rigley, T.H., Marsh, C.L., Stevens, R.B.: Prolonged preservation of the human pancreas prior to islet isolation using the two-layer (University of Wisconsin solution [UW]/perfluorocarbon) method. Transplantation **69**(8), 384 (2000)
194. Maillard, E., Sanchez-Dominguez, M., Kleiss, C., Langlois, A., Sencier, M.C., Vodouhe, C., et al.: Perfluorocarbons: New tool for islets preservation in vitro. Transplant. Proc. **40**(2), 372–374 (2008)
195. Sigrist, S., Mechine-Neuville, A., Mandes, K., Calenda, V., Braun, S., Legeay, G., et al.: Influence of VEGF on the viability of encapsulated pancreatic rat islets after transplantation in diabetic mice. Cell Transplant. **12**(6), 627–635 (2003)
196. Sigrist, S., Mechine-Neuville, A., Mandes, K., Calenda, V., Legeay, G., Bellocq, J.P., et al.: Induction of angiogenesis in omentum with vascular endothelial growth factor: Influence on the viability of encapsulated rat pancreatic islets during transplantation. J. Vasc. Res. **40**(4), 359–367 (2003)
197. Lai, Y., Schneider, D., Kidszun, A., Hauck-Schmalenberger, I., Breier, G., Brandhorst, D., et al.: Vascular endothelial growth factor increases functional beta-cell mass by improvement of angiogenesis of isolated human and murine pancreatic islets. Transplantation **79**(11), 1530–1536 (2005)
198. Lembert, N., Wesche, J., Petersen, P., Doser, M., Zschocke, P., Becker, H.D., et al.: Encapsulation of islets in rough surface, hydroxymethylated polysulfone capillaries stimulates VEGF release and promotes vascularization after transplantation. Cell Transplant. **14**(2–3), 97–108 (2005)
199. Juang, J., Hsu, B., Kuo, C., Ueng, S.: Beneficial effects of hyperbaric oxygen therapy on islet transplantation. Cell Transplant. **11**(2), 95–101 (2002)
200. Lakey, J.R.T., Mirbolooki, M., Shapiro, A.M.J.: Current status of clinical islet cell transplantation. Transplant. Immunol. **333**, 47–103 (2006)
201. Salcedo, R., Ponce, M.L., Young, H.A., Wasserman, K., Ward, J.M., Kleinman, H.K., et al.: Human endothelial cells express CCR2 and respond to MCP-1: direct role of MCP-1 in angiogenesis and tumor progression. Blood **96**(1), 34–40 (2000)
202. Paule, M.F., McColl, S.R., Simeonovic, C.J.: Murine chemokine gene expression in rejecting pig proislet xenografts. Transplant. Proc. **32**(5), 1062 (2000)
203. de Vos, P., Hillebrands, J.-L., De Haan, B.J., Strubbe, J.H., Van Schilfgaarde, R.: Efficacy of a prevascularized expanded polytetrafluoroethylene solid support system as a transplantation site for pancreatic islets 1. Transplantation **63**(6), 824–830 (1997)
204. Sen, C.: Wound healing essentials: let there be oxygen. Wound Repair Regen. **17**(1), 1–18 (2009)
205. Tandara, A.A., Mustoe, T.A.: Oxygen in wound healing – More than a nutrient. World J. Surg. **28**(3), 294–300 (2004)
206. Greif, R., Akça, O., Horn, E.-P., Kurz, A., Sessler, D.I.: Supplemental perioperative oxygen to reduce the incidence of surgical-wound infection. N. Engl. J. Med. **342**(3), 161–167 (2000)
207. Kumari, R., Willing, L.B., Krady, J.K., Vannucci, S.J., Simpson, I.A.: Impaired wound healing after cerebral hypoxia-ischemia in the diabetic mouse. J. Cereb. Blood Flow Metab. **27**(4), 710–718 (2006)
208. Distler, O., Distler, J.H.W., Scheid, A., Acker, T., Hirth, A., Rethage, J., et al.: Uncontrolled expression of vascular endothelial growth factor and its receptors leads to insufficient skin angiogenesis in patients with systemic sclerosis. Circ. Res. **95**(1), 109–116 (2004)
209. Salaman, R.A., Harding, K.G.: The aetiology and healing rates of chronic leg ulcers. J. Wound Care **4**(7), 320–323 (1995)
210. Shai, A., Maibach, H.I.: Wound healing and ulcers of the skin diagnosis and therapy – The practical approach. Springer, Berlin, Heidelberg (2005)
211. McGill, M., Collins, P., Bolton, T., Yue, D.K.: Management of neuropathic ulceration. J. Wound Care **5**(2), 52–54 (1996)
212. Centers for Disease Control and Prevention. National diabetes fact sheet: national estimates and general information on diabetes and prediabetes in the United States, 2011. Atlanta,

GA: U.S. Department of Health and Human Services, Centers for Disease Control and Prevention, 2011.
213. Hafner, J., Schaad, I., Schneider, E., Seifert, B., Burg, G., Cassina, P.C.: Leg ulcers in peripheral arterial disease (arterial leg ulcers): Impaired wound healing above the threshold of chronic critical limb ischemia. J. Am. Acad. Dermatol. **43**(6), 1001–1008 (2000)
214. Salaman, J.H., Miller, L., Harding, K.G.: Management of foot ulceration in a patient with diabetes mellitus. J. Wound Care **4**(10), 443–444 (1995)
215. Lait, M.E., Smith, L.N.: Wound management: a literature review. J. Clin. Nurs. **7**(1), 11–17 (1998)
216. Gordillo, G., Roy, S., Khanna, S., Schlanger, R., Khandelwal, S., Phillips, G., et al.: Topical oxygen therapy induces vascular endothelial growth factor expression and improves closure of clinically presented chronic wounds. Clin. Exp. Pharmacol. Physiol. **35**(8), 957–964 (2008)
217. Kalliainen, L., Gordillo, G., Schlanger, R., Sen, C.: Topical oxygen as an adjunct to wound healing: a clinical case series. Pathophysiology **9**(2), 81–87 (2003)
218. Fries, R., Wallace, W., Roy, S., Kuppusamy, P., Bergdall, V., Gordillo, G., et al.: Dermal excisional wound healing in pigs following treatment with topically applied pure oxygen. Mutat. Res. **579**(1–2), 172–181 (2005)
219. Davis, S., Cazzaniga, A., Ricotti, C., Zalesky, P., Hsu, L., Creech, J., et al.: Topical oxygen emulsion: a novel wound therapy. Arch. Dermatol. **143**(10), 1252 (2007)
220. Scadden, D.T.: The stem-cell niche as an entity of action. Nature **441**(7097), 1075–1079 (2006)
221. Mohyeldin, A., Garzon-Muvdi, T., Quinones-Hinojosa, A.: Oxygen in stem cell biology: a critical component of the stem cell niche. Cell Stem Cell **7**(2), 150–161 (2010)
222. Engler, A.J., Sen, S., Sweeney, H.L., Discher, D.E.: Matrix elasticity directs stem cell lineage specification. Cell **126**(4), 677–689 (2006)
223. Yoshida, Y., Takahashi, K., Okita, K., Ichisaka, T., Yamanaka, S.: Hypoxia enhances the generation of induced pluripotent stem cells. Cell Stem Cell **5**(3), 237–241 (2009)
224. Grayson, W.L., Zhao, F., Izadpanah, R., Bunnell, B., Ma, T.: Effects of hypoxia on human mesenchymal stem cell expansion and plasticity in 3D constructs. J. Cell. Physiol. **207**(2), 331–339 (2006)
225. Ma, T., Grayson, W.L., Fröhlich, M., Vunjak-Novakovic, G.: Hypoxia and stem cell-based engineering of mesenchymal tissues. Biotechnol. Prog. **25**(1), 32–42 (2009)
226. Zhao, F., Veldhuis, J.J., Duan, Y., Yang, Y., Christoforou, N., Ma, T., et al.: Low oxygen tension and synthetic nanogratings improve the uniformity and stemness of human mesenchymal stem cell layer. Mol. Ther. **18**(5), 1010–1018 (2010)
227. Simon, M.C., Keith, B.: The role of oxygen availability in embryonic development and stem cell function. Nat. Rev. Mol. Cell Biol. **9**(4), 285–296 (2008)
228. Eliasson, P., Jönsson, J.: The hematopoietic stem cell niche: low in oxygen but a nice place to be. J. Cell. Physiol. **222**(1), 17–22 (2010)
229. dos Santos, F., Andrade, P.Z., Boura, J.S., Abecasis, M.M., dos Silva, C.L., Cabral, J.M.S.: Ex vivo expansion of human mesenchymal stem cells: A more effective cell proliferation kinetics and metabolism under hypoxia. J. Cell. Physiol. **223**(1), 27–35 (2010)
230. Tottey, S., Corselli, M., Jeffries, E.M., Londono, R., Peault, B., Badylak, S.F.: Extracellular matrix degradation products and low-oxygen conditions enhance the regenerative potential of perivascular stem cells. Tissue Eng. Part A **17**(1–2), 37–44 (2011)
231. Cipolleschi, M.G., Dello Sbarba, P., Olivotto, M.: The role of hypoxia in the maintenance of hematopoietic stem cells. Blood **82**(7), 2031–2037 (1993)
232. Chow, D.C., Wenning, L.A., Miller, W.M., Papoutsakis, E.T.: Modeling pO_2 distributions in the bone marrow hematopoietic compartment. II. Modified Kroghian Models. Biophys. J. **81**(2), 685–696 (2001)
233. Nilsson, S.K., Johnston, H.M., Coverdale, J.A.: Spatial localization of transplanted hemopoietic stem cells: inferences for the localization of stem cell niches. Blood **97**(8), 2293–2299 (2001)

234. Parmar, K., Mauch, P., Vergilio, J.-A., Sackstein, R., Down, J.D.: Distribution of hematopoietic stem cells in the bone marrow according to regional hypoxia. Proc. Natl Acad. Sci. USA **104**(13), 5431–5436 (2007)
235. Abdollahi, H., Harris, L., Zhang, P., McIlhenny, S., Srinivas, V., Tulenko, T., et al.: The role of hypoxia in stem cell differentiation and therapeutics. J. Surg. Res. **1**(6), 1 (2009)
236. Ivanovic, Z.: Hypoxia or in situ normoxia: The stem cell paradigm. J. Cell. Physiol. **219**(2), 271–275 (2009)
237. Raheja, L.F., Genetos, D.C., Yellowley, C.E.: The effect of oxygen tension on the long-term osteogenic differentiation and MMP/TIMP expression of human mesenchymal stem cells. Cells Tissues Organs **191**(3), 175–184 (2010)
238. Takahashi, K., Tanabe, K., Ohnuki, M., Narita, M., Ichisaka, T., Tomoda, K., et al.: Induction of pluripotent stem cells from adult human fibroblasts by defined factors. Cell **131**(5), 861–872 (2007)
239. Nakagawa, M., Koyanagi, M., Tanabe, K., Takahashi, K., Ichisaka, T., Aoi, T., et al.: Generation of induced pluripotent stem cells without Myc from mouse and human fibroblasts. Nat. Biotech. **26**(1), 101–106 (2008). doi:10.1038/nbt1374
240. Millman, J.R., Tan, J.H., Colton, C.K.: The effects of low oxygen on self-renewal and differentiation of embryonic stem cells. Curr. Opin. Organ Transplant. **14**(6), 694–700 (2009)
241. Ji, A.R., Ku, S.Y., Cho, M.S., Kim, Y.Y., Kim, Y.J., Oh, S.K., et al.: Reactive oxygen species enhance differentiation of human embryonic stem cells into mesendodermal lineage. Exp. Mol. Med. **42**(3), 175–186 (2010)
242. Robertson, E.J.: Teratocarcinomas and Embryonic Stem Cells: A Practical Approach. IRL, Oxford (1987)
243. Boiani, M., Eckardt, S., Schöler, H.R., McLaughlin, K.J.: Oct4 distribution and level in mouse clones: consequences for pluripotency. Genes Dev. **16**(10), 1209–1219 (2002)
244. Forristal, C.E., Wright, K.L., Hanley, N.A., Oreffo, R.O.C., Houghton, F.D.: Hypoxia inducible factors regulate pluripotency and proliferation in human embryonic stem cells cultured at reduced oxygen tensions. Reproduction **139**(1), 85–97 (2010)
245. Takahashi, K., Yamanaka, S.: Induction of pluripotent stem cells from mouse embryonic and adult fibroblast cultures by defined factors. Cell **126**(4), 663–676 (2006)
246. Boyer, L.A., Lee, T.I., Cole, M.F., Johnstone, S.E., Levine, S.S., Zucker, J.P., et al.: Core transcriptional regulatory circuitry in human embryonic stem cells. Cell **122**(6), 947–956 (2005)
247. Keith, B., Simon, M.C.: Hypoxia-inducible factors, stem cells, and cancer. Cell **129**(3), 465–472 (2007)
248. Gustafsson, M.V., Zheng, X., Pereira, T., Gradin, K., Jin, S., Lundkvist, J., et al.: Hypoxia requires notch signaling to maintain the undifferentiated cell state. Dev. Cell **9**(5), 617–628 (2005)
249. Panchision, D.M.: The role of oxygen in regulating neural stem cells in development and disease. J. Cell. Physiol. **220**(3), 562–568 (2009)
250. Main, H., Lee, K.L., Yang, H., Haapa-Paananen, S., Edgren, H., Jin, S.B., et al.: Interactions between Notch- and hypoxia-induced transcriptomes in embryonic stem cells. Exp. Cell Res. **316**(9), 1610–1624 (2010)
251. Zachar, V., Prasad, S., Weli, S., Gabrielsen, A., Petersen, K., Petersen, M., et al.: The effect of human embryonic stem cells (hESCs) long-term normoxic and hypoxic cultures on the maintenance of pluripotency. In Vitro Cell. Dev. Biol. Animal. **46**(3), 276–283 (2010)
252. Pear, W.S., Simon, M.C.: Lasting longer without oxygen: The influence of hypoxia on Notch signaling. Cancer Cell **8**(6), 435–437 (2005)
253. Kirouac, D.C., Zandstra, P.W.: The systematic production of cells for cell therapies. Cell Stem Cell **3**(4), 369–381 (2008)
254. Rosová, I., Dao, M., Capoccia, B., Link, D., Nolta, J.A.: Hypoxic preconditioning results in increased motility and improved therapeutic potential of human mesenchymal stem cells. Stem Cells **26**(8), 2173–2182 (2008)

255. Li, Z., Leung, M., Hopper, R., Ellenbogen, R., Zhang, M.: Feeder-free self-renewal of human embryonic stem cells in 3D porous natural polymer scaffolds. Biomaterials **31**(3), 404–412 (2010)
256. Leach, J.B., Powell, E.M.: Understanding hypoxic environments: biomaterials approaches to neural stabilization and regeneration after ischemia. In: Roy, K. (ed.) Biomaterials as Stem Cell Niche, pp. 247–274. Springer, Berlin Heidelberg (2010)
257. Furth, M.E., Atala, A.: Stem cell sources to treat diabetes. J. Cell. Biochem. **106**(4), 507–511 (2009)
258. Holle, A.W., Engler, A.J.: Cell rheology: Stressed-out stem cells. Nat. Mater. **9**(1), 4–6 (2010)
259. Siti-Ismail, N., Bishop, A.E., Polak, J.M., Mantalaris, A.: The benefit of human embryonic stem cell encapsulation for prolonged feeder-free maintenance. Biomaterials **29**(29), 3946–3952 (2008)
260. Liu, H., Collins, S.F., Suggs, L.J.: Three-dimensional culture for expansion and differentiation of mouse embryonic stem cells. Biomaterials **27**(36), 6004–6014 (2006)
261. Fisher, O.Z., Khademhosseini, A., Langer, R., Peppas, N.A.: Bioinspired materials for controlling stem cell fate. Acc. Chem. Res. **43**(3), 419–428 (2009)
262. Bratt-Leal, A.M., Carpenedo, R.L., Ungrin, M.D., Zandstra, P.W., McDevitt, T.C.: Incorporation of biomaterials in multicellular aggregates modulates pluripotent stem cell differentiation. Biomaterials **32**(1), 48–56 (2011)
263. Hwang, Y.-S., Cho, J., Tay, F., Heng, J.Y.Y., Ho, R., Kazarian, S.G., et al.: The use of murine embryonic stem cells, alginate encapsulation, and rotary microgravity bioreactor in bone tissue engineering. Biomaterials **30**(4), 499–507 (2009)
264. Sengupta, S., Park, S.-H., Patel, A., Carn, J., Lee, K., Kaplan, D.L.: Hypoxia and amino acid supplementation synergistically promote the osteogenesis of human mesenchymal stem cells on silk protein scaffolds. Tissue Eng. Part A **16**(12), 3623–3634 (2010)
265. Fridley, K.M., Fernandez, I., Li, M.-T.A., Kettlewell, R.B., Roy, K.: Unique differentiation profile of mouse embryonic stem cells in rotary and stirred tank bioreactors. Tissue Eng. Part A **16**(11), 3285–3298 (2010)
266. Serra, M., Brito, C., Sousa, M.F.Q., Jensen, J., Tostoes, R., Clemente, J., et al.: Improving expansion of pluripotent human embryonic stem cells in perfused bioreactors through oxygen control. J. Biotechnol. **148**(4), 208–215 (2010)
267. Lovett, M., Rockwood, D., Baryshyan, A., Kaplan, D.L.: Simple modular bioreactors for tissue engineering: a system for characterization of oxygen gradients, human mesenchymal stem cell differentiation, and prevascularization. Tissue Eng. Part C Methods **16**(6), 1565–1573 (2010)
268. Malda, J., Martens, D.E., Tramper, J., van Blitterswijk, C.A., Riesle, J.: Cartilage tissue engineering: controversy in the effect of oxygen. Crit. Rev. Biotechnol. **23**(3), 175–194 (2003)
269. Barbero, A., Grogan, S., Schäfer, D., Heberer, M., Mainil-Varlet, P., Martin, I.: Age related changes in human articular chondrocyte yield, proliferation and post-expansion chondrogenic capacity. Osteoarthritis Cartilage **12**(6), 476–484 (2004)
270. Kuo, C.K., Li, W.-J., Mauck, R.L., Tuan, R.S.: Cartilage tissue engineering: its potential and uses. Curr. Opin. Rheumatol. **18**(1), 64–73 (2006)
271. Grimshaw, M.J., Mason, R.M.: Bovine articular chondrocyte function in vitro depends upon oxygen tension. Osteoarthritis Cartilage **8**(5), 386–392 (2000)
272. Chen, J., Wang, C., Lü, S., Wu, J., Guo, X., Duan, C., et al.: In vivo chondrogenesis of adult bone-marrow-derived autologous mesenchymal stem cells. Cell Tissue Res. **319**(3), 429–38 (2005)
273. Xu, Y., Malladi, P., Chiou, M., Bekerman, E., Giaccia, A.J., Longaker, M.T.: In vitro expansion of adipose-derived adult stromal cells in hypoxia enhances early chondrogenesis. Tissue Eng. **13**(12), 2981–2993 (2007)

274. Poole, A.R., Kojima, T., Yasuda, T., Mwale, F., Kobayashi, M., Laverty, S.: Composition and structure of articular cartilage: A template for tissue repair. Clin. Orthop. Relat. Res. **391**, S26–S33 (2001)
275. Schnabel, M., Marlovits, S., Eckhoff, G., Fichtel, I., Gotzen, L., Vécsei, V., et al.: Dedifferentiation-associated changes in morphology and gene expression in primary human articular chondrocytes in cell culture. Osteoarthritis Cartilage **10**(1), 62–70 (2002)
276. Lafont, J.E., Talma, S., Murphy, C.L.: Hypoxia-inducible factor 2α is essential for hypoxic induction of the human articular chondrocyte phenotype. Arthritis Rheum. **56**(10), 3297–3306 (2007)
277. Domm, C., Schünke, M., Christesen, K., Kurz, B.: Redifferentiation of dedifferentiated bovine articular chondrocytes in alginate culture under low oxygen tension. Osteoarthritis Cartilage **10**(1), 13–22 (2002)
278. Domm, C., Schünke, M., Steinhagen, J., Freitag, S., Kurz, B.: Influence of various alginate brands on the redifferentiation of dedifferentiated bovine articular chondrocytes in alginate bead culture under high and low oxygen tension. Tissue Eng. **10**(11–12), 1796–1805 (2004)
279. Vinatier, C., Mrugala, D., Jorgensen, C., Guicheux, J., Noël, D.: Cartilage engineering: a crucial combination of cells, biomaterials and biofactors. Trends Biotechnol. **27**(5), 307–314 (2009)
280. Malladi, P., Xu, Y., Chiou, M., Giaccia, A.J., Longaker, M.T.: Effect of reduced oxygen tension on chondrogenesis and osteogenesis in adipose-derived mesenchymal cells. Am. J. Physiol. Cell Physiol. **290**(4), C1139–C1146 (2006)
281. Zscharnack, M., Poesel, C., Galle, J., Bader, A.: Low oxygen expansion improves subsequent chondrogenesis of ovine bone-marrow-derived mesenchymal stem cells in collagen type I hydrogel. Cells Tissues Organs **190**(2), 81–93 (2008)
282. Mizuno, S., Glowacki, J.: Low oxygen tension enhances chondroinduction by demineralized bone matrix in human dermal fibroblasts in vitro. Cells Tissues Organs **180**(3), 151–158 (2005)
283. Buxton, A.N., Bahney, C.S., Yoo, J.U., Johnstone, B.: Temporal exposure to chondrogenic factors modulates human mesenchymal stem cell chondrogenesis in hydrogels. Tissue Eng. Part A **17**(3–4), 371–380 (2011)
284. Grande, D.A., Breitbart, A.S., Mason, J., Paulino, C., Laser, J., Schwartz, R.E.: Cartilage tissue engineering: Current limitations and solutions. Clin. Orthop. Relat. Res. **367**, S176–S185 (1999)
285. Mostafa, S.S., Miller, W.M., Papoutsakis, E.T.: Oxygen tension influences the differentiation, maturation and apoptosis of human megakaryocytes. Br. J. Haematol. **111**(3), 879–889 (2000)

Part III
Tuning of Mechanical Properties

Chapter 4
Adhesion Behavior of Soft Materials

Santanu Kundu and Edwin P. Chan

Abstract Adhesion is defined as the strength of an interface. The study of adhesion involves understanding the development of interfacial properties when two materials come into contact. Thus, it is a field that has relevance in nearly every aspect of our lives ranging from biological adhesion to microelectronics. In most instances, it is the control of adhesion that is important to the specific application. Additionally, adhesion is important to a diverse set of materials that ranges from soft tissues to hard inorganic materials. Therefore, it is important to discuss the general concepts and key materials properties that are involved in the adhesion and separation of an interface. As the scope of this book addresses properties of biomaterials, this chapter will focus on the adhesion of soft materials. To aid in this understanding, the theories of Hertz and JKR will be discussed as these theories address the coupling between contact geometry of the interfacial and materials properties. We will also discuss examples of the applications of these theories for characterization adhesion of different soft material applications. With the recent interests in biomimetic adhesion, i.e. gecko adhesion, we will also use these theories as foundation for understanding how patterned surfaces can tune interfacial properties and impact macroscopic performance.

Introduction

Adhesion, which is the science of understanding the strength of an interface, is a common phenomenon that has relevance in everyday life ranging from microbial adhesion on eating surfaces to tissue adhesives [1–5], to dermatological patches [6–8], to micro/nanoelectronics [9], and to bioimplants [10–13]. For electronic

S. Kundu (✉) • E.P. Chan (✉)
University of Massachusetts-Amherst, MA, USA

Polymers Division, National Institute of Standards and Technology, Gaithersburg, MD, USA
e-mail: santanukundu@gmail.com; edwin.chan@nist.gov

S.K. Bhatia (ed.), *Engineering Biomaterials for Regenerative Medicine: Novel Technologies for Clinical Applications*, DOI 10.1007/978-1-4614-1080-5_4,

applications [9] and tissue adhesives [1–3], strong adhesion is desirable, whereas for some bioimplants, such as contact lenses, low adhesion with contact lens and cornea/eyelid can improve the comfort level for the lens wearer [10–12]. As adhesion involves interfacial processes between two materials, the properties of both materials contribute to the adhesive strength. For instance, adhesive forces can be considered negligible in comparison to the forces needed to mechanical deform for surfaces that are very stiff [14–16]. In contrast, if the contacting surfaces are compliant and highly deformable, the contributions due to adhesive forces can become significant. The adhesion of smooth, deformable, and primarily elastic materials is well described based on the theory developed by Johnson, Kendall, and Roberts (JKR) [14, 17]. It is difficult to implement this theory to predict the adhesion of rough surfaces. It has been generally accepted that adhesion decreases if surface roughness consists of a statistical distribution of asperities [14, 18–20]. However, this concept does not always hold true. For example, small lizards such as Geckos have hierarchical topological structures on their feet that facilitate very strong but reversible adhesion to many different surfaces [21–23]. Inspired by these creatures, synthetic materials with various topological features have been developed toward enhanced materials with reversible adhesive properties [24–32].

In this chapter, we discuss the adhesion behavior of various soft materials such as elastomers and hydrogels. Our discussions are based on well-established contact mechanics theories including the theories of Hertz and JKR [14–18, 33]. We show the importance and interrelationships between the interface, near interface, and mechanical properties in determining the adhesion behavior. These theories will provide the framework for the recent developments of patterned surfaces for adhesion control. Specifically, we will discuss the effects of such patterns on adhesion and illustrate the importance of the coupling between contact geometry and material properties on performance.

Adhesion of Smooth Surfaces

Significance of Energy Release Rate, G

Adhesion quantifies the energetic processes during the formation and separation of an interface by two materials. If we consider adhesion from a thermodynamic viewpoint, adhesion can be described as the amount of energy required to form two new surfaces by separating one interface. The amount of work, expressed in energy per area, required to perform this interfacial separation is defined by the thermodynamic work of adhesion (w). This term is related to the surface energies of the two new surfaces (γ_1, γ_2) and the interfacial energy prior to separation (γ_{12}) [15, 34].

$$w = \gamma_1 + \gamma_2 - \gamma_{12}. \tag{4.1}$$

From (4.1), we can see that adhesion is defined by the property of both materials surfaces that contribute to the formation and separation of the interface.

Conceptually, (4.1) describes the surface energy contributions to controlling adhesion. Materials with large surface energies relative to the interfacial energy lead to higher adhesion or greater resistance to interfacial separation. However, the energy required to cause separation for soft materials is often significantly higher than the thermodynamic work of adhesion [35]. A classic example for this discrepancy is the adhesion of pressure sensitive adhesives (i.e. Scotch tape) to glass substrates. While the energy required for interface formation (~0.1 J/m^2) approaches the thermodynamic limit as predicted by (4.1), the energy of separation can be orders of magnitude greater (~1000 J/m^2). This discrepancy suggests that adhesion of soft materials, such as polymers, is not solely a function of the properties at the interface but includes contributions from material regions in proximity to the interface. This region is often referred to as the "near-interfacial" region, and the size-scale of this region will depend on the materials of interest as well as the mechanical deformation history during an adhesion test [36].

Generally, polymer adhesion involves the coupling of the interfacial properties and bulk properties away from the interface. To describe this multiplicative contribution to adhesion for primarily elastic materials, an energy per area quantity termed as the critical energy release rate (G_c) is often used [15, 16, 37]. Similar to surface energy, this parameter describes the materials property of an interface. However, unlike the surface energy, the critical energy release rate captures the interfacial and near-interfacial contributions to adhesion by quantifying the critical energy required to change the contact area by an incremental amount. In other words, the critical energy release rate is considered as the critical driving force required for separation of an interface. Because the critical energy release rate, elastic modulus, and contact area of an interface are intimately linked to macroscopic metrics such as load and displacement, several theories have been developed to quantify the contact mechanics and adhesion of soft materials. The primary theories include Hertz theory [14, 33], JKR [14, 17], and DMT [38]. In the following sections, we will discuss two basic theories, Hertz and JKR, that are often used to describe soft materials adhesion.

Hertz and JKR Theories

We begin this section by discussing the contact mechanics of two elastic bodies in the absence of adhesion. The original solution to this problem was developed by Heinrich Hertz in 1882 [33] and this solution is still used today in many engineering problems including nanomechanics and tribology [39, 40]. The Hertz theory considered the contact between two elastic spheres with radii of curvature (R_1, R_2), elastic moduli (E_1, E_2), and Poisson's ratios (ν_1, ν_2), respectively (Fig. 4.1a). Assuming that the deformation is small such that linear elastic mechanics applies, the average load, referred to as the Hertz load (P_H) and displacement (δ_H) grow in

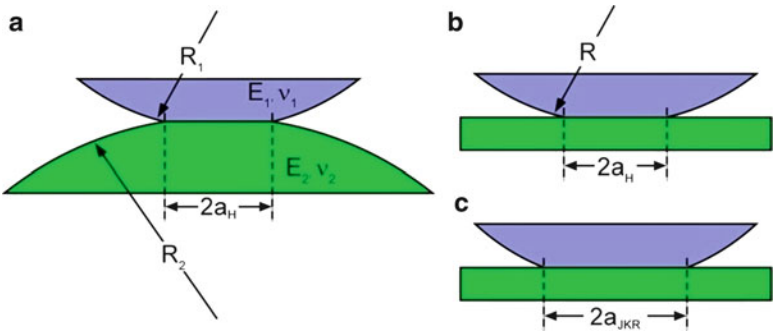

Fig. 4.1 (**a**) The Hertz contact mechanics problem between two elastic half-spheres. (**b**) Hertz contact between an elastic half-sphere and a flat substrate where a contact area $\pi a_H{}^2$ is established. (**c**) In the presence of adhesion, the contact area is greater than the Hertz contact as predicted by the JKR theory and now becomes $\pi a_{JKR}{}^2$

proportion to the contact area $A = \pi a^2$ and they are related to the contact radius a by the following [14–16]:

$$P_H = \frac{4E^* a^3}{3R}, \tag{4.2}$$

$$\delta_H = \frac{a^2}{R}. \tag{4.3}$$

Here, R is the harmonic mean of radii R_1 and R_2:

$$\frac{1}{R} = \frac{1}{R_1} + \frac{1}{R_2}. \tag{4.4}$$

E^* is an effective elastic constant:

$$\frac{1}{E^*} = \frac{1 - \nu_1^2}{E_1} + \frac{1 - \nu_2^2}{E_2}. \tag{4.5}$$

The theory is not only limited to the contact between two spheres but also to the contact of a sphere with a flat substrate (Fig. 4.1b). In this scenario, the mean curvature is defined by the radius of curvature of the sphere R_1 (as $R_2 \to \infty$). Because the Hertz theory did not consider the presence of adhesion, both the Hertz load and displacement depend only on the contact radius. In other words, the Hertz load and displacement are zero when the contact radius is zero, which implies that the stress state between the two spheres is purely compressive.

If we now consider the case when adhesion is present, the Hertz theory does not give a complete picture of the relationships between load, displacement, and contact area. Considering the contact between a sphere and a flat surface (Fig. 4.1c),

the contact area will be larger than that of the Hertz contact under the same applied load because of adhesion. Almost 100 years after the Hertz theory, in 1971, Johnson, Kendall, and Roberts used a similar approach to develop the JKR theory that considered the contact between two bodies when adhesion is present [17]. The relationship between load and contact area has a similar form to the Hertz theory except there are additional load terms to describe the exact relationship between load and contact area when adhesion is present [14–16].

$$\frac{4E^*a^3}{3R} = P + 3\pi GR + \sqrt{6\pi GRP + (3\pi GR)^2}. \tag{4.6}$$

The uniqueness in the JKR theory is that it was developed from a thermodynamic viewpoint. In other words, it is an elastic analysis that assumes all the applied energy is used to cause the change in interfacial contact area. This interfacial energy term required to separate the two bodies is known as the energy release rate (G) and has units of energy per area. Maugis and Barquins [18, 37, 41] reworked the JKR theory to provide a more straightforward relationship by presenting the expressions between energy release rate, load, and contact area in the context of fracture mechanics. The reworked expression relates the energy release rate to the applied load and the change in compliance (inverse to the stiffness of the system) with contact area ($\mathrm{d}C/\mathrm{d}A$) [16, 18, 37, 41].

$$G = -\frac{(P - P_{\mathrm{H}})^2}{2}\frac{\mathrm{d}C}{\mathrm{d}A}. \tag{4.7}$$

Once the exact relationships for the Hertz load (P_{H}) and compliance change with area are known, then (4.7) can be used to predict the energy release rate of an interface. For the contact geometry presented here, at any instance, the compliance C is equivalent to that of a cylinder under axial loading [15, 42]:

$$C = \frac{1}{2E^*a}. \tag{4.8}$$

Substitution of (4.2) and (4.8) into (4.7), we obtain the exact relationship between the material properties of the interface (G and E^*) and contact geometry (R and a).

$$G = \frac{(P - 4E^*a^3/3R)^2}{8\pi E^*a^3}. \tag{4.9}$$

The JKR theory can accurately describe the adhesion of soft materials for systems that are considered as primarily elastic. The typical experimental approach for quantifying adhesion of soft materials is known as contact adhesion test

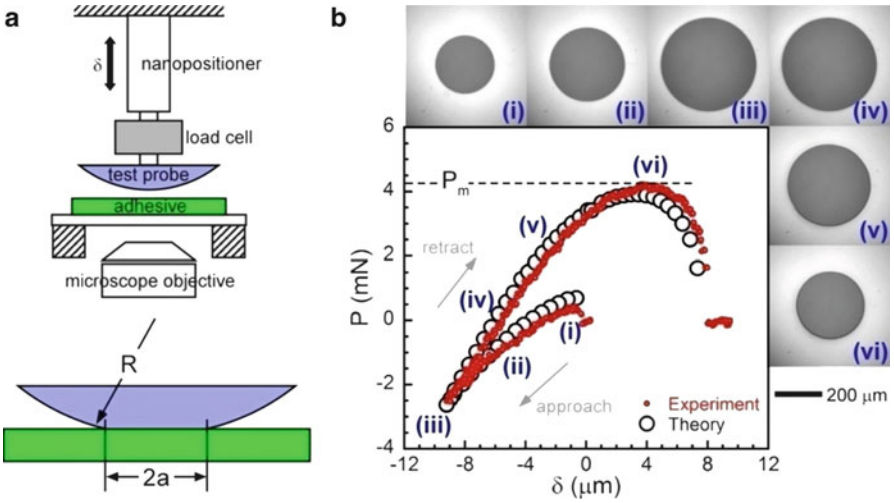

Fig. 4.2 Typical contact adhesion test. (**a**) A hemispherical glass probe is brought into contact with an elastomeric material. The probe is connected to nanopositioner and load cell. The nanopositioner controls the motion of the probe and the load cell records the corresponding load value. The contact area ($A = \pi a^2$) is recorded during the entire adhesion test. (**b**) Load vs. displacement curve for a contact adhesion test between a glass probe and cross-linked polydimethylsiloxane (PDMS). Images show contact area between spherical probe and flat surface. The dark circles define the contact area. Also shown is the JKR fit (4.13)

(Fig. 4.2a) [15–17, 24, 43–46]. This type of test is analogous to measuring the tackiness of a material by pressing our finger into an adhesive and pulling against it. In a typical contact adhesion test, a rigid probe is brought into contact with the soft adhesive of interest. The goal of this test is to form the interface by bringing the probe into contact with the adhesive and then subsequently fracturing the interface by retracting the probe from the adhesive. The approach and retraction motion of the probe is controlled by a nanopostioner, whereas the corresponding load is measured with a load cell. The entire setup is placed on an microscope stage to capture the contact area during the experiments [24, 43, 44].

Figure 4.2b is an illustrative example of the adhesion between a glass probe and cross-linked polydimethylsiloxane (PDMS) adhesive measured by contact adhesion testing. During the first part of the test, the probe is brought into contact with the adhesive to form the interface (approach in Fig. 4.2b) until a defined compressive load is reached. This compressive load can be somewhat arbitrary as long as it is not significantly high to cause nonlinear deformation or significantly low where the contact area is unstable. Past this defined load, the second part of the test occurs where the interface is made to separate by retracting the probe away from the adhesive. To cause interfacial separation, a tensile load is required to cause failure. Specifically, a maximum tensile load, often referred as P_{m}, develops prior to complete separation,

if adhesion is present. For this contact geometry, the maximum tensile load was originally derived by the JKR theory and is defined by [14, 16]:

$$P_{\mathrm{m}} = \frac{3}{2}\pi G_{\mathrm{c}} R. \tag{4.10}$$

There are several interesting aspects of (4.10). First, P_{m} is independent of E^*. Thus, the only material property P_{m} is related to is G_{c}. Second, this maximum load is related only to R and independent of A. Therefore, (4.10) provides a quick assessment of G_{c} if R is known and P_{m} is measured. For most soft materials that is characterized as primarily elastic, (4.10) gives quite reasonable values of G_{c} [24, 35, 45, 47]. However, we caution that it is more accurate to use (4.9) to quantify G_{c}. Additionally, (4.10) appears to contradict with our previous discussions of load and contact area. However, it was actually derived by the JKR theory as presented in (4.6) [17] and is self-consistent. The exact derivation of (4.10) will be discussed in the next section.

One final note we would like to make pertains to the experimental approach. So far, we have only discussed the contact between a hemispherical probe and a flat substrate. Another testing geometry often used is the contact between a flat cylindrical punch and a flat substrate. The advantage in this approach is that the stress distribution underneath the punch is significantly more simple than the hemispherical contact regardless of adhesion [14]. The difficulty of the approach lies in using it experimentally because one must ensure that the punch and the substrate is in uniform contact across the surface to maintain a uniform stress profile. Since this probe develops a uniform stress profile, (4.9) for a flat punch on a flat substrate is [16],

$$G = \frac{P^2}{8\pi E^* a^3}. \tag{4.11}$$

Determination of Material Properties: $\mathbf{E}^*$ *and* $\mathbf{G}_c$

To determine the material properties of the interface using the JKR theory, Shull and coworkers [15, 16] provided a thorough discussion on the fracture mechanics treatment originally presented by Maugis and Barquins [37, 41]. In this section, we briefly go through Shull's approach to extrapolate E^* and G_{c} of the interface [15, 16].

The basic assumption in this fracture mechanics treatment is that the interface is characterized as primarily linear elastic. Then, we can determine the C of the interface by the following relationship [16]:

$$C = \left.\frac{\delta_1 - \delta_2}{P_1 - P_2}\right|_a, \tag{4.12}$$

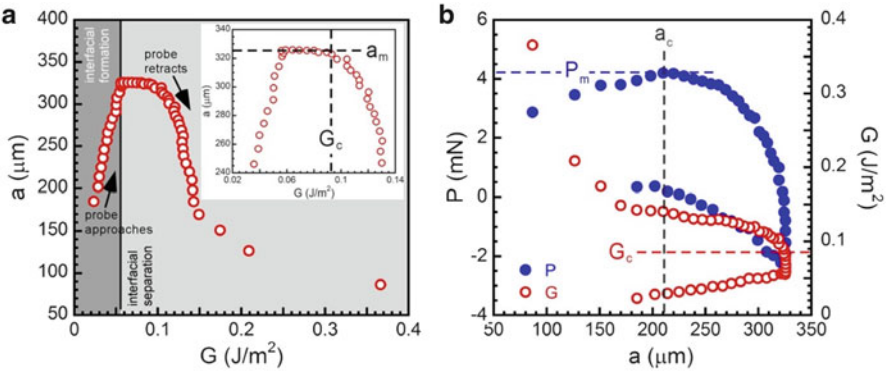

Fig. 4.3 (**a**) Relationship between G and a for the adhesion of PDMS flat film and a glass hemispherical probe. The inset illustrates the extrapolation of G_c when a advances. (**b**) Relationship between P_m and a_c

where the displacements (δ_1, δ_2) and loads (P_1, P_2) are directly obtained from the tack curve of a contact adhesion test. Equation (4.12) is valid when there is no change in a when δ_1 and P_1 reaches δ_2 and P_2, respectively. This condition occurs, if we assume that adhesion is not present at δ_1 and P_1 (Hertzian contact), then adhesion is present at δ_2 and P_2 to maintain the same a. In other words, $\delta_2 = \delta$ and $P_2 = P$. Based on these assumptions, we can relate E^* to P, δ, and a by substituting (4.3) and (4.8) into (4.12).

$$\delta = \frac{a^2}{3R} + \frac{P}{2E^* a}, \tag{4.13}$$

where δ and P are the displacement and load values measured from contact adhesion, respectively. We can fit (4.13) to the load–displacement curve obtained from a contact adhesion test to predict E^*. The results for this fitted curved are overlaid onto the load–displacement curve as shown in Fig. 4.2b. In this case where the modulus of the glass is orders of magnitude greater than that of the soft PDMS, this process directly determines the elastic modulus of the PDMS because $1/E^* = (1-\nu^2)/E_{PDMS} = 1/E_{PDMS}{}^*$. The best fit value of $E_{PDMS}{}^*$ is 1.6 MPa, which is similar to that reported using dynamic mechanical analysis [47].

Once the elastic modulus is obtained, (4.9) can be used to determine the energy release rate, G. The results of G as a function of a for the PDMS–glass system is shown in Fig. 4.3. Typically, G is plotted as the dependent variable that changes as a function of a. In reality, G is the energy supplied to cause the contact area to change. Therefore, we reverse the arrangement to illustrate how the applied energy changes the contact area of the interface to extrapolate G_c, which is a materials property that defines the critical driving force for changes in the interfacial contact.

Specifically, Fig. 4.3 allows us to extrapolate G_c experimentally by considering the interfacial separation as a dynamic process involving stability of the contact area. The stability of the interface is related to the applied values of P or δ, and the stability can be inferred by visualizing contact radius, a. In the loading portion of the test (approach in Fig. 4.2b), a grows in dimensions until a_m is reached. Upon establishing this maximum contact area, the probe withdraws from the interface (retract in Fig. 4.2b) which leads to a decrease in a. Based on the Hertz theory, we would expect a progressive decrease in a as the probe is withdrawn. An interesting observation is that due to adhesion, a does not decrease in this expected manner. Instead, a remains at the value of a_m until a critical value of G is reached. This critical point of G is the G_c typically reported for soft polymer adhesives. Physically, it establishes the stability point of the contact area. Prior to reaching G_c, the crack is stable because there is insufficient energy to advance the crack ($G < G_c$). In order for a to decrease, G has to continue increasing until G_c can be reached. Past this critical value of G, there is sufficient energy to advance the crack as indicated by Fig. 4.3a ($G \geq G_c$). Beyond this point, a decreases with G until the interface completely separates. Due to this requirement, we can consider G_c for polymers as a kinetic property rather than a thermodynamic one since this process is path dependent; a "build-up" of sufficient energy at the crack tip is required to drive the movement of the crack. Additionally, as this point is an extrapolated quantity where we assume that a suddenly reduces from a_m, great care must be taken to ensure that there is sufficient sets of G and a values collected from the adhesion test.

This G consideration as a function of a can also allow us to understand the relationship between P_m and G_c from (4.10). Figure 4.3b is a composite plot of P vs. a, and G vs. a. This plot links the two curves together by the contact area, which defines a critical contact radius (a_c). The meaning of a_c is a critical contact radius when the contact area is stable. Prior to reaching a_c ($a > a_c$), the contact area is stable because more energy is needed to cause the contact area to reduce. After a_c is reached ($a < a_c$), the contact area is no longer stable because there is already an excess of applied energy and the contact area will self-propagate to cause separation. If we first consider the P vs. a, the point of P_c occurs when $dP/da = 0$. When we evaluate (4.9) using this crack stability condition, it leads to the relationship for a_c:

$$a_c = \left(\frac{9\pi G_c R^2}{8E^*}\right)^{1/3}. \tag{4.14}$$

Substitution of (4.14) into (4.9) leads to (4.10). One interesting point to make in Fig. 4.3b is that when we evaluate G at a_c, it is slightly greater than the G_c. This difference is due to the sensitivity of G_c to crack velocity changes for polymer interfaces and will be discussed in "Size-Scale of Energy Dissipation Within Contacting Region" Section. Therefore, (4.10) should only be used to estimate G_c and not be treated as an absolute quantity.

Application of Contact Mechanics

Biomaterials

In the field of biomaterials, cells and material constructs are often combined to provide replacement or improvement of biological functions in the human body [48–52]. In general, cells and material constructs must have or provide specific mechanical properties to facilitate proper functioning [48–50]. Thus, understanding and measuring the mechanical properties of these materials are critical to the design of biomaterials as suitable replacement materials. From a materials perspective, many of these materials can be considered as very soft elastic solids. Thus, the contact mechanics theory discussed in the previous sections is applicable to describe the mechanical properties of biomaterials. In the next three sections, we will present examples on the application of contact mechanics to characterize the properties of cells, organs, and contact lenses.

Adhesion of Cells

From a materials perspective, living cells can be considered as a very soft elastic solid. Therefore, Hertz and JKR theories provide a rough description of the mechanical properties of a cell when it adopts well-defined shapes. Chu et al. used micropipetting to contact and to separate murine sarcoma S180 cells (Fig. 4.4) [53]. These cells do not adhere spontaneously. They were made to adhere through a depletion effect in the suspending medium (highly concentrated dextran solution). In their test, the cells were attached to the tips of micropipettes and were brought into contact by pressurizing the micropipettes. After the cells adhered, the micropipettes were pulled apart. During this process, the separation force was estimated from the last aspiration pressure. The adhesion energy (G), the upper limit of G_c, was estimated from the separation force (4.10).The change of contact radius during the separation process was measured and the elastic modulus ($K = 4/3E^*$) was estimated using (4.6). A constant value of G was used in this estimation. Despite this simplification, the estimated elastic modulus of the cells of 3,500 $\pm$ 1,500 Pa is similar to the values reported in literature. The applicability of JKR theory requires a small deformation with a finite contact area at separation. It was hypothesized that the cytoskeleton provided the cells with a 3D structure, which was sufficiently elastic and had a sufficiently low deformability.

Local Mechanics of Soft Tissue

Measuring the local mechanical properties of tissue in vivo is critical to understanding their complex and heterogeneous organization with itself as well as the surrounding materials. This understanding is not only important in tissue engineering applications, but is also crucial for understanding how the properties of tissue change

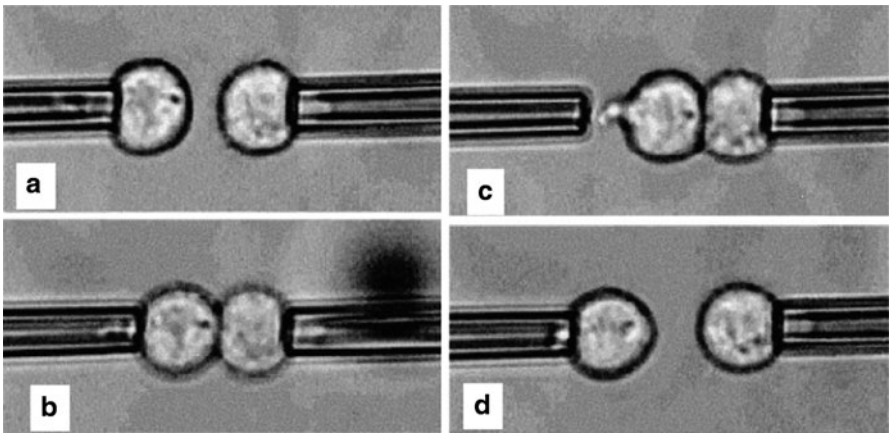

Fig. 4.4 Adhesion between two murine sarcoma S180 cells quantified using micropipette aspiration, for different concentrations of the suspending dextran medium [53]. (**a**) The cells were held under weak aspiration. (**b**) The cells were brought into contact and they adhered after 1 s of contact. The aspiration pressure of the right micropipette was then increased, and that pipette was moved to the right at an approximate velocity of 20 μm/s. During this process, the left cell, which was tightly adhered to the right cell could leave the left micropipette (**c**), or the two cells separated (**d**). The cell separation force was estimated from the final aspiration pressure. Reproduced by permission of the American Physical Society

with age or progression of a disease. Advanced imaging techniques can map the strain response to an applied stress. However, it is challenging to correlate information to elastic modulus since this requires knowledge of the constitutive relationships between the applied stress and the resultant strain.

Recently, the Crosby group developed a simple technique to measure the local mechanical properties of tissue based on a technique termed cavitation rheology [54, 55]. Strictly speaking, this technique is different from the conventional contact mechanics approaches discussed previously. However, cavitation rheology shares the common feature of characterizing the adhesion and mechanics of an interface. The technique involves forming an elastic instability, i.e., a bubble, within the material by injecting a volume of air or liquid via a syringe needle [54–57]. To form this bubble, a critical pressure must be reached to overcome (1) the mechanical resistance of the local tissue surrounding the bubble and (2) the energy penalty to forming this new bubble–tissue interface. Therefore, by measuring the critical pressure (P_c) required to develop a bubble within the tissue, the modulus of the tissue (E) and the surface tension between the bubble and tissue (γ) can be determined [55].

$$P_c = \frac{5}{6}E + \frac{2\gamma}{r}. \tag{4.15}$$

Experimentally, a series of cavitation experiments with different needle radii are performed that allows for the extrapolation of the material properties. By relating the critical pressure to the radius of the needle, a linear relationship can be

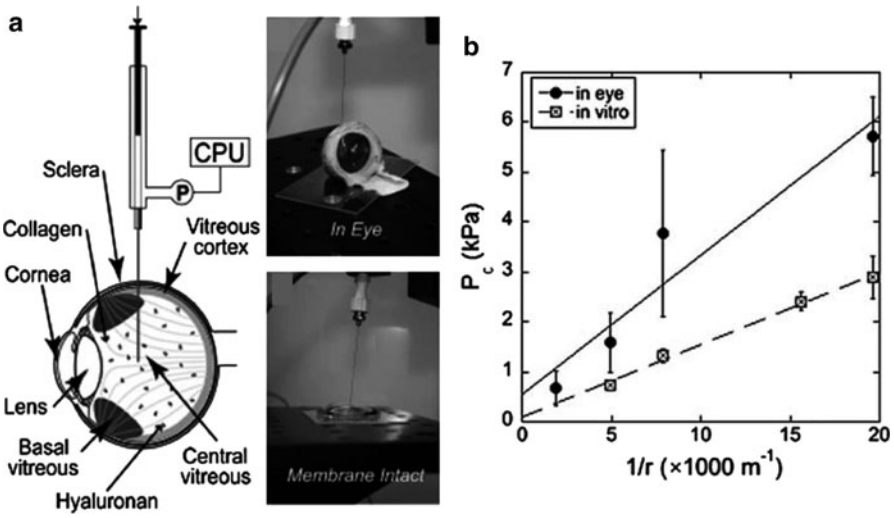

Fig. 4.5 (**a**) Cavitation rheology measurement of the bovine eye [54]. The micrographs illustrate the approach to measure the critical pressure to cause a cavity in the eye (*top image*) and the vitreous membrane (*bottom image*). (**b**) The elastic modulus of the eye can be determined by relating the critical pressure (P_c) to cause cavitation as a function of the needle radius (r). Specifically, the elastic modulus is directly related to the critical pressure at infinitely large needle radius ($1/r \rightarrow 0$). Reproduced by permission of the Royal Society of Chemistry

established as defined by 4.15 [55]. The elastic modulus of the material is directly related to the critical pressure for an infinitely large needle radius ($1/r \rightarrow 0$) and the surface tension can be obtained from the slope of the linear curve.

This approach has been demonstrated to characterize a variety of biomaterials including soft hydrogels and bovine eyes (Fig. 4.5) [54–57]. Depending on the specific materials, the elastic modulus values measured ranged from 600 to 5,000 Pa, which is consistent with literature values. The key advantage in the technique is that the local mechanical properties can be easily probe via (1) changing the needle size or (2) changing the penetration depth of the needle. Since the length scale of the measurement is related to the bubble size, reducing the radius of the needle (r) will facilitate more localized measurements. If depth profiling of the tissue is needed, this can be easily achieved simple by positioning the needle to the correct location within the tissue.

Pressure Sensitive Adhesives

Pressure sensitive adhesives (PSAs) are soft polymers whose adhesive properties are sensitive to the applied pressure [58]. Scotch Tape® is the most common example of PSAs; however, PSAs are increasingly being used as transdermal drug delivery patches [6–8]. Unlike structural adhesives or glues, PSAs can be

reused as the mechanisms of adhesion are determined primarily by secondary bonding (i.e., van der Waals). Because the properties of PSAs are reversible, the theory of JKR is appropriate to describe their adhesion, and many researchers have used the theory to describe "model" PSAs [59–61]. Most of these materials are lightly cross-linked polymers with a low glass transition (T_g) because the mobility of the polymer chains facilitate flow and good wetting with a substrate. Some examples include silicone rubbers, thermoplastic elastomers, and chemically cross-linked acrylates [58]. These materials are ideal materials as PSAs since a PSA is designed with a balance of viscous and elastic properties. To incorporate this balance of viscous and elastic characteristics, most PSAs are designed with some degree of viscoelasticity. The interfacial strength develops because the adhesive is soft enough to wet the substrate and has sufficient elasticity to resist deformation when stress is applied to the cause separation.

Because PSAs are quite thin in film thickness (~10 μm), it is difficult to use bulk rheological measurement techniques to quantify their viscoelasticity properties. One interesting approach to measuring the viscoelasticity of thin PSAs was demonstrated by Crosby et al [59]. The novelty in the approach is that it takes advantage of adhesion between a rigid indenter and the PSA as a means to apply a small oscillatory strain. Specifically, the approach involves bringing the probe into contact with the PSA and compressing it to a predefined compressive load (P_o). At this fixed load, the probe was sinusoidally oscillated at small displacements such that the contact area was kept constant. This is the key aspect of the technique; the contact area must be kept constant in order for a constant stress to be applied, which is facilitated by adhesion near the periphery of the contact area. When this condition is satisfied, then the applied displacement is:

$$\delta = \delta_o \sin(\omega t), \tag{4.16}$$

where, δ_o is the initial displacement amplitude and ω is the frequency. The resultant load is related to the frequency and phase lag (ϕ) by,

$$P = P_o \sin(\omega t - \phi). \tag{4.17}$$

By measuring the phase lag between the applied displacement and the resultant load, the loss and storage moduli were calculated. The complex modulus $E(\omega)$ can be determined by the compliance of the interface (4.12) and is the sum contribution of the storage modulus E' and loss modulus E''.

$$\begin{aligned} E(w) &= E' \sin(\omega t) + iE'' \cos(\omega t) \\ &= (E(w) \cos \phi) \sin(\omega t) + i(E(w) \sin(\phi)) \cos(\omega t). \end{aligned} \tag{4.18}$$

A good agreement was obtained between the bulk rheology and contact mechanics data [59, 62]. The benefit of performing this contact mechanics-based approach is that the technique can be applied to thin materials, where traditional measurements are difficult to implement.

Effects of Geometric Confinement

Since most PSAs are quite thin in thickness, the relationships presented in "Determination of Material Properties: E^* and G_c" section do not accurately their material properties since these relationships were developed for materials that are considered semi-infinite in dimensions. To properly describe the properties of thin PSAs, correction factors have been developed that properly relates the load, displacement, and compliance to the contact area [15, 16]. Here, we briefly go through the specific relationships because the approach is not limited to PSAs but to other materials whose thickness is sufficiently thin to be considered "geometrically confined" [15, 16].

The definition of geometrically confined in this discussion refers to the condition where the thickness of the film is commensurate with or less than the contact radius during deformation. In our previous discussions of the Hertz and JKR theories, the relationships for displacement and load assume that the deformation of a PSA to be semi-infinite in dimensions. Specifically, the region of material under deformation, as described by the contact radius (a), is significantly smaller than the thickness (h) of the material itself ($a << h$). Thus, the stiffness of the substrate does not affect the properties at the probe–PSA interface since the stress and strain fields do not couple with the properties of the substrate. When the contact radius is commensurate with the PSA thickness ($a \sim h$), the deformation behavior cannot be described by the Hertz and JKR theories since the relationships between load, displacement, and contact area are affected due to contributions by the underlying rigid substrate.

This geometric confinement effect is described by the ratio of a/h and has a significant impact on the separation behavior of PSAs. A variety of separation mechanisms can develop depending on the degree of geometric confinement. Therefore, a PSA is designed with a specific thickness that aims at developing a particular separation mechanism that aids its performance. Some examples of separation mechanisms besides simple interfacial separation ("Hertz and JKR Theories" section) include fingering instability and bulk cavitation. Both of these separation mechanisms are unique in that a significant portion of the applied energy is dissipated within the bulk of the adhesive via formation of cavities or localized yielding. Thus, the Hertz and JKR theories cannot adequately describe their mechanical behavior. As this subject is beyond the scope of this chapter, we recommend the following references for the interested reader [58, 60, 63, 64].

For PSAs that separate by simple interfacial separation, a significant portion of the applied energy is supplied to cause separation at the probe–PSA interface. Thus, a modified version of the Hertz and JKR theories can be used to describe the adhesion and mechanical properties of these materials. We can understand the effects of geometric confinement by comparing the load versus contact radius relationships for a PSA considered to be geometrically unconfined versus one that is geometrically confined. In the geometrically unconfined case, establishing contact radius a requires that a load of P_H (4.2) be reached. To reach the same a for the geometrically confined case, a load larger than P_H is required. Specifically, the increase in load relative to the Hertz load is defined as [15]:

$$P\left(\frac{a}{h}\right) = P_{\mathrm{H}} \times f_{\mathrm{P}}\left(\frac{a}{h}\right) = \frac{4E^{*}a^{3}}{3R} \times \left(1 + \beta\left(\frac{a}{h}\right)^{3}\right), \tag{4.19}$$

where β is 0.33 and 0.15 for the friction and frictionless interface, respectively. The corresponding displacement change relative to the Hertz displacement is defined as [15]:

$$\delta\left(\frac{a}{h}\right) = \delta_{\mathrm{H}} \times f_{\delta}\left(\frac{a}{h}\right) = \frac{a^{2}}{R} \times \left(0.4 + 0.6\exp\left(\frac{-1.8a}{h}\right)\right). \tag{4.20}$$

The compliance of the interface now becomes,

$$\begin{aligned} C\left(\frac{a}{h}\right) &= \frac{1}{2E^{*}a} \times f_{\mathrm{C}}\left(\frac{a}{h}\right) \\ &= \frac{1}{2E^{*}a} \times \left(1 + \left(\frac{0.75}{(a/h) + (a/h)^{3}} + \frac{2.8(1-2\nu)}{(a/h)}\right)^{-1}\right)^{-1}. \end{aligned} \tag{4.21}$$

Generally, PSAs can be approximated as soft incompressible solids ($\nu = 0.5$), thus, the compliance correction function can be simplified to:

$$f_{\mathrm{C}}\left(\frac{a}{h}, \nu = 0.5\right) = \left(1 + 1.33\left(\frac{a}{h}\right) + 1.33\left(\frac{a}{h}\right)^{3}\right)^{-1}. \tag{4.22}$$

The steps to determining the elastic modulus and energy release rate of the geometrically confined PSA are identical to the steps outlined in "Determination of Material Properties: E^{*} and G_{c}" section. To determine the elastic modulus, we fit the load–displacement curve using the following displacement relationship.

$$\delta = \frac{a^{2}}{R} \times f_{\delta}\left(\frac{a}{h}\right) + \frac{f_{\mathrm{C}}(a/h)}{2E^{*}a} \times \left(P - \frac{4E^{*}a^{3}}{3R} \times f_{\mathrm{P}}\left(\frac{a}{h}\right)\right). \tag{4.23}$$

Once the elastic modulus is extrapolated, the energy release rate can be determined. To properly determine the energy release rate for a geometrically confined PSA, these relationships must be substituted into (4.6). For an incompressible PSA, G is defined as:

$$\begin{aligned} G\left(\frac{a}{h}\right) &= \frac{\left(P - (4E^{*}a^{3}/3R) \times f_{\mathrm{P}}(a/h)\right)^{2}}{8\pi E^{*}a^{3}} \\ &\quad \times \left(\frac{0.56 + 1.5(a/h) + 3(a/h)^{3}}{\left(0.75 + (a/h) + (a/h)^{3}\right)^{2}}\right). \end{aligned} \tag{4.24}$$

Generally, the full friction condition ($\beta = 0.33$) is used to describe the adhesion of an interface. It is noted that for $a/h << 1$, all the confinement relationships reduces back to the original relationships for the geometrically unconfined system.

Contact Lenses

Hydrogels are polymer-based materials consisting of either physically or chemically cross-linked polymer chains that are highly soluble in water [48–50]. Because the mechanical and chemical properties can be tuned to mimic the properties of human tissue, they have been widely used in biomedical engineering as tissue scaffolds, drug delivery vehicles, as well as contact lenses [48–50]. Hertz and JKR contact mechanics have been applied to investigate the adhesion and mechanical properties of hydrogels [10–12, 55]. In this section, we discuss the application of contact mechanics to study the adhesion and mechanical behavior of contact lenses.

Contact lenses are typically made of poly(2-hydroxyethyl methacrylate) (polyHEMA) cross-linked with ethylene glycol dimethacrylate (EGDMA) [10, 11]. Because the lens has to secure to the cornea of the human eye, the comfort and general performance of contact lenses are directly linked to the adhesion, friction, and mechanical properties of the lens–cornea interface. Additionally, the biological responses of contact lenses such as protein adhesion and bacterial infection depend on the mechanical and chemical properties of the interface. Thus, improvements for the contact lens design are dependent upon the proper characterization of the relevant interface, near-interface, and mechanical properties.

Local Mechanics of Contact Lenses

The previous sections described the measurement of mechanical properties of biomaterials on the macroscopic length scale and they can be used to characterize the properties of contact lenses. For characterization of properties on the nanometer length scale, similar contact mechanics approaches can also be adapted as well. For example, Kim et al. used atomic force microscopy (AFM) to study the surface properties of contact lenses [10]. Two types of contact-mode cantilevers, V-shaped, silicon nitride cantilever with a tip curvature of 50 nm and polystyrene bead ($R = 2.03$ μm) affixed to a V-shaped, silicon nitride cantilever were used to perform contact adhesion tests on the polypropylene supported contact lenses (Fig. 4.6). Experiments were performed in both air and saline solution. The elastic modulus and adhesion of the contact lens surface were calculated from the force vs. displacement curves obtained by recording the normal deflection signal of the cantilever during the tip approach and retraction. During these tests, the contact areas could not be measured. Instead, the authors used Hertz mechanics for the contact of a sphere and a plane (4.2 and 4.3) to estimate the elastic modulus.

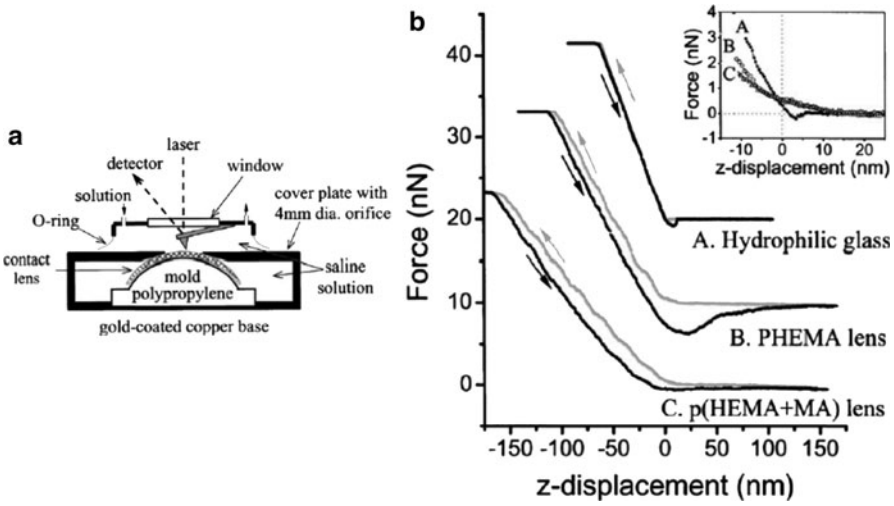

Fig. 4.6 **(a)** AFM setup to measure surface and mechanical properties of contact lenses. **(b)** Force vs. displacement curves of (**A**) hydrophilic glass (control) and two contact lenses, (**B**) pHEMA lens, and (**C**) p(HEMA + MA) lens. Experiments were performed in saline solution using a PS bead tip. Approach is shown in *gray*, whereas retraction is shown in *black*. The magnified view of the approach curves near the contact region is shown in inset. Note than sign convention used in these experiments are opposite of Fig. 4.2. Copyright Wiley-VCH Verlag GmbH & Co. KGaA. Reproduced with permission [10]

The estimated values are 1.347 ± 0.13 MPa for the pHEMA lens and 0.477 ± 0.04 MPa for the p(HEMA + MA) lens. These values are in agreement with the bulk elastic moduli of these contact lenses in saline solution.

The minimum in the force–displacement curve was used as a descriptor for adhesion between the PS bead tip and the contact lens surface (P_m in the earlier section). From the minimum in the force–displacement curve, G, was estimated using (4.10), $G = P_m/(3\pi R/2)$, where R is the radius of the PS bead. We should comment that G represents the upper limit for G_c of the interface. For the hydrophilic glass/PS bead contact in saline solution, P_m was ~0.9 ± 0.2 nN and G was ~ 0.2 mJ/m^2. These results are within reasonable values for the glass/organic surface contact in water. For the pHEMA lens/PS bead sample, P_m was 3.7 ± 0.4 nN and G was ~ 0.8 mJ/m^2. The p(HEMA + MA) lens/PS bead sample did not show significant adhesion in the saline solution. In saline solution, the adhesion to a polystyrene surface was much lower for the ionic-hydrogel (p(HEMA + MA)) contact lens than the neutral-hydrogel (pHEMA)contact lens. This reduction in adhesion was hypothesized to be attributed to the interactions of ionizable carboxylic acid groups at the p(HEMA + MA) lens surface with water. Absence of ionizable carboxylic acid group at pHEMA lens surface caused the expulsion of water at the PS/lens interface, which resulted in strong hydrophobic interaction.

Limitations of the JKR Theory

As evidenced by the numerous publications that reference the pioneering work by Johnson, Kendall and Roberts, many researchers have utilize the theory of JKR to describe numerous contact mechanics problem where adhesion plays a significant role. While this theory is applicable to a range of contact mechanics problems of soft materials, there are some instances where it is difficult to apply the JKR theory.

Size-Scale of Energy Dissipation Within Contacting Region

As discussed previously, the JKR theory is an energy balance approach that relates G to measurable quantities of P, δ, and a. This theory assumes that the deformation behavior can be described by linear elastic fracture mechanics, and the relationships between P, δ, and a can be easily defined. However, the materials where adhesive interactions are important, i.e. soft deformable polymers, are inherently viscoelastic. This has important implications in quantifying polymer adhesion since viscoelastic effects imply that the deformation process is history-dependent.

If the deformation processes are dominated by global viscoelastic effects, i.e. large-scale viscoelasticity, a significant amount of the elastic energy supplied is dissipated by deforming the bulk polymer rather than applying it to cause interfacial separation. As a result, G cannot be used to describe adhesion because the relationships between the measured quantities of P, δ, and a cannot be easily described using linear elastic theory. Instead, their specific relationships will depend on the viscoelastic response of the polymers of interest; whether they undergo creep or stress relaxation, which would also be affected by the type of adhesion test performed. In this case when "large-scale viscoelasticity" dominates the deformation processes, it is more appropriate to quantify adhesion in terms of the total energy rather than the energy release rate. As this topic is beyond the scope of the chapter, we refer the reader to the following references [58–60, 63–67].

The use of G to describe adhesion is only appropriate when the energy dissipated is confined within a region that is small in comparison to the volume of interfacial material deformed ($\approx a^3$). If this dissipation region is small in comparison to the deformation volume, then the elastic analysis described by the JKR theory is still adequate, even though viscoelastic contributions may be important. Viscoelastic contributions confined to this dissipation zone are defined as "small-scale viscoelasticity." Because the region around the crack tip experiences the highest tensile stresses, we have effectively assumed a specific viscoelastic behavior for the materials within this small region. Specifically, elastic modulus within this dissipation zone is considered to have decayed to the long-time, steady-state limit of the modulus. In this case, G can be clearly defined and appropriately used to quantify adhesion. We note that this concept of "small-scale viscoelasticity" does not assume that the material is behaving elastically. It merely assumes that the contributions due to viscoelasticity are confined to a highly localized region that

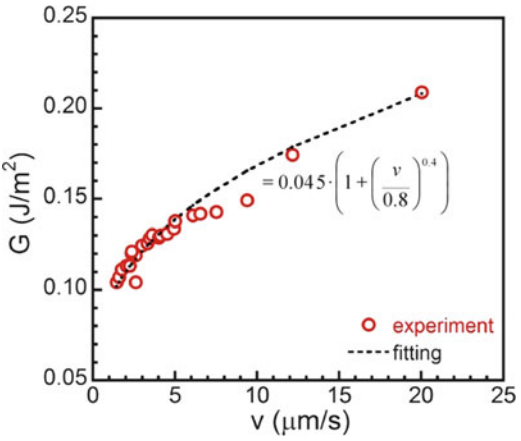

Fig. 4.7 Relationship between G and v for the adhesion of PDMS flat film and a glass hemispherical probe

can be appropriately described by G. As a result, it leads to an empirically derived relationship that links the energy release rate for the interface to the crack-tip velocity (v). Similar to fracture mechanics terminology, the contact perimeter can be defined as crack [16, 68].

$$G = G_{\mathrm{o}} \times \Phi(v) = G_o\left(1 + \left(\frac{v}{v^*}\right)^n\right). \tag{4.25}$$

G_{o} is the threshold adhesion energy, v^* is the characteristic crack velocity, and n is an adjustable parameter, which determines the shape of the curve. The function $\Phi(v)$ captures the dissipation processes near the crack tip and v is defined as:

$$v = -\frac{\mathrm{d}a}{\mathrm{d}t}. \tag{4.26}$$

Figure 4.7 illustrates the empirical relationship between G and v for the same PDMS system presented in Fig. 4.2. The value of G_{o} is extrapolated to be 0.045 J/m^2. This value corresponds to the energy required to cause separation when the crack velocity approaches zero, i.e. a value that approaches the thermodynamic limit of the energy release rate (w) [45]. We note that the change in v is determined based on the measured a with a constant cross-head velocity. The practical implication of (4.25) is that if two adhering surfaces are separated slowly, it will experience lower adhesion compared with the separation at higher rates. For a practical application of this result, if one wishes to remove a band-aid from skin, it would be advantageous to peel it at a very slow speed to minimize the adhesion between the skin and the band-aid.

Descriptors of Adhesion

In addition to large-scale viscoelasticity, many commercial PSAs can undergo irreversible separation processes such as bulk cavitation or fingering instabilities. These mechanisms of debonding are typically observed when we peel a piece of tape from a surface where long and slender fibrils are stretched to large extensions during separation. Because these deformation processes are history-dependent events related to the bulk properties of the adhesive, it is difficult to use the JKR theory to describe the adhesion of these materials. Hence, other adhesion performance metrics is used.

The use of these adhesion metrics is also prevalent in the field of biomimetic or patterned adhesion (discussed in the following section) primarily because the relationships between P, δ, and a are not straightforward. Thus, it is difficult to quantify the G for a discontinuous interface. Table 4.1 summarizes some of the common adhesion descriptors used in the literature.

While most of these parameters are not fundamental material properties, however, all of them have some relationship to G. For example, it is very common to use normalized maximum separation load ($P_{m,n}$) as a metric to relate the maximum separation load between a patterned surface versus a smooth analog. For a smooth interface, P_m can be derived from the JKR theory and can be experimentally extrapolated from the load–displacement curve of an adhesion test by taking the maximum load measured during interfacial separation. Another adhesion descriptor is the work of adhesion (W_{adh}), which is different from the thermodynamic work of adhesion, w. Experimentally, W_{adh} is calculated by integrating the load–displacement curve normalized by the maximum contact area. This energy descriptor is especially useful for polymer interfaces whose adhesion is dependent on deformation history. Specifically, for interfaces where significant hysteresis develops between the loading and unloading cycle of the test, W_{adh} will be a non-zero value. Thus, these descriptors should not be discounted, but one should be aware of their physical meaning.

To circumvent the difficulty in quantifying G for a patterned interface, the recent work by Vajpayee et al. have provided an alternative approach to extrapolate G without utilizing the Hertz and JKR theories [69]. The approach still assumes linear elastic fracture mechanics. However, the uniqueness of the approach lies in the treatment of the dynamic process for a and the subsequent determination of the energy release rate without developing exact relationships between P vs. a and δ vs. a. The interested reader should refer to the following reference [69].

Topography and Adhesion

In the previous sections, we have discussed the adhesion of smooth surfaces. In real world problems, the surfaces and interfaces are not necessarily smooth, and the presence of random, periodic, or hierarchical roughness has significant implications

Table 4.1 Summary of adhesion descriptors for a spherical probe

	Descriptor	Definition	Pros	Cons
Load	P_{m}, maximum separation load	$\frac{3}{2}\pi G_{\mathrm{c}} R$	• Simple metric	• Extensive property • Ignores contact area
	$P_{\mathrm{m,n}}$, normalized maximum separation load	$\frac{P_{\mathrm{m,material}}}{P_{\mathrm{m,smooth}}}$	• Useful comparison with Smooth interface	• Extensive property • Ignores contact area
	σ_{m}, maximum separation strength	$\frac{3/2\pi G_{\mathrm{c}} R}{\pi a^2}$	• Simple metric	• Extensive property
	$\sigma_{\mathrm{m,n}}$, normalized maximum separation strength	$\frac{\sigma_{\mathrm{m,material}}}{\sigma_{\mathrm{m,smooth}}}$	• Useful comparison with smooth interface	• Extensive property
Energy	G_{c}, critical energy release rate		• Intensive property • Classic descriptor	• Cannot be rigorously implemented for viscoelastic effects and patterned interfaces
	U_{adh}, energy of adhesion	$\oint P\mathrm{d}\delta$	• Accounts for total energy including viscoelastic effects	• Extensive property • Ignores contact area
	W_{adh}, work of adhesion	$\frac{\oint P\mathrm{d}\delta}{\pi a^2}$	• Accounts for total energy per area including viscoelastic effects and patterned interfaces	• Extensive property • Depends on contact area
	$W_{\mathrm{adh,n}}$, normalized work of adhesion	$\frac{W_{\mathrm{adh,material}}}{W_{\mathrm{wadh,smooth}}}$	• Useful comparison with smooth interface	• Extensive property • Depends on contact area

on the adhesion of an interface. In the following sections, we provide insight into the mechanisms that lead to changes in adhesion as a function of topography.

Contact of Randomly Rough Surfaces: The Theory of Fuller and Tabor

Often times, a surface consists of topographic features or asperities that are statistical in their dimensions and distribution. Its relationship to adhesion is quite complex because the nature of the roughness can enhance or suppress adhesion,

which is ultimately related to how the asperities couple individually or collectively to interact with the other surface. However, this topic is quite relevant in real world applications. Specifically, Post-it notes actually take advantage of statistical roughness as a way to tune the adhesion and release properties of the material. To give an overview on the effects of statistical roughness on adhesion of soft materials, we briefly discuss the theory of Fuller and Tabor [19] to explain these effects.

In the theory, the rough surface is described as a surface consisting of N asperities that make contact with a smooth rigid plane over a nominal area A_o. Each asperity is approximated as an individual elastic hemisphere with radius R. The heights z of the asperities are measured with respect to a datum level. The separation of each individual asperity is assumed to be uncoupled. Due to the presence of adhesion, the separation of a single asperity can be determined using (4.13):

$$\delta = \frac{2E^* a^3 + 3PR}{6E^* a^3 R}. \tag{4.27}$$

The maximum separation force is again defined by (4.10) and associated maximum displacement (δ_c) can be determined by substituting (4.10) and (4.14) into (4.27).

$$\delta_c = \left(\frac{3}{16}\frac{P_m^2}{E^{*2}R}\right)^{1/3}. \tag{4.28}$$

Because the feature size scales of the asperities are statistical, the total separation load and displacement over the area A_o involves the contributions from all the asperities. From JKR theory, the amount of compressive or tensile load of each asperity will depend on its dimensions. Therefore, a relative or dimensionless separation force and displacement must be defined for each asperity, which enables the determination of the relative change in adhesion as a function of roughness collectively. For a single asperity, the dimensionless load and displacement relationships can be established with the aid of (4.27) and (4.6) [18–20].

$$\frac{\delta}{\delta_c} = (3\chi - 1)((\chi + 1)/9)^{1/3}, \quad \chi \geq 0, \frac{\delta}{\delta_c} \geq 3^{-2/3}, \tag{4.29}$$

$$\frac{\delta}{\delta_c} = (3\chi - 1)((1 - \chi)/9)^{1/3}, \quad 0 \leq \chi \leq 1/3, \frac{\delta}{\delta_c} \leq 3^{-2/3}, \tag{4.30}$$

where $\chi = \left(1 - \left(\frac{P}{P_m}\right)\right)^{1/2}$.

Inverting (4.29) and (4.30) we obtain

$$\frac{P}{P_m} = f\left(\frac{\delta}{\delta_c}\right). \tag{4.31}$$

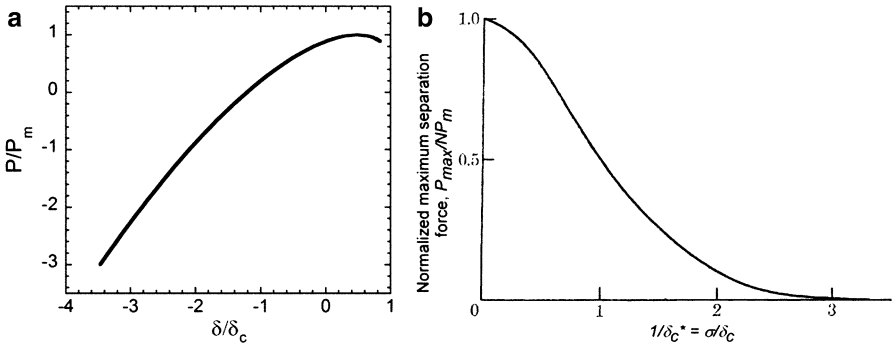

Fig. 4.8 (**a**) Dimensionless force as a function of dimensionless displacement for a single asperity. (**b**) Normalized maximum separation force of random rough surface as a function $1/\delta_c^* = \sigma/\delta_c$. (**b**) is reproduced by permission of Royal Society (Fig. 4.6, ref. [19])

The function is plotted in Fig. 4.8a. It is important to note that similar plot will be obtained if the Fig. 4.2b is presented in the dimensionless form.

An asperity will be in contact with the smooth surface of its height z is greater than a separation distance d. d is the distance between the smooth plane and the datum level. For N asperities within A_o, the probability for n asperities to be in contact with the smooth plane at a distance d is defined as:

$$n = N \int_d^\infty \phi_s(z)\, \mathrm{d}z \tag{4.32}$$

with the probability function, $\phi_s(z) = \left(1/(2\pi)^{1/2}\right) \exp(-z^2/2\sigma^2)$, where σ is the standard deviation of the mean height of the asperities.

Because we are only concerned about the separation process, (4.32) should be modified such that the limits of the integral become:

$$n = \frac{N}{\sigma(2\pi)^{1/2}} \int_{d-\delta_c}^\infty \exp\left(-\frac{z^2}{2\sigma^2}\right) \mathrm{d}z. \tag{4.33}$$

This new lower limit accounts for the asperities that are separated when their separations exceed δ_c. Therefore, the total separation force is the sum of the forces exerted by each asperity (P_i) in contact. Invoking (4.31), the total separation force is:

$$P = N \int_{d-\delta_c}^\infty P_i \phi_z(z)\, \mathrm{d}z = \frac{NP_m}{\sigma(2\pi)^{1/2}} \int_{d-\delta_c}^\infty f\left(\frac{\delta_i}{\delta_c}\right) \exp\left(-\frac{z^2}{2\sigma^2}\right) \mathrm{d}z. \tag{4.34}$$

In dimensionless form, (4.34) becomes:

$$\frac{P}{NP_{\mathrm{m}}} = \frac{1}{(2\pi)^{1/2}} \int_{-\delta_{\mathrm{c}}^{*}}^{\infty} f\left(\frac{\delta^{*}}{\delta_{\mathrm{c}}^{*}}\right) \exp\left(-\frac{1}{2}(\delta^{*} + d^{*})^{2}\right) \mathrm{d}\delta^{*}, \tag{4.35}$$

where $\delta^{*} = \delta/\sigma$, $\delta = z - d$, $\delta_{\mathrm{c}}^{*} = \delta_{\mathrm{c}}/\sigma$, $d^{*} = d/\sigma$. We can compute $P/(NP_{\mathrm{m}})$ as a function of δ^{*} for different values of δ_{c}^{*} using (4.35). From these results, the computed normalized maximum separation force $P_{\max}/(NP_{\mathrm{m}})$ as a function of $1/\delta_{\mathrm{c}}^{*} = \sigma/\delta_{\mathrm{c}}$ is shown in Fig. 4.8b. Here $P_{\max}$ is the maximum separation force for the entire surface. As $P_{\max}/(NP_{\mathrm{m}}) < 1$, the adhesion of a rough surface is lower than that of smooth surface. By rearranging (4.28), we obtain:

$$\left(\frac{\sigma}{\delta_{\mathrm{c}}}\right)^{1/2} = \frac{4}{3^{1/2}} \frac{E^{*}R^{1/2}\sigma^{3/2}}{P_{\mathrm{m}}}. \tag{4.36}$$

This is proportional to the ratio of the Hertzian force required to flatten an asperity of radius R by σ to the adherence force of this asperity. In dimensionless form, we can write [19],

$$\theta = \frac{E^{*}R^{1/2}\sigma^{3/2}}{G_{\mathrm{c}}R}. \tag{4.37}$$

This dimensionless parameter θ is known as Fuller and Tabor adhesion parameter. Fuller and Tabor have shown that adhesion of a rough interface decreases significantly, if $\theta > 10$. Qualitatively, this adhesion parameter describes the decrease in adhesion due to the large distribution of small roughness asperities as captured by the ratio of σ/R. Contrary to the prediction of Fuller and Tabor, Briggs and Briscoe reported an enhancement of adhesion for rough surfaces at certain dimensions of roughness [20]. One final note we like to point out is that this theory is applicable for two planar surfaces where one of the surfaces is rough. In cases where the surfaces are nonplanar, the description of effect of roughness on adhesion is significantly more challenging.

Periodic Roughness: The Principle of Contact Splitting

Another form of roughness is characterized as a topographic surface with asperities that are periodic in spatial arrangement with well-defined dimensions. There are many examples found in Nature that utilizes such periodic roughness to control adhesion [21, 22]. In particular, the footpad of some insects and geckos are decorated with long, fibrillar hyperstructures for the purposes of locomotion (Fig. 4.9) [21, 22]. Depending on the animal species, the fibrils can vary in complexity (sometimes hierarchically arranged), dimensions (fibrils spanning from

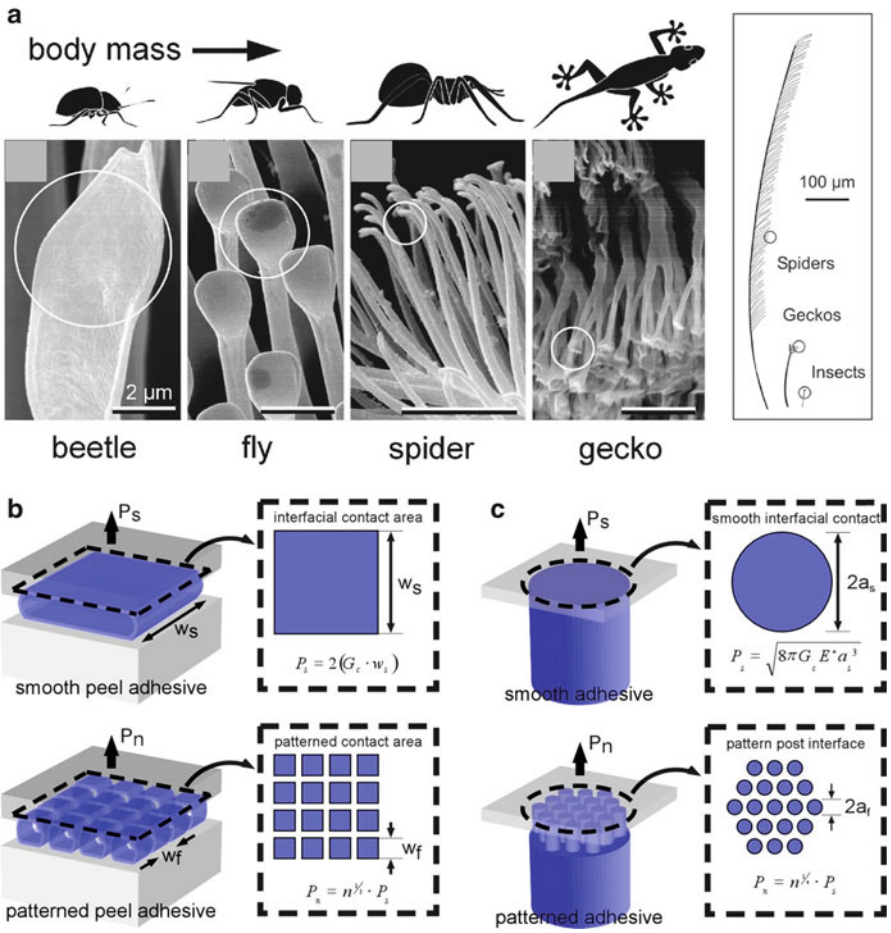

Fig. 4.9 Examples of natural and synthetic attachment structures. (**a**) Hierarchical fibrillar microstructure of the attachment foot pads of the beetle, fly, spider, and gecko. (**b**, **c**) Examples demonstrating the principle of contact splitting. For both peel geometry and cylindrical punch geometry, the separation force of the patterned adhesive (P_n) increases with the total number of split-up contacts (n), which illustrates that the enhancement in strength is associated with the increase in contact line, as opposed to contact area. (**b**) In a peel geometry, $P_n \sim n^{1/2}$. (**c**) In a flat punch geometry, $P_n \sim n^{1/4}$. G_c is critical energy release rate, a_s is the smooth contact radius, E^* is the reduced Young's modulus, and P_s is the separation force for a smooth surface. (**a**) is reproduced by permission of the National Academy of Sciences, USA. Copyright (2003). (**b**, **c**) are reproduced by permission of the MRS Bulletin

nanometers to millimeters in diameter), and material properties. These structures maximize adhesion and release to a variety of rough surfaces while enabling attachment and detachment over millions of cycles. It has been hypothesized that a fibrillar surface enhances adhesion based on the mechanism of "contact splitting" [21, 25, 43]. Here, we will briefly go through the mechanism.

The underlying principle of contact splitting is that a patterned surface can enhance adhesion compared with a smooth surface. The pattern surface does not increase the total contact area, rather, the total contact line per area is enhanced. In order for this mechanism to work, several conditions must be satisfied. First, the individual features are uncoupled with neighboring features during separation to maximize the total contact line. If they are coupled, then the total contact line is reduced. Second, the principle of equal load sharing of the patterns is assumed, i.e., the individual features are all loaded simultaneously. Third, the separation process for each feature can be considered as a crack initiation process. In other words, the separation process of a single feature is considered a stability point of the contact and the perimeter of the feature defines this point. To explain the mechanism, we begin the discussion by performing two adhesion experiments (Fig. 4.9b). The first experiment involves peeling a smooth adhesive with area, $A_s = {w_s}^2$, from a surface. The force required to peel the adhesive is defined by the Kaeble equation (P_s) [70].

$$P_s = 2G_c w_s, \tag{4.38}$$

where w_s is the width of the adhesive. For a constant value of G_c, this expression relates the peel force to the width or contact line of the adhesive during separation. Because there are two contact lines during separation, $P_s \sim 2w_s$. Instead of force, we can express (4.38) in terms of a separation stress (σ_s), which is the force normalized by A_s. Then, we have the following relationship where the separation stress scales inversely with the contact line.

$$\sigma_s = 2G_c \frac{w_s}{A_s} = 2G_c / w_s. \tag{4.39}$$

In the second adhesion experiment, we take the same adhesive except we pattern it by sectioning the adhesive into n smaller squares each with contact area, $A_f = {w_f}^2$. The separation stress of a single square is similar to (4.39). Since all of the adhesive squares separate simultaneously based on the principle of equal load sharing, the separation stress for the total area is dependent on the n number of adhesive squares present.

$$\sigma_n = 2n \frac{G_c}{w_f}. \tag{4.40}$$

To maintain the same total contact area as in the smooth case, we relate the total contact area of the smooth adhesive versus the patterned one by n.

$$n = \frac{w_s^2}{w_f^2}. \tag{4.41}$$

If we take the ratio of (4.40) and (4.39), i.e., σ_n/σ_s, we can define an adhesion metric that provides a measure of performance between the patterned versus the smooth adhesive. Substitution of (4.41) into this metric leads to an expression that describes the effect of contact line on adhesion.

$$\frac{\sigma_n}{\sigma_s} = \frac{P_n}{P_s} = n^{1/2}. \tag{4.42}$$

This scaling relationship suggests that a patterned interface can enhance adhesion relative to a smooth one since the separation force or stress depends on the total contact line or perimeter per area during separation. Similar scaling relationships can be developed for other contact geometries such as arrays of end-on cylinders (Fig. 4.9c) or arrays of hemispheres. Generally, they all scale as $n^{1/c}$, where c depends on the specific shape of the individual contact. Additionally, (4.42) illustrates the benefit of breaking up a smooth contact area into finer and denser patterns as it enhances the total contact line per area. This scaling argument is similar to the discussion of the critical separation force for a smooth hemisphere from a surface ("Hertz and JKR Theories" and "Determination of Material Properties: E^* and G_c" sections), where the separation force scales with the length R (4.10). The similarity between these cases is that the separation force or stress is determined by a stability point defined by dP/da. Thus, the primary length scale of control is related to the contact line during separation as this separation stage is determined by the stability of the contact.

Adhesion of Wrinkled Surfaces

Over the past decade, many research groups have made great strides in developing bio-inspired patterned adhesives for enhanced control of polymer adhesion [24–32, 71]. In most instances, the patterned adhesives consisted of dense array of pillars fabricated using lithographic-based approaches. While lithography can generate patterns with high fidelity, it involves multiple steps and may not be the most scalable approach [72]. As an alternative, surface wrinkling can be used to obtain functional patterns on a surface [55, 71, 73–77]. Surface wrinkling is a type of elastic instability that occurs in a variety of materials in response to a critical compressive stress. This approach is attractive because (1) the size scales (i.e., wavelength and amplitude) of the wrinkles are well defined and is geometrically determined, (2) the process occurs spontaneously, and (3) is highly scalable. Hence, many approaches have been developed to harness surface wrinkling to pattern polymeric materials. It is not our intent to discuss the approaches used to generate wrinkled surfaces. We recommend the interested reader to refer to the following references [71, 76–85]. Rather, we are interested in discussing the application of wrinkled surfaces to control polymer adhesion. This section will be divided into three parts. The first part will be a brief overview on developing wrinkled surfaces. Next, we will discuss the adhesion of

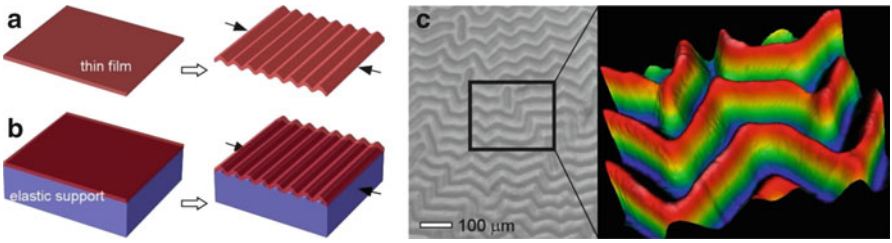

Fig. 4.10 (**a**) Compression of a freestanding thin film to cause wrinkling. (**b**) Typical approach to generating surface wrinkles on polymeric materials by supporting the thin film on an elastic support and compressing the support. (**c**) Example of a wrinkled surface by swelling-induced wrinkling [44]. (**c**) is reproduced by permission of the John Wiley and Sons

surface wrinkles with a planar surface and the role of wrinkle morphology in demonstrating the contact splitting mechanism. Finally, we will present a brief discussion on the adhesion of non-planar wrinkled surfaces with a planar surface

General Approach to Fabricate Wrinkled Surfaces

Surface wrinkling is a phenomenon that is ubiquitous both in nature and man-made materials [71, 76–86]. One example found in nature is wrinkling of human skin. Here, it is easy to demonstrate the formation of wrinkles simply by compressing a section of the skin along one direction. This results in the formation of wrinkles normal to the direction of compression. Wrinkles are also very common in man-made materials such as the patterns found in dried paints. In this example, wrinkles form due to the drying process of the paint that leads to the development of the compression. Regardless of the specific process to wrinkle formation, surface wrinkling in different materials has similar governing principles that determine the morphology of the structures. Here, we will give a brief overview of surface wrinkling in polymeric materials.

In general, wrinkling occurs in a thin film geometry that is placed in compression. We can consider the following example of a thin film under uniaxial compression (Fig. 4.10a). Because the film is thin in the thickness dimension, there is a geometric preference for the film to bend out-of-plane as opposed to compressing in-plane to relieve the deformation. Thus, many research groups have harnessed this attribute of thin films to generate wrinkled surfaces. Rather than directly compressing the thin film, an elastic support such as PDMS elastomer is used (Fig. 4.10b) to apply the compression. The resultant wrinkle morphology can be described by two characteristic size scale. The first is the wrinkle wavelength (λ), which is defined as [78, 79, 87, 88]:

$$\lambda = 2\pi h_f \left(\frac{E_f^*}{3E_s^*} \right)^{1/3}, \tag{4.43}$$

where h_f is the thickness of the thin film, E_f^* and E_s^* are the plane-strain elastic modulus of the film and elastic support, respectively. Equation (4.43) predicts that the wavelength of the wrinkles scale linearly with the thickness of the thin film and independent of the thickness of the elastic support. This assumption is valid as long as the support can be considered semi-infinitely thick in comparison to the thin film. Generally, this condition is met because the thin film is ~100 nm thick, whereas the elastic support is ~1 mm thick. Additionally, (4.43) was derived with the assumption that wrinkles have already formed, in other words, the compressive strain has been reached or exceeded the critical compressive strain for wrinkling (ε_c) defined as [87–89]:

$$\varepsilon_c = \frac{\left(3E_s^*/E_f^*\right)^{2/3}}{4}. \tag{4.44}$$

The critical strain is typically on the order of (1 MPa/10^3 MPa) ~ 0.1% for wrinkling a glassy polymeric thin film supported by an elastomer. The resultant amplitude of the wrinkles is related to this critical strain by [79, 88]:

$$A = h_f\left(\frac{\varepsilon}{\varepsilon_c} - 1\right)^{1/2}. \tag{4.45}$$

Reaching this critical strain is straightforward, however, the challenge is that most glassy polymers are quite sensitive to small strains and can yield at a few percent strains. While a large range of wrinkle wavelengths on the order of 1 μm can be accessed simply by changing the film thickness, the amplitude, which is typically on the order of 100 nm, is more challenging to vary due to material restrictions. Additionally, the glassy polymer films used are not ideally suited as soft adhesive materials. Thus, over the past several years, there has been a shift toward using swelling as an alternative approach to generating surfaces wrinkles in polymers [44, 71, 74–76]. In addition to overcoming pattern size-scale limitations, swelling-induced wrinkling opens new avenues for tuning the surface properties of the materials.

While swelling-induced wrinkling has been demonstrated since the 1960s, its application as patterned adhesives was only demonstrated recently. For adhesion studies, stable surface wrinkles are typically created from soft elastomers such as lightly cross-linked poly(*n*-butyl acrylate) (PnBA) or PDMS (Fig. 4.10c) [43, 44, 90]. For PnBA wrinkles, the fabrication process begins with photopolymerizing a PnBA elastomeric film with a desired film thickness onto a glass substrate. Next, this PnBA film is swollen with a photocurable swelling agent to induce wrinkling. Since the PnBA film is pinned to the glass substrate, the expansion due to swelling is constrained laterally. As a result, a net compressive strain develops within the film, which leads to the formation of surface wrinkles. To stabilize the surface wrinkles, the film is irradiated with UV to photopolymerize the swelling agent to form the final wrinkled adhesive. The initial film thickness is critical in controlling the

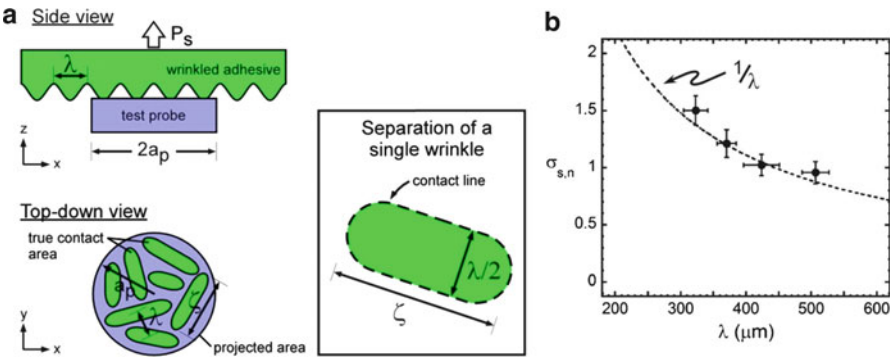

Fig. 4.11 (**a**) Schematic of the wrinkle adhesive during separation from a flat cylindrical probe. At P_s, only the crest of each wrinkle is in contact (*side view*). Hence, the true contact area consists of crest of the wrinkles in contact with the probe (*top-down view*). At separation, all the wrinkles separate simultaneously and the contribution from each wrinkle is determined by its contact line. As the inset illustrates, at separation, the contact line of a single wrinkle is defined by its perimeter, which is approximated as $\lambda + 2\zeta$. (**b**) Separation strength of the wrinkled adhesives normalized by the separation strength of a smooth non-wrinkled surface as a function of (λ). The *dashed line* is the empirical fit, where $\sigma_{s,n} \sim 1/\lambda$ (4.48). Copyright Wiley-VCH Verlag GmbH & Co. KGaA. Reproduced with permission

wavelength and amplitude of the wrinkles. For swelling-induced wrinkling, it has been experimentally observed that the wavelength scales directly with the wavelength. As the typical thickness of the polymer film is ~100 μm, the wavelength is also on the order of ~100 μm.

Adhesion of Wrinkles with a Flat Surface

In this section, we will discuss the adhesion of a surface wrinkled soft elastomer with a flat surface. This approach is interesting because it demonstrates the mechanism of contact splitting for a wrinkled surface in enhancing adhesion.

To realize the principle of equal load sharing required for contact splitting, contact adhesion tests on the wrinkled PnBA films were performed using a cylindrical punch of radius a_p (Fig. 4.11a) [43]. The experimental protocol is similar to that described previously (see "Hertz and JKR Theories" section). Using the maximum separation stress (σ_s) as the descriptor, the maximum separation stress for a non-patterned interface is [43]:

$$\sigma_{s,s} = \frac{P_m}{\pi a_p^2} = \frac{\left(8\pi G_c E^* a_p^3\right)^{1/2}}{\pi a_p^2}. \tag{4.46}$$

For the adhesion of n surface wrinkles with the flat punch, we can approximate each wrinkle as a short cylinder with its perimeter peeling away from the punch surface. For a cylinder of length $\zeta = k_1\lambda$ and width $\lambda/2$, the separation force is estimated as $P_c \sim G_c(\lambda + 2\zeta)$. Assuming equal load sharing, the maximum separation force for n cylinders occupying the contact area πa_p^2 is [43]

$$\sigma_{s,w} = \frac{nP_{c,w}}{\pi a_p^2} = \frac{\left(\pi a_p^2/\zeta\lambda\right)(G_c(\lambda + 2\zeta))}{\pi a_p^2} = \left(\frac{1}{k_1} + 2\right)\frac{G_c}{\lambda}, \tag{4.47}$$

where $n = (\pi a_p^2)/(\zeta\lambda)$ and k_1 defines the aspect ratio between the persistence length and width of the wrinkle.

Equation (4.47) indicates that the separation strength is determined by the wrinkle wavelength and the enhancement in adhesion increases as the size of the wrinkles decreases with increasing aerial density of wrinkles. In other words, this enhancement is associated with the increase in contact line per contact area. Normalizing $\sigma_{s,w}$ with $\sigma_{s,s}$, the dimensionless adhesion stress descriptor $(\sigma_{s,n})$ is obtained [43]:

$$\sigma_{s,n} = \left(\frac{1}{k_1} + 2\right)\left(\frac{\pi a_p}{2}\right)^{1/2}\left(\frac{G_c}{E^*}\right)^{1/2}\frac{1}{\lambda}. \tag{4.48}$$

Figure 4.11b demonstrates that there is good agreement between (4.48) and the experimental results. Additionally, (4.48) shows that the degree of enhancement scales with the material properties of the interface. In other words, the ratio of G_c/E^* defines a critical wavelength when adhesion enhancement is expected. Therefore, the critical wavelength of enhancement will depend on the specific materials of interest.

Adhesion of Non-planar Wrinkled Surfaces

Besides adhesion of wrinkles with a planar surface, there are real-world applications where the adhesion of wrinkles with a curved surface is important. One example is in contact lens application. Here, it may be advantageous to decorate a contact lens with surface wrinkles [12, 91] to control adhesion and friction with the cornea. We have developed a methodology to form surface wrinkles on a PDMS lens based on swelling-induced wrinkling [44]. This approach is a well-established process and involves forming a silicate-like thin film on the PDMS lens by UVO treatment [44, 74, 92]. Then, this silicate-PDMS composite is swollen with a solvent and the pattern is immediately replicated by molding against an optical adhesive (Norland 81). The replicated lens is then used as a negative mold to form wrinkled PDMS lenses. Using this procedure, we develop wrinkled PDMS lenses ($R \sim 7$ mm) with wrinkle wavelength (λ) and amplitude (A) in the range of 30–70 μm and 0.3–5.0 μm, respectively. Since the samples were prepared

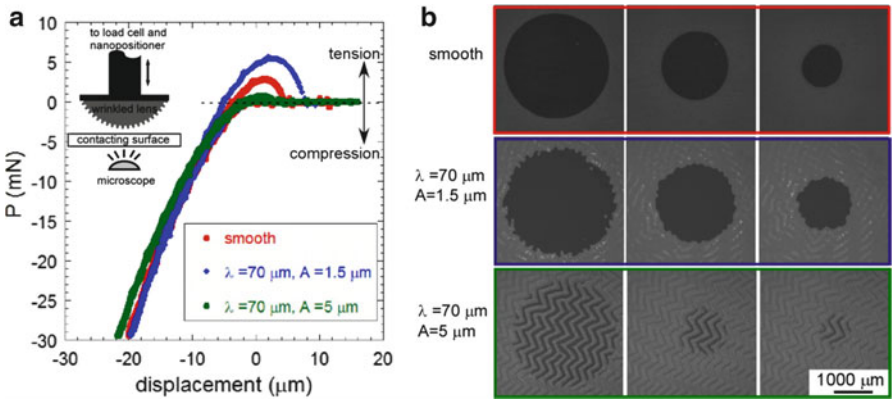

Fig. 4.12 (**a**) Force vs. displacement responses for three representative PDMS lenses [44]. Inset shows the experimental setup to measure adhesion. (**b**) Contact micrographs during separation process. Reproduced by permission of the John Wiley and Sons

using molding technique, no residual strain due to wrinkling was present in these samples.

Figure 4.12a illustrates the force vs. displacement curves from the contact adhesion tests of two lenses with similar wrinkle wavelength of ≈70 μm but with two different wrinkle amplitudes, 5 and 1.5 μm, respectively. Also shown is the adhesion for a smooth PDMS lens for comparison purposes. Again, we use the maximum separation force ($P_{m,w}$) as a descriptor of adhesion. The change of P_m as a function of wrinkle dimensions demonstrates that adhesion of a soft elastomer is influenced by the presence of wrinkled patterns.

The adhesion behavior of a surface depends on the local separation mechanism and the optical micrographs in Fig. 4.12b illustrate the different separation processes. In all the systems, the contact area decreases as the probe separates from the surface. However, the difference between the samples is the shape of the contact area and changes in the contact area during separation. For the smooth lens, the contact area is circular and the separation process occurs via a smooth recession of the circular contact. In the case of the smaller amplitude wrinkles, the perimeter of contact is no longer smooth, but its local curvature is influenced by the presence of the wrinkles. Finally, in the case of the high amplitude wrinkles, the contact area is not continuous. Instead, the height of the wrinkles is sufficient tall such that the shape of the wrinkles significantly influences the contact area and also the separation pathway.

Although the representative results in Fig. 4.12 suggest that adhesion decreases with the increase of wrinkle amplitude, experiments across a range of λ and A indicate that their trends are not straightforward. It is evident from Fig. 4.13a that for different combinations of λ and A, the maximum separation force can be enhanced or suppressed relative to the smooth surface. A phenomenological model has been derived that describes the change of adhesion behavior as a function of wrinkle dimensions [44]. It is shown that

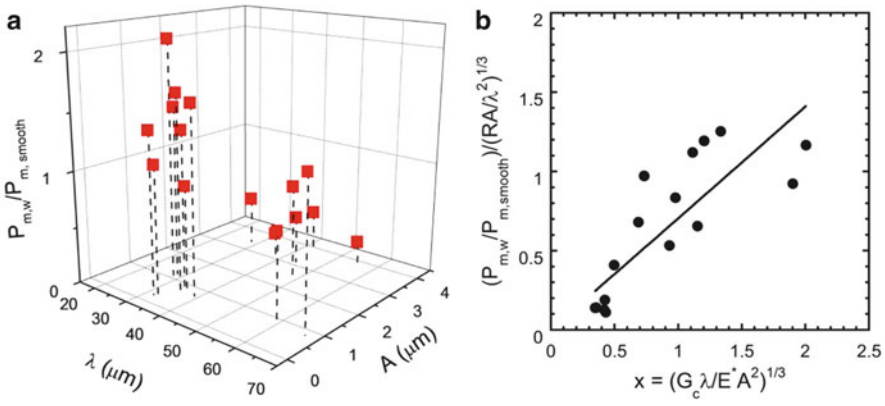

Fig. 4.13 (**a**) Normalized maximum separation force as a function of wavelength, λ and amplitude, A $P_{m,w}$ represents the maximum separation force of wrinkle surfaces, whereas $P_{m,smooth}$ is the maximum separation forces for smooth surfaces. $P_{m,w}$ normalized against $P_{m,smooth}$ are shown as a function of wrinkle wavelength (λ) and amplitude (A). (**b**) Normalized maximum separation force as a function of x. (**b**) is reproduced by permission of the John Wiley and Sons

$$\frac{P_{m,w}}{P_{m,smooth}} \sim \left(\frac{RG_c}{\lambda AE^*}\right)^{1/3} \approx \left(\frac{RA}{\lambda^2} \times \frac{G_c\lambda}{A^2E^*}\right) \approx \left(\frac{RA}{\lambda^2}\right)^{1/3} x. \tag{4.49}$$

Here, the radius of curvature of the PDMS probe and the amplitude and wavelength of the wrinkles are related through a dimensionless geometric parameter $\left(RA/\lambda^2\right)^{1/3}$. The ratio of adhesion force to elastic force the wrinkles experience is represented by a dimensionless parameter $x = \left(G_c\lambda/A^2E^*\right)^{1/3}$. The parameter x is very similar to the adhesion parameter (θ) presented by Fuller and Tabor (see "Contact of Randomly Rough Surfaces: The Theory of Fuller and Tabor" section), $x \sim (1/\theta)^{1/3}$. As displayed in Fig. 4.13b, (4.49) can fit the normalized experimental data reasonably.

In another study by Lin et al. [90], the adhesion behavior of oxygen plasma treated wrinkle surfaces was varied by changing the wrinkle dimensions real-time. They have shown a decrease of P_m with the increase of wrinkle amplitude with maintaining constant frequency. Their results are in overall agreement with the results presented above.

Concluding Remarks

As we have discussed in this chapter, the theories of Hertz and JKR provide the framework for understanding the contact mechanics of a variety of soft materials. Although significant progress has been made in understanding the adhesion and mechanical behavior of soft materials, most of these studies are limited to synthetic materials. A major direction of the ongoing research is extending and adapting the

contact mechanics theories and approaches to the biological systems. The primary challenge lies in establishing experimental techniques that is sufficiently sensitive to probe weak forces typically observed in biological systems and developing theoretical models to describe their mechanical properties which include viscoelastic and nonlinear responses. Additionally, it would be advantageous to develop measurement approaches that can probe these interfacial properties dynamically since the properties of most biological systems change with environmental conditions.

For synthetic materials, it is evident from our discussion that the next generation adhesive will be more complex, possibly incorporating structured surfaces for improved attachment and release properties. While experimentalists will continue to innovate and develop novel materials, as Nature has illustrated, it will difficult to explore the large design parameter space available for patterned adhesives. Hence, the challenge lies in developing theoretical models that can help predict the relationships between structure and performance that can greatly speed up the design process. From an applications perspective, it will be especially helpful if specific relationships between structure and adhesion metrics can be developed. From the fundamental science perspective, a unifying theory that links material structure to material properties such as G_c and E would be highly desirable.

References

1. Bhatia, S.K., Arthur, S.D., Chenault, H.K., Figuly, G.D., Kodokian, G.K.: Polysaccharide-based tissue adhesives for sealing corneal incisions. Curr. Eye Res. **32**, 1045–1050 (2007)
2. Bhatia, S.K., Arthur, S.D., Chenault, H.K., Kodokian, G.K.: Interactions of polysaccharide-based tissue adhesives with clinically relevant fibroblast and macrophage cell lines. Biotechnol. Lett. **29**, 1645–1649 (2007)
3. Mo, X., Iwata, H., Matsuda, S., Ikada, Y.: Soft tissue adhesive composed of modified gelatin and polysaccharides. J. Biomater. Sci. Polym. Ed. **11**, 341–351 (2000)
4. Ryou, M., Thompson, C.C.: Tissue Adhesives: A Review. Tech. Gastrointest. Endosc. **8**, 33–37 (2006)
5. Strehin, I., Nahas, Z., Arora, K., Nguyen, T., Elisseeff, J.: A versatile pH sensitive chondroitin sulfate-PEG tissue adhesive and hydrogel. Biomaterials **31**, 2788–2797 (2010)
6. Bait, N., Grassl, B., Derail, C. & Benaboura, A. Hydrogel nanocomposites as pressure-sensitive adhesives for skin-contact applications. *Soft Matter* **7**, 2025–2032 (2011)
7. Onuki, Y., et al.: Formulation optimization of photocrosslinked polyacrylic acid modified with 2-hydroxyethyl methacrylate hydrogel as an adhesive for a dermatological patch. J. Control. Release **108**, 331–340 (2005)
8. Venkatraman, S., Gale, R.: Skin adhesives and skin adhesion: 1. Transdermal drug delivery systems. Biomaterials **19**, 1119–1136 (1998)
9. Lee, K.J., et al.: Large-area, selective transfer of microstructured silicon: a printing-based approach to high-performance thin-film transistors supported on flexible substrates. Adv. Mater. **17**, 2332–2336 (2005)
10. Kim, S.H., Opdahl, A., Marmo, C., Somorjai, G.A.: AFM and SFG studies of pHEMA-based hydrogel contact lens surfaces in saline solution: adhesion, friction, and the presence of non-cross-linked polymer chains at the surface. Biomaterials **23**, 1657–1666 (2002)

11. Opdahl, A., Kim, S.H., Koffas, T.S., Marmo, C., Somorjai, G.A.: Surface mechanical properties of pHEMA contact lenses: Viscoelastic and adhesive property changes on exposure to controlled humidity. J. Biomed. Mater. Res. **67A**, 350–356 (2003)
12. Kundu, S., Sharma, R., Crosby, A.J.: Adhesion of contact lenses. (unpublished work)
13. Kurella, A., Dahotre, N.B.: Review paper: surface modification for bioimplants: the role of laser surface engineering. J. Biomater. Appl. **20**, 5–50 (2005)
14. Johnson, K.L.: Contact Mechanics. Cambridge University Press, Cambridge (1987)
15. Shull, K.R., Ahn, D., Chen, W., Flanigan, C.M., Crosby, A.J.: Axisymmetric adhesion tests of soft materials. Macromol. Chem. Phys. **199**, 489–511 (1998)
16. Shull, K.R.: Contact mechanics and the adhesion of soft solids. Mater. Sci. Eng.: R: Reports **36**, 1–45 (2002)
17. Johnson, K.L., Kendall, K., Roberts, A.D.: Surface energy and the contact of elastic solids. Proc. R. Soc. Lond. A Math. Phys. Sci. **324**, 301–313 (1971)
18. Maugis, D.: Contact Adhesion and Rupture of Elastic Solids. Springer, Berlin, New York (2000)
19. Fuller, K.N.G., Tabor, D.: The effect of surface roughness on the adhesion of elastic solids. Proc. R. Soc. Lond. A Math. Phys. Sci. **345**, 327–342 (1975)
20. Briggs, G.A.D., Briscoe, B.J.: The effect of surface topography on the adhesion of elastic solids. J. Phys. D: Appl. Phys. **10**, 2453 (1977)
21. Arzt, E., Gorb, S., Spolenak, R.: From micro to nano contacts in biological attachment devices. Proc. Natl Acad. Sci. USA **100**, 10603–10606 (2003)
22. Autumn, K., et al.: Adhesive force of a single gecko foot-hair. Nature **405**, 681–685 (2000)
23. Pennisi, E.: Biomechanics:Geckos Climb by the Hairs of Their Toes. Science **288**, 1717a–1718a (2000)
24. Crosby, A., Hageman, M., Duncan, A.: Controlling polymer adhesion with “Pancakes”. Langmuir **21**, 11738–11743 (2005)
25. Chan, E.P., Greiner, C., Arzt, E., Crosby, A.J.: Designing model systems for enhanced adhesion. MRS Bull. **32**, 496–503 (2007)
26. Boesel, L.F., Greiner, C., Arzt, E., del Campo, A.: Gecko-inspired surfaces: A path to strong and reversible dry adhesives. Adv. Mater. **22**, 2125–2137 (2010)
27. Murphy, M.P., Aksak, B., Sitti, M.: Gecko-inspired directional and controllable adhesion. Small **5**, 170–175 (2009)
28. Geim, A.K., Grigorieva, S., Novoselov, K.S., Zhukov, A.A., Shapoval, S.Y.: Microfabricated adhesive mimicking gecko foot-hair. Nat. Mater. **2**, 461–463 (2003)
29. Lee, H., Lee, B.P., Messersmith, P.B.: A reversible wet/dry adhesive inspired by mussels and geckos. Nature **448**, 338–341 (2007)
30. Jeong, H.E., Suh, K.Y.: Nanohairs and nanotubes: Efficient structural elements for gecko-inspired artificial dry adhesives. Nano Today **4**, 335–346 (2009)
31. Mahdavi, A., et al.: A biodegradable and biocompatible gecko-inspired tissue adhesive. Proc. Natl Acad. Sci. USA **105**, 2307 (2008)
32. Jeong, H.E., Lee, J.K., Kim, H.N., Moon, S.H., Suh, K.Y.: A nontransferring dry adhesive with hierarchical polymer nanohairs. Proc. Natl Acad. Sci. USA **106**, 5639 (2009)
33. Hertz, H.: On the contact of elastic solids. J. Reine Angew. Math. **92**, 156–171 (1881)
34. Israelachvili, J.N.: Intermolecular and Surface Forces, Second Edition: With Applications to Colloidal and Biological Systems. Academic Press, San Diego, CA (1992)
35. Perutz, S., Kramer, E.J., Baney, J., Hui, C., Cohen, C.: Investigation of adhesion hysteresis in poly(dimethylsiloxane) networks using the JKR technique. J. Polym. Sci. B Polym. Phys. **36**, 2129–2139 (1998)
36. Creton, C., Leibler, L.: How does tack depend on time of contact and contact pressure? J. Polym. Sci. B Polym. Phys. **34**, 545–554 (1996)
37. Maugis, D., Barquins, M.: Fracture mechanics and the adherence of viscoelastic bodies. J. Phys. D Appl. Phys. **11**, 1989 (1978)
38. Derjaguin, B.V., Muller, V.M., Toporov, Y.P.: Effect of contact deformations on the adhesion of particles. J. Colloid Interface Sci. **53**, 314–326 (1975)

39. Butt, H., Cappella, B., Kappl, M.: Force measurements with the atomic force microscope: Technique, interpretation and applications. Surf. Sci. Reports **59**, 1–152 (2005)
40. Dimitriadis, E.K., Horkay, F., Maresca, J., Kachar, B., Chadwick, R.S.: Determination of elastic moduli of thin layers of soft material using the atomic force microscope. Biophys. J. **82**, 2798–2810 (2002)
41. Maugis, D., Barquins, M.: Adhesive contact of sectionally smooth-ended punches on elastic half-spaces: theory and experiment. J. Phys. D: Appl. Phys. **16**, 1843 (1983)
42. Sneddon, I.N.: The relation between load and penetration in the axisymmetric Boussinesq problem for a punch of arbitrary profile. Int. J. Eng. Sci. **3**, 47–57 (1965)
43. Chan, E.P., Smith, E., Hayward, R., Crosby, A.: Surface wrinkles for smart adhesion. Adv. Mater. **20**, 711–716 (2008)
44. Kundu, S., Davis, C.S., Long, T., Sharma, R., Crosby, A.J.: Adhesion of nonplanar wrinkled surfaces. J. Polym. Sci. B Polym. Phys. **49**, 179–185 (2011)
45. Chaudhury, M., Whitesides, G.: Direct measurement of interfacial interactions between semispherical lenses and flat sheets of poly(dimethylsiloxane) and their chemical derivatives. Langmuir **7**, 1013–1025 (1991)
46. Silberzan, P., Perutz, S., Kramer, E.J., Chaudhury, M.K.: Study of the self-adhesion hysteresis of a siloxane elastomer using the JKR method. Langmuir **10**, 2466–2470 (1994)
47. Rand, C.J., Crosby, A.J.: Insight into the periodicity of Schallamach waves in soft material friction. Appl. Phys. Lett. **89**, 261907 (2006)
48. Lee, K.Y., Mooney, D.J.: Hydrogels for Tissue Engineering. Chem. Rev. **101**, 1869–1880 (2001)
49. Langer, R., Vacanti, J.: Tissue engineering. Science **260**, 920–926 (1993)
50. Kopecek, J.: Hydrogel biomaterials: A smart future? Biomaterials **28**, 5185–5192 (2007)
51. Lauffenburger, D.A., Griffith, L.G.: Who's got pull around here? Cell organization in development and tissue engineering. Proc. Natl Acad Sci. USA **98**, 4282–4284 (2001)
52. Ma, P.X.: Scaffolds for tissue fabrication. Materials Today **7**, 30–40 (2004)
53. Chu, Y., Dufour, S., Thiery, J.P., Perez, E., Pincet, F.: Johnson-Kendall-Roberts theory applied to living cells. Phys. Rev. Lett. **94**, 028102 (2005)
54. Zimberlin, J.A., McManus, J.J., Crosby, A.J.: Cavitation rheology of the vitreous: mechanical properties of biological tissue. Soft Matter **6**, 3632–3635 (2010)
55. Kundu, S., Crosby, A.J.: Cavitation and fracture behavior of polyacrylamide hydrogels. Soft Matter **5**, 3963–3968 (2009)
56. Zimberlin, J.A., Crosby, A.J.: Water cavitation of hydrogels. J. Polym. Sci. B Polym. Phys. **48**, 1423–1427 (2010)
57. Zimberlin, J.A., Sanabria-DeLong, N., Tew, G.N., Crosby, A.J.: Cavitation rheology for soft materials. Soft Matter **3**, 763–767 (2007)
58. Creton, C.: Pressure-sensitive adhesives: an introductory course. MRS Bull. **28**, 434–439 (2003)
59. Crosby, A., Shull, K., Lin, Y., Hui, C.: Rheological properties and adhesive failure of thin viscoelastic layers. J. Rheol. **46**, 273–294 (2002)
60. Crosby, A.J., Shull, K.R., Lakrout, H., Creton, C.: Deformation and failure modes of adhesively bonded elastic layers. J. Appl. Phys. **88**, 2956–2966 (2000)
61. Li, L., Tirrell, M., Korba, G.A., Pocius, A.V.: Surface Energy and Adhesion Studies on Acrylic Pressure Sensitive Adhesives. J. Adhes. **76**, 307 (2001)
62. Fabbroni, E.F., Shull, K.R., Hersam, M.C.: Adhesive and mechanical properties of soft nanocomposites: Model studies with blended latex films. J. Polym. Sci. B: Polym. Phys. **39**, 3090–3102 (2001)
63. Gay, C., Leibler, L.: Theory of Tackiness. Phys. Rev. Lett. **82**, 936 (1999)
64. Brown, K., Creton, C.: Nucleation and growth of cavities in soft viscoelastic layers under tensile stress. Eur. Phys. J. E: Soft Matter Biol. Phys. **9**, 35–40 (2002)
65. Hui, C., Baney, J.M., Kramer, E.J.: Contact mechanics and adhesion of viscoelastic spheres. Langmuir **14**, 6570–6578 (1998)

66. Hui, C., Xu, D., Kramer, E.J.: A fracture model for a weak interface in a viscoelastic material (small scale yielding analysis). J. Appl. Phys. **72**, 3294–3304 (1992)
67. Lin, Y.Y., Hui, C.Y., Baney, J.M.: Viscoelastic contract, work of adhesion and the JKR technique. J. Phys. D Appl. Phys. **32**, 2250 (1999)
68. Ahn, D., Shull, K.R.: Effects of substrate modification on the interfacial adhesion of acrylic elastomers. Langmuir **14**, 3646–3654 (1998)
69. Vajpayee, S., Hui, C., Jagota, A.: Model-independent extraction of adhesion energy from indentation experiments. Langmuir **24**, 9401–9409 (2008)
70. Kaelble, D.H.: Theory and analysis of peel adhesion: bond stresses and distributions. Trans. Soc. Rheol. **4**, 45–73 (1960)
71. Breid, D., Crosby, A.J.: Surface wrinkling behavior of finite circular plates. Soft Matter **5**, 425–431 (2009)
72. Nie, Z., Kumacheva, E.: Patterning surfaces with functional polymers. Nat. Mater. **7**, 277–290 (2008)
73. Bowden, N., Brittain, S., Evans, A.G., Hutchinson, J.W., Whitesides, G.M.: Spontaneous formation of ordered structures in thin films of metals supported on an elastomeric polymer. Nature **393**, 146–149 (1998)
74. Chan, E.P., Crosby, A.J.: Spontaneous formation of stable aligned wrinkling patterns. Soft Matter **2**, 324–328 (2006)
75. Chan, E.P., Crosby, A.: Fabricating microlens arrays by surface wrinkling. Adv. Mater. **18**, 3238–3242 (2006)
76. Vandeparre, H., Damman, P.: Wrinkling of stimuloresponsive surfaces: mechanical instability coupled to diffusion. Phys. Rev. Lett. **101**, 124301 (2008)
77. Kim, J., Yoon, J., Hayward, R.C.: Dynamic display of biomolecular patterns through an elastic creasing instability of stimuli-responsive hydrogels. Nat. Mater. **9**, 159–164 (2009)
78. Genzer, J., Groenewold, J.: Soft matter with hard skin: From skin wrinkles to templating and material characterization. Soft Matter **2**, 310–323 (2006)
79. Cerda, E., Mahadevan, L.: Geometry and physics of wrinkling. Phys. Rev. Lett. **90**, 74302 (2003)
80. Stafford, C.M., et al.: A buckling-based metrology for measuring the elastic moduli of polymeric thin films. Nat. Mater. **3**, 545–550 (2004)
81. Chung, J.Y., Nolte, A.J., Stafford, C.M.: Diffusion-controlled, self-organized growth of symmetric wrinkling patterns. Adv. Mater. **21**, 1358–1362 (2009)
82. Efimenko, K., et al.: Nested self-similar wrinkling patterns in skins. Nat. Mater. **4**, 293–297 (2005)
83. Southern, E., Thomas, A.G.: Effect of constraints on the equilibrium swelling of rubber vulcanizates. J. Polym. Sci. A General Papers **3**, 641–646 (1965)
84. Tanaka, T., et al.: Mechanical instability of gels at the phase transition. Nature **325**, 796–798 (1987)
85. Khang, D., Jiang, H., Huang, Y., Rogers, J.: A stretchable form of single-crystal silicon for high-performance electronics on rubber substrates. Science **311**, 208–212 (2006)
86. Kücken, M., Newell, A.C.: Fingerprint formation. J. Theor. Biol. **235**, 71–83 (2005)
87. Chen, X., Hutchinson, J.W.: Herringbone buckling patterns of compressed thin films on compliant substrates. J. Appl. Mech. **71**, 597–603 (2004)
88. Huang, Z., Hong, W., Suo, Z.: Nonlinear analyses of wrinkles in a film bonded to a compliant substrate. J. Mech. Phys. Solids **53**, 2101–2118 (2005)
89. Chung, J.Y., Chastek, T.Q., Fasolka, M.J., Ro, H.W., Stafford, C.M.: Quantifying residual stress in nanoscale thin polymer films via surface wrinkling. ACS Nano **3**, 844–852 (2009)
90. Lin, P.C., Vajpayee, S., Jagota, A., Hui, C.Y., Yang, S.: Mechanically tunable dry adhesive from wrinkled elastomers. Soft Matter **4**, 1830–1835 (2008)
91. Sharma, R., Braun, R.M., Ammon Jr, D.M., Kunzler, J.F., Lai, Y.C. Silicone contact lenses with wrinkled surface. US Patent# 7625598, published 12/01/2009.
92. Efimenko, K., Wallace, W.E., Genzer, J.: Surface modification of Sylgard-184 poly (dimethyl siloxane) networks by ultraviolet and ultraviolet/ozone treatment. J. Colloid Interface Sci. **254**, 306–315 (2002)

Chapter 5
PLA–PEO–PLA Hydrogels and Their Mechanical Properties

Gregory N. Tew and Surita R. Bhatia

Abstract Poly(lactide) – *block* – poly(ethylene oxide) – *block* – poly(lactide) [PLA–PEO–PLA] triblock copolymers are known to form physical hydrogels in water, due to the polymer's amphiphilic architecture. Their biodegradability has made them attractive for use as soft tissue scaffolds and other biological applications such as drug delivery. In many cases, their mechanical properties have been poorly investigated and "rules" for tuning their stiffness are missing. Often the network junction points are only physical cross-links, not covalent, and in a highly aqueous environment, these hydrogels will absorb more water, transform from gel to sol, and lose the designed mechanical properties. New insights into the self-assembly of these materials have resulted in new PLA–PEO–PLA gels with novel structural and mechanical properties. Here, we summarize our recent efforts to understand these novel hydrogels and control their mechanical properties. This is highlighted by a new approach in which the system is allowed to self-assemble and then it is covalently cross-linked to capture this self-assembled architecture. This produces hydrogels with permanent cross-links and allows their mechanical properties to be studied in much more detail.

G.N. Tew (✉)
Department of Polymer Science and Engineering, University of Massachusetts Amherst, Amherst, MA 01003, USA
e-mail: tew@mail.pse.umass.edu

S.R. Bhatia (✉)
Department of Chemical Engineering, University of Massachusetts Amherst, Amherst, MA 01003, USA
e-mail: sbhatia@ecs.umass.edu

S.K. Bhatia (ed.), *Engineering Biomaterials for Regenerative Medicine: Novel Technologies for Clinical Applications*, DOI 10.1007/978-1-4614-1080-5_5,

Introduction

Hydrogels have gained interest in the area of biomaterials for their many attractive qualities [1–4]. These qualities allow the integration of such materials in the body as tissue scaffolds by offering structural support and other features such as the influx of cell metabolites and efflux of cell waste. To this end, many researchers have investigated synthetic polymer hydrogels. In general, ABA amphiphilic block copolymers form associative networks in water where the A block is hydrophobic and the B block is hydrophilic. This self-assembly is driven by the association of the hydrophobic endblocks into micelles, which are bridged by the water-soluble midblocks forming physically cross-linked networks (see Fig. 5.1-top). These physical hydrogels are attractive because no cross-linking agent is necessary and the gelation can be triggered (body temperature and pH). However, chemically cross-linked systems have also been studied [5–8]. Chemical cross-linking leads to a more permanent three-dimensional structure than the physically cross-linked counter-parts, but can still be degraded with time.

One class of richly studied hydrogels is ABA triblock copolymers in which the A block is composed of a biodegradable polyester. Polyesters remain a candidate for many biomaterials applications including small area tissue repair to new organ growth. The chemical structures of three such polyesters are shown in Fig. 5.1-bottom. The overwhelmingly attractive feature of these materials is their biodegradation and ease of synthesis; however, in relation to the optimal requirements of a scaffold, these polymers (pure polyesters) are far from ideal. They are very hydrophobic making their compatibility with biological environments poor. They also suffer from unwanted responses in vivo including foreign body response [9]. At the same time, the homopolyester's modulus can be quite far from those of biological tissues. Although PLA and other synthetic polyesters represent important medical materials, they all suffer from a variety of critical limitations. Another class of polyesters, which has seen limited but promising exploration in biomedical applications, is poly(hydroxyalkanoates) (PHAs) [10–12]. Many researchers have investigated synthetic ABA triblock polymers containing the biocompatible hydrophilic poly(ethylene oxide) (PEO) segments along with biodegradable polyester domains, including poly(lactide) (PLA), poly(caprolactone) (PCL), and poly (glycolic acid) (PGA) [2, 13–22].

Cells respond to chemical signals and this is well documented. There is mounting evidence that mechanical cues can have similarly large influences on cellular response. Cells have biomechanical response systems and so the concept that the matrix material can significantly impact cellular cycles and behavior is logical. Mechanical properties impact cellular structure, metabolism, transcription and/or translation of various genes, and even viability [23–29]. Pioneering work showed NIH3T3 fibroblasts and rat kidney epithelial cells underwent compliance dependent motility and cytoskeletal adhesion changes [28, 30]. This is striking. Similar studies examined endothelial cells, myocytes, hepatocytes, neural/glial cells, and chondrocytes [31–35]. Myoblasts formed myotubes but only exhibited striations

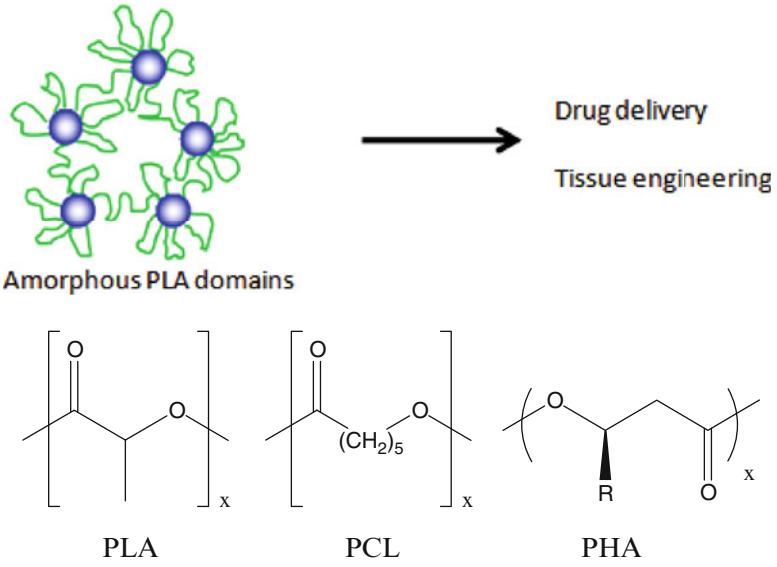

Fig. 5.1 (*top*) ABA triblock copolymer micelle and bridging micelle formation along with the typical applications for these materials. (*bottom*) Three polyesters used as tissue engineering scaffolds

on intermediate stiffness substrates [32]. The modulus of healthy muscle tissue is within this intermediate stiffness. Glial cells were unable to survive in soft materials, unlike neurons [31, 33, 36, 37]. The use of hydrogels has been proposed to limit scar tissue as a result of the mechanical properties at the wound site [31].

A variety of cross-linking techniques, polymer structures, and architectures have been used to synthesize biodegradable hydrogels; however, the corresponding mechanical properties are not as well characterized. Since the overall mechanical environment affects cell proliferation and growth this is unfortunate [31, 38, 39]. Cells typically bind to the extracellular matrix via surface receptors to generate traction forces. Thus, the underlying substrate must withstand these traction forces so that the cell can grow and spread properly. It has shown that cells can sense the restraining force of the substrate and can respond by locally strengthening cytoskeleton linkages [27]. Since the healthy survival of cells so greatly depends on the mechanical properties, it is important to consider the mechanical properties of both the target native tissue (see Table 5.1) and the hydrogel when designing materials for cell scaffolds.

In this chapter, a summary of recent efforts to understand and control the mechanical properties of PLA–PEO–PLA triblock copolymer hydrogels is provided. This includes the ability to varying the stiffness of these hydrogels by manipulating the length of the PLA endblocks [44], by changing the physical cross-links from amorphous to crystalline PLA [45], by varying the synthetic technique [46], by incorporating nanoparticles [47], and by covalently capturing the self-assembled

Table 5.1 Modulus values for some tissues

Material	Modulus (kPa)
Human nasal cartilage [40, 41]	234 ± 27
Bovine articular cartilage [40, 41]	990 ± 50
Pig thoracic aorta [42]	43.2 ± 15
Nucleus pulposus and eye lens [43]	~1
Canine kidney cortex [43]	~10

structure [48]. This last approach is particularly intriguing since it combines the advantages of self-assembly with the stability of covalent cross-links. This appears to be the first time covalently cross-linked hydrogels have been formed in this way.

PLA–PEO–PLA Triblock Copolymers Synthesis

Lactide has two stereoisomers: D-lactide and L-lactide. Poly(D-lactide) (PDLA) and poly(L-lactide) (PLLA) are isotactic and semicrystalline. Meanwhile, materials formed by atactic poly(D,L-lactide), or racemic poly(R-lactide) (PRLA), are amorphous [45]. This allowed direct control over the crystallinity of the hydrophobic micelle formed by these triblock copolymers. In general, the polymers can be prepared in solution or in the bulk. This can impact the mechanical properties of the resulting hydrogel since the molecular weight distribution (MWD), specifically the symmetry of the triblock copolymer, is influenced [46]. Generally, triblock copolymers produced through bulk-synthesis are more asymmetric, which reduced the mechanical stiffness of the gel phase (such as system relaxation time and junction lifetime). This had a larger impact on amorphous PRLA materials than on containing crystalline PLLA [46].

Triblock formation begins by ring-opening polymerization of the lactide monomer by a preformed dihydroxylated PEG [49–54]. Catalysts such as stannous octoate, SnO, SnO_2, Sb_2O_3, PbO, GeO_2, $SnCl_2$, and NaOH have been used [50, 52, 55–60]. Stannous octoate is the most frequently used catalyst [53, 55, 57, 61]. The polymerization conditions and mechanisms used to produce triblock copolymers can affect their biological, material, and chemical properties [53]. The copolymers described here were prepared by ring-opening polymerization of L-lactide either in the bulk or in solution using stannous (II) 2-ethylhexanoate as catalyst. Although a number of copolymers has been prepared, the PEO block length is held constant and the degree of polymerization (DP) for PLLA is varied, but typically from ~52 to ~72 [44, 61]. In all cases, the polymerization was not run to completion since this broadens the MWD. Thermal and diffraction studies of these polymers in the bulk always show PEO crystallization as well as PLLA crystallization when the block length is sufficiently long [62]. When both blocks crystallize, the PEO segments are confined between PLA lamellae [62].

To covalently capture the assembled hydrogel, the PLA–PEO–PLA triblock copolymer endgroups where functionalized with acrylates so that the self-assembled structure could be locked in by initiating photocrosslinking with ultra-violet radiation.

Mechanical Properties of These Hydrogels

Mechanical properties of physically cross-linked hydrogels are typically characterized using shear rheometry, by exposing the material to an oscillatory shear stress at various frequencies. This leads to a determination of the storage modulus (G') and the loss modulus (G''), providing insight on the elastic and viscous components of the material, respectively. Chemically cross-linked hydrogels are more typically characterized by measuring the stress in the material as strain is applied in compression. Implementing Hooke's law ($\sigma = E\varepsilon$, where σ is stress, ε is strain, and E is the Young's or elastic modulus) for the slope of the linear region at low strains corresponds to the elastic modulus. However, Hooke's law only applies to linearly elastic materials, while hydrogels typically have nonlinear stress–strain responses in compression. Models based on rubber networks such as a modified Neo-Hookean model [63–65] or a model defined by Mooney [66] and Rivlin [67] better describe the nonlinear behavior. Regardless, many researchers only apply Hooke's law despite the nonlinear behavior of their materials.

Addition of water to these ABA triblock copolymers produces hard, physically associated gels typically above 16 wt.%. The length of the PLA block directly impacts the wt.% of this sol–gel transition. The longer the PLA block (up to a solubility limit), the lower the transition [44]. For example, a triblock with total PLA of 72 units forms a viscous liquid 14 wt.% but a stiff gel at 16 wt.% (see inset Fig. 5.2). Characteristics of gel formation were seen to vary with the length of the hydrophobic blocks. Solutions of the triblock with the smaller hydrophobes (total PLA 52 units) did not gel up to concentrations of 20 wt.% polymer. To better quantify the mechanical properties of these hydrogels, dynamic mechanical shear rheology was employed.

Figure 5.2 shows G' vs. frequency for the two polymers described above at 25°C (filled symbols) and 37°C (open symbols). The gel of the shorter PLA materials (total PLA 52 units) was prepared in 20 wt.% but still forms a weaker gel than the one with the longer PLA blocks which only contains 16 wt.% polymer. It is clear from these results that the hydrophobic length, or DP, significantly influences elastic modulus. Comparing these two materials, the stiffness increases by more than two decades, from ~100 Pa to 10,000 Pa, as the length of the hydrophobic block is increased.

The stiffer gel is quite elastic, with G' only weakly dependent on frequency and greater than G'' over the entire frequency range. Looking to other systems, PEO-containing alkyl hydrophobe end-caps show qualitatively similar trends for the high-frequency limit of G'; [68] although the dependence of G' on hydrophobe length is weaker for the alkyl-capped systems than in these PLLA–PEO–PLLA gels.

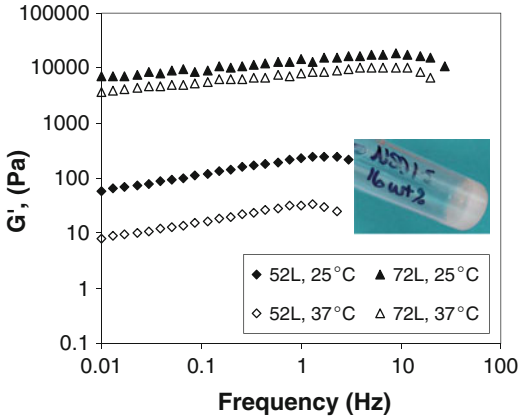

Fig. 5.2 Elastic modulus for two hydrogels at 20 and 16 wt.%, respectively. The *filled and open symbols* were collected at 25 and 37°C. The stiff 18 kPa gel is less sensitive to temperature changes than the softer gel made from shorter PLLA blocks. The photograph at room temperature shows the stiff gel does not flow

The elastic moduli of fluoroalkyl-capped PEO gels were insensitive to hydrophobe length at high frequency [69, 70]. Increasing the PLA length, or wt.%, increased G' over 10 kPa.

This ability to create gels with elastic modulus greater than 10 kPa provides materials that are almost an order of magnitude stiffer than any previous reports for polymers composed of similar chemistry. A copolymer of PMG_{19}–PEO_{33}–-PMG_{19} (PMG = poly(D,L-3-methyl-glycolide)) had an elastic modulus less than 500 Pa for a 27 wt.% sample [71]. Other hydrogels from stereocomplexed $PLLA_{18}$–PEO_{105}–$PLLA_{18}$ and $PDLA_{15}$–PEO_{105}–$PDLA_{15}$ (10 wt.%) had an elastic modulus up to 1,000 Pa at 37°C [21]. Solutions of either polymer independently at 10 wt.% did not form a hydrogel. These reports have focused on relatively small molecular weight (MW) polymers, which are quite different from the ones we have studied. Further, much of the data in the literature is reported at a single frequency and strain, so the dependence of modulus on frequency and strain is completely unknown [44]. Creating hydrogels with roughly kPa modulus values are of widespread interest since many native tissues have moduli in this range, although most have nonlinear response to strain (see Table 5.1). These values show the need for hydrogels with stiffer modulus values.

The network structure shown in Fig. 5.2-top is dynamic so a polymer may pull out of one micelle core and insert into another. As more water is added, as would happen in the body, the distance between micelles increases, lowering the density of junction points. Since there are no covalent bonds holding the junctions in place, at a certain critical concentration an associative network can no longer form. At this critical concentration, the hydrogel loses its mechanical integrity. However, by introducing a photocrosslinkable moiety (see Fig. 5.3), the self-assembled structure can be captured by irradiation with UV light (see Fig. 5.3). This method allows the differences between chemical and physical cross-linking in the same polymer hydrogel system to be studied. It also represents a new strategy to form hydrogels and is likely to lead to novel properties since it has the advantages of self-assembly and covalent, permanent cross-links.

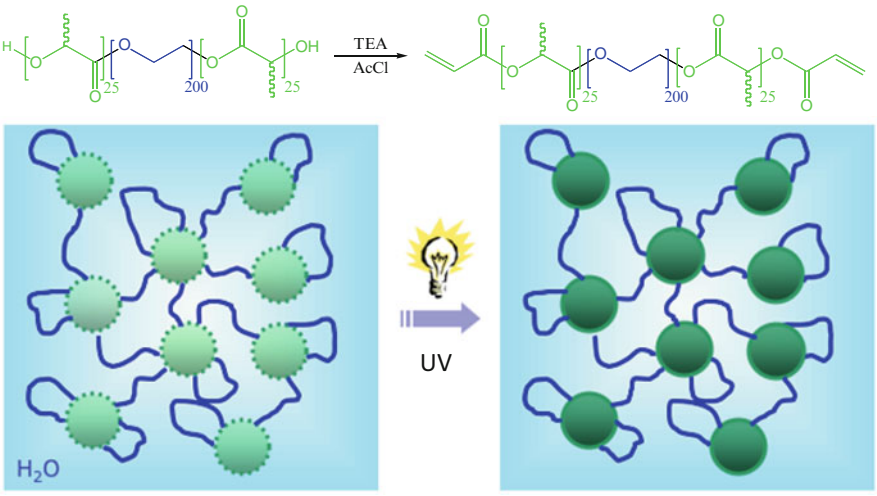

Fig. 5.3 PLA–PEO–PLA is reacted with acryloyl chloride using triethylamine as a basic catalyst to yield the acrylate end-functionalized triblock copolymer. Hydrophobic PLA is illustrated in *green*, while hydrophilic PEO is in *blue*. This triblock copolymer forms physical cross-links which are dynamic as illustrated by the *dashed lines* around the micellar cores (*left*), but once photocrosslinked the junction points are permanent, as shown using *solid lines* around the micelle cores (*right*)

The photocrosslinked PLA–PEO–PLA hydrogels remained intact when swollen in phosphate-buffered saline solution (pH 7.4) at body temperature (37°C) for extended periods of time. This is in contrast to the physical hydrogels which swell with excess solution until the system transforms from a gel to a sol. The performance of these photocrosslinked PLA–PEO–PLA hydrogels was evaluated in compression. Typical stress–strain curves from compression testing demonstrated the expected nonlinear behavior exhibited by soft networks. To analyze the data, the Neo-Hookean constitutive relationship for rubbers was utilized.

In this model, the specific form of the strain energy function (U) is dependent on the first invariant of the deformation tensor (I_1) by the constant, C_1:

$$U = C_1(I_1 - 3)$$
$$U = C_1\left(\lambda_1^2 + \lambda_2^2 + \lambda_3^2 - 3\right),$$

where λ_i is equal to the extension ratio in the i-principal direction, or more specifically, the length in the i-direction over the initial (pre-stressed) length in the i-direction. The extension ratio is related to the strain, ε, by the following expression: $\lambda = \varepsilon + 1$. For the case of uniaxial compression and assuming the material to be incompressible:

$$\lambda_1^2 = \lambda^2, \lambda_2^2 = \lambda_3^2 = \lambda^{-1}$$
$$\lambda_1^2\lambda_2^2\lambda_3^2 = 1.$$

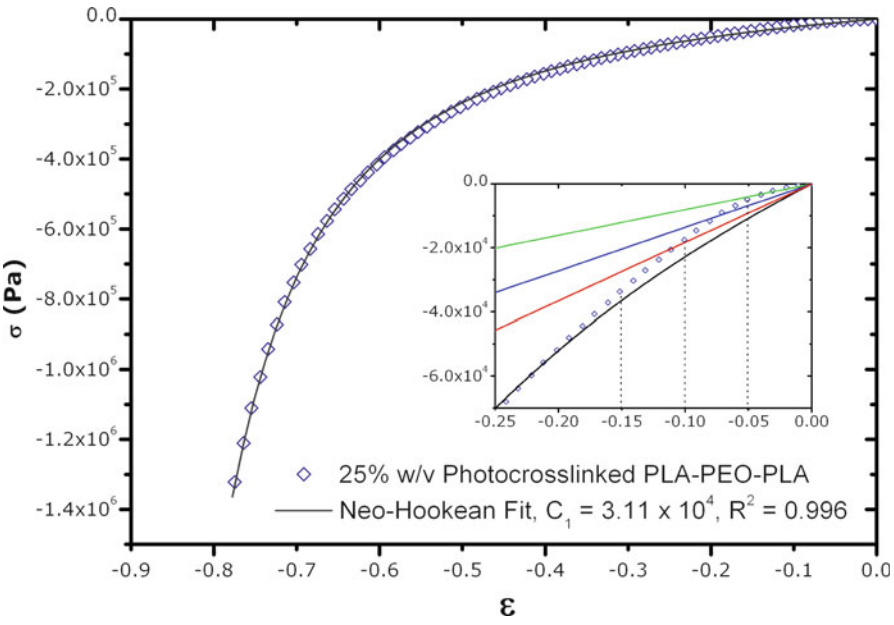

Fig. 5.4 Typical stress versus strain curve in compression. 25% w/v photocrosslinked PLA–PEO–PLA before degradation. Stress curve is nonlinear and typical of soft-rubbery materials. (*inset*) The Hookean model (shown in *green*, *blue*, and *red* at 5, 10, and 15% strain range, respectively) does not capture the nonlinearity in the stress–strain curve, while the Neo-Hookean fit (*in black*) does. The zoom into the small strain region shows that even at low strains, the curve is nonlinear

By substituting into the strain energy expression and differentiating with respect to the extension ratio, an expression for stress (σ) is derived:

$$U = C_1\left(\lambda^2 + \frac{2}{\lambda} - 3\right)$$

$$\sigma = \frac{\partial U}{\partial \lambda} = 2C_1\left(\lambda - \frac{1}{\lambda^2}\right) = 2C_1\left[(\varepsilon + 1) - \frac{1}{(\varepsilon + 1)^2}\right],$$

where the single parameter C_1 is defined as half of the shear modulus, G ($C_1 = G/2$). The same relationship can be derived using a statistical thermodynamic approach in which the distribution of end-to-end distances between cross-links is assumed to be Gaussian [63–65].

A typical stress–strain curve is shown in Fig. 5.4 along with its fit using this Neo-Hookean model. The fit agrees well with the data and predicts the observed nonlinear behavior, implying that the distribution of chains is Gaussian and that there is little contribution from entanglements and looping chains to the overall network. Using the Neo-Hookean fit, we observed the change in the gel stiffness as they were swollen and degraded with time in an aqueous environment [48].

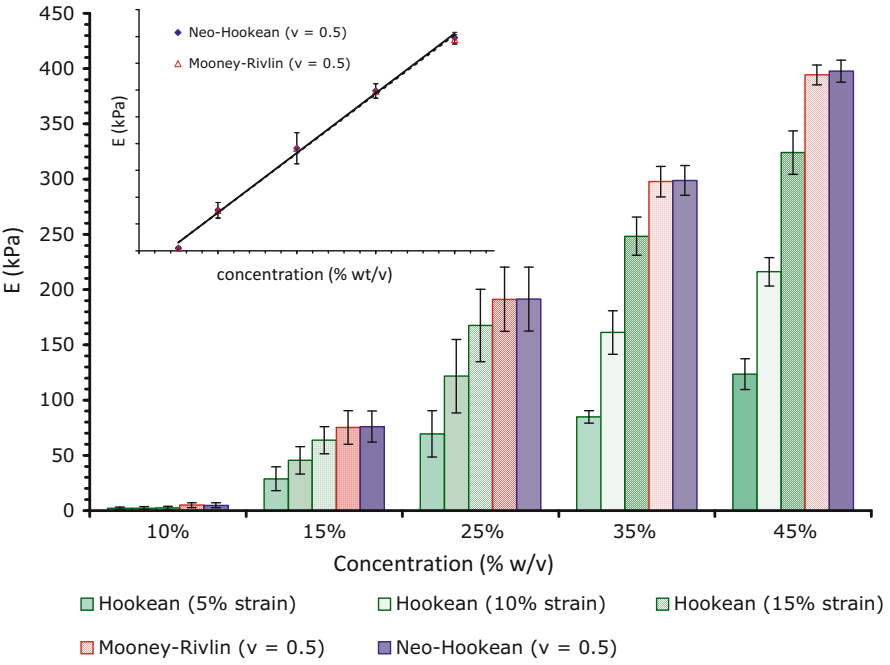

Fig. 5.5 Comparing elastic modulus using various fits. The reported modulus values are highly dependent on which constitutive relationship is assumed. (*inset*) Elastic modulus vs. concentration using rubber models. The two-parameter Mooney–Rivlin model calculates the same modulus as the one-parameter Neo-Hookean model (Note that these models assume incompressibility and a Poisson's ration of 0.5)

Initially, the 25% w/v hydrogels started with a shear modulus of ~ 64 kPa, but as they degraded, the shear modulus decreased exponentially to a value of ~ 7 kPa over a time scale of 35 days until a major drop in modulus occurred. The exponential decrease was in good agreement with the swelling data. The rate of hydrolysis is assumed to be proportional to the cross-link density (ρ_c), since as ester bonds are degraded, cross-links are eliminated. This kinetic behavior was evident in the swelling data, as ρ_c and Q were inversely proportional ($Q \sim 1/\rho_c$), and accounts for the exponential decrease in modulus with time ($G \sim \rho_c$) [72].

To probe the range of attainable moduli using photocrosslinkable PLA–PEO–PLA,, hydrogels were prepared at various concentrations: 10, 15, 25, 35, and 45% (weight of polymer per volume of PBS). As gels were less concentrated they became softer, and as they were more concentrated they became stiffer, as expected. More specifically, there was a linear dependence of shear modulus on the hydrogel concentration (Fig. 5.5-inset). This effect can be explained by considering the hydrogel structure. As already described, the physical cross-links in the network structure occur within the micelle core prior to photocrosslinking, effectively equating the number of micelles to the number of junction points. A critical aggregation number (N_{agg}) of polymer chains is necessary to form

a micelle. Assuming the critical N_{agg} remains constant and all micelles contribute to the network, then as the number of polymer chains (or the overall concentration) are increased linearly, so does the number of micelles (or cross-links). Since modulus is directly proportional to cross-link density, the linear relationship between modulus and concentration is well explained, demonstrating that the photocrosslinking process successfully locks in the pre-formed physical hydrogel structure.

The compression behavior of these polymer hydrogels shows the typical nonlinearity of soft rubbery materials and fits very well with the Neo-Hookean constitutive relationship described above. However, a more common and simple method used to determine modulus is the linear fit of the Hookean constitutive relationship, $[\sigma = E\varepsilon = E(\lambda - 1)]$, where stress is related to strain by the elastic modulus (E). While this relation only holds for the low strain, linear, elastic regime, it is often applied to hydrogel materials displaying nonlinear behavior. Our data can also be fit using a more general two-parameter Mooney–Rivlin model [66, 67]. The shear modulus in the Mooney–Rivlin constitutive relationship is two times the summation of the fit parameters ($G = 2[C_1 + C_2]$). This model, like the Neo-Hookean model, also fits well for nonlinear rubbery materials, but the second parameter allows for closer fits at high extension ratios. When fitting with the Mooney–Rivlin Model, C_1 was set to be equal to the C_1 determined from the Neo-Hookean fit, and C_2 was allowed to float to best fit the data.

Each of the above models fitted the data to various degrees; however, only the Neo-Hookean and Mooney–Rivlin models captured the nonlinear behavior of the hydrogels in compression over the entire strain range. For photocrosslinked PLA–PEO–PLA hydrogels, there was no linear elastic region, even at low strains (see inset of Fig. 5.4), that could be adequately described by the Hookean relationship. Because of the gel's nonlinear behavior, the modulus values obtained from fits using a Hookean relationship were dependent on the strain range to which the data was fit. Since at higher strains more of the downward sloping nonlinear region is taken into account, different values of the elastic modulus were measured. The extent of these effects was measured by fitting a Hookean relationship at 5, 10, and 15% strain with varying hydrogel concentrations (Fig. 5.4-inset). All of the Hookean fits showed a linear dependence on hydrogel concentration as already described, but as the fitted strain range increased so did the modulus. Furthermore, for stiffer hydrogels, the differences in moduli were more pronounced.

To compare the modulus values obtained from the Hookean model to those obtained from the Neo-Hookean and Mooney–Rivlin models, the shear modulus was converted to an elastic modulus, $[E = 2G(1 + \nu)]$, where ν is the Poisson's ratio or the ratio of lateral tension to longitudinal compression. Most commonly, rubbers and gels are assumed to be incompressible with a Poisson's ratio equal to 0.5, which was assumed in the Neo-Hookean and Mooney–Rivlin models. Again all the fits showed a linear dependence on concentration. Interestingly, the two-parameter Mooney–Rivlin fits determined modulus values that were almost identical to the one-parameter Neo-Hookean fit. Although the two-parameter model takes more of the high strain region into account, the one parameter model fits the data well enough that not much is gained in fitting with two parameters.

Furthermore, although most rubbers are assumed to have a Poisson's ratio of 0.5, significantly lower Poisson's ratios have been measured for several hydrogels [73–75]. For example, a Poisson's ratio as low as 0.33 has been reported for poly (vinyl alcohol) gels [76]. Therefore, if the actual Poisson's ratio of a material is not measured and is lower than that assumed, then a discrepancy between the real elastic modulus of the material and the measured elastic modulus will arise. The modulus values from all the fits are compared in Fig. 5.5, and again illustrate that the value obtained is dependent on the fit used. The Hookean model at small strains (5%) gave the lowest elastic moduli, while the Neo-Hookean and Mooney–Rivlin models gave the highest moduli.

Structural Properties of the Gel Phase

The structure of a hydrogel can be used to help determine its mechanical properties. For example, mechanical properties are often dependent upon both the nanoscale and microscale structures [77, 78]. We investigated the microscale structure of these hydrogels containing crystalline PLLA domains through ultra small angle X-ray scattering (USAXS), ultra small angle neutron scattering (USANS), and confocal microscopy techniques. The goal was to correlate changes in the hydrogel structure as the molecular weight of the PLA block was increased. All gel samples exhibited scattering in the low q range that followed power law behavior [78], indicating scattering from fractal structures [79, 80]. The power law exponents were found to be less than or equal to three, which is indicative of a mass fractal structure. These scattering results lead us to infer that hydrogel structure becomes denser as the molecular weight of the PLA domains increases. Although more work is necessary to fully understand the subtleties of the PLLA–PEO–PLLA system, these differences might be related to the crystalline nature of the PLLA hydrophobic domains. WAXD studies on these gels show strong diffraction peaks at $2\theta = 17$ and 19° corresponding to crystalline PLLA, while the PRLA-based hydrogel showed no such peaks [45].

Conclusions

PLA–PEO–PLA triblock copolymers have been extensively studied over the years and have found use in a wide variety of applications. Although we are beginning to understand this copolymer system at a more fundamental level, further study is required before we can fully understand and predict the material properties relevant to specific biomedical applications. We have demonstrated a number of ways to influence the mechanical properties of the resulting hydrogel including at the monomer level by alternating the stereo-center as well as at the nanometer scale by covalently capturing the self-assembled physical network. Unlike physical hydrogels,

the photocrosslinked systems remain intact in a highly aqueous environment giving better properties for various applications. We highlight how modulus values are influenced by the method of data analysis. The modulus of the hydrogel can be determined by choosing either a linear elastic Hookean model or the nonlinear Neo-Hookean and Mooney–Rivlin models. However, the Hookean model can only be applied to small strain regions and does not capture the nonlinear behavior of these soft rubbery materials.

Acknowledgments Data appearing in this review was supported by the central facilities of the NSF-funded Center for Hierarchical Manufacturing (CMMI-0531171 and CMMI-1025020) and the NSF-funded MRSEC on Polymers (DMR-0213695). We thank a number of agencies and companies for their support of the years including ARO, ONR, NSF, 3 M, and DuPont.

References

1. Hoffman, A.S.: Adv. Drug Deliv. Rev. **54**, 3 (2002)
2. Kissel, T., Li, Y., Unger, F.: Adv. Drug Deliv. Rev. **54**, 99 (2002)
3. Lee, K.Y., Mooney, D.J.: Chem. Rev. **101**, 1869 (2001)
4. Kim, B.-S., Mooney, D.J.: TIBTECH **16**, 224 (1998)
5. Tirelli, N., Lutolf, M.P., Napoli, A., Hubbell, J.A.: Rev. Mol. Biotechnol. **90**, 3 (2002)
6. Lutolf, M.P., Hubbell, J.A.: Nat. Biotechnol. **23**, 47 (2005)
7. Nuttelman, C.R., Rice, M.A., Rydholm, A.E., Salinas, C.N., Shah, D.N., Anseth, K.S.: Prog. Polym. Sci. **33**, 167 (2008)
8. Elisseeff, J., Anseth, K., Sims, D., McIntosh, W., Randolph, M., Langer, R.: Proc. Natl Acad. Sci. USA **96**, 3104 (1999)
9. Rotter, N., Ung, F., Roy, A.K., Vacanti, M., Eavey, R.D., Vacanti, C.A., Bonassar, L.J.: Tissue Eng. **11**, 192 (2005)
10. Sudesh, K., Doi, A.Y.: Prog. Polym. Sci. **25**, 1503 (2000)
11. Marois, Y.; Zhang, Z.; Vert, M.; Deng, X.; Lenz, R.W.; Guidoin, R. Bacterial Polyesters for Biomedical Applications: In vitro and in vivo Assessments of Sterilization, Degradation Rate and Biocompatihility of Poly ([3-beta-gydroxyoctaanoate) (PHO). In: Agrawal, C. M., Parr, J. E., Lin, S. T. (Eds.) Synthetic Bioabsorbably Polymers for Implants, ASTM, West Conshohocken, PA (2000).
12. Amass, W., Amass, A., Tighe, B.: Polym. Int. **47**, 89 (1998)
13. Li, S., Vert, M.: Macromolecules **36**, 8008 (2003)
14. Molina, I., Li, S., Martinez, M.B., Vert, M.: Biomaterials **22**, 363 (2001)
15. Bae, S.J., Joo, M.K., Jeong, Y., Kim, S.W., Lee, W.-K., Sohn, Y.S., Jeong, B.: Macromolecules **39**, 4873 (2006)
16. Kwon, K.-W., Park, M.J., Bae, Y.H., Kim, H.D., Char, K.: Polymer **43**, 3353 (2002)
17. Kim, M.S., Hyun, H., Khang, G., Lee, H.B.: Macromolecules **39**, 3099 (2006)
18. Lee, H.T., Lee, D.S.: Macromol. Res. **10**, 359 (2002)
19. Lee, D.S., Shim, M.S., Kim, S.W., Lee, H., Park, I., Chang, T.: Macromol. Rapid Commun. **22**, 587 (2001)
20. Zhong, Z., Dijkstra, P., Feijen, J., Kwon, Y.M., Bae, Y.H., Kim, S.W.: Macromol. Chem. Phys. **203**, 1797 (2002)
21. Fujiwara, T., Mukose, T., Yamaoka, T., Yamane, H., Sakurai, S., Kimura, Y.: Macromol. Biosci. **1**, 204 (2001)
22. Shim, W.S., Yoo, J.S., Bae, Y.H., Lee, D.S.: Biomacromolecules **6**, 2930 (2005)
23. Huang, S., Ingber, D.E.: Nat. Cell Biol. **1**, 131 (1999)

24. Lee, K.Y., Peters, M.C., Anderson, K.W., Mooney, D.J.: Nature **408**, 998 (2000)
25. Chicurel, M.E., Chen, C.S., Ingber, D.E.: Curr. Opin. Cell Biol. **10**, 232 (1998)
26. Kim, B.S., Nikolovski, J., Bonadio, J., Mooney, D.J.: Nat. Biotechnol. **17**, 979 (1999)
27. Choquet, D., Felsenfeld, D.P., Sheetz, M.P.: Cell **88**, 39 (1997)
28. Pelham, R.J., Wang, Y.L.: Proc. Natl Acad. Sci. USA **94**, 13661 (1997)
29. Wang, H.B., Dembo, M., Wang, Y.L.: Am. J. Physiol. Cell Physiol. **279**, C1345 (2000)
30. Pelham, R.J., Wang, Y.L.: Mol. Biol. Cell **10**, 935 (1999)
31. Georges, P.C., Janmey, P.A.: J. Appl. Physiol. **98**, 1547 (2005)
32. Engler, A.J., Griffin, M.A., Sen, S., Bonnetnann, C.G., Sweeney, H.L., Discher, D.E.: J. Cell Biol. **166**, 877 (2004)
33. Flanagan, L.A., Ju, Y.E., Marg, B., Osterfield, M., Janmey, P.A.: Neuroreport **13**, 2411 (2002)
34. Bryant, S.J., Bender, R.J., Durand, K.L., Anseth, K.S.: Biotechnol. Bioeng. **86**, 747 (2004)
35. Moran, J.M., Pazzano, D., Bonassar, L.J.: Tissue Eng. **9**, 63 (2003)
36. Teng, Y.D., Lavik, E.B., Qu, X.L., Park, K.I., Ourednik, J., Zurakowski, D., Langer, R., Snyder, E.Y.: Proc. Natl Acad. Sci. USA **99**, 3024 (2002)
37. Woerly, S., Doan, V.D., Sosa, N., de Vellis, J., Espinosa-Jeffrey, A.: J. Neurosci. Res. **75**, 262 (2004)
38. Brandl, F., Sommer, F., Goepferich, A.: Biomaterials **28**, 134 (2007)
39. Huang, S., Ingber, D.E.: Nat. Cell Biol. **1**, 131 (1999)
40. Frank, E.H., Grodzinsky, A.J.: J. Biomech. Eng. **20**, 629 (1987)
41. Stockwell, R.; Meachim, G. In: Adult Articular Cartilage, Pitman Medical London (1979).
42. Yu, Q.L., Zhou, J.B., Fung, Y.C.: Am. J. Physiol. **265**, H52 (1993)
43. Erkamp, R.Q., Wiggins, P., Skovoroda, A.R., Emelianov, Ss.Y., O'Donnell, M.: Ultrason. Imaging **20**, 17 (1998)
44. Aamer, K., Sardina, H.A., Bhatia, S., Tew, G.N.: Biomaterials **25**, 1087 (2004)
45. Sanabria-DeLong, N., Agrawal, S.K., Bhatia, S.R., Tew, G.N.: Macromolecules **39**, 1308 (2006)
46. Sanabria-DeLong, N., Agrawal, S.K., Bhatia, S.R., Tew, G.N.: Macromolecules **40**, 7864 (2007)
47. Agrawal, S.K., Sanabria-DeLong, N., Bhatia, S.K., Tew, G.N., Bhatia, S.R.: Langmuir **26**, 17330 (2010)
48. Sanabria-DeLong, N., Crosby, A.J., Tew, G.N.: Biomacromolecules **9**, 2784 (2008)
49. Li, Y.X., Kissel, T.: J. Control. Release **27**, 247 (1993)
50. Zhu, K.J., Lin, X.Z., Yang, S.L.: J. Appl. Polym. Sci. **39**, 1 (1990)
51. Li, F., Li, S.M., Vert, M.: Macromol. Biosci. **5**, 1125 (2005)
52. Rashkov, I., Manolova, N., Li, S.M., Espartero, J.L., Vert, M.: Macromolecules **29**, 50 (1996)
53. Li, S.M., Rashkov, I., Espartero, J.L., Manolova, N., Vert, M.: Macromolecules **29**, 57 (1996)
54. Mai, S.M., Abbot, A., Norton, D., McKean, R., Ryan, A.: J. Macromol. Chem. Phys. **210**, 840 (2009)
55. Cohn, D., Younes, H.: J. Biomed. Mater. Res. **22**, 993 (1988)
56. Kricheldorf, H.R., Meierhaack, J.: Makromolekulare Chemie-Macromol. Chem. Phys. **194**, 715 (1993)
57. Hu, D.S.G., Liu, H.J.: Polym. Bull. **30**, 669 (1993)
58. Cerrai, P., Tricoli, M., Lelli, L., Guerra, G.D., Delguerra, R.S., Cascone, M.G., Giusti, P.: J. Mater. Sci.-Mater. Med. **5**, 308 (1994)
59. Jedlinski, Z., Kurcok, P., Walach, W., Janeczek, H., Radecka, I.: Makromolekulare Chemie-Macromol. Chem. Phys. **194**, 1681 (1993)
60. Sawhney, A.S., Pathak, C.P., Hubbell, J.A.: Macromolecules **26**, 581 (1993)
61. Agrawal, S. K.; Sanabria-DeLong, N.; Aamer, K.; Sardina, H. A.; Bhatia, S.; Tew, G. N. Agrawal, S.K., Sardinha, H., Aamer, K.A., Sanabria-DeLong, N., Bhatia, S.R., Tew, G.N. Triblock PLLA-PEO-PLLA Hydrogels: Structure and Mechanical Properties. In: Svenson, S. (Ed.), Polymeric Drug Delivery volume II – Polymeric Matrices and Drug Particle Engineering, ACS Symposium Series, Washington, DC (2006).
62. Shin, D., Shin, K., Aamer, K.A., Tew, G.N., Russell, T.P., Lee, J.H., Jho, J.Y.: Macromolecules **38**, 104 (2005)

63. Wall, F.T.: J. Chem. Phys. **10**, 485 (1942)
64. Flory, P.J., Rehner, J.: J. Chem. Phys. **11**, 512 (1943)
65. Treloar, L.R.G.: Trans. Faraday Soc. **39**, 241 (1943)
66. Mooney, M.: J. Appl. Phys. **11**, 582 (1940)
67. Rivlin, R.S.: Philos. Trans. R. Soc. Lond. A Math. Phys. Sci. **241**, 379 (1948)
68. Pham, Q.T., Russel, W.B., Thibeault, J.C., Lau, W.: Macromolecules **32**, 5139 (1999)
69. Tae, G., Kornfield, J.A., Hubbell, J.A., Johannsmann, D., Hogen-Esch, T.E.: Macromolecules **34**, 6409 (2001)
70. Tae, G., Kornfield, J.A., Hubbell, J.A., Lai, J.: Macromolecules **5**, 4448 (2002)
71. Zhong, Z.Y., Dijkstra, P.J., Jan, F.J., Kwon, Y.M., Bae, Y.H., Kim, S.W.: Macromol. Chem. Phys. **203**, 1797 (2002)
72. Flory, P.J., Rehner, J.: J. Chem. Phys. **11**, 521 (1943)
73. De, S.K., Aluru, N.R., Johnson, B., Crone, W.C., Beebe, D.J., Moore, J.: J. Microelectromech. Syst. **11**, 544 (2002)
74. Takigawa, T., Ikeda, T., Takakura, Y., Masuda, T.: J. Chem. Phys. **117**, 7306 (2002)
75. Li, Y., Hu, Z., Li, C.: J. Appl. Polym. Sci. **50**, 1107 (1993)
76. Urayama, K., Takigawa, T., Masuda, T.: Macromolecules **26**, 3092 (1993)
77. Sieminski, A.L., Gooch, K.J.: Biomaterials **21**, 2233 (2000)
78. Agrawal, S.K., Sanabria-DeLong, N., Jemian, P.R., Tew, G.N., Bhatia, S.R.: Langmuir **23**, 5039 (2007)
79. Crichton, M., Bhatia, S.: J. Appl. Crystallogr. **36**, 652 (2003)
80. Schmidt, P.W.: J. Appl. Crystallogr. **24**, 414 (1991)

Part IV
Control of Inflammation and Host Response

Chapter 6
Host Response to Biomaterials

Anjelica L. Gonzalez-Simon and Omolola Eniola-Adefeso

Abstract The implantation of a biomaterial-based device or drug carrier will elicit a localized or systemic inflammatory response. An immune response occurs regardless of the method of introduction of biomaterial into the body, as all methods of biomaterial insertion, including surgery and injection, result in the disruption of the host's tissue. The extent of the inflammatory response, however, is dependent upon the location, implantation procedure, and compatibility of biomaterial. In general, inflammatory responses can be classified as acute or chronic, defined primarily by the duration of the response and the type of cells infiltrating a tissue in response to pro-inflammatory signals. This chapter discusses the general process of acute and chronic inflammatory response and gives details on the key immune cells and soluble blood plasma factors involved. Information is also provided on biomaterial design approaches employed to minimizing inflammatory response.

General Introduction

As in the case of a general injury or trauma to any tissue, the implantation of a biomaterial-based device or drug carrier will elicit a localized or systemic inflammatory response. An immune response occurs regardless of the method of introduction of biomaterial into the body, as all methods of biomaterial insertion, including surgery and injection, result in the disruption of the host's tissue. The extent of the inflammatory response, however, is dependent upon the location, implantation procedure, and compatibility of biomaterial. The consistent aspect of biomaterial implantation is that there will be a biological response driven by

A.L. Gonzalez-Simon (✉)
Department of Biomedical Engineering, Yale University, New Haven, CT, USA
e-mail: anjelica.gonzalez@yale.edu

O. Eniola-Adefeso
Department of Chemical Engineering, University of Michigan, Ann Arbor, MI, USA

S.K. Bhatia (ed.), *Engineering Biomaterials for Regenerative Medicine: Novel Technologies for Clinical Applications*, DOI 10.1007/978-1-4614-1080-5_6,

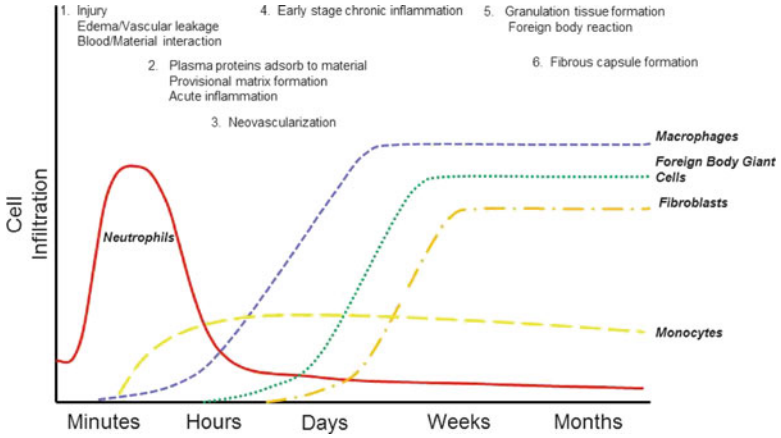

Fig. 6.1 Timeline of inflammatory response to tissue implanted biomaterials. Shortly following injury or implantation of biomaterials, neutrophil infiltration, edema, and vascular leakage occur. Biomaterials interface with blood leading to plasma protein adsorption on to the material surface. Neutrophil infiltration and influx of plasma protein causes tissue matrix reorganization and the initiation of complement and coagulation cascades. Neovascularization occurs as a result of provisional matrix formation. Early stage chronic inflammation is marked by increased monocyte and macrophage infiltration and neutrophil clearance. True chronic inflammation is marked by persistent macrophage activation and infiltration, foreign body response and formation of granulation tissue. Ultimately, biomaterial rejection is preceded by fibrous capsule formation and enclosure of the foreign object. Adapted from J. M Anderson. Mechanisms of Inflammation and Infection with Implanted Devices. Cardiovascascular Pathology. Vol. 2, No. 3 (Suppl.)1993: 33 S–41S [3]

blood and tissue proteins that initiate the coagulation and complement cascades, and result in a cellular immune response. *Localized inflammatory response* is an isolated physiological effort to heal and reestablish tissue homeostasis, whereas a *systemic inflammatory response* is a whole body reaction to a foreign entity that can result in organ damage and serious complications related to immunological reactions [1]. Inflammatory responses can be further classified as *acute* or *chronic*, defined primarily by the duration of the response and the type of cells infiltrating a tissue in response to pro-inflammatory signals (Fig. 6.1). The development of biocompatible biomaterials for use in medical devices and tissue replacement/regeneration is done with the goal of minimizing the acute phase response and thus avoiding the chronic phase inflammatory response that occurs when acute response is not resolved. Figure 6.1 outlines the general temporal sequence marking cell infiltration and persistence, delineating the acute and chronic phases of inflammation. Each phase and type of immunological response to biomaterials is driven by a tightly choreographed series of cellular processes; each interrelated between blood cells, tissue protein composition, tissue resident cells, and their pro-inflammatory protective response. In this chapter, we identify and outline the role of the most abundant and relevant cell types related to the immunological processes that drive biomaterial implant acceptance or rejection in association with wound healing.

Acute Inflammatory Response

The acute inflammatory response to injury or implanted materials is initiated by *innate immunity*. This response is driven by fast acting white blood cells, mostly neutrophils and macrophages, as the *primary* defense against *nonspecific* infecting entities. The goal of innate immunity is to recognize foreign pathogens or materials, clear them from the body, and remove apoptotic cell debris. The immune cell response to implanted biomaterials is ultimately dictated by the adsorption of endogenous proteins from blood or interstitial fluid onto the surface of a device, rather than the physical presence of the material itself. Devices become exposed to blood plasma proteins and tissue fluid or matrix proteins during implantation through surgery or injection. The immune cell identification of adsorbed protein is responsible for the initiation and severity of the immune response. Of course, the protein profile on an implant will depend on the chemical characteristic of the biomaterial involved and to a lesser extent the physical geometry (size and shape) of the implant as discussed later [2]. The inflammatory response is further characterized by the changes in cellularly released chemical factors that mediate additional cell recruitment and activity. As a robust means of systemic protection, the innate immune response is replicated each time an exogenous object is introduced into the body. This requires precise choreography between multiple cell types, including *neutrophils, macrophages, monocytes, endothelial cells* (ECs), and *fibroblasts* (Fig. 6.1) [3].

Neutrophils (Polymorphonuclear Granulocytes)

Neutrophils, the first responders in the initiation of innate immunity, are phagocytic white blood cells or leukocytes. Phagocytosis is a special form of endocytosis – the process by which a cell uptakes or eats (in the case of phagocytosis) solid particles. The life of the mature neutrophil is spent in the blood stream or surrounding tissue, with its primary role being to remove foreign particles from the body via phagocytosis. Additionally, the mature neutrophil rids the body of contaminants in the microenvironment through exocytosis – the process of secreting proteins, proteases, and reactive oxygen metabolites stored within mobilizable granules. Through exocytosis, the neutrophil reorganizes the surrounding microenvironment and promotes recruitment of additional immune responsive cells to the point of infection. The release of additional proteases and reactive oxygen species is done to damage and destroy the infecting entity. The normal life-time of neutrophils in the vasculature is approximately 12 h, during which time they may react to pro-inflammatory *cytokines* and *leukocyte adhesion molecules* (LAMs) presented by the endothelium (a monolayer of ECs that line the lumen of blood vessels) upon injury during implantation or injection [4]. Cytokines are a large family of proteins, peptides, or glycoproteins that are recognized as intercellular signaling immunomodulators.

LAMs are receptors on the surface of ECs that bind to ligands (or counter receptors) on the surface of leukocytes. For example, the *selectins* support cell–cell adhesion through recognition of carbohydrates, while members of the *immunoglobulins*, namely *intercellular adhesion molecule 1* (ICAM1) and *vascular cell-adhesion molecule 1* (VCAM1), bind to the leukocyte surface receptors known as *integrins*. Under quiescent conditions, the endothelium does not present large amounts of LAMs, however, upon damage through implantation or injection of a biomaterial, the endothelium becomes inflamed as EC upregulate a significant number of LAMs and produce pro-inflammatory signals. These molecular signals activate the cells to upregulate their own integrins, enabling neutrophils to become adherent to the blood vessel wall and ultimately migrate into the tissue. The life span of the neutrophil outside of the blood vessel and in the tissue is extended to 24–48 h [4].

The process of neutrophil capture to the endothelial wall (or margination) and their eventual migration into the extravascular space (or *transmigration*) occurs through a series of intricately choreographed steps known as the *leukocyte adhesion cascade* [5]. Instrumental to each step are LAMs, integrins, cytokines, and carbohydrates expressed or produced by the endothelium and the neutrophil. The acute phase of the inflammatory response begins with the initial *capture* from free stream to EC surface – the first step of the leukocyte adhesion cascade, in which neutrophil expressed L-selectin and P-selectin glycoprotein ligand 1 (PSGL1) engage endothelial expressed E-selectin, P-selectin, and PSGL1 [6, 7] to transiently tether the neutrophil to the endothelium. Capture is followed by *rolling* (transient adhesion), during which the inflamed endothelial cell is triggered to release neutrophil-activating cytokines and chemoattractants. These cytokines are physiological activators of the neutrophil integrins lymphocyte function-associated antigen 1 (LFA1, $\alpha_L\beta_2$) and very late antigen 4 (VLA4, $\alpha_4\beta_1$) that bind to EC expressed ICAM1 and VCAM1, respectively, promoting almost instantaneous *firm arrest* on the vascular lumen. Both increased integrin expression on the surface of neutrophils and modulation of affinity for integrin ligands contribute to the bond strength established between the adherent neutrophil and the EC. Once neutrophils are firmly arrested onto the endothelium, intravascular *crawling* can commence, in which integrin macrophage antigen 1 (MAC1, $\alpha_M\beta_2$) on the neutrophil surface engages ICAM1 on the endothelial surface to form traction forces that propel the cell forward. Finally, cell intravascular crawling brings the cell to a point at which it can migrate across the endothelial layer into the extravascular space, i.e. *transmigration*, to obtain direct access to the implanted biomaterial.

Transmigration is the most poorly understood event in the leukocyte adhesion cascade and continues to be investigated. The current understanding is that ICAM1 and MAC1 interact to trigger the formation of neutrophil protrusions at the leading edge of the transmigrating neutrophil. At this point, the neutrophil engages with additional adhesion and junctional molecules on the EC to transmigrate paracellularly (between two or more endothelial cells) or transcellularly (through the body of the endothelial cell). Subsequent interactions between neutrophil integrins, vascular endothelial cadherin (VE-cadherin), platelet/endothelial cell adhesion molecule 1 (PECAM1), junctional adhesion molecule A (JAMA),

endothelial cell selective adhesion molecule (ESAM), ICAM2, and CD99 are indeterminately involved in migration through the endothelial layer, the basement membrane and the pericyte sheath.

Migration within the extravascular space is heavily regulated by the chemotactic factors released by resident macrophages, protein components of the extracellular matrix (ECM), and the ability of the neutrophil to access these matrix components for anchoring, degradation, and migration. Using a number of non-redundant tissue matrix binding integrins, the neutrophil responds directly to the microenvironment by adhering to and remodeling the surrounding ECM. Each tissue in the body (connective, pulmonary, cardicac, etc.) contains a unique composition of ECM fibrous and non-fibrous proteins, largely collagens, elastin, proteoglycans, fibronectin, and laminins, that serve to anchor resident cells and maintain the structure of the organ. Specific integrins are responsible for *firm adhesion* of neutrophils to ECM proteins that contain adhesive amino acid motifs, including the widely studied arginine–glycine–aspartic acid (RGD) residues [8]. It is also understood that neutrophil integrins have specificity for sequences in the fibrinogen and fibronectin proteins that can generate functional cell activity, including adhesion and motility [9]. As the neutrophil invades, it maneuvers itself through globular and along fibrous structures of the ECM in response to chemical mediators released by injured and activated tissue or vascular cells. Neutrophils respond to these chemical mediators by migrating toward the injury or implant site through unidirectional movement toward the increasing gradient of chemical signal in a process known as chemotaxis. Once localized to the site of implantation, the presence and conformation of tissue ECM proteins and blood proteins deposited onto the surface of an implanted biomaterial will determine the neutrophil response to the implant. In response to protein identification, the neutrophil will begin the process of phagocytosis if the implant chemistry and geometry allows, the material may be degraded and endocytosed by the cell, and the dead neutrophil and material debris are later cleared by macrophages. However, phagocytosis and clearance is not possible with implants much larger than the size of the cell (10 μm). Thus, neutrophils of often respond to large implants by degranulating, releasing lysosomal protease and reactive oxygen species that remodel the native tissue and the implanted material, providing pathways not only for additional neutrophil invasion but also recruited macrophages. The duration and amount of enzyme released during this process is highly dependent upon the surface composition and the size of the biomaterial (particulate versus bulk).

Monocytes

Monocytes are blood flowing macrophage and dendritic cell precursors, making up 1–6% of the total circulating leukocyte population. As the number of neutrophils in the damaged or infected tissue begins to decline, cytokines, and chemotactic factors released by these cells and resident macrophages recruit monocytes to the site of injury, marking the initiation of the chronic inflammatory response. As a slow

migrating cell, compared with neutrophils, monocytes provide a secondary source of defense against pro-inflammatory mediators by differentiating into macrophage or dendritic cell populations following migration into the tissue, serving to amplify and, later, resolve inflammation.

Chronic Inflammatory Response

Chronic inflammation is most commonly associated with disease states and inflammatory disorders; however, a chronic inflammatory response to implanted biomaterials often leads to rejection and extraction. The persistence of inflammation may be related to the composition of the implant itself, degradation of the biomaterial through motion, or continued injury to the implant site through motion. In either case, when the acute phase of inflammation has not sufficed to clear the source of infection within the first 1–2 days of implantation, macrophages become the dominating force in the persisting inflammatory response through continued release of leukocyte recruiting chemotactic factors, reactive oxygen metabolites, growth factors, and cytokines. Macrophages operate to release these factors with the intent of degrading the biomaterial in an attempt to clear the infecting reagent.

Macrophages (Mononuclear Phagocytes)

The macrophage, greek for "large eater," is a monocyte derived specialized phagocytic and secretory white cell that is distributed throughout tissues. Tissue resident macrophages, within the lung, skin, liver, spleen, and gut serve the primary function of identifying and reacting to exogenous materials or infecting organisms. These cells have an elongated life (up to months) providing a continuous population of cells available to emigrate into an infected tissue for an extended duration, sustaining the chronic phase of inflammation. In a unique manner, the macrophage bridge innate and adaptive immunity by (1) phagocytosing and destroying invading microbes, (2) fusing to become multinucleated giant body cells, and (3) acting as antigen presenting cells, presenting proteins from digested microbes to activate the white blood cells responsible for adaptive immunity. Much like the neutrophil, in response to microbes and foreign entities, the macrophage ingests large microbes and proteins, releases tissue damaging proteases, reactive oxygen and nitrogen metabolites, and releases pro-inflammatory cytokines, chemokines, and lipid mediators. Specifically, the macrophage releases tumor necrosis factor-alpha (TNFα), interleukin-1 (IL-1), interleukin-6 (IL-6), and interleukin-8 (IL-8) to induce recruitment of additional neutrophils (exacerbating the innate inflammatory response), endothelial cells (for formation of new microvessels), and fibroblasts (for formation of fibrous scar tissue) [10]. Macrophages are also responsible for ridding the inflamed tissue of apoptotic cell debris, including aged neutrophils, marking the

resolution of acute inflammation. In general, macrophages are able to successfully ingest microbes and materials sized up to 10 μm as with neutrophils. For larger sized materials as in the case of most implants for regenerative medicine, multiple macrophages may fuse together forming a multinucleated *foreign body giant cell* (FBGC) that remains adherent to the surface of the large (>100 μm) biomaterial for the lifetime of the implant [11]. FBGCs may experience phagocytic frustration when the material is too large for ingestion, causing the release of cytokines, reactive oxygen species, and proteolytic enzymes, in hopes of degrading the large biomaterial [12]. The extended longevity of activated resident macrophages and FBGCs at the site of biomaterial implant contribute substantially to the *chronic* inflammatory response, in which inflammation is not effectively resolved and macrophages persist in respiratory burst and protease release, leading to damage of host tissue.

Foreign Body Reaction

Macrophages, like neutrophils, adhere to the surface of implanted biomaterials when unable to phagocytose the material due to large material to cell size ratio. In this condition, the fusion of macrophages to form FBGCs serves to prolong the life span of the frustrated macrophages, allowing continued release of cytokines and growth factors. Within the 3–5 days of monocyte invasion and activation of resident macrophages, the formation of *granulation tissue* occurs. Granulation tissue is a *wound healing* response in which fibroblasts, and often vascular endothelial cells, invade and proliferate within the infected tissue in an attempt to establish structure and homeostasis at the local inflammation site. In the granulation tissue, fibroblasts deposit non-fibrillar proteoglycans followed by collagen deposition, contributing to the initiation of the fibrous capsule. Likewise, endothelial cells invasion and proliferation contribute to the development of neovascularization of the wounded tissue in an attempt to deliver increased cytokines and growth factors that promote the wound healing response. The persistent presence of macrophages within the granulation tissue ensures constant remodeling of the tissue matrix and constant recruitment of fibroblasts, endothelial cells, and other cells. This process may continue from days to months, dependent upon the gravity, site and size of the infection, and implant.

Fibroblasts

While recruiting additional leukocytes to the milieu of inflamed tissue, macrophages also release growth factors and cytokines to activate and recruit fibroblasts to the site of injury, promoting cellular proliferation, and tissue remodeling. Fibroblasts are mesenchyme-derived cells with their primary function

being to produce and remodel the ECM, providing scaffolding and framework in various organs and specialized tissues. In a cyclical manner, the synthetic and degradative functions of fibroblasts are controlled and regulated by signals from the matrix, as well as leukocyte contributed cytokines and growth factors. Through its ability to generate matrix proteins, the fibroblast is primarily responsible for the generation and remodeling of fibrotic scar tissue and foreign body encapsulating matrices. The assembly of an acellular fibrous capsule, composed of dense and compacted collagen, is a method of resolving the inflammatory response to an implanted biomaterial, by walling off the damage induced by a foreign implant. While providing a resolution to the local immune response, the formation of the fibrous capsule may lead to implant failure/rejection, deformation at the site of implantation or loss of implant function.

Fibrous Encapsulation

As a means of resolving the inflammatory process, both stable and proliferating cells, resident to the infected tissue, contribute to the formation of a matrix-composed capsule surrounding the implanted biomaterial. Specifically, fibroblasts within the granulation tissue are deposit proteoglycans (nonfibrillar components of the ECM with the ability to bind growth factors), cytokines, matrix adhesion molecules, while contributing to the formation collagen fibers that form a base for the capsular structure. Subsequent deposition of collagens, fibronectins, laminins, thrombospondins, tenascin, and syndecans contribute to the advanced formation of a biomaterial encapsulating fibrous tissue that aids in integrating the new scaffold with the existing tissue. Unfortunately, over-development of the fibrotic capsule can lead to physical deformation of the host tissue and, ultimately, interrupt the intended function of the implanted device. When this occurs, surgical removal of the device is the preferred method of resolution.

Chemical Mediators of the Inflammatory Response to Biomaterials

The two phases of the foreign body response, acute and chronic phases, are distinguished by the time of the response and the type of cell involved in each phase. Because protein adsorption predicts the biological response to an implanted material, it is important to understand the protein-mediated cascades that result in inflammation. Here we describe the contributions of the *coagulation and complement cascades* to acute and chronic inflammation. The coagulation and complement systems act together as a physiological defense against injury and non-self in a manner that is complementary to leukocyte function in healing and ridding the body

of foreign entities [13]. Each system is composed of a number of proteins that interact with a biomaterial or implant surface, leading to biocompatibility or incompatibility [14, 15]. The initiation of both systems is highly dependent upon the ability of proteins to become surface bound and subsequently become activated through cleavage or conformational change [16]. Structural changes of coagulation and complement system proteins directly enable stimulation of neutrophils, monocytes, macrophages, and platelets typically leading to disadvantageous inflammation and biomaterial rejection.

The Complement Cascade

The complement system is composed of approximately 30 proteins and protein subunits whose function is to recruit and activate leukocytes to purge foreign substances and objects from the body. Three primary pathways make up the complement system. The first, the *classical pathway*, is triggered by the formation of antigen–antibody complexes, C-reactive protein, or identification of debris from damaged cells. The second pathway, the *mannose-binding lectin* (MBL) *pathway* (LP), is triggered by MBL binding to specific carbohydrates found on the surface of invading microorganisms. The third pathway, the *alternative pathway* (AP), is one in which non-self surfaces, including biomaterial surfaces, directly trigger complement activation. While the alternative pathway is most clearly associated with biomaterial implantation and rejection, the other pathways remain relevant as they can become amplified by alternative complement activation in response to foreign body implants. Within each of these pathways proteins complement component 3 (C3), component 4 (C4), and component (C5) are among the most abundant proteins. Complement C3 is most closely identified in the alternative pathway in response to biomaterial rejection. As a blood plasma component, C3 comes in contact with the implant surface during implantation. C3 can directly bind to a biomaterial surface and become conformationally altered to bind factor B from blood plasma, inducing an almost immediate complement initiated inflammatory response [12, 17]. The main event in activation of the alternative complement pathway is C3 conformational change into a C3b-like presentation or enzymatic cleavage into subunits C3b and C3a (Fig. 6.2). The C3b molecule can become bound to a biomaterial surface through binding to adsorbed proteins and carbohydrates via free hydroxyl or amine groups [18]. The structure of absorbed blood plasma proteins, including human serum albumin and immunoglobulin G (IgG) allows them to act as acceptors, covalently binding and stabilizing C3b [19–21]. Free hydroxyl groups provide the transient covalent ester bond necessary for the biological activity of C3b. Exposed amine group provides a stable covalent bond, also necessary for the C3b molecule activation [22]. Activated surface bound C3b is available to bind Factor B [23], forming C3bB, a complex that is further cleaved by Factor D for the formation of C3bBa and C3bBb. C3bBb is also known as C3 convertase and serves to further activate bound and free C3, amplifying the

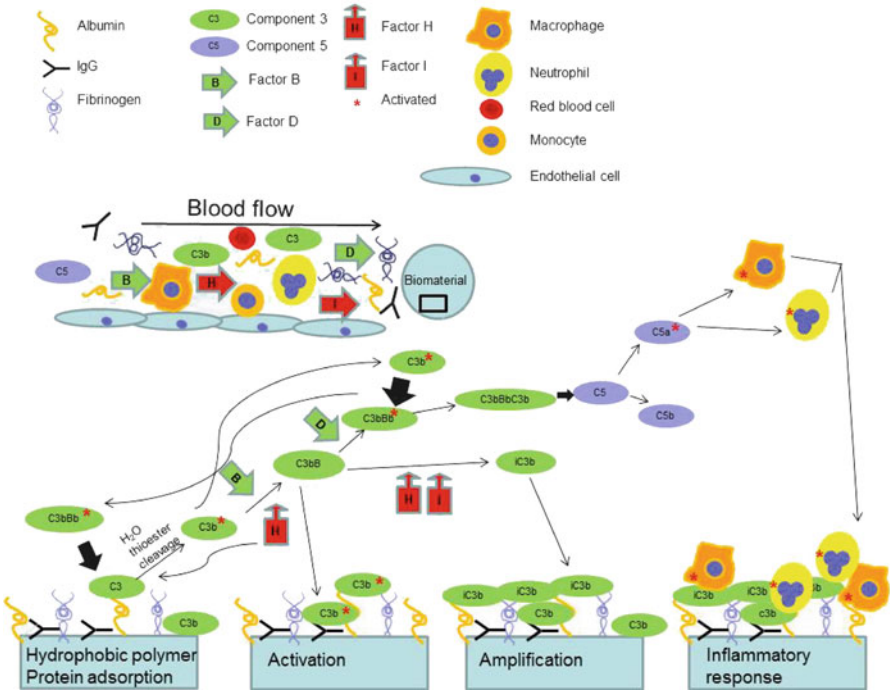

Fig. 6.2 Biomaterial activation of alternative complement pathway. Implanted biomaterials initially adsorb protein from blood plasma, including albumin, IgG, fibronectin, free C3, and C3b. C3 can be hydrolized for thioester cleavage (C3b) or can bind polymers surfaces in a C3b-like conformation for optimal binding of Factor B. Factor H competes with Factor B for binding to C3b, preventing Factor D binding and cleavage into C3 convertase, C3bBb. Factor H and I can act in tandem to regulate C3 convertase activity by creating inactive C3b (iC3b), which binds the surface of the biomaterial and directly binds activated leukocyte receptors. Otherwise, C3 convertase can act on C3 to amplify complement signal progression or bind C3b to become C5 convertase (C3bBbC3b), cleaving C5 into anaphylatoxic C5a. C5a activates granulocytes for recognition of binding ligands, including iC3b

complement system. Surface or protein bound C3b can subsequently interact with AP proteins to form C3 convertase, leading to additional surface deposition of C3b. An overabundance of deposited C3b on the surface causes C3 convertase progression to C3bBbC3b that preferentially targets C5, resulting in C5 cleavage and generation of subunits C5a and C5b. Anaphylatoxic peptides C3a and C5a are particularly dangerous, due to their ability to induce tissue damage through direct effects on monocytes, macrophages, and neutrophils. A secondary byproduct of C3b cleavage is iC3b, an MAC1-specific ligand, providing a means by which macrophages and neutrophils can bind directly to iC3b-coated surfaces, initiating phagocytosis and granule release.

Biomaterials surfaces initially become involved in the activation of complement through direct deposition of C3 when the device or material comes in contact with

blood or plasma from tissue injury during implantation or even interstitial tissue fluid (e.g., synovial fluid) that will have proteins with the same capability of adsorbing onto the material, enabling resident tissue macrophages to identify the material and bind, initiating the inflammatory cascade. Studies have indicated that C4 activation can also be triggered when C4 binds directly to an implant surface, causing an initial CP and or C4-dependent LP complement response, followed by AP activation. Beyond complement activation through direct binding of blood plasma proteins on biomaterial surface, we now know that complement activation, specifically C5 conversion to C5a can be initiated by proteins and enzymes from the coagulation system. For example, thrombin can become an active C5 convertase, promoting neutrophil, and monocyte activation and their response to C5a and C5b subunits.

While complement activation can cause excessive immune response, activation and creation of complement subunits and convertases can be internally regulated by complement components themselves. Internal regulator Factor H competes with Factor B for binding to C3b, prohibiting the formation of C3bB and subsequent convertases. Additionally, Factors H and I cleave C3bB to form the inactive C3b (iC3b) complex. As shown in Fig. 6.2, accumulation of iC3b can provide a binding site to which neutrophils and macrophages can adhere. Ultimately, the adsorption of C3, its cleavage and conversion to C3b, the amplification of C3 convertase, and accumulation of C3b, iC3b, and C5a are responsible for biomaterial driven complement-mediated inflammatory responses. A summary of the proteins initiating complement pathway bioincompatible responses to biomaterials is given below [24]:

1. Soluble C3a and C5a can react directly to receptors on neutrophils and monocytes to trigger chemotaxis, enhanced expression of C3b receptors, increased expression of MAC1, enhanced adhesion to endothelial cells, increased oxygen consumption and generation of free oxygen radicals and granule secretion.
2. Surface bound C3b and iC3b can generate leukocyte responses by binding C3b receptors on the cell membrane and signal release of granular enzymes and generation of active oxygen species [25].

Material Characteristic in Inflammation

As biomedical engineering has progressed, so has the development of biomaterials (typically polymer systems) and the understanding of the need for biocompatibility. Today, implanted systems are commonly functionalized to release anti-coagulant drugs, eliminating the complications of the coagulation cascade during implantation. However, the problem of blood–material interaction elicitation of inflammation remains. Polymers can elicit an inflammatory response through physiochemical properties that control the amount and conformation of proteins adsorbed to the material surface. Polymers chemistry can be functionally specified to create polymer

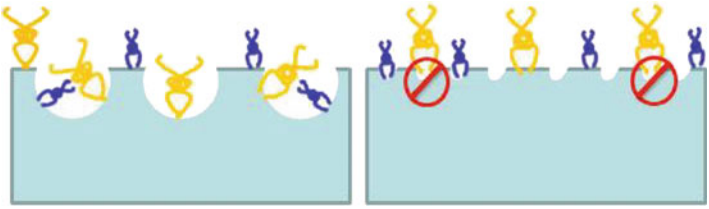

Fig. 6.3 Pore size exclusion of surface protein adsorption. Large pores on a biomaterial surface increase the surface area for interaction with protein. Smaller pores lead to loss of available surface area, as large and medium size proteins are unable to access the walls of the pores for adsorption

matrices that are acidic, basic or neutral, hydrophobic or hydrophilic and vary in pore size, and changes in these physiochemical properties can create a polymer system that will uniquely alter its capabilities of protein adsorption. Specifically, hydrophobicity is a characteristic that promotes protein adsorption because water can be easily displaced from a hydrophobic surface by proteins. A hydrophilic surface has a higher affinity for water than protein, creating a surface that is not favorable for protein adsorption. Protected from protein adsorption, the hydrophilic surface is less likely to elicit a direct inflammatory response. However, hydrophilic polymers may activate the complement system when another characteristic is altered. For example, it has been shown that hydrophilic, charged polymers can elicit complement activation due to the electrostatic interact between the protein charge and the density of electrons contributed by negatively charged polymers [26]. In this case, a negatively charged polymer can bind blood plasma proteins including complement components and IgGs that can induce complement activation and leukocyte response, overcoming the protection provided by hydrophilicity.

Because polymers are a cross-linked network of monomeric subunits, they form a porous network. The physical property of pore size can facilitate steric hindrance between proteins and the polymer surface. A small polymer pore size can limit the total accessible surface area for proteins to bind and also limit the size of proteins that can bind. A surface with large pores will not interfere with protein binding, allowing both large and small proteins to bind around and within pores for optimal protein presentation [26]. This is because pores of larger size are indented into the surface of the material, creating more surface area along the edges of the pores. Most sized (small, medium, and large) proteins can fit into and line the large pores. However, surfaces with small pore sizes do not provide enough area for the most protein to fit into the pore, thus the pore becomes a loss of accessible surface area (Fig. 6.3).

Functionalization of polymer systems is not limited to the charge, hydrophobicity, and pore size. More often now, researchers are exploring the ability to preferentially graft proteins or specific protein domains onto polymer chains to direct physiologic responses. Peptide sequences from blood proteins can be grafted to a polymer to provide a surface that will elicit a specific cell response. Polymers engrafted with the RGD peptide sequence can bind cells via integrins, creating a surface

upon which cells are firmly attached but immobile [9]. Taking advantage of integrin specificity and signaling, peptide sequences from blood proteins can also be used to promote specific cell activity, including protease and reactive oxygen release, cell polarization, and motility. As biomaterials research continues, methods to modify biomaterials surfaces to assure biocompatibility and minimize coagulation, protein adsorption, and complement activation are under development.

While chemical structure can alter basic characteristics of polymer systems, the manner in which proteins adsorb to the surface can also drive the cell response to a material. For example, an hydrophobic polymer surface predominately binds C3 in a manner that exposes the binding site to which factor H can attach, inhibiting the conversion of C3b to C3 convertase (C3bBb) or C5 convertase (C3bBbC3b) [27]. In this case, the surface bound Factor H creates a "nonactivating surface," inhibiting convertase formation and accelerating the dissociation of C3 convertase formed. This nonactivating surface should be incapable of covalently binding C3b or proteins that can subsequently bind C3b in an inactivating conformation. Likewise a surface that can preferentially bind regulatory factor H to prevent the conversion of C3b to a convertase in turn preventing amplification would be considered nonactivating. Heparin coatings are extensively used to inhibit coagulation and complement activation, by binding regulators such as factor H and anti-thrombin. Through the use of polymers such as polyethylene oxide (PEO) and polyethylene glycol (PEG), protein adsorption is minimized, though PEO modified surfaces can act as potent complement activators [28–31]. New advances suggest that hybrid surfaces, those that contain attributes of being protein resistant, anti-coagulatory, and present regulators of complement activation are likely the best models for biocompatible materials. Andersson et al. demonstrated in 2006 that factor H covalently bound to a functionalized PEO-coated polystyrene surfaces demonstrated the protein resistant and coagulation-inert properties of PEO, supplemented with complement inhibitory effects mediated by factor H [32].

Immune Response to Degradable Biomaterials

The many molecular and cellular events that are part of the inflammatory response to foreign objects have been adapted to enhance biomaterial effectiveness as drug delivery devices. The ability of a natural matrix protein to be degraded by hydrolysis, proteolysis, and oxidation are characteristics that have been incorporated into polymer systems. By creating a water or protease sensitive polymer chain, the polymer-based device can be rendered degradable in the presence of tissue fluid and inflammatory cells. In the same manner by which leukocytes use proteases and reactive oxidants to degrade a device for rejection, proteases and oxidants can degrade the polymer cross-links of an implanted device that carries a drug. By altering the severity of the mounted immunological response or the sensitivity of the polymer cross-links to degradation, the material can be tuned to create a device with a specific drug release profile. The most common example of a tunable

polymer system that used the tissue microenvironment (i.e., tissue fluids) and innate immune responses for drug delivery purposes is the co-block polymer poly(lactic-glycolic) acid (PLGA). By altering the ratio of glycolic to lactic acid in the co-block polymer. The higher the ratio (up to 50%) of glycolic acid, the faster the rate of erosion. Early reports of degradation of this copolymer were observed in wound closing sutures [33] and upon implantation of vascular stents into a porcine model, in which inflammation was noticed [34]. Hydrolysis, along with monocyte, neutrophil, lymphocyte, and giant cells activation, was implicated as the cause of degradation of implanted PLGA devices [35].

Beyond direct chemical modification of the polymer backbone, the polymer system can be functionalized, with protease sensitive peptide sequences. Leukocyte degranulation results in the release of elastases and collagenases that are known to cleave specific peptide sequences within elastin and collagens. By creating polymer systems that include an elastase- or collagenase-sensitive peptide, a non-degradable polymer can be rendered degradable [36].

Immune Response to Cell-Grafted Biomaterials

Very often cells are grafted on or embedded within the matrix (microencapsulation) of many implants for tissue regeneration. Transplanted cells are often of autologous (cells from implant host or host species), allogenic (cells of same species as host, though genetically altered), or xenogeneic (cells from species differing from host) origin. Grafted cells can serve (1) to produce therapeutic biomolecules, e.g., insulin-producing islet cells, (2) as a nucleation point for tissue regeneration, or (3) to guide host cell in growth and injury repair. The presence of cells in engineered tissue constructs can induce adaptive immune response in addition to the innate immune response to the biomaterial as previously described. Here, it is the macrophages (tissue or recruited) that primarily bridge the gap between innate and adaptive response. In their adaptive immunity role, macrophages ingest a pathogen, digest the organism and present digested fragments on the cell surface to signal adaptive immune cells for a more specialized immune response. Macrophages do this by presenting major histocompatability complex (MHC) class II for T-cell recognition and presenting costimulatory molecules, CD80 and CD86, for T-cell activation [37, 38], which often leads to immune rejection of the transplanted cells and overall failure of the implanted device. In this way, macrophages provide crossover between innate (nonspecific) and adaptive (specific) immunity. Alternatively, host T-cells in proximity of implanted device may recognize implanted cells directly by binding to MHC on allogeneic cells. Xenogeneic and allogeneic more than autogenic cells induce immune response in tissue regeneration owing to their "non-self" characteristics. However, excessive ex vivo processing or genetic modification of autogenic cells can render them immunogenic. Overall, immune response to cell-containing tissue engineered constructs can be controlled by

embedding cells within the polymer matrix and employing pore sizes that allow nutrient exchange between matrix and surrounding while preventing access of inflammation and immune cells.

Summary

While a number of factors contribute to the degree of biocompatibility elicited by an implanted or injected biomaterial, including size and shape, the overriding characteristic that drives the physiological response is the ability of the biomaterial to adsorb protein to its surface. In all conditions, blood plasma or tissue fluid/ECM proteins will come in contact with the biomaterial surface, and the subsequent presentation of these proteins will drive the acute cellular response of neutrophils and monocytes, followed by the chronic inflammatory response of macrophages and the wound healing response of foreign body cells and fibroblasts. Protein adsorption can be controlled by a number of factors, including surface hydrophobicity, charge, and porosity. The cellular responses can be exploited through biomaterial modification to elicit a very specific cellular activity, including adhesion, protein deposition, or protease and oxidant release. Controlling cellular function through biomaterial modification can create functional materials, useful in drug delivery and biological acceptance of engineered tissue constructs.

References

1. Chu, C.-C.: Wound Closure Biomaterials and Devices. CRC, LLC, Boca Raton (1996)
2. Lundqvist, M., Stigler, J., Elia, G., Lynch, I., Cedervall, T., Dawson, K.A.: Nanoparticle size and surface properties determine the protein corona with possible implications for biological impacts. Proc. Natl Acad. Sci. USA **105**, 14265–14270 (2008)
3. Anderson, J.M.: Mechanisms of inflammation and infection with implanted devices. Cardiovasc. Pathol. **2**, 33S–41S (1993)
4. Zarbock, A., Ley, K.: New insights into leukocyte recruitment by intravital microscopy. Curr. Top. Microbiol. Immunol. **334**, 129–152 (2009)
5. Ley, K., Laudanna, C., Cybulsky, M.I., Nourshargh, S.: Getting to the site of inflammation: the leukocyte adhesion cascade updated. Nat. Rev. Immunol. **7**, 678–689 (2007)
6. da Costa Martins, P., Garcia-Vallejo, J.J., van Thienen, J.V., Fernandez-Borja, M., van Gils, J. M., Beckers, C., Horrevoets, A.J., Hordijk, P.L., Zwaginga, J.J.: P-selectin glycoprotein ligand-1 is expressed on endothelial cells and mediates monocyte adhesion to activated endothelium. Arterioscler. Thromb. Vasc. Biol. **27**, 1023–1029 (2007)
7. Rivera-Nieves, J., Burcin, T.L., Olson, T.S., Morris, M.A., McDuffie, M., Cominelli, F., Ley, K.: Critical role of endothelial P-selectin glycoprotein ligand 1 in chronic murine ileitis. J. Exp. Med. **203**, 907–917 (2006)
8. Gonzalez, A.L., Gobin, A.S., West, J.L., McIntire, L.V., Smith, C.W.: Integrin interactions with immobilized peptides in polyethylene glycol diacrylate hydrogels. Tissue Eng. **10**, 1775–1786 (2004)

9. Gonzalez, A.L., El-Bjeirami, W., West, J.L., McIntire, L.V., Smith, C.W.: Transendothelial migration enhances integrin-dependent human neutrophil chemokinesis. J. Leukoc. Biol. **81**, 686–695 (2007)
10. Mantovani, A., Sica, A., Sozzani, S., Allavena, P., Vecchi, A., Locati, M.: The chemokine system in diverse forms of macrophage activation and polarization. Trends Immunol. **25**, 677–686 (2004)
11. Kou, P.M., Babensee, J.E.: Macrophage and dendritic cell phenotypic diversity in the context of biomaterials. J Biomed Mater Res A **96**, 239–260 (2011)
12. Anderson, J.M., Rodriguez, A., Chang, D.T.: Foreign body reaction to biomaterials. Semin. Immunol. **20**, 86–100 (2008)
13. Markiewski, M.M., Nilsson, B., Ekdahl, K.N., Mollnes, T.E., Lambris, J.D.: Complement and coagulation: strangers or partners in crime? Trends Immunol. **28**, 184–192 (2007)
14. Tang, L., Hu, W.: Molecular determinants of biocompatibility. Expert Rev. Med. Devices **2**, 493–500 (2005)
15. Kao, W.J., Hubbell, J.A., Anderson, J.M.: Protein-mediated macrophage adhesion and activation on biomaterials: a model for modulating cell behavior. J. Mater. Sci. Mater. Med. **10**, 601–605 (1999)
16. Thiele, L., Diederichs, J.E., Reszka, R., Merkle, H.P., Walter, E.: Competitive adsorption of serum proteins at microparticles affects phagocytosis by dendritic cells. Biomaterials **24**, 1409–1418 (2003)
17. Nilsson, B., Ekdahl, K.N., Mollnes, T.E., Lambris, J.D.: The role of complement in biomaterial-induced inflammation. Mol. Immunol. **44**, 82–94 (2007)
18. Andersson, J., Ekdahl, K.N., Larsson, R., Nilsson, U.R., Nilsson, B.: C3 adsorbed to a polymer surface can form an initiating alternative pathway convertase. J. Immunol. **168**, 5786–5791 (2002)
19. Jenney, C.R., Anderson, J.M.: Adsorbed IgG: a potent adhesive substrate for human macrophages. J. Biomed. Mater. Res. **50**, 281–290 (2000)
20. McNally, A.K., Anderson, J.M.: Complement C3 participation in monocyte adhesion to different surfaces. Proc. Natl Acad. Sci. USA **91**, 10119–10123 (1994)
21. Wilson, C.J., Clegg, R.E., Leavesley, D.I., Pearcy, M.J.: Mediation of biomaterial-cell interactions by adsorbed proteins: a review. Tissue Eng. **11**, 1–18 (2005)
22. Ekdahl, K., Nilsson, B., Golander, C., Elwing, H., Lassen, B., Nilsson, U.R.: Complement activation on radiofrequency plasma modified poystyrene surfaces. J. Colloid Interface Sci. **158**, 121–128 (1993)
23. Chenoweth, D.E.: Complement activation in extracorporeal circuits. Ann. N. Y. Acad. Sci. **516**, 306–313 (1987)
24. Kazatchkine, M.D., Carreno, M.P.: Activation of the complement system at the interface between blood and artificial surfaces. Biomaterials **9**, 30–35 (1988)
25. Fearon, D.T., Wong, W.W.: Complement ligand-receptor interactions that mediate biological responses. Annu. Rev. Immunol. **1**, 243–271 (1983)
26. Engberg, A.E., Rosengren-Holmberg, J.P., Chen, H., Nilsson, B., Lambris, J.D., Nicholls, I.A., Ekdahl, K.N.: Blood protein–polymer adsorption: Implications for understanding complement-mediated hemocompatibility. J. Biomed. Mater. Res. A **97A**, 74–84 (2011)
27. Lin, Y.S., Hlady, V., Janatova, J.: Adsorption of complement proteins on surfaces with a hydrophobicity gradient. Biomaterials **13**, 497–504 (1992)
28. Amiji, M., Park, K.: Prevention of protein adsorption and platelet adhesion on surfaces by PEO/PPO/PEO triblock copolymers. Biomaterials **13**, 682–692 (1992)
29. Hansson, K.M., Tosatti, S., Isaksson, J., Wetterö, J., Textor, M., Lindahl, T.L., Tengvall, P.: Whole blood coagulation on protein adsorption-resistant PEG and peptide functionalised PEG-coated titanium surfaces. Biomaterials **26**, 861–872 (2005)
30. Kidane, A., Park, K.: Complement activation by PEO-grafted glass surfaces. J. Biomed. Mater. Res. **48**, 640–647 (1999)

31. Kidane, A., Lantz, G.C., Jo, S., Park, K.: Surface modification with PEO-containing triblock copolymer for improved biocompatibility: in vitro and ex vivo studies. J. Biomater. Sci. Polym. Ed. **10**, 1089–1105 (1999)
32. Andersson, J., Bexborn, F., Klinth, J., Nilsson, B., Ekdahl, K.N.: Surface-attached PEO in the form of activated Pluronic with immobilized factor H reduces both coagulation and complement activation in a whole-blood model. J. Biomed. Mater. Res. A **76**, 25–34 (2006)
33. Heller, J.: Biodegradable polymers in controlled drug delivery. Crit. Rev. Ther. Drug Carrier Syst. **1**, 39–90 (1984)
34. Gogolewski, S.: Resorbable polymers for internal fixation. Clin. Mater. **10**, 13–20 (1992)
35. van der Giessen, W.J., Lincoff, A.M., Schwartz, R.S., van Beusekom, H.M., Serruys, P.W., Holmes, D.R., Ellis, S.G., Topol, E.J.: Marked inflammatory sequelae to implantation of biodegradable and nonbiodegradable polymers in porcine coronary arteries. Circulation **94**, 1690–1697 (1996)
36. Lee, S.H., Moon, J.J., Miller, J.S., West, J.L.: Poly(ethylene glycol) hydrogels conjugated with a collagenase-sensitive fluorogenic substrate to visualize collagenase activity during three-dimensional cell migration. Biomaterials **28**, 3163–3170 (2007)
37. Thiele, L., Merkle, H.P., Walter, E.: Phagocytosis and phagosomal fate of surface-modified microparticles in dendritic cells and macrophages. Pharm. Res. **20**, 221–228 (2003)
38. Thiele, L., Rothen-Rutishauser, B., Jilek, S., Wunderli-Allenspach, H., Merkle, H.P., Walter, E.: Evaluation of particle uptake in human blood monocyte-derived cells in vitro. Does phagocytosis activity of dendritic cells measure up with macrophages? J. Control. Release **76**, 59–71 (2001)

Chapter 7
Modulation of the Wound Healing Response Through Oxidation Active Materials

Paritosh P. Wattamwar and Thomas D. Dziubla

Abstract Oxidative stress originally gained attention as key pathological process in a variety of disease states and conditions (e.g., acute lung injury, sepsis, chronic degenerative neurological diseases). Furthermore, it oxidative stress has also been identified as one of the key mechanisms to tissue toxicity brought on by nanomaterials and implant biomaterials. Yet, despite these origins, newer research has started to view oxidative stress and not simply pathology, but as a physiologically relevant signaling system, working in concert with the more traditional cell signaling cascades (e.g., growth factor signaling, cytokine release). As a result, a reinvigoration of research in regenerative medicine has begun looking at oxidative stress as a potential tuning mechanism to enhance the natural wound healing process. In this chapter, a summary of the biological aspects of oxidative stress is presented as well as a current state of the art approaches used in designing biomaterials to actively participate in the oxidative stress signaling.

Introduction

Any successful regenerative medicine strategy requires the ability to effectively orchestrate the complex wound healing process, which is classically broken down into four distinct yet overlapping phases – immediate formation of a blood clot, inflammation, new tissue formation followed by vascularization/remodeling of the tissue. If any step becomes compromised (e.g., excessive inflammation), a chronic wound environment can result, negatively impacting the regenerative outcome. As a result, much attention has been made to the effects of cytokines, signaling molecules, and growth factors on the wound response and using these to control

P.P. Wattamwar • T.D. Dziubla (✉)
Department of Chemical and Materials Engineering, University of Kentucky, Lexington, KY, USA
e-mail: dziubla@engr.uky.edu

S.K. Bhatia (ed.), *Engineering Biomaterials for Regenerative Medicine: Novel Technologies for Clinical Applications*, DOI 10.1007/978-1-4614-1080-5_7,

healing. However, in addition to these agents, a parallel process of oxidative stress has been generating growing consideration as a means of tuning wound healing. In this chapter, a review of oxidative stress and its relationship to wound healing is provided. This review is then followed by a summary of approaches that has been and can be used to intervene in the reduction/oxidation (Red/ox) cycles as a way of additional control over wound healing, providing an additional tool by which to design novel regenerative medicine strategies.

Oxidative Stress

Under normal physiological conditions, cells maintain a balanced redox state by evening the production and consumption of reactive oxygen species/reactive nitrogen species (ROS/RNS). While not fully elucidated, these ROS/RNS play an important role in cell signaling directly via the oxidation of cysteine residues on proteins [1] or indirectly by stimulating inflammatory signals (e.g., upregulation of cytokines and cell adhesion molecules, CAMs) [2] and mediate cellular responses such as differentiation, proliferation, apoptosis, and migration [3–7]. When ROS/RNS production exceeds the cells antioxidant capacity, a degenerative pathological state known as oxidative stress can occur, which is known to be a primary and/or a secondary mechanism in many disease states such as hypertension [8], atherosclerosis [9], ischemia–reperfusion injury [10], acute lung injury [11, 12], and aging and neurodegenerative diseases [13, 14].

Mechanism and Chemistry

Generation of various ROS/RNS by different reactions is highlighted in Fig. 7.1. Oxidative stress is often initiated by the generation of the superoxide anion ($O_2^{\bullet -}$) during mitochondrial respiration or by enzymes such as NADPH-oxidase (NADPHox), xanthine oxidase (XO), cyclooxygenases (COX), and P450 reductase. Upon activation, NADPHox converts molecular O_2 to $O_2^{\bullet -}$, which can then react with nitric oxide ($NO^{\bullet}$) to form peroxynitrite anion ($ONOO^-$). $NO^{\cdot}$ is a diffusible gaseous signaling molecule produced by enzyme nitric oxide synthase (NOS) and affects vasorelaxation and platelet inhibition. Preventing the oxidation of species by superoxide, $O_2^{\bullet -}$ is enzymatically converted to H_2O_2 (hydrogen peroxide) by superoxide dismutase (SOD). In the presence of the chloride anion (Cl^-), myeloperoxidase (MPO) converts H_2O_2 into a very potent oxidant, hypochlorous acid (HOCl). H_2O_2 can also react with reduced transition metals such as Fe^{2+} and Cu^+ to form hydroxyl radicals ($OH^{\bullet}$) [15], which can react with polyunsaturated fatty acid (LH) to cause lipid peroxidation and form a carbon-centered lipid radical ($L^{\bullet}$) which further reacts with molecular oxygen to give a lipid peroxyl radical ($LOO^{\bullet}$). A Lipid peroxidation cycle can begin LOOH reacts with Fe^{2+} to form lipid

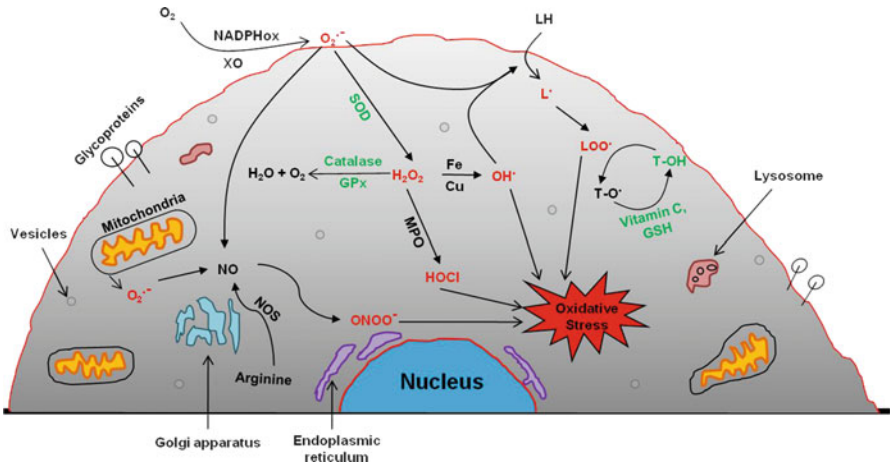

Fig. 7.1 A simplified view of the cellular generation of ROS/RNS

alkoxyl radical ($LO^{\bullet}$) or with Fe^{3+} to form $LOO^{\bullet}$. These radicals, in turn, oxidize more lipids and propagate the cycle.

When compared with other molecules, ROS/RNS are relatively unstable, having a very short half-life on account of their ability to react with and oxidatively damage cellular proteins, DNA, and lipids affecting normal functioning of cells/tissue. Even though ROS/RNS have a random destructive effect, in many conditions that are subject to redox-sensitive pathways, production of ROS/RNS is tightly regulated with a specific downstream target. Depending on the scenario and the enzymes involved, ROS/RNS can be generated within the cell, in cell lipid membrane or extracellularly. Extracellular milieu and outer leaflet of plasma membrane are the first target of extracellular ROS/RNS attack, where as intracellular ROS/RNS damage intracellular proteins and inner leaflet of plasma membrane [16]. Location of the ROS/RNS generation should, therefore, be considered while designing an antioxidant therapy.

Antioxidants

Antioxidants are the primary way cells and tissues are able to maintain a balance in the redox state (Fig. 7.1). Antioxidants can be classified into two major categories: small molecule oxidant scavengers (e.g., tocopherol, glutathione, quercetin, etc.) and antioxidant enzymes (e.g., SOD, catalase, etc.). Depending on their octanol/water partitioning coefficient, small molecule antioxidants can either localize in cellular cytoplasm or cellular and intracellular lipid membranes. For example, Vitamin E (T-OH), which can partition itself in lipid bilayer, scavenges $LOO^{\cdot}$ to reduce it to lipid hydroperoxide (LOOH) and in the process forms a vitamin E

radical (T-O$^{\bullet}$). Vitamin C/ascorbic acid (AscH) or glutathione (GSH) react with T-O$^{\bullet}$ to regenerate T-OH. Water soluble antioxidants such as vitamin C and GSH can also react with cytoplasmic ROS/RNS. Small molecule antioxidants are generally nonspecific and scavenge a variety of ROS and RNS. Also, they are well tolerated, stable for long-term storage, resistant to complex and/or aggressive formulation processing methods and relatively inexpensive. However, these small molecule scavengers typically reduce free radicals and other oxidizing species in stoichiometric ratios, being consumed in the process [17, 18]. Hence, large sustained doses are expected to be required to observe a significant clinical effect.

Antioxidant enzymes, on the other hand, are not consumed in reaction, allowing a single enzyme to react with millions of copies of radicals before becoming inactivated. For instance, catalase, which reduces H_2O_2 to water and oxygen, has a turnover number of 40 million molecules hydrogen peroxide molecules degraded per second, allowing for even small delivered amounts to have profound cellular effects [19]. The enzyme glutathione peroxidase (GPx) can reduce lipid hydroperoxides and free H_2O_2 to corresponding alcohols and water, respectively. The redox cycle of GPx requires an electron obtained from NADPH via GSH and glutathione reductase to catalyze the reduction of peroxides [20, 21]. Peroxiredoxins is another class of enzymes that use either thioredoxin or GSH or both as an electron donor to catalyze the reduction of H_2O_2, other hydroperoxides (e.g., LOOH) and $ONOO^-$ [22, 23]. Besides this high potency, antioxidant enzymes are also highly selective, allowing for a more targeted approach to antioxidant therapy not possible with small molecule antioxidants. However, antioxidant enzymes are relatively fragile and expensive, limiting the set of conditions which can be used for their formulation [24]. Further, they are prone to proteolytic and pH-dependant inactivation, which can limit their therapeutic duration [25, 26].

Role of Oxidative Stress in Wound Healing

The complex wound healing process can be broken down into four main phases: (a) formation of blood clot and platelet plug, (b) inflammation, (c) new tissue formation, and (d) tissue remodeling (Fig. 7.2). The immediate first step response to a wound is to stop blood flow by initiating thrombosis. This fibrin clot serves as a temporary seal to the wound and provides a scaffold where other cells can migrate and proliferate. The hemostasis process is followed by inflammatory phase where the fibrin clot acts as a pool for variety of cytokines (e.g., interleukins, interferons, and tumor necrosis factors) and growth factors (e.g., platelet-derived growth factor, transforming growth factor, etc.) that are released from degranulating activated platelets and the immune cells. Chemoattractants, which include growth factors released from the platelets and other cues like by-products of fibrin proteolysis or peptides cleaved from bacteria, result in the accumulation of inflammatory cells (neutrophils and monocytes) from the circulation. Also, cytokines and ROS

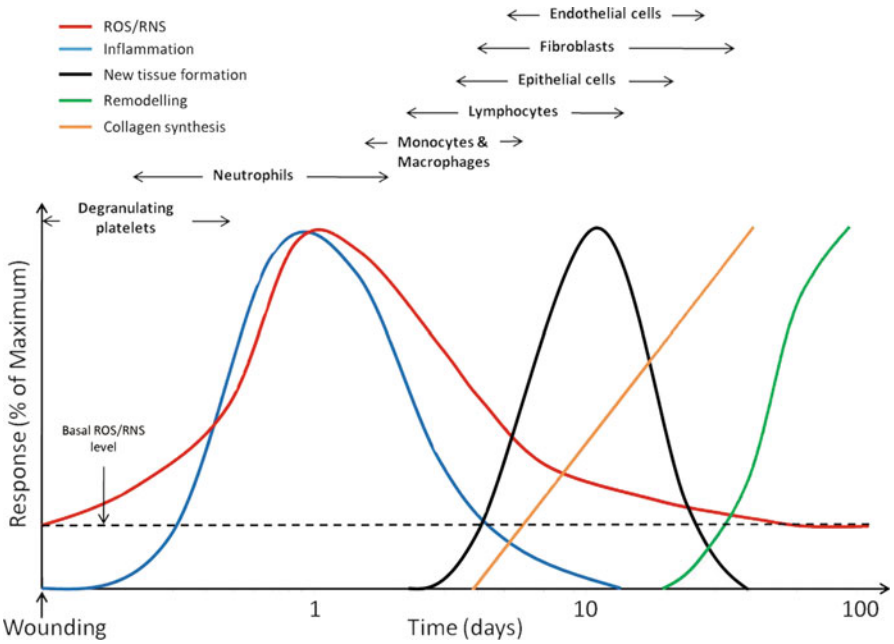

Fig. 7.2 The temporal compositional changes expected at the wound site

upregulate expression of CAMs (e.g., CD54) which recruit neutrophils and monocytes from circulation [16, 27].

One of the major roles of neutrophils is to combat wound infection by eliminating the invading microorganisms (e.g., bacteria) through burst release of oxidative species [28]. Monocytes at the inflamed wound site differentiate into macrophages which phagocytose apoptotic neutrophils and other cellular/bacterial debris. Macrophages are responsible for the long-term wound repair process not only by amplifying the inflammatory response but also by initiating the growth of new tissue. Macrophages and other inflammatory cells also release cytokines and other growth factors that can activate fibroblasts and keratinocytes [29].

One to two days after wounding, new tissue formation begins and is marked by migration and proliferation of various cells such as endothelial cells, fibroblasts, keratinocytes, and inflammatory cells. Keratinocytes (in case of dermal wounds) migrate over the injured dermis with concomitant angiogenesis to restore blood flow at the wound site. Fibroblasts along with macrophages replace the fibrin matrix with granulation tissue (called so due to appearance of several small capillaries) which also serves as a substrate for keratinocyte migration and proliferation. Macrophages activate fibroblasts to differentiate into myofibroblasts, which contract the wound gradually bringing edges of the wound closer together. Fibroblasts and myofibroblasts together also produce collagen-rich extracellular matrix which forms bulk of the scar. The wound healing process is completed by a long phase of

tissue remodeling that can last up to a year or more and is characterized by the attenuation of all the activated processes. Many of the recruited cells (endothelial, fibroblasts, and macrophages) either undergo apoptosis or exit the wound leaving behind an acellular tissue mostly composed of collagen and some extracellular–matrix proteins. Matrix metalloproteinases (e.g., MMP-1 and MMP-9) that are secreted by the cells replace type III collagen in the granulation tissue with type I collagen [30].

ROS and RNS are involved in redox-sensitive cell signaling pathways that induce various responses such as chemotaxis, proliferation, differentiation, etc. and therefore oxidative stress (ROS and RNS) play a critical role in orchestration of each of these wound healing phases [31]. A better understanding of role and effect (both positive and negative) of oxidative stress in each of the wound healing phases is necessary for optimal design of the therapeutic intervention strategy by using antioxidants.

The following sections include detailed discussion of the role of ROS/RNS in the inflammatory phase and new tissue formation phase of wound healing. Redox state plays an important role in the hemostasis process and is reviewed in detail by Gorlach and Sen et al. [31, 32].

Inflammation

ROS at the wound site play an important role in the recruitment/chemotaxis and the function of neutrophils and other immune cells. Chemotaxis is the migration of cells based on the concentration gradient cues. In a recent study with a zebrafish wound model, it has been shown that during the initial phase of wound detection, H_2O_2 gradient at low concentration (~ 0.5–50 μM) induces chemotaxis in leukocytes [33, 34]. Experiments have also shown that the inhibition of NADPHox within the neutrophils affected their chemotactic migration, possibly by affecting ROS-based intracellular signaling [35]. Elevated levels of thioredoxin, an important redox protein, in circulation inhibit lipopolysaccharide-stimulated (LPS) chemotaxis as well as the recruitment of leukocytes induced by murine chemokine KC/GROα, RANTES (regulated upon activation, normal T-cell expressed and secreted) and monocyte chemoattractant protein-1 (MCP-1) [36]. Immune response to a kill a pathogen is composed of a respiratory burst by the immune cells. Neutrophils, phagocytes as well as other immune cells undergo respiratory burst, a rapid and non-mitochondrial conversion of O_2 to battery of ROS and RNS by the activation of membrane-bound NADPHox via chemoattractants or other inflammatory stimuli, to eliminate bacteria or other microorganisms that could cause an infection [37–39]. Any defect in the NADPHox system, which is critical for the respiratory burst, results in the loss of resistance to infections [40, 41].

Leukocytes are recruited to the wound site by a variety of chemoattractants, including fragmented extracellular matrix protein, tumor necrosis factor (TNF), transforming growth factor β (TGF-β), MCP-1, granulocyte colony-stimulating factor

Table 7.1 ROS/RNS play an important role in inflammatory phase by affecting expression and release of various cytokines and chemoattractants

Cytokines and Chemoattractants	Source	Effect of ROS/RNS	Reference
MIP-1α	Rat alveolar macrophages	• H_2O_2 treatment induced MIP-1α mRNA expression	[43]
MIP-2	Rat alveolar macrophages, rat lung epithelial cells	• H_2O_2 increased MIP-2 mRNA expression • Quartz, TiO2, and crocidolite asbestos particles induced oxidative stress, resulting in increased MIP-2 expression	[42, 46]
MCP-1	Human aortic smooth muscle cells, monocytes	• PDGF stimulated $O2^{\cdot-}$ release resulting in increased MCP-1 mRNA expression • X/XO stimulated monocyte to produce MCP-1	[44]
CSF-1	Endothelial cells	• TGF-β1 stimulated macrophage CSF via H_2O_2 based signaling	[47]
TNF-α	Human dendritic cells, Rat alveolar epithelial cells	• H_2O_2 stimulated production of TNF-α • LPS induced glutathione depletion resulted in release of cytokines	[48, 50]
IL-8	Human dendritic cells, Rat alveolar epithelial cells, Monocytes	• H_2O_2 stimulated production of IL-8 • LPS induced glutathione depletion resulted in release of cytokines • X/XO stimulated monocyte to produce IL-8	[48–50]
IL-1β	Rat alveolar epithelial cells	• LPS induced glutathione depletion resulted in release of cytokines	[50]
IL-6	Rat alveolar epithelial cells	• LPS induced glutathione depletion resulted in release of cytokines	[50]

(G-CSF), granulocyte/macrophage CSF (GM-CSF), and macrophage-inflammatory protein (MIP). Through ROS such as H_2O_2 and $O_2^{\bullet-}$, oxidative stress increases the production of MIP-1α, MIP-2, MCP-1, CSF-1, and other chemoattractants and is very critical in the recruitment of immune cells at the wound site [42–47]. Oxidative stress also upregulates the production of cytokines by cells. Expression of inflammatory cytokines expected at the wound site (e.g., TNFα, IL-8, IL-1β, and IL-6) is stimulated by oxidative stress [48–50]. Effect of oxidative stress on expression and release of various inflammatory cytokines is summarized in Table 7.1.

ROS and RNS are important in the functioning of immune cells. Exogenous H_2O_2 induces calcium release from the intracellular compartments of neutrophils increasing their phagocytic activity [51]. H_2O_2 also modulates the respiratory burst of monocytes and neutrophils, where low concentrations of H_2O_2 stimulate $O_2^{\bullet-}$ production where as higher concentrations inhibit $O_2^{\bullet-}$ production [52–54]. Monocytes and macrophages protect themselves from the respiratory burst by H_2O_2 triggered

increase in the uptake of GSH [55]. High mobility group box-1 (HMGB1), an endogenous pro-inflammatory cytokine, is passively released by necrotic cells or actively secreted by monocytes/macrophages to exogenous and endogenous stimuli such as TNF-α, IL-1, endotoxins, and interferon-γ (IFN-γ) [56]. HMGB1 also mediates innate and adaptive immune responses by promoting dendritic cell maturation [57]. Oxidative stress induces HMGB1 release, both actively and passively, from monocytes and macrophages in a mitogen-activated protein kinase (MAPK) and chromosome region maintenance (CRM1)-dependent mechanism. At nontoxic concentrations of H_2O_2 (<0.125 mM), it stimulated interaction of HMGB1 with the nuclear export factor CRM1, whereas at higher concentrations of 0.25 mM, H_2O_2 exhibited cell toxicity triggering active and passive release of HMGB1 [58]. Hypoxia-induced HMGB1 release by hepatocytes during ischemia/reperfusion injury is also regulated via toll-like receptor 4 (TLR4)-dependent ROS production and downstream calcium-mediated signaling [59].

Neutrophils and monocytes are recruited from the circulation due to their receptivity to certain molecular signals that are expressed on the endothelial cells as a response to the wound. Expression of surface molecular signals on the endothelium alters as the wound healing progresses allowing for sequential recruitment of different classes of leukocytes at the wound site. Initially, selectin family of CAMs expressed on the endothelium mediate tethering of leukocytes to the vessel wall, allowing for their rolling in the direction of the blood flow. The light adhesion to selectins is followed by tighter adhesions and arrest mediated by β2 subfamily of integrins. Attached leukocytes then follow directional cues from chemoattractants using integrins for traction and then crawl across the endothelium into extravascular space [27, 60]. Once the leukocytes leave the circulation and enter the extracellular matrix, they interact with matricellular proteins through the β1 subfamily of integrins. Both β1 and β2 integrins induce different signaling pathways in monocytes which are important for their functioning (migration and phagocytocis) and differentiation into the repairing macrophages [61].

H_2O_2 promotes β2-integrin leukocyte function-associated antigen-1 (LFA-1)-dependent attachment of neutrophils to cardiac myocytes and in the presence of exogenous chemoattractants (e.g., c5a), there is a transition from LFA-1 to macrophage 1 antigen (Mac-1)-dependent adhesion, resulting in prolonged attachment of neutrophils to myocytes [62, 63]. Also, neutrophils at early stages utilize the interaction of LFA-1 with intercellular adhesion molecule-1 (ICAM-1) to trigger H_2O_2 production without requiring chemotactic stimulation, whereas the cytokine-induced respiratory burst of neutrophils is augmented by Mac-1-dependent adhesion of neutrophils [64–66]. This mechanism could result in additional recruitment of neutrophils by neutrophils whose ROS production is based on Mac-1-dependent adherence to myocytes. Cellular redox state affects the expression of LFA-1 in myeloid lineage, where exogenous use of antioxidants such as *N*-acetyl-L-cysteine (NAC) and pyrrolidine dithiocarbamate (PDTC) suppressed expression of protein CD11a/LFA-1α [67]. Exposure of leukocytes to H_2O_2 and superoxide upregulated the expression of leukocyte adhesion molecules and promoted leukocyte–endothelial adhesion [68].

Mediators of inflammation (e.g., TNFα, IL-1, and IFγ), including ROS, modulate expression of endothelial surface adhesion molecules. Both endogenously and exogenously (as a result of attached leukocytes) released ROS from the endothelium upregulates the expression of intercellular adhesion molecule-1 (ICAM-1, CD54), vascular cellular adhesion molecule-1 (VCAM-1), and P-selectin on surface of endothelial cells recruiting more leukocytes from the circulation [69–72]. Antioxidants NAC and PDTC inhibited H_2O_2-induced and cytokine-induced expression of ICAM-1, respectively [73, 74].

Redox state of the cell also plays an important role in regulating chemokines and their receptors. Antioxidants PDTC, NAC, and 2-mercaptoethanol inhibited mRNA expression of chemokine receptors CCR2 (CC chemokine receptor-2), CCR5, and CXCR4 (CXC chemokine receptor-4) in human monocytes. Oxidative stress induced either by xanthine/xanthine oxidase, H_2O_2, or buthionine sulfoximine (a glutathione-depleting drug) counteracted the inhibitory effects of antioxidants and increased the expression of chemokine receptors [75, 76]. TNFα and bacterial lipopolysaccharide-mediated inhibition of CCR5 and CXCR4 mRNA expressions was opposed by the generation of ROS (xanthine/xanthine oxidase), which increased both CCR5 and CXCR4 mRNA expressions and cell migration (threefold) in response to MIP-1β [75]. Homocysteine-induced stimulation of CCR2 mRNA level is also mediated through superoxide formation [77]. Oxidative stress upregulates the production of cytokines by cells. ROS-stimulated synthesis of IL-8 and TNFα by dendritic cells [48]. A flow diagram of the relationship between oxidative stress and inflammation is provided in Fig. 7.3. As shown, a failure to resolve oxidative stress can lead to chronic inflammation and, thereby, aberrant healing.

New Tissue Formation

Two to ten days after the injury, wound closure and new tissue formation starts, which is characterized by the migration of epithelial cells and, in the case of dermal wounds, keratinocytes. Any defect in the migration mechanism of the keratinocytes can result in a chronic non-healing wound [78]. Insulin-like growth factor-1 (IGF-1) facilitates cell spreading, stimulates membrane protrusion and migration of keratinocytes [79]. IGF-1-induced signaling events are subject to redox control and ROS-induced oxidative stress can upregulate IGF-1 action by increasing the expression of IGF-1 and IGF-1 receptor (IGF-1R) [80–82].

Oxidative stress can induce proliferation and migration of smooth muscle cells and epithelial cells [83, 84]. Extracellular oxidative stress activates redox-sensitive pathways that increase Nox1-based NADPHox expression and vascular smooth muscle cell (VSMC) proliferation [7]. Matrix metalloproteinases (MMPs) are a class of enzymes that can degrade various components of cell–cell junction, cell–matrix contacts, and extracellular matrix allowing different cells to migrate across the wound to promote reepithelialization. Exogenous oxidative stress can activate MMP-2 and MMP-9 secreted from VSMCs [85]. Cells produce MMP-1 via

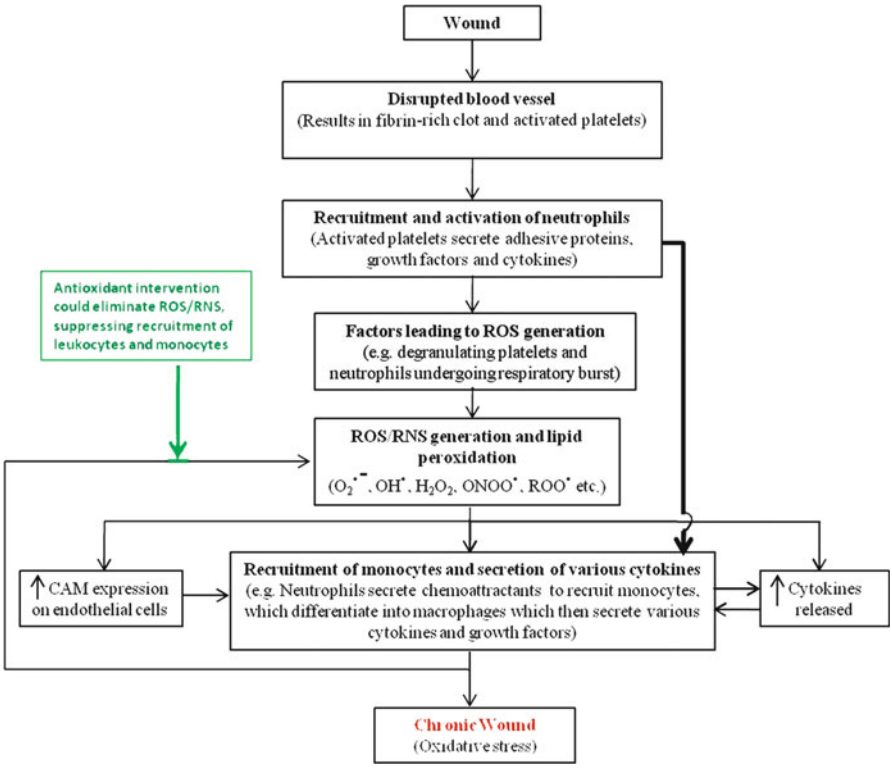

Fig. 7.3 Initiation and propagation of oxidative stress after wounding. Failure to suppress excessive generation of ROS/RNS could result in prolonged inflammatory phase, finally resulting in a chronic non-healing wound. *CAM* cell adhesion molecules

Nox4-mediated and ROS-dependent pathways [86] and sustained exposure to ROS-induced activation of pro-MMP-2 and increased cell motility [87]. Epidermal growth factor (EGF), transforming growth factor-α (TGF-α), and keratinocyte growth factor (KGF) are required for the proliferation of epidermal cells behind the migrating front [88]. ROS are capable of triggering EGF- and KGF-dependent signaling and can also induce TGF-α in fibroblasts [31]. Fibroblast proliferation results in a collagen-rich scar tissue (granulation tissue) along with the formation of new blood vessels for nutrients and oxygen supply.

The importance of ROS in angiogenesis and tissue vascularization can be inferred from the study by Roy et al. where decomposition of H_2O_2 by adenoviral gene transfer of catalase resulted in impaired wound tissue vascularization [89]. Also, Nox1-induced molecular markers of angiogenesis [e.g., vascular endothelial growth factor (VEGF)] were eliminated after coexpression of Nox1 and catalase, indicating that H_2O_2 plays an important role in the angiogenic switch [90]. Oxidants not only induce VEGF expression but also play a central role in VEGF

signaling and are discussed in detail by Sen and Roy [31]. Several small molecule antioxidants such as GSH, vitamin C, vitamin E, and polyphenols (quercetin, curcumin, resveratrol, etc.) have anti-angiogenic properties which suggest positive role of oxidants in tissue vascularization [31, 91].

Role of Antioxidants in Wound Healing

Evidence of Oxidative Stress in Wound Healing

In this section, a systematic review of the various oxidants and their markers present at the wound site is presented.

Direct Evidence of the Oxidants

As ROS/RNS are very unstable, they have a very short half-life and are present at low concentrations, ROS/RNS detection at the wound site is difficult. Oxidative stress is generally correlated with the actual levels of small molecule antioxidant scavengers and antioxidant enzymes or biomarkers such as uric acid:allantoin ratio, protein carbonyls, and 3-nitrotyrosine (3-NT) (for protein oxidation), malondialdehyde, and protein bound 4-hydroxyl-2-trans nonenal (HNE) (for lipid peroxidation), in the wound fluid and wound tissue. However, in the work done by Roy et al., micromolar concentrations of H_2O_2 (150–250 μM) were detected in the wound fluid from full-thickness murine excisional wounds using a real-time electrochemical technique [89, 92]. Even though H_2O_2 concentration peaked during the inflammatory phase 2-days postinjury, H_2O_2 was also detected in the post-inflammatory phase 5-days postinjury (Fig. 7.4). Superoxide production at the wound edge tissue was also found to be much higher when compared with the normal skin. H_2O_2 at lower concentration facilitated angiogenesis at the wound site, whereas at high concentration adversely affected the healing process. The same group also confirmed these findings in another recent study where non-invasive electron paramagnetic resonance spectroscopy was used to measure oxidative state of the wound site after topical application of ^{15}N-perdeuterated tempone [93]. Concentration of oxidants at the wound site peaked during the inflammatory phase 2-days after the injury was induced. In the same study, lower superoxide levels were found in the wound fluid of mice deficient in Rac2, an essential subunit of NADPHox. This low superoxide and H_2O_2 concentration at the wound site correlated with poor healing response from Rac2 knockout mice. Findings of this group suggest that low levels of ROS are important for wound angiogenesis and healing [89, 93].

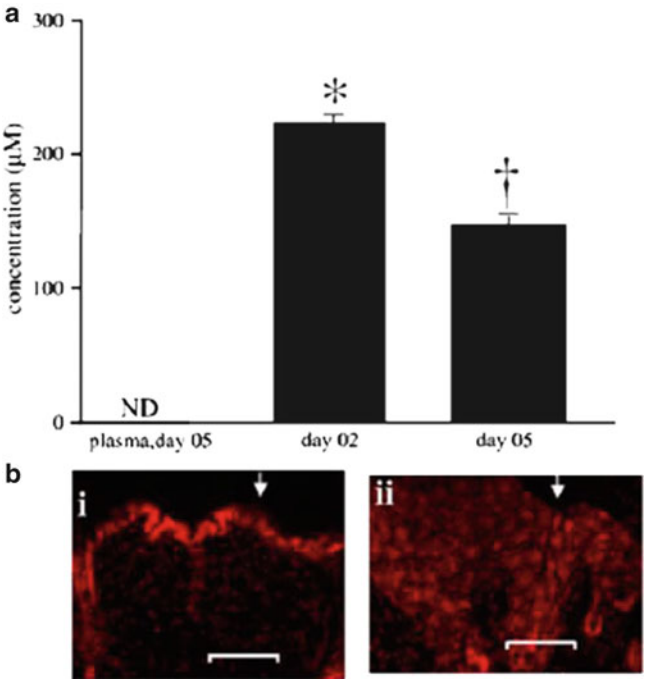

Fig. 7.4 Presence of ROS (H_2O_2 and superoxide) at the wound-site. (**a**) Wound fluid contains detectable concentration of H_2O_2 during inflammatory phase (day 2) and at slightly reduced level in the post-inflammatory phase (day 5). (**b**) Dihydroethidium (*red fluorescence*) as a marker of superoxide production in normal skin (i) and 12 h wound edge tissue (ii). Superoxide production in the wound edge tissue is much higher as compared to that of normal skin. Scale bar is 100 μm. (Figure reproduced from [89])

Protein Oxidation as Marker of Oxidative Stress

Exposure of proteins to ROS and RNS results in its oxidation. Measure of carbonyl content of protein is a commonly used method for the estimation of general oxidative stress-mediated protein oxidation [94]. Higher protein carbonyl content in the wound fluid/tissue as compared to plasma or uninjured tissue has been reported. Blister fluid obtained from patients with superfacial or partial thickness burns had 50% more protein carbonyl content as compared to normal serum, which also correlated with reduced antioxidant scavenging capacity of the blister fluid [95]. Traumatic brain and spinal cord injury also triggers oxidative stress causing oxidative damage to the nearby tissue, as evident by the higher protein carbonyl content in a rat injury model [96–98]. Wound tissue lysates of peroxiredoxin six knockout mice had higher levels of oxidized proteins as compared to intact skin [99]. Surprisingly, immunoblot analysis of acute wound fluids revealed higher

protein carbonyl content as compared to chronic wound fluid [100]. However, analysis of wound tissue lysates could have given better understanding of redox state at the wound site.

3-Nitrotyrosine (3-NT) and protein-bound 4-hydroxy-2-nonenal (HNE) are other specific markers of protein oxidation by RNS (peroxynitrite) and lipid peroxidation, respectively. Peroxynitrite can nitrate position 3 of tyrosine residues in proteins and measurement of 3-NT accumulation on proteins provides an estimate for protein oxidation by peroxynitrite. Oxidative damage to the tissue after spinal cord injury to the rats was also supported by elevated levels of 3-NT [97]. Immunostaining of granulation tissue of peroxiredoxin 6 knockout mice with an antibody against 3-NT indicated the presence of more 3-NT positive cells as compared to the wild-type mice [99]. mRNA levels of p66Shc, also an redox enzyme that upon phosphorylation on serine 36, can translocate into the mitochondrial intermembrane space and catalyze production of hydrogen peroxide, in peripheral blood mononuclear cells of type-2 diabetic patients were significantly higher than normal subjects and correlated with their total plasma 8-isoprostane levels, a marker of oxidative stress [101]. p66Shc was involved in the delayed wound healing in diabetic mice model. Deletion of p66Shc reversed the non-healing feature and showed reduced nitrotyrosine levels in wounded skin as compared to wild-type diabetic mice [102].

HNE is one of the major products of membrane lipid peroxidation that can also react with sulfhydryl groups, primary amino groups or histidine residues of proteins [103]. Protein-bound HNE is, therefore, a specific marker of protein oxidation by lipid peroxidation. Spinal cord injury resulted in the accumulation of HNE in injured tissue and immunohistochemical results of tissue indicated the colocalization of 3-NT and HNE, indicating that peroxynitrite is involved in the oxidation of both proteins and lipids [97]. Immunohistochemical result obtained by staining for HNE at the edge of murine excisional wound indicated the colocalization of HNE with neutrophils, suggesting that respiratory burst of the neutrophils causes lipid peroxidation. Rac2 knockout mice had lower HNE level in the wound tissue further suggesting that superoxide production by NADPHox has a major role in lipid peroxidation [93]. Malondialdehyde (MDA) is another byproduct of lipid peroxidation, which was found at higher levels after spinal cord injury in rats and in wounds of hydrocortisone-treated healing-impaired rats [104, 105]. MDA levels in the wound fluids from acute and chronic wound patients were similar, which was unexpected. However, normalization of the MDA levels in wound fluid with MDA levels in normal plasma/serum would have been a better biomarker of lipid peroxidation in wounds [100].

Allantoin: Uric Acid Ratio (AUR)

Uric acid, which is generated in the human body by oxidation of purines, is found in plasma at concentrations up to 500 μM and can acts as an antioxidant. Allantoin is a non-enzymatic oxidation product of uric acid, and AUR could serve as a marker of

oxidative stress [106]. Wound fluid from chronic leg ulcers had an elevated AUR as compared to both paired plasma and acute surgical wound drain fluid. However, AUR levels between the chronic wounds that healed and those that failed to heal were not significantly different [107].

8-Isoprostane as Marker of Lipid Peroxidation

Isoprostanoids are prostaglandin-like compounds that are formed as a result of free-radical-induced oxidation of essential fatty acids (primarily arachidonic acid) and are an established marker for lipid peroxidation [108, 109]. 8-Isoprostane levels were elevated in the chronic leg ulcer fluid compared to the acute wound fluid, suggesting a greater oxidative activity in the chronic ulcers [110]. This also confirms with the higher AUR in chronic ulcer fluid [107]. Even though 8-isoprostanes are formed non-enzymatically in situ on phospholipids, there release in to the circulation as free form is regulated by phospholipase activity (e.g., PLA_2) [108, 111]. The higher levels of 8-isoprostane in chronic wounds could possibly be a result of increased phospholipase activity in the chronic wound. Similar to the AUR, there was no significant difference in 8-isoprostane levels in healing and non-healing chronic leg ulcer fluid suggesting the continuation of ROS/RNS generation in chronic wounds [110].

As discussed in the above sections, cells use ROS for intracellular as well as intercellular cell–cell signaling and there by switch ON/OFF different responses in a timely manner to orchester wound healing. Two sources of ROS production at wound site are (1) respiratory burst by immune cells and (2) ROS producing Nox/Duox family of enzymes (e.g., NADPHox, NOS, and SOD) that are also expressed in other cells such as endothelial cells, fibroblasts, and keratinocytes. ROS levels at the wound site are modulated by small molecule antioxidant scavengers and antioxidant enzymes.

Role of Small Molecule Antioxidants in Wound Healing

The importance of small molecule antioxidant scavengers in the wound healing process is evident from the findings that the levels of antioxidants decrease post-injury and their sustained deficiency results in an impaired or chronic wound. Small molecule antioxidants such as glutathione, vitamin C, vitamin E (tocopherol), and polyphenols (e.g., catechins, flavanoids, etc.) regulate redox state at wound site by eliminating free radicals. Table 7.2 provides a summary of effect of antioxidants on wound healing outcomes and their mechanism of action. Kamencic et al. showed that oxidative stress caused after spinal cord injury resulted in reduced GSH levels. Post-injury administration of L-2-oxothiazolidine-4-carboxylate (OTC), a compound used to increase intracellular cysteine level required for GSH synthesis,

Table 7.2 Role of antioxidants in wound healing

Antioxidants		Administration route	Wound healing parameters affected	Mechanism	Reference
Antioxidant Enzymes	Catalase	Overexpression of catalase by adenoviral gene delivery, topical application	Impaired wound angiogenesis, closure and slowed tissue remodeling Improved dental pulp tissue healing in	Low concentrations of H_2O_2 mediate wound angiogenesis by VEGF expression	[89, 156]
	SOD	Intravenous SOD and SOD mimetic, cutaneous gene therapy of MnSOD	Reduced wound edema, increased collagen synthesis and new blood vessel formation	Reduced hyperglycemia-induced ROS	[143, 150, 152]
	Peroxiredoxin	Transgenic overexpression of Prdx6	Enhancement of wound closure in aged mice and reduced number of apoptotic cells after UVA/UVB irradiation	Prdx6 deficient endothelial and inflammatory cells are more susceptible to ROS treatment Prdx6 knockout mice showed severe hemorrhage in granulation tissue	[159, 161]
Small molecule antioxidants	Glutathione	Topical application of glutathione monoester, administration of OTC	Faster healing	Restoring cellular redox potential by suppressing oxidative stress	[98, 114]
	Vitamin E	Oral	Faster wound closure	Suppressed lipid peroxidation	[118]
	Ascorbic acid (Vitamin C)	Oral, topical	Increased proliferation of fibroblasts and improved collagen synthesis	Allows normal collagen hydroxylation (of proline residues) and is required to reduce Fe^{3+} In human dermal fibroblasts, improved cell motility as a result of increased expression of uPA, hyaluronan-mediated motility receptor and IL-6 expression	[136, 137, 139, 141]
	Curcumin	Topical	Faster wound closure, increased migration of fibroblasts and myofibroblasts resulting in higher collagen deposition	Reduced lipid peroxidation Upregulation of levels of TGF-β1 and uPA Anti-inflammatory properties – In cultured A549 cells, suppressed H_2O_2 and TNF-α induced release of NF-κβ, AP-1, IL-8, and increased GSH biosynthesis	[127, 133, 135]

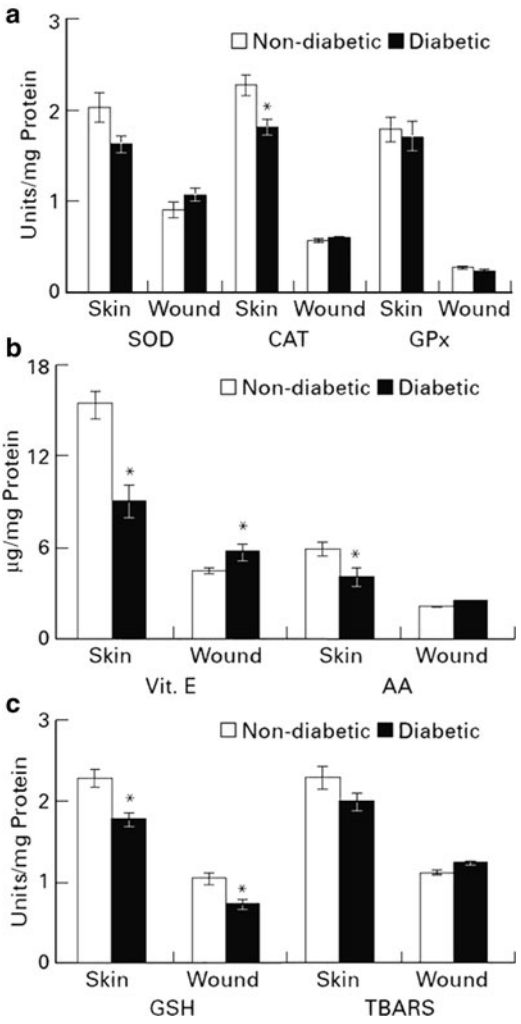

Fig. 7.5 Antioxidant status of skin and 7-day wound tissue of diabetic and non-diabetic rats. Level of antioxidants is lower in wound tissue as compared to normal skin. Reduced GSH level in the wound tissue of diabetic rats could be responsible for delayed wound healing observed in diabetic rats. (Figure reproduced from [113])

elevated previously reduced GSH levels allowing tissue preservation in spinal cord [98]. Analysis of the antioxidant status of a self-healing cutaneous wound at different times after wounding demonstrated that the levels of small molecule antioxidants (GSH, vitamins C and E) in injured tissue decreased by 60–70% as compared to normal skin (Fig. 7.5) and only GSH levels were recovered completely 14 days post-wounding [112]. The same group found that glutathione and vitamin E levels in wound tissue of aged rats were lower as compared to young rats, which could explain the delayed wound healing observed in the aged rats. In streptozotocin-induced diabetic rats, the 7-day wound tissue had lower levels of GSH (in contrast to elevated levels of vitamin E) which indicates that reduced levels of GSH could be responsible for delayed wound healing [113] (Fig. 7.5).

Among diabetic patients with foot ulcers, the wound edge tissue as compared to control tissue had lower levels of GSH and cysteine, whereas elevated levels of mixed protein disulfides. Lower GSH levels were found in wound tissues of diabetic mice as compared to non-diabetic mice [114]. Hydrocortisone-treated immunocompromised rats also showed reduced levels of GSH, vitamins C and E in both normal and wounded skin (2 days post-wounding) as compared to immunocompetent rats. Seven days post-wounding, levels of vitamins C and E in wound tissue of immunocompromised were similar to that of immunocompetent rats, but GSH level remained depleted even after 2 weeks [105]. When rats were depleted of GSH using L-buthionine-(*S*,*R*)-sulfoximine (BSO), an inhibitor of rate-limiting enzyme in biosynthesis of GSH (γ-glutamylcysteine synthetase), there was a reduction in wound bursting strength as compared to untreated animals [115]. The same group also demonstrated that GSH levels are significantly lower in ischemic skin flaps, but preconditioning enhances skin flap survival by increasing activity of glutathione reductase and maintaining GSH levels [116]. All these results considered together indicate that depletion of small molecule antioxidants disturb the redox state of the wound and result in an impaired healing response. Restoring the redox balance in the wounds by application/delivery of small molecule antioxidants would be a viable strategy to improve the healing response.

Topical application of glutathione monoester (GME), a drug used to increase intracellular GSH content, using carboxymethylcellulose (CMC) vehicle in a diabetic mice wound model resulted in significantly faster healing [114, 117].

Dietary supplementation of diabetic rats with palm vitamin E (70% tocotrienols and 30% tocopherols) extract (PVE) and α-tocopherol in an excisional wound model showed that PVE was more effective at enhancing wound healing and inducing antioxidant enzyme levels in the wounds of diabetic rats as compared to α-tocopherol. However, both antioxidants were able to reduce lipid peroxidation in healing wounds, as measured by lower MDA levels [118]. The difference in the potencies of PVE and α-tocopherol could be attributed to the higher percent tocotrienols content of PVE or preferential pharmacokinetic distribution of tocotrienols in skin. Orally administered tocotrienols have better distribution in skin (15% tocotrienols distributed in the skin as compared to 1% tocopherols) and in some conditions tocotrienols have been reported as more potent antioxidants against lipid peroxidation than tocopherols [119–121]. Although the reasons for impaired wound healing in diabetic mice are not completely understood, an altered VEGF mRNA expression as a result of lipid peroxidation is one of the characteristics of wound healing defect among diabetic mice. Inhibition of lipid peroxidation in diabetic mice by systemic treatment with raxofelast, a hydrophilic vitamin E-like inhibitor of lipid peroxidation, normalized VEGF mRNA expression and secretion resulting in improved wound healing and angiogenesis [122, 123]. This effect of raxofelast was not seen in non-diabetic mice [123].

Curcumin (diferuloylmethane), a yellow pigment present in the Indian spice turmeric, is a polyphenolic antioxidant that also interacts with several cell signaling proteins and thereby exert its anti-cancer, anti-inflammatory, anti-angiogenic, etc. effects [124–126]. Enhancement of wound healing by curcumin has been

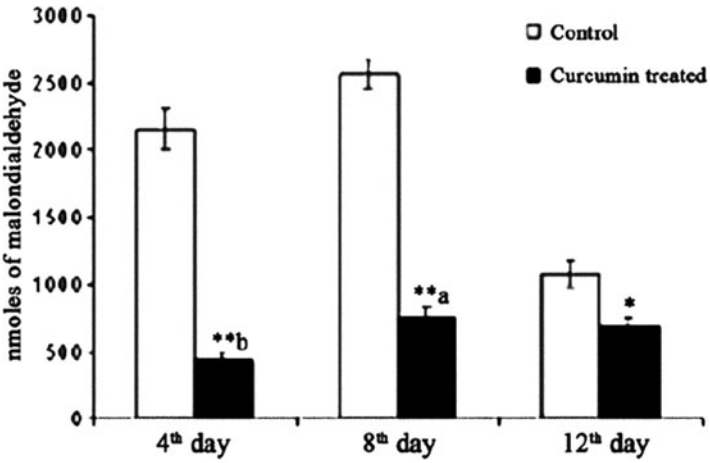

Fig. 7.6 Lipid peroxide levels in the granulation tissue of control and curcumin-treated wounds on rats. (Figure reproduced from [128])

demonstrated in several studies [127]. Topical application of curcumin in full thickness excision wound model resulted in increased cellular proliferation and collagen synthesis at the wound site and making wound heal faster. Curcumin exerted antioxidant effect at the wound site by decreasing lipid peroxidation (Fig. 7.6) and topical treatment resulted in increased activity of antioxidant enzymes SOD, catalase, and GPx [128]. Biopsies of curcumin-treated animal wounds showed increased migration of fibroblasts, myofibroblasts, macrophages, improved neovascularization and higher collagen deposition at wound site. Immunohistochemical, in situ hybridization and polymerase chain reaction analysis showed an increase in transforming growth factor-β1 (TGF-β1) levels and TGF-β1 mRNA expression, indicating that curcumin treatment-induced endogenous production of TGF-β1 in the wound of both diabetic and non-diabetic mice [129, 130]. TGF-β1stimulates fibroblast proliferation and enhances fibroblast production of collagen and fibronectin, thereby playing an important role in production of extracellular matrix [131]. TGF-β1 has also been suggested to induce epidermal keratinocytes to express integrins that facilitate the migratory component of re-epithelialization [132]. Madhyastha et al. have observed curcumin-induced and JNK and p38 MAPK-mediated upregulation of urokinase plasminogen activator (uPA) gene expression and that uPA upregulation is important in promoting fibrinolysis, matrix remodeling, and cell migration, two mechanisms that are vital for wound healing [133, 134]. Faster wound closure and enhanced collagen deposition in curcumin-treated wounds could be a result of curcumin-induced TGF-β1 production and uPA upregulation. In cultured alveolar epithelial cells (A549), curcumin suppressed H_2O_2-induced and TNF-α-induced NF-κβ, activator protein-1 (AP-1), and IL-8 release, exerting its anti-inflammatory properties. In the same study, curcumin-treatment of A549 cells resulted in an increased GSH biosynthesis and glutamylcysteine ligase catalytic subunit mRNA expression, suggesting that antioxidant properties of curcumin do not depend only on its free radical scavenging ability [135].

Beneficial effects of vitamin C (ascorbic acid) on wound healing in humans were reported by Ringsdorf and Cheraskin [136]. Topical application of vitamin C in an incisional wound model resulted in faster wound healing marked by reduced number of macrophages, increased proliferation of fibroblasts and new vessels, and thicker and more organized collagen fibers in the wounds [137]. Intraperitoneal administration of vitamin C prior to γ-radiation resulted in elevated wound contraction in a dose-dependent manner and improved healing of the wounds after whole body exposure to γ-radiation [138]. Ascorbic acid can regulate the extracellular matrix synthesis by inducing increased collagen synthesis in human dermal fibroblasts. Stimulatory effect of vitamin C on collagen production results from its action in allowing normal collagen hydroxylation and restoring efficient collagen secretion [139]. Enzymatic mechanism suggested for hydroxylation of collagen (proline residues) occurs through a reactive iron–oxygen complex (the ferryl ion) and that ascorbic acid is required to reduce Fe^{3+} formed during the reaction [140]. Long-term treatment of human dermal fibroblasts with L-ascorbic acid 2-phosphate (AA2P), a stable vitamin C derivative, resulted an increase in cell motility in context of wound healing. Microarray analysis showed that AA2P treatment increased the expression of uPA, upregulated the hyaluronan-mediated motility receptor which is required for fibroblast migration in the context of wound healing and IL-6, which also promotes cell motility and matrix remodeling during wound healing [141].

Studies with other small molecule antioxidants such as quercetin, allopurinol, retinoids (e.g., vitamin A and tretinoin), and uric acid have shown enhanced wound healing and improved collagen content at wound site, indicating that scavenging free radicals has a beneficial effect on overall wound healing process [142–145].

Role of Antioxidant Enzymes in Wound Healing

SOD

Importance of SOD in wound healing can be inferred from the finding that SOD1 deficiency resulted in a delayed wound healing response [146]. Steiling et al. have studied spatial and temporal expression of different antioxidant enzymes during cutaneous wound repair and found that SOD1 and SOD2 mRNA levels were upregulated during early phase of wound repair when the oxidative burst occurs. In situ hybridization and immunofluorescence data indicated that Cu/ZnSOD is expressed in basal cells of the hyperproliferative epithelium at wound edge and in the granulation tissue. SOD2 was expressed in both basal and suprabasal cells of hyperproliferative epidermis [147]. Contrary to this data, Shukla et al. had reported reduced activity of SOD after cutaneous injury and that SOD activity was not recovered even after 14 days [112]. This inconsistency in the mRNA expression and enzyme activity reported in the two studies could be a result of loss of

enzymatic activity of SOD at wound site due to oxidative environment at the wound site [148, 149].

Intravenous administration of SOD in an ischemic skin injury model resulted in a reduction in edema and increased the wound breaking strength and collagen synthesis at wound site [143]. Delayed healing in streptozotocin-induced type 1 diabetic mice was restored by a single regimen of cutaneous gene therapy of MnSOD, marked by reduced superoxide levels, and increased cutaneous MnSOD and NOS activity [150]. The same group also demonstrated that poor wound healing in diabetic mice is a result of decreased MnSOD expression and activity in endothelial progenitor cells (EPCs), which normally assist angiogenesis at wound site. By restoring diabetic EPC function after ex vivo, MnSOD gene transfer prior to their transplantation at the wound site resulted in an enhanced and accelerated wound healing. Enhanced wound healing effect was also observed by increasing the number of transplanted diabetic EPCs [151]. Also, transgenic diabetic mice that overexpress MnSOD or treatment of diabetic mice with SOD mimetic corrected post-ischemic defects in neovascularization, oxygen delivery, chemokine expression, and normalized tissue survival [152]. These results taken together demonstrate that scavenging superoxide can correct impaired wound healing process.

Catalase and Glutathione Peroxidase

Catalase and GPx at the wound site keep a check on the levels of H_2O_2 generated by SOD from superoxide anion. Steiling et al. showed that catalase and GPx were coexpressed along with SOD in the wound. Along with Cu/ZnSOD and MnSOD, only the levels of selenoenzymes GPx (SeGPx) mRNA were upregulated during early phase of wound repair where as catalase and phospholipid hydroperoxide GPx (PhGPx) mRNA levels did not alter after injury. Like SOD, catalase and GPx mRNA expressions were also prominent in the hyperproliferative endothelium but were found in lower levels in the granulation tissue. Similar expression pattern of SOD, catalase and GPx suggest that H_2O_2 produced by SOD is detoxified by catalase and GPx before it could react with transition metal ions to generate deleterious hydroxyl radicals [147]. However, Shukla et al. have shown that catalase activity in the healing wounds decreased during the first week post-wounding and activity level of catalase was recovered to its original level at 2 weeks post-wounding [112]. Again as mentioned above, the discrepancy in the mRNA expression of catalase and the activity of catalase could be a result of enzyme inactivation or translational failure to code protein to due to the oxidative environment at the wound site.

Unexpectedly, catalase overexpression by adenoviral gene delivery impaired wound angiogenesis, closure and slowed tissue remodeling [89]. H_2O_2 by itself or H_2O_2 generated by the overexpression of SOD1 via gene transfer induces VEGF expression in wound-related cells [153–155] and low concentration of H_2O_2 present at the wound was important, mediating angiogenesis by upregulating VEGF expression. However, in a separate study by Alacam et al., topical application of catalase

as a pulp-capping agent improved long-term (after 90 days) dental pulp tissue healing in a canine injury model [156].

Peroxiredoxins

Kümin et al. studied the expression of peroxiredoxins post-injury in a full-thickness excisional wound model and found enhanced expression of Prdx6 and moderate increase in the expression of Prdx4 as compared to unaltered expression of Prdx1 and Prdx2 [99]. Levels of Prdx6 mRNA were highest at day 1 after injury, remained elevated till day 7 and levels reduced back to normal skin level 14 days post-wounding when the wound was completely healed [157]. Using an in situ hybridization technique, it was found that in vivo, Prdx6 mRNA was highly expressed by keratinocytes of the hyperproliferative epidermis of skin wounds, although other cells in the granulation tissue also expressed Prdx6 mRNA [158]. Since wound healing response was associated with altered Prdx6 levels as compared to other five peroxiredoxins, Kümin et al. have studied effect of Prdx6 overexpression and underexpression on wound healing [99, 159]. Although Prdx6 knockout mice develops normally, they were found to be more susceptible to oxidative stress injury induced by intraperitoneal injection of paraquat, suggesting that Prdx6 aides in the regulation of superoxide-mediated oxidative stress. Also, macrophages from these Prdx6 knockout mice had lower survival rates against oxidative insult induced by H_2O_2, *t*-butyl hydroperoxide, and paraquat [160]. Even though Prdx6 expression was predominant in the hyperproliferative epidermis of skin, cutaneous injury to the Prdx6 knockout mice resulted in normal wound epithelialization indicating that other antioxidant enzymes in these cells can compensate for the absence of Prdx6. However, severe hemorrhage in the granulation tissue of the knockout mice was observed and the extent of hemorrhage correlated with the oxidative damage to the granulation tissue as indicated by the presence of oxidized proteins and nitrotyrosine positive cells. At the ultrastructural level in the wound tissue of Prdx6 knockout mice, endothelial cells appeared to be damaged and their rate of apoptosis was also enhanced. Increased susceptibility of cultured endothelial cells to oxidative stress after siRNA-mediated knockdown of Prdx6 confirmed sensitivity of endothelial cells to the loss of Prdx6. Wound healing studies in the bone marrow chimeric mice indicate that Prdx6-deficient inflammatory and endothelial cells contribute to the hemorrhage observed in the granulation tissue. This study also revealed the ROS-mediated cross-talk between hematopoietic cells and resident cells at the wound [99]. Overexpression of Prdx6 in transgenic mice did not affect their skin morphogenesis and homeostatis. Keratinocytes cultured from Prdx6 overexpressing mice showed enhanced resistance to ultraviolet A (UVA) and menadione-induced oxidative damage. Upon skin injury to these transgenic mice, enhanced wound closure was observed in aged animals, suggesting that the overexpression of Prdx6 protected the skin from age-related accumulative oxidative damage which is responsible for poor wound healing in aged animals [159].

"Antioxidant Materials" for Wound Healing

As described, antioxidants clearly play an important role in ROS-mediated intercellular and intracellular signaling and pro-healing effects of several antioxidants. However, suboptimal delivery of antioxidants to the wound site has complicated their use as a regenerative medicine strategy. Antioxidants could be delivered at wound site via oral route (or dietary supplementation), intravenously or direct dermal application to the wound. Several studies have shown that oral administration of antioxidants has beneficial effect on the wound healing [118, 162]. However, unfavorable pharmacological distribution of these antioxidants means that large doses are required for the antioxidants to reach a therapeutic concentration at the wound site, and the wound healing effect if any would be slow. Large doses of antioxidants for prolonged period could also result in other side effects. Some studies have found that antioxidants have no effect on the wound healing process when administered orally. Also, oral delivery of AOE has been at best marginally effective [24]. All these drawbacks make oral delivery a less attractive option for wound healing applications. Direct application of antioxidants on the wound (e.g., topical application) seems to be an easier and effective way of antioxidant delivery to the wound site. However, direct application of antioxidants is limited by (1) rapid clearance, (2) stability, and (3) choice of material used to deliver antioxidants.

Loading antioxidants into a synthetic scaffold, a film, or a porous 3D network that acts as a diffusion barrier could be used for slow and controlled release of antioxidants from the scaffolds. Full thickness dermal wounds in rats that were treated with curcumin and quercetin incorporated collagen films showed increased wound reduction and enhanced cell proliferation as compared to control and collagen-treated animals [142, 163]. Incorporation of curcumin in electrospun nanofiber mats of cellulose acetate and poly(ε-caprolactone) (PCL) resulted in a sustained release of curcumin over ~ 3 days [164, 165]. Fibroblasts cultured on curcumin-loaded PCL nanofibers showed resistance to H_2O_2-induced oxidative stress and mouse macrophages cultured on curcumin-loaded PCL nanofibers reduced LPS-induced IL-6 expression, a marker of inflammation. In a streptozotocin-induced diabetic mice wound model, curcumin-loaded PCL nanofibers had a pro-wound healing effect as evidenced by increased rate of wound closure [164]. Hydrogels, three-dimensional network of hydrophilic polymers, can be used for immobilizing antioxidant enzymes to prevent inactivation of enzymes otherwise caused by direct application. Study by Chiumiento et al. where they loaded carboxymethylcellulose (CMC) hydrogels with SOD and treated the rat wounds with CMC-SOD found that CMC-SOD reduced the time necessary for wound healing. Also, CMC-SOD had a proliferative effect on primary human fibroblasts [166].

Effectiveness of scaffold based antioxidant therapy would also depend on the biomaterial used for the synthesis of the scaffold, since in some settings biomaterials could themselves induce an inflammatory response from the host tissue [167]. This inflammatory response is often the result of local accumulation

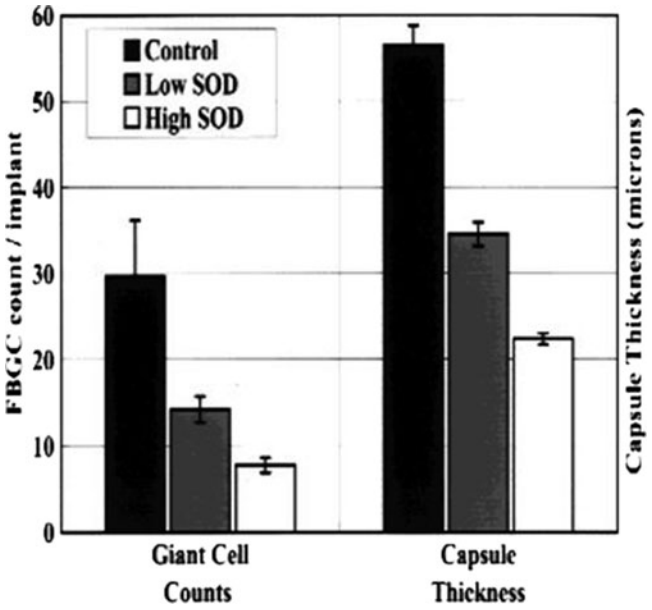

Fig. 7.7 Surface functionalization of polyethylene (PE) implants with low molecular weight SOD mimetic (SODm) suppress biomaterial-induced chronic inflammatory response. Count of foreign body giant cells (FBGCs) adherent to the PE implant (*left*) and capsule thickness (*right*) for the control and SODm-treated PE implants after 28 days. (Figure reproduced from [176])

of the polymer degradation byproducts or leachouts, inducing cellular oxidative stress [168–171]. One of the approaches to suppress biomaterial-induced inflammatory response could be to conjugate small molecule antioxidants such as ascorbic acid, vitamin E, GSH, gallic acid, catechin, etc. to the polymer ('antioxidant polymers') [172–175]. Conjugation of low molecular weight superoxide dismutase mimetic (SODm) to implanted biomedical materials such as ultra-high molecular weight polyethylene (UHMWPE), poly(etherurethane urea), and tantalum metal suppressed both chronic and inflammatory responses to the implants as evident by fewer neutrophils (after 3 days), fewer foreign body giant cells (FBGCs) (after 28 days), and inhibition of fibrous capsule formation (Fig. 7.7) [176]. Also, the incorporation of NAC in poly(methyl methacrylate) (PMMA) bone cement reduced cytotoxicity of PMMA by scavenging free radicals and increasing GSH levels in osteoblasts, resulting in increased bone formation with higher strength [177]. Antioxidant polymers could not only be used to improve biocompatibility, but could also serve as a means of delivering antioxidants at the wound site. Some of the above mentioned examples of antioxidant polymers [173, 175] are limited by low percentage of antioxidant content as compared to the bulk material. If designed appropriately by increasing their percent antioxidant content and controlling the degradation rate (rate of release of antioxidants), antioxidant polymers can be used effectively for antioxidant delivery at the wound site. In our previous work, we have

polymerized trolox, a water-soluble analog of vitamin E, to synthesize poly(trolox ester) with 100% antioxidant content which undergoes biodegradation to release trolox [178]. Nanoparticles of poly(trolox ester) suppressed oxidative stress in human U937 monocytes in an in vitro metal nanoparticle-based injury model. Another advantage of incorporating antioxidants in polymer backbone [172, 178] as compared to pendant conjugation strategies [174] is that it protects the antioxidant from premature oxidation and allows for sustained release over longer time periods. As a similar approach to incorporate polyphenolic antioxidants (e.g., quercetin and curcumin) into the polymer backbone, our lab has synthesized poly (antioxidant β-amino esters) with varying percent antioxidant content and tunable degradation rate [179]. Poly(antioxidant β-amino esters) chemistry can be extended to other polyphenolic antioxidants and provides a platform to develop antioxidant polymers with tunable degradation properties.

Conclusions and Perspective

In conclusion, the role of oxidants during the wound healing process is a result of a complex interaction between cells, extracellular matrix, and biomolecules. The dynamic role of oxidative stress in wound healing is evident from the fact that excess oxidants during the inflammatory phase of healing could result in a chronic non-healing wound, but certain level of ROS/RNS are necessary for tissue vascularization. Studies with the use of a scaffold or the use of growth factors (e.g., PDGF) alone have not yet met success in wound healing applications [31, 180], which indicates the necessity to modulate the wound environment at different levels simultaneously. Since various aspects of wound-healing are redox-dependent, the use of antioxidants to modulate redox state of the wound could provide an effective leverage in controlling the wound healing response. Temporal control over the delivery of antioxidants at the wound site will be a major factor in determining the effectiveness of antioxidant therapy in wound healing.

References

1. Hancock, J.T.: The role of redox mechanisms in cell signalling. Mol. Biotechnol. **43**(2), 162–166 (2009)
2. Muzykantov, V.R.: Delivery of antioxidant enzyme proteins to the lung. Antioxid. Redox Signal. **3**(1), 39–62 (2001)
3. Cataldi, A.: Cell responses to oxidative stressors. Curr. Pharm. Des. **16**(12), 1387–1395 (2010)
4. Ogasawara, M.A., Zhang, H.: Redox regulation and its emerging roles in stem cells and stem-like cancer cells. Antioxid. Redox Signal. **11**(5), 1107–1122 (2009)
5. Sharma, R.K., Zhou, Q., Netland, P.A.: Effect of oxidative preconditioning on neural progenitor cells. Brain Res. **1243**, 19–26 (2008)

6. Smith, J., et al.: Redox state is a central modulator of the balance between self-renewal and differentiation in a dividing glial precursor cell. Proc. Natl Acad. Sci. USA **97**(18), 10032–10037 (2000)
7. Stanic, B., Katsuyama, M., Miller Jr., F.J.: An oxidized extracellular oxidation-reduction state increases Nox1 expression and proliferation in vascular smooth muscle cells via epidermal growth factor receptor activation. Arterioscler. Thromb. Vasc. Biol. **30**, 2234–2241 (2010)
8. Delles, C., Miller, W.H., Dominiczak, A.F.: targeting reactive oxygen species in hypertension. Antioxid. Redox Signal. **10**(6), 1061–1077 (2008)
9. Heinecke, J.W.: Oxidants and antioxidants in the pathogenesis of atherosclerosis: implications for the oxidized low density lipoprotein hypothesis. Atherosclerosis **141**(1), 1–15 (1998)
10. Wei, Z., et al.: Simulated ischemia in flow-adapted endothelial cells leads to generation of reactive oxygen species and cell signaling. Circ. Res. **85**(8), 682–689 (1999)
11. Chow, C.W., et al.: Oxidative stress and acute lung injury. Am. J. Respir. Cell Mol. Biol. **29**(4), 427–431 (2003)
12. Kirkham, P.: Oxidative stress and macrophage function: a failure to resolve the inflammatory response. Biochem. Soc. Trans. **35**(Pt 2), 284–287 (2007)
13. Barnham, K.J., Masters, C.L., Bush, A.I.: Neurodegenerative diseases and oxidative stress. Nat. Rev. Drug Discov. **3**(3), 205–214 (2004)
14. Finkel, T., Holbrook, N.J.: Oxidants, oxidative stress and the biology of ageing. Nature **408** (6809), 239–247 (2000)
15. Jomova, K., Valko, M.: Advances in metal-induced oxidative stress and human disease. Toxicology **283**(2–3), 65–87 (2011)
16. Muzykantov, V.R.: Targeting of superoxide dismutase and catalase to vascular endothelium. J. Control. Release **71**(1), 1–21 (2001)
17. Parkhurs, R.M., Skinner, W.A.: Oxidation products of vitamin E and its model 6-hydroxy-2,2,5,7,8-pentamethylchroman.8. oxidation with benzoyl peroxide. J. Organic Chem. **31**(4), 1248–51 (1966)
18. Villano, D., et al.: Radical scavenging ability of polyphenolic compounds towards DPPH free radical. Talanta **71**(1), 230–235 (2007)
19. Stenesh, J.: Biochemistry, p. xxvii, 568. Plenum, New York (1998)
20. Papp, L.V., et al.: From selenium to selenoproteins: synthesis, identity, and their role in human health. Antioxid. Redox Signal. **9**(7), 775–806 (2007)
21. Lu, J., Holmgren, A.: Selenoproteins. J. Biol. Chem. **284**(2), 723–727 (2009)
22. Manevich, Y., Fisher, A.B.: Peroxiredoxin 6, a 1-Cys peroxiredoxin, functions in antioxidant defense and lung phospholipid metabolism. Free Radic. Biol. Med. **38**(11), 1422–1432 (2005)
23. Rhee, S.G., Chae, H.Z., Kim, K.: Peroxiredoxins: a historical overview and speculative preview of novel mechanisms and emerging concepts in cell signaling. Free Radic. Biol. Med. **38**(12), 1543–1552 (2005)
24. Hood*, E., Simone, E., Wattamwar, P.P., Dziubla, T.D., Muzykantov, V.R.: Polymeric Carriers for Antioxidant Enzymes and Small Molecules. Review article. Nanomedicine (Accepted)
25. Muro, S., et al.: Slow intracellular trafficking of catalase nanoparticles targeted to ICAM-1 protects endothelial cells from oxidative stress. Am. J. Physiol. Cell Physiol. **285**(5), C1339–C1347 (2003)
26. Dziubla, T.D., Karim, A., Muzykantov, V.R.: Polymer nanocarriers protecting active enzyme cargo against proteolysis. J. Control. Release **102**(2), 427–439 (2005)
27. Martin, P.: Wound healing–aiming for perfect skin regeneration. Science **276**(5309), 75–81 (1997)
28. Nathan, C.: Neutrophils and immunity: challenges and opportunities. Nat. Rev. Immunol. **6**(3), 173–182 (2006)

29. Hubner, G., et al.: Differential regulation of pro-inflammatory cytokines during wound healing in normal and glucocorticoid-treated mice. Cytokine **8**(7), 548–556 (1996)
30. Lovvorn, H.N., et al.: Relative distribution and crosslinking of collagen distinguish fetal from adult sheep wound repair. J. Pediatr. Surg. **34**(1), 218–223 (1999)
31. Sen, C.K., Roy, S.: Redox signals in wound healing. Biochimica Et Biophysica Acta-General Subjects **1780**(11), 1348–1361 (2008)
32. Gorlach, A.: Redox regulation of the coagulation cascade. Antioxid. Redox Signal. **7**(9–10), 1398–1404 (2005)
33. Klyubin, I.V., Kirpichnikova, K.M., Gamaley, I.A.: Hydrogen peroxide-induced chemotaxis of mouse peritoneal neutrophils. Eur. J. Cell Biol. **70**(4), 347–351 (1996)
34. Niethammer, P., et al.: A tissue-scale gradient of hydrogen peroxide mediates rapid wound detection in zebrafish. Nature **459**(7249), 996–999 (2009)
35. Hattori, H., et al.: Small-molecule screen identifies reactive oxygen species as key regulators of neutrophil chemotaxis. Proc. Natl Acad. Sci. USA **107**(8), 3546–3551 (2010)
36. Nakamura, H., et al.: Circulating thioredoxin suppresses lipopolysaccharide-induced neutrophil chemotaxis. Proc. Natl Acad. Sci. USA **98**(26), 15143–15148 (2001)
37. Nathan, C.F.: Neutrophil activation on biological surfaces. Massive secretion of hydrogen peroxide in response to products of macrophages and lymphocytes. J. Clin. Invest. **80**(6), 1550–1560 (1987)
38. Babior, B.M.: Phagocytes and oxidative stress. Am. J. Med. **109**(1), 33–44 (2000)
39. Baggiolini, M., et al.: Activation of neutrophil leukocytes – chemoattractant receptors and respiratory burst. FASEB J. **7**(11), 1004–1010 (1993)
40. Leto, T.L., Geiszt, M.: Role of Nox family NADPH oxidases in host defense. Antioxid. Redox Signal. **8**(9–10), 1549–1561 (2006)
41. Meischl, C., Roos, D.: The molecular basis of chronic granulomatous disease. Springer Semin. Immunopathol. **19**(4), 417–434 (1998)
42. Shi, M.M., et al.: Regulation of macrophage inflammatory protein-2 gene expression by oxidative stress in rat alveolar macrophages. Immunology **97**(2), 309–315 (1999)
43. Shi, M.M., Godleski, J.J., Paulauskis, J.D.: Regulation of macrophage inflammatory protein-1 alpha mRNA by oxidative stress. J. Biol. Chem. **271**(10), 5878–5883 (1996)
44. Marumo, T., et al.: Platelet-derived growth factor-stimulated superoxide anion production modulates activation of transcription factor NF-kappa B and expression of monocyte chemoattractant protein 1 in human aortic smooth muscle cells. Circulation **96**(7), 2361–2367 (1997)
45. Soneja, A., Drews, M., Malinski, T.: Role of nitric oxide, nitroxidative and oxidative stress in wound healing. Pharmacol. Rep. **57**(Suppl), 108–119 (2005)
46. Driscoll, K.E.: TNFalpha and MIP-2: role in particle-induced inflammation and regulation by oxidative stress. Toxicol. Lett. **112–113**, 177–183 (2000)
47. Hong, Y.H., et al.: Hydrogen peroxide-mediated transcriptional induction of macrophage colony-stimulating factor by TGF-beta 1. J. Immunol. **159**(5), 2418–2423 (1997)
48. Verhasselt, V., Goldman, M., Willems, F.: Oxidative stress up-regulates IL-8 and TNF-alpha synthesis by human dendritic cells. Eur. J. Immunol. **28**(11), 3886–3890 (1998)
49. Lee, J.S., et al.: Modulation of monocyte chemokine production and nuclear factor kappa B activity by oxidants. J. Interferon Cytokine Res. **19**(7), 761–767 (1999)
50. Haddad, J.J.: Redox regulation of pro-inflammatory cytokines and I kappa B-alpha/NF-kappa B nuclear translocation and activation (vol 296, pg 847, 2002). Biochem. Biophys. Res. Commun. **301**(2), 625–625 (2003)
51. Bejarano, I., et al.: Hydrogen peroxide increases the phagocytic function of human neutrophils by calcium mobilisation. Mol. Cell. Biochem. **296**(1–2), 77–84 (2007)
52. Winn, J.S., et al.: Hydrogen-peroxide modulation of the respiratory burst of human neutrophils. Biochem. Pharmacol. **41**(1), 31–36 (1991)
53. Krjukov, A.A., et al.: Activation of redox-systems of monocytes by hydrogen peroxide. Biofactors **26**(4), 283–292 (2006)

54. Murphy, J.K., et al.: Modulation of the alveolar macrophage respiratory burst by hydroperoxides. Free Radic. Biol. Med. **18**(1), 37–45 (1995)
55. Seres, T., et al.: The phagocytosis-associated respiratory burst in human monocytes is associated with increased uptake of glutathione. J. Immunol. **165**(6), 3333–3340 (2000)
56. Klune, J.R., et al.: HMGB1: Endogenous danger signaling. Mol. Med. **14**(7–8), 476–484 (2008)
57. Bianchi, M.E., Manfredi, A.A.: High-mobility group box 1 (HMGB1) protein at the crossroads between innate and adaptive immunity. Immunol. Rev. **220**, 35–46 (2007)
58. Tang, D., et al.: Hydrogen peroxide stimulates macrophages and monocytes to actively release HMGB1. J. Leukoc. Biol. **81**(3), 741–747 (2007)
59. Tsung, A., et al.: HMGB1 release induced by liver ischemia involves Toll-like receptor 4 dependent reactive oxygen species production and calcium-mediated signaling. J. Exp. Med. **204**(12), 2913–2923 (2007)
60. Springer, T.A.: Traffic signals for lymphocyte recirculation and leukocyte emigration – the multistep paradigm. Cell **76**(2), 301–314 (1994)
61. Reyes-Reyes, M., et al.: Beta 1 and beta 2 integrins activate different signalling pathways in monocytes. Biochem. J. **363**, 273–280 (2002)
62. Lu, H.F., et al.: Hydrogen peroxide induces LFA-1-dependent neutrophil adherence to cardiac myocytes. Am. J. Physiol. Heart Circ. Physiol. **278**(3), H835–H842 (2000)
63. Blouin, E., Halbwachs-Mecarelli, L., Rieu, P.: Redox regulation of beta 2-integrin CD11b/CD18 activation. Eur. J. Immunol. **29**(11), 3419–3431 (1999)
64. Lu, H.F., Ballantyne, C., Smith, C.W.: LFA-1 (CD11a/CD18) triggers hydrogen peroxide production by canine neutrophils. J. Leukoc. Biol. **68**(1), 73–80 (2000)
65. Nathan, C., et al.: Cytokine-induced respiratory burst of human-neutrophils – dependence on extracellular-matrix proteins and Cd11/Cd18 integrins. J. Cell Biol. **109**(3), 1341–1349 (1989)
66. Shappell, S.B., et al.: Mac-1 (Cd11b Cd18) mediates adherence-dependent hydrogen-peroxide production by human and canine neutrophils. J. Immunol. **144**(7), 2702–2711 (1990)
67. Hashizume, K., et al.: N-acetyl-L-cysteine suppresses constitutive expression of CD11a/LFA-1 alpha protein in myeloid lineage. Leuk. Res. **26**(10), 939–944 (2002)
68. Fraticelli, A., et al.: Hydrogen peroxide and superoxide modulate leukocyte adhesion molecule expression and leukocyte endothelial adhesion. Biochimica Et Biophysica Acta-Molecular Cell Research **1310**(3), 251–259 (1996)
69. Cai, H.: Hydrogen peroxide regulation of endothelial function: Origins, mechanisms, and consequences. Cardiovasc. Res. **68**(1), 26–36 (2005)
70. Carnemolla, R., Shuvaev, V.V., Muzykantov, V.R.: Targeting antioxidant and antithrombotic biotherapeutics to endothelium. Semin. Thromb. Hemost. **36**(3), 332–342 (2010)
71. Bradley, J.R., Johnson, D.R., Pober, J.S.: Endothelial activation by hydrogen-peroxide – selective increases of intercellular-adhesion molecule-1 and major histocompatibility complex class-I. Am. J. Pathol. **142**(5), 1598–1609 (1993)
72. Hubbard, A.K., Rothlein, R.: Intercellular adhesion molecule-1 (ICAM-1) expression and cell signaling cascades. Free Radic. Biol. Med. **28**(9), 1379–1386 (2000)
73. Roebuck, K.A., et al.: H2o2 and tumor-necrosis-factor-alpha activate intercellular-adhesion molecule-1 (Icam-1) gene-transcription through distinct cis-regulatory elements within the Icam-1 Promoter. J. Biol. Chem. **270**(32), 18966–18974 (1995)
74. Kawai, M., et al.: Pyrrolidine dithiocarbamate inhibits intercellular-adhesion molecule-1 biosynthesis induced by cytokines in human fibroblasts. J. Immunol. **154**(5), 2333–2341 (1995)
75. Saccani, A., et al.: Redox regulation of chemokine receptor expression. Proc. Natl. Acad. Sci. USA **97**(6), 2761–2766 (2000)
76. Lehoux, G., et al.: Upregulation of expression of the chemokine receptor CCR5 by hydrogen peroxide in human monocytes. Mediators Inflamm. **12**(1), 29–35 (2003)

77. Sung, F.L., Siow, X.L., Wang, G., Lynn, E.G., and Karmin, O.: Homocysteine stimulates the expression of monocyte chemoattractant protein-1 receptor (CCR2) in human monocytes: possible involvement of oxygen free radicals. Biochem. J. **357**(Pt 1), 233–240 (2001)
78. Raja, et al.: Wound re-epithelialization: modulating keratinocyte migration in wound healing. Front. Biosci. **12**, 2249–2268 (2007)
79. Haase, I., et al.: Regulation of keratinocyte shape, migration and wound epithelialization by IGF-1- and EGF-dependent signalling pathways. J. Cell Sci. **116**(15), 3227–3238 (2003)
80. Vardatsikos, G., Sahu, A., Srivastava, A.K.: The insulin-like growth factor family: molecular mechanisms, redox regulation, and clinical implications. Antioxid. Redox Signal. **11**(5), 1165–1190 (2009)
81. Higashi, Y., et al.: A redox-sensitive pathway mediates oxidized LDL-induced downregulation of insulin-like growth factor-1 receptor. J. Lipid Res. **46**(6), 1266–1277 (2005)
82. Hober, S., et al.: Insulin-like growth factors I and II are unable to form and maintain their native disulfides under in vivo redox conditions. FEBS Lett. **443**(3), 271–276 (1999)
83. Nishio, E., Watanabe, Y.: The involvement of reactive oxygen species and arachidonic acid in alpha 1-adrenoceptor-induced smooth muscle cell proliferation and migration. Br. J. Pharmacol. **121**(4), 665–670 (1997)
84. Ranjan, P., et al.: Redox-dependent expression of cyclin D1 and cell proliferation by Nox1 in mouse lung epithelial cells. Antioxid. Redox Signal. **8**(9–10), 1447–1459 (2006)
85. Rajagopalan, S., et al.: Reactive oxygen species produced by macrophage-derived foam cells regulate the activity of vascular matrix metalloproteinases in vitro. Implications for atherosclerotic plaque stability. J. Clin. Invest. **98**(11), 2572–2579 (1996)
86. Grange, L., et al.: NAD(P)H oxidase activity of Nox4 in chondrocytes is both inducible and involved in collagenase expression. Antioxid. Redox Signal. **8**(9–10), 1485–1496 (2006)
87. Yoon, S.O., et al.: Sustained production of H(2)O(2) activates pro-matrix metalloproteinase-2 through receptor tyrosine kinases/phosphatidylinositol 3-kinase/NF-kappa B pathway. J. Biol. Chem. **277**(33), 30271–30282 (2002)
88. Clark, R.A.F.: The Molecular and Cellular Biology of Wound Repair, 2nd edn. Plenum, New York (1996)
89. Roy, S., et al.: Dermal wound healing is subject to redox control. Mol. Ther. **13**(1), 211–220 (2006)
90. Arbiser, J.L., et al.: Reactive oxygen generated by Nox1 triggers the angiogenic switch. Proc. Natl Acad. Sci. USA **99**(2), 715–720 (2002)
91. West, X.Z., et al.: Oxidative stress induces angiogenesis by activating TLR2 with novel endogenous ligands. Nature **467**(7318), 972–976 (2010)
92. Liu, X.P., Zweier, J.L.: A real-time electrochemical technique for measurement of cellular hydrogen peroxide generation and consumption: Evaluation in human polymorphonuclear leukocytes. Free Radic. Biol. Med. **31**(7), 894–901 (2001)
93. Ojha, N., et al.: Assessment of wound-site redox environment and the significance of Rac2 in cutaneous healing. Free Radic. Biol. Med. **44**(4), 682–691 (2008)
94. Stadtman, E.R.: Protein oxidation and aging. Free Radic. Res. **40**(12), 1250–1258 (2006)
95. Haycock, J.W., et al.: Oxidative damage to protein and alterations to antioxidant levels in human cutaneous thermal injury. Burns **23**(7–8), 533–540 (1997)
96. Aksenova, M., et al.: Increased protein oxidation and decreased creatine kinase BB expression and activity after spinal cord contusion injury. J. Neurotrauma **19**(4), 491–502 (2002)
97. Xiong, Y.Q., Rabchevsky, A.G., Hall, E.D.: Role of peroxynitrite in secondary oxidative damage after spinal cord injury. J. Neurochem. **100**(3), 639–649 (2007)
98. Kamencic, H., et al.: Promoting glutathione synthesis after spinal cord trauma decreases secondary damage and promotes retention of function. FASEB J. **15**(1), 243–250 (2001)
99. Kumin, A., et al.: Peroxiredoxin 6 is required for blood vessel integrity in wounded skin. J. Cell Biol. **179**(4), 747–760 (2007)

100. Moseley, R., et al.: Comparison of oxidative stress biomarker profiles between acute and chronic wound environments. Wound Repair Regen. **12**(4), 419–429 (2004)
101. Pagnin, E., et al.: Diabetes induces p66(shc) gene expression in human peripheral blood mononuclear cells: Relationship to oxidative stress. J. Clin. Endocrinol. Metab. **90**(2), 1130–1136 (2005)
102. Fadini, G.P., et al.: The redox enzyme p66Shc contributes to diabetes and ischemia-induced delay in cutaneous wound healing. Diabetes **59**(9), 2306–2314 (2010)
103. Uchida, K., Stadtman, E.R.: Modification of histidine-residues in proteins by reaction with 4-hydroxynonenal. Proc. Natl. Acad. Sci. USA **89**(10), 4544–4548 (1992)
104. Cao, Y., et al.: Neuroprotective effect of baicalin on compression spinal cord injury in rats. Brain Res. **1357**, 115–123 (2010)
105. Gupta, A., Singh, R.L., Raghubir, R.: Antioxidant status during cutaneous wound healing in immunocompromised rats. Mol. Cell. Biochem. **241**(1–2), 1–7 (2002)
106. Grootveld, M., Halliwell, B.: Measurement of allantoin and uric-acid in human-body fluids – a potential index of free-radical reactions invivo. Biochem. J. **243**(3), 803–808 (1987)
107. James, T.J., et al.: Evidence of oxidative stress in chronic venous ulcers. Wound Repair Regen. **11**(3), 172–176 (2003)
108. Morrow, J.D., et al.: Non-cyclooxygenase-derived prostanoids (F2-isoprostanes) are formed insitu on phospholipids. Proc. Natl Acad. Sci. USA **89**(22), 10721–10725 (1992)
109. Meagher, E.A., Fitzgerald, G.A.: Indices of lipid peroxidation in vivo: Strengths and limitations. Free Radic. Biol. Med. **28**(12), 1745–1750 (2000)
110. Yeoh-Ellerton, S., Stacey, M.C.: Iron and 8-isoprostane levels in acute and chronic wounds. J. Invest. Dermatol. **121**(4), 918–925 (2003)
111. Awad, J.A., Morrow, J.D.: Excretion of F-2-isoprostanes in bile – a novel index of hepatic lipid-peroxidation. Hepatology **22**(3), 962–968 (1995)
112. Shukla, A., Rasik, A.M., Patnaik, G.K.: Depletion of reduced glutathione, ascorbic acid, vitamin E and antioxidant defence enzymes in a healing cutaneous wound. Free Radic. Res. **26**(2), 93–101 (1997)
113. Rasik, A.M., Shukla, A.: Antioxidant status in delayed healing type of wounds. Int. J. Exp. Pathol. **81**(4), 257–263 (2000)
114. Mudge, B.P., et al.: Role of glutathione redox dysfunction in diabetic wounds. Wound Repair Regen. **10**(1), 52–58 (2002)
115. Adamson, B., et al.: Delayed repair: The role of glutathione in a rat incisional wound model. J. Surg. Res. **62**(2), 159–164 (1996)
116. Rees, R.S., et al.: Oxidant stress – the role of the glutathione redox cycle in skin preconditioning. J. Surg. Res. **58**(4), 395–400 (1995)
117. Levy, E.J., Anderson, M.E., Meister, A.: Transport of glutathione diethyl ester into human-cells. Proc. Natl Acad. Sci. USA **90**(19), 9171–9175 (1993)
118. Musalmah, M., et al.: Comparative effects of palm vitamin E and alpha-tocopherol on healing and wound tissue antioxidant enzyme levels in diabetic rats. Lipids **40**(6), 575–580 (2005)
119. Traber, M.G., Podda, M., Weber, C., Yan, L.J., Packer, L.: Diet derived and topically applied tocotrienols accumulate in skin and protect the tissue against UV-induced oxidative stress. Asia Pac. J. Clin. Nutr. **6**, 63–67 (1997)
120. Serbinova, E., et al.: Free-radical recycling and intramembrane mobility in the antioxidant properties of alpha-tocopherol and alpha-tocotrienol. Free Radic. Biol. Med. **10**(5), 263–275 (1991)
121. Suzuki, Y., et al.: Structural and dynamic membrane-properties of alpha-tocopherol and alpha-tocotrienol - implication to the molecular mechanism of their antioxidant potency. Biochemistry **32**(40), 10692–10699 (1993)
122. Altavilla, D., et al.: Lipid peroxidation inhibition by raxofelast improves angiogenesis and wound healing in experimental burn wounds. Shock **24**(1), 85–91 (2005)

123. Altavilla, D., et al.: Inhibition of lipid peroxidation restores impaired vascular endothelial growth factor expression and stimulates wound healing and angiogenesis in the genetically diabetic mouse. Diabetes **50**(3), 667–674 (2001)
124. Ruby, A.J., et al.: Antitumor and antioxidant activity of natural curcuminoids. Cancer Lett. **94**(1), 79–83 (1995)
125. Kunnumakkara, A.B., Anand, P., Aggarwal, B.B.: Curcumin inhibits proliferation, invasion, angiogenesis and metastasis of different cancers through interaction with multiple cell signaling proteins. Cancer Lett. **269**(2), 199–225 (2008)
126. Maheshwari, R.K., et al.: Multiple biological activities of curcumin: a short review. Life Sci. **78**(18), 2081–2087 (2006)
127. Thangapazham, R.L., Sharma, A., Maheshwari, R.K.: Beneficial role of curcumin in skin diseases. Adv. Exp. Med. Biol. **595**, 343–357 (2007)
128. Panchatcharam, M., et al.: Curcumin improves wound healing by modulating collagen and decreasing reactive oxygen species. Mol. Cell. Biochem. **290**(1–2), 87–96 (2006)
129. Sidhu, G.S., et al.: Enhancement of wound healing by curcumin in animals. Wound Repair Regen. **6**(2), 167–177 (1998)
130. Sidhu, G.S., et al.: Curcumin enhances wound healing in streptozotocin induced diabetic rats and genetically diabetic mice. Wound Repair Regen. **7**(5), 362–374 (1999)
131. Faler, B.J., et al.: Transforming growth factor-beta and wound healing. Perspect. Vasc. Surg. Endovasc. Ther. **18**(1), 55–62 (2006)
132. Gailit, J., Welch, M.P., Clark, R.A.: TGF-beta 1 stimulates expression of keratinocyte integrins during re-epithelialization of cutaneous wounds. J. Invest. Dermatol. **103**(2), 221–227 (1994)
133. Madhyastha, R., et al.: Curcumin facilitates fibrinolysis and cellular migration during wound healing by modulating urokinase plasminogen activator expression. Pathophysiol. Haemost. Thromb. **37**(2–4), 59–66 (2010)
134. Choong, P.F., Nadesapillai, A.P.: Urokinase plasminogen activator system: a multifunctional role in tumor progression and metastasis. Clin. Orthop. Relat. Res. **415 (Suppl)**, S46–S58 (2003)
135. Biswas, S.K., et al.: Curcumin induces glutathione biosynthesis and inhibits NF-kappa B activation and interleukin-8 release in alveolar epithelial cells: Mechanism of free radical scavenging activity. Antioxid. Redox Signal. **7**(1–2), 32–41 (2005)
136. Ringsdorf Jr., W.M., Cheraskin, E.: Vitamin C and human wound healing. Oral. Surg. Oral. Med. Oral. Pathol. **53**(3), 231–236 (1982)
137. Lima, C.C., et al.: Ascorbic acid for the healing of skin wounds in rats. Braz. J. Biol. **69**(4), 1195–1201 (2009)
138. Jagetia, G.C., et al.: Augmentation of wound healing by ascorbic acid treatment in mice exposed to gamma-radiation. Int. J. Radiat. Biol. **80**(5), 347–354 (2004)
139. Chan, D., et al.: Regulation of procollagen synthesis and processing during ascorbate-induced extracellular matrix accumulation in vitro. Biochem. J. **269**(1), 175–181 (1990)
140. Peterkofsky, B.: Ascorbate requirement for hydroxylation and secretion of procollagen: relationship to inhibition of collagen synthesis in scurvy. Am. J. Clin. Nutr. **54**(6 Suppl), 1135S–1140S (1991)
141. Duarte, T.L., Cooke, M.S., Jones, G.D.: Gene expression profiling reveals new protective roles for vitamin C in human skin cells. Free Radic. Biol. Med. **46**(1), 78–87 (2009)
142. Gomathi, K., et al.: Quercetin incorporated collagen matrices for dermal wound healing processes in rat. Biomaterials **24**(16), 2767–2772 (2003)
143. Senel, O., et al.: Oxygen free radicals impair wound healing in ischemic rat skin. Ann. Plast. Surg. **39**(5), 516–523 (1997)
144. Abdelmalek, M., Spencer, J.: Retinoids and wound healing. Dermatol. Surg. **32**(10), 1219–1230 (2006)
145. Chigurupati, S., et al.: A synthetic uric acid analog accelerates cutaneous wound healing in mice. PLoS One **5**(4), e10044 (2010)

146. Iuchi, Y., et al.: Spontaneous skin damage and delayed wound healing in SOD1-deficient mice. Mol. Cell. Biochem. **341**(1–2), 181–194 (2010)
147. Steiling, H., et al.: Different types of ROS-scavenging enzymes are expressed during cutaneous wound repair. Exp. Cell Res. **247**(2), 484–494 (1999)
148. Bayir, H., et al.: Neuronal NOS-mediated nitration and inactivation of manganese superoxide dismutase in brain after experimental and human brain injury. J. Neurochem. **101**(1), 168–181 (2007)
149. Pigeolet, E., et al.: Glutathione peroxidase, superoxide dismutase, and catalase inactivation by peroxides and oxygen derived free radicals. Mech. Ageing Dev. **51**(3), 283–297 (1990)
150. Luo, J.D., et al.: Gene therapy of endothelial nitric oxide synthase and manganese superoxide dismutase restores delayed wound healing in type 1 diabetic mice. Circulation **110**(16), 2484–2493 (2004)
151. Marrotte, E.J., et al.: Manganese superoxide dismutase expression in endothelial progenitor cells accelerates wound healing in diabetic mice. J. Clin. Invest. **120**(12), 4207–4219 (2010)
152. Ceradini, D.J., et al.: Decreasing intracellular superoxide corrects defective ischemia-induced new vessel formation in diabetic mice. J. Biol. Chem. **283**(16), 10930–10938 (2008)
153. Sen, C.K., et al.: Oxidant-induced vascular endothelial growth factor expression in human keratinocytes and cutaneous wound healing. J. Biol. Chem. **277**(36), 33284–33290 (2002)
154. Grzenkowicz-Wydra, J., et al.: Gene transfer of CuZn superoxide dismutase enhances the synthesis of vascular endothelial growth factor. Mol. Cell. Biochem. **264**(1–2), 169–181 (2004)
155. Ushio-Fukai, M., Alexander, R.W.: Reactive oxygen species as mediators of angiogenesis signaling - Role of NAD(P)H oxidase. Mol. Cell. Biochem. **264**(1–2), 85–97 (2004)
156. Alacam, A., et al.: Effects of topical Catalase application on dental pulp tissue: a histopathological evaluation. J. Dent. **28**(5), 333–339 (2000)
157. Auf dem Keller, U., et al.: Reactive oxygen species and their detoxification in healing skin wounds. J. Investig. Dermatol. Symp. Proc. **11**(1), 106–111 (2006)
158. Munz, B., et al.: A novel type of glutathione peroxidase: expression and regulation during wound repair. Biochem. J. **326**(Pt 2), 579–585 (1997)
159. Kumin, A., et al.: Peroxiredoxin 6 is a potent cytoprotective enzyme in the epidermis. Am. J. Pathol. **169**(4), 1194–1205 (2006)
160. Wang, X., et al.: Mice with targeted mutation of peroxiredoxin 6 develop normally but are susceptible to oxidative stress. J. Biol. Chem. **278**(27), 25179–25190 (2003)
161. Schafer, M., Werner, S.: Oxidative stress in normal and impaired wound repair. Pharmacol. Res. **58**(2), 165–171 (2008)
162. Wicke, C., et al.: Effects of steroids and retinoids on wound healing. Arch. Surg. **135**(11), 1265–1270 (2000)
163. Gopinath, D., et al.: Dermal wound healing processes with curcumin incorporated collagen films. Biomaterials **25**(10), 1911–1917 (2004)
164. Merrell, J.G., et al.: Curcumin-loaded poly(epsilon-caprolactone) nanofibres: Diabetic wound dressing with anti-oxidant and anti-inflammatory properties. Clin. Exp. Pharmacol. Physiol. **36**(12), 1149–1156 (2009)
165. Suwantong, O., et al.: Electrospun cellulose acetate fiber mats containing curcumin and release characteristic of the herbal substance. Polymer **48**(26), 7546–7557 (2007)
166. Chiumiento, A., et al.: Immobilizing Cu, Zn-superoxide dismutase in hydrogels of carboxymethylcellulose improves its stability and wound healing properties. Biochem.-Moscow **71**(12), 1324–1328 (2006)
167. Kao, W.Y.J., Kleinbeck, K.R., Faucher, L.D.: Biomaterials modulate interleukin-8 and other inflammatory proteins during reepithelialization in cutaneous partial-thickness wounds in pigs. Wound Repair Regen. **18**(5), 486–498 (2010)
168. Jiang, W.W., et al.: Phagocyte responses to degradable polymers. J. Biomed. Mater. Res. A **82A**(2), 492–497 (2007)

169. Geurtsen, W., et al.: Cytotoxicity of 35 dental resin composite monomers/additives in permanent 3 T3 and three human primary fibroblast cultures. J. Biomed. Mater. Res. **41**(3), 474–480 (1998)
170. Lefeuvre, M., et al.: TEGDMA induces mitochondrial damage and oxidative stress in human gingival fibroblasts. Biomaterials **26**(25), 5130–5137 (2005)
171. Serrano, M.C., et al.: Transitory oxidative stress in L929 fibroblasts cultured on poly(epsilon-caprolactone) films. Biomaterials **26**(29), 5827–5834 (2005)
172. Fleming, C., et al.: A carbohydrate-antioxidant hybrid polymer reduces oxidative damage in spermatozoa and enhances fertility. Nat. Chem. Biol. **1**(5), 270–274 (2005)
173. Spizzirri, U.G., et al.: Synthesis of antioxidant polymers by grafting of gallic acid and catechin on gelatin. Biomacromolecules **10**(7), 1923–1930 (2009)
174. Wang, Y.Z., et al.: Expansion and osteogenic differentiation of bone marrow-derived mesenchymal stem cells on a vitamin C functionalized polymer. Biomaterials **27**(17), 3265–3273 (2006)
175. Williams, S.R., et al.: Synthesis and characterization of poly(ethylene glycol)-glutathione conjugate self-assembled nanoparticles for antioxidant delivery. Biomacromolecules **10**(1), 155–161 (2009)
176. Udipi, K., et al.: Modification of inflammatory response to implanted biomedical materials in vivo by surface bound superoxide dismutase mimics. J. Biomed. Mater. Res. **51**(4), 549–560 (2000)
177. Tsukimura, N., et al.: N-acetyl cysteine (NAC)-mediated detoxification and functionalization of poly(methyl methacrylate) bone cement. Biomaterials **30**(20), 3378–3389 (2009)
178. Wattamwar, P.P., et al.: Antioxidant activity of degradable polymer poly(trolox ester) to suppress oxidative stress injury in the cells. Adv. Funct. Mater. **20**(1), 147–154 (2010)
179. Vasilakes, A., Byarski, J.P., Biswal, D., Wattamwar, P.P., Peyyala, R., Hilt, J.Z., and Dzivbla, T.D.: Controlled release of catalase and vancomycin from poly(β-amino ester) Hydrogels J. Control. Release. (submitted)
180. Macri, L., Clark, R.A.F.: Tissue Engineering for cutaneous wounds: selecting the proper time and space for growth factors, cells and the extracellular matrix. Skin Pharmacol. Physiol. **22**(2), 83–93 (2009)

Part V
Biologically Inspired Materials for Tissue Regeneration

Chapter 8
Gecko-Inspired Tape-Based Adhesives

Woo Kyung Cho, Maria José Maio Nunes Pereira, Nora Lang, Kyungheon Lee, Shwetha Mureli, Andreas Zumbuehl, Cathryn Sundback, Peter T. Masiakos, David J.D. Carter, Jeffrey Borenstein, Lino Ferreira, Robert Langer, and Jeffrey M. Karp

Abstract The next generation of surgical adhesives that are intended for internal applications will present considerable functional and regulatory challenges compared with topical adhesives that are currently available. These new adhesives must strongly adhere to wet surfaces and remain in place until the wound is leak-proof, while not being easily monitored. As adjuncts to current technologies such as

W.K. Cho
Harvard-MIT Division of Health Science and Technology, Massachusetts Institute of Technology, Cambridge, MA 02139, USA

Department of Medicine, Brigham and Women's Hospital, Harvard Medical School, Boston, MA 02115, USA

M.J.M.N. Pereira
Department of Medicine, Brigham and Women's Hospital, Harvard Medical School, Boston, MA 02115, USA

Center for Neuroscience and Cell Biology, University of Coimbra, Coimbra, Portugal

Biocant-Center of Innovation and Biotechnology, Cantanhede, Portugal

N. Lang
Department of Cardiac Surgery, Children's Hospital, Harvard Medical School, Boston, MA 02115, USA

K. Lee
Department of Medicine, Brigham and Women's Hospital, Harvard Medical School, Boston, MA 02115, USA

School of Mechanical, Aerospace and Systems Engineering, KAIST, Daejeon, South Korea

S. Mureli
Department of Medicine, Brigham and Women's Hospital, Harvard Medical School, Boston, MA 02115, USA

School of Chemical and Biotechnology, SASTRA University, Thanjavur 613401, India

A. Zumbuehl
Department of Organic Chemistry, University of Geneva, Geneva, Switzerland

S.K. Bhatia (ed.), *Engineering Biomaterials for Regenerative Medicine: Novel Technologies for Clinical Applications*, DOI 10.1007/978-1-4614-1080-5_8,

sutures, staples, and tissue glue, there is a growing interest to reduce the incidence of trauma associated with surgical incisions and suture lines. Novel approaches are under development that can facilitate wound closure without causing excessive inflammation, ischemia, or necrosis to the wound. Degradable tissue adhesive tapes have recently been suggested as a potential method for wound closure/healing. One strategy to implement this technology utilizes biomimicry to achieve high levels of adhesion by replicating the nanotopography of the gecko's footpad in biocompatible and biodegradable elastomers. Geckos can walk up vertical surfaces because the bottoms of their feet are covered with hierarchical fibrillar arrays which can maximize the interfacial adhesion to surfaces. Tissue adhesion of structures that mimic the gecko footpad can be further enhanced by applying a thin coating of a tissue-reactive biocompatible "glue" to the nanotopographically patterned surface. Using this two-component design, a tape-based adhesive can adapt to physiologic mechanical forces, while remaining strongly attached to the underlying tissue and eliciting minimal inflammatory response, eventually resorbing harmlessly without the damage caused by removal associated with other adhesives. These strongly adherent and minimally inflammatory biodegradable taped-based adhesives will provide a platform for many practical additions to the surgical armamentarium.

C. Sundback
Center of Regenerative Medicine, Massachusetts General Hospital, Boston, MA 02114, USA

Harvard Medical School, Boston, MA 02115, USA

P.T. Masiakos
Department of Pediatric Surgery, Massachusetts General Hospital, Boston, MA 02114, USA

Laboratory of Tissue Engineering, Harvard Medical School, Boston, MA 02115, USA

D.J.D. Carter • J. Borenstein
The Charles Stark Draper Laboratory, Cambridge, MA 02139, USA

L. Ferreira
Center for Neuroscience and Cell Biology, University of Coimbra, Coimbra, Portugal

Biocant-Center of Innovation and Biotechnology, Cantanhede, Portugal

R. Langer (✉)
Harvard-MIT Division of Health Science and Technology, Massachusetts Institute of Technology, Cambridge, MA 02139, USA

Department of Chemical Engineering, Massachusetts Institute of Technology, Cambridge, MA 02139, USA
e-mail: rlanger@mit.edu

J.M. Karp (✉)
Harvard-MIT Division of Health Science and Technology, Massachusetts Institute of Technology, Cambridge, MA 02139, USA

Department of Medicine, Brigham and Women's Hospital, Harvard Medical School, Boston, MA 02115, USA

Harvard Stem Cell Institute, Cambridge, MA, USA
e-mail: jkarp@rics.bwh.harvard.edu

The Need for Tough, Biocompatible, and Biodegradable Polymer Adhesives for Wound Closure

Mechanical wound closure is a necessary first step to wound healing. Sutures and surgical clips prevent leaks, stop bleeding, provide an antimicrobial barrier and ultimately permit the healing process to begin. Although sutures, staples, and glues have been widely used for many applications, there is a significant medical need for tough, biodegradable adhesives that can be used to close wounds or incisions that can accommodate various mechanical deformations while remaining strongly attached to the underlying tissue [1, 2]. These materials would be particularly useful as replacements or support to sutures and/or could be used as patches to aid in hemostasis to improve the visibility of the operative field. Furthermore, these technologies may be useful as drug delivery patches for internal use. The potential advantages of using these materials include reduction in operating time and increase ease of tissue handling, and mitigation of surgical complications such as infection. Although numerous tissue adhesives exist, presently none of them can withstand high tensile strength nor can be rapidly applied in a tape or sheet format that matches the compliance of underlying tissue with a programmable rate of degradation [1, 3].

Disadvantages of Current Technologies for Wound Closure

Current technologies for wound closure have been recently reviewed [4]. The purpose of this section is to highlight the limitations associated with the main technologies used in the clinic.

Suture and Staple

Sutures and staples represent the gold standard for wound closure. However, there are many potential complications and drawbacks associated with their use. First, suturing can be time consuming. Second, repaired tissue must be manipulated before each pass of the suture's needle which can cause wound edge necrosis. Sutures also do not work effectively for repair of dura mater [5], urethral defects [6], lung tissue (fluid and air leakage) [7], or nerve repair (scarring and lack of conductions) [8]. The imprecise placement of sutures or staples may necessitate their removal and replacement that can lead to damage of delicate tissues, and sutures or staples may lead to scar formation [9].

Tissue Glue

Tissue glues such as fibrin and cyanoacrylate have been used to augment sutures or staples. Most tissue glues are liquid during application and can be easily applied to

wounds in comparison with sutures. However, they are difficult to apply to a specific location during endoscopic procedures and it is difficult to minimize migration of the glue away from the application site.

Fibrin glue is formed by the reaction of virus-inactivated human fibrinogen and human thrombin. In the presence of calcium ions, thrombin cleaves fibrinogen chains to form fibrin monomers, which then assemble to produce a fibrin clot. Typically, physiologic fibrinolysis degrades the fibrin clot in approximately 2 weeks [4]. Fibrin glues are advantageous as they do not induce substantial inflammation, foreign body reaction, tissue necrosis, or extensive fibrosis. In addition to stoppage of bleeding, fibrin glues have been utilized during endoscopic procedures for the treatment of peptic ulcers [10] and for the prevention of anastomotic leaks during gastric bypass surgery [11]. However, the bond strength of fibrin glue (~1.3 N/cm^2) is low for many wound closing applications [4]; fibrin glue is typically used in conjunction with sutures to reinforce repair [12].

Cyanoacrylate glue forms strong bonds with most tissues (~7 N/cm^2) [4]. Cyanoacrylate is an acrylic resin that rapidly polymerizes in a heat-generating, exothermic reaction in the presence of water or a weak base. Cyanoacrylates are potentially useful in many surgical procedures because they form strong bonds to tissue under wet conditions. However, the clinic use of cyanoacrylates has been limited because of the possible thermal damage to underlying tissues during polymerization and due to concerns related to the cytotoxic (or histotoxic) properties of the glues and their degradation by-products. The cyanoacrylate monomers with short alkyl chains (i.e., ethyl-2-cyanoacrylate) can be toxic either directly or through their degradation products, which include cyanoacetate and formaldehyde [13] If these by-products accumulate in tissues, significant histotoxicity occurs, characterized by both acute and chronic inflammation. Consequently, most uses of cyanoacrylates have not been approved by the FDA, despite widespread application in thoracic, gastrointestinal, neurologic, cardiovascular, ophthalmologic, and vascular surgeries [14].

In an attempt to decrease cytotoxicity, the degradation rate of cyanoacrylate was slowed by incorporating monomers with longer alkyl chains such as *n*-butyl-2-cyanoacrylate and 2-octyl cyanoacrylate (Dermabond™). Cytotoxicity and histotoxicity was still observed, particularly in well-vascularized soft tissues [13].

The undesirable inflammatory response to cyanoacrylate and its degradation products continues to limit their clinical use.

Biocompatible and Biodegradable Tape-Based Adhesive

In addition to sutures, staples, and glues, tapes have been shown to be effective for closure of skin wounds and are often the preferred alternative [15, 16]. In a study in which 5-mm trocar closure sites were sealed with vicryl sutures, cyanoacrylate glue, or skin tape, patients preferred either sutures or tape over cyanoacrylate glue, both in terms of wound appearance and minimization of pain. The cyanoacrylate

glue negatively affected wound healing and led to greater scar formation [16]. Tapes for skin wound closure may eliminate tissue strangulation, needle puncture marks, and suture canal scarring as well as lead to lower rates of infection and tissue morbidity [15]. Tapes may reduce operating time as tapes can be applied significantly faster than glues [17].

In addition to the external application described above, biocompatible and biodegradable tissue-compliant adhesive tapes have been suggested for internal applications [18] to address the disadvantages of current methods for wound closure. Similar to external use applications, tape-based adhesives may reduce operating times and enhance tissue handling. In addition, tape adhesives could be used internally as a patch to aid in hemostasis and as replacement or support for sutures that are difficult to manipulate during laparoscopic or microscopic procedures. Adhesive tapes may also be useful as an internal equivalent of a transdermal drug delivery patch.

Currently Used Tapes or Films for Internal Uses in Clinic and Their Disadvantages

Adhesion Barriers

Postoperative intra-abdominal and pelvic adhesions are associated with complications including small bowel obstruction, difficult and dangerous reoperations, chronic pelvic pain, and infertility. It was reported that the incidence of postoperative adhesion ranges between 55 and 95% after abdominal or pelvic surgery [19]. To prevent adhesions, barrier films such as Seprafilm (Genzyme, Cambridge, MA) can be applied between manipulated tissue layers before the incision site is closed. Seprafilm is a clear film composed of sodium hyaluronate and carboxymethylcellulose. It will attach strongly to any tissue it touches and is resorbed over 7 days. While in place, Seprafilm acts as a physical barrier to separate traumatized tissue surfaces, preventing them from adhering to one another while the tissue surfaces to be healed [20]. Seprafilm has been used to seal retinal tears, permitting migration of retinal pigment epithelial cells [21], and to prevent peridural fibrosis during spinal surgery [22]. This barrier product has been shown to decrease the incidence and extent of adhesion formation in women undergoing myomectomy [23]. However, the film is brittle, must be accurately placed as it cannot be moved once applied and cannot be used laparoscopically [24]. Seprafilm also lacks sufficient tensile strength for use as an adhesive to seal holes in tissue and to prevent dehiscence.

Meshes for Hernia Repair

Hernias are fascial defects through which internal structures can pass. To repair a hernia appropriately, a tension-free repair is sought. Sutures and synthetic meshes

have been commonly used in the clinic to fix hernias with great success, albeit with specific complications associated with their use (pain from inflammation and recurrence). Hernias may be treated by a standard open surgical approach or laparoscopically: a preperitoneal prosthetic mesh is applied over the hernia creating a tension-free repair [25, 26]. The mesh is fixed in place using metal staples or tacks to prevent graft displacement or hernia recurrence [27]. However, the metal staples or tacks can cause numerous complications including nerve damage, sensory nerve entrapment with neuralgia [28], bleeding and hematomas, and chronic unexplained groin pain [29]. To replace the staples or tacks, alternatives have been investigated including fibrin sealant [30]. The meshes for hernia repair are typically made of non-biodegradable polypropylene, polyester, polytetrafluoroethylene, and composite material [30]. There is a growing interest to replace permanent prosthetic implants with biodegradable synthetic materials or biological-based materials. The ideal mesh should be capable of conforming to the abdominal/inguinal wall, be resistant to physical manipulation, and be capable of resisting mechanical forces exerted by underlying or surrounding tissue. It should also not adhere to surrounding tissue, should gradually be remodeled overtime, and should not shrink upon implantation [31].

Although numerous tissue adhesives exist, presently none of them have sufficient tensile strength to close a hernia defect or are able to be rapidly applied in a tape or sheet format that matches the compliance of underlying tissue with a programmable rate of degradation [1, 3]. Ideally, a tissue adhesive should provide the following properties: (1) biocompatibility and biodegradability, (2) mechanical compliance with underlying substrate (i.e., the tissue), (3) strong adhesion under wet conditions, (4) minimal inflammatory response, (5) ability to form a water tight seal, and preferably, (6) the ability to direct the formation of reparative tissue during wound healing. However, a paradox exists: namely, strong tissue adhesion typically requires highly reactive chemistry that also promotes an intense inflammatory response. This significantly limits the potential medical applications of strongly adherent tissue glues.

New Concept from Nature

Bioinspiration or biomimetics has become an important field to help overcome barriers when developing technology to address unmet needs. For example, the exquisite silica structure generated under inherently mild physiological conditions in diatom and sponges has provided a new route to cost-effective and low-energy fabrication of inorganic films [32]. Work to understand and mimic (or making an exact copy of the natural substrate [33]) the super-hydrophobic properties of lotus leaves have evolved into self-cleaning surfaces for windows or painted surfaces and for transporting fluids within microfluidic devices [34–36]. During the past decade, geckos, a type of lizard, have been studied as part of an effort to develop dry adhesives by mimicking the gecko's amazing ability to attach to vertical surfaces

and support its body weight [37, 38]. The gecko is not only able to attach to smooth and vertical surfaces, but also able to walk upright, and even cross indoor ceilings with ease. Interestingly (and importantly), the adhesion of gecko is both strong and reversible. This extraordinary ability arises from the unique structure of its footpad, which is composed of nearly 500,000 keratinous hairs called setae [39, 40]. The tips of setae contain hundreds of smaller hairs called spatula with typical diameters on the order of a few hundreds of nanometers. The adhesion mechanism of gecko's footpad is discussed below.

Adhesion Mechanism of Gecko's FootPad

A clear understanding of the adhesion mechanism of the gecko's footpad presents a major challenge as there are at least 11 components for the forces between two narrow-gapped surfaces [41] and the componential forces including ionic bonding, covalent bonding, van der Waals forces, and capillary forces rarely exist individually in nature. However, from the remarkable work of several research groups, contact line splitting [42, 43], van der Waals interactions [40, 44–47], and capillary forces [45, 48] have been shown to be dominant components contributing to the adhesion of a gecko's footpad.

From the hierarchical structure of a gecko's footpad, it would seem counterproductive to have a patterned interface because hierarchical patterning reduces the overall contact area compared with a smooth surface of the same projected area. Interestingly, the total contact line for a patterned interface, defined by the sum contribution of each setae, can be significantly greater than that of a smooth interface. The contact line per interfacial area relationship is critical for maximizing the adhesion. For example, for a triangular piece of scotch tape, it is more difficult to peel the tape from the base of the triangle than it is from the tip, even though the area is constant. The difference between these two cases is the length of the contact line that is being peeled at the interface. This can also be found in nature [49].

As shown in Fig. 8.1, the setae diameter decreases as the mass of the animal increases. Both the reduction in setae diameter and an associated increase in setae density may result in an enhancement in the adhesion at the interface. Van der Waals forces and capillary forces lead to levels of adhesion on the order of 1–10 N/cm^2 and are typical values for most interfacial surfaces [40]. Additionally, the hierarchical micro- and nano-design increases the mechanical compliance of the footpad and permits the gecko foot to conform and adhere to surfaces with various roughness. This can increase the interfacial contact to enhance van der Waals/capillary forces, producing an increase of contact line splitting. Herein, the contribution of each force to the gecko adhesion is described below.

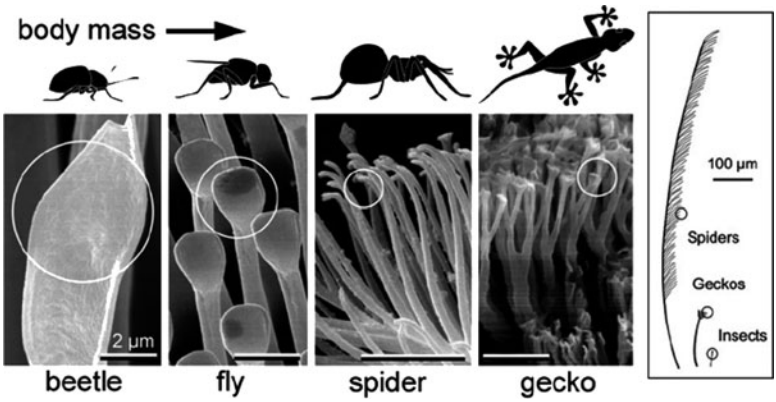

Fig. 8.1 FE-SEM images of the terminal elements (indicated as *circles*) in animals with hairy design for attachment pads. Generally, heavier animals exhibit finer terminal pads [49]. Reprinted with permission from ref. [49]. Copyright (2003) National Academy of Sciences, USA. Interestingly, it has been argued that when some of setae are buckled, the contact area cannot be uniform, resulting in the reduction of adhesion force. In this case, hierarchical fibrillar structures might produce lower adhesion than that of flat surface [50, 51]

Van der Waals Force

Van der Waals forces, which include attractive or repulsive forces between atoms, molecules, and surfaces, are known to be one of the weakest intermolecular forces. However, significant numbers of spatulae (by some estimates over 1 billion on the footpads of a single Tokay gecko) facilitate significant van der Waals forces to sustain the gecko's body weight through large surface contact area [44]. The fibrillar structure of a gecko's footpad can thus be a useful system to mimic to develop dry adhesives.

Van der Waals forces between a planar substrate and a circular planar spatula and circular curved spatula of radius R are described as follows [52]:

$$F_{vdw} = \frac{AR^2}{6D^3}, F_{vdw} = \frac{AR}{6D^2}$$

The first equation describes van der Waals forces between a planar substrate and circular planar spatula, and the latter equation shows van der Waals force between the planar substrate and circular curved spatula, where A is the Hamaker constant, D is the gap distance between two surfaces, and R is the radius of circular planar spatula. In addition to these equations, the adhesion force can be a function of the spatula geometry of gecko's foot, therefore, van der Waals adhesion force in the gecko setae can be described by adapting a useful theory of adhesion such as Johnson–Kendall–Roberts (JKR), Maugis-Dugadale and the Derjaguin-Muller-Toporov models, which are known as the approximated models to describe the adhesion force of a single elastic spatula. All of these models assumed the profile of tip shape as $z = r^2/R$, where z is the height or sphere, and r is the planar radius of tip

cross-section. However, for the cylindrical spatula having hemispherical tip with diameter 2R, the profile of the hemispherical tip should be described by a function $z = R - \sqrt{R^2 - r^2}$ when the tip is in contact with smooth surface. In this case, the theoretical strength of the van der Waals interaction (σ_0) is dominant factor for the van der Waals adhesion strength. The pull-off force (P_C) for a single hemispherical tip shape spatula can be calculated as follows [52]:

$$P_C = \int_0^R 2\pi r\sigma \, dr$$

Moreover, the deformability of hemispherical spatula should also be considered to calculate the pull-off force through van der Waals interaction. If the end shape of the tip is not a deformable spatula, the following equation, which is based on Dugdale interaction law [53], may be useful.

$$\frac{P_C}{\pi R^2 \sigma_0} = \begin{cases} 2\eta - \eta^2 & \eta < 1 \\ 1 & \eta \geq 1 \end{cases},$$

where $\eta = \Delta\gamma/(R\sigma_0)$. When η is smaller than 1, the radius of spatula is smaller than the ratio of the van der Waals interaction energy ($\Delta\gamma$) to theoretical strength of the van der Waals interaction (σ_0). Then, the maximum adhesive strength is limited from the described theoretical strength and it should be less than the theoretical maximum value. And when η is larger than 1, the radius of spatula is small enough to obtain the maximum theoretical strength. The adhesion force of the deformable spatula can be evaluated using numerical approaches such as Lenard–Jones type interaction law [53], which can be used to calculate the pull-off force between an elastic spatula and a rigid substrate.

These theoretical approaches enable a calculation of the maximum adhesion force of a spatula having a hemispherical tip through van der Waals interactions. However, there is always the presence of sites of stress concentration at certain points when two real surfaces are in contact. Because of this stress concentration, the adhesion force can be decreased, and thus the theoretical maximum adhesion may be different from the true maximum adhesion force [49]. The theoretical maximum adhesion strength by van der Waals force can be achieved only at the atomic level. Theoretical approaches to determine the adhesion force from the spatula of a gecko require optimization and are a subject of intense research.

Capillary Force

Capillary forces are considered as one of key mechanisms contributing to gecko's adhesion force. The general equation for the capillary force between a sphere of radius R and a flat surface is [52]

$$F = 2\pi R\gamma_L(\cos\theta_1 + \cos\theta_2),$$

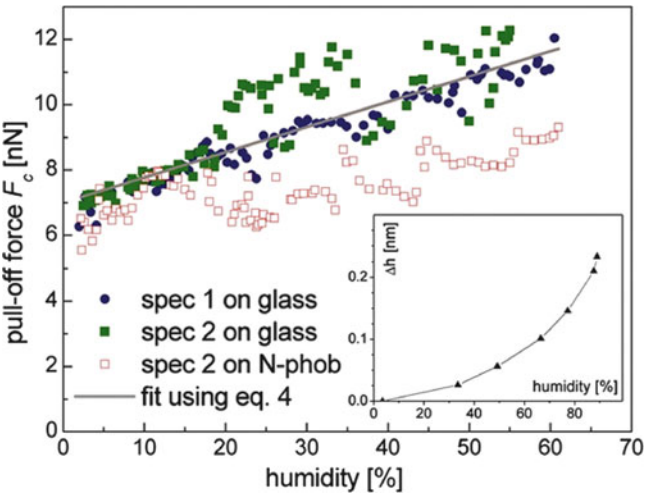

Fig. 8.2 Spatular pull-off forces on glass and *N*-phob (hydrophobic surface) vs. humidity at ambient temperature. The straight line corresponds to the calculations of previous equation the increase Δhin water-film thickness on a Si wafer with increasing humidity as measured by ellipsometry [48]. Reprinted with permission from ref. [48], Copyright (2005) National Academy of Sciences, USA

where θ_1 and θ_2 are the contact angles on each surface, and γ_{L1} is the liquid/vapor surface tension. However, the capillary forces generated by the gecko's spatula depend on the relative humidity, which is a critical element in determining capillary force in a real-world environment. For example, at 90% relative humidity liquid bridges between fibrillar structures may be generated, and capillary forces can be a dominant factor for the gecko's adhesion force. Because of the complexity of capillary condensation at different levels of humidity, many research groups have studied the adhesion of the gecko structure in the presence of small amounts of water through controlling environmental humidity (Fig. 8.2) [48]. The total adhesion force by capillary forces can be described as:

$$F = F_{\text{dry}}\left(1 + \rho g \frac{A_{\text{wet}}}{A_{\text{dry}}}\right) \approx F_{\text{dry}}\left(1 + 1.22\text{Hg}\sqrt{\frac{A_{\text{w}}}{A_{\text{s}}}}\right),$$

where $g = f'/f$is a geometrical factor. $f$is assumed to be the true fraction of the spatula that contact directly with surface, f' is in contact with the substrate through a monolayer of water, A_{wet} and A_{dry} are the Hamaker constants with and without a monolayer of water. Assuming the liquid (e.g., water) is in thermal equilibrium with the vapor phase, the relative water coverage ρ is:

$$\rho = \frac{H}{H + \exp(-E/k_{\text{B}}T)} \approx H \exp\left(\frac{E}{k_{\text{B}}T}\right) \approx 1.22H,$$

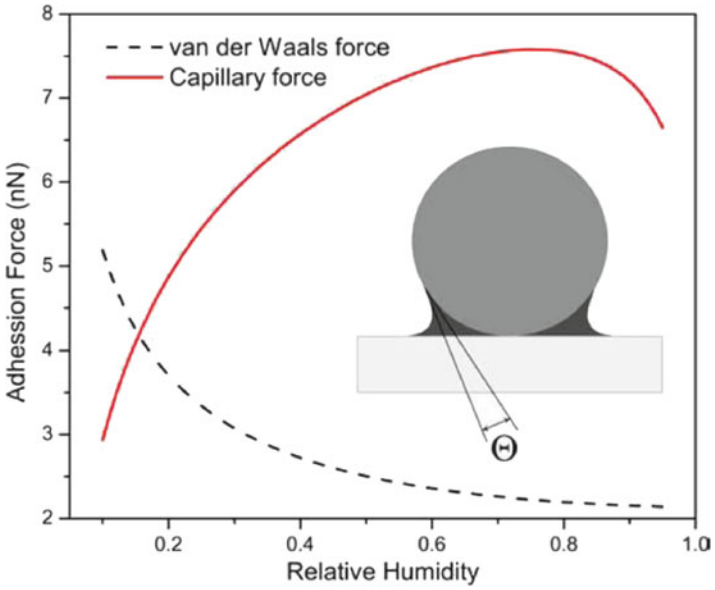

Fig. 8.3 Computer simulation of the adhesion forces between a silicon nitride sphere with the radius R of 15 nm and mica, at relative humidity varied from 0.10 to 0.95. The contact angles of Si_3N_4 and mica are 60 and 0°, respectively. The simulation configuration is shown in the inset [41]. Reprinted with permission from ref. [41]. Copyright © (2005) Elsevier

where H is the humidity, E is absorption energy for a wet surface. E is generally much less than k_BT at room temperature.

Recently, some research groups have attempted to determine the adhesion forces between a hemispherical tip end and a flat surface. For example, Wanxin et al. calculated the adhesion force between a hemispherical surface and flat surface as a function of relative humidity [41]. The magnitudes of van der Waals forces and capillary forces are inversely proportional to each other as a function of relative humidity (Fig. 8.3). Specifically, the dry adhesion force depends on the relative humidity of the environment. It is critical to consider that capillary forces and van der Waals forces may not be beneficial, if the surface is submerged under water, as is often the case with application of adhesives to tissue.

Contact Line Splitting Mechanism

Although strong evidence exists that both van der Waals forces and capillary forces contribute to the adhesion of the gecko's foodpad, the magnitude of the measured adhesive force is not fully accounted for from these contributions. Contact line splitting at the interface has been suggested as another contributor to the gecko's adhesion. The contact line splitting refers to the contact line per interfacial area that

affects the magnitude of adhesion force. Based on van der Waals forces, the general equation of peel-off force of the interfacial contact area is described with the following equation [42, 43].

$$P_s = G_c w_s.$$

where P_s is peel-off force for a single spatula, G_c is interfacial energy, and w_s is the width of the contacted interface. However, if the whole close-packed and patterned area is peeled off simultaneously, the width of the interfacial area increases as the number of patterns increases. Thus, peel-off force also increases. Because the tip shape of spatula determines the contact line between surface and spatula, the peel-off force is also influenced by the shape of spatula tip. When tips of surface structures are flat, the total peel-off forces from n structures (P_n) are described as [42]:

$$P_n = n^{1/4} P_s.$$

If the tip end is spherical with radius of curvature R, the JKR model can be applied:

$$P_n = n^{1/2} P_s,$$

where n is the number of patterns on the contact line. Additionally, not only the interfacial energy dissipation but the 3D geometry of the patterned interface also serves an important role. Contact area conformability can be manipulated by aspect ratio: higher compliance is obtained by patterns with higher aspect ratios. Controllable conformability may be useful to design tape-based tissue adhesives which make good contact with tissue.

Fabrication and Characterization of Gecko-Inspired Nanopatterns

Synthetic gecko patterns have been fabricated in a variety of polymers through many different top-down fabrication techniques including contact lithography [58], nanodrawing [54], photolithography followed by etching [55], micro/nanomolding [56], or nanocasting using vertically aligned multiwalled carbon nanotubes [57]. The merit of top-down approaches is the inherent ability to generate patterned surfaces with highly defined feature length scales. In the application of these approaches for developing tape-based adhesives, such techniques are particularly attractive since they are capable of generating solid-state devices that can be placed with greater accuracy (i.e., glues may leak into unwanted regions). Additionally, the fibrillar design of gecko's footpad can be mimicked in polymeric materials to enhance mechanical compliance for the interface and therefore provides good

conformability to a variety of surfaces. This enhancement in compliance can improve contact with surfaces having various degrees of small-scale roughness and large-scale curvature.

Despite the growing interest in developing gecko-inspired adhesives, the reduced adhesive strength of single gecko setae to wet surfaces has shown that the adhesive strength of the gecko surfaces depends on the hydrophobic and hydrophilic nature of substrates and that wet adhesion strength is significantly lower than dry adhesion [58, 59]. This observation is not surprising given the nature of the adhesive contributions of the setae interface (van der Waals and capillary forces) and their likely interaction with water rather than the substrate of interest (or blood in the case of medical adhesives). Furthermore, only a few adhesive structures have been optimized for a wet tissue-like environment. Important work from P. Messersmith's group, for example, has led to a synthetic gecko adhesive that is effective under water with reversible, non-covalent bonding to inorganic surfaces [60]. The bond strengths of gecko-inspired adhesives are typically evaluated through sub-micron atomic force microscopy (AFM) measurements which provide evidence for adhesion strength of different pillar geometries [60]. However, it is difficult to accurately predict the large area adhesion strength of arrays of millions of nano- or micropatterns from single pillar measurements: the scaling of single measurement by the area of array assumed the perfect contact of all pillars with target surface, however, the contact of the array with target surface is rarely perfect. In addition, AFM measurement could not consider the stress concentration and interaction between lots of nanopillars and the backing structure. Unlike the gecko-inspired dry adhesives created to date (and the reversible adhesive mechanism the gecko uses for locomotion), adhesives for medical applications require strong irreversible bonds to organic substrates to avoid disruption by the movement of underlying or nearby tissues. Thus, it may be more appropriate to consider a gecko "inspired" medical adhesive than a gecko "mimicking" adhesive given the need for additional mechanisms that are not required for gecko adhesion to dry surfaces. Additionally, translation of existing gecko-inspired adhesives for medical applications is complex as multiple parameters must be optimized, including: biocompatibility, biodegradation, strong adhesive tissue bonding, as well as compliance and conformability to tissue surfaces. Ideally, these adhesives would also have the ability to deliver drugs or growth factors to promote healing.

Development of Biocompatible and Biodegradable Elastomers with Controllable Mechanical Properties

For the development of a tape-based tissue adhesive, it is critical to consider the use of materials that possess properties such as biocompatibility, biodegradability, and tissue compliance [61]. Elastomers may be useful substrates to enable achievement of these requirements.

Elastomers

Current trends and needs in the biomedical field are stimulating the development of new biodegradable polymeric materials. Given the softness of most tissues, materials which can mimic their mechanical properties, are essential in applications where tissue compliance is a design criteria [62]. Hence, "rubbery" materials, also called as "elastomers" have emerged in the medical field. Synthetic elastomers have been used for medical applications since vulcanized natural rubber was introduced in medical devices (e.g., surgical gloves, tubing, catheters, balloons, etc.) [63]. The characteristic property of such materials is their "viscoelasticity": they exhibit both viscous and elastic characteristics and are able to recover to their initial size/shape while undergoing mechanical stresses [62]. Elastomers have been widely used in the medical field as they can provide mechanical compliance to different tissues and are able to facilitate regeneration of host neo-tissue [64].

Structurally, elastomers are polymers predominantly developed from hydrocarbon chains with several thousand chemical repeating units, called monomers which are linked together by covalent bonds [65]. The carbon bonds that are present within their backbones contribute to the flexibility of the elastomer. A physical parameter of elastomer elasticity is given by the "glass transition temperature (T_g)." For most elastomers, the critical glass transition temperature is below room temperature which maintains their soft, pliable, and flexible properties at body temperature [66]. A common example of a commercial elastomer is polydimethyl siloxane ($T_g = -125°C$), which in addition to elasticity has a low interfacial free energy that facilitates micro- and nanomolding, and good chemical and thermal stability. Some of the currently used biodegradable elastomers and their mechanical properties are provided in Table 8.1 along with the mechanical properties of relevant tissues [62].

Synthesis and Mechanical Properties of Elastomers for Tape-Based Adhesive Applications

The mechanical compliance of elastomers with various tissues make them attractive materials for tape-based tissue adhesives as they potentially can withstand repeated mechanical stress without failure and without interfering with the dynamics of the surrounding tissues [67]. Among degradable elastomers, in addition to degradable poly(urethane) materials, poly (glycerol sebacate) (PGS), and its derivatives have become one of a few well-established materials that have shown significant potential in the field of regenerative medicine, given its biocompatibility, biodegradability, and ease of processing [68–70].

PGS was first synthesized by Langer and coworkers in 2002 by the polycondensation of glycerol and sebacic acid, two endogenous monomers (Scheme 8.1). Therefore, its degradation products are likely metabolized by the human body thereby reducing potential cytotoxic effects [72].

Table 8.1 Mechanical properties of biodegradable elastomers and natural tissues

	Tensile stress (MPa)	Young's modulus (MPa)	Elongation (%)	Degradation (months)
Elastomers				
Poly(ε-caprolactone)	20.7–34.5	0.21–0.34	300–500	>24
Poly(3-hydroxybutyrate)	36	2,400	3	24
Poly(4-hydroxybutyrate)	50	70	~1,000	2–12
Copolymers of 3-hydroxybutyrate and 3-hydroxyvalerate	25	–	20	10% HV
Copolymers of 3-hydroxybutyrate and 3-hydroxyhexanoate	21	–	400	10% HHx
Poly(3-hydroxyoctanoate)	45.1	10.4	198	–
Poly(glycolic acid)	70	6,900	<3	1.5
Poly(L-lactic acid)	28–50	1,200–1,700	6	16–60
Poly(glycolid-*co*-caprolactone)	<1	–	250	>1.5
Poly(trimethylene carbonate-*co*-caprolactone) (10:90)	23	140	7	<11
Poly(trimethylene carbonate-*co*-D, L-lactide) (20:80)	51	1,900	7	<11
Poly(trimethylene carbonate-*co*-D, L-lactide) (50:50)	10	16	570	<11
Poly(glycerol sebacate)	>0.5	0.282	>267	1
Poly(1,8-octanediol-co-citrate)	<6.7	0.92–16.4	265	Variable
Natural tissues				
Ulnar cadaveric peripheral nerve	0.5–0.6	–	8.21	–
Human inferior cava vein	1.17	–	84	–
Human ascending aorta	0.069	–	81	–
Rat abdominal aorta	0.4	0.17	–	–
Porcine aortic heart valve (radial)	1.4	6.4	134.8	–
Porcine aortic heart valve (circumferential)	8.3	44.7	48.7	–
Bovine elastin	–	1.1	–	–
Collagen fibers	–	100	50	–
Smooth muscle relaxed	–	0.006	300	–
Smooth muscle contracted	–	0.01	300	–
Cartilage	24–112	65–541	–	–
Trabecular bone	0.15–116.4	1–9,800	–	–
Cortical bone	–	23.8	–	Tibia, wet bone

Reprinted with permission from ref. [62]. Copyright (2010) Wiley-VCH

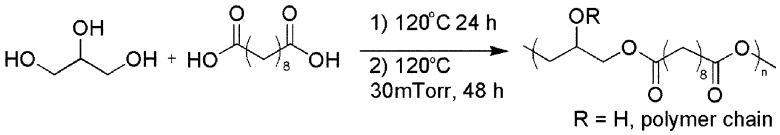

Scheme 8.1 Synthesis of poly(glycerol sebacate)

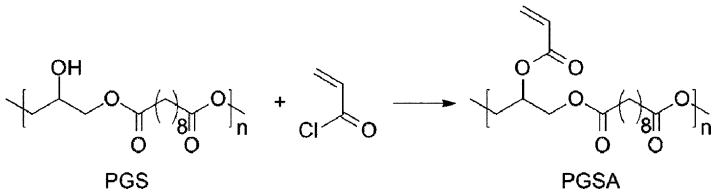

Scheme 8.2 Acrylation of the PGS prepolymer yielding PGSA

Though the majority of Food and Drug Administration (FDA) approved products containing degradable materials are based on stiff materials such as poly (lactic acid) (PLA) and poly(glycolic acid) (PGA) [62], PGS offers a broad and tunable range of mechanical properties and degradation in vivo. PGS is highly elastic and its Young's modulus (0.282 ± 0.0250 MPa) lies in the range of soft tissues properties [71]. In addition to its ability to elicit a minimum inflammatory response in vivo and facilitate the growth of host neo-tissue, the tunable mechanical properties of PGS are critical in making it suitable for a variety of clinical applications. Nevertheless, PGS synthesis presents a number of shortcomings for certain applications, including the need for use high temperatures, intense vacuum, and long curing times. For example, it cannot be directly polymerized on tissue, and due to high temperatures required for synthesis, temperature-sensitive molecules or cells cannot be easily incorporated into it. Therefore, there was a need to develop a PGS elastomeric derivative, synthesized through less harsher conditions, but which could maintain the excellent properties of PGS.

A method that has been practiced widely for fast and simple polymer cross-linking is to utilize free-radical polymerization to synthesize a photocurable version of a desired pre-polymer. Hence, an acrylated form of PGS, poly(glycerol-*co*-sebacate) acrylate (PGSA) was synthesized (Scheme 8.2) [72]. This material can be cross-linked after UV exposure through photo-induced free radical polymerization [72].

Depending on the degree of acrylation (DA) in PGSA, a broad range of mechanical (Young's modulus and ultimate tensile strength) and degradation properties can be obtained. Other parameters that can potentially determine the final characteristics of the material are the curing times and the molecular weight of PGS pre-polymer. Importantly, the mechanical properties of the material vary linearly with DA. As shown in Fig. 8.4, tensile tests demonstrate control of the Young's modulus from 0.05 to 1.38 MPa, ultimate strength from 0.05 to 0.50 MPa and elongation at break between 42 and 189%, thereby affirming that the material's mechanical properties may be tailored according to the needs of the desired applications [72].

In vitro biocompatibility studies of photocured PGSA shows that it is highly supportive of cellular attachment. Viability assays were performed to confirm that the cells remained alive and their proliferation capacities were not compromised due to the presence of PGSA [72]. Given its elastic properties, tunable mechanical properties, and easy processing for micro- and nanomolding, PGSA may be a useful material for the development of tape-based adhesives [18].

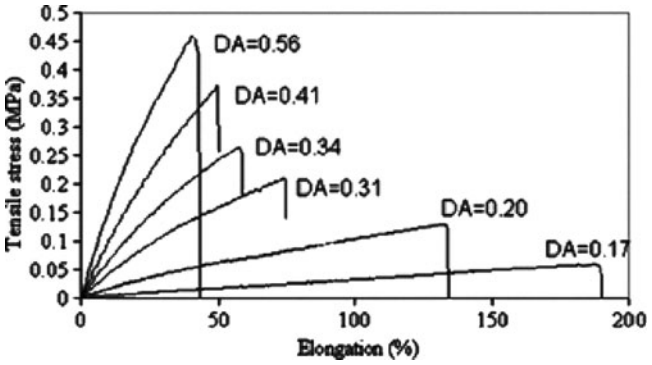

Fig. 8.4 Stress–strain curves of photocured PGSA elastomer [72]. Reprinted with permission from ref. [72]. Copyright (2007) American Chemical Society

Fabrication of Gecko-Inspired PGSA Adhesives and Their Tissue Adhesion

It is critical to consider that strong tissue adhesion typically requires highly reactive chemistry that also promotes an intense inflammatory response. This significantly limits the potential medical applications of strongly adherent tissue glues. As an alternative, a textured surface design may be used to increase the surface area of contact of the reactive adhesive interface with tissue. Through increasing the surface area of contact, the approach to use gecko-inspired nanopatterns could be effective in reducing the reactivity of the chemistry required to achieve strong tissue bonding without promoting an intense inflammatory response. It was postulated that the patterned surface may be useful to enhance adhesion through mechanical interlocking with the underlying compliant tissue substrate.

To develop a general platform for biocompatible tissue adhesives that can be manufactured with a variety of materials (and is amendable to temperature sensitive drugs for drug delivery applications), PGSA was used. The fabrication procedure to manufacture the PGSA tissue adhesives was based on replica molding that avoids high temperature and harsh chemical conditions. Replica molding is an efficient method for the duplication of structural information present in mold [70, 71]. UV or thermally curable polymers, as long as they do not contain solvent, usually have a shrinkage of less than 3% on curing, and therefore, the cured polymers can have almost the same surface topography as the mold [73]. To make gecko-inspired nanopatterns by replica molding, firstly, several silicon templates with different geometries were prepared by using photolithography and reactive ion etching. PGSA polymer solution was cast on silicon templates with nanosized cavities, without using high vacuum, and cured by UV light at room temperature for 5 min. By peeling-off the cured PGSA films, polymeric nanopatterns were obtained (Fig. 8.5a). To determine the effect of pattern dimensions on PGSA adhesion with tissue, pillar arrays were fabricated in PGSA with tip diameters ranging from $\approx$ 100 nm to 1 μm and pillar height from $\approx$ 0.8 to $\approx$ 3 μm

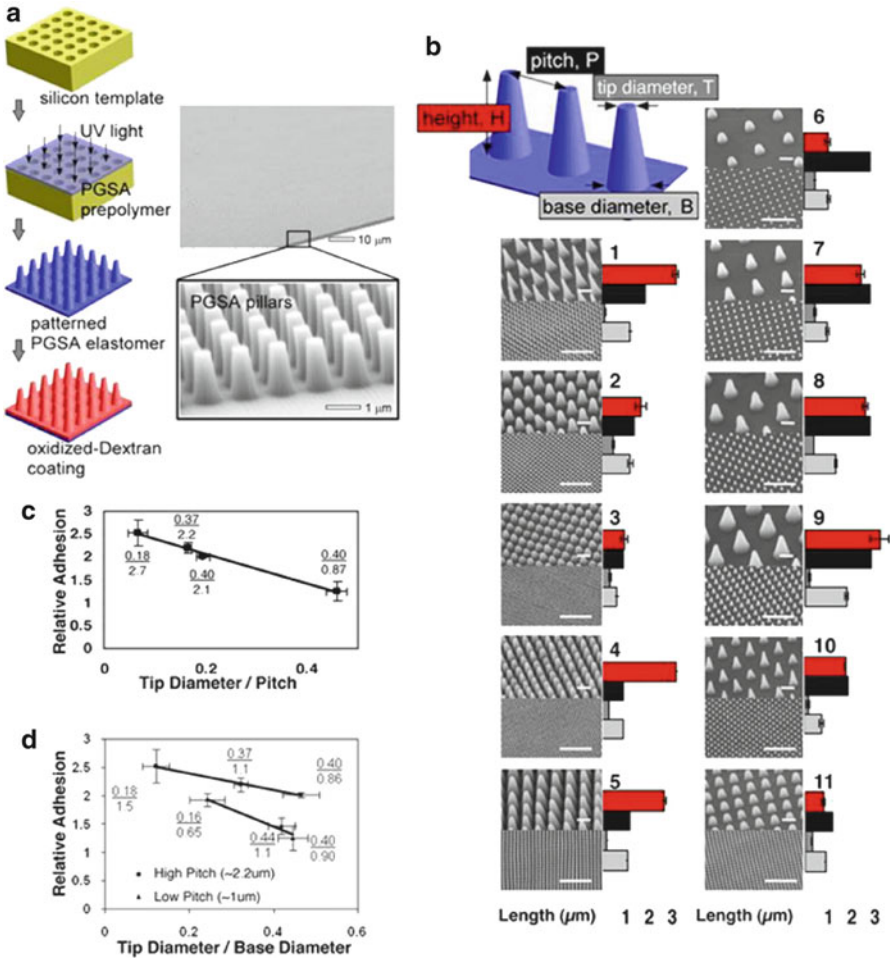

Fig. 8.5 Development of biodegradable synthetic gecko patterns. (**a**) Nanomolding of the PGSA prepolymer is accomplished by photocuring the prepolymer under UV light followed by removal of the pattern and subsequent spin-coating of oxidized dextran on the surface of the pillars. Scanning electron microscopy (SEM) demonstrated excellent pattern transfer and fidelity. (**b**) Gecko patterns having different pillar size and center to center pitch were developed as illustrated by the SEM images. Pillar dimensions were measured by using optical profilometry as represented by the *bar graphs*, with *red* representing the height of pillars; *black*, the center to center pitch; *light gray*, diameter of pillar base; and *dark gray*, diameter of the tip. (*Small and large scale bars*, 1 and 10 μm, respectively.) (**c**) Adhesion trend of the longest pillar heights (2.4 μm) shows adhesion of nanopattern with respect to flat polymer as a function of ratio of tip diameter to pitch. R^2 value of linear fit is 0.99. (**d**) Adhesion trend of the patterns is plotted as a function of ratio of tip diameter to base diameter of pillars. R^2 values of linear fit for the low- and high-pitch patterns are 0.96 and 0.99, respectively. Reprinted with permission from ref. [18]. Copyright (2008) National Academy of Sciences, USA

(Fig. 8.5b). The adhesive strength of PGSA patterned surfaces to tissue was evaluated using porcine intestinal tissue. Shear or sliding forces were measured to mimic the potential shear forces between the adhesive and underlying tissue after surgical placement [74]. The adhesion strength of nanopatterned PGSA surface was nearly two-fold higher than that of flat unpatterned PGSA (Fig. 8.5c, d).

The tissue adhesion strengths of PGSA nanopatterns were also tested as a function of tip diameter to pitch length for the patterns with the highest pillars, 2.4 μm. As shown in Fig. 8.5c, tissue adhesion increases as the ratio of tip diameter to pitch decreases. To prove the importance of pillar geometry on adhesion independently of pillar height, tissue adhesion was measured as a function of ratio of tip diameter to base diameter. As demonstrated in Fig. 8.5d, an increase of this ratio leads to a decrease in adhesion. Pitch was also important parameter for tissue adhesion. A decrease in pitch leads to a decrease in overall adhesion and an even sharper decrease in adhesion strength with increasing ratio of tip diameter to base diameter of the nanopillars (Fig. 8.5b). Of the patterns tested, pattern 9 provided the highest tissue adhesion.

Surface Modification of PGSA Gecko Patterns for Enhanced Wet Tissue Adhesion

The gecko-inspired/mimetic adhesives including PGSA nanopillars are valuable in a variety of applications where adhesion reversibility and absence of glue residues after peeling are important. However, the direct translation of gecko-inspired adhesive efficiency to a wet environment has been a difficult task. For example, the maximum tissue adhesion achieved by PGSA nanopatterns was ~0.3 N/cm [2], which was not strong enough for clinical application. Van der Waals forces, one of the main adhesion mechanisms of the adhesives, are not interface selective, and thus the presence of water molecules can reduce the number of direct contacts between the patterned surface and its target [75]. Therefore, translating the gecko-mimetic approach to the biomedical field is challenging: the adhesives will have to adhere to complex wet surfaces and maintain their biocompatibility and biodegradability over a defined time range. These requirements are crucial for wound closure applications, especially for internal application.

Recent trends in the field make use of combinatorial approaches between topography and chemistry to achieve high underwater adhesive forces [60]. For example, *Geckel* reversible adhesive, which was developed by Messersmith's group, can maintain its strength for over a thousand contact cycles under wet and dry conditions. Its properties derive from merging two bioinspired strategies: the nanopatterned surface inspired by geckos contributes to the reversibility of the system and the coating with a layer of mussel-derived protein residues (3,4,-dihydroxy-L-phenylalanine) contributes to a strong attachment to surfaces in the presence of water [76]. Strikingly, the adhesion of each fibril under wet condition is comparable to a gecko spatulae on a dry surface. However, the system was not

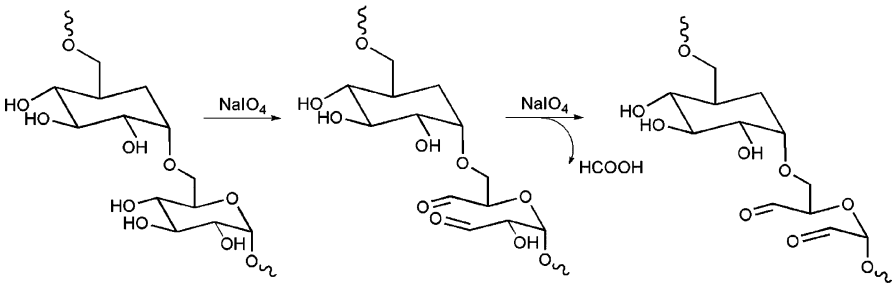

Scheme 8.3 Oxidation of dextran by sodium periodate. Degree of oxidation can be tuned by changing the molar ratio of sodium periodate to dextran glucopyranoside residues

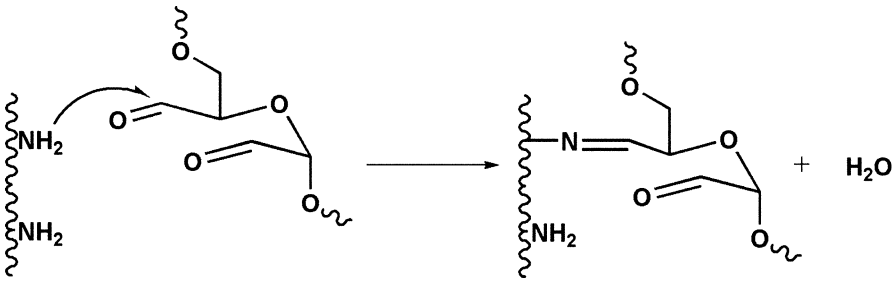

Scheme 8.4 Oxidized dextran aldehydes react with amines on tissue surface, forming a covalent linkage through an imine group

studied at macroscale and not investigated for tissue adhesive applications. To examine the effectiveness of the adhesive on biological tissues, in vivo compatibility studies, degradation properties, and the effectiveness on a macroscale under physiological conditions would have to be assessed.

As the first demonstration of tape-based tissue adhesive, Mahdavi et al. took advantage of mild chemistry to synergistically enhance the adhesive capacity of the nanopatterned PGSA in a complex physiological environment [18]. In order for a coating to be suitable for biomedical application as a tissue adhesive: (1) it has to be biocompatible and biodegradable, (2) covalently attach to chemical functionalities present at tissue surface, (3) the reactivity should be easily tuned to minimize the inflammatory response while maximizing adhesion, and (4) it should be easily integrated in the PGSA patch without interfering with the surface topography. To address these criteria, the authors developed a thin coating of a sugar-based material (Dextran; DXT) which was selectively oxidized (Scheme 8.3) to present aldehyde groups at its surface (Dextran aldehyde; DXTA).

Aldehydes react with amine functionality present on the tissue surface (e.g., extracellular matrix proteins, cell surface receptors, and cell membrane) through nucleophilic reactions: a hemiaminal intermediate is formed which is further dehydrated to form imine linkages (Scheme 8.4). pH variability from tissue to tissue and different pathophysiological states, will determine different reaction

yields, that control the adhesive forces that are obtained in each application [77]. Other relevant factors that mediate bonding to tissue include the surface amine density and its steric availability [78]. Therefore, given the intimacy of the contact between material and tissue, adhesive forces might change depending on the tissue type, its physiological properties and surrounding environment even if the aldehyde content remains the same.

Adhesives that utilize aldehyde chemistry have been explored in medical glues (e.g., gelatin-resorcinol-formalin [79] or albumin-glutaraldehyde [80]), however, these compositions employ highly reactive small molecular weight aldehydes as cross-linkers, which are limited given their diffusion capacity to the surrounding tissue and consequent toxicity. The limited biocompatibility of aldehyde-based glues has restricted their use. Recently, novel materials based on aldehyde chemistry were developed that slow release of its degradation products and whose reactivity can be tuned for specific tissues. DXTA-based systems have emerged as one of the most promising candidates, given their high molecular weight, water solubility, controllable reactivity, and good biocompatibility [78, 81]. Of special relevance, injectable two-component hydrogels have been explored for applications including corneal incision [82]. In this example, DXTA and an amine-terminated component (e.g., branched polyethylene glycol diamine) are mixed and form an adhesive gel over a defined time period. The aldehyde component has the double function of cross-linker in the bulk material and adhesive component by establishing a second bond with tissue amines.

The initial design of the gecko-inspired approach included a nanoscale thin film of DXTA with a 14% degree of oxidation that was spin-coated on top of PGSA patterns and extensively rinsed to remove excess glue. The thin layer was important to prevent occlusion of the space between the pillars. Covalent immobilization was possible given the reaction between free hydroxyl groups of the elastomer and aldehyde functionalities of DXTA. PGSA with lower DA showed a high cumulative effect in relative adhesion when nanopatterns were coated with DXTA. This may have resulted from its higher content of free hydroxyl group and consequently more efficient DXTA retention. Alternatively, DXTA retention may have resulted from the relatively high porosity and physical entrapment of the macromonomer in PGSA with lower DA. In contrast, PGSA with higher DA showed less synergistic effect between chemistry and topography. Therefore, an efficient immobilization of the glue to the tape was essential for the stabilization of the DXTA-coated elastomer system to help ensure that the adhesive peeling will result from failure at the coating–tissue interface.

Biocompatibility and Biodegradability of the Tape-Based Tissue Adhesive

Tissue Biocompatibility of the Adhesive Tape

The adhesive tape should promote only a very minimal inflammatory reaction. To assess the effect of polymer composition and nanotopography on tissue response, for example, the disks of patterned PGSA polymer were implanted subcutaneously

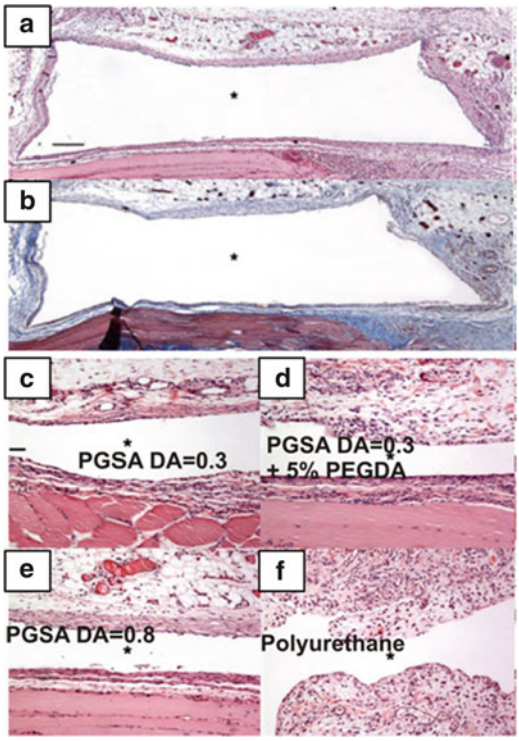

Fig. 8.6 Tissue response to nanopatterned PGSA disks with DA 0.8, subcutaneously implanted in the rat dorsum. Low magnification photo-micrographs of (**a**) H&E and (**b**) Masson's trichrome-stained tissue sections immediately adjacent to PGSA implants. PGSA implants formerly occupied open spaces denoted by *asterisk*. Nanotopography was placed next to muscle tissue (*down*), and samples were harvested after 1-week implantation. A mild response was observed with a thin inflammatory infiltrate without collagen deposition. (Scale bar, 400 μm). (**c**–**f**) High magnification photomicrographs of H&E-stained tissue sections immediately adjacent to PGSA implants with (**c**) DA 0.3, (**d**) DA 0.3 with 5% PEGDA, and (**e**) DA 0.8 and (**f**) unpatterned polyurethane implants. Nanotopography was placed next to muscle tissue (*down*), and samples were harvested after 1-week implantation. The tissue responses were mild in all PGSA implantation but more pronounced in the polyurethane implantation. (Scale bar, 100 μm). Reproduced with permission from ref. [18]. Copyright (2008) National Academy of Sciences, USA

in the backs of rats for 7 days. The tissue response was mild (Fig. 8.6a, b) and independent of PGSA nanotopography or formulation (Fig. 8.6c–e). This tendency was consistent with the previous reports with native PGSA polymer [68, 71]. A thin inflammatory infiltrate layer with little vascularization encircled the implant cavity and there was no giant cell reaction. As a control, non-resorbable polyurethane exhibited a significant inflammatory response (Fig. 8.6f). The minimal inflammatory response observed for the adhesive tape suggest potential as an alternative to medical grade cyanoacrylate glue (i.e., DermabondTM) and albumin-glutaraldehyde (i.e., BioGlueTM), which exhibit significant inflammatory responses for

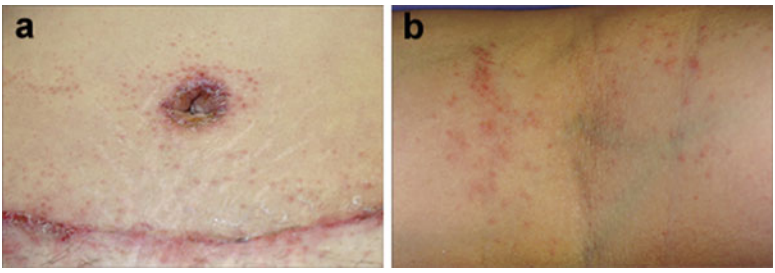

Fig. 8.7 Adverse reactions after postsurgical repair with 2-octylcyanoacrylate. (**a**) Erythematous and eczematous linearity directly over the superficial closure sites where the 2-octylcyanoacrylate was placed. (**b**) Itchy, red papules arose 2 days after application of 2-octylcyanoacrylate on the forearm (*left side*) with an interesting complementary reaction on the biceps (*right side*). Reprinted with permission from ref. [86]. Copyright © (2008) American Medical Association All rights reserved

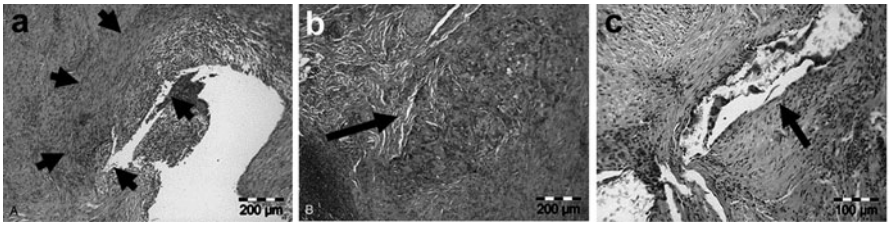

Fig. 8.8 (**a**) Photomicrograph of a paravascular abscess after albumin–glutaraldehyde (AG) glue application. A high concentration of leukocytes and giant foreign body cells surround the cavity *(arrows)* as a result of a continuously ongoing inflammatory reaction. (**b**) Histologic section showing a detailed magnification of a giant foreign-body cell *(arrow)* after AG application. (**c**) Photomicrograph showing a deposit of cyanoacrylate glue *(arrow)* with moderate inflammatory reaction including the presence of lymphocytes. Reprinted with permission from ref. [87]. Copyright © (2006) Elsevier

dermal and internal applications [83, 84]: it is important to consider that adverse reactions such as allergic contact dermatitis or foreign body reaction have been described after skin closure with 2-octylcyanoacrylate (Fig. 8.7) [85]. Moderate/severe inflammatory reactions, which are associated with the use of albumin–glutaraldehyde tissue glue or *n*-butyl-2-cyanoacrylate glue, were also reported when the adhesives were used for porcine coronary artery surgery (Fig. 8.8) [86].

In Vitro and In Vivo Biodegradability of the Tissue Adhesive

Tape-based adhesives for internal uses should exhibit biodegradability to reduce the foreign material left in the body and limit the requirement for a subsequent surgical procedure to remove the adhesive system. Ideally, the degradation of the

tape would coincide with tissue infiltration where the mechanical role of the adhesive would be transitioned to the developing tissue interface. Importantly, the patterned PGSA adhesive was shown to be degradable when it was immersed in cholesterol esterase solution (1 U/mL), which is a suitable model for the esterase associated with macrophages that is known to degrade polyesters [87]. Importantly, the in vitro/in vivo degradation rate of the adhesive could be controlled by adjusting DA of PGSA. For adhesives tapes that include nano- or microfeatures, it is critical to consider that the degradation the surface features may occur much faster than the bulk material. To circumvent this, different materials may be chosen for the surface and bulk of degradable adhesive tape designed for internal procedures.

Perspectives

Adhesives tapes have been suggested as alternatives to current technologies such as sutures, staples, and tissue glues for closing and sealing wounds. Bioinspiration from the amazing adhesion ability of geckos has lead to the development of a new generation of tape-based adhesives that are biocompatible and biodegradable and can attach to wet tissue. However, more work is required to increase the adhesion strength upwards of 5–15 N/cm^2 to enable use for multiple clinical applications. One approach may involve increasing the chemical cross-linking and mechanical interlocking with tissue. Mechanical interlocking may be promoted through altering the morphology or aspect ratio of the patterned substrate, perhaps through use of hierarchical structures that include both nano- and microtopography [88–90].

It is critical to consider that the performance of the patterned adhesive is likely tissue-specific as the extent of mechanical interlocking depends on the ability of the tissue to conform to the surface of the adhesives. Although the reactivity of the chemistry used to promote bonding with tissue can be useful to enhance adhesion, one needs to be careful to balance this with a minimal inflammatory response. Through combining mechanical interlocking with adequate surface reactivity, a tape-based tissue adhesive platform may be developed and tailored for both external and internal applications, ranging from suture/staple replacement/supplement, waterproof sealants for hollow organ anatomoses, air-tight seals to prevent air leaks following lung section procedures, mesh grafts to treat hernias, ulcers, and burns, and haemostatic wound healings.

Acknowledgements Funding for this research was provided by the NSF NIRT grant 0609182, NIH grant DE013023, NIH grant GM086433, and American Heart Association Grant 0835601D. The content of the information does not necessarily reflect the position or the policy of the Government, and no official endorsement should be inferred. Part of this chapter was published by Jeff Karp as part of a Pressure Sensitive Tape Council Technical Seminar.

References

1. Saltz, R., Sierra, D.H.: Surgical Adhesives and Sealants: Current Technology and Applications. Lancaster, PA, Technomic Pub (1996)
2. Wilson, D.J., Chenery, D.H., Bowring, H.K., Wilson, K., Turner, R., Maughan, J., West, P.J., Ansell, C.W.: Physical and biological properties of a novel siloxane adhesive for soft tissue applications. J. Biomater. Sci. Polym. Ed. **16**, 449–472 (2005)
3. Singer, A.J., Thode Jr., H.C.: A review of the literature on octylcyanoacrylate tissue adhesive. Am. J. Surg. **187**, 238–248 (2004)
4. Lauto, A., Mawad, D., Foster, L.J.R.J.: Adhesive biomaterials for tissue reconstruction. Chem. Technol. Biotechnol. **83**, 464–472 (2008)
5. Hida, K., Yamaguchi, S., Seki, T., Yano, S., Akino, M., Terasaka, S., Uchida, T., Iwasaki, Y.: Nonsuture dural repair using polyglycolic acid mesh and fibrin glue: clinical application to spinal surgery. Surg. Neurol. **65**, 136–142 (2006)
6. Cimador, M., Castagnetti, M., Milazzo, M., Sergio, M., De Grazia, E.: Suture materials: Do they affect fistula and stricture rates in flap urethroplasties? Urol. Int. **73**, 320–324 (2004)
7. Murray, K.D., Ho, C.H., Hsia, J.Y.J., Little, A.G.: The influence of pulmonary staple line reinforcement on air leaks. Chest **122**, 2146–2149 (2002)
8. Millesi, H.: PERIPHERAL-NERVE INJURIES - NERVE SUTURES AND NERVE GRAFTING. Scand. J Plast. Reconstr. Surg. Hand Surg. **19**, 25–37 (1982)
9. Dziki, A.J., Duncan, M.D., Harmon, J.W., Saini, N., Malthaner, R.A., Trad, K.S., Fernicola, M.T., Hakki, F., Ugarte, R.M.: ADVANTAGES OF HANDSEWN OVER STAPLED BOWEL ANASTOMOSIS. Dis. Colon Rectum **34**, 442–448 (1991)
10. Rutgeerts, P., Rauws, E., Wara, P., Swain, P., Hoose, A., Solleder, E., Halttunen, J., Dobrilla, G., Richter, G., Prassler, R.: Randomized trials of a single and repeated fibrin glue compared with injection of polidocanol in treatment of bleeding peptic ulcer. Lancet **350**, 692–696 (1997)
11. Silecchia, G., Boru, C.E., Mouiel, J., Rossi, M., Anselmino, M., Tacchino, R.M., Foco, M., Gaspari, A.L., Gentileschi, P., Morino, M., Toppino, M., Basso, N.: Clinical evaluation of fibrin glue in the prevention of anastomotic leak and internal hernia after laparoscopic gastric bypass: preliminary results of a prospective, randomized multicenter trial. Obes. Surg. **16**, 125–131 (2006)
12. Ono, K., Saito, Y., Yura, H., Ishikawa, K., Kurita, A., Akaike, T., Ishihara, M.: Photocrosslinkable chitosan as a biological adhesive. J. Biomed. Mater. Res. **49**, 289–295 (2000)
13. Vote, B.J., Elder, M.J.: Cyanoacrylate glue for corneal perforations: a description of a surgical technique and a review of the literature. Clin. Experiment. Ophthalmol. **28**, 437–442 (2000)
14. Mattama, G.J.: US FDA perspective on the regulations of medical-grade polymers: cyanoacrylate polymer medical device tissue adhesives. Expert Rev. Med. Devices **5**, 41–49 (2008)
15. Pepicello, J., Yavorek, H.: Five year experience with tape closure of abdominal wounds. Surg. Gynecol. Obstet. **169**, 310–314 (1989)
16. Harold, K.L., Goldstein, S.L., Nelms, C.D., Matthews, B.D., Sing, R.F., Kercher, K.W., Lincourt, A., Heniford, B.T.: Optimal closure method of five-millimeter trocar sites. Am. J. Surg. **187**, 24–27 (2004)
17. Coulthard, P., Esposito, M., Worthington, H.V., van der Elst, M., van Waes, O.J., Darcey, J.: Tissue adhesives for closure of surgical incisions. Cochrane Database Syst. Rev. **5**, CD004287 (2010)
18. Mahdavi, A., Ferreira, L., Sundback, C., Nichol, J.W., Chan, E.P., Carter, D.J., Bettinger, C.J., Patanavanich, S., Chignozha, L., Ben-Joseph, E., Galakatos, A., Pryor, H., Pomerantseva, I., Masiakos, P.T., Faquin, W., Zumbuehl, A., Hong, S., Borenstein, J., Vacanti, J., Langer, R., Karp, J.M.: A biodegradable and biocompatible gecko-inspired tissue adhesive. Proc. Natl Acad. Sci. USA **105**, 2307–2312 (2008)
19. Diamond, M.P., Nezhat, F.: ADHESIONS AFTER RESECTION OF OVARIAN ENDOMETRIOMAS. Fertil. Steril. **59**, 934–935 (1993)

20. Becker, J.M., Dayton, M.T., Fazio, V.W., Beck, D.E., Stryker, S.J., Wexner, S.D., Wolff, B.G., Roberts, P.L., Smith, L.E., Sweeney, S.A., Moore, M.: Prevention of postoperative: Abdominal adhesions by a sodium hyaluronate-based bioresorbable membrane: A prospective, randomized, double-blind multicenter study. J. Am. Coll. Surg. **183**, 297–306 (1996)
21. Sueda, J., Sakuma, T., Nakamura, H., Usumoto, N., Okuno, T., Arai, M., Hirose, T.: In vivo and in vitro feasibility studies of Intraocular use of Seprafilm to close retinal breaks in bovine and rabbit eyes. Invest. Ophthalmol. Vis. Sci. **47**, 1142–1148 (2006)
22. Topsakal, C., Akpolat, N., Erol, F.S., Ozveren, M.F., Akdemir, I., Kaplan, M., Tiftikci, M., Kilic, N.: Seprafilm superior to Gore-Tex in the prevention of peridural fibrosis. J. Neurosurg. **101**, 295–302 (2004)
23. Tsuji, S., Takahashi, K., Yomo, H., Fujiwara, M., Kita, N., Takebayashi, K., Miyazaki, K., Noda, Y.: Effectiveness of antiadhesion barriers in preventing adhesion after myomectomy in patients with uterine leiomyoma. Eur. J. Obstet. Gynecol. Reprod. Biol. **123**, 244–248 (2005)
24. Weis, C., Odermatt, E.K., Kressler, J., Funke, Z., Wehner, T., Freytag, D.: Poly(vinyl alcohol) membranes for adhesion prevention. J. Biomed. Mater. Res. B Appl. Biomater. **70B**, 191–202 (2004)
25. Fitzgibbons Jr., R.J., Salerno, G.M., Filipi, C.J., Hunter, W.J., Watson, P.: A laparoscopic intraperitoneal onlay mesh technique for the repair of an indirect inguinal hernia. Ann. Surg. **219**, 144–156 (1994)
26. Katkhouda, N., Campos, G.M.R., Mavor, E., Trussler, A., Khalil, M., Stoppa, R.: Laparoscopic extraperitoneal inguinal hernia repair – A safe approach based on the understanding of rectus sheath anatomy. Surg. Endosc. – Ultrasound Interventional Tech **13**, 1243–1246 (1999)
27. Powell, J.J., Murray, G.D., O'Dwyer, P.J.J.: Evaluation of staples and prostheses for use in laparoscopic inguinal hernia repair. Laparoensc. Surg. **4**, 109–112 (1994)
28. Kraus, M.A.: NERVE INJURY DURING LAPAROSCOPIC INGUINAL-HERNIA REPAIR. Surg. Laparosc. Endosc. **3**, 342–345 (1993)
29. Phillips, E.H., Arregui, M., Carroll, B.J., Corbitt, J., Crafton, W.B., Fallas, M.J., Filipi, C., Fitzgibbons, R.J., Franklin, M.J., McKernan, B., Olsen, D., Ortega, A., Payne, J.H., Peters, J., Rodriguez, R., Rosette, P., Schultz, L., Seid, A., Sewell, R., Smoot, R., Toy, F., Waddell, R., Watson, S.: INCIDENCE OF COMPLICATIONS FOLLOWING LAPAROSCOPIC HERNIOPLASTY. Surg. Endosc. – Ultrasound Interventional Tech. **9**, 16–21 (1995)
30. McGinty, J.J., Hogle, N.J., McCarthy, H., Fowler, D.L.: A comparative study of adhesion formation and abdominal wall ingrowth after laparoscopic ventral hernia repair in a porcine model using multiple types of mesh. Surg. Endosc. Other Interventional Tech. **19**, 786–790 (2005)
31. Eriksen, J.R., Gögenur, I., Rosenberg, J.: Choice of mesh for laparoscopic ventral hernia repair. Hernia **11**, 481–492 (2007)
32. Brutchey, R.L., Morse, D.E.: Silicatein and the translation of its molecular mechanism of biosilicification into low temperature nanomaterial synthesis. Chem. Rev. **108**, 4915–4934 (2008)
33. Sun, M., Luo, C., Xu, L., Ji, H., Ouyang, Q., Yu, D., Chen, Y.: Artificial lotus leaf by nanocasting. Langmuir **21**, 8978–8981 (2005)
34. Blossey, R.: Self-cleaning surfaces–virtual realities. Nat. Mater. **2**, 301–306 (2003)
35. Yabu, H., Shimomura, M.: Single-step fabrication of transparent superhydrophobic porous polymer films. Chem. Mater. **17**, 5231–5234 (2005)
36. Nakajima, A., Hashimoto, K., Watanabe, T.: Recent studies on super-hydrophobic films. Monatshefte Fur Chemie **132**, 31–41 (2001)
37. Jeong, H.E., Lee, J.K., Kim, H.N., Moon, S.H., Suh, K.Y.: A nontransferring dry adhesive with hierarchical polymer nanohairs. Proc. Natl Acad. Sci. USA **106**, 5639–5644 (2009)
38. Jeong, H.E., Suh, K.Y.: Nanohairs and nanotubes: Efficient structural elements for geckoinspired artificial dry adhesives. Nano Today **4**, 335–346 (2009)
39. Hansen, W.R., Autumn, K.: Evidence for self-cleaning in gecko setae. Proc. Natl Acad. Sci. USA **102**, 385–389 (2005)
40. Autumn, K., Liang, Y.A., Hsieh, S.T., Zesch, W., Chan, W.P., Kenny, T.W., Fearing, R., Full, R.J.: Adhesive force of a single gecko foot-seta. Nature **405**, 5 (2000)

41. Wanxin Sun, P.N., Tanu Suryadi Kustandi, Sharon Oh, Victor D. Samper: The Nature of the Gecko Lizard Adhesive Force. *Biophys. J.: Biophys. Lett.* 4, (2005)
42. Chan, E.P., Eduard Arzt, C.G., Crosby, A.J.: Designing Model Systems for Enhanced Adhesion. MRS Bull. **32**, 8 (2006)
43. Arzt, E., Gorb, S., Spolenak, R.: From micro to nano contacts in biological attachment devices. Proc. Natl Acad. Sci. USA **100**, 4 (2003)
44. Autumn, K., Sitti, M., Liang, Y.A., Peattie, A.M., Hansen, W., Sponberg, S., Kenny, T.W., Fearing, T., Israelachvili, J.N., Hsieh, S.T., Zesch, W., Chan, W.P., Kenny, T.W., Fearing, R., Full, R.J.: Evidence for van der Waals adhesion in gecko setae. Proceedings of the National Academy of Sciences of the United States of America **99**, 5 (2002)
45. Atutumn, K.: Properties, Principles, and Parameters of the Gecko Adhesive System. Springer, Berlin (2006)
46. Gao, H., Wang, X., Yao, H., Gorb, S., Arzt, E.: Mechanics of hierarchical adhesion structures of geckos. Mechanics of Materials **37**, 11 (2004)
47. Yao, H.Ga.H.: Shape insensitive optimal adhesion of nanoscale fibrillar structures. Proc. Natl. Acad. Sci. USA **101**, 6 (2004)
48. Huber, G., Mantz, H., Spolenak, R., Mecke, K., Jacobs, K., Gorb, S.N., Arzt, E.: Evidence for capillarity contributions to gecko adhesion from single spatula nanomechanical measurements. Proc. Natl Acad. Sci. USA **102**, 16293–16296 (2005)
49. Arzt, E., Gorb, S., Spolenak, R.: From micro to nano contacts in biological attachment devices. Proc. Natl Acad. Sci. USA **100**, 10603–10606 (2003)
50. Glassmaker, N.J., Jagota, A., Hui, C.Y., Kim, J.: Design of biomimetic fibrillar interfaces: 1. Making contact. J. R. Soc. Interface **1**, 23–33 (2004)
51. Tang, T., Hui, C.Y., Glassmaker, N.J.: Can a fibrillar interface be stronger and tougher than a non-fibrillar one? J. R. Soc. Interface **2**, 505–516 (2005)
52. Israelachvili, J.N.: Intermolecular and Surface Forces, 2nd edn. Academic, New York (1992)
53. Greenwood, J.A.: Adhesion of elastic spheres. Proc. Math. Phys. Eng. Sci. **453**, 21 (1997)
54. Jeong, H.E., Lee, S.H., Kim, P., Suh, K.Y.: Stretched Polymer Nanohairs by Nanodrawing. Nano Lett. **6**, 1508–1513 (2006)
55. Geim, A.K., Dubonos, S.V., Grigorieva, I.V., Novoselov, K.S., Zhukov, A.A., Shapoval, S.Y.: Microfabricated adhesive mimicking gecko foot-hair. Nat. Mater. **2**, 461–463 (2003)
56. del Campo, A., Greiner, C., Arzt, E.: Contact shape controls adhesion of bioinspired fibrillar surfaces. Langmuir **23**, 10235–10243 (2007)
57. Yurdumakan, B., Raravikar, N.R., Ajayan, P.M., Dhinojwala, A.: Synthetic gecko foot-hairs from multiwalled carbon nanotubes. Chem Commun (Camb) **14**(30), 3799–801 (2005)
58. Autumn, K., Sitti, M., Liang, Y.A., Peattie, A.M., Hansen, W.R., Sponberg, S., Kenny, T.W., Fearing, R., Israelachvili, J.N., Full, R.J.: Evidence for van der Waals adhesion in gecko setae. Proc. Natl Acad. Sci. USA **99**, 12252–12256 (2002)
59. Huber, G., Mantz, H., Spolenak, R., Mecke, K., Jacobs, K., Gorb, S.N., Arzt, E.: Evidence for capillarity contributions to gecko adhesion from single spatula nanomechanical measurements. Proc. Natl Acad. Sci. USA **102**, 16293–16296 (2005)
60. Lee, H., Lee, B.P., Messersmith, P.B.: A reversible wet/dry adhesive inspired by mussels and geckos. Nature **448**, 338–341 (2007)
61. Chen, Q.Z., Harding, S.E., Ali, N.N., Lyon, A.R., Boccaccini, A.R.: Biomaterials in cardiac tissue engineering: Ten years of research survey. Mater. Sci. Eng. R-Reports **59**, 1–37 (2008)
62. Serrano, M.C., Chung, E.J., Ameer, G.A.: Advances and Applications of Biodegradable Elastomers in Regenerative Medicine. Adv. Funct. Mater. **20**, 192–208 (2010)
63. Yoda, R.: Elastomers for biomedical applications. J. Biomater. Sci. Polym. Ed. **9**, 561–626 (1998)
64. Kang, Y., Yang, J., Khan, S., Anissian, L., Ameer, G.A.: A new biodegradable polyester elastomer for cartilage tissue engineering. J. Biomed. Mater. Res. A **77A**, 331–339 (2006)
65. Spontak, R.J., Patel, N.P.: Thermoplastic elastomers: fundamentals and applications. Curr. Opin. Colloid Interface Sci. **5**, 334–341 (2000)

66. Sircar, A.K., Galaska, M.L., Rodrigues, S., Chartoff, R.P.: Glass transition of elastomers using thermal analysis techniques. Rubber Chem. Technol. **72**, 513–552 (1999)
67. Amsden, B.: Curable, biodegradable elastomers: emerging biomaterials for drug delivery and tissue engineering. Soft Matter **3**, 1335–1348 (2007)
68. Sundback, C.A., Shyu, J.Y., Wang, Y.D., Faquin, W.C., Langer, R.S., Vacanti, J.P., Hadlock, T.A.: Biocompatibility analysis of poly(glycerol sebacate) as a nerve guide material. Biomaterials **26**, 5454–5464 (2005)
69. Chen, Q.Z., Ishii, H., Thouas, G.A., Lyon, A.R., Wright, J.S., Blaker, J.J., Chrzanowski, W., Boccaccini, A.R., Ali, N.N., Knowles, J.C., Harding, S.E.: An elastomeric patch derived from poly(glycerol sebacate) for delivery of embryonic stem cells to the heart. Biomaterials **31**, 3885–3893 (2010)
70. Gao, J., Crapo, P.M., Wang, Y.D.: Macroporous elastomeric scaffolds with extensive micropores for soft tissue engineering. Tissue Eng. **12**, 917–925 (2006)
71. Wang, Y.D., Ameer, G.A., Sheppard, B.J., Langer, R.: A tough biodegradable elastomer. Nat. Biotechnol. **20**, 602–606 (2002)
72. Nijst, C.L.E., Bruggeman, J.P., Karp, J.M., Ferreira, L., Zumbuehl, A., Bettinger, C.J., Langer, R.: Synthesis and characterization of photocurable elastomers from poly(glycerol-co-sebacate). Biomacromolecules **8**, 3067–3073 (2007)
73. Xia, Y.N., Whitesides, G.M.: Soft lithography. Annu. Rev. Mater. Sci. **28**, 153–184 (1998)
74. Autumn, K., Dittmore, A., Santos, D., Spenko, M., Cutkosky, M.: Frictional adhesion: a new angle on gecko attachment. J. Exp. Biol. **209**, 3569–3579 (2006)
75. Buhl, S., Greiner, C., del Campo, A., Arzt, E.: Humidity influence on the adhesion of biomimetic fibrillar surfaces. Int. J. Mater. Res. **100**, 1119–1126 (2009)
76. Waite, J.H., Tanzer, M.L.: POLYPHENOLIC SUBSTANCE OF MYTILUS-EDULIS-NOVEL ADHESIVE CONTAINING L-DOPA AND HYDROXYPROLINE. Science **212**, 1038–1040 (1981)
77. Artzi, N., Shazly, T., Baker, A.B., Bon, A., Edelman, E.R.: Aldehyde-Amine Chemistry Enables Modulated Biosealants with Tissue-Specific Adhesion. Adv. Mater. **21**, 3399–3403 (2009)
78. Artzi, N., Shazly, T., Crespo, C., Ramos, A.B., Chenault, H.K., Edelman, E.R.: Characterization of Star Adhesive Sealants Based On PEG/Dextran Hydrogels. Macromol. Biosci. **9**, 754–765 (2009)
79. Fukunaga, S., Karck, M., Harringer, W., Cremer, J., Rhein, C., Haverich, A.: The use of gelatinresorcin-formalin glue in acute aortic dissection type A. Eur. J. Cardiothorac. Surg. **15**, 564–569 (1999)
80. Kumar, A., Maartens, N.F., Kaye, A.H.: Evaluation of the use of BioGlue (R) in neurosurgical procedures. J. Clin. Neurosci. **10**, 661–664 (2003)
81. Bhatia, S.K., Arthur, S.D., Chenault, H.K., Kodokian, G.K.: Interactions of polysaccharide-based tissue adhesives with clinically relevant fibroblast and macrophage cell lines. Biotechnol. Lett. **29**, 1645–1649 (2007)
82. Bhatia, S.K., Arthur, S.D., Chenault, H.K., Figuly, G.D., Kodokian, G.K.: Polysaccharide-based tissue adhesives for sealing corneal incisions. Curr. Eye Res. **32**, 1045–1050 (2007)
83. Dragu, A., Unglaub, F., Schwarz, S., Beier, J.P., Kneser, U., Bach, A.D., Horch, R.E.: Foreign body reaction after usage of tissue adhesives for skin closure: a case report and review of the literature. Arch. Orthop. Trauma Surg. **129**, 167–169 (2009)
84. Schiller, W., Rudorf, H., Welzel, C.B., Kiderlen, M.J., Probst, C., Dewald, O., Welz, A.: Sutureless anastomoses of rabbit carotid arteries with BioGlue. J. Thorac. Cardiovasc. Surg. **134**, 1513–1518 (2007)
85. Hivnor, C.M., Hudkins, M.L.: Allergic contact dermatitis after postsurgical repair with 2-octylcyanoacrylate. Arch. Dermatol. **144**, 814–815 (2008)
86. Wippermann, J., Konstas, C., Breuer, M., Kosmehl, H., Wahlers, T., Albes, J.M.: Long-term effects in distal coronary anastomoses using different adhesives in a porcine off-pump model. J. Thorac. Cardiovasc. Surg. **132**, 325–331 (2006)

87. Santerre, J.P., Labow, R.S.: The effect of hard segment size on the hydrolytic stability of polyether-urea-urethanes when exposed to cholesterol esterase. J. Biomed. Mater. Res. **36**, 223–232 (1997)
88. Kustandi, T.S., Samper, V.D., Ng, W.S., Chong, A.S., Gao, H.: Fabrication of a gecko-like hierarchical fibril array using a bonded porous alumina template. J. Micromech. Microeng. **17**, N75–N81 (2007)
89. del Campo, A., Greiner, C.: SU-8: a photoresist for high-aspect-ratio and 3D submicron lithography. J. Micromech. Microeng. **17**, R81–R95 (2007)
90. Murphy, M.P., Kim, S., Sitti, M.: Enhanced Adhesion by Gecko-Inspired Hierarchical Fibrillar Adhesives. ACS Appl. Mater. Interfaces **1**, 849–855 (2009)

Chapter 9
Heparin-Functionalized Materials in Tissue Engineering Applications

Christopher McGann and Kristi Kiick

Abstract Over the past decade, the tissue engineering field has placed increasing emphasis on the development of materials that mimic the natural cellular microenvironment and the complexity inherent to biological systems. Understanding cell and molecular biology has become as important to the development of tissue engineering scaffolds as traditional material science. This emphasis on biological mimicry has led to interest in materials that incorporate the dynamic and complex interactions found in the native extracellular matrix (ECM); protein-saccharide interactions in the ECM are one such example. In particular, over the past decade the glycosaminoglycan (GAG) heparin has found a tremendous amount of use in the design of tissue engineering scaffolds and drug delivery devices, as well as in more traditional applications. Both heparin and its biological counterpart, heparan sulfate, interact – mainly electrostatically – with a number of proteins and play an important role in many biological processes. This has been put to use in tissue engineering approaches to sequester and deliver the factors that drive regenerative processes. Additionally, heparin has been utilized in the development of novel responsive materials that form hydrogels through physical assembly. The versatility provided by these approaches has afforded opportunities not only in the design of scaffolds for tissue engineering but also in the development of drug delivery devices.

Extracellular Matrix Mimicry in Tissue Engineering Scaffolds

The ECM was once considered to be passive scaffolding with a purpose relegated to maintaining structural support for body tissue and serving as an anchor for cells [1]. Early tissue engineering scaffolds, likewise, were not designed with specific

C. McGann • K. Kiick (✉)
Department of Materials Science and Engineering, University of Delaware Newark, 201 DuPont Hall, DE 19716, USA
e-mail: kiick@udel.edu

S.K. Bhatia (ed.), *Engineering Biomaterials for Regenerative Medicine: Novel Technologies for Clinical Applications*, DOI 10.1007/978-1-4614-1080-5_9,

biological activity in mind. The native ECM, as now widely modeled in the biomaterials community, is a dynamic and evolving microenvironment that plays a vital role in the promotion and regulation of cell behavior. It comprises a complex network of biomacromolecules including polysaccharides, proteins, glycoproteins, proteoglycans, and GAGs. These molecules are undergoing constant degradation and reassembly as cells remodel the microenvironment in response to external signals [2]. Thus, the proliferation and survival, migration, and differentiation of cells are all guided in part by the ECM; it is especially important in modulating gene expression and the establishment of cellular phenotype, which directs cellular fate and tissue morphogenesis [1, 2]. For these reasons, the design criteria for novel tissue engineering scaffolds have increasingly incorporated principles from cell and molecular biology in addition to the more traditional material sciences [3].

A ubiquitous constituent of the ECM is the polysaccharides, which are found to function in numerous biological roles such as protein ligand receptors, as in the case of heparan sulfate [4–6], as well as roles in mechanical integrity, such as the case of high molecular weight hyaluronic acid in cartilage tissue. Many polysaccharides, even nonmammalian ones, are readily available, biocompatible and non-immunogenic, which has led to their application as tissue engineering scaffolds [4]. For example, tissue engineering scaffolds have been constructed from chitin and chitosan [5–10], dextran [11–15], hyaluronan [16–21], and heparin (or heparan sulfate) [22–25].

In addition to the widespread use of polysaccharides, researchers have had great success engineering into scaffolds such biological signals as cell adhesion moieties [26, 27], enzyme-specific degradation domains [3, 28], as well as the capacity for growth factor sequestration and controlled release [29]. Cell adhesion moieties, apart from providing a means of anchorage to the scaffold, are particularly important in processes such as cell growth and differentiation, wound healing, and the immune response [26, 30]. The incorporation of enzyme-specific degradation domains, which contrasts the original hydrolytic degradation mechanisms employed in biomaterials design, [28], provides mechanisms for scaffold remodeling that mimic those that occur in natural regenerative processes. With the incorporation of these enzymatic cleavage domains, tissue scaffold degradation is cell-directed and localized; the bulk mechanical integrity of the tissue scaffold is retained while the microenvironment is remodeled.

The inclusion of growth factors, a class of proliferative or anti-proliferative signaling proteins that modulate cellular behavior, into tissue scaffolds, provides strategies to modulate desired cellular signaling pathways such as cell adhesion, migration, gene expression, and differentiation [3, 31]. These factors are present in vivo not only as soluble macromolecules but also sequestered in the ECM; the differential sequestration of growth factors contributes to variations in their activities and outcomes [32–35]. Evidence has demonstrated that molecules in the ECM, such as heparan sulfate, can bind and localize these signals providing an important mechanism in the regulation of their activity [29]. Borrowing from these models, growth factors have been widely incorporated into scaffolds, with passive or direct loading of growth factors as the most facile way of incorporating these

molecules into a polymeric matrix. Commonly observed burst release from scaffolds has motivated development of systems that sequester growth factors via their interactions with heparin and heparan sulfate [29]. Examples include the engineering of scaffolds with affinity-based delivery through the use of electrostatic interactions between growth factor and a binding domain [27, 29] and covalently bound growth factors with enzymatically regulated release [36–38].

Many laboratories, including our own, have taken a keen interest in utilizing these interactions for the development of hydrogel-based tissue engineering scaffolds that are functionalized with or that assemble based upon these protein–polysaccharide interactions. Drawing inspiration from the affinity/assembly interactions between proteins, which have been utilized widely for the formation of physical gels [39–41], physical hydrogels assembled on the basis of heparin–peptide and heparin–protein interactions mark an important step in the application of heparin in tissue engineering.

Heparin and Heparan Sulfate

Heparin and heparan sulfate (HS) are heterogeneous and highly sulfated linear polysaccharides composed of uronic acid–(1 → 4)-D-glucosamine disaccharide repeat units. These macromolecules are the most structurally complex in the family of GAGs that includes chondroitin sulfate, dermatan sulfate, and keratin sulfate [42]. Heparin is particularly unique in that it has the highest negative charge density of any known biological macromolecule [43]. Heparin and HS have been shown to mediate a wide range of biological functions including: cell adhesion, regulation of cellular growth and proliferation, inhibition of blood coagulation, and cell surface binding [42]. Their interactions with a variety of proteins yield useful biological activity that has motivated their use for nearly a century in medical applications; a summary of this evolution is given below.

Discovery and History of Heparin/Heparan Sulfate

Although heparin was first discovered in 1916 in the laboratory of physiologist William Howell at Johns Hopkins University [44, 45], the exact structure and chemistry of heparin would require an additional 15 years for elucidation. The uronic acid was the first sugar of the disaccharide repeat unit to be correctly identified in 1928, and identification of glucosamine as the second saccharide in the repeat unit occurred in 1935–1936. Shortly thereafter heparin was found to contain significant levels of covalently linked sulfate, which made the linear polysaccharide one of the strongest biological acids found in nature [44]. Heparan sulfate was discovered as an impurity of heparin with low anticoagulating potential and was initially named heparitin sulfate [42, 46]. However, it was later established that HS

served an important purpose in modulating signaling between the cell and ECM signaling molecules [47].

Heparin has been used as an anticoagulant since 1935, specifically as a prophylaxis against post-operative thrombosis. Improvements in characterization of heparin in the latter half of the twentieth century have yielded various low molecular weight heparins (LMWH) with better defined chemistry and as a result, more predictable activity and improved bioavailability. These LMWHs have replaced traditional heparin as the primary clinical anticoagulant in the twenty-first century [44].

Chemistry, Structure, and Biosynthesis of Heparin/Heparan Sulfate

Heparin, as indicated above, is a heterogeneous linear polysaccharide that consists of 1–4-linked disaccharide repeat units consisting of pyranosyluronic acid (90% L-idopyranosyluronic acid and 10% D-glucopyranosyluronic acid) and 2-amino-2-deoxyglucopyranose (glucosamine). The heterogeneity of the heparin molecule stems from different arrangements of hydroxyl, acetyl, amine, and sulfate functional groups substituted along the chain of the polysaccharide. Represented by the "X" in Fig. 9.1, the 3- and 6-positions of the glucosamine and the 2-position of either the L-iduronic or D-glucuronic acid will carry an *O*-linked sulfo group or will be unsubstituted. The amino group on the glucosamine residue, represented by the "Y" on Fig. 9.1, is N-linked to an acetyl group, a sulfo group or similarly left unsubstituted. Despite these variations, the trisulfated disaccharide (with sulfates occupying the 3-, 6- and amino-positions) – also known as the "major sequence" – is by far the most common in the heparin chain. Heparin averages ~2.7 sulfate groups per disaccharide, with an overall charge of −75 for a 15 kDa chain [4, 42, 44, 48].

Heparan sulfate is structurally similar to heparin as it is also a linear polysaccharide with uronic acid 1 → 4-linked to glucosamine disaccharide repeat units. However, it is the D-glucuronic acid that is the primary uronic acid and there is far less sulfation (an average of only one per disaccharide). HS contains the same functional group substitutions as heparin (see Fig. 9.1), but there is greater heterogeneity in the sequence, which results in increased structural complexity and a wider range of biological functionality [42, 44, 48].

The polydispersity and the variability of the disaccharide sequences in both heparin and HS preclude any complete structural analysis of even the most highly purified preparations of heparin. Therefore, one can only generalize based upon analysis of chemically discrete fragments of depolymerized heparin and HS [42]. However, from these analyses, it has been determined that heparin has an extended, right-handed helical structure that cannot fold due to restricted rotation around the glycosidic bond. For this reason, heparin cannot form any of the tertiary structures found commonly in proteins [42, 44].

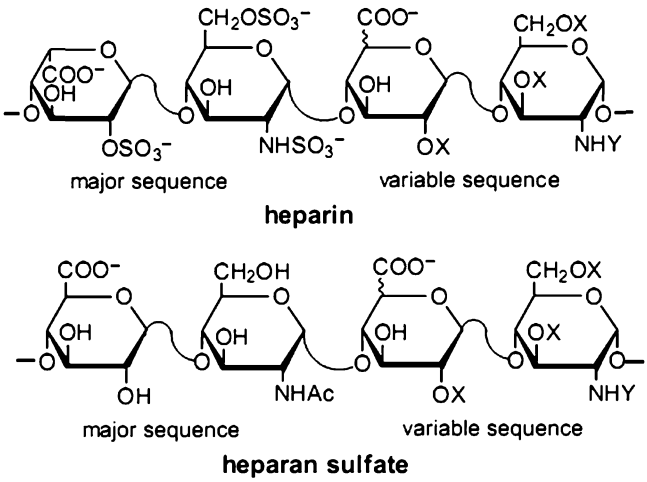

Fig. 9.1 A diagram indicating the major and variable sequences of heparin and heparan sulfate. (X = H or SO_3^-, Y = H, acetyl, or SO_3^-) Reproduced from ref. [44], permission granted from WILEY-VCH

Studies of heparin biosynthesis [44] have elucidated that heparin is synthesized as a heparin proteoglycan where a unique core protein (serglycin) acts as a support for the polymerization of the heparin chains (see Fig. 9.2) [42]. The biosynthesis involves a cascade of various enzymatic modifications of the growing GAG chain, and variations in the degree to which these reactions occur is the cause for the heterogeneity in the final heparin product [42]. Following chain modification, the core protein, acted on by proteases, releases a 100-kDa peptidoglycan heparin polymer, which is then immediately cleaved into a number of smaller (15 kDa) GAG heparin chains by β-endoglucuronidases [44]. These final heparin GAG chains are found localized in the secretory granules of mast cells [42]. An increased understanding of the details of this biosynthesis has afforded chemoenzymatic forms of heparin that are of absolute homogeneity; the expansion of these methods will provide important mechanisms to selectively tailor the bioactivities of biomaterials matrices [49–52].

The biosynthesis of HS follows the same general steps as those of heparin biosynthesis, with the notable difference that the chain modifications tend to be more localized in HS than in heparin, owing to increased substrate selectivity of the enzymes responsible for the chain modifications. This is consistent with the greater heterogeneity and limited sulfate substitution seen in the HS chains; it also explains why the primary structure of HS varies from tissue to tissue and from cell to cell [42]. In addition, as heparan sulfate serves a much wider range of biological function in vivo less can be said about specific cell types that express HS. More importantly, the expression of HS can change during development, aging, and disease. Another major difference between HS and heparin is that the HS GAG

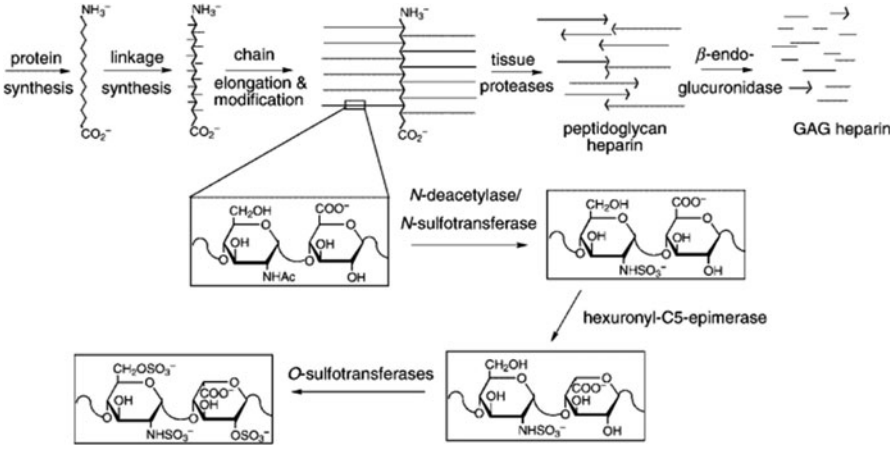

Fig. 9.2 Schematic representation of the steps involved in heparin/HS biosynthesis. Heparan sulfate remains a proteoglycan and attached to its core protein [syndecan or glypican (not shown)]. Reproduced from ref. [44], permission granted from WILEY-VCH

chains remain connected to the core protein: syndecan or glypican. The final heparan sulfate proteoglycans are found on cell surfaces and in the ECM [44].

Protein–Heparin/HS Interactions

The primary mechanism of binding between heparin/HS and protein is electrostatic; it involves the interaction of basic residues along the peptide chain with the anionic functional groups of the heparin/HS [42], with minor likely contributions from hydrogen bonding and hydrophobic forces [44]. Many heparin-binding proteins have been identified, and proposed heparin-binding consensus sequences include: XBBBXXBX, XBBXBX, XBBBXXBBBBXXBBX, and TXXBXXTBXXXTBB, where B is a basic residue, T is a turn, and X is a hydropathic residue [42, 44, 53]. It is clear from these sequences that both local proximity of basic residues, as well as their spatial orientation, drive heparin-binding capacity [44, 53]. These consensus sequences provide an archetype for the design of synthetic or biosynthetic peptides that can be incorporated into a scaffold material to endow it with heparin-binding properties.

The first well-studied protein–heparin interaction was the association of heparin to antithrombin III, a serine protease inhibitor. Antithrombin III (AT-III), the natural inhibitor of the blood coagulation protein, thrombin, was found to be potentiated by heparin [43]. While only a small pentasaccharide oligomer of heparin is required for AT-III binding [54] a 16-saccharide chain of heparin is necessary to effectively increase AT-III–thrombin binding and to inhibit thrombin [44]. Following the elucidation of the heparin–AT-III interaction, many other heparin/heparan sulfate

interactions have been identified. Heparan sulfate proteoglycans located on the cell surfaces of hepatocytes have been found to play an important role in lipoprotein clearance [42, 55]. The role of HS proteoglycans as cell-surface receptor proteins means that they are also important in pathogenesis. The Dengue virus, HIV-1, and HSV, as well as some parasites, utilize HS proteoglycans to target and infect cells. HS has also demonstrated importance in determining tumor progression; depending on the location and structure, HS may have inhibitory or proliferative consequences for tumor development [50]. Adhesion proteins also interact with heparin and heparan sulfate with important implications in inflammation, nerve tissue growth, and the formation of amyloid deposits in the brain [44]. The discovery of numerous protein–heparin/HS interactions indicates their importance in the regulation of many biological activities. In particular, the behavior of cell-surface HS proteoglycans may have important consequences in the signaling events that choreograph regenerative processes; understanding the role of these proteoglycans and utilizing these interactions may prove to be critical to the development of scaffold materials that guide desired cell behavior.

Growth Factor Interactions

Heparin/HS interactions with extracellular signaling molecules, such as growth factors and chemokines, are particularly important to the fields of tissue engineering and regenerative medicine. Heparin has been found to stabilize growth factors and increase binding affinity for cell receptors [56, 57]. Heparin-binding growth factors include fibroblast growth factors (FGFs), endothelial growth factors, and numerous others [42]. However, the interactions between heparin/HS and FGFs are probably the most well studied (after the AT-III–heparin interaction). FGFs are a large family of signaling proteins that have important roles in developmental processes such as cell proliferation, differentiation, morphogenesis, and angiogenesis [44]. The FGF growth factors effect biological and physiological change through binding events with their cell-surface, FGF receptors. Through crystallography studies, it has been revealed that heparin decasaccharides stabilize the growth factor–receptor interaction [53]. Signal transduction is only initiated when all three macromolecules (heparin, growth factor, and receptor) interact simultaneously [44].

Other growth factors, including bone morphogenetic protein 7 (BMP-7), neurgulin-1, vascular endothelial growth factors (VEGF), heparin-binding epidermal growth factor (HB-EGF), platelet-derived growth factor (PDGF), transforming growth factor-β1 (TGF-β1), and hepatocyte growth factor (HGF) have all been found to interact with heparin, isolated HS, or with the HS proteoglycans [44, 55]. HGF has been found to bind with HS and may act as a tumor suppressor, morphogen, and angiogenic factor. Heparin has been shown to modulate the activity of TGF-β1, which is important to cell migration and proliferation, immune activities, and ECM synthesis [44]. The binding of VEGF to HS has shown to be important in the morphogenesis of mouse vasculature. Differences in the distributions of soluble and heparin-binding forms of VEGF results in variations in local signaling that alter

blood vessel formation; for example, the sprouting of vessels is promoted by tethered isoforms of VEGF, while the dilation of vessels is induced by soluble forms [32–38]. This evidence supports that tissue patterning is driven by a relationship between soluble and bound VEGF, which is determined by the form and distribution of HS present in the tissue microenvironment as well as by the relative amounts of various isoforms of VEGF. A similar relationship between FGF-10 and HS, relevant to lung morphogenesis, strengthens the supposition that HS behaves as a "growth factor tethering" agent whose distribution throughout the ECM affects growth factor gradient and in some way dictates development [55]. Thus, greater understanding of the HS-growth factor relationship will be fruitful for tissue engineering; materials that can control the spatial/temporal distribution of soluble or tethered factors could potentially guide tissue morphogenesis [58, 59].

Cytokine/Chemokine Interactions

Another group of important interactions between soluble signals and heparin/HS are those involving cytokines and chemokines such as monocyte chemoattractant protein 1 (MCP-1), stromal cell-derived factor 1 (SDF-1α), tumor necrosis factor α (TNF-α), interleukin 5 (IL-5), interleukin 6 (IL-6), interleukin 8 (IL-8), interleukin 10 (IL-10), and platelet factor 4 (PF-4) [55]. HS has been shown to localize these signals in extracellular compartments in addition to exerting control over the activity of the signals. Studies have shown PF-4 and SDF-1α appear to play important roles in inflammatory and wound healing processes; SDF-1α, in particular, has demonstrated potency as a chemoattractant for monocytes and T-cells [44]. It is believe that HS proteoglycans bind and localize these signaling molecules on cell surfaces, effectively clustering these signal molecules, which circulate in vivo at low concentrations. Similarly, it is likely that HS proteoglycans located in the ECM create and maintain signal gradients that may be important to cells that migrate through tissue and organs [55].

Heparin in Biomaterials and Tissue Engineering

The incorporation of heparin in biomaterials and tissue engineering scaffolds has been widely explored due to heparin's antithrombogenic properties as well as its ability to interact with numerous soluble proteins. Biomaterials with incorporated heparin are very often used for anticoagulative purposes; vascular grafts, which often fail due to early thrombosis, provide an example of this application of heparin [60].

Tissue engineering scaffolds containing heparin have also been produced. Heparin's affinity for numerous soluble signals, as described in detail above, has driven much of this interest. It has provided enhanced biological functionality for

synthetic-based scaffolds and has given tissue engineers a powerful mechanism for delivering factors that guide regenerative processes. Some applications involve investigation of cell phenotype and differentiation [61–65], while others attempt to utilize heparin for controlled factor delivery applications [66–71].

Antithrombogenic Materials

Some of the earliest examples of materials that contained heparin had the explicit goal of taking advantage of heparin's antithrombotic properties [72, 73]. Researchers functionalized the surfaces of these materials, usually those to be implanted or used during surgery, with heparin in order to improve blood compatibility [74]. Examples where heparin has been implemented as an anticoagulant agent include polyurethanes [75], polylactide [76, 77], a collagen/chitosan complex [10], a silk fibroin/chitosan complex [8], a poly(vinyl alcohol) composites [78], decelluarized porcine arterial tissue [60], and multi-polymer composites [79, 80].

A variety of applications for these materials exist, including coatings for coronary stents [77–80] and tissue engineering applications. Two of the major complications resulting from the implantation of coronary stents are restenosis of the arterial tissue and thrombosis; heparinized stents demonstrate less platelet adhesion [77, 78, 80] or less platelet activation, indicating lower thrombogenic potential. Tissue engineering scaffolds have also been functionalized with heparin in the attempt to provide the scaffold material with antithrombotic properties. Liao et al. investigated heparinizing the surface of decellularized porcine arteries as a means of resolving current issues with synthetic vascular grafts, which suffer clinically due to thrombosis [60]. Similarly, studies have explored heparinizing collagen/chitosan [10] and silk fibroin/chitosan scaffolds [8] in an effort to limit the materials' thrombogenic properties.

Enhanced Biological Functionality

Heparin has also been utilized to increase the biological activity of synthetic tissue engineering scaffolds. Synthetic materials have advantages over their naturally derived counterparts in that they are inexpensive and standardized; in particular, naturally derived matrices suffer from variability based upon source and purification technique. Further, synthetic materials are more versatile and the mechanical properties can be tailored for a wide range of final applications. However, synthetics suffer from a lack of biologically relevant functionality. To create synthetic materials with biological activity, a widely adopted approach has been the simple incorporation of components from the ECM, such as heparin and HS.

In particular, researchers have heparinized synthetic scaffolds to promote growth factor activation [81] and localization/concentration [82]. Nilasaroya et al.

created photopolymerized hydrogels of methacrylated poly(vinyl alcohol) and heparin macromers. The conjugation of heparin to the methacrylate and its subsequent polymerization into a hydrogel did not interfere with heparin's anticoagulative properties or its ability to interact with bFGF [81]. Bezuidenhout et al. heparinized porous polyurethane scaffolds to promote vascularization and angiogenesis. It was reported that the heparinized scaffolds resulted in increased numbers of capillaries and arterioles without significant change in the inflammatory response. The authors suggest that by binding and stabilizing growth factor in vivo the heparinized polyurethane encouraged vascularization within the scaffold [82]. Along similar lines, Cabric et al. recently explored the use of heparin to bind vascular endothelial growth factor-A as a means of attracting endothelial cells to induce revascularization of pancreatic islet transplants [83].

Heparinized materials have also been explored as means of controlling cell proliferation and phenotype [61–63]. Beamish et al. [63] and Cushing et al. [61, 62] both investigated heparin's capacity to influence cell phenotype. Beamish et al. found that the incorporation and slow release of heparin from poly(ethylene glycol) (PEG) diacrylate hydrogels could effectively upregulate markers of contractile SMCs [63]. Cushing et al. found that heparin covalently linked to a PEG hydrogel could induce a myofibroblast phenotype through the inhibition of FGFR activation. FGF receptor (FGFR) activation by FGF serves to naturally repress valvular interstitial cells (VICs) from adopting the myofibroblast phenotype. Thus, the inhibition of FGFR activation, via sequestration of FGF in the PEG–heparin hydrogel that reduced the concentration of FGF at the receptor, induced a myofibroblast phenotype in VICs that could be useful in the temporal regulation of heart valve repair [62]. Benoit et al. used PEG hydrogels functionalized with heparin to investigate the differentiation of human mesenchymal stem cells (hMSCs). The heparin hydrogels supported hMSCs and induced their osteogenic differentiation as evidenced by the increased alkaline phosphatase production and increased osteopontin and collagen I gene expression [65]. Furthermore, the presence of heparin in the hydrogels served to sequester and localize BMP-2 contributing to greater osteogenic differentiation [64]. The combination of these studies suggests intriguing opportunities to manipulate growth factor signaling via the use of heparinized materials, in manners that can purposefully direct a cellular outcome. The development of materials in which a specific GF can be targeted will expand the selectivity of these materials.

In covalently cross-linked PEG-LMWH systems developed in our laboratories, the effect of hydrogel mechanical properties on human aortic adventitial fibroblasts (AoAF) and other cardiovascular cell types has been investigated [84, 85]. It is widely reported that the mechanical properties of a matrix can affect cell adhesion, proliferation, and differentiation [86]. In this study, maleimide- and thiol-terminated star PEGs provided the hydrogel support structure to which biological functionality was incorporated. The biological domains included maleimide-functionalized heparin, a thiol-functionalized adhesion peptide (RGDSP) and fibronectin (FN). These components were differentially combined to form a set of four hydrogel structures illustrated in Fig. 9.3. Interestingly, modification of the gels, by

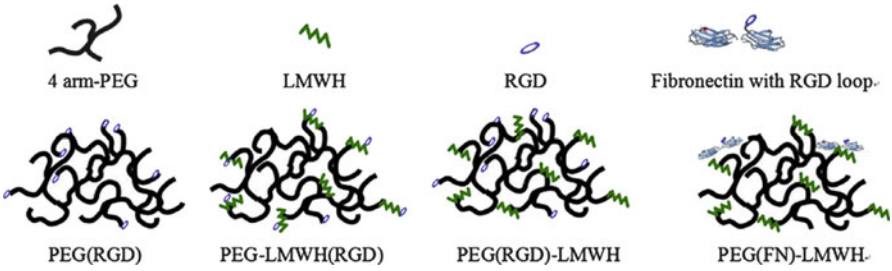

Fig. 9.3 Illustration depicting the hydrogel systems incorporating cell adhesion and heparin functionality. Reproduced from ref. [84], permission granted from Elsevier

the attachment of fibronectin to PEG, was required to improve adhesion of cells to these matrices; modification of gels with RGDSP did not provide useful cell adhesion, and attachment of the RGDSP to LMWH was particularly ineffective [84]. Studies of the adhesion of AoAFs to the FN-modified PEG-LMWH gels indicated that the AoAFs demonstrate the greatest affinity for the more mechanically sturdy gels ($G' = 2.8$ kPa in these studies) [84].

In more recent studies on multiple cardiovascular cell types [85], we have further illustrated the impact of mechanical properties on gene expression of human AoAFs, vascular smooth muscle cells (T/G-HA vSMCs), and human umbilical vein endothelial cells (HUVECs). In these studies, each cell type showed preferred proliferation on materials of a specific modulus [e.g., AoAFs to high-modulus materials ($G' = 13.7$ kPa) and HUVECs to low-modulus materials ($G' = 0.4$ kPa)], with corresponding differences in the up- and down-regulation of signaling pathways that also suggested phenotypic differences in addition to these proliferation preferences. These studies highlight that the modulation of the biochemical and mechanical properties of these heparinized scaffolds will be necessary for the proliferation of a given cell type for a given scaffold. They also suggest interesting opportunities to spatially control the phenotypes of cells in complex multicellular constructs via the modulation of matrix mechanical properties.

Growth Factor Delivery

One highly studied application of heparin in biomaterials has been as a vehicle for growth factor delivery in tissue engineering scaffolds. A notable application of heparin in this regard has been the controlled release of angiogenic factors such as VEGF, bFGF, and TGF-β [29, 87]. The materials used for controlling the delivery of growth factors through heparin sequestration have varied greatly from particulate or micellar systems [22, 70, 88–90] to synthetic hydrogel systems [4, 23, 25, 68, 84, 91–106], to demineralized bone matrices [107]. A great variety of materials, methods, and applications are found in the literature; we focus below

mainly on hydrogel matrices derived from either natural sources (fibrin, collagen) or synthetic polymers (PEG).

Natural Materials

There are a number of examples in the literature that involve the heparinization of polysaccharide matrices for the purposes of growth factor delivery [4, 105, 108–113]. Liu et al. created hyaluronate–heparin conjugate gels for the controlled delivery of bFGF [114], while Chinen et al. and Tanihara et al. created alginate–heparin systems in which the objective was to localize and control delivery of bFGF for the induction of angiogenesis [70, 115]. More recent examples of polysaccharide-based scaffolds include the alginate-chitosan gels produced by Ho et al. [113] and the alginate gels produced by Freeman and Cohen [112]. Both of these systems incorporated heparin as the mechanism for controlled delivery of growth factor; but the study performed by Freeman and Cohen was particularly interesting as the system sequentially delivered three angiogenic factors: VEGF, PDGF-BB, and TGF-β1 [112].

The addition of heparin to collagen-based matrices has mainly been in pursuit of controlled delivery of angiogenic growth factors [116–120], with an increasing number of alternative uses. For example, Bladergroen et al. recently incubated collagen–heparin gels with SDF-1α, a potent chemotactic cytokine, to encourage in vivo recruitment of hematopoietic cells. The scaffolds supported the recruitment of hematopoietic progenitor cells and the cells continued development along several different lineages [69]. Additionally, von Walter et al. loaded a heparinized collagen filler for a TiO_2/glass composite (Ecopore) with BMP-2 to induce bone regrowth. Following implantation into rabbit bone defect models, energy dispersive X-ray spectroscopy measurements revealed that the implants with the heparinized collagen demonstrated greater bone regrowth than the controls lacking heparin or the heparinized-collagen filler [120].

However, much of the literature dedicated to heparinized collagen matrices involves the loading of angiogenic factors such as bFGF and VEGF [116–119, 121]. Most cases involve the use of only one factor such as bFGF [122–124] or VEGF [116, 119, 121], but Nillesen et al. investigated a combinatory approach revealing that the loading of both rat recombinant bFGF and VEGF led to enhanced and well-developed vasculature in adult Wistar rats as compared to either factor by itself [117]. Highlighting the complexity of signaling inherent to vascularization, a third factor, angiogenin (ANG), found to activate various individual events responsible for angiogensis, was explored by Shi et al. in a heparinized collage-chitosan scaffold. The heparinized scaffold was effective at the controlled release of ANG in an in vitro study and also demonstrated faster development of vasculature in rabbit models compared with ANG-free controls [118]. Most recently, Grieb et al. heparinized collagen sponges to sequester and release VEGF in an attempt to address the poor angiogenic potential of artificial dermis materials such as Alloderm®, Apligraf®, and Integra®. In this study, heparin was found to sequester and slowly release VEGF providing the surrounding cells with a consistent angiogenic stimulus [116].

The work of Sakiyama-Elbert and coworkers has focused on the development of heparin–fibrin matrices for controlled delivery. In comparison to the above examples involving collagen [69, 116–121], heparin is immobilized in the fibrin scaffolds through affinity interactions with heparin-binding peptides (HBPs) conjugated to the matrix. Appropriate choice of peptide:heparin:growth factor ratios permits the sequestration of the GF in the matrix, while simultaneously affording release of both the GF and the heparin on desired timescales. This work has utilized heparin-binding capacity of a number of growth factors, including bFGF [67], beta-nerve growth factor (β-NGF) [66], neurotrophin-3 (NT-3) [125–128], and glial-derived neurotrophic factor (GDNF) [129], for potential treatment of nerve injury. This work has demonstrated the utility of heparin as a controlled delivery element in matrix scaffolds for even weakly associating factors such as NT-3 and β-NGF [66, 125, 126, 128]. These fibrin–heparin affinity matrices have also been utilized for the delivery of growth factor for the repair of tendon tissue [130–134]. Most recently, Thompoulous et al. investigated the impact of a fibrin–heparin affinity system that bound bFGF or platelet-derived growth factor BB (PDGF-BB) on the proliferation and gene expression of canine tendon fibroblasts. The scaffolds containing the heparin retained the bFGF compared with negative controls. Furthermore, the delivery of the both growth factors stimulated tendon fibroblast proliferation and caused changes in the expression of matrix genes [130].

Synthetic Materials

In some of the earliest such studies, Ishihara et al. conjugated heparin to polystyrene monomers for the creation of heparinized polystyrene plates. Heparin was first exposed to periodate and cleaved in an alkaline bath before functionalized with *p*-vinylbenzylamine and coated onto well-suspension culture plates. These plates were shown to increase the activity of both VEGF and bFGF [135, 136]. The success of this work led to the widespread adoption of heparin-synthetic polymer systems for the purpose of controlled growth-factor delivery.

As mentioned previously, heparin-conjugated PEG has been utilized to investigate differentiation and phenotype of hMSCs and VICs [62, 64, 65]; in addition, heparin–PEG hydrogels have been examined for tissue engineering scaffolds and growth factor delivery applications [23, 25, 68, 91–94, 97, 105]. Benoit et al. copolymerized macromolecular heparin monomers with dimethacrylated poly(ethylene glycol) monomers to form synthetic ECM capable of bFGF delivery. These heparinized-PEG hydrogels demonstrated sustained release of bFGF following zero-order kinetics over a 5-week time period. Additionally, the adhesion, proliferation, and osteogenic differentiation of hMSCs was reported to be enhanced by heparin–PEG gels as compared to unmodified PEG gels [68]. Another example of a heparin–PEG conjugate includes a synthetic composite consisting of heparin, PEG, and either hyaluronan (HA) or chondroitin sulfate (CS) constructed for the delivery of bFGF. The GAGs were modified through the addition of a thiol group before conjugation with PEG diacrylate into a hydrogel. These scaffolds demonstrated

sustained release of bFGF for 28 days and in vivo mouse models demonstrated increased neovascularization [105]. Tae et al. modified the carboxylic acid groups of heparin through EDC/HOBt chemistry to form hydrazides, which were subsequently reacted with *N*-hydroxysuccinimidyl esters of PEG-bis-butanoic acid to form PEG–heparin hydrogels. These hydrogels provided controlled release of VEGF over the course of 3 weeks and preserved its biological activity in vitro, as measured by the survival/proliferation of HUVECs [25]. A more recent study involving this heparin–PEG system utilized a different pro-angiogenic factor, osteoprotegerin (OPG). Heparin was modified through its carboxylic acid groups with cystamine to yield thiols, which were subsequently reacted via Michael-type addition with a PEG-diacrylate to form the hydrogel. The mild cross-linking meant that the procedure could be utilized in combination with cells, but the gels exhibited little degradation in vivo and it was determined that little OPG actually diffused from the gel [23].

The utility of adding heparin to tissue engineering scaffolds is clear. The incorporation of heparin into natural matrices endows antithrombogenic properties, while the addition of heparin to synthetic matrices provides desired biological functionality. Both synthetic and naturally derived tissue engineering scaffolds benefit from heparin incorporation when the objective is to provide controlled factor release. In addition, heparin has also been utilized as a mechanically integral part of hydrogel matrices cross-linked via physical interactions.

Heparin-Based Physical Assembly of Hydrogels

Interest in physical assembly is largely borne out of the potential for forming hydrogels that can reversibly assemble upon application of an environmental stimulus, which could include pH, temperature, mechanical stress, or the presence of some exogenous factor. Advantages include not only the potential for injection but also the absence of potentially toxic cross-linking chemicals. Physical assembly through protein interactions has been thoroughly studied and involves mechanisms such as coiled coil formation [137–143], antigen–antibody recognition [144–148], or supramolecular assembly [149–152]. The success of many of these systems has led to the exploration of hydrogels that physically assemble through different mechanisms such as protein–saccharide affinity interactions. Heparin, due to its interactions with varied peptides and growth factors, has been of particular interest in studies of such physically assembled systems [99].

Peptide–Polymer/Heparin Physical Assembly

Initial work on the physical assembly of heparin–polymer matrices was presented by Seal and Panitch in 2003 [102], in which heparin served as the cross-linking agent for a synthetic matrix comprising a PEG star polymer that was terminally functionalized with a small HBP (see Fig. 9.4). The peptide, covalently linked to the PEG star

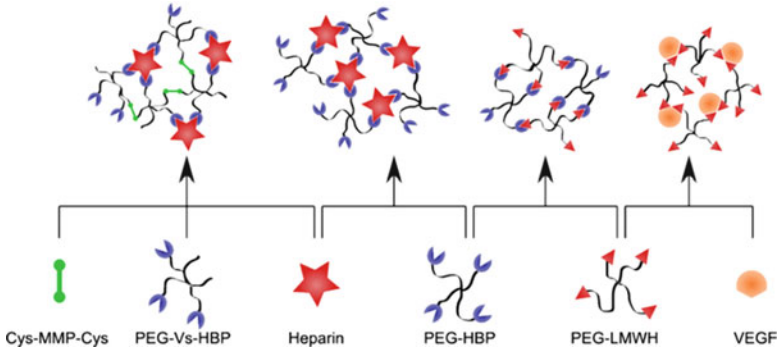

Fig. 9.4 Illustration of the methods for heparin-based physical assembly. This figure demonstrates the systems pursued by the Panitch (*two on left*) and Kiick laboratories (*two on right*). Reproduced from ref. [4]; permission granted from WILEY-VCH

polymer was capable of electrostatic interactions with the heparin and when the components were mixed it formed a viscoelastic material. The formation of a physical hydrogel avoided the use of toxic initiators, which complicate the in situ gelation for certain hydrogel systems. Additionally, this approach afforded the use of biological components which could offer a pathway to enhanced interaction with target tissues and thereby mimic specific biological activity native to the ECM [102].

The peptide-linkers were designed using the previously identified heparin-binding domains (HBD) of AT-III and TAT, a transduction peptide derived from an HIV regulator protein. The terminal ends of four-arm star PEG were functionalized with vinyl sulfone moieties, to limit hydrolytic degradation of the gels and permit Michael-type addition of the cysteine residue of the peptide. The peptide–PEG conjugates were mixed with heparin derived from porcine intestinal mucosa to form the physical hydrogels. Oscillatory rheology demonstrated strong frequency dependence, as well as temperature dependence, of the mechanical properties of these gels, but a release study indicated that the gels could sequester and release peptide at different rates dependent on the relative affinity of the peptide for heparin [102]. The addition of covalent cross-links to physical interactions (see Fig. 9.4) was subsequently developed by Panitch and coworkers [103, 104]. An eight-arm star PEG, functionalized with a vinyl sulfone moiety, was conjugated with both mono- and bis-thiolated peptides to introduce both covalent and noncovalent cross-linking points in the network. The bis-thiolated cross-linker, a short peptide sequence that could be enzymatically degraded by collagenese I, afforded the final hydrogels useful degradation properties. Oscillatory rheology, a degradation study, and a hemolysis assay suggested the useful properties of these materials. The oscillatory rheology revealed the frequency-independent elasticity of the matrix and demonstrated improvement in mechanical properties as compared to the previous system. Interestingly, the addition of heparin not only contributed to the overall mechanical properties of the gels (i.e., shear storage modulus), but led to faster gelation

times as well. While the mechanical integrity of the materials was increased, however, the reversible gelation of the system was lost, highlighting a possible trade-off in terms of material design of these types of systems. The degradation studies demonstrated that gels only responded to the collagenese, though they were also tested using heparinase and thrombin. Finally, the hemolysis assay demonstrated very low toxicity to erythrocytes [103, 104].

Heparin–Polymer/Peptide Physical Assembly

Complementary to the above approaches, our group has investigated the assembly of heparinized, four-arm star PEGs. The star PEG was terminally functionalized with low molecular weight heparin (LMWH) (see Fig. 9.4) and was used to form physical cross-links with heparin-binding polymers and proteins. We have demonstrated the physical gelation of these PEG-LMWH macromolecules with PEG star polymers functionalized with HBPs, as well as gelation with heparin-binding growth factors. Most recently, we have explored the physical assembly of recombinant, modular polypeptides equipped with heparin-binding sequences.

Noncovalently Assembled Materials [91, 93–95]

The choice of a PEG star copolymer provided the system hydrophilicity, biocompatibility, low protein fouling and low immunogenicity; while the terminal conjugation of LMWH to the PEG star polymer ($\geq$ 73% functionalization) [93, 94] ensured not only the requisite binding affinity needed for physical gelation, but also ensured the formation of a soluble macromolecule competent for the formation of networks. HMWH (~18 kDa) was avoided owing to the likelihood of its functionalization with greater than one moiety used for conjugation to the PEG, which would lead to the formation of an insoluble network. The incorporation of heparin in this manner was not expected to impair its ability to bind factor and might be useful in applications where multivalent presentation of the GAG is relevant.

Different peptide sequences were utilized for the HBP: ones isolated from the heparin-binding domains of AT-III and the heparin-interacting protein (HIP), as well as a coiled-coil peptide mimic of platelet factor 4. All were conjugated via reaction of a cysteine residue with vinyl sulfone-terminated four-arm star PEG. Sufficient degrees of functionalization of the PEG-LMWH and PEG-HBPs were observed for the formation of networks.

The combination of any of the PEG-HBPs with the PEG-LMWH (which itself exhibited weak mechanical properties owing to the self-association of the polyelectrolyte heparin) [95] led to self-supporting gels that after syneresis were estimated to contain 7 wt.% polymer. These results contrasted with the mixing of the PEG-HBP with unconjugated LMWH, which did not form hydrogels. Further, preformed hydrogels could be liquefied through the addition of exogenous LMWH or HBP,

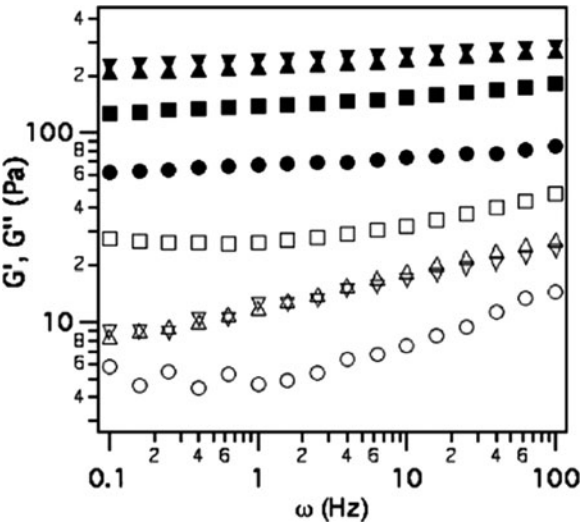

Fig. 9.5 Graph of the oscillatory rheology data for PEG-LMWH/PEG-HIP system. Storage moduli indicated by the *closed symbols*; loss moduli indicated by the *open symbols*. The PEG-LMWH/PEG-HIPs were mixed in different amounts based upon molar of LMWH to HIP: 9:1 (*squares*), 8:2 (*triangles*), and 6:4 (*inverted triangles*). The response of PEG-LMWH alone (7.2 wt.%) was added for comparison and is indicated by the *circles*. Reproduced from ref. [94]; permission granted form the American Chemical Society

indicating that the gels were in fact formed through physical interactions that could be reversed through competition with unconjugated peptide or heparin. Oscillatory rheology characterization of these hydrogels revealed the elastic properties of the gels at all frequencies (see Fig. 9.5) as the storage modulus exceeded the loss modulus, but overall, the moduli of these hydrogels were rather low. Limitation in the number of cross-linking sites for certain HBP–LMWH pairs may prevent the maximum possible elastic modulus; the development of homogeneous LMWH species with affinities for specific binding partners, as well as the utilization of other polymer architectures with a greater number of binding sites, may provide a strategy to maximize cross-linking pairs and enhance the mechanical properties of these materials.

The ability of LMWH to bind with multiple partners was exploited for the sequestration and delivery of growth factors from these matrices. Incubation of PEG–LMWH solutions with growth factor prior to the introduction of the PEG-HBP provided a facile manner to incorporate GFs into the hydrogels. These materials were found to sequester and passively release bFGF over a 2-week period; additionally, the release kinetics correlated well with the storage modulus of the hydrogel. Furthermore, the delivery of growth factor strongly matched the matrix dissolution kinetics (see Fig. 9.6); this suggests that the release of growth factor was triggered by matrix erosion and that it could be controlled by adjusting the mechanical properties of the matrices. The results from these growth factor release kinetics studies of these gels present an enticing opportunity for potential tissue engineering applications or for the treatment of ischemic tissue.

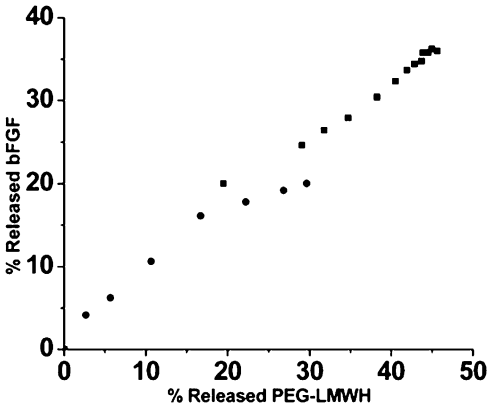

Fig. 9.6 The percentage released bFGF versus the percentage of released PEG-LMWH for the PEG-LMWH/PEG-PF4$_{zip}$ hydrogel (*square*, slope of 0.77) and the PEG-LMWH/PEG-HIP hydrogel (*circle*, slope 0.81). Reproduced from ref. [99]; permission granted from The Royal Society of Chemistry

Growth Factor Cross-Linked Hydrogels [92, 153]

The initial studies of the PEG–LMWH system demonstrated the utility of the polymer heparinization approach and the utility of erosion for controlling growth factor release. The potential for release to control erosion was thus also explored. As growth factors mainly bind short-heparin sequences, it was postulated that if the growth factor contained more than one heparin-binding domain it could act as functional cross-link for PEG-LMWH with functionality ≥ 3. Such a system could deliver factor selectively; it would be sensitive to ligand-exchange mechanisms, such as those with growth factor receptors, and would result in biologically relevant and targeted erosion of the hydrogel.

To this end, a system incorporating the PEG-LMWH and dimeric VEGF was investigated (see Fig. 9.7). Upon mixing of the two components, a self-supporting, viscoelastic hydrogel was immediately formed, as confirmed via optical tweezer microrheological methods. The lack of gelation of a bovine serum albumin (BSA)/PEG-LMWH control suggested that gelation was mediated by the interaction of LMWH with VEGF. Furthermore, the addition of exogenous LMWH to the preformed gel caused it to liquefy.

The erosion of these hydrogels was monitored in the absence and presence of the primary VEGF receptor (VEGFR-2); the release of ^{125}I-labeled VEGF was monitored. Polystyrene particles with covalently attached VEGFR-2 were added to the VEGF/PEG-LMWH hydrogels to induce targeted erosion. In comparison to controls containing only PBS buffer or polystyrene particles passivated with anti-IgG, the VEGFR-2-containing systems demonstrated significantly greater release of VEGF (see Fig. 9.8).

Studies employing porcine aortic endothelial cells equipped with the VEGFR-2 receptor (PAE KDR) confirmed the cell-responsiveness of these materials [153]. In particular, PAE cells overexpressing the VEGFR-2 receptor caused greater rates of VEGF release from PEG-LMWH hydrogels, with consequently greater rates of hydrogel erosion. Notably, cells that did not overexpress the receptor did not cause

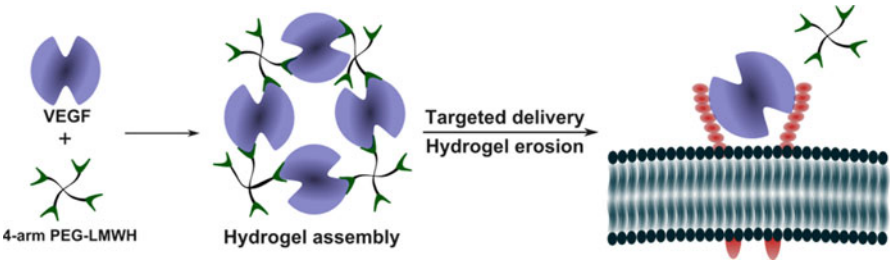

Fig. 9.7 Noncovalently assembled hydrogel for targeted delivery of VEGF. PEG is poly(ethylene glycol); LMWH is low molecular weight heparin; VEGF is vascular endothelial growth factor. Reproduced from ref. [153]; permission granted from WILEY-VCH

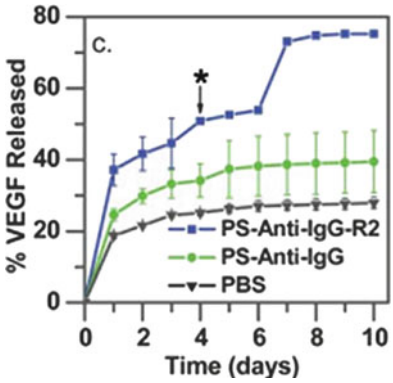

Fig. 9.8 The percentage released of vascular endothelial growth factor from VEGF-cross-linked hydrogels as a function of time in the absence and presence of the VEGFR-2 receptor. The *blue line* indicates the polystyrene nanoparticle containing the VEGFR-2; the *green line* is a control containing the polystyrene nanoparticle without the receptor; and the *black line* is a PBS control. The *asterisk* indicates that the VEGFR-2 containing system was visibly eroded at day 4. Reproduced from ref. [92]; permission granted from the American Chemical Society

hydrogel erosion. These results clearly demonstrate that therapeutic proteins can function as cross-links in non-covalently assembled hydrogel networks and that they can be selectively eroded in the presence of a specific receptor for targeted, delivery-mediated erosion of hydrogels.

Heparin-Binding Recombinant Polypeptide Hydrogels

Recombinantly derived, heparin-binding polypeptides with responsive and useful mechanical properties would also offer interesting opportunities in the design of tissue engineering scaffolds of complex biological functionality. The use of

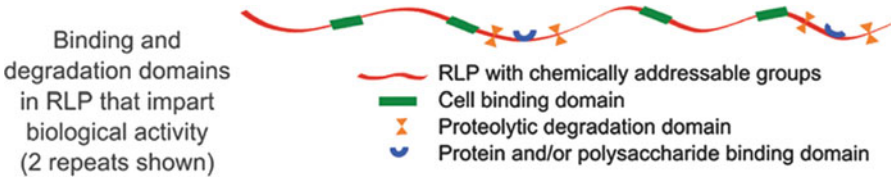

Fig. 9.9 Illustration of the modularly designed resilin-like polypeptide (RLP). Reproduced from ref. [155]; permission granted from The Royal Society of Chemistry

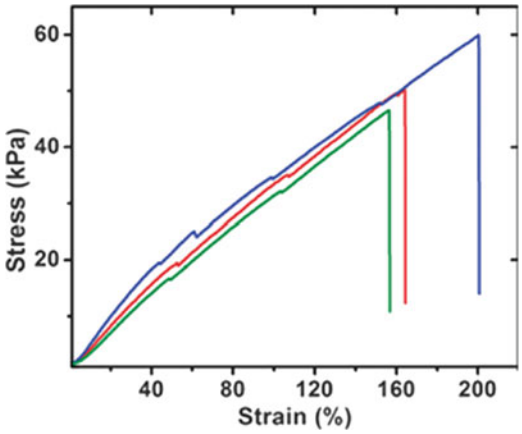

Fig. 9.10 Tensile testing data for resilin-like polypeptide hydrogels conducted at strain rate 10% gauge length per minute at 25°C. Results from three separate films of identical composition are shown. Reproduced from ref. [155]; permission granted from The Royal Society of Chemistry

recombinant methods permits the facile incorporation of multiple biological domains, such as cell adhesion sequences, heparin-binding domains, and enzymatic degradation sites. These modules are simply encoded directly into a desired gene, which is then expressed by an expression host and purified. Modules of various length and sequence can be encoded and swapped readily to permit tuning of multiple properties of the matrix (see Fig. 9.9). While recent work on elastin-like polypeptides demonstrates this approach [154], we have employed polypeptide sequences based on the insect protein resilin, owing to its hydrophilicity, excellent resilience, and high-frequency responsiveness [155].

We have described the biosynthesis and initial characterization of RLP12, a resilin-like polypeptide that carries 12 repeats of the elastomeric consensus repeat sequence of native resilin and is equipped with a heparin-binding domain. Mechanical testing, both by tensile testing and oscillatory rheology, has demonstrated the excellent bulk mechanical properties of the RLP12 in terms of extensibility (ca. 200%, Fig. 9.10) and resilience (ca. 96%, not shown). The cytocompatibility of this matrix has been confirmed. We have also preliminarily demonstrated the sensitivity of the mechanical properties of this matrix to the addition of heparin. The gelation time for the networks is significantly reduced in the presence of heparin, and the ultimate storage modulus is increased, consistent with the previous reports by Panitch and coworkers [115, 117, 118]. In addition, the heparin-binding domain will provide

affinity interactions to permit the sequestration of growth factor as described in previous examples. These matrices will offer unique properties for engineering highly mechanically active tissues, such as cardiovascular and vocal fold.

Conclusions and Outlook: Heparin in Tissue Engineering

The applications of heparin and heparan sulfate discussed in this chapter highlight the utility and importance of these macromolecules to tissue engineering and biomaterials. Devices incorporating these heterogeneous GAGs demonstrate better blood compatibility as well as the capacity to sequester and deliver important biological factors. In addition, heparinized materials have demonstrated physical assembly through affinity interactions and have presented a novel strategy for the formation of noncovalently assembled, biologically responsive materials. However, the mechanical properties of noncovalently assembled networks require additional engineering to expand the utility of those matrices. In addition, the complexity and heterogeneity of heparin raises both challenges and opportunities in their application in biomaterials. The heterogeneity of heparin affords it versatility, but may limit the number of crosslinks that it can form in a given matrix and/or make difficult the targeting of select proteins in vivo. Understanding the molecular details of heparin–peptide binding specificity would open up new opportunities for greater modulation of physiological and pathological processes and may lead to the introduction of new therapeutics. Additionally, it may improve the tunability of interactions between peptide and saccharide having implications in both growth factor delivery and physical assembly. As mentioned above, continued efforts toward the synthesis of homogeneous heparin species will also have importance in this regard. On a broader scale, increased understanding of the multitude of interactions within the ECM, and exploitation of these interactions in the design of materials, will remain important in the creation of regenerative medicine solutions.

Acknowledgments Related work in the author's laboratories has been supported by the University of Delaware Research Foundation, the Arnold and Mabel Beckman Foundation, the National Center for Research Resources (NCRR, a component of the National Institutes of Health), and the National Institutes of Health (NIH; 1-RO1-EB003172, 1-P20-RR017716, and P30-RR031160). Its contents are solely the responsibility of the authors and do not necessarily represent the official views of NCRR or NIH.

References

1. Daley, W.P., Peters, S.B., Larsen, M.: J. Cell Sci. **121**, 255–264 (2008)
2. Zagris, N.: Micron **32**, 427–438 (2001)
3. Lutolf, M.P., Hubbell, J.A.: Nat. Biotechnol. **23**, 47–55 (2005)
4. Baldwin, A.D., Kiick, K.L.: Biopolymers **94**, 128–140 (2010)

5. Khor, E., Lim, L.Y.: Biomaterials **24**, 2339–2349 (2003)
6. Kim, I.Y., Seo, S.J., Moon, H.S., Yoo, M.K., Park, I.Y., Kim, B.C., Cho, C.S.: Biotechnol. Adv. **26**, 1–21 (2008)
7. Senel, S., McClure, S.J.: Adv. Drug Deliv. Rev. **56**, 1467–1480 (2004)
8. She, Z.D., Liu, W.Q., Feng, Q.L.: Polym. Int. **59**, 55–61 (2010)
9. Wang, X.H., Yan, Y.N., Lin, F., Xiong, Z., Wu, R.D., Zhang, R.J., Lu, Q.P.: J. Biomater. Sci. Polym. Ed. **16**, 1063–1080 (2005)
10. Yu, X., Bichtelen, A., Wang, X.H., Yan, Y.N., Lin, F., Xiong, Z., Wu, R.D., Zhang, R.J., Lu, Q.P.: J. Bioact. Compat. Pol. **20**, 15–28 (2005)
11. Zhang, X.Z., Wu, D.Q., Chu, C.C.: Biomaterials **25**, 4719–4730 (2004)
12. Bajgai, M.P., Aryal, S., Bhattarai, S.R., Bahadur, K.C.R., Kim, K.W., Kim, H.Y.: J. Appl. Polym. Sci. **108**, 1447–1454 (2008)
13. Jukes, J.M., van der Aa, L.J., Hiemstra, C., van Veen, T., Dijkstra, P.J., Zhong, Z.Y., Feijen, J., van Blitterswijk, C.A., de Boer, J.: Tissue Eng. Part A **16**, 565–573 (2010)
14. Levesque, S.G., Shoichet, M.S.: Biomaterials **27**, 5277–5285 (2006)
15. Plieva, F., Oknianska, A., Degerman, E., Galaev, I.Y., Mattiasson, B.: J. Biomater. Sci. Polym. Ed. **17**, 1075–1092 (2006)
16. Horn, E.M., Beaumont, M., Shu, X.Z., Harvey, A., Prestwich, G.D., Horn, K.M., Gibson, A. R., Preul, M.C., Panitch, A.: J. Neurosurg. Spine **6**, 133–140 (2007)
17. Jia, X.Q., Burdick, J.A., Kobler, J., Clifton, R.J., Rosowski, J.J., Zeitels, S.M., Langer, R.: Macromolecules **37**, 3239–3248 (2004)
18. Leach, J.B., Bivens, K.A., Patrick, C.W., Schmidt, C.E.: Biotechnol. Bioeng. **82**, 578–589 (2003)
19. Park, Y.D., Tirelli, N., Hubbell, J.A.: Biomaterials **24**, 893–900 (2003)
20. Prestwich, G.D., Kuo, J.: Curr. Pharm. Biotechnol. **9**, 242–245 (2008)
21. Sahiner, N., Jha, A.K., Nguyen, D., Jia, X.Q.: J. Biomater. Sci. Polym. Ed. **19**, 223–243 (2008)
22. Lee, J.S., Go, D.H., Bae, J.W., Lee, S.J., Park, K.D.: J. Control. Release **117**, 204–209 (2007)
23. McGonigle, J.S., Tae, G., Stayton, P.S., Hoffman, A.S., Scatena, M.: J. Biomater. Sci. Polym. Ed. **19**, 1021–1034 (2008)
24. Tae, G., Kim, Y.J., Choi, W.I., Kim, M., Stayton, P.S., Hoffman, A.S.: Biomacromolecules **8**, 1979–1986 (2007)
25. Tae, G., Scatena, M., Stayton, P.S., Hoffman, A.S.: J. Biomater. Sci. Polym. Ed. **17**, 187–197 (2006)
26. Hersel, U., Dahmen, C., Kessler, H.: Biomaterials **24**, 4385–4415 (2003)
27. Sakiyama-Elbert, S.E., Hubbell, J.A.: Anni. Rev. Mater. Res. **31**, 183–201 (2001)
28. Kim, S., Healy, K.E.: Biomacromolecules **4**, 1214–1223 (2003)
29. Silva, A.K.A., Richard, C., Bessodes, M., Scherman, D., Merten, O.W.: Biomacromolecules **10**, 9–18 (2009)
30. Albelda, S.M., Buck, C.A.: FASEB J. **4**, 2868–2880 (1990)
31. Nimni, M.E.: Biomaterials **18**, 1201–1225 (1997)
32. Ferrara, N., Gerber, H.P., LeCouter, J.: Nat. Med. **9**, 669–676 (2003)
33. Lee, S., Jilani, S.M., Nikolova, G.V., Carpizo, D., Iruela-Arispe, M.L.: J. Cell Biol. **169**, 681–691 (2005)
34. Ozawa, C.R., Banfi, A., Glazer, N.L., Thurston, G., Springer, M.L., Kraft, P.E., McDonald, D.M., Blau, H.M.: J. Clin. Invest. **113**, 516–527 (2004)
35. Fischbach, C., Mooney, D.J.: Biomaterials **28**, 2069–2076 (2007)
36. Zisch, A.H., Lutolf, M.P., Ehrbar, M., Raeber, G.P., Rizzi, S.C., Davies, N., Schmokel, H., Bezuidenhout, D., Djonov, V., Zilla, P., Hubbell, J.A.: FASEB J. **17**, 2260–2262 (2003)
37. Ehrbar, M., Djonov, V.G., Schnell, C., Tschanz, S.A., Martiny-Baron, G., Schenk, U., Wood, J., Burri, P.H., Hubbell, J.A., Zisch, A.H.: Circ. Res. **94**, 1124–1132 (2004)
38. Ehrbar, M., Metters, A., Zammaretti, P., Hubbell, J.A., Zisch, A.H.: J. Control. Release **101**, 93–109 (2005)

39. Krishna, O.D., Kiick, K.L.: Biopolymers **94**, 32–48 (2010)
40. Kopecek, J., Yang, J.Y.: Polym. Int. **56**, 1078–1098 (2007)
41. Kopecek, J., Yang, J.Y.: Acta Biomater. **5**, 805–816 (2009)
42. Rabenstein, D.L.: Nat. Prod. Rep. **19**, 312–331 (2002)
43. Nelson, D.L., Lehninger, A.L., Cox, M.M.: Lehninger Principles of Biochemistry. W.H. Freeman, New York (2008)
44. Capila, I., Linhardt, R.J.: Angew. Chem. Int. Ed. **41**, 391–412 (2002)
45. McLean, J.: Circulation **19**, 75–78 (1959)
46. Linker, A., Hoffman, P., Sampson, P., Meyer, K.: Biochim. Biophys. Acta **29**, 443–444 (1958)
47. Sasisekharan, R., Shriver, Z., Venkataraman, G., Narayanasami, U.: Nat. Rev. Cancer **2**, 521–528 (2002)
48. Sun, Z.C., Wei, Z., Wei, K.M.: Prog. Chem. **20**, 1136–1142 (2008)
49. Linhardt, R.J., Dordick, J.S., Deangelis, P.L., Liu, J.: Semin. Thromb. Hemost. **33**, 453–465 (2007)
50. Weiwer, M., Sherwood, T., Green, D.E., Chen, M., DeAngelis, P.L., Liu, J., Linhardt, R.J.: J. Org. Chem. **73**, 7631–7637 (2008)
51. Arungundram, S., Al-Mafraji, K., Asong, J., Leach, F.E., Amster, I.J., Venot, A., Turnbull, J. E., Boons, G.J.: J. Am. Chem. Soc. **131**, 17394–17405 (2009)
52. Laremore, T.N., Zhang, F.M., Dordick, J.S., Liu, J., Linhardt, R.J.: Curr. Opin. Chem. Biol. **13**, 633–640 (2009)
53. Gandhi, N.S., Mancera, R.L.: Chem. Biol. Drug Des. **72**, 455–482 (2008)
54. Vanboeckel, C.A.A., Petitou, M.: Angew. Chem. Int. Ed. Engl. **32**, 1671–1690 (1993)
55. Whitelock, J.M., Iozzo, R.V.: Chem. Rev. **105**, 2745–2764 (2005)
56. Gospodarowicz, D., Cheng, J.: J. Cell. Physiol. **128**, 475–484 (1986)
57. Neufeld, G., Cohen, T., Gengrinovitch, S., Poltorak, Z.: FASEB J. **13**, 9–22 (1999)
58. Singh, M., Berkland, C., Detamore, M.S.: Tissue Eng. Part B Rev. **14**, 341–366 (2008)
59. Tayalia, P., Mooney, D.J.: Adv. Mater. **21**, 3269–3285 (2009)
60. Liao, D., Wang, X.W., Lin, P.H., Yao, Q.Z., Chen, C.Y.: J. Cell. Mol. Med. **13**, 2736–2743 (2009)
61. Cushing, M.C., Liao, J.T., Anseth, K.S.: Matrix Biol. **24**, 428–437 (2005)
62. Cushing, M.C., Liao, J.T., Jaeggli, M.P., Anseth, K.S.: Biomaterials **28**, 3378–3387 (2007)
63. Beamish, J.A., Geyer, L.C., Haq-Siddiqi, N.A., Kottke-Marchant, K., Marchant, R.E.: Biomaterials **30**, 6286–6294 (2009)
64. Benoit, D.S., Collins, S.D., Anseth, K.S.: Adv. Funct. Mater. **17**, 2085–2093 (2007)
65. Benoit, D.S.W., Durney, A.R., Anseth, K.S.: Biomaterials **28**, 66–77 (2007)
66. Sakiyama-Elbert, S.E., Hubbell, J.A.: J. Control. Release **69**, 149–158 (2000)
67. Sakiyama-Elbert, S.E., Hubbell, J.A.: J. Control. Release **65**, 389–402 (2000)
68. Benoit, D.S.W., Anseth, K.S.: Acta Biomater. **1**, 461–470 (2005)
69. Bladergroen, B.A., Siebum, B., Siebers-Vermeulen, K.G.C., Van Kuppevelt, T.H., Poot, A. A., Feijen, J., Figdor, C.G., Torensma, R.: Tissue Eng. Part A **15**, 1591–1599 (2009)
70. Chinen, N., Tanihara, M., Nakagawa, M., Shinozaki, K., Yamamoto, E., Mizushima, Y., Suzuki, Y.: J. Biomed. Mater. Res. A **67A**, 61–68 (2003)
71. Chung, H.J., Kim, H.K., Yoon, J.J., Park, T.G.: Pharm. Res. **23**, 1835–1841 (2006)
72. Goosen, M.F.A., Sefton, M.V., Hatton, M.W.C.: Thromb. Res. **20**, 543–554 (1980)
73. Miura, Y., Aoyagi, S., Kusada, Y., Miyamoto, K.: J. Biomed. Mater. Res. **14**, 619–630 (1980)
74. Engbers, G.H., Feijen, J.: Int. J. Artif. Organs **14**(1), 99–215 (1991)
75. Magoshi, T., Matsuda, T.: Biomacromolecules **3**, 976–983 (2002)
76. Jee, K.S., Dal Park, H., Park, K.D., Ha Kim, Y., Shin, J.W.: Biomacromolecules **5**, 1877–1881 (2004)
77. Gong, F.R., Cheng, X.Y., Wang, S.F., Zhao, Y.C., Gao, Y., Cai, H.B.: Acta Biomater. **6**, 534–546 (2010)
78. Jiang, T., Wang, G.X., Qiu, J.H., Luo, L.L., Zhang, G.Q.: Biomed. Mater. **4**, 10 (2009)
79. Kim, T.G., Lee, H., Jang, Y., Park, T.G.: Biomacromolecules **10**, 1532–1539 (2009)

80. Lee, Y.K., Park, J.H., Moon, H.T., Lee, D.Y., Yun, J.H., Byun, Y.: Biomaterials **28**, 1523–1530 (2007)
81. Nilasaroya, A., Poole-Warren, L.A., Whitelock, J.M., Martens, P.J.: Biomaterials **29**, 4658–4664 (2008)
82. Bezuidenhout, D., Davies, N., Black, M., Schmidt, C., Oosthuysen, A., Zilla, P.: J. Biomater. Appl. **24**, 401–418 (2010)
83. Cabric, S., Sanchez, J., Johansson, U., Larsson, R., Nilsson, B., Korsgren, O., Magnusson, P. U.: Tissue Eng. Part A **16**, 961–970 (2010)
84. Nie, T., Akins, R.E., Kiick, K.L.: Acta Biomater. **5**, 865–875 (2009)
85. Robinson, K.G., Nie, T., Baldwin, A., Yang, E., Kiick, K.L., Akins, J., R.E. Soft Matter J. Biomed. Mater. Res. (2011, in review)
86. Ghosh, K., Pan, Z., Guan, E., Ge, S.R., Liu, Y.J., Nakamura, T., Ren, X.D., Rafailovich, M., Clark, R.A.F.: Biomaterials **28**, 671–679 (2007)
87. Spadaccio, C., Chello, M., Trombetta, M., Rainer, A., Toyoda, Y., Genovese, J.A.: J. Cell. Mol. Med. **13**, 422–439 (2009)
88. Chu, C.L., Goerges, A.L., Nugent, M.A.: Biochemistry **44**, 12203–12213 (2005)
89. Joung, Y.K., Bae, J.W., Park, K.D.: Expert Opin. Drug Deliv. **5**, 1173–1184 (2008)
90. Jung, Y., Chung, Y.I., Kim, S.H., Tae, G., Kim, Y.H., Rhie, J.W.: Biomaterials **30**, 4657–4664 (2009)
91. Zhang, L., Furst, E.M., Kiick, K.L.: J. Control. Release **114**, 130–142 (2006)
92. Yamaguchi, N., Zhang, L., Chae, B.S., Palla, C.S., Furst, E.M., Kiick, K.L.: J. Am. Chem. Soc. **129**, 3040–3041 (2007)
93. Yamaguchi, N., Kiick, K.L.: Biomacromolecules **6**, 1921–1930 (2005)
94. Yamaguchi, N., Chae, B.S., Zhang, L., Kiick, K.L., Furst, E.M.: Biomacromolecules **6**, 1931–1940 (2005)
95. Spinelli, F.J., Kiick, K.L., Furst, E.M.: Biomaterials **29**, 1299–1306 (2008)
96. Schultz, K.M., Baldwin, A.D., Kiick, K.L., Furst, E.M.: Macromolecules **42**, 5310–5316 (2009)
97. Nie, T., Baldwin, A., Yamaguchi, N., Kiick, K.L.: J. Control. Release **122**, 287–296 (2007)
98. Kim, S.H., Kiick, K.L.: Peptides **28**, 2125–2136 (2007)
99. Kiick, K.L.: Soft Matter **4**, 29–37 (2008)
100. Jia, X.Q., Kiick, K.L.: Macromol. Biosci. **9**, 140–156 (2009)
101. Jeong, K.J., Panitch, A.: Biomacromolecules **10**, 1090–1099 (2009)
102. Seal, B.L., Panitch, A.: Biomacromolecules **4**, 1572–1582 (2003)
103. Seal, B.L., Panitch, A.: Acta Biomater. **2**, 241–251 (2006)
104. Seal, B.L., Panitch, A.: Macromolecules **39**, 2268–2274 (2006)
105. Cai, S.S., Liu, Y.C., Shu, X.Z., Prestwich, G.D.: Biomaterials **26**, 6054–6067 (2005)
106. Yoon, J.J., Chung, H.J., Lee, H.J., Park, T.G.: J. Biomed. Mater. Res. A **79A**, 934–942 (2006)
107. Chen, L., He, Z.Q., Chen, B., Yang, M.J., Zhao, Y.N., Sun, W.J., Xiao, Z.F., Zhang, J., Dai, J. W.: J. Mater. Sci. Mater. Med. **21**, 309–317 (2010)
108. Ho, Y.C., Wu, S.J., Mi, F.L., Chiu, Y.L., Yu, S.H., Panda, N., Sung, H.W.: Bioconjug. Chem. **21**, 28–38 (2010)
109. Lee, K.W., Yoon, J.J., Lee, J.H., Kim, S.Y., Jung, H.J., Kim, S.J., Joh, J.W., Lee, H.H., Lee, D.S., Lee, S.K.: Transplant. Proc. **36**, 2464–2465 (2004)
110. Mi, F.L., Shyu, S.S., Peng, C.K., Wu, Y.B., Sung, H.W., Wang, P.S., Huang, C.C.: J. Biomed. Mater. Res. A **76A**, 1–15 (2006)
111. Jiang, T., Kumbar, S.G., Nair, L.S., Laurencin, C.T.: Curr. Top. Med. Chem. **8**, 354–364 (2008)
112. Freeman, I., Cohen, S.: Biomaterials **30**, 2122–2131 (2009)
113. Ho, Y.C., Mi, F.L., Sung, H.W., Kuo, P.L.: Int. J. Pharm. **376**, 69–75 (2009)
114. Liu, L.S., Ng, C.K., Thompson, A.Y., Poser, J.W., Spiro, R.C.: J. Biomed. Mater. Res. **62**, 128–135 (2002)
115. Tanihara, M., Suzuki, Y., Yamamoto, E., Noguchi, A., Mizushima, Y.: J. Biomed. Mater. Res. **56**, 216–221 (2001)

116. Grieb, G., Groger, A., Piatkowski, A., Markowicz, M., Steffens, G.C.M., Pallua, N.: Cells Tissues Organs **191**, 96–104 (2010)
117. Nillesen, S.T.M., Geutjes, P.J., Wismans, R., Schalkwijk, J., Daamen, W.F., van Kuppevelt, T.H.: Biomaterials **28**, 1123–1131 (2007)
118. Shi, H.F., Han, C.M., Mao, Z.W., Ma, L., Gao, C.Y.: Tissue Eng. Part A **14**, 1775–1785 (2008)
119. Steffens, G.C.M., Yao, C., Prevel, P., Markowicz, M., Schenck, P., Noah, E.M., Pallua, N.: Tissue Eng. **10**, 1502–1509 (2004)
120. von Walter, M., Herren, C., Gensior, T.J., Steffens, G.C.M., Hermanns-Sachweh, B., Jahnen-Dechent, W., Ruger, M., Erli, H.J.: Acta Biomater. **4**, 997–1004 (2008)
121. Yao, C., Markowicz, M., Pallua, N., Noah, E.M., Steffens, G.: Biomaterials **29**, 66–74 (2008)
122. Wissink, M.J.B., Beernink, R., Poot, A.A., Engbers, G.H.M., Beugeling, T., van Aken, W.G., Feijen, J.: J. Control. Release **64**, 103–114 (2000)
123. Wissink, M.J.B., Beernink, R., Pieper, J.S., Poot, A.A., Engbers, G.H.M., Beugeling, T., van Aken, W.G., Feijen, J.: Biomaterials **22**, 2291–2299 (2001)
124. Pieper, J.S., Hafmans, T., van Wachem, P.B., van Luyn, M.J.A., Brouwer, L.A., Veerkamp, J. H., van Kuppevelt, T.H.: J. Biomed. Mater. Res. **62**, 185–194 (2002)
125. Taylor, S.J., Rosenzweig, E.S., McDonald Iii, J.W., Sakiyama-Elbert, S.E.: J. Control. Release **113**, 226–235 (2006)
126. Taylor, S.J., Sakiyama-Elbert, S.E.: J. Control. Release **116**, 204–210 (2006)
127. Johnson, P.J., Parker, S.R., Sakiyama-Elbert, S.E.: Biotechnol. Bioeng. **104**, 1207–1214 (2009)
128. Taylor, S.J., McDonald, J.W., Sakiyama-Elbert, S.E.: J. Control. Release **98**, 281–294 (2004)
129. Wood, M.D., Borschel, G.H., Sakiyama-Elbert, S.E.: J. Biomed. Mater. Res. A **89A**, 909–918 (2009)
130. Thomopoulos, S., Das, R., Sakiyama-Elbert, S., Silva, M.J., Charlton, N., Gelberman, R.H.: Ann. Biomed. Eng. **38**, 225–234 (2010)
131. Gelberman, R.H., Thomopoulos, S., Sakiyama-Elbert, S.E., Das, R., Silva, M.J.: J. Hand Surg.-Am. **32A**, 373–379 (2007)
132. Thomopoulos, S., Zaegel, M., Das, R., Harwood, F.L., Silva, M.J., Amiel, D., Sakiyama-Elbert, S., Gelberman, R.H.: J. Orthop. Res. **25**, 1358–1368 (2007)
133. Sakiyama-Elbert, S.E., Das, R., Gelberman, R.H., Harwood, F., Amiel, D., Thomopoulos, S.: J. Hand Surg.-Am. **33A**, 1548–1557 (2008)
134. Thomopoulos, S., Das, R., Silva, M.J., Sakiyama-Elbert, S., Harwood, F.L., Zampiakis, E., Kim, H.M., Amiel, D., Gelberman, R.H.: J. Orthop. Res. **27**, 1209–1215 (2009)
135. Ishihara, M., Saito, Y., Yura, H., Ono, K., Ishikawa, K., Hattori, H., Akaike, T., Kurita, A.: J. Biomed. Mater. Res. **50**, 144–152 (2000)
136. Ishihara, M., Sato, M., Hattori, H., Saito, Y., Yura, H., Ono, K., Masuoka, K., Kikuchi, M., Fujikawa, K., Kurita, A.: J. Biomed. Mater. Res. **56**, 536–544 (2001)
137. Dusek, K., Duskova-Smrckova, M., Yang, J., Kopecek, J.: Macromolecules **42**, 2265–2274 (2009)
138. Liu, B., Lewis, A.K., Shen, W.: Biomacromolecules **10**, 3182–3187 (2009)
139. Montclare, J.K., Son, S., Clark, G.A., Kumar, K., Tirrell, D.A.: Chembiochem **10**, 84–86 (2009)
140. Shen, W., Kornfield, J.A., Tirrell, D.A.: Soft Matter **3**, 99–107 (2007)
141. Shen, W., Kornfield, J.A., Tirrell, D.A.: Macromolecules **40**, 689–692 (2007)
142. Shen, W., Zhang, K.C., Kornfield, J.A., Tirrell, D.A.: Nat. Mater. **5**, 153–158 (2006)
143. Xu, C.Y., Kopecek, J.: Pharm. Res. **25**, 674–682 (2008)
144. Kim, J., Singh, N., Lyon, L.A.: Biomacromolecules **8**, 1157–1161 (2007)
145. Kim, J.S., Singh, N., Lyon, L.A.: Chem. Mater. **19**, 2527–2532 (2007)
146. Lu, Z.R., Kopeckova, P., Kopecek, J.: Macromol. Biosci. **3**, 296–300 (2003)
147. Miyata, T., Asami, N., Uragami, T.: J. Polym. Sci. B-Polym. Phys. **47**, 2144–2157 (2009)
148. Zhang, R., Bowyer, A., Eisenthal, R., Hubble, J.: Biotechnol. Bioeng. **97**, 976–984 (2007)

149. Deming, T.J.: Soft Matter **1**, 28–35 (2005)
150. Yang, S.J., Zhang, S.G.: Supramol. Chem. **18**, 389–396 (2006)
151. Zhao, X.J., Zhang, S.G.: Chem. Soc. Rev. **35**, 1105–1110 (2006)
152. Zhao, X.J., Zhang, S.G.: Macromol. Biosci. **7**, 13–22 (2007)
153. Kim, S.H., Kiick, K.L.: Macromol. Rapid Comm. **31**(14), 1231–1240 (2010)
154. Straley, K.S., Heilshorn, S.C.: Soft Matter **5**, 114–124 (2009)
155. Charati, M.B., Ifkovits, J.L., Burdick, J.A., Linhardt, J.G., Kiick, K.L.: Soft Matter **5**, 3412–3416 (2009)

Part VI
Clinical Applications of Tissue Regeneration

Chapter 10
Tissue Engineering Strategies for Vocal Fold Repair and Regeneration

Alexandra J.E. Farran, Zhixiang Tong, Robert L. Witt, and Xinqiao Jia

Abstract Vocal fold is one of the most mechanically active tissues in the human body, producing a great variety of sounds through a regular, wave-like motion of the lamina propria (LP) at frequencies of 100-1,000 Hz and strains up to 30% [1]. Each vocal fold consists of a pliable vibratory layer of connective tissue, known as the lamina propria (LP), sandwiched between epithelium and muscle [2, 3]. The lamina propria plays a critical role in the production of voice as its shape and tension determine the vibratory characteristics of the vocal folds. Numerous environmental factors and pathological conditions can damage the delicate tissue; and patients suffering from vocal fold disorders are socially isolated due to their inability to phonate. This chapter summarizes recent endeavors in vocal fold regeneration using biomaterial-based, tissue engineering methodologies. Successful repair and regeneration of vocal fold lamina propria relies on the attainment of vocal fold-specific, biomimetic matrices that not only foster the attachment and proliferation of vocal fold fibroblast-like cells, but also induce the production of an extracellular matrix (ECM) that approximates the native tissue in terms of the biochemical composition, structural organization, and mechanical characteristics. The performance of the artificial matrices can be further enhanced by incorporating morphogenic factors and physiologically relevant biomechanical stimulations. Strategic combination of polymeric scaffolds, multipotent cells, defined biological factors, and biomechanical signals will lead to the successful reconstruction of functional vocal fold tissues that can be used as an alternative treatment modality for patients suffering from severe vocal fold disorders.

A.J.E. Farran • Z. Tong • X. Jia (✉)
Department of Materials Science and Engineering, Delaware Biotechnology Institute
University of Delaware, 201 DuPont Hall, Newark, DE 19716, USA
e-mail: xjia@udel.edu

R.L. Witt
Christiana Care Hospital, Medical Arts Pavilion, I-Suite 112, 475 Ogletown-Stanton Rd., Newark, DE 19713, USA

S.K. Bhatia (ed.), *Engineering Biomaterials for Regenerative Medicine: Novel Technologies for Clinical Applications*, DOI 10.1007/978-1-4614-1080-5_10,

Vocal Fold Physiology

One of the most remarkable mechanical devices Nature has engineered consists of the two small folds of tissue comprising the vocal folds, which move together and apart in a wave-like motion at frequencies of 100 to 1,000 Hz during sound production. This great mechanical versatility is due to the unique structure, composition, and mechanical properties of the vocal folds.

Vocal Fold Structure and Composition

The human vocal folds are located in the larynx between the epiglottis and the trachea. Two sets of folds appear in the larynx, the ventricular folds or false vocal folds above and the true vocal folds below (Fig. 10.1) [1]. The true vocal folds are a paired structure of roughly 11–21 mm in length and 1.6–2.6 mm in thickness, muscle excluded. Upon exhalation, the vocal folds are driven into a wave-like motion, creating a great variety of sounds. Structurally, the human vocal folds are composed of five distinct layers: the vocalis muscle, the main body of the vocal folds, is covered by the mucosa, which consists of a stratified squamous epithelium and the lamina propria (LP). The lamina propria (LP) is a pliable layer of connective tissue which can be subdivided into three layers: the superficial lamina propria (SLP), the intermediate lamina propria (ILP), and the deep lamina propria (DLP) [3]. While all three layers are required for phonation, the vocal fold cover, composed of the epithelium and the SLP, is the most important component of the vocal fold vibrating structure. The ILP and DLP combined is called the ligament [2].

Vocal fold LP is an anisotropic, gradient structure, containing fibrous proteins, interstitial substances, and cells that vary in concentration depending on the tissue depth. The fibrous proteins, such as collagen and elastin, and the interstitial molecules, such as hyaluronic acid (HA), constitute the extracellular matrix (ECM) of the vocal fold LP [2]. By weight, collagen (predominantly type I and III) is the most abundant protein in human vocal folds, representing 43% of the total protein [4]. Collagen content is the highest in the DLP and is the lowest in the SLP [3, 5]. The collagen fiber orientation, thickness, and density increase from the ILP to the DLP [6, 7]. Elastin is the second most abundant protein by weight, taking up an estimated 8.5% of the total protein. The mature elastic fibers are mostly present in the ILP, although some elastic fibers can be found in the DLP [4, 8, 9]. As opposed to collagen, the elastin content decreases as the vocalis muscle is approached [4]. The elastic and collagenous fibers in SLP are immature and exhibit smaller diameters, rendering the SLP loose and pliable [3]. On the other hand, the ligament is mostly composed of those two fibers aligned almost parallel to the edges of the vocal folds. The fibrous proteins provide vocal fold LP with structural support, shape, form, and the ability to withstand stress [10, 11]. While collagen contributes to the tissue tensile strength and stability, elastin is responsible for the

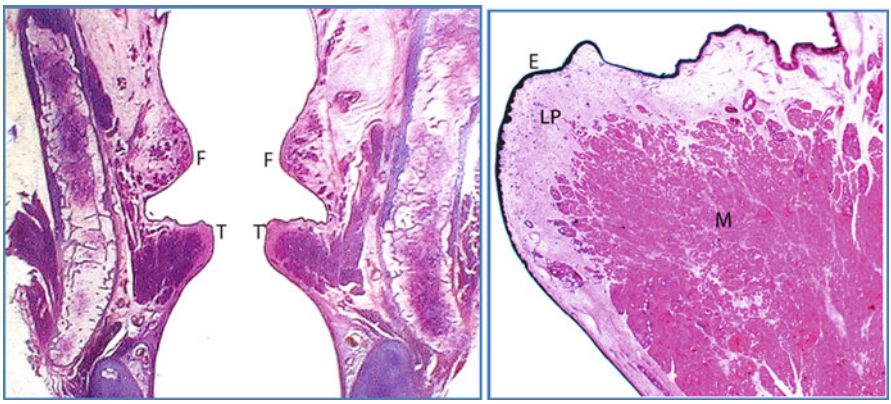

Fig. 10.1 H&E staining of healthy human vocal folds. *F* false vocal folds, *T* true vocal folds, *E* squamous epithelium, *LP* lamina propria, *M* vocalis muscle. Courtesy of Dr. James B. Kobler, Massachusetts General Hospital

tissue elasticity [4, 5, 9, 11, 12]. The presence of elastin in the vocal fold tissue allows it to be stretched up to two times its normal length without losing its resilience [9].

The interstitial components in the lamina propria surround the fibrous elements [10]. Relatively minute by weight, they serve as space fillers in the tissue due to their high molecular weight, abundant negative charges, and strong affinity for water. Generally amorphous in nature, the interstitial components found in human vocal fold LP include HA, fibronectin, fibromodulin, decorin, versican, and perlecan [13]. HA is the major glycosaminoglycan found in LP and is differentially enriched in the intermediate layer of the LP [4, 8, 9]. In addition to providing shock absorbing properties, HA is a major modulator of the tissue viscosity [2, 14, 15]. HA's presence in human vocal folds is evolutionarily beneficial due to the constant trauma they are subjected to during phonation. Moreover, HA's shear-thinning properties create optimum conditions for phonation by decreasing the tissue stiffness while vibrating [16]. Fibronectin is the most common glycoprotein found in the vocal fold ECM and is present throughout the layers, facilitating cell–cell and cell–ECM adhesion, cell migration, and differentiation, as well as the maintenance of extracellular structure [15, 17]. Vocal fold composition varies with age and gender, with men having 30% higher collagen content and three times more HA than women [4, 9, 18]. On the other hand, elastin varies more by age than by gender, with the elastin content increasing from the infant to the geriatric stage [8].

The vocal fold LP contains three types of cells: fibroblasts, myofibroblasts, and macrophages [19]. Macrophages are the least abundant of the three cell types, being present mostly in the SLP and playing a vital role in inflammatory responses. Myofibroblasts are differentiated fibroblasts that contain muscle-specific actin. They are most abundant in the SLP and are known to be involved in the reorganization and repair of the injured vocal fold tissue. Fibroblasts constitute the main cellular component of the LP, accounting for 80% of cells in normal adult human

LP, and are responsible for the general maintenance of the connective tissue by depositing, degrading, and rearranging the ECM. Vocal fold fibroblasts are present throughout the layers of the LP. Despite the presence of those three different types of cells, the human vocal fold remains hypocellular, with a total of 18 millions fibroblasts per gram of wet tissue [7]. As a comparison, dermis accounts for 100 millions fibroblasts per gram of wet tissue.

Vocal Fold Development

Newborn vocal folds differ greatly from the adult ones, not only in composition but also in structure. Newborn vocal fold LP is structurally and compositionally uniform, consisting of only one layer rich in ground substances such as HA and fibronectin, with sparse, immature fibrous components homogeneously distributed throughout the LP. The layered structure starts to evolve in infancy and does not become fully developed until adolescence. The fibroblasts in the newborn vocal fold LP are immature, showing an oval shape and a large nucleus–cytoplasm ratio. During infancy, fibroblasts are still sparse, but become spindle-shaped, and start to secrete ECM molecules adjacent to the cell body. The elastic fibers remain sparse and immature, mostly made of microfibrils. As the vocal folds continue to develop, the amount of the fibrous components increase gradually and the ground substance decreases proportionally, thereby slowly altering the microstructure of the vocal fold LP [20]. This difference in the vocal fold composition, along with the absence of vocal ligament, is thought to be responsible for newborns' inability to articulate sounds [21].

Parallel to the evolution of LP ECM is the differentiation of the cellular components. The LP monolayer at birth and shortly thereafter is hypercellular. By 2 months of age, the vocal fold starts to differentiate into a bilaminar structure of distinct cellular concentrations. Between 11 months and 7 years of age, a three-layered structure starts to appear, showing different cellular population densities. Although young vocal folds start to display a layered structure, such structure is not comparable to the trilaminar structure seen in adult tissues, where the layers are defined by their differential elastin and collagen fiber compositions. By 13 years of age, the vocal fold becomes mature, displaying a hypocellular SLP, an ILP composed mostly of elastin fibers, and a DLP composed mostly of collagen fibers, similar to that seen in adult vocal folds [22, 23].

Vocal Fold Biomechanics

Fundamental understanding of the mechanical properties of the native vocal fold tissues, both in tension and in shear, is an essential first step toward the development of biomaterials-based strategies for vocal fold repair and regeneration. Titze and coworkers assessed the stiffness of the vocal fold ligament using a home-made tensile

tester. They found that the vocal ligament exhibits a nonlinear Young's modulus–strain relationship, with a Young's modulus ranging from 33 kPa at low strain up to 600 kPa at 40% strain [24]. This method is considered valid since the vocal ligament experiences cyclic tensions at low frequencies of 1–10 Hz [25]. A commercially available, parallel-plate rotational rheometer has been utilized to measure the mucosa viscoelastic properties [26]. The results show that elastic shear modulus of the human vocal fold mucosa varies from 10 to 1,000 Pa at frequencies of 0.01–15 Hz. Within this frequency range, the dynamic viscosity of the tissue decreases monotonically with frequency. Since the vocal fold vibrates at frequencies well above 100 Hz, these low frequency data may not accurately depict the true viscoelasticity of the tissue. To overcome this limitation, a strain-controlled torsional rheometer was introduced, thus extending the upper frequency limit to 50 Hz [27]. The results are consistent with the previous measurements.

Rheometric tests are based on the assumption that the stress is uniform throughout the thickness of the sample. For soft tissues such as vocal fold LP, such an assumption is only valid at frequencies well below the lower limit of phonation frequency [28]. Although other methods have been developed to measure the viscoelastic properties of materials at high frequencies [29, 30], they either do not allow the direct measurement of the shear modulus or are not compatible with the small, thin sample geometries of the vocal fold tissue [31]. An alternative technique has been invented by Clifton and Jia, treating the deformation of the sample as a wave propagation problem [31–33]. Referred to as the torsional wave analysis (TWA), this method allows the measurement of viscoelastic properties of soft materials, including thin vocal fold tissues, at frequencies of 20–2,000 Hz.

In a typical setup, a thin cylindrical sample is mounted between two hexagonal plates. The assembly is enclosed in an environmental chamber to maintain the temperature and relative humidity at in vivo conditions. The bottom plate is subjected to small oscillations by means of a galvanometer driven by a frequency generator that steps through a sequence of frequencies. The motion of the top and the bottom plates is monitored by a laser passing through a series of optical lenses. The optical signal is collected by a photodiode detector and processed by an oscilloscope (Fig. 10.2). At each frequency, measured rotations of the top and bottom plates are used to determine the ratio of the amplitudes of the rotations of the two plates. Comparison of the frequency dependence of this ratio with that predicted for torsional waves in a linear viscoelastic material allows the storage modulus and the loss angle (δ), in shear, to be calculated by a best-fit procedure. The reliability of this method has been validated theoretically and experimentally [31, 32, 34]. TWA has been applied to measure the viscoelastic properties of the native vocal fold tissues, as well as the hydrogel replacement materials at human phonation frequencies [31, 33–36]. Accumulated data on porcine vocal folds indicate that the newborn piglets have a softer vocal fold LP, with an average elastic modulus in the range of 250–315 Pa. The vocal fold LP becomes stiffer as the animal matures; the measured elastic modulus for pigs 2–3 years of age varies from 1,000 to 3,000 Pa. The elastic modulus of human vocal folds from donors 60–90 years old (collected from National Disease Research Interchange, NDRI) lies

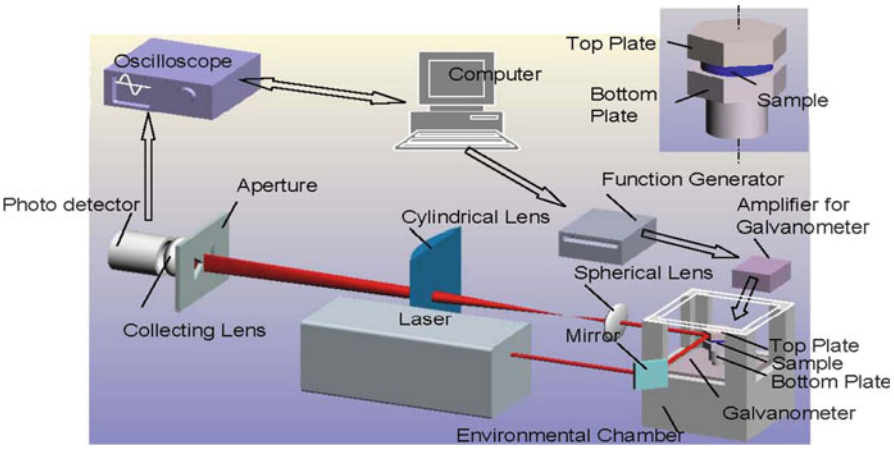

Fig. 10.2 Schematic representation of the experimental setup for torsional wave analysis.[31] Copyright permission from Springer

in the range of 500–1,700 Pa. When compared with the synthetic hydrogels, vocal fold tissues are significantly more viscous, with a tan(δ) value generally greater than 0.2. A perfect elastic hydrogel material has a tan(δ) close to zero. Combining TWA and histological analysis, we are constructing a database correlating the viscoelastic properties of vocal fold tissues with their composition and organization.

Vocal Fold Disorders

Voice plays a defining role in human social life. It is essential for a good quality of life and is indispensible for about 25% of the American working population. The occupations at the greatest risk for vocal fold disorders are singers, social workers, teachers, lawyers, clergy, and telemarketers [37]. An estimated 3–9% of Americans are affected by voice disorders [37]. Vocal folds can be damaged by intubation, traumas, radiation, voice overuse and abuse, esophageal reflux, chemical exposure, frequent cold/sinus infections [38], surgical treatments of benign lesions and infectious and malignant lesions [25, 39]. The susceptibility to vocal fold disorders varies depending on gender, age, and voice use patterns and demand.

Vocal Fold Scarring

Vocal fold scarring represents the leading cause of voice impairment [39], and the SLP is particularly prone to scarring [40]. The decreased pliability and increased

stiffness associated with the scar tissues hinder the ability of vocal folds to vibrate readily and continuously. Located at the edges of the vocal folds, the scar tissue prevents the full closure of the vocal folds and disrupts the normal vibrational patterns [41]. Microscopic changes in the vocal fold LP are responsible for the increased stiffness and reduced pliability of the mucosal tissue [41]. Comprehensive understanding of vocal fold scarring and wound healing are essential to the development of novel biomaterials for the restoration of the vibratory functions of damaged vocal folds.

The vocal fold wound healing responses, ranging from regenerative healing to pathological scarring, depend on the cause of injury [25]. Unlike most soft tissues in the human body, vocal folds are subjected to high-impact collisions on a regular basis. Despite this high mechanical demand, the vocal fold function is not easily compromised. This apparent resistance to mechanical stress originates from the LP's unique composition and structure, and the tissue's limited capacity to repair itself. All normal vocal fold LP contain differentiated fibroblasts (myofibroblasts) with reparative properties [2]. The SLP has the highest myofibroblast density, and the number of myofibroblasts decreases as the tissue depth increases [2]. In fact, the epithelium and the SLP are competent at repairing microscopic injuries without either engaging a full-scale wound healing response or compromising the normal tissue function. However, when the scars reach a macroscopic scale, or when vocal fold self-repair mechanism is inhibited (as in the case of a chronic exposure to injurious stimuli), serious vocal fold pathologies will develop [2, 42].

Acute phonotrauma, caused by voice overuse, usually resolves on its own. The injury causes vascular network disruption, damages the basement membrane zone, and disrupts the ECM homeostasis. Patients present vocal fold edema (or laryngitis) and inflammation at the site of greatest stress. The healing response usually manifests as an increase in inflammatory mediators such as interleukin 1β (IL-1β), tumor necrosis factor α (TNF-α), and matrix metalloproteinase 8 (MMP-8). If the acute phonotrauma persists, it becomes chronic. In this case, the tissue is in a permanent tissue repair and scarring state. The edema of the acute phonotrauma is then replaced by a benign vocal fold lesion and/or a scar. Examples of those lesions are nodules, polyps, and cysts. While nodules are the result of a disruption of the basement membrane zone with a separation of the epithelium from the ECM, polyps appear as a more vascular injury, with less fibronectin deposition and less basement membrane disruption [42]. Chemical injuries caused by inhalation of chemical irritants such as cigarette smoke or gastroesophageal reflux, usually cause a vast diffuse vocal fold edema. This edema is associated with hemorrhage, increased fibronectin deposition, and thickening of the basement membrane zone [42]. Most of those benign lesions can be resolved by treating the underlying cause combined with speech therapy [25]. Carefully selected patients that do not respond to those treatments may be candidates for phonomicrosurgery [25]. Non-phonatory mechanical trauma is another important cause of vocal fold injury. Intubation and complications from benign lesion removal by phonomicrosurgery can both lead to permanent vocal fold scarring.

Biochemistry of Vocal Fold Scars

To develop effective methods for the prevention and the treatment of vocal fold scarring, it is important to understand the histological differences that lie between scarred and normal vocal fold tissues, as well as the roles that ECM molecules play during the wound healing process. Inspections of the scarred animal vocal fold tissues reveal the presence of dense and disorganized collagen deposition, decrease or total loss of elastin, increase of fibronectin, decrease or unchanged amount of HA, and decrease of decorin and fibromodulin compared with the uninjured controls [39, 43–47]. A recent study on human vocal folds confirmed the excessive deposition of collagen, and decrease of decorin in the scarred tissues [43]. Immediately after the injury, there is a rapid increase in collagen production for up to 4 weeks. Thereafter, the collagen synthesis starts to decline [48]. Initially, collagen fiber bundles are fine, but progressively become thicker and more organized during the wound healing and tissue remodeling process. This collagen maturation can last from 20 days to 1 year. In contrast to collagen, elastin is found to be significantly less present in scarred VF tissue, thus accounting for the poor elasticity of the latter [44].

In addition to being a key factor in controlling the viscoelastic properties of the vocal folds, HA plays a wide variety of roles in all steps of wound healing. In the early phase of inflammatory response, HA is abundant in the tissues, acting as a promoter and a mediator of inflammation. Soluble fragments of HA upregulate the expression of a few cytokines and induce the expression of inflammatory genes in macrophages. HA's presence in granular tissues is correlated to its role to facilitate cell migration, cell proliferation, and matrix organization. HA accomplishes its unique biological functions through its unique physicochemical properties and its specific interactions with cells and ECM molecules such as collagen and fibrin. In spite of HA's important role in wound healing, there is no significant difference in its content between the scarred and the healthy vocal folds [44]. Although HA production peaks 48–72 h after injury in adult wounds, it quickly falls back to normal or below thereafter [41]. In contrast, in fetal wounds, HA is present at high levels for weeks. This high content of HA in fetal wounds, combined with the ability of HA to suppress collagen synthesis, is thought to be responsible for the scarless nature of fetal wound healing [49, 50]. Finally, fibronectin's increase in scar tissue seems to be directly related to its essential wound healing properties [14, 16, 51]. Its mediating role is particularly critical in basement membrane zone repair and reepithelialization [47].

As a result of the structural and compositional changes, the rheological properties of scarred vocal folds are distinctly different from those of the normal tissues. The scarred vocal fold LP exhibits an increase in elastic shear modulus and the dynamic viscosity, thereby impairing its normal vibratory function [44]. It is important to note that the alteration of the mechanical properties of the scarred vocal folds is just a result of changes in the concentration of various ECM molecules; the disruption of the normal relationship between ECM molecules and their organization also contributes to the stiffness and viscosity increase in the scarred vocal folds.

Tissue Engineering Strategies for Vocal Fold Repair and Regeneration

Clinically available treatment methods for vocal fold disorders include voice therapy, injection laryngoplasty, phonomicrosurgery, and framework surgery [41, 52]. While voice therapy is effective in treating mild vocal fold abnormalities, laryngoplasty and framework surgery are commonly applied to treat vocal fold paralysis. For the treatment of vocal fold scarring, increasingly precise phonosurgical techniques and microinstrument innovations have been developed [53, 54]. Unfortunately, these techniques will only be minimally successful unless coupled with synthetic SLP substitutes. To date, optimal treatment for vocal fold scarring has not yet been realized, and new approaches need to be considered to restore the properties of the scarred vocal fold to normal.

Tissue engineering holds great promise in reestablishing normal vibratory characteristics to the damaged vocal folds, ultimately helping patients regain their normal voice. Two basic paradigms for vocal fold tissue engineering can be employed. The first method is based on a minimally invasive technique whereby smart, responsive, and multifunctional biomaterials are directly injected into the damaged vocal folds so as to afford in vivo synthesis of vocal fold ECM. The second method relies on in vitro functional tissue formation by the appropriate combination of cells, artificial scaffolds, biological cues, and mechanical stimulation. A combination of both approaches will likely be critical for addressing the significant challenges posed by the tissue engineering of functional vocal folds. The field of vocal fold tissue engineering is a fertile area that promises to bring exciting discoveries and help reestablish normal vibratory characteristics to damaged vocal folds.

In Vivo Vocal Fold Treatment

Traditionally, injection laryngoplasty is applied to increase the bulk of the vocal folds, improve the glottal closure, and alter the shape of the larynx, with the vocalis muscle being the common injection site [55]. These approaches are not regenerative in nature, and its long-term efficacy has been limited due to the implant migration and resorption, chronic inflammation and foreign body reactions induced by various implant materials that include Teflon [56, 57], calcium hydroxylapatite [58], polydimethylsiloxane (PDMS) [59], polypropylene [60], fascia [61], fat [62], and collagen [63, 64]. In the context of vocal fold repair and regeneration, we limit our discussions to the direct injection of bioactive molecules, cells, biomaterials, or their combinations to the vocal folds using minimally invasive procedures.

Growth Factor Therapy

Due to their critical roles in modulating the wound healing process, many growth factors have been used as therapeutic agents for the treatment of vocal fold scarring,

by direct injection to the injured vocal folds. The proven antifibrotic activity of HGF in liver cirrhosis and lung fibrosis has motivated Ford and coworkers to investigate the effects of HGF injection (with or without normal vocal fold fibroblasts) into scarred vocal folds in a canine model. The HGF group presented much better results than both the sham (saline injection) and the fibroblast/HGF groups in terms of mucosal wave amplitude and incidence of vocal fold bowing, glottal incompetence, and phase asymmetry. The histological data suggest that the HGF injection prevents excessive collagen deposition and tissue contraction, thus reducing the effects of scarring on the vibratory properties of the vocal folds [65]. Similar studies using rabbit models confirmed previous observations. Moreover, rheological analysis showed that the HGF treatment helps to maintain the viscoelastic shear properties of the vocal fold [66]. In vitro studies show that HGF stimulated the production of HA and decreased the production of collagen type I from the cultured fibroblasts, whereas fibronectin production was not affected [67, 68].

Basic fibroblast growth factor (bFGF), known to stimulate fibroblast growth and HA production, has been shown to restore the viscoelastic properties of vocal folds in various animal models [69, 70]. In a recent human studies, Hirano et al. [69, 71] treated patients with atrophied aging vocal folds by unilateral bFGF injection. A significant improvement of aged vocal fold properties, with respect to mucosal vibration, glottal closure, and voice quality, has been demonstrated. The beneficial effects are attributed to the rapid bioactivity of bFGF that triggers many downstream biological mechanisms, altering vocal fold tissue properties a week after the treatment [71]. Collectively, these studies suggest the therapeutic potential of growth factor injection in the prevention and the treatment of vocal fold scarring.

The short half life and high diffusivity of growth factor molecules necessitate the utilization of a drug delivery system to prolong their therapeutic effects. Direct injection of HGF-laden, glutaraldehyde-crosslinked gelatin to the scarred dog vocal folds has resulted in an enhanced mucosal movement and reduced scar formation 3 months later, highlighting the potential of a HGF delivery system in the treatment of chronic vocal fold scarring [72]. Although this study represents a step forward in the growth factor therapy, the hydrogel materials utilized do not provide ideal growth factor release kinetics at the injection site. As discussed above, the wound healing process is tightly controlled by various cytokins and chemokins that are released by specific type of cells at the specific time and tissue location. Later in this chapter, we discuss our efforts in engineering growth factor delivery systems that recapitulate the scenario occurring in nature.

Injectable/Implantable Biomaterials for the Treatment of Vocal Fold Scarring

Although temporary relief has been observed after various growth factor injections in animal models, long-term repair has not been accomplished. Injectable biomaterials are attractive alternatives for the treatment of vocal fold scarring. Biomaterials designed for in vivo vocal fold repair should be injectable or readily

implantable using minimally invasive procedures. Once injected, the material must fill up the space, take up a defined geometry and smooth the edges of the vocal folds. The materials must exhibit matching viscoelasticity to the native tissue at the injection site and maintain their structure and properties during phonation. The injectable materials should be biocompatible and remain at the site of injection for a prolonged period of time (preferably more than 6 months) without inducing chronic inflammatory responses. To imitate the active tissue repair process, the biomaterials should be engineered to foster cell infiltration and enhance the scarless wound healing process.

For in vivo vocal fold repair, HA-based matrices are the most attractive candidates and have dominated the field because of HA's relevance in vocal fold physiology, wound healing, and biomechanics, as well as its biocompatibility and non-immunogeneity, unique viscoelastic properties, commercial availability and the presence of readily accessible reactive handles for chemical modification and covalent crosslinking. In the following sections, we discuss various HA-based hydrogels and insoluble meshes, either commercially established or under development, for in vivo repair of the scarred vocal folds.

Commercially Available HA-Based Materials

Prophylactic use of HA or chemically modified HA derivatives has produced favorable results in terms of vocal fold repair and subsequent functional recovery [73]. Hylaform, a divinyl sulfone crosslinked HA gel, is commercially available and has been injected into the vocalis muscle/vocal ligament of patients with glottal insufficiency. Superior vocal fold status was observed 1 year after the initial treatment [74]. However, the underlying mechanism for the long-lasting effect is unknown. Restylane, a 1,4-butanediol diglycidyl ether crosslinked HA gel, has been applied to treat vocal fold immobility; temporary medialization in animal models [75] and in patients has been observed [76].

Another category of commercial HA derivatives that has been tested in clinical settings is HYAFF produced by esterification of the carboxylic acid groups of HA. Depending on the chemical structure of the ester group and the degree of esterification, the products exhibit varying water solubility and in vivo residence time [77]. Finck et al. implanted the fibrous mesh of HYAFF 11, 100% benzyl ester of HA, into the LP of human patients after microdissection and removal of benign lesions. The meshes remained at the implantation site for an estimated 2–6 weeks. The implants are reported to be well tolerated by the majority of the patients with no evidence of scarring. Patients treated with HYAFF 11 showed an overall improvement in vocal performance [78]. It is unclear, however, whether the benign lesions returned after the implant was completely resorbed.

A novel HA-based, synthetic extracellular matrix (sECM) system, originally developed in the Prestwich lab at the University of Utah, is composed of di(thiopropionyl) bishydrazide-modified hyaluronic acid (HA-DTPH), di(thiopropionyl) bishydrazide-modified gelatin (Gln-DTPH), and poly(ethylene glycol) diacrylate (PEGDA).

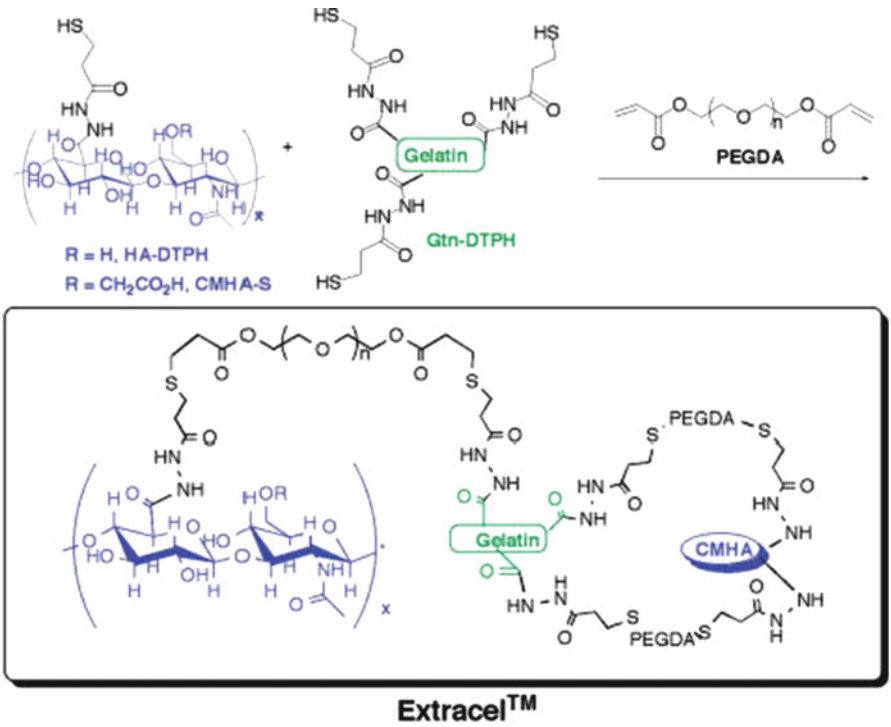

Fig. 10.3 Formation of Extracel™ by the covalent crosslinking of HA-DTPH, Gln-DTPH, and PEGDA [79]. Copyright permission from the American Chemical Society

HA-DTPH can be further stabilized against enzymatic degradation by hyaluronidase using carboxymethylated HA (Fig. 10.3, CMHA-S). Under appropriate conditions, crosslinking occurs through a Michael-type addition reaction between the thiol and the acrylate groups. Mixing of HA-DTPH, Gln-DTPH, and PEGDA results in the formation of viscoelastic gels; no toxic by-products are produced during the crosslinking [79]. The cytocompatible nature of the soluble precursors and the crosslinking chemistry permits in situ cell encapsulation and in vivo implantation. The mechanical properties of the hydrogels can be varied by changing the concentrations of each component and their relative ratio. This type of sECMs has been recently commercialized by several companies using different trade names. Carbylan-SX™ refers to CMHA-S crosslinked by PEGDA, and Carbylan-GSX™ refers to the product containing CMHA-S, Gtn-DTPH, and PEGDA. Extracel™ is reserved for products used for 3D in vitro culture, as well as in vivo and in vitro tissue engineering. These novel modular sECMs have been shown to support the attachment, growth, and proliferation of a great variety of cells in a 3D environment. In vivo studies also prove its efficacy in the engineering and repair of both soft and hard tissues [80–82].

Hansen et al. studied the effects of the Carbylan™ HA hydrogels on the tissue repair of rabbit vocal folds. Bilaterally biopsied rabbit vocal folds were injected with

Carbylan™-SX, HA-DTPH crosslinked by PEGDA and saline. Histological, biochemical, and biomechanical evaluations of the vocal folds 3 weeks after the treatment showed that Carbylan™-SX induced significantly less fibrosis than the saline-treated controls; tissue elasticity and viscosity were improved in this group as well [83]. In a parallel study, Duflo et al. compared the short-term (3 weeks after injection) effects of Carbylan™-GSX and Carbylan-SX in the repair and regeneration of rabbit models upon biopsy [84]. Although both Carbylan-SX and Carbylan-GSX significantly improved tissue elasticity and viscosity, elevated hyaluronidase mRNA levels were detected only in the Carbylan-GSX (with 20% w/w gelatin)-treated groups. Another recent study focused on the late effects of HA-Gln gels in the remodeling of the scarred vocal folds. Extracel™ was injected into the biopsied rabbit vocal folds. Six months post-injection, similar therapeutic effects, in terms of tissue fibrosis, transcription levels of ECM molecules and tissue biomechanics, were observed [85].

To further enhance the therapeutic potential of the Extracel™ products, human bone marrow-derived, mesenchymal stem cells (MSCs) were mixed with the soluble components before being injected into scarred rat vocal fold LP. After 1 month of repeated unilateral injections, quantitative PCR analysis and immunofluorescence characterization revealed that the MSCs embedded in sECM exhibited elevated levels of procollagen-III, fibronectin, TGF-β1, hyaluronidase, and decreased levels of smooth muscle actin (SMA) gene expression compared with MSCs alone controls. The embedded MSCs survived the injection and continued to grow 1 month after the injection. This evidence suggests that injected MSCs–sECM mixture is conducive to vocal fold ECM remodeling [86]. In summary, the injectable Extracel™ can provide therapeutic effects to the scarred vocal folds by improving the tissue viscoelastic properties and providing a benign environment for vocal fold wound healing.

Novel HA-Based Materials Currently Under Development

There are some limitations associated with the commercial HA-based matrices. For example, the crosslinking chemistries for Hylaform and Restylane are not compatible with cells and tissues. Hydrogels have to be synthesized prior to the injection. The commercial products are in fact dilute suspensions of mechanically fragmented hydrogel particles (HGPs). Consequently, the injectable formulations may not exhibit the desired mechanical properties. Moreover, the chemistries do not permit ready adjustment of the crosslinking density, thus the in vivo residence time of the gels cannot be prolonged on demand. The Extracel™ technology overcomes many of the limitations associated with the traditional HA hydrogels in that gels with the desired viscoelasticity [87] can be formed in situ at the injection site and that the gel stiffness can be modulated by varying the concentration of the constituent building blocks. Depending on the formulation, gelation occurs within 5–30 min through the addition reaction between the thiol and the acrylate groups [81].

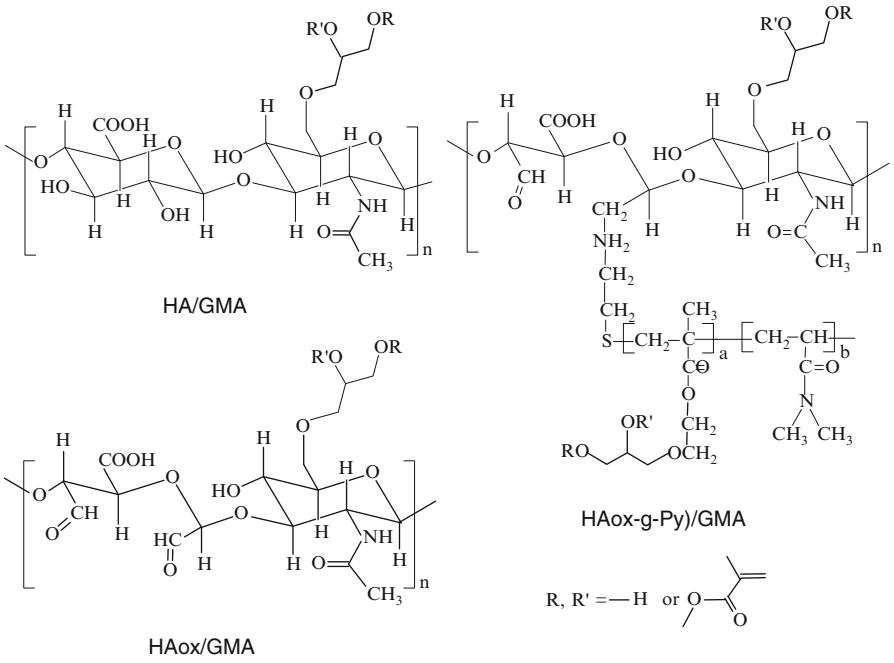

Fig. 10.4 Chemical structures of HA-based photocrosslinkable macromonomers. y%: grafting density. Revised from Ref. [33]

An alternative chemistry at our disposal is photochemically induced radical polymerization. Photocrosslinking is particularly attractive because the liquid precursor can fill irregular tissue defects and becomes solidified within minutes of UV irradiation. The UV light can be delivered locally to the vocal fold LP using a minimally invasive surgical procedure and the viscoelastic properties of the resultant gels can be readily tuned to match those of the normal tissue. Jia et al. have developed a photocrosslinkable hydrogel system using a synthetic polymer-grafted HA as the soluble precursor [33]. The conjugation of synthetic polymers to HA offers a versatile method to fine tune the properties of the resulting copolymer. The synthetic polymer employed was oligomeric random copolymers of 2-hydroxyethyl methacrylate (HEMA) with *N*,*N*-dimethylacrylamide (DMAM). The resulting graft copolymers were referred to as (HAox-g-Py) (y%: grafting percent) (Fig. 10.4). HA and oxidized HA (HAox) were included as the controls. Modification of these polymers with glycidyl methacrylate (GMA) rendered them radically crosslinkable. Hydrogels were obtained by subjecting the aqueous macromonomer solutions to UV irradiation in the presence of a photoinitiator. Grafting of 1.9 mol% P(HEMA-*co*-DMAM) to the oxidized HA reduced the hydrogel swelling and improved their enzymatic stability, and at the same time increased the gel stiffness. NIH 3T3 fibroblasts photoencapsulated in the HA-based networks remained viable immediately after encapsulation and after 3 and 7 days of culture, demonstrating the compatibility of hydrogels derived from (HAox-g-P1.9)/GMA.

The HA hydrogels discussed so far are macroscopic polymer networks derived from molecularly dispersed, soluble precursors (monomers and multifunctional crosslinkers or macromers) that are randomly interconnected, lacking the structural complexity, mechanical integrity, and functional diversity seen in the natural ECM. In most cases, increasing crosslinking density results in hydrogels with desirable enzymatic stability. Unfortunately, the pliability of the hydrogels is compromised, i.e., gels become too stiff relative to the target tissue. The inability to control the degradation profiles and mechanical properties of the hydrogels independently limits their utility in vocal fold tissue engineering. To overcome this limitation, the Jia group at the University of Delaware has developed HA-based doubly crosslinked networks (DXNs) using HA hydrogel particles (HGPs) as the microscopic crosslinkers [34, 35, 88]. We have developed techniques for the production of HA-based, covalently crosslinked HGPs of micron to submicron dimensions. In our initial study, HA HGPs with an average diameter of 10 μm (HGP10) were prepared by crosslinking HA derivatives carrying hydrazide (HAADH) and aldehyde (HAALD) functionalities [89] within the inverse emulsion droplets (water in mineral oil) stabilized by Span 80 [35]. In a follow-up work, Jha et al. were able to decrease the particle size down to 0.9 μm (HGP0.9) by crosslinking HA with divinyl sulfone employing a sodium bis(2-ethylhexyl)sulfosuccinate) (AOT)/isooctane reverse micelle system in the presence of 1-heptanol [34, 88]. While HGP10 exhibit residual functional groups (aldehyde and hydrazide) after the synthesis, sodium periodate oxidation was used to introduce aldehyde groups to HGP0.9. Alternatively, modification of HGP0.9 with GMA rendered the particles photocrosslinkable (HGP0.9-GMA) without altering their sizes significantly [90]. All three types of particles are nanoporous and cytocompatible; they are significantly more stable against enzymatic degradations than their respective macroscopic gels of the same chemical make-up.

The reactive groups in HGPs (aldehyde or methacrylate) were used as reactive handles for subsequent crosslinking with an HA derivative containing hydrazide (HAADH) or methacrylate groups (HAGMA). The resultant macroscopic gels contain densely crosslinked, nanoporous HA HGPs covalently interconnected by a loose secondary network that is also HA-based, thereby hierarchical in nature (Fig. 10.5). The viscoelasticity of the DXNs can be readily modulated by varying the particle size, their surface functional group, intra- and inter-particle crosslinking. The hydrogel viscoelasticity was quantified at low frequencies (0.1–10 Hz) using a controlled stress rheometer and at high frequencies (up to 200 Hz) with a home-built torsional wave apparatus. The DXNs are stable, elastic gels that become stiffer at higher frequencies; the dynamic viscosity decreases linearly with frequency in log–log scale. The mechanical characteristics of DXN are similar to that of vocal fold lamina propria. A close inspection of the cryoSEM image (Fig. 10.5) for DXNs indicates a diffuse interphase between individual oxHGPs and the matrix, which proves that the secondary network originates from the particle surface. As a result, the secondary network can exert mechanical constraints on the HGPs, leading to the deformation of HGP through the covalent linkage between the secondary network and the HGP surface.

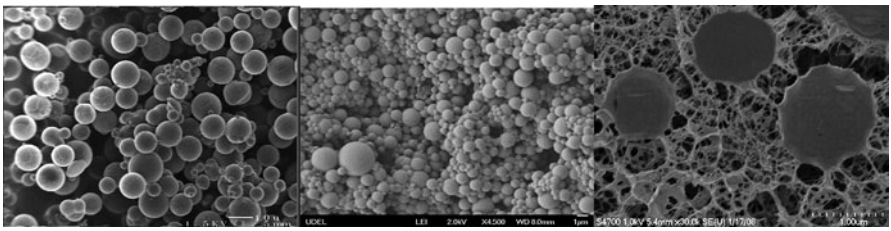

Fig. 10.5 Scanning electron micrographs of HA hydrogel particles (*Left*: HGP10; *Middle*: HGP0.9) and cryogenic scanning electron micrograph (cryoSEM) of HA DXN (*right*) [34, 35, 88]. Copyright permission from the American Chemical Society and Brill

We are interested in utilizing HA-based HGP for the treatment of vocal fold scarring, not just as an inert filler material, but instead as smart entities that can actively remodel the scar tissue. As discussed above, injection of growth factor solutions into vocal folds does not lead to long-lasting therapeutic effects. It is well known that the biological activity of growth factors depends not only upon its identity, but also upon how it is presented to the cells in space and over time [91]. In the HA DXN system, the controlled release of pharmaceutically active compounds can be achieved through their anchorage at predetermined locales of the particulate hydrogel system. For example, when model drug molecules of low and high molecular weights (rhodamine 6 G: R6G; bone morphogenetic protein 2: BMP-2) were loaded into HGPs prior to the formation of DXNs, a near zero-order release kinetic with minimal initial burst has been observed [88, 90].

In the native ECM, growth factors are stored as an intact, latent complex through their specific binding to ECM molecules including heparan sulfate proteoglycans (HSPGs). HSPGs, alone or through their specific binding with heparin binding growth factors, effectively modulate cellular growth, development, angiogenesis, and tissue regeneration [92]. To emulate this feature in vitro, we [93] covalently immobilized domain I of perlecan (PlnDI), an important HSPG expressed in many ECM and basement membranes, to HA HGPs through a flexible PEG linker. When compared with HGPs without PlnDI, PlnDI-conjugated HGPs (HGP-P1) exhibited significantly higher BMP-2 binding capacity and distinctly different BMP-2 release kinetics. Heparitinase treatment increased the amount of BMP-2 released from HGP-P1, confirming the HS-dependent BMP-2 binding. While BMP-2 was released from HGPs with a distinct burst release followed by a minimal cumulative release, its release from HGP-P1 exhibited a minimal burst release followed by linear release kinetics over 15 days. The bioactivity of the HGPs was evaluated using micromass culture of multipotent MSCs, and the chondrogenic differentiation was assessed by the production of glycosaminoglycan, aggrecan, and collagen-type II. Our results revealed that BMP-2-loaded HGP-P1 stimulates more robust cartilage-specific ECM production as compared to BMP-2-loaded HGP, due to the ability of HGP-P1 to potentiate BMP-2 and modulate its release with near zero-order release

kinetics. Although R6G and BMP-2 are not applicable to the repair and regeneration of vocal folds, the technology we have developed can be readily translated to physiologically relevant molecules such as HGF and bFGF.

In Vitro Vocal Fold Tissue Engineering

In vitro tissue engineering aims to regenerate functional tissues or organs via the strategic combination of polymeric scaffolds, viable cells, biological factors, and biomechanical stimulations. The goal of vocal fold tissue engineering is to recapitulate the vocal-like microenvironment in vitro so that cells residing in the artificial matrices can maintain the vocal fold fibroblastic phenotype, readily proliferate and produce an ECM that is structurally and compositionally similar to that of the native tissue. Functional vocal fold tissue engineering relies on the rational investigation of the roles of biological and mechanical factors in tissue repair and regeneration [94]. The engineered tissue will then be implanted in the body, as a replacement for the injured one. While cells are the major players in this process, artificial matrices are indispensible for initiation of the proper cellular responses.

Biomaterials as Vocal Fold Tissue Engineering Scaffolds

Polymeric scaffolding to be used as the transient artificial ECM should (1) be biocompatible and cell adhesive; (2) exhibit mechanical responses comparable to the natural tissue; (3) be able to sustain repetitive high frequency vibration without fatigue; (4) effectively transmit forces from the environment to the growing tissue over prolonged periods of time; (5) have a degradation profile that mirrors the ECM deposition; and (6) exhibit a spatial and temporal distribution of biological cues. Many of the hydrogels described above for use as injectable materials have also been evaluated for their potential in in vitro tissue engineering. For example, Chen et al. assessed the potential of Carbylan-GSX in vocal fold wound repair and tissue regeneration using the immortalized human vocal fold fibroblasts (see below). When compared with cells cultured in Matrigel, similar morphology, cell marker protein expression, proliferation, viability and apoptosis of the immortalized cells were observed with Carbylan-GSX after 1 week of in vitro culture. Gene expression levels for fibromodulin, transforming growth factor-beta I, and TNF-α were similar between Carbylan GSX and Matrigel. Fibronectin, hyaluronidase 1, and cyclooxygenase II expression levels were induced by Carbylan-GSX, whereas interleukins 6 and 8, Col I, and hyaluronic acid synthase 3 expression levels were decreased by Carbylan-GSX. While the immortalized cells adopted an elongated spindle-shaped morphology when cultured on the surface of Carbylan-GSX, they were spherical in shape, with the fibroblast marker clustered around the cell nuclei, after 72 h of culture in the gel [95].

Using readily available source materials, Hahn et al. investigated the ability of collagen-alginate and collagen-HA composite hydrogels to support the ECM synthesis by vocal fold fibroblasts. The composite gels are physical mixtures of collagen and HA (or alginate) without any covalent stabilization. Collagen-HA composites showed significant mass loss over 28 days of culture, with little evidence of new matrix production. Collagen-alginate composites, in contrast, resisted scaffold compaction and mass loss for at least 42 days in culture while allowing for ECM synthesis. The authors conclude that collagen-alginate hydrogels appear to be promising materials for vocal fold restoration [40].

The combination of chemically modified, covalently crosslinkable HA derivatives with self-assembling collagen monomers offers an attractive strategy to provide custom-made matrices that overcome the limitations associated with the use of matrices based on HA or collagen alone. Farran et al. developed two types of collagen/HA-based scaffolds for in vitro 3D culture of primary vocal fold fibroblasts [36]. These scaffolds differ from one another in terms of the chemical composition, structural organization, and mechanical characteristics. While type A gels were composed of self-assembled mature collagen fibers reinforced by HAALD, type B matrices contained immature collagen fibrils interpenetrated in an amorphous matrix formed by HAADH and HAALD. The encapsulated vocal fold fibroblasts attached to the matrix and proliferated over the 28 days of cell culture (Fig. 10.6). In addition, cells maintained their fibroblastic morphology, and expressed the genes related to ECM proteins present in vocal fold tissue. Type B gels retained lower amounts of collagen and higher amounts of HA than type A gels over the course of culture. Difference in the viscoelastic properties of the scaffolds have also been observed, but interestingly such difference was reduced over the course of culture. In fact, our results suggest the ability of the encapsulated fibroblasts to reorganize the matrices and modulate their viscoelastic properties. Comparison of the end point viscoelastic properties and histological structures of both scaffolds to those of porcine vocal fold tissues revealed striking similarities, implicating utility of these scaffolds for vocal fold tissue engineering.

For 3D cell culture, gelation should take place in the presence of homogeneously dispersed cells, thus entrapping them in a macroscopic network when the crosslinking (either physical or chemical in nature) is complete. In many synthetic hydrogel systems, intact ECM components (e.g. collagen) or fragments of cell adhesive domains, in combination with MMP sensitive peptide [96], have to be incorporated in the matrices to enhance integrin-mediated cell attachment in the matrix. In the absence of these bioactive components, however, the nanometer-scale mesh size of many synthetic crosslinked hydrogel networks restricts the encapsulated cells to a rounded morphology. Consequently, cellular processes such as proliferation and migration that are essential for the early stages of remodeling and tissue formation are severely inhibited. Webb and coworkers investigated an approach for accelerating cellular remodeling based on the creation of semi-interpenetrating networks (IPNs) composed of hydrolytically degradable PEGDA macromers and native, enzymatically degradable HA. Although both HA and PEG are well known for their non-adhesive properties, the addition of HA at

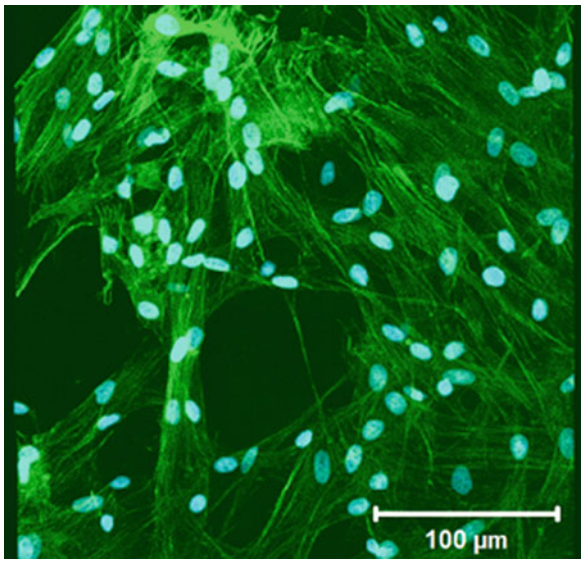

Fig. 10.6 Cytoskeleton staining of the cell–gel constructs cultured under static conditions for 14 days. F-actin (*green*) and nuclei (*blue*) were stained with phalloidin Alexa Fluor 488 and Draq-5, respectively [36]. Copyright permission from Mary Ann Liebert, Inc.

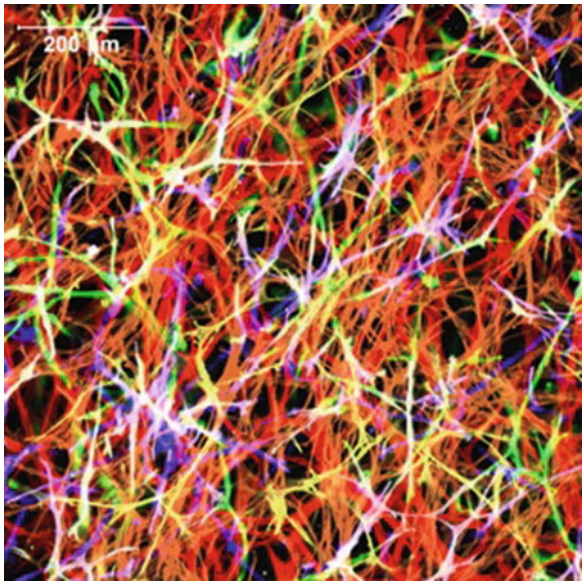

Fig. 10.7 Representative pseudo-colored composite of confocal image sections of fibroblasts at varying depths within 6% w/v w/v PEG-bis-AP-based semi-IPN containing 0.12% w/v hyaluronic acid after 14 days in culture. Color scheme – *red* (0 µm), *orange* (100 µm), *yellow* (200 µm), *green* (300 µm), *pink* (400 µm), and *blue* (500 µm).[97] Copyright permission from Elsevier

concentrations of 0.12% w/v and greater supported fibroblast spreading throughout the three-dimensional network (Fig. 10.7) and significantly increased proliferation relative to control hydrogels without HA. Incorporation of HA resulted in relatively small changes in hydrogel physical/chemical properties such as swelling, degradation rate, and elastic modulus. Fibroblast spreading was eliminated by the addition of hyaluronidase inhibitors, demonstrating that cell-mediated enzymatic degradation

of HA is a necessary mechanism responsible for the observed increases in fibroblast activity. By tailoring the mechanical properties of the hydrogel matrix, at the same time, accelerating early cellular remodeling and growth these semi-IPNs may be useful vehicles for cell transplantation in vocal fold tissue engineering applications [97].

HA-based hydrogels complemented with collagen and/or biocompatible synthetic polymers have been the dominating choice of materials so far. There exist a wide variety of other synthetic materials that have been proven promising as tissue engineering scaffolds. Particularly, a 15 amino acid-long, facially amphiphilic peptide has been commercialized as PuraMatrix™ by BD Bioscience for 3D cell culture purposes. This peptide contains alternating hydrophilic and hydrophobic amino acid residues. The hydrophilic residues, in turn, alternate between being positively and negatively charged. Upon exposure to cell-culture media, the peptide self-assembles into β-sheets that further stack to form double-walled nano-ribbons, which further entangle physically to form macroscopic gels. The resulting hydrogels contain nanofibers of 7–10 nm in diameter, and 50–400 nm sized nanopores, reminiscent of the morphological characteristics of natural ECM. Despite their low mechanical strength, these hydrogels have been used for the 3D culture of vocal fold fibroblasts in a condition medium containing various growth factors including TGF-β1, bFGF, or HGF. After 21 days of cultures, it was found that TGF-β1 induced matrix contraction and enhanced collagen and sulfated glycosaminoglycan production, bFGF effectively increased cell proliferation, and HGF stimulated synthesis of hyaluronic acid and elastin with less collagen accumulation than other conditions. It was concluded that HGF is most useful for stimulating essential tissue components for restoring vocal fold pliability [98].

One of the major limitations of the materials discussed above is their low mechanical strength. Abundant literature suggests that mechanical signals have profound effects on cellular functions including growth, differentiation, apoptosis, motility, and gene expression [99]. Furthermore, cells are known to preferentially differentiate on artificial extracellular matrices that have mechanical stiffness similar to that of their natural tissues [100, 101]. These discoveries underscore the importance of engineering hydrogel matrices with high strength and appropriate elasticity to maintain the desired cell phenotype and to effectively transmit the external mechanical forces to the encapsulated cells [102, 103]. This is particularly important for the engineering of the most mechanically active tissue in the human body.

Our group has developed elastomeric hydrogels by mimicking the molecular architecture and mechanical properties of natural elastin. Elastin achieves its excellent mechanical properties through a multiblock copolypeptide structure composed largely of two types of short segments that alternate along the polypeptide chain: highly flexible hydrophobic segments composed of VPGVG repeats, with many transient structures that can easily change their conformation when stretched; and alanine- and lysine-rich α-helical segments, which form crosslinks between adjacent molecules via the action of lysyl oxidase in the ECM [104]. Our strategy involves the synthesis of multiblock hybrid polymers consisting of flexible synthetic polymers alternating with alanine-rich, lysine-containing peptides that are the

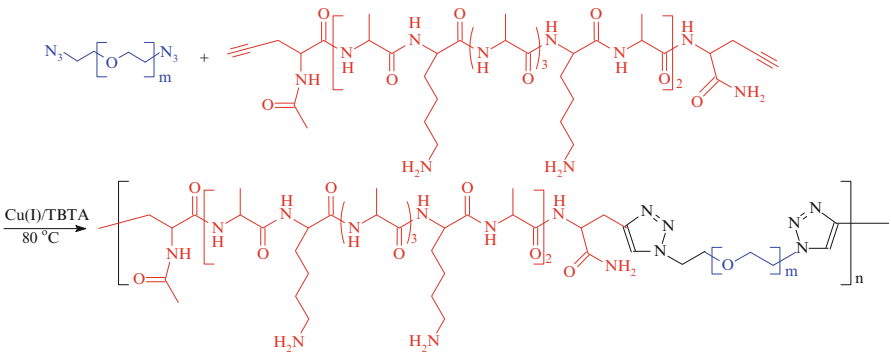

Fig. 10.8 Elastin mimetic hybrid polymer (EMHP) synthesized by step growth polymerization using orthogonal click chemistry [107]. Copyright permission from the American Chemical Society

structural component of the hydrophilic crosslinking domains of natural elastin (Fig. 10.8) [105]. Specifically, multiblock elastin mimetic hybrid polymers were synthesized via a condensation polymerization approach employing orthogonal click chemistry using azide-functionalized, telechelic PEG and alkyne-terminated peptides [X(AKAAAKA)2X, X: propargyl glycine, A: alanine, K: lysine] as the macromonomers. Covalent crosslinking of the resulting multiblock copolymers by hexamethylene diisocyanate (HMDI) was achieved universally through the lysine side chains of the peptide domain to form urea linkages. When compared with the dry samples, the fully swollen hybrid hydrogels are softer and more compressible, consistent with results observed for natural elastin [106]. Moreover, the hybrid hydrogels exhibit similar compressive properties to a hydrophobic polyurethane elastomer (Tecoflex™ SG80A) widely used for tissue engineering applications. The elastin mimetic hybrid hydrogels are capable of rapid recovery from mechanical stress, as evidenced by the remarkable overlapping loading–unloading curves in the cyclic compression tests. To promote integrin-mediated cell adhesion to these gels, fibronectin-derived GRGDSP domains have been included in the peptide building blocks. Human neonatal foreskin fibroblasts are able to attach and proliferate readily on RGD-containing, HMDI-crosslinked copolymers. The modular nature of the design, coupled with the chemical nature of the synthesis, permits facile adjustment of mechanical, morphological, and biological properties of the resulting polymers [107]. Although the elastin mimetic hybrid copolymers have desirable material properties, their production requires multi-step chemical transformations and solid phase peptide synthesis, thus making it difficult to scale up.

Cell Source

Currently, available cell sources for vocal fold tissue engineering include mature vocal fold fibroblasts, immortalized vocal fold fibroblasts and multipotent MSCs.

The use of primary vocal fold fibroblasts of human origin has been problematic because normal vocal fold is difficult to obtain without compromising the integrity of the tissue, and if obtained, the number of cells is hardly sufficient for tissue engineering purposes. Under current in vitro conditions, human vocal fold fibroblasts possess a relatively short replicative life span. After a series of population doublings, primary cells enter a state where they no longer divide, marked by distinct change in cell morphology, gene expression, and metabolism. Recently, Thibeault and coworker developed the immortalized human vocal fold fibroblasts by transducing primary vocal fold fibroblasts with a retroviral vector-containing human telomerase reverse transcriptase (hTERT) gene [108]. Although the immortalized human vocal fold fibroblasts are a suitable model system for in vivo studies, translation into the clinic will be challenging [95]. On the other hand, skin fibroblasts can be easily extracted from the patients by skin biopsy and be expanded in culture. They can be genetically reprogrammed by vocal fold-specific mechanical and chemical signals to produce vocal fold LP-like ECM [109, 110].

Alternatively, multipotent MSCs can be obtained from a variety of adult tissues and be readily expanded in culture without signs of senescence [111, 112]. MSCs have been successfully differentiated into osteoblasts, chondrocytes, adipocytes, and nerve cells under defined in vitro culture conditions [113]. Hertegard et al. injected MSCs into scarred rabbit vocal folds. Rheological analysis 4 weeks post-injection showed that the injection of MSCs resulted in a decrease in elastic shear modulus and dynamic viscosity, compared with the saline-treated vocal folds [114]. Pluoripotent human embryonic stem cells (hESCs) are also potential sources for cell transplantations. Cedervall et al. were the first to report the injection of hESCs into lesions of scarred rabbit vocal mucosa and superficial thyroarytenoid muscle. While the hESC injection improved the viscoelastic properties of the injured vocal folds, compared with the saline-treated controls, a low degree of cell survival was detected [115]. In both cases, it is unclear how the injected cells behave in the tissue and whether they eventually differentiated, and if so, into what lineages. The long-term effects of stem cell injection remain unanswered. Direct injection of hESCs into the vocal fold carries the risk of tumor formation. Systematic investigations on the differentiation of MSCs in a well-controlled, biomimetic in vitro environment are necessary for the establishment of stem cell technology in vocal fold regeneration.

Biomechanical Stimulations

Recent studies have underscored the importance of mechanical signals in mediating cellular functions [102, 116]. Mechanical stress, in a tissue or in a construct, can regulate the synthesis of ECM molecules indirectly by stimulating the release of growth factors, or directly by triggering an intracellular pathway that will activate the corresponding genes [116]. Fibroblasts sense force-induced deformations in their ECM through integrin and transduce them into biochemical responses

[102, 116]. Although the effects of mechanical stimulations on the behavior of chondrocytes, osteoblasts, smooth muscle cells, and fibroblasts (skin and muscle) have been well documented [105, 116–120], only a few studies have examined such effects on vocal fold fibroblasts due to the difficulty in replicating the demanding biomechanical environment in vitro [121, 122].

It has been postulated that the development of the vocal folds is shaped by the tasks that are required [23]. In other words, the mechanical tasks that the vocal folds are asked to engage in and accomplish increase in complexity over time. This mechanical stimulation prompts cellular differentiation and tissue development and maturation. To provide a biomimetic microenvironment for vocal fold tissue engineering, it is critical to impose high frequency vibrations coupled with longitudinal tension to the tissue engineering scaffolds to simulate the mechanical environment experienced by the cells. Titze et al. were the first to describe a bioreactor for the cultivation of vocal fold fibroblasts under vibratory stimulation [2, 121, 123]. In their design (Fig. 10.9), a low frequency (or static) actuator was coupled to a series of connectors and levers to provide axial substrate elongation. The high frequency vibratory stimulus to the scaffolds was generated using a voice coil actuator connected to a lever, which is attached to a vibrational bar. This bar moves the four vibrator arms in the flask, creating a vocal fold-like biomechanical environment. A porous polyurethane substrate containing primary vocal fold fibroblasts was subjected to vibrational stimulations at frequencies of 20–200 Hz. Results showed that the vibrational stress altered the expression levels of many ECM-related genes, as well as the spatial distribution of both cells and the matrix components. Particularly, 20% axial strain and vibration at 100 Hz for 6 h resulted in a significant increase in fibronectin, MMP-1, HA synthase 2, and CD44, with respect to static control.

Alternatively, the Jia group has designed a bioreactor which not only allows the vibration of constructs at phonation frequencies, but also vibrates them in a wave-like motion similar to that of vocal folds during phonation [124]. The bioreactor is composed of an enclosed speaker driven by a function generator and a power amplifier, a T-75 flask modified to accommodate the vibration tubes and a collagen-coated, silicone membrane covering the vibration tube. A rigid plastic tubing effectively secures the membrane, creating a small vibration chamber (13 mm wide and 3 mm deep) for dynamic cell culture. Our preliminary data show that neonatal foreskin fibroblasts cultured on the silicone membrane respond to the vibrational stimulations through the alteration of their gene expression levels of essential ECM proteins in a frequency- and amplitude-dependent manner. These results confirm our hypothesis that fibroblasts can be manipulated by physiologically relevant mechanical stimulations to produce the ECM molecules necessary for vocal fold tissue repair or regeneration.

A more user-friendly, readily adjustable and microscope-compatible bioreactor (Fig. 10.10) has been recently fabricated. The overall bioreactor design consists of a silicone membrane sandwiched between a pair of mountable acrylic blocks containing matching ridges and grooves that lock the membrane in place. Four corner screws connect the top and the bottom plates, essentially creating a water-tight vibration chamber that allows for cells to be cultured dynamically. Upon completion of cell

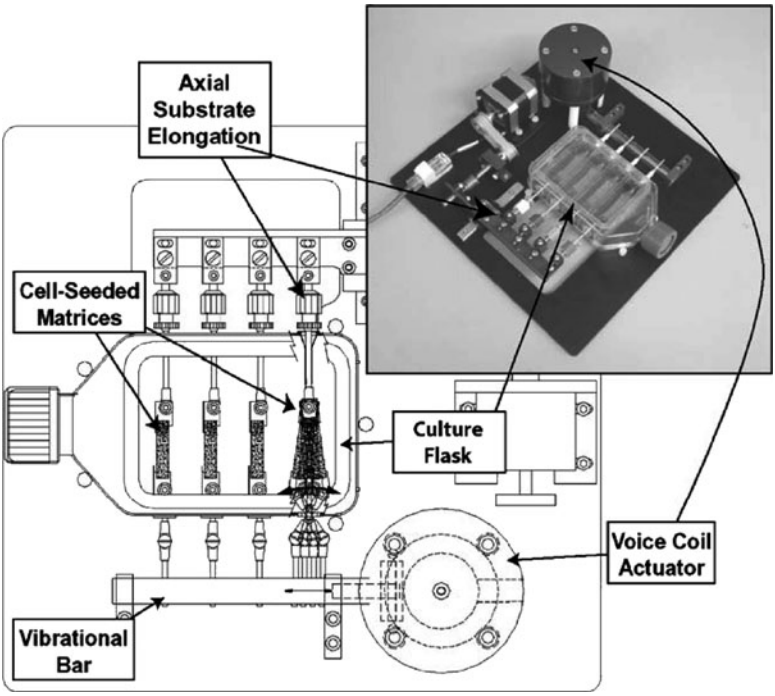

Fig. 10.9 Vocal fold bioreactor designed by Titze and coworkers [121]. Copyright permission from Elsevier

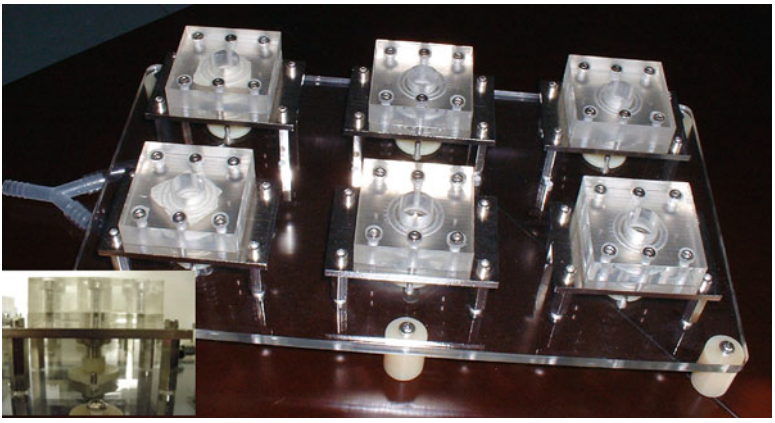

Fig. 10.10 Digital picture of the Delaware bioreactor showing six parallel vibration chambers assembled on a portable stage. Insert shows the side view of the vibration chamber [124]

culture, the acrylic blocks containing cultured cells and media can be readily removed from the platform, allowing cells to be directly imaged without having to disassemble the acrylic plates and disrupting the cultured cells. The new design also incorporates an adjustable knob underneath the membrane, through which the pre-stress across the membrane can be adjusted prior to the initiation of vibration. The entire bioreactor is portable and can be fitted into an incubator easily. Our invention has been described in a US non-provisional patent recently filed [124]. With the bioreactor fully characterized, we are exploring the possibility of engineering vocal fold LP using human bone marrow-derived MSCs and the synthetic ECMs.

In Vitro Vocal Fold Tissue Engineering

Successful in vitro engineering of vocal fold tissue requires that the interplay of cellular, molecular, and physical factors present in vivo be replicated with high precision. Essential tissue engineering components are (1) biologically active, synthetic scaffolds, (2) multipotent cells, (3) morphogenic factors presented in a spatial and temporal manner, and (4) physiologically relevant biomechanical stimulations. Innovative systems have to provide a tight control over the environmental parameters so that the cellular responses can be readily mediated.

Vocal fold tissue engineering is an unexplored field; only a limited number of groups in the USA, us included, are actively pursuing this goal. In a recent study, Webb and coworkers [125] investigated the effects of physiologically relevant vibratory stimulations on gene expression and protein production by fibroblasts encapsulated within HA hydrogels that approximate the viscoelastic properties of vocal mucosa. Primary human dermal fibroblasts were used in the place of vocal fold fibroblasts and photocrosslinkable, methacrylated HA, in conjunction with fibronectin-derived cell adhesion peptide (GRGDS), was used to create the artificial matrix. The vocal fold bioreactor previously designed by Titze et al. was used to generate high frequency mechanical stimulations. After overnight equilibration under static conditions, the constructs were subjected to a 2 s on/2 s off vibrational regimen for 4 h/day at 100 Hz for up to 10 days. Their results show that vibrational stimulations significantly increased the mRNA levels of HA synthase 2, decorin, fibromodulin, and MMP-1, but did not lead to significant changes in collagen and elastin expressions. Interestingly, the expression levels exhibited a temporal response, with maximum increases observed after 3 and 5 days of vibratory stimulation and significant downregulation observed at day 10. Furthermore, the stimulations increased the production of sulphated glycosaminoglycans, but decreased the amount of collagen accumulated after 5 and 10 days of culture. Cell-mediated cellular and matrix remodeling has also been observed. This study undoubtedly confirms that vibration is a critical epigenetic factor in regulating vocal fold ECM. The recreation of the phonatory microenvironment in vitro is a promising strategy for the engineering of functional vocal fold tissue.

Conclusion

This chapter describes the basic physiology of healthy and diseased vocal folds and highlights efforts toward in vivo tissue repair and in vitro tissue engineering. Although the principle of tissue engineering has been established for over 30 years, only until very recently was it applied to target the vocal folds. While direct injection of cells, growth factors, biomaterials or their combinations has improved histological, rheological, and/or functional outcomes relative to untreated control injuries, long-term repair, or complete recovery of native tissue structure and function, has not been achieved. Biomaterials that not only meet the biochemical and biomechanical requirements of the vocal folds, but also elicit an active cell remodeling and a scarless wound healing process have yet to be synthesized. On the other hand, Nature provides ample inspirations for the development of biocompatible and biodegradable materials, whose material properties and biological responses can be readily tailored for specific tissues. Recapturing the molecular architecture, multiscale organization, chemical, and mechanical responsiveness of the native ECM will likely lead to the generation of robust, dynamic, and information-rich biomaterials that will provide guidance cues to the embedded cells. As insight continues to be gleaned from vocal fold physiology and developmental biology, more intelligent and complex hydrogel materials will likely emerge as conducive matrices for vocal fold tissue repair and regeneration [107, 126, 127]. Future studies integrating biomimetic scaffolds, multipotent cells, soluble factor delivery, and mechanical stimulation into unifying constructs are likely to achieve synergistic improvements. Successful engineering of functional vocal folds cannot be successful without interdisciplinary collaborations between clinical otolaryngologists, molecular biologists, and materials scientists.

Acknowledgements We acknowledge funding from the US National Institutes of Health (National Institute on Deafness and Other Communication Disorders, National Center for Research Resources), the US National Science Foundation (Division of Materials Research, Biomaterials Program) and the University of Delaware Research Foundation.

References

1. Titze, I.R. (ed.): Principles of Voice Production, 2nd edn, p. 409. National Center for Voice and Speech, Iowa City (2000)
2. Gray, S.D.: Cellular physiology of the vocal folds. Otolaryngol. Clin. North Am. **33**(4), 679–697 (2000)
3. Hirano, M., Kurita, S., Nakashima, T.: Vocal Fold Physiology: Contemporary Research and Clinical Issues. In Vocal Fold Physiology, Conference. College-Hill, San Diego, CA (1981)
4. Hahn, M.S., Kobler, J.B., Starcher, B.C., Zeitels, S.M., Langer, R.: Quantitative and comparative studies of the vocal fold extracellular matrix - I: Elastic fibers and hyaluronic acid. Ann. Otol. Rhinol. Laryngol. **115**(2), 156–164 (2006)

5. Hahn, M.S., Kobler, J.B., Zeitels, S.M., Langer, R.: Quantitative and comparative studies of the vocal fold extracellular matrix II: Collagen. Ann. Otol. Rhinol. Laryngol. **115**(3), 225–232 (2006)
6. Hahn, M.S., Jao, C.Y., Faquin, W., Grande-Allen, K.J.: Glycosaminoglycan composition of the vocal fold lamina propria in relation to function. Ann. Otol. Rhinol. Laryngol. **117**(5), 371–381 (2008)
7. Munoz-Pinto, D., Whittaker, P., Hahn, M.S.: Lamina propria cellularity and collagen composition: an integrated assessment of structure in humans. Ann. Otol. Rhinol. Laryngol. **118** (4), 299–306 (2009)
8. Hammond, T.H., Gray, S.D., Butler, J., Zhou, R., Hammond, E.: Age- and gender-related elastin distribution changes in human vocal folds. Otolaryngol. Head Neck Surg. **119**(4), 314–322 (1998)
9. Hammond, T.H., Zhou, R., Hammond, E.H., Pawlak, A., Gray, S.D.: The intermediate layer: A morphologic study of the elastin and hyaluronic acid constituents of normal human vocal folds. J. Voice **11**(1), 59–66 (1997)
10. Ward, P.D., Thibeault, S.L., Gray, S.D.: Hyaluronic acid: Its role in voice. J. Voice **16**(3), 303–309 (2002)
11. Gray, S.D., Titze, I.R., Alipour, F., Hammond, T.H.: Biomechanical and histologic observations of vocal fold fibrous proteins. Ann. Otol. Rhinol. Laryngol. **109**(1), 77–85 (2000)
12. Chan, R.W., Fu, M., Young, L., Tirunagari, N.: Relative contributions of collagen and elastin to elasticity of the vocal fold under tension. Ann. Biomed. Eng. **35**(8), 1471–1483 (2007)
13. Pawlak, A.S., Hammond, T., Hammond, E., Gray, S.D.: Immunocytochemical study of proteoglycans in vocal folds. Ann. Otol. Rhinol. Laryngol. **105**(1), 6–11 (1996)
14. Chan, R.W., Titze, I.R.: Hyaluronic acid (with fibronectin) as a bioimplant for the vocal fold mucosa. Laryngoscope **109**(7), 1142–1149 (1999)
15. Gray, S.D., Titze, I.R., Chan, R., Hammond, T.H.: Vocal fold proteoglycans and their influence on biomechanics. Laryngoscope **109**(6), 845–854 (1999)
16. Chan, R.W., Gray, S.D., I.R. Titze.: The importance of hyaluronic acid in vocal fold biomechanics. Otolaryngol. Head Neck Surg. **124**(6), 607–614 (2001)
17. Ruoslahti, E.: Fibronectin and its receptors. Annu. Rev. Biochem. **57**, 375–413 (1988)
18. Hammond, T.H., Gray, S.D., Butler, J.E.: Age- and gender-related collagen distribution in human vocal folds. Ann. Otol. Rhinol. Laryngol. **109**(10), 913–920 (2000)
19. Catten, M., Gray, S.D., Hammond, T.H., Zhou, R., Hammond, E.: Analysis of cellular location and concentration in vocal fold lamina propria. Otolaryngol. Head Neck Surg. **118**(5), 663–667 (1998)
20. Sato, K., Hirano, M., Nakashima, T.: Fine structure of the human newborn and infant vocal fold mucosae. Ann. Otol. Rhinol. Laryngol. **110**(5), 417–424 (2001)
21. Schweinfurth, J.M., Thibeault, S.L.: Does hyaluronic acid distribution in the larynx relate to the newborn's capacity for crying? Laryngoscope **118**(9), 1692–1699 (2008)
22. Boseley, M.E., Hartnick, C.J.: Development of the human true vocal fold: Depth of cell layers and quantifying cell types within the lamina propria. Ann. Otol. Rhinol. Laryngol. **115**(10), 784–7888 (2006)
23. Hartnick, C.J., Rehbar, R., Prasad, V.: Development and maturation of the pediatric human vocal fold lamina propria. Laryngoscope **115**(1), 4–15 (2005)
24. Min, Y.B., Titze, I.R., Alipourhaghighi, F.: Stress–strain response of the human vocal ligament. Ann. Otol. Rhinol. Laryngol. **104**(7), 563–569 (1995)
25. Kutty, J.K., Webb, K.: Tissue engineering therapies for the vocal fold lamina propria. Tissue Eng. Part B Rev. **15**(3), 249–262 (2009)
26. Chan, R.W., Titze, I.R.: Viscoelastic shear properties of human vocal fold mucosa: Measurement methodology and empirical results. J. Acoust. Soc. Am. **106**(4), 2008–2021 (1999)
27. Chan, R.W.: Measurements of vocal fold tissue viscoelasticity: Approaching the male phonatory frequency range. J. Acoust. Soc. Am. **115**(6), 3161–3170 (2004)

28. Clifton, R.J., Jiao, T., Bull, C.: Methods and apparatus for measuring the viscoelastic response of vocal fold tissues and scaffolds across a frequency range, US Patent Application, Pub. No. US 2006/0207343 A1, 2004
29. Deng, T.H., Knauss, W.G.: The temperature and frequency dependence of the bulk compliance of poly(vinyl acetate). A re-examination. Mech. Time-Depend. Mater. **1**(1), 33–49 (1997)
30. Trunov, M., Bilanich, V., Dub, S.: Nanoindentation study of the time-dependent mechanical behavior of materials. Tech. Phys. **7710**, 50–57 (2007)
31. Jiao, T., Farran, A., Jia, X., Clifton, R.: High frequency measurements of viscoelastic properties of hydrogels for vocal fold regeneration. Exp. Mech. **49**, 235–246 (2009)
32. Clifton, R.J., Jia, X., Jiao, T., Bull, C., Hahn, M.S.: Viscoelastic response of vocal fold tissues and scaffolds at high frequencies, in Mechanics of Biological Tissue. In: Holzapfel, G.A., Ogden, R.W. (Eds.), New York, NY, Springer, 445–455 (2006)
33. Jia, X.Q., Burdick, J.A., Kobler, J., Clifton, R.J., Rosowski, J.J., Zeitels, S.M., Langer, R.: Synthesis and characterization of in situ cross-linkable hyaluronic acid-based hydrogels with potential application for vocal fold regeneration. Macromolecules **37**(9), 3239–3248 (2004)
34. Jha, A.K., Hule, R.A., Jiao, T., Teller, S.S., Clifton, R.J., Duncan, R.L., Pochan, D.J., Jia, X.Q.: Structural analysis and mechanical characterization of hyaluronic acid-based doubly cross-linked networks. Macromolecules **42**(2), 537–546 (2009)
35. Jia, X.Q., Yeo, Y., Clifton, R.J., Jiao, T., Kohane, D.S., Kobler, J.B., Zeitels, S.M., Langer, R.: Hyaluronic acid-based microgels and microgel networks for vocal fold regeneration. Biomacromolecules **7**(12), 3336–3344 (2006)
36. Farran, A.J.E., Teller, S.S., Jha, A.K., Jiao, T., Hule, R.A., Clifton, R.J., Pochan, D.P., Duncan, R.L., Jia, X.Q.: Effects of matrix composition, microstructure, and viscoelasticity on the behaviors of vocal fold fibroblasts cultured in three-dimensional hydrogel networks. Tissue Eng. Part A **16**(4), 1247–1261 (2010)
37. Williams, N.R.: Occupational groups at risk of voice disorders: a review of the literature. Occup. Med. (Lond.) **53**(7), 456–460 (2003)
38. Roy, N., Merrill, R.M., Gray, S.D., Smith, E.M.: Voice disorders in the general population: Prevalence, risk factors, and occupational impact. Laryngoscope **115**(11), 1988–1995 (2005)
39. Hansen, J.K., Thibeault, S.L.: Current understanding and review of the literature: Vocal fold scarring. J. Voice **20**(1), 110–120 (2006)
40. Hahn, M.S., Teply, B.A., Stevens, M.M., Zeitels, S.M., Langer, R.: Collagen composite hydrogels for vocal fold lamina propria restoration. Biomaterials **27**(7), 1104–1109 (2006)
41. Hirano, S.: Current treatment of vocal fold scarring. Curr. Opin. Otolaryngol. Head Neck Surg. **13**(3), 143–147 (2005)
42. Branski, R.C., Verdolini, K., Sandulache, V., Rosen, C.A., Hebda, P.A.: Vocal fold wound healing: A review for clinicians. J. Voice **20**(3), 432–442 (2006)
43. Hirano, S., Minamiguchi, S., Yamashita, M., Ohno, T., Kanemaru, S.-I., Kitamura, M.: Histologic characterization of human scarred vocal folds. J. Voice **23**(4), 399–407 (2009)
44. Thibeault, S.L., Gray, S.D., Bless, D.M., Chan, R.W., Ford, C.N.: Histologic and rheologic characterization of vocal fold scarring. J. Voice **16**(1), 96–104 (2002)
45. Rousseau, B., Hirano, S., Chan, R.W., Welham, N.V., Thibeault, S.L., Ford, C.N., Bless, D.M.: Characterization of chronic vocal fold scarring in a rabbit model. J. Voice **18**(1), 116–124 (2004)
46. Rousseau, B., Hirano, S., Scheidt, T.D., Welham, N.V., Thibeault, S.L., Chan, R.W., Bless, D.M.: Characterization of vocal fold scarring in a canine model. Laryngoscope **113**(4), 620–627 (2003)
47. Thibeault, S.L., Bless, D.M., Gray, S.D.: Interstitial protein alterations in rabbit vocal fold with scar. J. Voice **17**(3), 377–383 (2003)
48. Ehrlich, H.P.: Collagen considerations in scarring and regenerative repair. In: Garg, H.G., Longaker, M.T. (eds.) Scarless Wound Healing, pp. 99–113. Marcel Dekker, New York (2000)
49. Chin, G.S., Stelnicki, E.J., Gittes, G.K., Longaker, M.T.: Characteristics of fetal wound repair. In: Garg, H.G., Longaker, M.T. (eds.) Scareless Wound Healing, pp. 239–262. Marcel Dekker, New York (2000)

50. Croce, M.A., Dyne, K., Boraldi, F., Quaglino, D., Cetta, G., Tiozzo, R., Ronchetti, I.P.: Hyaluronan affects protein and collagen synthesis by in vitro human skin fibroblasts. Tissue Cell **33**(4), 326–331 (2001)
51. Gray, S.D., Hammond, E., Hanson, D.F.: Benign pathological responses of the larynx. Ann. Otol. Rhinol. Laryngol. **104**(1), 13–18 (1995)
52. Benninger, M.S., Alessi, D., Archer, S., Bastian, R., Ford, C., Koufman, J., Sataloff, R.T., Spiegel, J.R., Woo, P.: Vocal fold scarring: Current concepts and management. Otolaryngol. Head Neck Surg. **115**(5), 474–482 (1996)
53. Zeitels, S.M.: Atlas of Phonomicrosurgery and Other Endolaryngeal Procedures for Benign and Malignant Disease. Singular Publishing Group, San Diego (2001)
54. Zeitels, S.M., Healy, G.B.: Laryngology and phonosurgery. N. Engl. J. Med. **349**(9), 882–892 (2003)
55. Costantino, P.D., Friedman, C.D.: Soft-tissue augmentation and replacement in the head and neck. General considerations. Otolaryngol. Clin. North Am. **27**(1), 1–12 (1994)
56. Lewy, R.B.: Teflon injection of the vocal cord: complications, errors, and precautions. Ann. Otol. Rhinol. Laryngol. **92**(5 Pt 1), 473–474 (1983)
57. Pohris, E., Kleinsasser, O.: Stenosis of the larynx following Teflon injection. Arch. Otorhinolaryngol. **244**(1), 44–48 (1987)
58. Rosen, C.A., Gartner-Schmidt, J., Casiano, R., Anderson, T.D., Johnson, F., Remacle, M., Sataloff, R.T., Abitbol, J., Shaw, G., Archer, S., Zraick, R.I.: Vocal fold augmentation with calcium hydroxylapatite: Twelve-month report. Laryngoscope **119**(5), 1033–1041 (2009)
59. Sittel, C., Thumfart, W.F., Pototschnig, C., Wittekindt, C., Eckel, H.E.: Textured polydimethylsiloxane elastomers in the human larynx: safety and efficiency of use. J. Biomed. Mater. Res. **53**(6), 646–650 (2000)
60. Yamashita, M., Kanemaru, S., Hirano, S., Umeda, H., Kitani, Y., Omori, K., Nakamura, T., Ito, J.: Glottal reconstruction with a tissue engineering technique using polypropylene mesh: a canine experiment. Ann. Otol. Rhinol. Laryngol. **119**(2), 110–117 (2010)
61. Cheng, Y., Li, Z.Q., Huang, J.Z., Xue, F., Jiang, M.J., Wu, K.M., Wang, Q.P.: Combination of autologous fascia lata and fat injection into the vocal fold via the cricothyroid gap for unilateral vocal fold paralysis. Arch. Otolaryngol. Head Neck Surg. **135**(8), 759–763 (2009)
62. Umeno, H., Shirouzu, H., Chitose, S., Nakashima, T.: Analysis of voice function following autologous fat injection for vocal fold paralysis. Otolaryngol. Head Neck Surg. **132**(1), 103–107 (2005)
63. Ford, C.N.: Histologic studies on the fate of soluble collagen injected into canine vocal folds. Laryngoscope **96**(11), 1248–1257 (1986)
64. Anderson, T.D., Sataloff, T.T.: Complications of collagen injection of the vocal fold: Report of several unusual cases and review of the literature. J. Voice **18**(3), 392–397 (2004)
65. Hirano, S., Bless, D.A., Nagai, H., Rousseau, B., Welham, N.V., Montequin, D.W., Ford, C.N.: Growth factor therapy for vocal fold scarring in a canine model. Ann. Otol. Rhinol. Laryngol. **113**(10), 777–785 (2004)
66. Hirano, S., Bless, D.M., Rousseau, B., Welham, N., Montequin, D., Chan, R.W., Ford, C.N.: Prevention of vocal fold scarring by topical injection of hepatocyte growth factor in a rabbit model. Laryngoscope **114**(3), 548–556 (2004)
67. Hirano, S., Bless, D., Heisey, D., Ford, C.: Roles of hepatocyte growth factor and transforming growth factor beta 1 in production of extracellular matrix by canine vocal fold fibroblasts. Laryngoscope **113**(1), 144–148 (2003)
68. Hirano, S., Bless, D.M., Massey, R.J., Hartig, G.K., Ford, C.N.: Morphological and functional changes of human vocal fold fibroblasts with hepatocyte growth factor. Ann. Otol. Rhinol. Laryngol. **112**(12), 1026–1033 (2003)
69. Hirano, S., Nagai, H., Tateya, I., Tateya, T., Ford, C.N., Bless, D.M.: Regeneration of aged vocal folds with basic fibroblast growth factor in a rat model: a preliminary report. Ann. Otol. Rhinol. Laryngol. **114**(4), 304–308 (2005)

70. Suehiro, A., Hirano, S., Kishimoto, Y., Rousseau, B., Nakamura, T., Ito, J.: Treatment of acute vocal fold scar with local injection of basic fibroblast growth factor: a canine study. Acta Otolaryngol. **130**(7), 844–850 (2010)
71. Hirano, S., Kishimoto, Y., Suehiro, A., Kanemaru, S., Ito, J.: Regeneration of aged vocal fold: first human case treated with fibroblast growth factor. Laryngoscope **118**(12), 2254–2259 (2008)
72. Kishimoto, Y., Hirano, S., Kitani, Y., Suehiro, A., Umeda, H., Tateya, I., Kanemaru, S., Tabata, Y., Ito, J.: Chronic vocal fold scar restoration with hepatocyte growth factor hydrogel. Laryngoscope **120**(1), 108–113 (2010)
73. Hallen, L., Johansson, C., Laurent, C.: Cross-linked hyaluronan (hylan B gel): a new injectable remedy for treatment of vocal fold insufficiency - an animal study. Acta Otolaryngol. **119**(1), 107–111 (1999)
74. Hertegard, S., Hallen, L., Laurent, C., Lindstrom, E., Olofsson, K., Testad, P., Dahlqvist, A.: Cross-linked hyaluronan used as augmentation substance for treatment of glottal insufficiency: Safety aspects and vocal fold function. Laryngoscope **112**(12), 2211–2219 (2002)
75. Perazzo, P.S., Duprat Ade, C., Lancellotti, C.L.: Histological behavior of the vocal fold after hyaluronic acid injection. J. Voice **23**(1), 95–98 (2009)
76. Lau, D.P., Lee, G.A., Wong, S.M., Lim, V.P., Chan, Y.H., Tan, N.G., Rammage, L.A., Morrison, M.D.: Injection laryngoplasty with hyaluronic acid for unilateral vocal cord paralysis. Randomized controlled trial comparing two different particle sizes. J. Voice **24**(1), 113–118 (2010)
77. Campoccia, D., Doherty, P., Radice, M., Brun, P., Abatangelo, G., Williams, D.F.: Semisynthetic resorbable materials from hyaluronan esterification. Biomaterials **19**(23), 2101–2127 (1998)
78. Finck, C., Lefebvre, P.: Implantation of esterified hyaluronic acid in microdissected Reinke's space after vocal fold microsurgery: First clinical experiences. Laryngoscope **115**(10), 1841–1847 (2005)
79. Prestwich, G.D.: Evaluating drug efficacy and toxicology in three dimensions: Using synthetic extracellular matrices in drug discovery. Acc. Chem. Res. **41**(1), 139–148 (2008)
80. Shu, X.Z., Liu, Y., Palumbo, F.S., Luo, Y., Prestwich, G.D.: In situ crosslinkable hyaluronan hydrogels for tissue engineering. Biomaterials **25**(7–8), 1339–1348 (2004)
81. Shu, X.Z., Prestwich, G.D.: Therapeutic biomaterials from chemically modified hyaluronan. In: Garg, H.G., Hales, C.A. (eds.) Chemistry and Biology of Hyaluronan, pp. 475–504. Elsevier, Oxford (2004)
82. Prestwich, G.D., Kuo, J.: Chemically-modified HA for therapy and regenerative medicine. Curr. Pharm. Biotechnol. **9**(4), 242–245 (2008)
83. Hansen, J.K., Thibeault, S.L., Walsh, J.F., Shu, X.Z., Prestwich, G.D.: In vivo engineering of the vocal fold extracellular matrix with injectable hyaluronic acid hydrogels: early effects on tissue repair and biomechanics in a rabbit model. Ann. Otol. Rhinol. Laryngol. **114**(9), 662–670 (2005)
84. Duflo, S., Thibeault, S.L., Li, W., Shu, X.Z., Prestwich, G.D.: Vocal fold tissue repair in vivo using a synthetic extracellular matrix. Tissue Eng. **12**(8), 2171–2180 (2006)
85. Thibeault, S.L., Klemuk, S.A., Chen, X., QuinchiaJohnson, B.H.: In vivo engineering of the vocal fold ECM with injectable HA hydrogels-late effects on tissue repair and biomechanics in a rabbit model. J. Voice **25**(2), 249–253 (2011)
86. Johnson, B.Q., Fox, R., Chen, X., Thibeault, S.: Tissue regeneration of the vocal fold using bone marrow mesenchymal stem cells and synthetic extracellular matrix injections in rats. Laryngoscope **120**(3), 537–545 (2010)
87. Caton, T., Thibeault, S.L., Klemuk, S., Smith, M.E.: Viscoelasticity of hyaluronan and nonhyaluronan based vocal fold injectables: Implications for mucosal versus muscle use. Laryngoscope **117**(3), 516–521 (2007)
88. Sahiner, N., Jha, A.K., Nguyen, D., Jia, X.Q.: Fabrication and characterization of crosslinkable hydrogel particles based on hyaluronic acid: potential application in vocal fold regeneration. J. Biomater. Sci. Polym. Ed. **19**(2), 223–243 (2008)

89. Jia, X.Q., Colombo, G., Padera, R., Langer, R., Kohane, D.S.: Prolongation of sciatic nerve blockade by in situ cross-linked hyaluronic acid. Biomaterials **25**(19), 4797–4804 (2004)
90. Jha, A.K., Malik, M.S., Farach-Carson, M.C., Duncan, R.L., Jia, X.: Hierarchically structured, hyaluronic acid-based hydrogel matrices via the covalent integration of microgels into macroscopic networks. Soft Matter **6**(20), 5045–5055 (2010). doi:10.1039/c0sm00101e
91. Biondi, M., Ungaro, F., Quaglia, F., Netti, P.A.: Controlled drug delivery in tissue engineering. Adv. Drug Deliv. Rev. **60**(2), 229–242 (2008)
92. Farach-Carson, M.C., Hecht, J.T., Carson, D.D.: Heparan sulfate proteoglycans: key players in cartilage biology. Crit. Rev. Eukaryot. Gene Expr. **15**(1), 29–48 (2005)
93. Jha, A.K., Yang, W.D., Kirn-Safran, C.B., Farach-Carson, M.C., Jia, X.Q.: Perlecan domain I-conjugated, hyaluronic acid-based hydrogel particles for enhanced chondrogenic differentiation via BMP-2 release. Biomaterials **30**(36), 6964–6975 (2009)
94. Freshney, R.I., Obradovic, B., Grayson, W., Cannizzaro, C., Vunjak-Novakovic, G.: Principles of tissue culture and bioreactor design. In: Lonza, R., Langer, R., Vacanti, J. (eds.) Principles of Tissue Engineering. Academic, Burlington (2007)
95. Chen, X., Thibeault, S.L.: Biocompatibility of a synthetic extracellular matrix on immortalized vocal fold fibroblasts in 3-D culture. Acta Biomater. **6**(8), 2940–2948 (2010)
96. Lutolf, M.P., Hubbell, J.A.: Synthetic biomaterials as instructive extracellular microenvironments for morphogenesis in tissue engineering. Nat. Biotechnol. **23**(1), 47–55 (2005)
97. Kutty, J.K., Cho, E., Lee, J.S., Vyavahare, N.R., Webb, K.: The effect of hyaluronic acid incorporation on fibroblast spreading and proliferation within PEG-diacrylate based semi-interpenetrating networks. Biomaterials **28**(33), 4928–4938 (2007)
98. Luo, Y., Kobler, J.B., Zeitels, S.M., Langer, R.: Effects of growth factors on extracellular matrix production by vocal fold fibroblasts in 3-dimensional culture. Tissue Eng. **12**(12), 3365–3374 (2006)
99. Chicurel, M.E., Chen, C.S., Ingber, D.E.: Cellular control lies in the balance of forces. Curr. Opin. Cell Biol. **10**, 232–239 (1998)
100. Discher, D.E., Janmey, P., Wang, Y.-L.: Tissue cells feel and respond to the stiffness of their substrate. Science **310**, 1139–1143 (2005)
101. Engler, A.J., Sen, S., Sweeney, H.L., Discher, D.E.: Matrix elasticity directs stem cell lineage specification. Cell **126**(4), 677–689 (2006)
102. Ingber, D.E.: Cellular mechanotransduction: putting all the pieces together again. FASEB J. **20**(7), 811–827 (2006)
103. Kung, C.: A possible unifying principle for mechanosensation. Nature **436**, 647–654 (2005)
104. Vrhovski, B., Weiss, A.S.: Biochemistry of tropoelastin. Eur. J. Biochem. **258**(1), 1–18 (1998)
105. Gardinier, J.D., Majumdar, S., Duncan, R.L., Wang, L.Y.: Cyclic hydraulic pressure and fluid flow differentially modulate cytoskeleton re-organization in MC3T3 osteoblasts. Cell. Mol. Bioeng. **2**(1), 133–143 (2009)
106. Lillie, M.A., Gosline, J.M.: The effects of hydration on the dynamic mechanical properties of elastin. Biopolymers **29**(8–9), 1147–1160 (1990)
107. Jia, X.Q., Kiick, K.L.: Hybrid multicomponent hydrogels for tissue engineering. Macromol. Biosci. **9**(2), 140–156 (2009)
108. Chen, X., Thibeault, S.L.: Novel isolation and biochemical characterization of immortalized fibroblasts for tissue engineering vocal fold lamina propria. Tissue Eng. Part C Methods **15**(2), 201–212 (2009)
109. Kim, B.S., Nikolovski, J., Bonadio, J., Mooney, D.J.: Cyclic mechanical strain regulates the development of engineered smooth muscle tissue. Nat. Biotech. **17**, 979–983 (1999)
110. Stamatas, G.N., McIntire, L.V.: Rapid flow-induced responses in endothelia cells. Biotechnol. Prog. **17**, 383–402 (2001)
111. Caplan, A.I.: Adult mesenchymal stem cells for tissue engineering versus regenerative medicine. J. Cell. Physiol. **213**(2), 341–347 (2007)

112. Jiang, Y.H., Jahagirdar, B.N., Reinhardt, R.L., Schwartz, R.E., Keene, C.D., Ortiz-Gonzalez, X.R., Reyes, M., Lenvik, T., Lund, T., Blackstad, M., Du, J.B., Aldrich, S., Lisberg, A., Low, W.C., Largaespada, D.A., Verfaillie, C.M.: Pluripotency of mesenchymal stem cells derived from adult marrow. Nature **418**(6893), 41–49 (2002)
113. Pittenger, M.F., Mackay, A.M., Beck, S.C., Jaiswal, R.K., Douglas, R., Mosca, J.D., Moorman, M.A., Simonetti, D.W., Craig, S., Marshak, D.R.: Multilineage potential of adult human mesenchymal stem cells. Science **284**(5411), 143–147 (1999)
114. Hertegard, S., Cedervall, J., Svensson, B., Forsberg, K., Maurer, F.H., Vidovska, D., Olivius, P., Ahrlund-Richter, L., Le Blanc, K.: Viscoelastic and histologic properties in scarred rabbit vocal folds after mesenchymal stem cell injection. Laryngoscope **116**(7), 1248–1254 (2006)
115. Cedervall, J., Ahrlund-Richter, L., Svensson, B., Forsgren, K., Maurer, F.H., Vidovska, D., Hertegard, S.: Injection of embryonic stem cells into scarred rabbit vocal folds enhances healing and improves viscoelasticity: Short-term results. Laryngoscope **117**(11), 2075–2081 (2007)
116. Chiquet, M., Renedo, A.S., Huber, F., Flück, M.: How do fibroblasts translate mechanical signals into changes in extracellular matrix production? Matrix Biol. **22**(1), 73–80 (2003)
117. Brown, M.A., Iver, R.K., Radisic, M.: Pulsatile perfusion bioreactor for cardiac tissue engineering. Biotechnol. Prog. **24**(4), 907–920 (2008)
118. Buschmann, M.D., Gluzband, Y.A., Grodzinsky, A.J., Hunziker, E.B.: Mechanical compression modulates matrix biosynthesis in chondrocyte/agarose culture. J. Cell Sci. **108**(4), 1497–1508 (1995)
119. Kim, Y.-J., Bonassar, L.J., Grodzinsky, A.J.: The role of cartilage streaming potential, fluid flow and pressure in the stimulation of chondrocyte biosynthesis during dynamic compression. J. Biomech. **28**(9), 1055–1066 (1995)
120. Mauck, R.L., Soltz, M.A., Wang, C.C.B., Wong, D.D., Chao, P.H.G., Valhmu, W.B., Hung, C.T., Ateshian, G.A.: Functional tissue engineering of articular cartilage through dynamic loading of chondrocyte-seeded agarose gels. J. Biomech. Eng.-Trans. ASME **122**(3), 252–260 (2000)
121. Titze, I.R., Hitchcock, R.W., Broadhead, K., Webb, K., Li, W., Gray, S.D., Tresco, P.A.: Design and validation of a bioreactor for engineering vocal fold tissues under combined tensile and vibrational stresses. J. Biomech. **37**(10), 1521–1529 (2004)
122. Webb, K., Hitchcock, R.W., Smeal, R.M., Li, W.H., Gray, S.D., Tresco, P.A.: Cyclic strain increases fibroblast proliferation, matrix accumulation, and elastic modulus of fibroblast-seeded polyurethane constructs. J. Biomech. **39**(6), 1136–1144 (2006)
123. Titze, I.R., Broadhead, K., Tresco, P., Gray, S.: Strain distribution in an elastic substrate vibrated in a bioreactor for vocal fold tissue engineering. J. Biomech. **38**(12), 2406–2414 (2005)
124. Jia, X., Jia, M., Jha, A.K., Farran, A.J.E., Tong, Z.: Dynamic vibrational method and device for vocal fold tissue growth, Non-provisional Patent Application, US 12/781,305, May 17, 2010
125. Kutty, J.K., Webb, K.: Vibration stimulates vocal mucosa-like matrix expression by hydrogel-encapsulated fibroblasts. J. Tissue Eng. Regen. Med. **4**(1), 62–72 (2010)
126. Place, E.S., Evans, N.D., Stevens, M.M.: Complexity in biomaterials for tissue engineering. Nat. Mater. **8**(6), 457–470 (2009)
127. Huebsch, N., Mooney, D.J.: Inspiration and application in the evolution of biomaterials. Nature **462**(7272), 426–432 (2009)

Chapter 11
Nonviral Gene Delivery for Applications in Regenerative Medicine

Kory Blocker and Millicent Sullivan

Abstract To promote tissue repair and regeneration, much research in the field of tissue engineering has been aimed at the development of synthetic three-dimensional scaffolds to maintain the space and provide the mechanical support necessary for tissue development. However, to regenerate functional tissue of the same quality as natural tissue, the release of biochemical cues from these synthetic matrices will be necessary. While both bolus injection as well as polymeric encapsulation of proteins has been shown to stimulate regenerative processes, proteins have a fragile three-dimensional structure, which can be costly and difficult to synthesize. Because of the increased stability of DNA in comparison with proteins, plasmids may be used to stimulate gene transfer and localized expression of plasmid-encoded proteins to promote tissue development. However, due to the multiple barriers to gene transfer, a gene delivery vehicle must be carefully designed to impart control over the spatial and temporal release of the DNA. Furthermore, as the cellular processes involved in directing tissue repair are complex, delivery must be well controlled and stimulate gene expression that mimics the natural release processes of target growth factors and other proteins. Thus, this chapter will discuss the delivery control imparted by various mechanisms of gene transfer including bolus, polymeric, and substrate-mediated delivery. Matrix-controlled delivery methods for regenerative medicine applications will be explored in depth. Ultimately, to reform tissue of the necessary quality and functionality, the appropriate spatial and temporal patterning of gene expression profiles within targeted cells will need to be attained by synthetic systems.

Tissue engineering approaches have great potential for facilitating functional tissue repair and regeneration. Thus, much effort has gone into the development of synthetic

K. Blocker • M. Sullivan (✉)
Department of Chemical Engineering, University of Delaware,
150 Academy Street, Newark, DE 19716, USA
e-mail: msullivan@udel.edu

S.K. Bhatia (ed.), *Engineering Biomaterials for Regenerative Medicine: Novel Technologies for Clinical Applications*, DOI 10.1007/978-1-4614-1080-5_11,

scaffolds that provide mechanical support and maintain the three-dimensional (3D) space necessary for tissue development. The paradigm of artificial extracellular matrix (aECM) creation involves biomimicry to produce well-organized materials that maintain a highly hydrated environment with strength, stability, and the ability to resist compressive forces [1]. The biodegradability, porosity, and mechanical properties of aECM are critical for tissue repair or regeneration, and must be carefully selected for a given application. For example, while large pores induce the infiltration of cells, they limit the ability to create vasculature given that endothelial cells cannot traverse pores greater than a cell diameter [2]. In addition to its structural role, aECM must also facilitate cellular adhesion and regulate the delivery of soluble proteins like growth factors, which are critical modulators of gene expression by cells in engineered tissues [1]. Natural ECM binds, stores, and releases soluble biochemical cues, enabling control over tissue remodeling and regeneration [3]. Synthetic matrices must have a similar capacity to guide gene expression [1].

The cellular processes that direct tissue repair are often complex, and involve coordinated cellular activities and coupled signaling pathways. For example, the wound healing response involves complex interactions between different cells, ECM, and soluble biochemical cues to induce the proliferation, migration, and differentiation of several cell types to create a new matrix and promote actions such as angiogenesis, nerve sprouting, and/or production of hair follicles and glands, depending on the location and severity of injury [4, 5]. The interconnections between external stimuli, cellular behaviors, and tissue impact are detailed in Fig. 11.1. In particular, the creation of mature blood vessels requires a cascade of morphogenetic processes consisting of the coordinated actions of several cytokines and cellular signaling pathways [11, 12]. These activities initiate neovessel formation by inducing endothelial cell activation, proliferation, and migration; vessel formation terminates with the stimulation of smooth muscle cells and pericytes, which surround the mature blood vessels and seal off the new vasculature [12, 13]. Therefore, materials must be generated that can couple cell–ECM and cell–cell adhesion patterns with spatially and temporally controlled delivery of soluble biochemical cues to direct cellular behavior toward the development of fully functional vessels or other tissues [2]. This chapter will detail the motivation and advantages of biomaterial-mediated nonviral gene delivery to promote tissue repair and regeneration. The general challenges to therapeutic delivery for tissue regeneration and the rationale behind nonviral gene therapy, in particular, will be reviewed. Mechanisms of gene transfer including bolus delivery, polymeric delivery, and substrate-mediated delivery will be discussed.

Requirements for Therapeutic Delivery

Both the rate of release of a given growth factor or cytokine and the sequence of delivery for all factors involved in a process are critical in therapeutic delivery. Growth factors enable cellular manipulation by binding to receptors on the

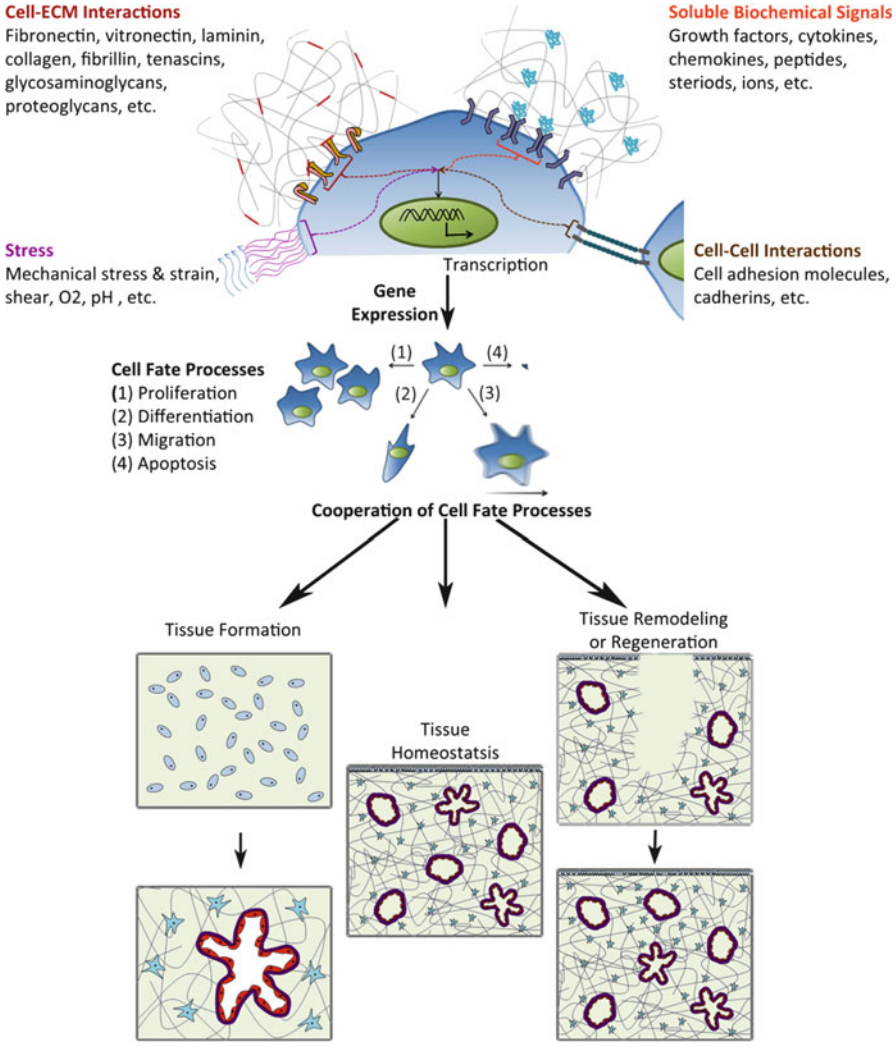

Fig. 11.1 Cellular behavior in tissues is regulated by complex signaling pathways that are influenced by interactions with ECM via integrins, binding to soluble biochemical cues, cell–cell interactions, and detection of external mechanical or chemical stress via cilia [6, 7] (as shown) or hemichannels [8]. These external cues control internal gene expression, determine cellular phenotype, and ultimately affect tissue growth response. Adapted by permission from ref. [9] (Copyright 2002 John Wiley &Sons, Inc.) and ref. [10] (Copyright 2005 Macmillan Publishers Ltd.)

cellular membrane and are able to mediate tissue development at very low concentrations [14, 15]. Furthermore, the complexity of processes such as angiogenesis may require multiple growth factors to be released to produce functional tissue [16]. For example, although vascular endothelial growth factor (VEGF) is considered to be the most potent stimulator of angiogenesis [17], members

of the VEGF family including VEGF-A, -B, -C, -D, -E, -F and placental growth factor (PlGF) [13, 17–20], members of the angiopoietin family [13, 18, 21], hepatocyte growth factor (HGF) [20], angiotensin-1 [20], and at least one member of the ephrin family [18] are collectively required to induce endothelial cells to produce neovessels. For mature blood vessel formation, other growth factors including platelet-derived growth factor (PDGF) [13, 21–24], transforming growth factor-β (TGF-β) [13, 19, 21–24], and fibroblast growth factor (FGF) [13, 19, 20] are required. FGF induces upregulation of VEGF, promotes endothelial cell proliferation and migration, and is critical in neovascularization, while PDGF and TGF-β are necessary to recruit smooth muscle cells and pericytes that promote ECM deposition and stabilize neovessels [13, 19]. Recently, heparin binding-epidermal growth factor (HB-EGF) has demonstrated a possible role in angiogenesis [19]. Additionally, transcription factors [22] and chemokines [19] have been shown to regulate the development of vasculature. For example, the use of transcription factors including homeobox protein Hox-A3 [25] and cardiac ankyrin repeat protein [26] have been shown to enhance cell migration and angiogenesis in several animal models. The process of delivering therapeutic biomolecules to induce the formation of functional vessels will require all of these factors to be delivered and used in a complementary and coordinated manner [18]. Thus, doses must be localized and carefully controlled by delivery strategies.

Therapeutic Protein Delivery

Previous studies have shown that regenerative processes can be stimulated by bolus delivery of growth factors or cytokines, either intravenously or via localized injection. For example, the delivery of angiopoietin-1 (Ang-1) combined with VEGF has been shown to increase the amount of neovascularization compared with the delivery of either Ang-1 or VEGF alone in both ex vivo and in vivo models [17]. However, even though high local concentrations of these factors are unnecessary [10], bolus administration of growth factor proteins requires large doses because most of the material is immediately cleared from the body [27]. Furthermore, current strategies suffer from an inherent loss of protein activity as well as decreased mobility due to the protein size [28].

Polymeric encapsulation of proteins has been shown to help in therapeutic delivery. The degradation profile and pore size of these polymeric release systems are important for controlling the protein release profile. For instance, in a murine hindlimb ischemic model, it was shown that releasing FGF-2 from gelatin crosslinked with poly(L-lysine) (PLL) or poly(L-glutamic acid) (PLG) produced substantial angiogenesis for 4 weeks, at which point the angiogenic capacity began to decrease due to growth factor exhaustion and scaffold biodegradation [29]. Similarly, $VEGF_{165}$ released from matrix metalloproteinase (MMP)-sensitive, Arg-Gly-Asp (RGD)-containing polyethylene glycol (PEG) networks induced complete remodeling of connective tissue containing new vasculature when the

networks were implanted subcutaneously in rats [30]. Prolonged growth factor presentation and retention have also been achieved by covalent immobilization of $VEGF_{121}$ to fibrin gels, which resulted in endothelial cell growth in a dose-dependent manner in vitro [27], and covalent crosslinking of VEGF in fibrin glue allowed for sustained release of bioactive VEGF from a subcutaneous implant in a mouse model [31]. However, in studies where FGF-1 and heparin were co-encapsulated in a fibrin glue, a burst release profile similar to bolus delivery profiles was observed with 70% of the growth factor released to the media after 24 h [32]. Thus, the materials used for polymeric delivery must be carefully manipulated such that a prolonged and sustained release profile may be obtained.

On the whole, protein therapies are well-established and have several benefits, including their predictable pharmacokinetics and therapeutic levels as well as the absence of long-term side effects [10]. Unfortunately, proteins have very short half-lives in vivo when delivered directly and may be denatured by encapsulation processes [12, 33–38]. Additionally, despite the high cost of recombinant proteins [12], they do not always provide the therapeutic benefit of natural proteins due to their atypical post-translational modifications [33, 34]. Therefore, a gene delivery approach in which cells would be modified to synthesize and deliver gene-encoded factors in a time-regulated and locally restricted manner to the desired location would overcome many limitations associated with the application of recombinant proteins [28]. The stability of plasmid DNA (pDNA) as well as the ability to manipulate the gene sequence to encode various proteins that introduce specific functions [39] have promoted the approach of transfecting cells with therapeutic protein-encoding DNA to enable cellular production of the encoded proteins in situ [40, 41].

Therapeutic Gene Delivery

Gene delivery is a newer area than protein delivery, and thus less is known about the long-term side effects and relative toxicity of delivered transgenes. Gene delivery can prolong and sustain the expression of transcription factors and/or growth factors as well as provide mechanisms to regulate the expression and delivery of multiple biochemical cues [12]. Reductions in gene expression by gene knock-out can also help with regenerative processes [17, 42–44], and have been accomplished by the use of antisense oligonucleotides and, more recently, small-interfering RNAs (siRNAs). DNA and RNA have been packaged within both viral and nonviral vehicles. Although viral delivery is currently more efficient than nonviral gene delivery, some viral vectors such as the adenoviral vector suffer from limitations on the gene size (36–38 kb) [45]. Viral vectors also raise safety concerns [46, 47] as they have the potential to mutate or recombine with wild-type viruses or cause cellular damage following repeated exposure [48]. These potential issues have led to the exploration of nonviral delivery methods, which provide control over the chemical and physical properties of the vehicle [49, 50]. pDNA can be manufactured using existing fermentation technology [28]. Low levels of transgene expression are sufficient for tissue repair and regeneration [28] and can be produced

via transient transfection [51]. Furthermore, nonviral gene delivery has the capability to coordinate delivery of the multiple growth factors that are required to form complex tissues such as vascular networks [20, 21].

Similar to the direct injection of proteins, the direct injection of plasmids has efficacy issues as it produces heterogeneous transgene expression in target tissues. Controlled design of a delivery vehicle may impart more control over the release profile, enable homogeneous transfection in a desired region [12, 20], and promote prolonged and sustained protein expression at adequate levels for tissue formation [21]. Additionally, it has been shown that the type of gene delivery vehicle employed has a large impact on the efficiency of gene transfer [28]. The vehicle must overcome multiple in vivo barriers to prevent degradation of the plasmid and promote localized and effective delivery [52]. The gene delivery systems discussed throughout this chapter will primarily be focused on nonviral methods to deliver pDNA. Bolus delivery methods will briefly be reviewed, and matrix-controlled delivery methods designed for regenerative medicine applications will be explored in depth.

Bolus Gene Delivery

Bolus gene delivery involves the direct introduction of a DNA formulation into the bloodstream or a tissue over a short period of time. Bolus delivery is limited by mass transport issues and deactivation process such as degradation, aggregation, and clearance from the system [53]. A successful gene delivery vehicle must traverse the bloodstream, localize to and be internalized by target cells, escape the endosome (if taken up via an endocytic pathway), enter the nucleus, and disassemble to enable transcription [54]. Thus, plasmids have been packaged into particles that are designed to overcome these extracellular and intracellular barriers (Fig.11.2). Spatial and temporal control over the administration of these particles can be achieved in vivo by a variety of methods, including delivery through catheters or direct tissue injection [55–65]. Additionally, modification of the delivery vehicle with receptor-specific ligands permits targeting to specific cells or tissues [66–70].

DNA complexes are typically formulated by the self-assembly of pDNA with cationic liposomes (to form lipoplexes) or polymers (to form polyplexes) as represented in Fig. 11.3. These complexes have been shown to protect DNA by providing a barrier against nucleases, serum factors, and liver scavengers, thus limiting certain paths of DNA elimination from the body [71, 72]. The positive charge of lipoplexes and polyplexes enables interaction with the negatively charged cell-surface glycosaminoglycans and promotes passive cellular internalization [52, 72–76]. Moreover, in many cases, the complexes are able to escape the endosome to be released to the cytosol [75, 77]. It is hypothesized that polyplexes are able to escape the endosome via the “proton sponge effect,” in which the buffering capacity of the cationic polymer leads to an osmotic pressure increase when the endosomal pH drops, ultimately causing the endosome to rupture and release the polyplexes to the cytosol [78]. Although a similar buffering effect may be active for lipoplexes [78], it is generally theorized that lipoplexes escape the

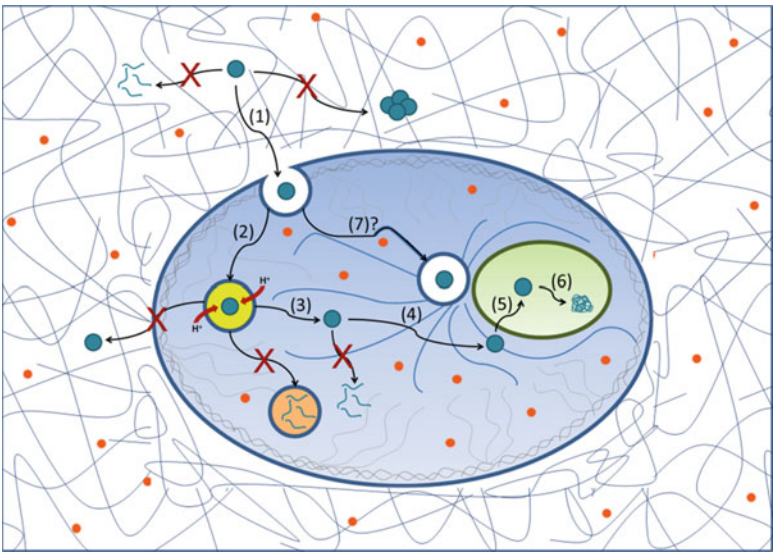

Fig. 11.2 There are several barriers to gene delivery. Primarily, the vehicle ( ) must avoid aggregation and degradation by extracellular and intracellular nucleases ( ) to target the cell and nucleus, respectively. Furthermore, the endosome may recycle the vehicle to the extracellular environment or the vehicle may be degraded by the lysosome upon lysosomal acidification, if it does not escape the endosome. Therefore, to transfect a cell, the vehicle must overcome the following barriers: (1) localize to a target cell; (2) internalize; (3) escape the endosome; (4) localize to the nucleus; (5) enter the nucleus; and (6) unpackage in the nucleus to be transcribed. Alternative intracellular trafficking patterns involving the trafficking of vehicle-containing endocytic vesicles to the nucleus via microtubules (7) may also occur

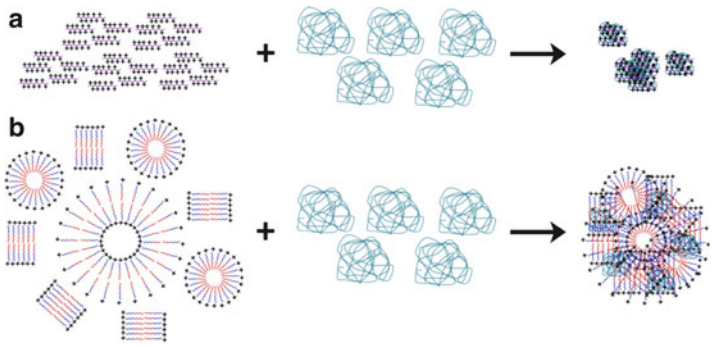

Fig. 11.3 (**a**) Polyplex formation spontaneously occurs when DNA (*blue*) is mixed with a cationic polymer (*purple*). Polyplexes typically form multimolecular aggregates containing one or several DNA molecules and many polymer molecules. (**b**) Lipoplex formation occurs when cationic amphiphiles are mixed with DNA. The amphiphiles are typically added at a concentration above the critical micelle concentration, and thus secondary structures such as micelles or liposomes exist in solution prior to the addition of DNA. Upon the addition of DNA, plasmids condense with these pre-formed amphiphilic assemblies to form lipoplexes

endosome by destabilizing the membrane through structural changes and interactions of the liposomal amphiphiles with the endosomal membrane, thus enabling the DNA release to the cytosol [79, 80]. Furthermore, to aid in specific cellular internalization, more efficient endosomal escape, vehicle trafficking through the cytosol, and vehicle nuclear internalization, additional components have been added to the complexes [54, 75, 81–93]. Lipoplex and polyplex materials have been extensively reviewed [52, 70, 79, 94–97]; consequently, the following paragraphs will provide a few brief highlights.

Lipoplexes have been formed from a variety of liposomal formulations, which often consist of a polyamine conjugated to a hydrophobic lipid tail [98–106]. Examples of amine-containing lipids capable of lipoplex formulation include 1,2-dimyristyloxypropyl-3-dimethyl-hydroxyethyl ammonium bromide (DMRIE) [107] and *n*-[1-(2,3-dioleoyloxy)propyl]-*n*,*n*,*n*-trimethylammonium methyl sulfate (DOTAP) [108]. Additionally, other novel liposomal vehicles have been formulated from guanidinium calixarenes, which were used to transfect RD-4 human rhabdomyosarcoma cells [109]. However, many of these liposomal agents require a helper agent [98, 102, 103, 106, 109] such as dioleoyl phophotidylethanolamine (DOPE) or dioleoyl phosphatidylcholine (DOPC) to aid in intermembrane interactions and enable cellular internalization as well as endosomal escape [79, 110, 111]. Some lipoplex formulations including Lipofectin® (*N*-[1-(2,3-dioleyloxy)propyl]-*n*,*n*,*n*-trimethylammonium chloride (DOTMA) and DOPE, 1:1 w/w) [61, 108, 112] and the Lipofectamine™ reagent family (proprietary formulations) [113–115] are highly potent in vitro. Lipofectin® has been shown to be capable of transfecting various mammalian cell lines including murine fibroblast cell lines, simian kidney cells, and rat hepatoma-derived cells [112]. Lipofectamine™ 2000 has also been shown to be capable of transfecting several mammalian cell lines with high efficiency in comparison to other currently available transfection agents [115]. In general, lipoplexes have been shown to be effective in transferring genes to endothelial cells in vitro and in vivo [61, 116–119]. Unfortunately, there is a cytotoxic effect associated with the delivery of lipoplexes, which increases with increasing lipid to DNA ratio; [120] this cytotoxicity is believed to be attributable to lipid disruption of the cellular and endosomal membranes. The poorly timed unpackaging of lipoplexes has also been suggested as a problematic issue with this mechanism of gene delivery [121].

DNA polyplexes have been created with various cationic polymers including PLL [122], poly-L-histidine [123], poly-L-ornithine [123], and chitosan [124]. Complexation with polyethylenimine (PEI) has been considered the gold standard in polyplex-mediated gene transfer due to the ability of PEI–DNA complexes to transfect many cell types with high efficiency in vitro [77]. However, PEI–DNA complexes have shown a limited ability to transfect certain types of cells, such as primary vascular endothelial cells [125], L929 murine fibroblasts [126], and non-dividing cells [127]. Additionally, PEI exhibits significant cytotoxicity both in vivo and in vitro [128, 129] and its non-biodegradability precludes repeated

administration [130]. Various degradable PEI and poly(amino esters) (PAE) derivatives have improved cytotoxicity profiles but maintain robust activities in a variety of cell types, including human endothelial cells [94, 129, 131, 132]. Dendritic polyamidoamines (PAMAMs) [133] such as starburst PAMAM dendrimers have also been shown to mediate DNA transfer to a number of cell types [134] including primary vascular endothelial cells [125]. These materials have low cytotoxicity, are non-immunogenic [135], and have been shown to transfect murine cardiac grafts in vivo [136, 137].

While all of these systems exhibit potential as therapeutics, in vivo bolus gene delivery using lipoplexes and polyplexes is still limited by poor availability and colloidal instability [52]. Most of these formulations have been shown to interact with serum components that cause aggregation or dissociation of the complexes [138]. As a result, complexes delivered intravenously are rapidly removed from the bloodstream (<30 min) [139]. Furthermore, the positive charge of the complexes induces reticuloendothelial clearance as well as protein adsorption and complex removal by macrophages [72]. PEG [140] and other polymers [141] can be used to screen lipo- or polyplex charge and thereby enable prolonged circulation times, improved biodistribution [142], reduced toxicity, and improved specificity [54]. Despite these improvements, only a small percentage of the DNA administered by bolus methods ever reaches its target cells, suggesting that mass transport issues remain a significant problem [53, 143].

Biomaterial-Controlled Gene Delivery

For regenerative medicine applications, there is often a desire to accomplish localized and sustained gene delivery, which has the potential to reduce the number of doses as well as the overall quantity of drug delivered [144]. While direct injection into a tissue of interest improves localization of gene expression, a series of injections would need to be conducted to ensure therapeutic benefit [17]. Alternatively, the structural scaffolds used in tissue engineering provide a convenient reservoir for the encapsulation and controlled release of plasmids or particles. Incorporation of plasmids or particles within a polymeric scaffold or immobilization of these particles onto a surface can significantly limit the extracellular barriers to gene delivery [145]. The scaffolds localize delivery to the site of healing or regeneration, and can be tailored to provide a desired drug release profile [52]. Numerous methods have been developed to provide controlled, localized, sustained, and triggered release of genes from scaffolds both in vitro and in vivo [46, 52, 75, 146–151]. These systems may be segregated into categories of gene-activated matrices (GAMs), substrate-mediated delivery materials, and multilayered thin films, as detailed in Fig. 11.4.

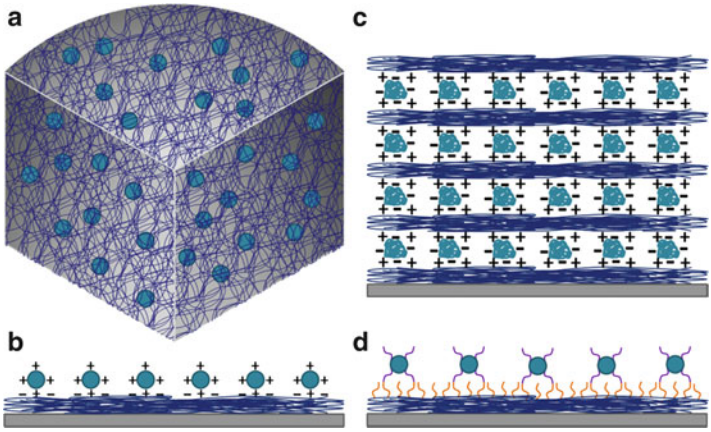

Fig. 11.4 Biomaterial-based gene delivery systems can be divided into several categories: (**a**) Gene-activated matrices or polymeric gene delivery consists of plasmids that are encapsulated in a 3D polymer scaffold or microparticle; (**b**) Nonspecific substrate-mediated gene delivery consists of plasmids or plasmid-containing vehicles that are physisorbed to a substrate. Most commonly cationic polyplexes are immobilized to negatively charged substrates as imaged; (**c**) Gene delivery multilayered thin films, which can be considered a class of nonspecific substrate-mediated gene delivery, are created primarily by immobilizing plasmids in layers of polycationic polymers; and (**d**) Specific substrate-mediated gene delivery is accomplished by immobilizing the plasmid or vehicle by chemical interactions or bonds

Polymeric Gene Delivery or Gene-Activated Matrices

Polymeric gene delivery has the potential to facilitate wound healing and tissue regeneration [152, 153] because of its ability to provide control over the location and release profile of delivered genes. Polymeric release systems are defined as polymer scaffolds that encapsulate DNA [46]. Depending on the material used, the scaffolds may need to be implanted or they may form the matrix upon injection [152, 153]. In all of these systems, DNA release may be accomplished by diffusion out of the scaffold and/or degradation of the matrix [46]. As a result, the release profile can be tailored by varying the material such that the DNA is delivered rapidly as in bolus delivery or in a prolonged fashion over a period of months [152, 154, 155].

DNA encapsulation provides several advantages in comparison with bolus methods for gene delivery during tissue regeneration. Encapsulation can provide some protection of the DNA from degradation [36, 46], thereby maintaining the bioactivity of the plasmid [156] and increasing the local concentration of active DNA such that the transfection efficiency is enhanced [36, 46, 157]. The matrix also promotes the interactions between cells and plasmids [39, 158], while simultaneously providing a 3D scaffold to maintain space [152, 153] and support the migration, proliferation, and differentiation of infiltrating cells [159]. In addition,

encapsulation allows for distribution of the vehicle throughout the 3D space [158], enabling sustained and prolonged gene delivery and the transfection of a large number of cells [152]. The mechanism of release, whether via diffusion or matrix degradation, can be tuned to control whether the cells in the surrounding tissue or cells migrating into the matrix are targeted [152, 153]. In general, matrices that deliver via scaffold degradation limit gene transfer to cells that infiltrate the matrix [152, 153, 160], whereas diffusion-controlled methods maintain the ability to target cells in the vicinity of the matrix [161] due to the limited transport of DNA through tissue [162]. The localized gene expression promoted by these delivery mechanisms can prevent the unwanted side effects caused by transfection in non-targeted tissues [163]. Finally, GAMs can be designed to deliver multiple plasmids simultaneously or sequentially to signal production of all of the therapeutic proteins that are necessary for tissue regeneration [164].

Different geometries and properties of GAMs can be achieved while maintaining the bioactivity of the encapsulated plasmid [165, 166]. Naked DNA has been encapsulated in scaffolds and microspheres composed of hydrophilic and hydrophobic polymers. Hydrophilic polymers that have been used include hyaluronan [39, 167], alginate [39], carboxymethyl cellulose [39], PEG [167], and collagen [39, 40, 153, 155, 167–169], whereas hydrophobic polymers that have been used include poly(lactide-*co*-glycolide) (PLGA) [39, 152, 156, 167, 170–172], polyanhydrides [167, 173], and ethylene vinyl-*co*-acetate (EVAc) [174, 175]. Collagen has generated particular interest because of its natural abundance in the body [52] and its inherent biocompatibility and biodegradability [176, 177]. Preformed collagen sponges have been shown to be capable of delivering DNA in vivo [40, 153, 155, 168, 169], and enable localized delivery and increased gene transfer efficiency and gene expression [39]. However, collagen matrices may deliver DNA via a burst release profile, thus requiring large quantities of DNA (100 mg) to achieve efficacy [153]. At this high dose of DNA, immune suppression may become significant [178]. Thus, to prevent dose dumping and improve efficacy, matrices that are able to prolong the release of pDNA, such as hybrid collagen gels [154, 179, 180] and polyanhydride matrices [173], are desirable. For example, when a PLGA sealant was added to a collagen GAM-coated stent, DNA release was extended beyond 24 h in a pig coronary model [181]. These PLGA-sealed collagen GAM-coated stents induced the transfection of $10.4 \pm 1.23\%$ of cells in the stented segment [181], whereas PLGA GAM-coated stents achieved levels of $1.14 \pm 0.7\%$ transfection with twice the quantity of DNA [182]. Similarly, EVAc polymers can provide sustained release of DNA on the time scale of weeks [174, 175] by solubilization of the drug and diffusion out of the matrix [183]. Control of plasmid release profiles from GAMs may be further exerted by the manipulation of polymer density [180, 184, 185] and extent of crosslinking [185, 186].

Multiple examples demonstrate the capacity of these extended release systems for controlling delivery such that appropriate physiological changes are observed. For example, in vivo implantation of a collagen or gelatin matrix incorporating PDGF, FGF-2, FGF-4, and FGF-6-encoding plasmids induced artery formation and

muscle repair [187–189]. Similarly, the use of a PLGA GAM formed by high pressure gas foaming resulted in sustained expression of plasmid-encoded PDGF and VEGF such that increases in vascularization (the size and density of blood vessels) and granulation tissue formation were observed in vivo [152, 188]. Small blood vessel formation was induced in a mouse model by the encapsulation of an endothelial locus-1-encoding plasmid in a PLGA scaffold [171]. In a rabbit model, the incorporation of VEGF-encoding plasmids in a phosphorylcholine polymer coating on a stent was able to increase endothelialization and recovery in comparison to a control stent [190]. Vascularization and matrix deposition have also been enhanced by the encapsulation of a PDGF-encoding plasmid in a PLGA implant in a rat subdermal model [152].

Further enhancements in GAM efficacy can be achieved when DNA is condensed with polycationic liposomes or polymers prior to encapsulation [46]. Condensation of the DNA is believed to protect it during the polymer processing required to create scaffolds [191, 192] and may increase the efficiency of DNA incorporation in the matrix [193]. For example, the level of plasmid encapsulation in both PLGA matrices and collagen sponges was increased by DNA complexation with PLL or PEI. In addition, the DNA condensation decreased the rate of release, thereby prolonging the release of DNA from the scaffold in vitro and in various rat and mouse models [155, 169, 194–197]. Similarly, the incorporation of polyplexes within PLGA scaffolds increased the efficiency of DNA encapsulation and facilitated the intracellular trafficking of the plasmid [195, 197, 198]. Condensation of DNA has also been shown to better protect it from nuclease degradation [78, 97] and promote cellular uptake [78, 199, 200]. Finally, complexation can protect DNA from the byproducts of scaffold degradation, as in the case of PLGA scaffolds, whose byproducts of lactic acid and glycolic acid can degrade the DNA [152].

Polymeric scaffolds can also be manipulated to interact with DNA vehicles to cause changes in the incorporation efficiency and rate of release [46]. For example, the encapsulation of lipoplexes within fibrin hydrogels achieved sustained release of the plasmid for 19 days in vitro. Unfortunately, there was a decreased transfection efficiency associated with the lipoplexes as compared to naked DNA that was ascribed to interactions between the lipoplexes and fibrinogen that were believed to inhibit DNA release [201]. In a rabbit ear wound model, the interaction between lipoplexes and fibrin enabled a high transfection efficiency to be achieved with lipoplexes encapsulated in a fibrin scaffold [202]. In this case, the interactions between the lipoplexes and the substrate were believed to maintain the bioactivity of the delivery vehicle and enhance cell uptake of the vector. PEI–DNA complexes have also been immobilized to the surface of or embedded within fibrin scaffolds, enabling control over the release rate of DNA and gene expression in vitro [203]. Immobilization to the polymeric scaffold can allow enhanced control of release via desorption from the substrate (if possible), diffusion, and degradation of the matrix [204].

Substrate-Mediated Gene Delivery

The interactions between DNA vehicles and delivery matrices have been explored in depth, such that a new class of matrix-mediated gene delivery has been established. As in the cases of PEI/DNA complexes and lipoplexes encapsulated in fibrin gels [201–203], these materials work by the immobilization of naked DNA or a vehicle onto a biomaterial surface and the subsequent release of the DNA into the cellular microenvironment [46]. This substrate-mediated or solid-phase gene delivery preserves the bioactivity of the vector [53] and reduces systemic removal of the vehicle from the body [205]. Gene delivery directly from a substrate mimics the natural delivery mechanisms of growth factors, which are sequestered by the ECM and are active either directly on the substrate or once they have been released [206]. Viruses are also known to bind to ECM to localize within the cellular microenvironment and thus more easily enter cells [161, 207–211]. Similarly, substrate immobilization of DNA increases the pDNA concentration near target cells and thereby increases the efficiency of gene transfer and gene expression in vitro and in vivo [50, 53, 143, 152, 157, 212–214]. Substrate binding also increases the concentration of DNA in the targeted tissue and localizes delivery to cells that adhere to the material [212, 215], avoiding the potentially cytotoxic and immunogenic effect of circulating vehicles [46]. The targeted nature of delivery may aid in tissue repair and regeneration [39], given that therapeutic proteins with the correct post-translational modifications are locally produced at physiological levels to provide biochemical cues to adherent cells [10, 143]. In addition to the increased ability to target delivery, surface immobilization of plasmids enables efficacy to be achieved at lower doses and provides additional opportunities to control the release profile [50, 216, 217]. For example, the immobilization of DNA to a substrate allows continuous release of plasmids for an extended period of time [53, 188, 218] and in a spatially controlled manner [143, 145, 212]. Depending on the mechanism of immobilization, DNA may be delivered to cells directly from the surface, or alternatively, tethers between the delivery vehicle and the substrate may need to be degraded before the vehicles are able to transfect cells [46]. In general, surface immobilization has been accomplished by utilizing both specific and nonspecific interactions [49, 53, 212]. In some cases, these interactions have been exploited to form multilayered thin films or cell-responsive materials.

Nonspecific (Physisorbtion) Immobilization of Vehicles

Depending on the molecular compositions of the vehicle and the surface, gene delivery vehicles can be immobilized to surfaces by nonspecific hydrophobic, electrostatic, and/or van der Waals interactions [46, 50, 219, 220]. Immobilization of lipoplexes or polyplexes onto self-assembled monolayer (SAM)-modified surfaces has been extensively explored because of the flexible chemistry of SAMs. For instance, lipoplexes were shown to preferentially immobilize onto

charged hydrophilic surfaces, to a lesser extent onto hydrophobic surfaces, and minimally onto uncharged hydrophilic substrates. Thus, electrostatic and hydrophobic interactions were shown to be the driving forces behind DNA sequestration. Release of the lipoplexes was controlled by serum component-mediated displacement of the complexes. Transfection efficiency was highest on the hydrophilic ionic surfaces and lowest on the hydrophobic substrates. Micropatterning SAMs allowed for spatial regulation of complex immobilization and transfection [145].

The use of SAM technology has also enabled exploration of PEG-modified surfaces through the use of EG-terminated alkanethiols. For example, as PEG is both hydrophobic as well as hydrophilic [221], hydrophobic interactions enabled PEI polyplex immobilization onto EG-terminated SAMs. The highest in vitro transgene expression levels were achieved on SAMs that combined EG and carboxylic acid head groups. In general, complexes immobilized to surfaces containing EG groups were smaller and less polydisperse than those immobilized onto non-EG surfaces, indicating decreased particle aggregation on the EG substrates. It is hypothesized that the EG groups increased the efficiency of transfection by preserving polyplex morphologies or by sterically hindering electrostatic interactions between the polyplexes and the surface [222].

Other methods of nonspecific immobilization involve the electrostatic interactions between DNA and cationic agents such as PLL [223], PEI [78, 169, 198], chitosan [124], *N*,*N*-(dimethylamino)ethylmethacrylate (DMAEMA) [224], or dendrimers such as PAMAM [133]. In one example, surfaces containing naked DNA bound to DMAEMA-modified poly(L-lactic acid) (PLLA) achieved high in vitro gene transfer efficiencies with low quantities of DNA, and also reduced the innate cytotoxicity of DMAEMA [224]. When applied to the skin of a hairless mouse, DNA complexed with PAMAM dendrimers and immobilized onto phosphatidyl glycerol-coated PLGA and collagen membranes achieved a six- to eight-fold increase in gene transfer efficiency in comparison to naked DNA delivery from the same substrates [218]. The immobilization of PEI polyplexes to silica nanoparticles [225, 226] and PLGA scaffolds [216] produced comparable or higher levels of gene expression with less DNA as compared to bolus delivery to various cell types in vitro. Furthermore, the cytotoxicity of PEI–DNA complexes may be reduced by immobilization, as in the case of PEI–DNA polyplexes that were adsorbed onto silica nanoparticles and used to transfect COS-1, Caco-2, and MH-S murine alveolar macrophages in vitro [225, 226].

In addition to promoting more efficient localized gene delivery with reduced cytotoxicity, immobilization has the potential to influence the method of cellular entry, and thereby impact the intracellular trafficking of the vehicle. For example, lipoplexes and polyplexes have been electrostatically immobilized to surfaces coated with recombinant fibronectin (FN) fragments and used to transfect NIH/3T3 cells in vitro. In comparison with polyplexes immobilized onto substrates coated with FN or a protein polymer of the same molecular weight as FN without cell adhesion sites, a larger number of the FN fragment-immobilized polyplexes were internalized by caveolae-mediated endocytosis. Furthermore, the FN-fragment immobilized polyplexes were shown to traffic via higher efficiency,

non-degradative pathways, displaying the potential for this system to promote effective gene transfer. This system demonstrates that the extracellular substrate can influence and manipulate the intracellular gene delivery processes, as well as impact vehicle immobilization and cellular entry [227].

The principles of nonspecific immobilization may be used with 3D scaffolds as well as with 2D surfaces. For example, the immobilization of PEI polyplexes onto porcine small intestinal submucosa (SIS) has shown utility for substrate-mediated gene delivery in vitro. Given that SIS is an ECM substrate composed of collagen intertwined with glycosaminoglycan chains and contains FGF-2, TGF-β, and VEGF, this system could provide the complex signaling necessary for tissue regeneration and wound repair [228]. In general, DNA immobilization onto 3D scaffolds enables space maintenance and promotes the efficient and localized delivery of therapeutics for tissue repair or regeneration.

Multilayered Thin Films

The principles of nonspecific immobilization have also been used to create multilayered thin films, which can both provide localized delivery of plasmids in vivo [181, 182, 190, 217, 229–232] and significantly sustain the release of a plasmid. These films have been created using many polyelectrolytes including PLL, PGA, chitosan, hyaluronan (HA), poly-(allylamine hydrochloride) (PAH), poly-(sodium-4-styrene-sulfonate) (PSS) [233], and β-cyclodextrin [234]. Multilayered thin films are created by alternately immersing a surface in a solution of a cationic molecule and in a solution of an anionic molecule in a process known as layer-by-layer (LbL) assembly [235–241]. The use of aqueous-based fabrication techniques in LbL assembly prevents the need for arduous wash steps to remove organic solvents [237]. Also, due to the simplicity of the assembly, thin films can easily be created on objects with complex geometries [242–244].

Gene delivery from thin films containing plasmids has been engineered through the use of materials that degrade or disassemble under physiological conditions [245, 246]. For example, hydrolytically degradable polyamines and LbL assembly have been used to electrostatically immobilize plasmid DNA within multilayered thin films on a stent [247]. The incorporation of plasmids within a multilayered thin film enables dose control based on the number of layers of DNA sequestered in the film [237]. By the sequestration of different DNA constructs between layers of polyamines, hydrolysis of the polyamine layers enables the release of multiple genes from a stent surface [247]. These nanometer-scale films were able to spatially and temporally control the gene delivery of multiple DNA constructs to promote transgene expression in vitro with various cell lines [237]. Additional hydrolytically degradable multilayered thin films have been created with LbL and poly(2-aminoethyl propylene phosphate) (PPE-EA) [248] or poly(glycoamidoamine)s [249]. A cationic poly(β-aminoester) ("polymer 1") was used to sequester DNA and promote cellular internalization upon hydrolytic degradation of the polycation and plasmid release [250–259]. Multilayered thin films fabricated with polymer 1

were capable of delivering bioactive plasmids for over 30 h in COS-7 cells [260]. The release profile was also altered to further extend the release period by increasing the hydrophobicity (and thereby decreasing the degradation rate) of the polymer [261–263]. This work indicates the ability to tailor plasmid release by altering polymer properties such as hydrophobicity, charge density, and side chain functionality, and thereby altering the degradation profile [237].

In addition to hydrolytic degradation, thin film disassembly/degradation and plasmid release have been initiated by changes in pH or ionic strength [264–269], chemical or enzymatic degradation of the polycationic layer [245, 246], competitive binding to disrupt receptor–ligand interactions [270–272], and external stimuli such as laser-induced degradation [243, 244, 273–275]. For example, degradation of LbL assemblies has been accomplished by creating thin films consisting of disulfide-bonded polycations which disassemble upon exposure to the reducing environments encountered in some biological systems [276]. The ability to disassemble a multilayered thin film upon enzymatic exposure was shown by the creation of a PLL/DNA LbL assembly, which sequestered and released plasmids upon exposure to alpha-chymotrypsin over a 35 h period in enzyme-containing buffer [277, 278]. Furthermore, polyvinyl alcohol-borate and chitosan multilayered thin films were shown to disassemble and release their payloads in a glucose solution based on competitive binding of glucose [279].

A recent and interesting approach toward thin film disassembly and plasmid release involves the alteration of the charge of the assembled cationic polymers. In these examples, the electrostatic bonds that drive film formation are disrupted when the side chains of the cationic polymers are hydrolyzed to introduce negative charge [280] or remove the cationic group [281–283]. The use of "charge-shifting" polymers allows degradation to occur in physiologically relevant systems over long time periods [284]. For instance, a poly(β-aminoester) incorporating "charge-shifting" ability was used to create a multilayered thin film capable of releasing bioactive plasmids continuously for at least 90 days in PBS solution [285]. Thus, multilayered thin films are capable of promoting sustained release of plasmids from a substrate via multiple types of degradative processes.

Specific Immobilization of Vehicles

In some cases, specific methods for immobilizing plasmids or vehicles onto substrates may enable more control over the release of a therapeutic from the substrate. Specific immobilization has been accomplished through the use of complementary functional groups on the vehicle and substrate, such as antigen–antibody interactions and biotin–avidin interactions [46]. The use of antigen–antibody interactions to immobilize gene delivery vehicles has primarily been explored with viruses [230, 286, 287]. For example, adenoviruses have been tethered to polyurethane films and collagen-coated polyurethane films using anti-adenovirus antibodies [286]. In an in vivo sheep model, the antibody-mediated specific immobilization of adenovirus to polyurethane films promoted localized

gene delivery to 25% of the cells attached to a polyurethane heart valve leaflet [288]. Using this same antigen–antibody interaction with a stent enabled localized arterial gene expression with no expression beyond the targeted tissue [215, 230, 287]. The immobilization of naked pDNA using antigen–antibody interactions has been explored by utilizing an anti-DNA antibody to immobilize a plasmid to a stent. In vivo, this stent was capable of delivering the plasmid with high efficiency and excellent target specificity, as no expression was observed outside of the area of implantation [289].

Specific immobilization using biotin–avidin interactions has been accomplished by complexing DNA with biotin-modified PLL [212] and PEI [53]and then binding the polyplexes to a neutravidin substrate. This method both protected the DNA from degradation by nucleases and inhibited aggregation of the polyplexes. The immobilization also maintained the DNA in the cellular microenvironment, and was thereby believed to enhance transfection efficiency and provide spatial control over transgene expression, as transfected cells were present only in areas where DNA had been tethered [53, 212]. When tested in vitro, release in this polyplex immobilization system was believed to occur via extracellular unpackaging of the DNA, such that the DNA was at least partially freed from the polycationic packaging materials prior to internalization. With the modified PEI system, release appeared to be dependent on the electrostatic interactions between the PEI amines and the neutravidin surface, given that transfection was independent of the biotin content. In all such systems, the binding affinity must be controlled to support substrate binding while still allowing the vehicle to be internalized by cells [53]. Thus, the vehicle and polymer used in substrate-mediated delivery systems must be adapted for both plasmid sequestration and a reasonable release profile [46].

Cell-Responsive Release

While many of the previously mentioned systems provide therapeutic delivery advantages, efficient transfection with these immobilized vehicles requires careful control to balance the binding of the vehicle and substrate with the ability to release the vehicle for cellular uptake [49, 50, 53, 143, 216]. Hence, the properties of the vehicle and/or substrate must be altered to manipulate the rate of vehicle release. Additionally, release is not cell-specific and occurs for any cell that comes into contact with the vehicle.

Cell-responsive release can allow for enhanced specificity over the types of cells that become transfected when growing on delivery substrates, and is needed in situations where transfection of locally growing cells other than the target cells is undesirable. Cell-responsive release has primarily been accomplished by having some portion of the delivery system degrade and release the vehicle upon exposure to an enzyme. One example of this is a system in which pDNA is semi-covalently immobilized onto a fibrin matrix as shown in Fig. 11.5. Upon exposure to plasmin, the matrix degrades and releases the plasmid. This system was created by condensing pDNA with a peptide containing an N-terminal transglutaminase substrate, as

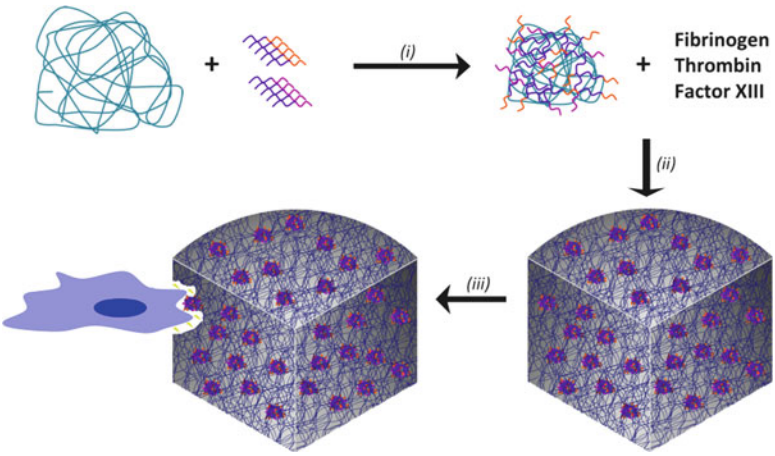

Fig. 11.5 Cell-responsive gene delivery has been accomplished through the use of a fibrin matrix [290, 291]. (i) Complexation of pDNA took place using two peptides, NQEQVSPLGGGCHK KKKKKHC and CHKKKKKKHCGGGPKKKRKVEDPY, which contained a fibrin-binding region (*pink*), DNA-binding regions (*purple*), and a nuclear localization sequence (*orange*). (ii) The complexes were covalently immobilized in fibrin gels by enzymatic crosslinking, which took place upon the addition of fibrinogen, thrombin, and factor XIII. (iii) Upon cellular production of plasminogen both in vitro and in vivo, localized degradation of the fibrin matrix took place and released the plasmids

well as multiple lysines to complex the DNA, and two cysteines to stabilize the complexes by forming disulfide bridges. These condensates were covalently immobilized onto fibrin matrices by the cross-linking activity of transglutaminase. Subsequently, the plasmid was released following cellular production of plasmin and local degradation of the fibrin matrix [290]. The effectiveness of this system was demonstrated in a mouse wound model, in which the localized delivery of hypoxia-inducible factor (HIF)-1α-encoding DNA induced the upregulation of proangiogenic factors and a subsequent fourfold increase in mature blood vessel formation, in comparison with the application of VEGF protein from fibrin gels [291]. However, because the immobilization process for this system is not carefully controlled, the system may promote some release via diffusion in addition to degradation. Also, the release of the plasmid is tied to the properties of the matrix and depends upon the use of fibrin.

To build upon the successes of previous work, our group has designed a cell-responsive substrate-mediated gene delivery system in which the physical and chemical properties of the vehicle and substrate are partially decoupled from the release mechanism [292]. This system, shown in Fig. 11.6, enables plasmid release upon cellular demand, given that the pDNA is semi-covalently bound to the substrate via an enzymatically labile peptide sequence. To accomplish this type of immobilization, pDNA is chemically functionalized with peptide nucleic acid (PNA) clamps that allow the peptide to be attached directly to the plasmid. The coupled peptide includes cell adhesive and MMP-degradable sequences to promote

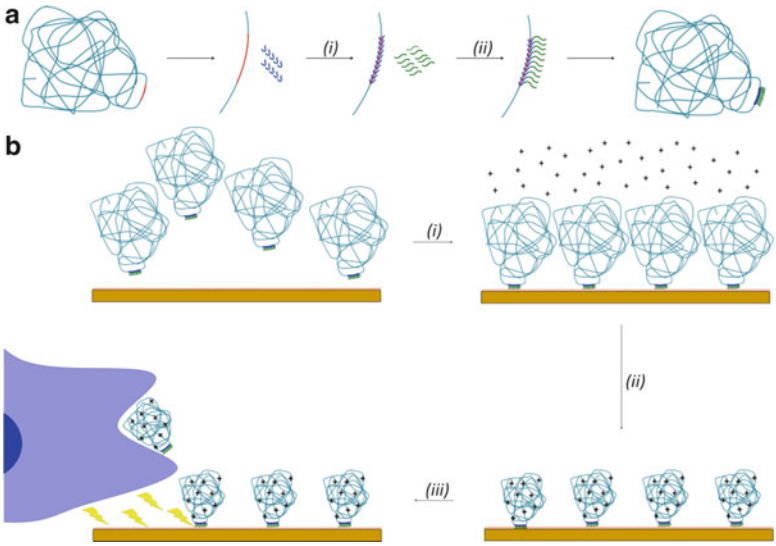

Fig. 11.6 Substrate-independent cell-responsive gene delivery can be accomplished through the use of an enzymatically labile peptide tether [292]. (**a**) Using a plasmid with PNA-binding regions (*red*), PNA is able to functionalize the plasmid (i). Following functionalization, peptides with enzymatically labile regions can be covalently tethered to the pDNA–PNA conjugate (ii). (**b**) pDNA–PNA–peptide conjugates were bound to a model substrate (i) and subsequently complexed with a polycation (ii). Upon exposure to cell-produced enzymes, the peptide tether is cleaved, releasing the plasmid in a local manner (iii)

the release and uptake of the plasmid in a cell-responsive manner. After pDNA-PNA-peptide (DPP) conjugate formation, the DPP conjugates may be directly linked to any of a variety of biomaterial surfaces. The system was established by attaching the conjugates to SAM-modified gold surfaces because of their well-defined nature [293, 294] and easily manipulated [295]. In vitro evidence details the specificity of the surface immobilization of the conjugates and the ability to transfect cells in a cell-responsive manner. Thus, this system allows for surface immobilization, independent control over the transfection agent and substrate, and overall greater control over cellular transfection.

Conclusions

The complex signaling processes involved in angiogenesis, wound healing, and tissue regeneration necessitate both a better understanding of regenerative processes, and improved methods for controlling the delivery of therapeutic genes and proteins within the healing environment. For example, the impact of specific genes and proteins within the angiogenic signaling cascade must be understood to promote the formation of functional blood vessels within new tissues [12].

The current lack of understanding is manifested by the inability to translate successes in animal models into clinical successes [20]. Strong angiogenic factors such as VEGF can cause many negative side effects [296–299], and thus the toxic levels must be determined to set maximal doses [300]. In the case of VEGF, successful angiogenesis seems to be produced by appropriate VEGF gradients within the target tissue [301], which may be more easily obtained by the use of tissue engineering substrates that can provide spatially controlled gene delivery.

Systems capable of the controlled delivery of multiple plasmids have the potential to improve the stability and functionality of newly formed tissues. For example, genes that regulate the production of proangiogenic proteins improve the vasculature produced [17], as shown in the case of the fibrin-mediated delivery of a HIF-1α encoding gene [291]. In general, biomaterial systems that sequester plasmids enable the localized and sustained delivery that is required for the formation of new tissues, while reducing the necessary doses for inducing efficacy and improving gene utilization. New understanding of the correlations between surface-vehicle chemistry and vehicle release, as well as improved appreciation for the role of the substrate in determining the efficiency of intracellular utilization have poised matrix-mediated delivery systems for success in the tissue engineering arena. Furthermore, the development of cell-responsive systems may enable release to targeted cells without restricting the choices of the transfection agent and/or surface. Plasmids covalently immobilized to fibrin matrices were released by the action of plasmin, and release was independent of the complexation agent. The release of DNA by cleavage of an MMP-labile peptide tether was independent of both the complexation agent and the substrate. In general, gene delivery systems for tissue regeneration must be highly tailorable such that the matrix substrates and the transfection agents may be selected for the application at hand, without reducing the potential for controlled release. Ultimately, efficacy will be dependent upon the appropriate spatial and temporal patterning of gene expression profiles within targeted cells, such that these cells are stimulated to reform natural and functional tissues.

References

1. Putnam, A.J., Mooney, D.J.: Tissue engineering using synthetic extracellular matrices. Nat. Med. **2**, 824–826 (1996)
2. Davis, M.E., Hsieh, P.C.H., Grodzinsky, A.J., Lee, R.T.: Custom design of the cardiac microenvironment with biomaterials. Circ. Res. **97**, 8–15 (2005)
3. Ramirez, F., Rifkin, D.B.: Cell signaling events: A view from the matrix. Matrix Biol. **22**, 101–107 (2003)
4. Martin, P.: Wound healing–Aiming for perfect skin regeneration. Science **276**, 75–81 (1997)
5. Singer, A.J., Clark, R.A.: Cutaneous wound healing. N. Engl. J. Med. **341**, 738–746 (1999)
6. Malone, A.M., Anderson, C.T., Tummala, P., Kwon, R.Y., Johnston, T.R., Stearns, T., Jacobs, C.R.: Primary cilia mediate mechanosensing in bone cells by a calcium-independent mechanism. Proc. Natl Acad. Sci. USA **104**, 13325–13330 (2007)

7. Nauli, S.M., Kawanabe, Y., Kaminski, J.J., Pearce, W.J., Ingber, D.E., Zhou, J.: Endothelial cilia are fluid shear sensors that regulate calcium signaling and nitric oxide production through polycystin-1. Circulation **117**, 1161–1171 (2008)
8. Burra, S., Nicolella, D.P., Francis, W.L., Freitas, C.J., Mueschke, N.J., Poole, K., Jiang, J.X.: Dendritic processes of osteocytes are mechanotransducers that induce the opening of hemichannels. Proc. Natl Acad. Sci. USA **107**, 13648–13653 (2010)
9. Bottaro, D.P., Liebmann-Vinson, A., Heidaran, M.A.: Molecular signaling in bioengineered tissue microenvironments. Ann. N. Y. Acad. Sci. **961**, 143–153 (2002)
10. Lutolf, M.P., Hubbell, J.A.: Synthetic biomaterials as instructive extracellular micro-environments for morphogenesis in tissue engineering. Nat. Biotechnol. **23**, 47–55 (2005)
11. Davis, G.E., Bayless, K.J., Mavila, A.: Molecular basis of endothelial cell morphogenesis in three-dimensional extracellular matrices. Anat. Rec. **268**, 252–275 (2002)
12. Laham, R.J., Mannam, A., Post, M.J., Sellke, F.: Gene transfer to induce angiogenesis in myocardial and limb ischaemia. Expert Opin. Biol. Ther. **1**, 985–994 (2001)
13. Hirschi, K.K., Skalak, T.C., Peirce, S.M., Little, C.D.: Vascular assembly in natural and engineered tissues. Ann. N. Y. Acad. Sci. **961**, 223–242 (2002)
14. Chen, R.R., Mooney, D.J.: Polymeric growth factor delivery strategies for tissue engineering. Pharm. Res. **20**, 1103–1112 (2003)
15. Alberts, B., Johnson, A., Lewis, J., Raff, M., Roberts, K., Walter, P.: Cell communication. In Gibbs, S. (ed.) Molecular Biology of the Cell; p. 831. Garland Science, New York (2002)
16. Fischbach, C.; Mooney, D.: Polymeric systems for bioinspired delivery of angiogenic molecules. Polymers for Regenerative Medicine. p. 191–221. (2006)
17. Uchida, C., Haas, T.L.: Evolving strategies in manipulating VEGF/VEGFR signaling for the promotion of angiogenesis in ischemic muscle. Curr. Pharm. Des. **15**, 411–421 (2009)
18. Gale, N.W., Yancopoulos, G.D.: Growth factors acting via endothelial cell-specific receptor tyrosine kinases: VEGFs, angiopoietins, and ephrins in vascular development. Genes Dev. **13**, 1055–1066 (1999)
19. Barrientos, S., Stojadinovic, O., Golinko, M.S., Brem, H., Tomic-Canic, M.: Growth factors and cytokines in wound healing. Wound Repair Regen. **16**, 585–601 (2008)
20. Brewster, L.P., Brey, E.M., Greisler, H.P.: Cardiovascular gene delivery: The good road is awaiting. Adv. Drug Deliv. Rev. **58**, 604–629 (2006)
21. von Degenfeld, G., Banfi, A., Springer, M.L., Blau, H.M.: Myoblast-mediated gene transfer for therapeutic angiogenesis and arteriogenesis. Br. J. Pharmacol. **140**, 620–626 (2003)
22. Carmeliet, P.: Mechanisms of angiogenesis and arteriogenesis. Nat. Med. **6**, 389–395 (2000)
23. Hellstrom, M., Kalen, M., Lindahl, P., Abramsson, A., Betsholtz, C.: Role of PDGF-B and PDGFR-β in recruitment of vascular smooth muscle cells and pericytes during embryonic blood vessel formation in the mouse. Development **126**, 3047–3055 (1999)
24. Hirschi, K.K., Rohovsky, S.A., Beck, L.H., Smith, S.R., D'Amore, P.A.: Endothelial cells modulate the proliferation of mural cell precursors via platelet-derived growth factor-BB and heterotypic cell contact. Circ. Res. **84**, 298–305 (1999)
25. Mace, K.A., Hansen, S.L., Myers, C., Young, D.M., Boudreau, N.: HOXA3 induces cell migration in endothelial and epithelial cells promoting angiogenesis and wound repair. J. Cell Sci. **118**, 2567–2577 (2005)
26. Shi, Y., Reitmaier, B., Regenbogen, J., Slowey, R.M., Opalenik, S.R., Wolf, E., Goppelt, A., Davidson, J.M.: CARP, a cardiac ankyrin repeat protein, is up-regulated during wound healing and induces angiogenesis in experimental granulation tissue. Am. J. Pathol. **166**, 303–312 (2005)
27. Zisch, A.H., Schenk, U., Schense, J.C., Sakiyama-Elbert, S.E., Hubbell, J.A.: Covalently conjugated VEGF-fibrin matrices for endothelialization. J. Control. Release **72**, 101–113 (2001)
28. Eming, S.A., Krieg, T., Davidson, J.M.: Gene therapy and wound healing. Clin. Dermatol. **25**, 79–92 (2007)

29. Layman, H., Spiga, M.G., Brooks, T., Pham, S., Webster, K.A., Andreopoulos, F.M.: The effect of the controlled release of basic fibroblast growth factor from ionic gelatin-based hydrogels on angiogenesis in a murine critical limb ischemic model. Biomaterials **28**, 2646–2654 (2007)
30. Lutolf, M.P., Raeber, G.P., Zisch, A.H., Tirelli, N., Hubbell, J.A.: Cell-responsive synthetic hydrogels. Adv. Mater. **15**, 888–892 (2003)
31. Ehrbar, M., Zeisberger, S.M., Raeber, G.P., Hubbell, J.A., Schnell, C., Zisch, A.H.: The role of actively released fibrin-conjugated VEGF for VEGF receptor 2 gene activation and the enhancement of angiogenesis. Biomaterials **29**, 1720–1729 (2008)
32. Shireman, P.K., Hampton, B., Burgess, W.H., Greisler, H.P.: Modulation of vascular cell growth kinetics by local cytokine delivery from fibrin glue suspensions. J. Vasc. Surg. **29**, 852–861 (1999)
33. Edelman, E.R., Nugent, M.A., Karnovsky, M.J.: Perivascular and intravenous administration of basic fibroblast growth factor: Vascular and solid organ deposition. Proc. Natl Acad. Sci. USA **90**, 1513–1517 (1993)
34. Bowenpope, D.F., Malpass, T.W., Foster, D.M., Ross, R.: Platelet-derived growth factor in vivo: Levels, activity, and rate of clearance. Blood **64**, 458–469 (1984)
35. Houchin-Ray, T., Swift, L.A., Jang, J.H., Shea, L.D.: Patterned PLG substrates for localized DNA delivery and directed neurite extension. Biomaterials **28**, 2603–2611 (2007)
36. Langer, R.: Drug delivery and targeting. Nature **392**, 5–10 (1998)
37. Fu, K., Klibanov, A.M., Langer, R.: Protein stability in controlled-release systems. Nat. Biotechnol. **18**, 24–25 (2000)
38. Zhu, G., Mallery, S.R., Schwendeman, S.P.: Stabilization of proteins encapsulated in injectable poly (lactide-coglycolide). Nat. Biotechnol. **18**, 52–57 (2000)
39. Bonadio, J.: Tissue engineering via local gene delivery: Update and future prospects for enhancing the technology. Adv. Drug Deliv. Rev. **44**, 185–194 (2000)
40. Bonadio, J.: Tissue engineering via local gene delivery. J. Mol. Med.-JMM **78**, 303–311 (2000)
41. Bonadio, J.: Genetic approaches to tissue repair. Reparative Medicine: Growing Tissues and Organs **961**, 58–60 (2002)
42. Nguyen, T., Menocal, E.M., Harborth, J., Fruehauf, J.H.: RNAi therapeutics: An update on delivery. Curr. Opin. Mol. Ther. **10**, 158–167 (2008)
43. In *Quark Pharmaceuticals* Fremont, CA, USA (2007)
44. Cheema, S.K., Chen, E., Shea, L.D., Mathur, A.B.: Regulation and guidance of cell behavior for tissue regeneration via the siRNA mechanism. Wound Repair Regen. **15**, 286–295 (2007)
45. Cattaneo, R., Miest, T., Shashkova, E.V., Barry, M.A.: Reprogrammed viruses as cancer therapeutics: Targeted, armed and shielded. Nat. Rev. Microbiol. **6**, 529–540 (2008)
46. Pannier, A.K., Shea, L.D.: Controlled release systems for DNA delivery. Mol. Ther. **10**, 19–26 (2004)
47. Nazir, S.A., Metcalf, J.P.: Innate immune response to adenovirus. J. Investig. Med. **53**, 292–304 (2005)
48. Felgner, P.L., Rhodes, G.: Gene therapeutics. Nature **349**, 351–352 (1991)
49. Bengali, Z., Pannier, A.K., Segura, T., Anderson, B.C., Jang, J.H., Mustoe, T.A., Shea, L.D.: Gene delivery through cell culture substrate adsorbed DNA complexes. Biotechnol. Bioeng. **90**, 290–302 (2005)
50. Bengali, Z., Shea, L.D.: Gene delivery by immobilization to cell-adhesive substrates. MRS Bull. **30**, 659–662 (2005)
51. Storrie, H., Mooney, D.J.: Sustained delivery of plasmid DNA from polymeric scaffolds for tissue engineering. Adv. Drug Deliv. Rev. **58**, 500–514 (2006)
52. Segura, T., Shea, L.D.: Materials for non-viral gene delivery. Annu. Rev. Mater. Res. **31**, 25–46 (2001)
53. Segura, T., Volk, M.J., Shea, L.D.: Substrate-mediated DNA delivery: Role of the cationic polymer structure and extent of modification. J. Control. Release **93**, 69–84 (2003)

54. Schaffer, D.V., Lauffenburger, D.A.: Targeted synthetic gene delivery vectors. Curr. Opin. Mol. Ther. **2**, 155–161 (2000)
55. Wolff, J.A., Malone, R.W., Williams, P., Chong, W., Acsadi, G., Jani, A., Felgner, P.L.: Direct gene transfer into mouse muscle in vivo. Science **247**, 1465–1468 (1990)
56. Wolff, J.A., Williams, P., Acsadi, G., Jiao, S., Jani, A., Chong, W.: Conditions affecting direct gene transfer into rodent muscle in vivo. Biotechniques **11**, 474–485 (1991)
57. Hickman, M.A., Malone, R.W., Lehmann-Bruinsma, K., Sih, T.R., Knoell, D., Szoka, F.C., Walzem, R., Carlson, D.M., Powell, J.S.: Gene expression following direct injection of DNA into liver. Hum. Gene Ther. **5**, 1477–1483 (1994)
58. Riessen, R., Isner, J.M.: Prospects for site-specific delivery of pharmacologic and molecular therapies. J. Am. Coll. Cardiol. **23**, 1234–1244 (1994)
59. Sikes, M.L., O'Malley Jr., B.W., Finegold, M.J., Ledley, F.D.: In vivo gene transfer into rabbit thyroid follicular cells by direct DNA injection. Hum. Gene Ther. **5**, 837–844 (1994)
60. Schwartz, B., Benoist, C., Abdallah, B., Rangara, R., Hassan, A., Scherman, D., Demeneix, B.A.: Gene transfer by naked DNA into adult mouse brain. Gene Ther. **3**, 405–411 (1996)
61. Laitinen, M., Hartikainen, J., Hiltunen, M.O., Eranen, J., Kiviniemi, M., Narvanen, O., Makinen, K., Manninen, H., Syvanne, M., Martin, J.F., Laakso, M., Yla-Herttuala, S.: Catheter-mediated vascular endothelial growth factor gene transfer to human coronary arteries after angioplasty. Hum. Gene Ther. **11**, 263–270 (2000)
62. Beeri, R., Guerrero, J.L., Supple, G., Sullivan, S., Levine, R.A., Hajjar, R.J.: New efficient catheter-based system for myocardial gene delivery. Circulation **106**, 1756–1759 (2002)
63. Eastman, S.J., Baskin, K.M., Hodges, B.L., Chu, Q., Gates, A., Dreusicke, R., Anderson, S., Scheule, R.K.: Development of catheter-based procedures for transducing the isolated rabbit liver with plasmid DNA. Hum. Gene Ther. **13**, 2065–2077 (2002)
64. Losordo, D.W., Vale, P.R., Hendel, R.C., Milliken, C.E., Fortuin, F.D., Cummings, N., Schatz, R.A., Asahara, T., Isner, J.M., Kuntz, R.E.: Phase 1/2 placebo-controlled, double-blind, dose-escalating trial of myocardial vascular endothelial growth factor 2 gene transfer by catheter delivery in patients with chronic myocardial ischemia. Circulation **105**, 2012–2018 (2002)
65. Sharif, F., Daly, K., Crowley, J., O'Brien, T.: Current status of catheter- and stent-based gene therapy. Cardiovasc. Res. **64**, 208–216 (2004)
66. Miller, N., Vile, R.: Targeted vectors for gene therapy. FASEB J. **9**, 190–199 (1995)
67. Sudimack, J., Lee, R.J.: Targeted drug delivery via the folate receptor. Adv. Drug Deliv. Rev. **41**, 147–162 (2000)
68. Hashida, M., Nishikawa, M., Yamashita, F., Takakura, Y.: Cell-specific delivery of genes with glycosylated carriers. Adv. Drug Deliv. Rev. **52**, 187–196 (2001)
69. Pardridge, W.M.: Drug and gene targeting to the brain with molecular Trojan horses. Nat. Rev. Drug Discov. **1**, 131–139 (2002)
70. Torchilin, V.P.: Recent advances with liposomes as pharmaceutical carriers. Nat. Rev. Drug Discov. **4**, 145–160 (2005)
71. Boeckle, S., von Gersdorff, K., van der Piepen, S., Culmsee, C., Wagner, E., Ogris, M.: Purification of polyethylenimine polyplexes highlights the role of free polycations in gene transfer. J. Gene Med. **6**, 1102–1111 (2004)
72. Mahato, R.I., Smith, L.C., Rolland, A.: Pharmaceutical perspectives of nonviral gene therapy. Adv. Genet. **41**, 95–156 (1999)
73. Ruponen, M., Yla-Herttuala, S., Urtti, A.: Interactions of polymeric and liposomal gene delivery systems with extracellular glycosaminoglycans: Physicochemical and transfection studies. Biochim. Biophys. Acta-Biomembr. **1415**, 331–341 (1999)
74. Mislick, K.A., Baldeschwieler, J.D.: Evidence for the role of proteoglycans in cation-mediated gene transfer. Proc. Natl Acad. Sci. USA **93**, 12349–12354 (1996)
75. Niidome, T., Huang, L.: Gene therapy progress and prospects: Nonviral vectors. Gene Ther. **9**, 1647–1652 (2002)

76. Herweijer, H., Wolff, J.A.: Progress and prospects: Naked DNA gene transfer and therapy. Gene Ther. **10**, 453–458 (2003)
77. Godbey, W.T., Wu, K.K., Mikos, A.G.: Poly(ethylenimine) and its role in gene delivery. J. Control. Release **60**, 149–160 (1999)
78. Boussif, O., Lezoualch, F., Zanta, M.A., Mergny, M.D., Scherman, D., Demeneix, B., Behr, J.P.: A versatile vector for gene and oligonucleotide transfer into cells in culture and in vivo - Polyethylenimine. Proc. Natl Acad. Sci. USA **92**, 7297–7301 (1995)
79. Wasungu, L., Hoekstra, D.: Cationic lipids, lipoplexes and intracellular delivery of genes. J. Control. Release **116**, 255–264 (2006)
80. Hoekstra, D., Rejman, J., Wasungu, L., Shi, F., Zuhorn, I.: Gene delivery by cationic lipids: In and out of an endosome. Biochem. Soc. Trans. **035**, 68–71 (2007)
81. Ogris, M., Steinlein, P., Carotta, S., Brunner, S., Wagner, E.: DNA/polyethylenimine transfection particles: Influence of ligands, polymer size, and PEGylation on international and gene expression. AAPS Pharmsci. **3**, E21 (2001)
82. Fisher, K.D., Ulbrich, K., Subr, V., Ward, C.M., Mautner, V., Blakey, D., Seymour, L.W.: A versatile system for receptor-mediated gene delivery permits increased entry of DNA into target cells, enhanced delivery to the nucleus and elevated rates of transgene expression. Gene Ther. **7**, 1337–1343 (2000)
83. Tan, P.H., King, W.J., Chen, D., Awad, H.M., Mackett, M., Lechler, R.I., Larkin, D.F.P., George, A.J.T.: Transferrin receptor-mediated gene transfer to the corneal endothelium. Transplantation **71**, 552–560 (2001)
84. Hart, S.L., Harbottle, R.P., Cooper, R., Miller, A., Williamson, R., Coutelle, C.: Gene delivery and expression mediated by an integrin-binding peptide. Gene Ther. **2**, 552–554 (1995)
85. Theoharis, S., Manunta, M., Tan, P.H.: Gene delivery to vascular endothelium using chemical vectors: implications for cardiovascular gene therapy. Expert Opin. Biol. Ther. **7**, 627–643 (2007)
86. Nicklin, S.A., White, S.J., Watkins, S.J., Hawkins, R.E., Baker, A.H.: Selective targeting of gene transfer to vascular endothelial cells by use of peptides isolated by phage display. Circulation **102**, 231–237 (2000)
87. White, S.J., Nicklin, S.A., Buning, H., Brosnan, M.J., Leike, K., Papadakis, E.D., Hallek, M., Baker, A.H.: Targeted gene delivery to vascular tissue in vivo by tropism-modified adeno-associated virus vectors. Circulation **109**, 513–519 (2004)
88. Morpurgo, M., Kirschner, M., Radu, A.: An approach to increased polyplex gene delivery by peptides selected from a phage display library. J. Biochem. Biophys. Methods **52**, 31–43 (2002)
89. Jost, P.J., Harbottle, R.P., Knight, A., Miller, A.D., Coutelle, C., Schneider, H.: A novel peptide, THALWHT, for the targeting of human airway epithelia. FEBS Lett. **489**, 263–269 (2001)
90. Tan, P.H., Beutelspacher, S.C., Wang, Y.H., McClure, M.O., Ritter, M.A., Lombardi, G., George, A.J.: Immunolipoplexes: an efficient, nonviral alternative for transfection of human dendritic cells with potential for clinical vaccination. Mol. Ther. **11**, 790–800 (2005)
91. Tan, P.H., Manunta, M., Ardjomand, N., Xue, S.A., Larkin, D.F., Haskard, D.O., Taylor, K. M., George, A.J.: Antibody targeted gene transfer to endothelium. J. Gene Med. **5**, 311–323 (2003)
92. Schaffer, D.V., Lauffenburger, D.A.: Optimization of cell surface binding enhances efficiency and specificity of molecular conjugate gene delivery. J. Biol. Chem. **273**, 28004–28009 (1998)
93. Ziady, A.G., Ferkol, T., Dawson, D.V., Perlmutter, D.H., Davis, P.B.: Chain length of the polylysine in receptortargeted gene transfer complexes affects duration of reporter gene expression both in vitro and in vivo. J. Biol. Chem. **274**, 4908–4916 (1999)
94. Wong, S.Y., Pelet, J.M., Putnam, D.: Polymer systems for gene delivery-past, present, and future. Prog. Polym. Sci. **32**, 799–837 (2007)

95. Thomas, M., Klibanov, A.M.: Non-viral gene therapy: polycation-mediated DNA delivery. Appl. Microbiol. Biotechnol. **62**, 27–34 (2003)
96. Brown, M.D., Schatzlein, A.G., Uchegbu, I.F.: Gene delivery with synthetic (non viral) carriers. Int. J. Pharm. **229**, 1–21 (2001)
97. Cullis, P.R., Chonn, A.: Recent advances in liposome technologies and their applications for systemic gene delivery. Adv. Drug Deliv. Rev. **30**, 73–83 (1998)
98. Felgner, J.H., Kumar, R., Sridhar, C.N., Wheeler, C.J., Tsai, Y.J., Border, R., Ramsey, P., Martin, M., Felgner, P.L.: Enhanced gene delivery and mechanism studies with a novel series of cationic lipid formulations. J. Biol. Chem. **269**, 2550–2561 (1994)
99. Remy, J.S., Sirlin, C., Vierling, P., Behr, Gene transfer with a series of lipophilic DNA-binding molecules. J.P.: Bioconjug. Chem. **5**, 647–654 (1994)
100. Gao, X., Huang, L.: Cationic liposome-mediated gene transfer. Gene Ther. **2**, 710–722 (1995)
101. Balasubramaniam, R.P., Bennett, M.J., Aberle, A.M., Malone, J.G., Nantz, M.H., Malone, R.W.: Structural and functional analysis of cationic transfection lipids: The hydrophobic domain. Gene Ther. **3**, 163–172 (1996)
102. Budker, V., Gurevich, V., Hagstrom, J.E., Bortzov, F., Wolff, J.A.: pH-sensitive, cationic liposomes: A new synthetic virus-like vector. Nat. Biotechnol. **14**, 760–764 (1996)
103. Stephan, D.J., Yang, Z.Y., San, H., Simari, R.D., Wheeler, C.J., Felgner, P.L., Gordon, D., Nabel, G.J., Nabel, E.G.: A new cationic liposome DNA complex enhances the efficiency of arterial gene transfer in vivo. Hum. Gene Ther. **7**, 1803–1812 (1996)
104. Lee, R.J., Huang, L.: Lipidic vector systems for gene transfer. Crit. Rev. Ther. Drug Carrier Syst. **14**, 173–206 (1997)
105. Rosenzweig, H.S., Rakhmanova, V.A., MacDonald, R.C.: Diquaternary ammonium compounds as transfection agents. Bioconjug. Chem. **12**, 258–263 (2001)
106. Serikawa, T., Suzuki, N., Kikuchi, H., Tanaka, K., Kitagawa, T.: A new cationic liposome for efficient gene delivery with serum into cultured human cells: A quantitative analysis using two independent fluorescent probes. Biochim. Biophys. Acta **1467**, 419–430 (2000)
107. Wheeler, C.J., Sukhu, L., Yang, G., Tsai, Y., Bustamente, C., Felgner, P., Norman, J., Manthorpe, M.: Converting an alcohol to an amine in a cationic lipid dramatically alters the co-lipid requirement, cellular transfection activity and the ultrastructure of DNA-cytofectin complexes. Biochim. Biophys. Acta **1280**, 1–11 (1996)
108. Porteous, D.J., Dorin, J.R., McLachlan, G., Davidson-Smith, H., Davidson, H., Stevenson, B.J., Carothers, A.D., Wallace, W.A., Moralee, S., Hoenes, C., Kallmeyer, G., Michaelis, U., Naujoks, K., Ho, L.P., Samways, J.M., Imrie, M., Greening, A.P., Innes, J.A.: Evidence for safety and efficacy of DOTAP cationic liposome mediated CFTR gene transfer to the nasal epithelium of patients with cystic fibrosis. Gene Ther. **4**, 210–218 (1997)
109. Sansone, F., Dudic, M., Donofrio, G., Rivetti, C., Baldini, L., Casnati, A., Cellai, S., Ungaro, R.: DNA condensation and cell transfection properties of guanidinium calixarenes: Dependence on macrocycle lipophilicity, size, and conformation. J. Am. Chem. Soc. **128**, 14528–14536 (2006)
110. Farhood, H., Serbina, N., Huang, L.: The role of dioleoyl phosphatidylethanolamine in cationic liposome mediated gene transfer. Biochim. Biophys. Acta **1235**, 289–295 (1995)
111. Hui, S.W., Langner, M., Zhao, Y.L., Ross, P., Hurley, E., Chan, K.: The role of helper lipids in cationic liposomemediated gene transfer. Biophys. J. **71**, 590–599 (1996)
112. Felgner, P. L.; Gadek, T. R.; Holm, M.; Roman, R.; Chan, H. W.; Wenz, M.; Northrop, J. P.; Ringold, G. M.; Danielsen, M. Lipofection: A highly efficient, lipid-mediated DNA-transfection procedure. *Proc Natl Acad Sci U S A***1987**, *84*, 7413-7.
113. Hawley-Nelson, P., Ciccarone, V., Gebeyehu, G., Jessee, J., Felgner, P.: LipofectAmine reagent: A new, higher efficiency polycationic liposome transfection reagent. Focus **15**, 73–79 (1993)
114. Dube, S.: Transfection using LipofectAmine Plus Reagent. Focus **19**, 57 (1997)
115. Ciccarone, V., Chu, Y., Schifferli, K., Pichet, J.P., Hawley-Nelson, P., Evans, K., Roy, L., Bennett, S.: LipofectAmine 2000 Reagent for rapid, efficient transfection of eukaryotic cells. Focus **21**, 54–55 (1999)

116. Kupatt, C., Dessy, C., Hinkel, R., Raake, P., Daneau, G., Bouzin, C., Boekstegers, P., Feron, O.: Heat shock protein 90 transfection reduces ischemia-reperfusion-induced myocardial dysfunction via reciprocal endothelial NO synthase serine 1177 phosphorylation and threonine 495 dephosphorylation. Arterioscler. Thromb. Vasc. Biol. **24**, 1435–1441 (2004)
117. Khurana, R., Shafi, S., Martin, J., Zachary, I.: Vascular endothelial growth factor gene transfer inhibits neointimal macrophage accumulation in hypercholesterolemic rabbits. Arterioscler. Thromb. Vasc. Biol. **24**, 1074–1080 (2004)
118. Kim, S.I., Kim, K.S., Kim, H.S., Kim, D.S., Jang, Y., Chung, K.H., Park, Y.S.: Inhibitory effect of the salmosin gene transferred by cationic liposomes on the progression of B16BL6 tumors. Cancer Res. **63**, 6458–6462 (2003)
119. Kaiser, S., Toborek, M.: Liposome-mediated high-efficiency transfection of human endothelial cells. J. Vasc. Res. **38**, 133–143 (2001)
120. Masotti, A., Mossa, G., Cametti, C., Ortaggi, G., Bianco, A., Grosso, N.D., Malizia, D., Esposito, C.: Comparison of different commercially available cationic liposome-DNA lipoplexes: Parameters influencing toxicity and transfection efficiency. Colloids Surf. B Biointerfaces **68**, 136–144 (2009)
121. Hama, S., Akita, H., Ito, R., Mizuguchi, H., Hayakawa, T., Harashima, H.: Quantitative comparison of intracellular trafficking and nuclear transcription between adenoviral and lipoplex systems. Mol. Ther. **13**, 786–794 (2006)
122. Kwoh, D.Y., Coffin, C.C., Lollo, C.P., Jovenal, J., Banaszczyk, M.G., Mullen, P., Phillips, A., Amini, A., Fabrycki, J., Bartholomew, R.M., Brostoff, S.W., Carlo, D.J.: Stabilization of poly-L-lysine/DNA polyplexes for in vivo gene delivery to the liver. Biochim. Biophys. Acta-Gene Struct. Expr. **1444**, 171–190 (1999)
123. Plank, C., Tang, M.X., Wolfe, A.R., Szoka, F.C.: Branched cationic peptides for gene delivery: Role of type and number of cationic residues in formation and in vitro activity of DNA polyplexes. Hum. Gene Ther. **10**, 319–332 (1999)
124. MacLaughlin, F.C., Mumper, R.J., Wang, J.J., Tagliaferri, J.M., Gill, I., Hinchcliffe, M., Rolland, A.P.: Chitosan and depolymerized chitosan oligomers as condensing carriers for in vivo plasmid delivery. J. Control. Release **56**, 259–272 (1998)
125. Tan, P.H., Xue, S.A., Manunta, M., Beutelspacher, S.C., Fazekasova, H., Alam, A.K., McClure, M.O., George, A.J.: Effect of vectors on human endothelial cell signal transduction: Implications for cardiovascular gene therapy. Arterioscler. Thromb. Vasc. Biol. **26**, 462–467 (2006)
126. Rémy-Kristensen, A., Clamme, J.-P., Vuilleumier, C., Kuhry, J.-G., Mély, Y.: Role of endocytosis in the transfection of L929 fibroblasts by polyethylenimine/DNA complexes. Biochim. Biophys. Acta-Biomembr. **1514**, 21–32 (2001)
127. Brunner, S., Sauer, T., Carotta, S., Cotten, M., Saltik, M., Wagner, E.: Cell cycle dependence of gene transfer by lipoplex, polyplex and recombinant adenovirus. Gene Ther. **7**, 401–407 (2000)
128. Hong, S., Leroueil, P.R., Janus, E.K., Peters, J.L., Kober, M.M., Islam, M.T., Orr, B.G., Baker Jr., J.R., Banaszak Holl, M.M.: Interaction of polycationic polymers with supported lipid bilayers and cells: Nanoscale hole formation and enhanced membrane permeability. Bioconjug. Chem. **17**, 728–734 (2006)
129. Breunig, M., Lungwitz, U., Liebl, R., Goepferich, A.: Breaking up the correlation between efficacy and toxicity for nonviral gene delivery. Proc Natl Acad. Sci. USA **104**, 14454–14459 (2007)
130. Schaffert, D., Wagner, E.: Gene therapy progress and prospects: synthetic polymer-based systems. Gene Ther. **15**, 1131–1138 (2008)
131. Lee, Y., Mo, H., Koo, H., Park, J.Y., Cho, M.Y., Jin, G.W., Park, J.S.: Visualization of the degradation of a disulfide polymer, linear poly(ethylenimine sulfide), for gene delivery. Bioconjug. Chem. **18**, 13–18 (2007)
132. Green, J.J., Shi, J., Chiu, E., Leshchiner, E.S., Langer, R., Anderson, D.G.: Biodegradable polymeric vectors for gene delivery to human endothelial cells. Bioconjug. Chem. **17**, 1162–1169 (2006)

133. KukowskaLatallo, J.F., Bielinska, A.U., Johnson, J., Spindler, R., Tomalia, D.A., Baker, J.R.: Efficient transfer of genetic material into mammalian cells using Starburst polyamidoamine dendrimers. Proc. Natl Acad. Sci. USA **93**, 4897–4902 (1996)
134. Haensler, J., Szoka Jr., F.C.: Polyamidoamine cascade polymers mediate efficient transfection of cells in culture. Bioconjug. Chem. **4**, 372–379 (1993)
135. Roberts, J.C., Bhalgat, M.K., Zera, R.T.: Preliminary biological evaluation of polyamidoamine (PAMAM) Starburst dendrimers. J. Biomed. Mater. Res. **30**, 53–65 (1996)
136. Wang, Y., Boros, P., Liu, J., Qin, L., Bai, Y., Bielinska, A.U., Kukowska-Latallo, J.F., Baker, J.R., Bromberg, J.S.: DNA/dendrimer complexes mediate gene transfer into murine cardiac transplants ex vivo. Mol. Ther. **2**, 602–608 (2000)
137. Qin, L., Pahud, D.R., Ding, Y., Bielinska, A.U., Kukowska-Latallo, J.F., Baker Jr., J.R., Bromberg, J.S.: Efficient transfer of genes into murine cardiac grafts by Starburst polyamidoamine dendrimers. Hum. Gene Ther. **9**, 553–560 (1998)
138. Ledley, F.D.: Pharmaceutical approach to somatic gene therapy. Pharm. Res. **13**, 1595–1614 (1996)
139. Dash, P.R., Read, M.L., Barrett, L.B., Wolfert, M.A., Seymour, L.W.: Factors affecting blood clearance and in vivo distribution of polyelectrolyte complexes for gene delivery. Gene Ther. **6**, 643–650 (1999)
140. Slepushkin, V.A., Simoes, S., Dazin, P., Newman, M.S., Guo, L.S., Pedroso de Lima, M.C., Duzgunes, N.: Sterically stabilized pH-sensitive liposomes. Intracellular delivery of aqueous contents and prolonged circulation in vivo. J Biol Chem. **272**, 2382–2388 (1997)
141. Woodle, M.C., Engbers, C.M., Zalipsky, S.: New amphipatic polymer-lipid conjugates forming long-circulating reticuloendothelial system-evading liposomes. Bioconjug. Chem. **5**, 493–496 (1994)
142. Ogris, M., Brunner, S., Schuller, S., Kircheis, R., Wagner, E.: PEGylated DNA/transferrin-PEI complexes: Reduced interaction with blood components, extended circulation in blood and potential for systemic gene delivery. Gene Ther. **6**, 595–605 (1999)
143. Segura, T., Chung, P.H., Shea, L.D.: DNA delivery from hyaluronic acid-collagen hydrogels via a substrate-mediated approach. Biomaterials **26**, 1575–1584 (2005)
144. Sanders, L.M., Kell, B.A., McRae, G.I., Whitehead, G.W.: Prolonged controlled-release of nafarelin, a luteinizing hormone-releasing hormone analogue, from biodegradable polymeric implants: Influence of composition and molecular weight of polymer. J. Pharm. Sci. **75**, 356–360 (1986)
145. Pannier, A.K., Anderson, B.C., Shea, L.D.: Substrate-mediated delivery from self-assembled monolayers: Effect of surface ionization, hydrophilicity, and patterning. Acta Biomater. **1**, 511–522 (2005)
146. Moses, J.W., Leon, M.B., Popma, J.J., Fitzgerald, P.J., Holmes, D.R., O'Shaughnessy, C., Caputo, R.P., Kereiakes, D.J., Williams, D.O., Teirstein, P.S., Jaeger, J.L., Kuntz, R.E.: Sirolimus-eluting stents versus standard stents in patients with stenosis in a native coronary artery. N. Engl. J. Med. **349**, 1315–1323 (2003)
147. Stone, G.W., Ellis, S.G., Cox, D.A., Hermiller, J., O'Shaughnessy, C., Mann, J.T., Turco, M., Caputo, R., Bergin, P., Greenberg, J., Popma, J.J., Russell, M.E.: A polymer-based, paclitaxel-eluting stent in patients with coronary artery disease. N. Engl. J. Med. **350**, 221–231 (2004)
148. Saltzman, W.M.: Delivering tissue regeneration. Nat. Biotechnol. **17**, 534–535 (1999)
149. Nishikawa, M., Huang, L.: Nonviral vectors in the new millennium: Delivery barriers in gene transfer. Hum. Gene Ther. **12**, 861–870 (2001)
150. Saltzman, W.M., Olbricht, W.L.: Building drug delivery into tissue engineering. Nat. Rev. Drug Discov. **1**, 177–186 (2002)
151. Panyam, J., Labhasetwar, V.: Biodegradable nanoparticles for drug and gene delivery to cells and tissue. Adv. Drug Deliv. Rev. **55**, 329–347 (2003)
152. Shea, L.D., Smiley, E., Bonadio, J., Mooney, D.J.: DNA delivery from polymer matrices for tissue engineering. Nat. Biotechnol. **17**, 551–554 (1999)

153. Bonadio, J., Smiley, E., Patil, P., Goldstein, S.: Localized, direct plasmid gene delivery in vivo: Prolonged therapy results in reproducible tissue regeneration. Nat. Med. **5**, 753–759 (1999)
154. Ochiya, T., Nagahara, S., Sano, A., Itoh, H., Terada, M.: Biomaterials for gene delivery: Atelocollagen-mediated controlled release of molecular medicines. Curr. Gene Ther. **1**, 31–52 (2001)
155. Scherer, F., Schillinger, U., Putz, U., Stemberger, A., Plank, C.: Nonviral vector loaded collagen sponges for sustained gene delivery in vitro and in vivo. J. Gene Med. **4**, 634–643 (2002)
156. Wang, D.Q., Robinson, D.R., Kwon, G.S., Samuel, J.: Encapsulation of plasmid DNA in biodegradable poly(D,Llactic-co-glycolic acid) microspheres as a novel approach for immunogene delivery. J. Control. Release **57**, 9–18 (1999)
157. Luo, D., Saltzman, W.M.: Enhancement of transfection by physical concentration of DNA at the cell surface. Nat. Biotechnol. **18**, 893–895 (2000)
158. Xie, Y., Yang, S.T., Kniss, D.A.: Three-dimensional cell-scaffold constructs promote efficient gene transfection: Implications for cell-based gene therapy. Tissue Eng. **7**, 585–598 (2001)
159. Bonadio, J., Goldstein, S.A., Levy, R.J.: Gene therapy for tissue repair and regeneration. Adv. Drug Deliv. Rev. **33**, 53–69 (1998)
160. Doukas, J., Chandler, L.A., Gonzalez, A.M., Gu, D., Hoganson, D.K., Ma, C., Nguyen, T., Printz, M.A., Nesbit, M., Herlyn, M., Crombleholme, T.M., Aukerman, S.L., Sosnowski, B.A., Pierce, G.F.: Matrix immobilization enhances the tissue repair activity of growth factor gene therapy vectors. Hum. Gene Ther. **12**, 783–798 (2001)
161. Bajaj, B., Lei, P., Andreadis, S.T.: High efficiencies of gene transfer with immobilized recombinant retrovirus: Kinetics and optimization. Biotechnol. Prog. **17**, 587–596 (2001)
162. Zaharoff, D.A., Barr, R.C., Li, C.Y., Yuan, F.: Electromobility of plasmid DNA in tumor tissues during electric fieldmediated gene delivery. Gene Ther. **9**, 1286–1290 (2002)
163. Yancopoulos, G.D., Davis, S., Gale, N.W., Rudge, J.S., Wiegand, S.J., Holash, J.: Vascular-specific growth factors and blood vessel formation. Nature **407**, 242–248 (2000)
164. Huang, Y.C., Kaigler, D., Rice, K.G., Krebsbach, P.H., Mooney, D.J.: Combined angiogenic and osteogenic factor delivery enhances bone marrow stromal cell-driven bone regeneration. J. Bone Miner. Res. **20**, 848–857 (2005)
165. Ando, S., Putnam, D., Pack, D.W., Langer, R.: PLGA microspheres containing plasmid DNA: Preservation of supercoiled DNA via cryopreparation and carbohydrate stabilization. J. Pharm. Sci. **88**, 126–130 (1999)
166. Jang, J.H., Shea, L.D.: Controllable delivery of non-viral DNA from porous scaffolds. J. Control. Release **86**, 157–168 (2003)
167. Varde, N.K., Pack, D.W.: Microspheres for controlled release drug delivery. Expert Opin. Biol. Ther. **4**, 35–51 (2004)
168. Fang, J.M., Zhu, Y.Y., Smiley, E., Bonadio, J., Rouleau, J.P., Goldstein, S.A., McCauley, L.K., Davidson, B.L., Roessler, B.J.: Stimulation of new bone formation by direct transfer of osteogenic plasmid genes. Proc. Natl Acad. Sci. USA **93**, 5753–5758 (1996)
169. Cohen-Sacks, H., Elazar, V., Gao, J.C., Golomb, A., Adwan, H., Korchov, N., Levy, R.J., Berger, M.R., Golomb, G.: Delivery and expression of pDNA embedded in collagen matrices. J. Control. Release **95**, 309–320 (2004)
170. Walter, E., Dreher, D., Kok, M., Thiele, L., Kiama, S.G., Gehr, P., Merkle, H.P.: Hydrophilic poly(DL-lactide-coglycolide) microspheres for the delivery of DNA to human-derived macrophages and dendritic cells. J. Control. Release **76**, 149–168 (2001)
171. Eliaz, R.E., Szoka, F.C.: Robust and prolonged gene expression from injectable polymeric implants. Gene Ther. **9**, 1230–1237 (2002)
172. Cohen, H., Levy, R.J., Gao, J., Fishbein, I., Kousaev, V., Sosnowski, S., Slomkowski, S., Golomb, G.: Sustained delivery and expression of DNA encapsulated in polymeric nanoparticles. Gene Ther. **7**, 1896–1905 (2000)

173. Peppas, N.A., Langer, R.: New challenges in biomaterials. Science **263**, 1715–1720 (1994)
174. Shen, H., Goldberg, E., Saltzman, W.M.: Gene expression and mucosal immune responses after vaginal DNA immunization in mice using a controlled delivery matrix. J. Control. Release **86**, 339–348 (2003)
175. Jong, Y.S., Jacob, J.S., Yip, K.P., Gardner, G., Seitelman, E., Whitney, M., Montgomery, S., Mathiowitz, E.: Controlled release of plasmid DNA. J. Control. Release **47**, 123–134 (1997)
176. Friess, W.: Collagen–biomaterial for drug delivery. Eur. J. Pharm. Biopharm. **45**, 113–136 (1998)
177. Pouton, C.W., Seymour, L.W.: Key issues in non-viral gene delivery. Adv. Drug Deliv. Rev. **34**, 3–19 (1998)
178. Scheule, R.K.: The role of CpG motifs in immunostimulation and gene therapy. Adv. Drug Deliv. Rev. **44**, 119–134 (2000)
179. Ochiya, T., Takahama, Y., Nagahara, S., Sumita, Y., Hisada, A., Itoh, H., Nagai, Y., Terada, M.: New delivery system for plasmid DNA in vivo using atelocollagen as a carrier material: The minipellet. Nat. Med. **5**, 707–710 (1999)
180. Samuel, R.E., Lee, C.R., Ghivizzani, S.C., Evans, C.H., Yannas, I.V., Olsen, B.R., Spector, M.: Delivery of plasmid DNA to articular chondrocytes via novel collagen-glycosaminoglycan matrices. Hum. Gene Ther. **13**, 791–802 (2002)
181. Perlstein, I., Connolly, J.M., Cui, X., Song, C., Li, Q., Jones, P.L., Lu, Z., DeFelice, S., Klugherz, B., Wilensky, R., Levy, R.J.: DNA delivery from an intravascular stent with a denatured collagen-polylactic-polyglycolic acid-controlled release coating: Mechanisms of enhanced transfection. Gene Ther. **10**, 1420–1428 (2003)
182. Klugherz, B.D., Jones, P.L., Cui, X., Chen, W., Meneveau, N.F., DeFelice, S., Connolly, J., Wilensky, R.L., Levy, R.J.: Gene delivery from a DNA controlled-release stent in porcine coronary arteries. Nat. Biotechnol. **18**, 1181–1184 (2000)
183. Baldwin, S.P., Mark Saltzman, W.: Materials for protein delivery in tissue engineering. Adv. Drug Deliv. Rev. **33**, 71–86 (1998)
184. Quick, D.J., Anseth, K.S.: Gene delivery in tissue engineering: a photopolymer platform to coencapsulate cells and plasmid DNA. Pharm. Res. **20**, 1730–1737 (2003)
185. Yun, Y.H., Goetz, D.J., Yellen, P., Chen, W.: Hyaluronan microspheres for sustained gene delivery and site-specific targeting. Biomaterials **25**, 147–157 (2004)
186. Kim, A., Checkla, D.M., Dehazya, P., Chen, W.: Characterization of DNA-hyaluronan matrix for sustained gene transfer. J. Control. Release **90**, 81–95 (2003)
187. Doukas, J., Blease, K., Craig, D., Ma, C., Chandler, L.A., Sosnowski, B.A., Pierce, G.F.: Delivery of FGF genes to wound repair cells enhances arteriogenesis and myogenesis in skeletal muscle. Mol. Ther. **5**, 517–527 (2002)
188. Jang, J.H., Rives, C.B., Shea, L.D.: Plasmid delivery in vivo from porous tissue-engineering scaffolds: Transgene expression and cellular transfection. Mol. Ther. **12**, 475–483 (2005)
189. Kasahara, H., Tanaka, E., Fukuyama, N., Sato, E., Sakamoto, H., Tabata, Y., Ando, K., Iseki, H., Shinozaki, Y., Kimura, K., Kuwabara, E., Koide, S., Nakazawa, H., Mori, H.: Biodegradable gelatin hydrogel potentiates the angiogenic effect of fibroblast growth factor 4 plasmid in rabbit hindlimb ischemia. J. Am. Coll. Cardiol. **41**, 1056–1062 (2003)
190. Walter, D.H., Cejna, M., Diaz-Sandoval, L., Willis, S., Kirkwood, L., Stratford, P.W., Tietz, A.B., Kirchmair, R., Silver, M., Curry, C., Wecker, A., Yoon, Y.S., Heidenreich, R., Hanley, A., Kearney, M., Tio, F.O., Kuenzler, P., Isner, J.M., Losordo, D.W.: Local gene transfer of phVEGF-2 plasmid by gene-eluting stents: An alternative strategy for inhibition of restenosis. Circulation **110**, 36–45 (2004)
191. Capan, Y., Woo, B.H., Gebrekidan, S., Ahmed, S., DeLuca, P.P.: Stability of poly(L-lysine)-complexed plasmid DNA during mechanical stress and DNase I treatment. Pharm. Dev. Technol. **4**, 491–498 (1999)
192. Capan, Y., Woo, B.H., Gebrekidan, S., Ahmed, S., DeLuca, P.P.: Influence of formulation parameters on the characteristics of poly(D,L-lactide-co-glycolide) microspheres containing poly(L-lysine) complexed plasmid DNA. J. Control. Release **60**, 279–286 (1999)

193. De Rosa, G., Quaglia, F., La Rotonda, M.I., Appel, M., Alphandary, H., Fattal, E.: Poly(lactide-co-glycolide) microspheres for the controlled release of oligonucleotide/polyethylenimine complexes. J. Pharm. Sci. **91**, 790–799 (2002)
194. Berry, M., Gonzalez, A.M., Clarke, W., Greenlees, L., Barrett, L., Tsang, W., Seymour, L., Bonadio, J., Logan, A., Baird, A.: Sustained effects of gene-activated matrices after CNS injury. Mol. Cell. Neurosci. **17**, 706–716 (2001)
195. Huang, Y.C., Connell, M., Park, Y., Mooney, D.J., Rice, K.G.J.: Fabrication and in vitro testing of polymeric delivery system for condensed DNA. Biomed. Materials Res. Part A **67A**, 1384–1392 (2003)
196. Huang, Y.C., Simmons, C., Kaigler, D., Rice, K.G., Mooney, D.J.: Bone regeneration in a rat cranial defect with delivery of PEI-condensed plasmid DNA encoding for bone morphogenetic protein-4 (BMP-4). Gene Ther. **12**, 418–426 (2005)
197. Huang, Y.C., Riddle, K., Rice, K.G., Mooney, D.J.: Long-term in vivo gene expression via delivery of PEI-DNA condensates from porous polymer scaffolds. Hum. Gene Ther. **16**, 609–617 (2005)
198. Zheng, J., Manuel, W.S., Hornsby, P.J.: Transfection of cells mediated by biodegradable polymer materials with surface-bound polyethyleneimine. Biotechnol. Prog. **16**, 254–257 (2000)
199. Gao, X., Huang, L.: Potentiation of cationic liposome-mediated gene delivery by polycations. Biochemistry **35**, 1027–1036 (1996)
200. Birchall, J.C., Marichal, C., Campbell, L., Alwan, A., Hadgraft, J., Gumbleton, M.: Gene expression in an intact exvivo skin tissue model following percutaneous delivery of cationic liposome-plasmid DNA complexes. Int. J. Pharm. **197**, 233–238 (2000)
201. des Rieux, A., Shikanov, A., Shea, L.D.: Fibrin hydrogels for non-viral vector delivery in vitro. J. Control. Release **136**, 148–154 (2009)
202. Kulkarni, M., Breen, A., Greiser, U., O'Brien, T., Pandit, A.: Fibrin-lipoplex system for controlled topical delivery of multiple genes. Biomacromolecules **10**, 1650–1654 (2009)
203. Saul, J.M., Linnes, M.P., Ratner, B.D., Giachelli, C.M., Pun, S.H.: Delivery of non-viral gene carriers from spheretemplated fibrin scaffolds for sustained transgene expression. Biomaterials **28**, 4705–4716 (2007)
204. Batycky, R.P., Hanes, J., Langer, R., Edwards, D.A.: A theoretical model of erosion and macromolecular drug release from biodegrading microspheres. J. Pharm. Sci. **86**, 1464–1477 (1997)
205. Gersbach, C.A., Coyer, S.R., Le Doux, J.M., Garcia, A.J.: Biomaterial-mediated retroviral gene transfer using selfassembled monolayers. Biomaterials **28**, 5121–5127 (2007)
206. Sakiyama-Elbert, S.E., Panitch, A., Hubbell, J.A.: Development of growth factor fusion proteins for cell-triggered drug delivery. FASEB J. **15**, 1300–1302 (2001)
207. Proctor, R.A.: Fibronectin: A brief overview of its structure, function, and physiology. Rev. Infect. Dis. **9**(Suppl 4), S317–S321 (1987)
208. Williams, D.A.: Retroviral-fibronectin interactions in transduction of mammalian cells. Hematopoietic Stem Cells **872**, 109–114 (1999)
209. Julkunen, I., Vartio, T., Keskioja, J.: Localization of "Viral-Envelope-Glycoprotein-Binding Sites in Fibronectin. Biochem. J. **219**, 425–428 (1984)
210. Hanenberg, H., Xiao, X.L., Dilloo, D., Hashino, K., Kato, I., Williams, D.A.: Colocalization of retrovirus and target cells on specific fibronectin fragments increases genetic transduction of mammalian cells. Nat. Med. **2**, 876–882 (1996)
211. Lei, P., Bajaj, B., Andreadis, S.T.: Retrovirus-associated heparan sulfate mediates immobilization and gene transfer on recombinant fibronectin. J. Virol. **76**, 8722–8728 (2002)
212. Segura, T., Shea, L.D.: Surface-tethered DNA complexes for enhanced gene delivery. Bioconjug. Chem. **13**, 621–629 (2002)
213. Shen, H., Tan, J., Saltzman, W.M.: Surface-mediated gene transfer from nanocomposites of controlled texture. Nat. Mater. **3**, 569–574 (2004)

214. Park, I.K., von Recum, H.A., Jiang, S., Pun, S.H.: Supramolecular assembly of cyclodextrin-based nanoparticles on solid surfaces for gene delivery. Langmuir **22**, 8478–8484 (2006)
215. Levy, R.J., Song, C., Tallapragada, S., DeFelice, S., Hinson, J.T., Vyavahare, N., Connolly, J., Ryan, K., Li, Q.: Localized adenovirus gene delivery using antiviral IgG complexation. Gene Ther. **8**, 659–667 (2001)
216. Jang, J.H., Bengali, Z., Houchin, T.L., Shea, L.D.: Surface adsorption of DNA to tissue engineering scaffolds for efficient gene delivery. J. Biomed. Mater. Res. Part A **77A**, 50–58 (2006)
217. Fishbein, I., Stachelek, S.J., Connolly, J.M., Wilensky, R.L., Alferiev, I., Levy, R.J.: Site specific gene delivery in the cardiovascular system. J. Control. Release **109**, 37–48 (2005)
218. Bielinska, A.U., Yen, A., Wu, H.L., Zahos, K.M., Sun, R., Weiner, N.D., Baker, J.R., Roessler, B.J.: Application of membrane-based dendrimer/DNA complexes for solid phase transfection in vitro and in vivo. Biomaterials **21**, 877–887 (2000)
219. Norde, W., Lyklema, J.: Why proteins prefer interfaces. J. Biomater. Sci. Polym. Ed. **2**, 183–202 (1991)
220. Putney, S.D., Burke, P.A.: Improving protein therapeutics with sustained-release formulations. Nat. Biotechnol. **16**, 153–157 (1998)
221. Zhang, F., Kang, E.T., Neoh, K.G., Huang, W.: Modification of gold surface by grafting of poly(ethylene glycol) for reduction in protein adsorption and platelet adhesion. J. Biomater. Sci. Polym. Ed. **12**, 515–531 (2001)
222. Pannier, A.K., Wieland, J.A., Shea, L.D.: Surface polyethylene glycol enhances substrate-mediated gene delivery by nonspecifically immobilized complexes. Acta Biomater. **4**, 26–39 (2008)
223. Gonsho, A., Irie, K., Susaki, H., Iwasawa, H., Okuno, S., Sugawara, T.: Tissue-Targeting Ability of Saccharide-Poly(L-Lysine) Conjugates. Biol. Pharm. Bull. **17**, 275–282 (1994)
224. Jiang, T.T., Chang, J.B., Wang, C.M., Ding, Z., Chen, J.N., Zhang, J.F., Kang, E.T.: Adsorption of plasmid DNA onto N,N-(dimethylamino)ethyl-methacrylate graft-polymerized poly-L-lactic acid film surface for promotion of insitu gene delivery. Biomacromolecules **8**, 1951–1957 (2007)
225. Kneuer, C., Sameti, M., Bakowsky, U., Schiestel, T., Schirra, H., Schmidt, H., Lehr, C.M.: A nonviral DNA delivery system based on surface modified silica-nanoparticles can efficiently transfect cells in vitro. Bioconjug. Chem. **11**, 926–932 (2000)
226. Manuel, W.S., Zheng, J.I., Hornsby, P.J.: Transfection by polyethyleneimine-coated microspheres. J. Drug Target. **9**, 15–22 (2001)
227. Rea, J.C., Gibly, R.F., Davis, N.E., Barron, A.E., Shea, L.D.: Engineering Surfaces for Substrate-Mediated Gene Delivery Using Recombinant Proteins. Biomacromolecules **10**, 2779–2786 (2009)
228. Tseng, S.: j.; Chuang, C.-J.; Tang, S.-C.: Electrostatic immobilization of DNA polyplexes on small intestinal submucosa for tissue substrate-mediated transfection. Acta Biomater. **4**, 799–807 (2008)
229. Nakayama, Y., Ji-Youn, K., Nishi, S., Ueno, H., Matsuda, T.: Development of high-performance stent: Gelatinous photogel-coated stent that permits drug delivery and gene transfer. J. Biomed. Mater. Res. **57**, 559–566 (2001)
230. Klugherz, B.D., Song, C.X., Defelice, S., Cui, X.M., Lu, Z.B., Connolly, J., Hinson, J.T., Wilensky, R.L., Levy, R.J.: Gene delivery to pig coronary arteries from stents carrying antibody-tethered adenovirus. Hum. Gene Ther. **13**, 443–454 (2002)
231. Takahashi, A., Palmer-Opolski, M., Smith, R.C., Walsh, K.: Transgene delivery of plasmid DNA to smooth muscle cells and macrophages from a biostable polymer-coated stent. Gene Ther. **10**, 1471–1478 (2003)
232. Fishbein, I., Alferiev, I.S., Nyanguile, O., Gaster, R., Vohs, J.M., Wong, G.S., Felderman, H., Chen, I.W., Choi, H., Wilensky, R.L., Levy, R.J.: Bisphosphonate-mediated gene vector delivery from the metal surfaces of stents. Proc. Natl Acad. Sci. USA **103**, 159–164 (2006)

233. Meyer, F., Ball, V., Schaaf, P., Voegel, J.C., Ogier, J.: Polyplex-embedding in polyelectrolyte multilayers for gene delivery. Biochim. Biophys. Acta-Biomembr. **1758**, 419–422 (2006)
234. Jessel, N., Oulad-Abdeighani, M., Meyer, F., Lavalle, P., Haikel, Y., Schaaf, P., Voegel, J.C.: Multiple and timescheduled in situ DNA delivery mediated by β-cyclodextrin embedded in a polyelectrolyte multilayer. Proc. Natl Acad. Sci. USA **103**, 8618–8621 (2006)
235. Decher, G.: Fuzzy nanoassemblies: Toward layered polymeric multicomposites. Science **277**, 1232–1237 (1997)
236. Bertrand, P., Jonas, A., Laschewsky, A., Legras, R.: Ultrathin polymer coatings by complexation of polyelectrolytes at interfaces: suitable materials, structure and properties. Macromol. Rapid Commun. **21**, 319–348 (2000)
237. Jewell, C.M., Lynn, D.M.: Multilayered polyelectrolyte assemblies as platforms for the delivery of DNA and other nucleic acid-based therapeutics. Adv. Drug Deliv. Rev. **60**, 979–999 (2008)
238. Vázquez, E., Dewitt, D.M., Hammond, P.T., Lynn, D.M.: Construction of hydrolytically-degradable thin films via layer-by-layer deposition of degradable polyelectrolytes. J. Am. Chem. Soc. **124**, 13992–13993 (2002)
239. Wood, K.C., Chuang, H.F., Batten, R.D., Lynn, D.M., Hammond, P.T.: Controlling interlayer diffusion to achieve sustained, multiagent delivery from layer-by-layer thin films. Proc. Natl Acad. Sci. USA **103**, 10207–10212 (2006)
240. Lowman, G.M., Tokuhisa, H., Lutkenhaus, J.L., Hammond, P.T.: Novel solid-state polymer electrolyte consisting of a porous layer-by-layer polyelectrolyte thin film and oligoethylene glycol. Langmuir **20**, 9791–9795 (2004)
241. Wood, K.C., Boedicker, J.Q., Lynn, D.M., Hammond, P.T.: Tunable drug release from hydrolytically degradable layer-by-layer thin films. Langmuir **21**, 1603–1609 (2005)
242. Peyratout, C.S., Dahne, L.: Tailor-made polyelectrolyte microcapsules: From multilayers to smart containers. Angew. Chem. Int. Ed. Engl. **43**, 3762–3783 (2004)
243. De Geest, B.G., Sanders, N.N., Sukhorukov, G.B., Demeester, J., De Smedt, S.C.: Release mechanisms for polyelectrolyte capsules. Chem. Soc. Rev. **36**, 636–649 (2007)
244. Sukhorukov, G.B., Rogach, A.L., Garstka, M., Springer, S., Parak, W.J., Munoz-Javier, A., Kreft, O., Skirtach, A.G., Susha, A.S., Ramaye, Y., Palankar, R., Winterhalter, M.: Multifunctionalized polymer microcapsules: Novel tools for biological and pharmacological applications. Small **3**, 944–955 (2007)
245. Lynn, D.M.: Layers of opportunity: Nanostructured polymer assemblies for the delivery of macromolecular therapeutics. Soft Matter **2**, 269–273 (2006)
246. Lynn, D.M.: Peeling back the layers: Controlled erosion and triggered disassembly of multilayered polyelectrolyte thin films. Adv. Mater. **19**, 4118–4130 (2007)
247. Jewell, C.M., Zhang, J., Fredin, N.J., Wolff, M.R., Hacker, T.A., Lynn, D.M.: Release of plasmid DNA from intravascular stents coated with ultrathin multilayered polyelectrolyte films. Biomacromolecules **7**, 2483–2491 (2006)
248. Lu, Z.Z., Wu, J., Sun, T.M., Ji, J., Yan, L.F., Wang, J.: Biodegradable polycation and plasmid DNA multilayer film for prolonged gene delivery to mouse osteoblasts. Biomaterials **29**, 733–741 (2008)
249. Taori, V.P., Liu, Y., Reineke, T.M.: DNA delivery in vitro via surface release from multilayer assemblies with poly(glycoamidoamine)s. Acta Biomater. **5**, 925–933 (2009)
250. Lynn, D.M., Anderson, D.G., Akinc, A.B., Langer, R.: In: Amiji, M. (ed.) Degradable poly(β-amino ester)s for gene delivery. In Polymeric Gene Delivery: Principles and Applications. CRC Press, New York (2004)
251. Lynn, D.M., Langer, R.: Degradable poly(β-amino esters): Synthesis, characterization, and self-assembly with plasmid DNA. J. Am. Chem. Soc. **122**, 10761–10768 (2000)
252. Lynn, D.M., Anderson, D.G., Putnam, D., Langer, R.: Accelerated discovery of synthetic transfection vectors: Parallel synthesis and screening of degradable polymer library. J. Am. Chem. Soc. **123**, 8155–8156 (2001)

253. Akinc, A., Lynn, D.M., Anderson, D.G., Langer, R.: Parallel synthesis and biophysical characterization of a degradable polymer library for gene delivery. J. Am. Chem. Soc. **125**, 5316–5323 (2003)
254. Akinc, A., Anderson, D.G., Lynn, D.M., Langer, R.: Synthesis of poly(β-amino ester)s optimized for highly effective gene delivery. Bioconjug. Chem. **14**, 979–988 (2003)
255. Anderson, D.G., Lynn, D.M., Langer, R.: Semi-automated synthesis and screening of a large library of degradable cationic polymers for gene delivery. Angew. Chem. Int. Ed. Engl. **42**, 3153–3158 (2003)
256. Anderson, D.G., Peng, W., Akinc, A., Hossain, N., Kohn, A., Padera, R., Langer, R., Sawicki, J.A.: A polymer library approach to suicide gene therapy for cancer. Proc. Natl Acad. Sci. USA **101**, 16028–16033 (2004)
257. Little, S.R., Lynn, D.M., Ge, Q., Anderson, D.G., Puram, S.V., Chen, J., Eisen, H.N., Langer, R.: Poly-β amino ester-containing microparticles enhance the activity of nonviral genetic vaccines. Proc. Natl Acad. Sci. USA **101**, 9534–9539 (2004)
258. Anderson, D.G., Akinc, A., Hossain, N., Langer, R.: Structure/property studies of polymeric gene delivery using a library of poly(β-amino esters). Mol. Ther. **11**, 426–434 (2005)
259. Greenland, J.R., Liu, H., Berry, D., Anderson, D.G., Kim, W.K., Irvine, D.J., Langer, R., Letvin, N.L.: β-amino ester polymers facilitate in vivo DNA transfection and adjuvant plasmid DNA immunization. Mol. Ther. **12**, 164–170 (2005)
260. Zhang, J., Chua, L.S., Lynn, D.M.: Multilayered thin films that sustain the release of functional DNA under physiological conditions. Langmuir **20**, 8015–8021 (2004)
261. Zhang, J., Fredin, N.J., Janz, J.F., Sun, B., Lynn, D.M.: Structure/property relationships in erodible multilayered films: influence of polycation structure on erosion profiles and the release of anionic polyelectrolytes. Langmuir **22**, 239–245 (2006)
262. Zhang, J.T., Fredin, N.J., Lynn, D.M.: Erosion of multilayered films fabricated from degradable polyamines: Characterization and evidence in support of a mechanism that involves polymer hydrolysis. J. Polym. Science Part A-Polym. Chem. **44**, 5161–5173 (2006)
263. Zhang, J., Lynn, D.M.: Multilayered films fabricated from combinations of degradable polyamines: Tunable erosion and release of anionic polyelectrolytes. Macromolecules **39**, 8928–8935 (2006)
264. Sukhishvili, S.A., Granick, S.: Layered, Erasable Polymer Multilayers Formed by Hydrogen-Bonded Sequential Self-Assembly. Macromolecules **35**, 301–310 (2002)
265. Dubas, S.T., Farhat, T.R., Schlenoff, J.B.: Multiple membranes from "true" polyelectrolyte multilayers. J. Am. Chem. Soc. **123**, 5368–5369 (2001)
266. Dubas, S.T., Schlenoff, J.B.: Polyelectrolyte multilayers containing a weak polyacid: Construction and deconstruction. Macromolecules **34**, 3736–3740 (2001)
267. Schuler, C., Caruso, F.: Decomposable hollow biopolymer-based capsules. Biomacromolecules **2**, 921–926 (2001)
268. Sukhishvili, S.A., Granick, S.: Layered, erasable, ultrathin polymer films. J. Am. Chem. Soc. **122**, 9550–9551 (2000)
269. Cho, J., Caruso, F.: Polymeric multilayer films comprising deconstructible hydrogen-bonded stacks confined between electrostatically assembled layers. Macromolecules **36**, 2845–2851 (2003)
270. Inoue, H., Anzai, J.: Stimuli-sensitive thin films prepared by a layer-by-layer deposition of 2-iminobiotin-labeled poly(ethyleneimine) and avidin. Langmuir **21**, 8354–8359 (2005)
271. Sato, K., Imoto, Y., Sugama, J., Seki, S., Inoue, H., Odagiri, T., Hoshi, T., Anzai, J.: Sugar-induced disintegration of layer-by-layer assemblies composed of concanavalin a and glycogen. Langmuir **21**, 797–799 (2005)
272. Inoue, H., Sato, K., Anzai, J.: Disintegration of layer-by-layer assemblies composed of 2-iminobiotin-labeled poly(ethyleneimine) and avidin. Biomacromolecules **6**, 27–29 (2005)
273. Radt, B., Smith, T.A., Caruso, F.: Optically addressable nanostructured capsules. Adv. Mater. **16**, 2184–2189 (2004)

274. Skirtach, A.G., Javier, A.M., Kreft, O., Kohler, K., Alberola, A.P., Mohwald, H., Parak, W.J., Sukhorukov, G.B.: Laser-induced release of encapsulated materials inside living cells. Angew. Chem. Int. Ed.Engl. **45**, 4612–4617 (2006)
275. Borden, M.A., Caskey, C.F., Little, E., Gillies, R.J., Ferrara, K.W.: DNA and polylysine adsorption and multilayer construction onto cationic lipid-coated microbubbles. Langmuir **23**, 9401–9408 (2007)
276. Blacklock, J., Handa, H., Soundara Manickam, D., Mao, G., Mukhopadhyay, A., Oupicky, D.: Disassembly of layerby-layer films of plasmid DNA and reducible TAT polypeptide. Biomaterials **28**, 117–124 (2007)
277. Ren, K.F., Ji, J., Shen, J.C.: Tunable DNA release from cross-linked ultrathin DNA/PLL multilayered films. Bioconjug. Chem. **17**, 77–83 (2006)
278. Ren, K., Ji, J., Shen, J.: Construction and enzymatic degradation of multilayered poly-l-lysine/DNA films. Biomaterials **27**, 1152–1159 (2006)
279. Manna, U., Patil, S.: Glucose-triggered drug delivery from borate mediated layer-by-layer self-assembly. ACS Appl. Mater. Interfaces **2**, 1521–1527 (2010)
280. Liu, X.H., Yang, J.W., Miller, A.D., Nack, E.A., Lynn, D.M.: Charge-shifting cationic polymers that promote selfassembly and self-disassembly with DNA. Macromolecules **38**, 7907–7914 (2005)
281. Funhoff, A.M., van Nostrum, C.F., Janssen, A.P., Fens, M.H., Crommelin, D.J., Hennink, W.E.: Polymer sidechain degradation as a tool to control the destabilization of polyplexes. Pharm. Res. **21**, 170–176 (2004)
282. Veron, L., Ganee, A., Charreyre, M.T., Pichot, C., Delair, T.: New hydrolyzable pH-responsive cationic polymers for gene delivery: A preliminary study. Macromol. Biosci. **4**, 431–444 (2004)
283. Luten, J., Akeroyd, N., Funhoff, A., Lok, M.C., Talsma, H., Hennink, W.E.: Methacrylamide polymers with hydrolysis-sensitive cationic side groups as degradable gene carriers. Bioconjug. Chem. **17**, 1077–1084 (2006)
284. De Geest, B.G., Vandenbroucke, R.E., Guenther, A.M., Sukhorukov, G.B., Hennink, W.E., Sanders, N.N., Demeester, J., De Smedt, S.C.: Intracellularly degradable polyelectrolyte microcapsules. Adv. Mater. **18**, 1005–1009 (2006)
285. Zhang, J.T., Lynn, D.M.: Ultrathin multilayered films assembled from "charge-shifting" cationic polymers: Extended, long-term release of plasmid DNA from surfaces. Adv. Mater. **19**, 4218–4223 (2007)
286. Stachelek, S.J., Song, C., Alferiev, I., Defelice, S., Cui, X., Connolly, J.M., Bianco, R.W., Levy, R.J.: Localized gene delivery using antibody tethered adenovirus from polyurethane heart valve cusps and intra-aortic implants. Gene Ther. **11**, 15–24 (2004)
287. Abrahams, J.M., Song, C.X., DeFelice, S., Grady, M.S., Diamond, S.L., Levy, R.J.: Endovascular microcoil gene delivery using immobilized anti-adenovirus antibody for vector tethering. Stroke **33**, 1376–1382 (2002)
288. Stachelek, S.J., Alferiev, I., Choi, H., Kronsteiner, A., Uttayarat, P., Gooch, K.J., Composto, R.J., Chen, I.W., Hebbel, R.P., Levy, R.J.: Cholesterol-derivatized polyurethane: Characterization and endothelial cell adhesion. J. Biomed. Mater. Res. A. **72**, 200–212 (2005)
289. Jin, X., Mei, L., Song, C.X., Liu, L.X., Leng, X.G., Sun, H.F., Kong, D.L., Levy, R.J.: Immobilization of plasmid DNA on an anti-DNA antibody modified coronary stent for intravascular site-specific gene therapy. J. Gene Med. **10**, 421–429 (2008)
290. Trentin, D., Hubbell, J., Hall, H.: Non-viral gene delivery for local and controlled DNA release. J. Control. Release **102**, 263–275 (2005)
291. Trentin, D., Hall, H., Wechsler, S., Hubbell, J.A.: Peptide-matrix-mediated gene transfer of an oxygen-insensitive hypoxia-inducible factor-1α variant for local induction of angiogenesis. Proc. Natl Acad. Sci. USA **103**, 2506–2511 (2006)
292. Blocker, K.M., Kiick, K.L., Sullivan, M.O.: Surface Immobilization of Plasmid DNA with a Cell-Responsive Tether for Substrate-Mediated Gene Delivery. Langmuir **27**, 2739–2746 (2011)
293. Mrksich, M., Whitesides, G.M.: Using self-assembled monolayers to understand the interactions of man-made surfaces with proteins and cells. Annu. Rev. Biophys. Biomol. Struct. **25**, 55–78 (1996)

294. Tidwell, C.D., Ertel, S.I., Ratner, B.D., Tarasevich, B.J., Atre, S., Allara, D.L.: Endothelial cell growth and protein adsorption on terminally functionalized, self-assembled monolayers of alkanethiolates on gold. Langmuir **13**, 3404–3413 (1997)
295. Whitesides, G.M., Kriebel, J.K., Love, J.C.: Molecular engineering of surfaces using self-assembled monolayers. Sci. Prog. **88**, 17–48 (2005)
296. Bhardwaj, S., Roy, H., Gruchala, M., Viita, H., Kholova, I., Kokina, I., Achen, M.G., Stacker, S.A., Hedman, M., Alitalo, K., Yla-Herttuala, S.: Angiogenic responses of vascular endothelial growth factors in periadventitial tissue. Hum. Gene Ther. **14**, 1451–1462 (2003)
297. Rissanen, T.T., Markkanen, J.E., Gruchala, M., Heikura, T., Puranen, A., Kettunen, M.I., Kholova, I., Kauppinen, R.A., Achen, M.G., Stacker, S.A., Alitalo, K., Yla-Herttuala, S.: VEGF-D is the strongest angiogenic and lymphangiogenic effector among VEGFs delivered into skeletal muscle via adenoviruses. Circ. Res. **92**, 1098–1106 (2003)
298. Rutanen, J., Rissanen, T.T., Markkanen, J.E., Gruchala, M., Silvennoinen, P., Kivela, A., Hedman, A., Hedman, M., Heikura, T., Orden, M.R., Stacker, S.A., Achen, M.G., Hartikainen, J., Yla-Herttuala, S.: Adenoviral cathetermediated intramyocardial gene transfer using the mature form of vascular endothelial growth factor-D induces transmural angiogenesis in porcine heart. Circulation **109**, 1029–1035 (2004)
299. Springer, M.L., Chen, A.S., Kraft, P.E., Bednarski, M., Blau, H.M.: VEGF gene delivery to muscle: Potential role for vasculogenesis in adults. Mol. Cell **2**, 549–558 (1998)
300. Yla-Herttuala, S., Alitalo, K.: Gene transfer as a tool to induce therapeutic vascular growth. Nat. Med. **9**, 694–701 (2003)
301. Yla-Herttuala, S., Markkanen, J.E., Rissanen, T.T.: Gene therapy for ischemic cardiovascular diseases: Some lessons learned from the first clinical trials. Trends Cardiovasc. Med. **14**, 295–300 (2004)

Chapter 12
Chitosan-Based Delivery System for Tissue Regeneration and Chemotherapy

Sungwoo Kim and Yunzhi Yang

Abstract A variety of polymeric devices have been widely studied as a means to deliver drugs at an appropriate dosage, delivery sequence, and time period to improve and optimize the treatment. In the conventional therapy of drug administration, a major limitation is the initial burst release of drugs, inducing a rapid loss of therapeutic efficacy and increasing the risk of harmful side effects to patients. As an alternative approach, single or multiple therapeutic agents can be incorporated into an appropriate material to well regulate its residence time and dosages. In this regard, numerous synthetic and natural polymers have been employed as drug carriers to control drug release for a desired administration. Recently, chitosan, a cationic natural polymer, has gained considerably attention due to its potential broad application in tissue regeneration, chemotherapy, and wound healing. In this chapter, chitosan is introduced as a drug carrier in a variety of forms. This chapter discusses several properties of chitosan such as biocompatibility, biodegradability, and functionality. It will also discuss techniques for preparation of chitosan-based delivery systems, and strategies of controlled drug release for potential biomedical and pharmaceutical applications, including tissue regeneration, chemotherapy, and wound healing.

Polymeric Drug Delivery System

A drug delivery system is a device that can maintain effective drug levels in the body over a desired time period. Current technical advances in drug delivery have enabled drugs to be incorporated into a variety of devices such as an osmotic pump, a transdermal patch, a liposomal encapsulation, and an implant [26, 68]. These delivery

S. Kim • Y. Yang (✉)
Orthopedic Surgery, Stanford University, 300 Pasteur Drive, Edwards R105,
Mail code 5341, Stanford, CA 94305, USA
e-mail: kim4@stanford.edu; ypyang@stanford.edu

S.K. Bhatia (ed.), *Engineering Biomaterials for Regenerative Medicine: Novel Technologies for Clinical Applications*, DOI 10.1007/978-1-4614-1080-5_12,

systems have been explored to optimize the therapeutic efficacy of drugs, biomolecules, and growth factors for long-term delivery regarding stability and safety.

One of the major considerations in drug delivery systems is biocompatibility. Polymeric devices are implantable and have consistent contact with the local tissues and body fluid; thus, polymers and their degradable products need to be nontoxic. In particular, biodegradable delivery systems alleviate the need for surgical removal of the implant, thereby increasing patient acceptance and compliance [31]. They are disintegrated by hydrolysis of the polymer chains into biologically acceptable polymer products over time. The biodegradable polymers have hydrolysable linkages such as ester, amide, anhydride, orthoester, urea, carbonate, and urethane linkages in their backbone [31]. They are absorbed or excreted from the body via normal metabolic pathways without any complications. The biodegradation of the polymers is attributed to factors such as chemical structure, composition, wettability, surface morphology, molecular weight, shape, size, etc. [26, 45]. Drugs released from biodegradable systems are governed by diffusion, initial drug loading, drug/polymer interactions, drug solubility, and polymer degradation [31]. In contrast, nonbiodegradable polymeric systems such as poly(methyl methacrylate) (PMMA) used in trauma infection treatment need minor surgery to remove the implant. The drug release is achieved by diffusion via pores in the nonbiodegradable polymer matrix or between polymer chains [26].

Chitosan

The choice of an ideal drug carrier is of importance because it can significantly affect the efficacy of therapeutics. A variety of materials have been studied as drug carriers. Among them, polysaccharides have shown their outstanding properties for being used as a drug carrier [11, 63, 77]. In particular, chitosan has been of great interest among polysaccharides due to the presence of a nitrogen group, allowing opportunities for chemical modification and beneficial biological properties. The presence of functional groups in chitosan allows for several synthetic modifications to improve specific properties of native chitosan [30, 48, 88, 109]. Chitosan exhibits a variety of physicochemical and biological properties, which are very attractive in diverse applications. The most studied biomedical applications include wound healing, tissue regeneration, and drug/gene delivery [57, 79].

Properties of Chitosan

Physicochemical Properties

Chitosan is the fully or partially *N*-deacetylated derivative of chitin, which is the most abundant natural amino polysaccharide, found in shellfish sources such as lobsters,

crabs, and shrimp [57, 79]. Chitosan and chitin have structural similarity to cellulose in plants, and they are copolymers consisting of *N*-acetyl-glucosamine and *N*-glucosamine units [14]. Chitin contains more than 50% of *N*-acetyl-glucosamine units, has limited solubility in common solvents, and is chemically less reactive than chitosan. In contrast, chitosan contains a higher proportion of *N*-glucosamine units (above 50%) in the polymer compared with chitin. It is soluble in dilute acids including hydrochloric, lactic, and acetic acids and has better reactivity for chemical reactions [51].

Chitosan contains groups that favor hydrogen bonding such as hydroxyl (–OH), amine ($–NH_2$), amide (–NH-C), and carbonyl (–C = O) groups [21]. Unlike other polysaccharides such as cellulose and dextran, chitosan is a positively charged polysaccharide in an acidic solvent along with its molecules, which causes electrostatic repulsion between chitosan molecules. The protonation (NH_3^+) of amine groups (NH_2) of chitosan in acidic solution provides important physicochemical properties. The parameters responsible for free amine groups of chitosan include the degree of deacetylation (DDA), molecular weight, and environmental factors such as pH, solvent, temperature, etc. [103]. An increase in the DDA significantly lowers the protonation constant (pKa), influencing hydrophobic interactions and hydrogen bonds between chitosan molecules [103]. An increase in the molecular weight of chitosan also lowers the protonation constant pKa. Chemical modification can provide specific functionality and alter physical properties of chitosan. For example, the functional groups of the chitosan can be used for side group attachment, affecting its crystallinity by increasing the amorphous structure. This modification alters the mechanical strength and solubility of chitosan. In addition, a sulfation process can make chitosan molecules anionic and water soluble, which are reverse characteristics of the natural properties of chitosan [27].

Chitosan has an outstanding viscosity in acidic environments with high molecular weight and behaves as a pseudoplastic material [104]. Its viscosity increases with an increase in concentration and DDA. Viscosity influences mechanical properties such as the elongation at break and the tensile strength of chitosan films [100, 104]. Viscous chitosan polymer produces significant biological activities in wound-healing and osteogenesis development [29]. Solubility of chitosan can be controlled by crosslinking reagents such as glutaraldehyde, which is commonly used for slow drug release [46].

Biological Properties

Chitosan exhibits various beneficial biological properties such as biocompatibility, biodegradability, nontoxicity, and low immunogenicity. It also exhibits antibacterial, anti-fungal, and anti-viral activity [57]. These properties have been used in numerous applications in pharmaceutical and biomedical fields. Chitosan has also been used in the field of dentistry, ophthalmology, and orthopedics due to its excellent mucoadhesive property [9, 52, 65]. It has been reported that after implantation in vivo, chitosan films did not induce inflammatory reactions in the surrounding tissues [14, 52, 100].

Chitosan is a biodegradable polymer and is hydrolyzed by different enzymes such as chitosanase and lysozyme [70, 76, 100]. Chitosanase is completely absent in mammals, but lysozyme is mainly responsible for the degradation of chitosan in human body. Lysozyme is present in tissues, saliva, blood, and tears, and it is used by phagocytic cells during the inflammatory response [79]. Lysozyme hydrolyses the glycosidic bonds of chitosan molecules, but it is less active on chitosans with higher DDA [76, 94]. The hydrolysis reaction of the lysozyme includes proton (H^+) transfer from a carboxyl group of a glutamic acid (Glu-35) to the substrate and then a hydroxyl group of a water molecule is added to a carbon atom in an amino sugar group [70].

Chitosan is degraded into amino sugar groups via the metabolic pathways of glycosaminoglycans and glycoproteins [14]. The degradation rate of chitosan polymers can be controlled by changing the DDA and molecular weight [61, 103]. The degradation rates of chitosan are inversely related to the DDA. Chitosan polymers with higher than 85% of DDA exhibit the lowest degradation rates and remain over several months in vivo [100].

The DDA of chitosan plays an important role in cell attachment and proliferation. These properties can be used for both soft and hard tissue regeneration [52]. Chatelet et al. investigated the effect of degree of deacetylation (DDA) on biological properties of chitosan films in vitro [14]. It was observed that chitosan films with a lower DDA induced better cell attachment, growth, and proliferation compared with those with a higher degree of DDA. In the wound area, chitosan films with lower DDA enhanced fibroblast attachment and provided a suitable environment for the proliferation of keratinocytes, inducing epidermal regeneration. This result indicated that chitosan films with a lower DDA are excellent candidates for wound healing applications [14, 37, 71]. In their work, all chitosan films were cytocompatible with culture cells such as keratinocytes and fibroblasts. Hoekstra et al. also demonstrated that chitosan is a potential bio-sealant to achieve hemostasis at the puncture site in vivo [39]. A created wound in dogs was sealed with the chitosan quickly without inflammation, presenting anti-thrombogenic properties.

In addition, chitosan itself has shown anti-proliferative and anti-angiogenesis effects on cancer cells [13, 69, 96]. Murata et al. investigated an inhibitory effect of anti-metastatic sulfated chitin derivatives on lung tumor metastasis. In their work, it was found that the sulfated chitin derivatives did not directly affect the viability and the growth of tumor cells and endothelial cells in vitro. However, the derivatives significantly reduced the number of vessels around tumor tissue, indicating an anti-angiogenetic effect [69]. Hasegawa et al. investigated the effect of chitosan on caspase-3 activity in human bladder tumor cells in vitro [35]. In their work, the caspase-3 activity of the chitosan treated cells was significantly elevated. The chitosan treated tumor cells showed nuclear fragmentation and chromatin condensation, indicating apoptosis of the cancer cells. The results suggested that the chitosan exhibited anti-canter properties by inducing apoptosis via the activation of caspase-3.

Chitosan is also considered a promising biodegradable carrier for controlled drug release in the field of drug delivery systems [44, 80]. Its positively charged

molecules interact with negatively charged therapeutic agents and biomolecules. Generally, drugs are chemically attached or dispersed into the chitosan matrix and released via slow and controllable diffusion or biodegradation [28, 42, 81]. Therefore, chitosan delivery systems can carry a variety of therapeutics such as polar drugs, peptides, proteins, vaccines, and DNA [2, 7, 9, 64, 77].

Preparation of Chitosan-Based Drug Carriers

Chitosan-based biomaterials have been developed in a variety of forms such as powders, films, sponges, hydrogels, composite fibers, and beads. Chitosan itself has an ability to form a 3D gelling structure, and it can be modified chemically or physically via various crosslinking mechanisms such as covalent bonds, ionic bonds, hydrogen bonds, hydrophobic interactions, etc. [103]. The chemical or physical modifications have been widely studied to improve its water solubility, control its drug release, and extend its applications [30, 48, 88, 109]. These modifications influence physicochemical and biological properties of chitosan as well as the efficacy of therapeutics. Therefore, designing a drug delivery carrier depends on application areas and properties of bioactive molecules.

Chemical Crosslinking Methods

Chitosan can form covalently crosslinked irreversible networks using small molecule crosslinking, secondary polymerization, irradiation, enzymatic reaction, pH, temperature, etc. [5, 6, 38, 62]. The chemical crosslinking methods have been used to control porosity, swellability, dissolution, degradation, and mechanical property of the drug delivery systems. Most of chemical crosslinking molecules react with amine groups of chitosan to form inter- or intra-molecular networks [5]. Alternatively, photo-reactive molecules or enzymatic sensitive molecules have been employed to form covalent crosslinks on the chitosan chains, followed by UV exposure irradiation [36, 38]. Even though covalent bonds are the main forces for the formation of the crosslinked polymer networks, secondary interactions such as hydrogen bonds and hydrophobic interactions are also important in the formation of the 3D polymer networks [36]. The covalent crosslinking density is affected by various parameters such as the concentration of crosslinking agents, molecular weight, and DDA of chitosan. Therefore, those parameters are important in determining properties of drug delivery systems such as controlled drug release and mechanical strength.

The covalently crosslinked chitosan polymers can be divided into different categories according to their structural differences [5, 36]: small molecule crosslinked network, hybrid polymer network, and interpenetrating polymer network (IPN). The simple covalent crosslinking method involves using small crosslinking molecules such as glutaraldehyde, diglycidyl ether, diisocyanate,

glyoxal, etc. [5, 36, 62]. Amino (–NH_2) and hydroxyl (–OH) groups of the chitosan are used to form the crosslinked chitosan network via various linkage mechanisms such as the Schiff base formation [5, 12]. Aldehyde groups of the crosslinking molecules such as glutaraldehyde form imine bonds with the amino groups of chitosan via a Schiff base [12]. The crosslinking molecules can improve the mechanical properties of the delivery system, but they also generate the main drawbacks such as toxicity and limited application. Therefore, it is desirable to investigate better crosslinking methods for chitosan as alternatives [5].

In another approach, the functionalized polymer chains can be used to crosslink chitosan to reduce the release of toxic chemicals during gelation. As an example of the hybrid polymer network, Tan et al. recently developed a composite hydrogel based on a water soluble chitosan and an oxidized hyaluronic acid for cartilage tissue engineering applications [98]. In their work, an *N*-succinyl-chitosan and an aldehyde hyaluronic acid (A-HA) were synthesized without the addition of chemical crosslinking agents for the preparation of composite hydrogels. *N*-succinyl-chitosan, a water soluble chitosan, was prepared by mixing a chitosan solution and a succinic anhydride solution, resulting in the addition of succinyl groups at the N-position of the chitosan. Separately, the aldehyde hyaluronic acid (A-HA) was prepared by adding a sodium periodate solution into a hyaluronic acid solution. The crosslinked composite hydrogels were formed by a Schiff's base reaction (-C = N–) between amino (-NH_2) groups of the *N*-succinyl-chitosan and aldehyde (-CHO) groups of aldehyde hyaluronic acid. The results demonstrated that the biocompatibility of the composite hydrogel was improved, and that the crosslinking density was dependent on the ratios of the *N*-succinyl-chitosan to the aldehyde hyaluronic acid. Weng et al. reported a similar result using an oxidized dextran and an *N*-carboxyethyl chitosan for controlled drug release [105]. In an attempt to improve the solubility of chitosan, an acrylic acid was introduced into a chitosan polymer to form a water soluble carboxyethyl chitosan. The chitosan polymer formed the crosslinked networks via a Schiff base reaction between aldehyde groups in the oxidized dextran and amino groups in the *N*-carboxyethyl chitosan. The chemical crosslinking density was closely related to the ratios of the oxidized dextran to the *N*-carboxyethyl chitosan, temperature, time, and the concentration of the polymers.

Alternatively, the chitosan polymer can be crosslinked with the functionalized polymer chains via the Michael-type addition reaction [53, 66]. The primary amino groups in the chitosan chains can react with the vinyl groups on the other polymers such as poly(ethylene oxide) (PEO) without any crosslinking agents. This crosslinked network can be readily formed under physiological conditions. Kim et al. recently reported a novel chitosan-poly(ethylene oxide) (PEO) hydrogel via the Michael-type addition reaction [53]. The chemically crosslinked chitosan–PEO network was formed using 2-carboxyethyl acrylate grafted chitosan and PEO with hexa-thiol. The acrylate end groups in the soluble chitosan were chemically crosslinked with thiol end groups in the PEO via the Michael-type reaction without the addition of crosslinking agents. Therefore, this approach can be applied for tissue engineering and drug delivery matrixes [66].

Photo-crosslinked chitosan hydrogels can be formed by adding photosensitive moieties to the chitosan chains with UV irradiation [43, 73, 75]. Ono et al. developed a photo-crosslinked chitosan hydrogel (Az-CH-LA) containing both lactose moieties (LA) and photo-reactive azide groups (Az) through a two-step condensation reaction [75]. In their work, amino groups of the chitosan were replaced by lactobionic acid moieties to form the lactose-linked chitosan (CH-LA), providing better solubility in water. Subsequently, the azide moieties were introduced to the lactose-linked chitosan (CH-LA) using azidobenzoic acid. As a result, the viscous Az-CH-LA solution became the crosslinked hydrogel after UV irradiation. The UV irradiation released N_2 from the azide groups ($–N_3$), which were converted into reactive nitrene groups. The interaction between amino groups of chitosan and the nitrene groups induced a gelation. The photo-crosslinked Az-CH-LA exhibited excellent potential as a biological adhesive and a drug carrier for the controlled release of growth factors [73, 75].

Similarly, the photo-crosslinked chitosan networks can be formed using functionalized Pluronic or PEG for the sustained release of different types of therapeutics [108, 110]. Yoo et al. developed a thermo-sensitive and photo-crosslinkable hydrogel by employing di-acrylated Pluronic and acrylated chitosan [110]. Pluronic chitosan, known as Poloxamer, is a nonionic triblock copolymer. It is composed of a central hydrophobic chain of poly(propylene oxide) and two hydrophilic chains of poly(ethylene oxide). It undergoes a sol–gel transition via hydrogen bonds between poly(propylene oxide) blocks with an increasing temperature above a lower critical solution temperature (LCST). In their study, Pluronic and chitosan were separately functionalized by reacting with photosensitive acryloyl chloride and glycidyl methacrylate, respectively. The functionalized Pluronic/acrylated chitosan formulations physically underwent thermal gelations with increasing temperature, and the concentration of the chitosan significantly affected gelation temperature. After preparing the thermo-sensitive gels above LCST, the Pluronic/chitosan hydrogels were photo-crosslinked by UV irradiation to form covalently crosslinked networks between the di-acryloyl pluronic and the glycidyl methacrylated chitosan. Swelling ratios and degradation rates of the crosslinked hydrogels were dependent on UV irradiation time and concentrations of the polymers. The hydrogels containing human growth hormone (hGH) exhibited sustained release with long photo-crosslinking times and high chitosan contents in the hydrogel.

Recently, the enzyme-catalyzed crosslinking method has gained significant attention in the fields of tissue engineering and drug delivery [15, 50, 85]. There have been numerous approaches using the action of natural tissue enzymes such as transglutaminase (TG) [49, 87, 93], tyrosinase [15], and horseradish peroxidase (HRP) with hydrogen peroxide (H_2O_2) [49, 50, 85]. For example, Sakai et al. developed a novel chitosan derivative that was soluble at neutral pH and became a hydrogel via a peroxidase-catalyzed reaction [85]. In their work, chitosan was conjugated with 3-(*p*-hydroxyphenyl) propionic acid (pHP) using the carboxyl groups of pHP and the amino groups of chitosan. This resulted in a formation of chitosan derivatives with phenolic hydroxyl groups (Ph). This step made the

chitosan soluble at neutral pH, and its solubility was dependent on the number of Ph groups. The Ph groups in the chitosan chains induced a crosslinkable chitosan hydrogel using HRP and hydrogen peroxide (H_2O_2). The crosslinked hydrogel was formed either between Ph groups or between Ph groups and amino groups via an enzyme-catalyzed oxidative reaction [15, 49, 50, 86]. The gelation time decreased with increasing concentration of HRP and with decreasing concentration of H_2O_2. The higher content of H_2O_2 deactivated HRP. Therefore, it is desirable to use lower concentration of H_2O_2 for faster gelation and better biocompatibility.

In the other approach, the covalently crosslinked network can be formed by adding non-reacting secondary polymers into the chitosan solution before crosslinking. These non-reacting polymers form a physically entangled polymer mesh, which is an interpenetrating polymer network (semi-IPN) [5, 32, 102]. If an additional polymer is crosslinked to have two entangled crosslinked networks, a full-IPN is formed. Several chitosan-based IPN hydrogels were studied [5, 9]. However, this technique has the limited applications because it requires the use of toxic chemicals during crosslinking or polymerization.

Physical Bonding Methods

Physically crosslinked polymers are formed under mild conditions without the addition of toxic crosslinkers [5, 36, 38, 62, 92]. They are biocompatible but exhibit weak mechanical strength [38, 91, 92]. Therefore, external environmental factors (e.g., ionic strength, pH, and temperature) can disrupt the polymer networks. Non-covalent polymer networks can be formed with ionic molecules, polyelectrolyte polymers, and neutral polymers [38]. The major physical interactions are electrostatic, hydrophobic, and hydrogen bonds between polymer chains [36]. The physically bonded polymers are suitable for short-term drug delivery.

The chitosan polymer can form ionic interactions with negatively charged molecules due to its cationic amino groups. The chitosan polymer can bind metal anions and anionic small molecules such as phosphates and sulfates with its protonated amino groups [5, 63, 100]. The charge density of chitosan is dependent on environmental pH, and the protonation constant pKa [89, 103]. Therefore, small anionic molecules containing a high charge density can form strong ionic interactions with the chitosan polymer. Secondary forces such as hydrophobic interactions and hydrogen bonds can be formed between hydroxyl groups of chitosan and the ionic molecules after neutralization of the cationic charges of the chitosan [5, 89]. Similarly, chitosan can form polyelectrolyte complexes (PECs) via electrostatic interactions with anionic macromolecules such as proteins, DNA, polysaccharides, and the other polymers [5, 6, 11]. The PECs are stronger than the other interactions including hydrogen bonds and van der Waals forces, but they are reversible if there are changes in charge density, pH, temperature, etc. [6]. The PECs are networks physically bonded without the addition of toxic chemicals such as catalysts, crosslinkers, and initiators under physiological conditions [5].

In addition, chitosan can form a 3D gelling structure using a neutralizing agent such as a sodium hydroxide (NaOH) [5, 56]. The neutralization reduces electrostatic repulsion between chitosan molecules and enhances the formation of hydrogen bonds and hydrophobic interactions [6]. Generally, chitosan molecules in an acidic solution immediately form a hydrated precipitate by adding a strong base due to the reduced charge density along chitosan chains, which subsequently induces extensive hydrogen bonding and hydrophobic interactions between chains [54, 62, 91]. This results in an inability to maintain chitosan molecules in a solution at a physiologically acceptable pH [5]. Therefore, the increase in the concentration of the neutralizing agent significantly affects the 3D chitosan network, resulting in shrinkage and depletion of the gelling system [99].

Recently, the thermo-sensitive gels have gained special attention due to its ability to deliver therapeutic agents, molecules or cells [4, 18, 67, 83, 96, 97]. The hydrophobic interactions and hydrogen bonds are essentially involved in the mechanism of a sol–gel transition in response to the change of temperature. The injectable gel system has several advantages over the implantable drug delivery systems [23, 33, 82, 83]. An injectable gel formulation is liquid at room temperature and becomes a gel at body temperature. It can be directly administered at the targeted site by a simple injection without surgical intervention. In addition, a variety of therapeutics can be encapsulated into the gel formulation. These include hydrophobic drugs, various types of growth factors, and even cells [4, 18, 23, 33, 82, 96]. This delivery method can reduce costs and surgical complications.

The thermo-sensitive chitosan hydrogel can be prepared either by neutralization of an acidic chitosan solution with various polyols such as glycerol, ethylene glycol, and sorbitol or by aggregation of copolymers in aqueous media [3, 18, 47, 56, 107]. These polyols maintain chitosan as a liquid. Polyols form a shield of water around chitosan chains in an acidic solution and maintain the solubility of chitosan at higher pH values at lower temperatures [5, 19, 21, 82, 106]. β-Glycerophosphate (β-GP) has attracted a lot of attention in forming thermo-sensitive chitosan-based gel delivery vehicles [19, 21–23, 40, 106]. Several interactions reported during the gelation process include the loss of electrostatic repulsion, hydrogen bonding, and increased hydrophobic interactions. Chitosan is positively charged in an acidic solution due to the protonation of the free amine groups, which causes electrostatic repulsion between chitosan molecules. When a weak base of disodium β-GP solution is added into an acidic chitosan solution, it increases pH and also induces electrostatic attractions between positively charged chitosan (NH_3^+) and negatively charged phosphate molecules ($-HPO_4^-$ or $-PO_4^{2-}$) of β-GP. It also reduces electrostatic repulsion between the chitosan chains due to charge neutralization by β-GP anions, which results in an increase in hydrogen bonding interactions along chitosan interchains [21]. With increasing temperature, chitosan–chitosan interactions become dominant resulting in a phase transition from a liquid to a gel, while hydrogen bonding interactions are reduced [19, 106]. After breaking of hydrogen bonding, phosphate groups function as a proton sink after chitosan chains release protons [96]. The chitosan chains subsequently are brought close to precipitation resulting in the gelation of the chitosan gel-forming solution (Fig. 12.1).

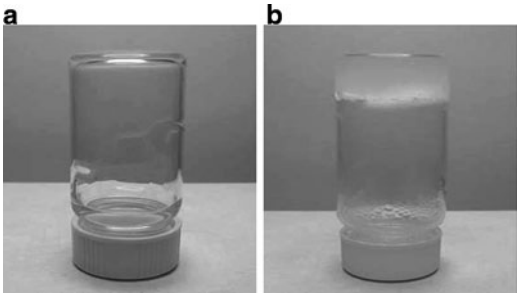

Fig. 12.1 Photograph showing the thermal gelation of the chitosan/β-GP solutions which were placed (**a**) at 5°C and (**b**) at 37°C for 30 min. 5 mL of chitosan solution contained 0.088 M of β-GP solution and the final pH was 7.23

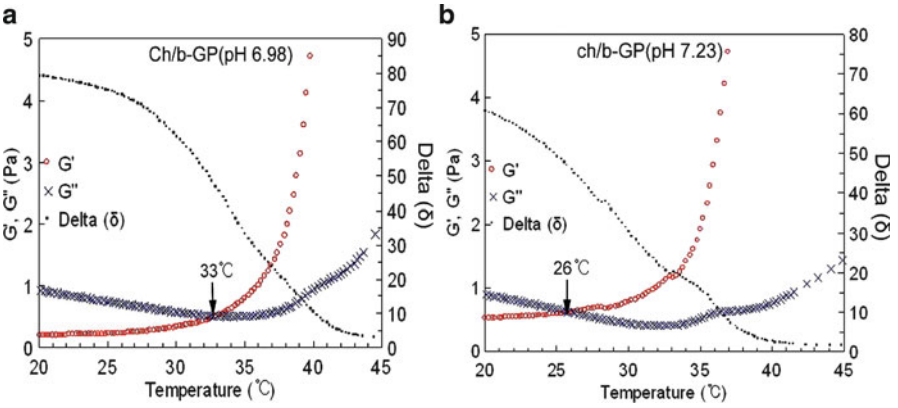

Fig. 12.2 The gelation temperature of the chitosan/β-GP solution at (**a**) pH 6.98 and (**b**) at pH 7.23. The storage modulus (G') and the loss modulus (G'') of the chitosan/β-GP solution were evaluated with regard to the effect of the final pH on the gelation temperature. The elastic modulus (G') and the viscous modulus (G'') are equivalent in value at $\delta = 45°$ [54]

Several studies have reported that phosphate groups of β-GP do not induce ionic crosslinking with the chitosan molecules. Instead, the hydrophobic effect has been considered the main force in inducing thermal gelation of the chitosan/β-GP system [3, 18, 21]. The gelation of the chitosan/β-GP system can be controlled by the DDA of chitosan, concentration of chitosan, the amount of polyol salt, temperature, and the final pH of the gel forming solution [21, 22, 97]. As shown in Fig. 12.2, the crossover of the storage modulus (G') and the loss modulus (G'') moved to the left with increasing final pH of the gel forming solution.

The phase angle (δ) of the chitosan/β-GP solution (final pH 6.98 or 7.23) decreased gradually as the temperature increased. The phase angle reached 45° where $G' = G''$ at which the temperature was 33°C for pH 6.98 and 26°C for pH 7.23, respectively. The rheological analysis indicated that the storage modulus (G') began to increase at lower temperature with the chitosan/β-GP solution at higher final pH 7.23 compared with lower final pH 6.98. This study demonstrated that the

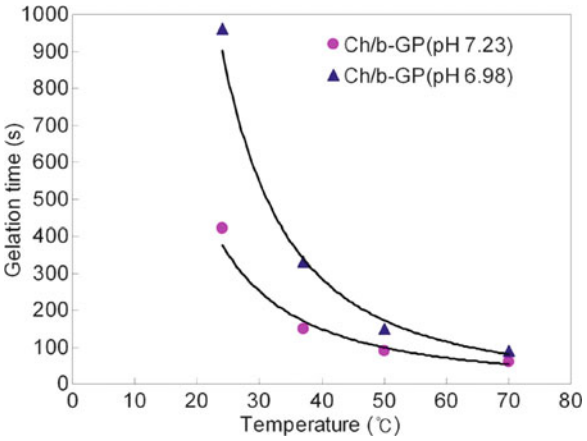

Fig. 12.3 The gelation time of the DCh/β-GP solution as a function of the temperature. The DCh/β-GP solutions were prepared with different final pHs which were 6.98 and 7.23, respectively [54]

gelation temperature was lowered with increasing final pH of the gel forming solution. Figure 12.3 shows that the gelation time decreases exponentially with increasing temperature. The chitosan/β-GP solution at pH 7.23 showed faster gelation time (150 s at 37°C) compared with that at pH 6.98 (330 s at 37°C).

Alternatively, similar thermo-sensitive chitosan gelation has been reported using a chitosan copolymer containing hydrophilic and hydrophobic moieties [10, 17]. The thermo-sensitive chitosan hydrogel can be formed by grafting a monohydroxy poly(ethylene glycol) onto the chitosan backbone (PEG-g-chitosan) [10]. In this study, PEG was covalently connected to chitosan chains to improve the solubility of chitosan via a Schiff base reaction, and then the aqueous copolymer solution became a semisolid hydrogel at body temperature. At low temperatures, hydrogen bonding was formed between hydrophilic groups of PEG and water molecules. With increasing temperature, hydrophobic interactions dominated between the polymer chains [78]. To induce a sustained release of proteins, the second crosslinking can be performed onto the PEG-g-chitosan gel with a chemical crosslinker, which transforms it from a physical gel to an insoluble chemical gel [10].

Applications of Chitosan-Based Drug Carriers

Controlled Drug Release for Tissue Engineering and Chemotherapy

Strategies of Drug Loading

The optimal function of a drug delivery system depends on both properties of the delivery device and the drug. Therefore, the choice of the material and the strategy of drug loading should be considered according to the characteristics of the drug such as

solubility, charge, and size for controlled release. There are several approaches of incorporating drugs into chitosan networks. Drugs can be directly added into chitosan carriers via a permeation method [38, 92]. In this method, chitosan hydrogels are placed into medium containing therapeutics, which slowly diffuse into the gels [91]. This method can be easily applied for small molecules and hydrophilic drugs, but is not appropriate for large molecules such as peptides and proteins [62]. It takes a long time to load drugs using this method. The drug release profile exhibits a rapid burst release during initial swelling. To deliver large molecules, chemical crosslinking methods can be used to encapsulate the drug agents into the delivery system [38]. A drug is directly added into the polymer solution with a crosslinking agent, inducing the entrapment of the drug into chitosan gel networks [34, 46]. However, unnecessary crosslinking between polymer chains and drug molecules decreases the therapeutic activity of the drug during the formation of the polymer network. To improve the crosslinking effect, a drug can be intentionally tethered to the polymer chains physically or chemically before the formation of the polymer network [38, 62]. This method can reduce the initial burst release of the drug from the delivery system, resulting in improved therapeutic residence. However, linkages between the polymer and drug should be broken down to increase drug exposure to the target tissue via environmental factors such as enzymes, pH, and temperature.

In another strategy, the polymer solution can be mixed with some additives such as amphiphilic molecules to load hydrophobic molecules or molecules with the same charge as the polymer components [62, 84]. For example, paclitaxel is one of popular anti-cancer drugs used to treat various cancers such as ovarian and lung cancer, head and neck carcinoma, acute leukemia, and breast cancers [72, 84]. However, it is hydrophobic and less soluble in water. To improve its therapeutic efficacy, several delivery strategies have been applied. Ruel-Gariepy et al. encapsulated paclitaxel into an injectable chitosan gel containing β-glycerophosphate (β-GP) for the sustained release of paclitaxel and investigated its in vivo anti-tumor activity using an EMT-6 murine mammary carcinoma model [84]. Addition of β-glycerophosphate (β-GP) to a chitosan solution induced a sol–gel transition at body temperature. The results showed the controlled release of paclitaxel from the injectable chitosan gel over 1 month in vitro. These experiments demonstrated that an intra-tumoral injection of the chitosan hydrogel containing paclitaxel was four times more effective compared with intravenous injections of Taxol. Similarly, camptothecin, an insoluble anti-cancer drug, was also loaded into the chitosan/β-glycerophosphate (β-GP) hydrogel for sustained intra-tumoral release into mouse tumor model (RIF-l) [8]. In vitro release profiles exhibited zero order release kinetics for 4 weeks with low initial burst effects (less than 5%). This injectable chitosan hydrogel maximized the therapeutic efficacy of camptothecin without toxicity. In another application, the chitosan/β-glycerophosphate (β-GP) hydrogel was prepared and evaluated as a potential delivery system for living cells and therapeutic proteins in tissue engineering applications [18]. In those studies, hydrophobic interaction was the main force that induced thermal gelation of the chitosan and affected drug loading rates in the chitosan/β-GP system [5, 21, 54, 106].

Alternatively, Obara et al. reported similar results using photo-crosslinked chitosan hydrogels [72]. In their work, Azide (*p*-azidebenzoic acid) and lactose (lactobionic acid) were added to amino groups in the chitosan via a condensation reaction prior to the drug loading [72, 75]. The addition of lactose induced a water soluble chitosan at neutral pH values. The chitosan (Az-CH-LA) solution containing paclitaxel became an insoluble hydrogel after UV irradiation. In vitro release profiles showed a slow release of paclitaxel molecules from the chitosan (Az-CH-LA) hydrogel via both diffusion and biodegradation. These results demonstrated that the paclitaxel loaded Az-CH-LA induced significant necrosis on tumor tissue and inhibited angiogenesis compared with control groups, which included delivering the drug or Az-CH-LA hydrogel alone.

In another strategy, a separate drug carrier is incorporated into another delivery system for long-term applications. Therapeutic agents are initially loaded into small vehicles such as micro/nanoparticles prior to encapsulation by another main delivery system such as hydrogels and scaffolds [41, 58–60]. Lee et al. encapsulated TGF-β1 loaded chitosan microspheres into a collagen/chitosan/glycosaminoglycan (GAG) scaffold for cartilage formation [59]. In their work, TGF-β1 was loaded into chitosan microspheres using an emulsion crosslinking method. The TGF-β1 loaded microspheres in 90% aqueous ethanol were then introduced into the scaffold and lyophilized. The results showed that the chitosan microspheres released TGF-β1 over 1 week in a controlled manner with an initial burst effect. However, the initial burst release of TGF-β1 was reduced due to additional encapsulation by the scaffold.

Strategies of Drug Release

The release mechanism of drug delivery systems varies according to the characteristics of the materials such as hydrophilicity, swellability, solubility, degradability, and crosslinking density [62]. Generally, different mechanisms are involved in the release profile of the therapeutics encapsulated in the polymer network, including diffusion, swelling, and degradation. In polymeric materials, diffusion is the most well-known mechanism of drug release. The porous structure of the delivery matrix significantly affects the rate of the drug release. Diffusion rate is highly related to the pore size of the delivery matrix in a similar manner as drug molecular size [62]. Small molecular drugs are released faster than macromolecules such as proteins and peptides from the delivery system. The diffusion of small molecules is not significantly affected by swelling of the polymer network, but the diffusion of large molecules can be controlled using the swelling behavior of the delivery system [62, 90]. Swelling of the delivery matrix accelerates the diffusion of drugs by opening pores of the polymer network. In addition, drugs can be chemically crosslinked to the polymer matrix for controlled and sustained drug release. In this case, polymer chains are broken down via hydrolytic or enzymatic degradation. The release of encapsulated or crosslinked drugs is accelerated via surface erosion, degradation of the polymer chains, and bulk

degradation of the polymer backbone [62, 90]. However, diffusion, swelling, or crosslinking mechanisms generate a nonspecific release profile of drugs.

In another strategy, environmental or biological stimulations such as pH, temperature, and enzymes are used to effectively control drug release for selective treatments. These methods can maintain therapeutic levels at local specific target sites without increasing toxicity for a designed time period [6, 62]. pH stimulation is one of the most promising methods for controlled drug release and effective treatment. The pH sensitivity is dependent on the presence of functional groups on the polymer backbone. Neutral and anionic polymers are less sensitive to the change of pH under acidic conditions. However, cationic polymers such as chitosan are very responsive to low pH (3–5), but they become insoluble at higher pH.

As an example of pH responsive release, Dai et al. developed an *N*-succinyl chitosan/alginate hydrogel crosslinked by Ca^{2+} ions for the controlled delivery of nifedipine [25]. In their work, the shrinkable characteristic of alginate at low pH was used to induce pH sensitive drug release. Ca^{2+} ions provide ionic crosslinks of alginate, inducing the formation of microencapsulated beads. Soluble *N*-succinyl chitosan was also crosslinked by Ca^{2+}, resulting in entangled alginate on the *N*-succinyl chitosan gel. The Ca^{2+} crosslinked hydrogel beads were sensitive to the changes in pH due to carboxylated groups (–COO–) in the polymer network. The results showed that the drug release from the beads was relatively slow (11.6%) at pH 1.5, while the release rate was increased to 76% at pH 7.4. This result indicated that the system is sensitive at higher pH and has a site specific property which makes it a potential drug carrier in the intestinal tract. At neutral pH, the release of nifedipine from the hydrogel beads was significantly increased due to enhanced swellability of the hydrogel network. At pH 1.5, hydrogen bonding between the alginate and the *N*-succinyl chitosan dominated, and the hydrogel beads were in a shrunken state. The ionization of carboxylic groups in the beads induced the best swelling characteristic and pH sensitivity at pH 7.4.

In a comparative study, the swelling behavior of the chitosan polymer can be controlled by adjusting the ratio of hydrophilic to hydrophobic groups and the crosslinking density in the polymer network [1, 32]. Recently, Guo et al. reported similar results using a semi-IPN hydrogel by combining a natural carboxymethyl (CM)-chitosan and a synthetic poly (*N*-isopropylacrylamide) (PNIPAm) to induce pH and temperature sensitivity [32]. They found that the cumulative release of coenzyme A (CoA) was 22.6% at pH 2.1 and 89.1% at pH 7.4 within 24 h. At pH 2.1, carboxyl groups (–COOH) formed hydrogen bonds between –OH groups in the CM-chitosan and –NHCO groups in the PNIPAm. The hydrogen bonds became dominant and made the gel shrink. However, at pH 7.4, carboxyl groups (–COOH) were negatively charged and the hydrogen bonds were dissociated, resulting in swelling of the hydrogel. In addition, the release rate of CoA was higher at 37°C than 25°C at pH 7.4 because the swelling ratio of the hydrogels decreased with increasing temperature at both pH 2.1 and 7.4. The decreased swellability of the polymer network was attributed to the collapse of the PNIPAm chains at 37°C. Hydrophilic groups (–NHCO) in the PNIPAm polymer formed intermolecular hydrogen bonds with the surrounding water at 25°C. With increasing temperature,

the water molecule gained an enthalpy, and the hydrophobic force of the PNIPAm became dominant. Consequently, the water molecules inside the hydrogel were released, resulting in a decreased swelling ratio of the hydrogels at 37°C. As a result, the crosslinking density of the semi-IPN hydrogel was reduced due to the precipitation of PNIPAm, and the porous size of the hydrogel became enlarged, thereby accelerating the CoA release.

In another study, Ahmed et al. reported pH-sensitive IPN microspheres, which were prepared by combining a chitosan polymer and an acrylamide-grafted hydroxyethylcellulose (AAm-g-HEC) using glutaraldehyde as a crosslinker [1]. The crosslinked chitosan was used as a pH-sensitive hydrogel due to its swellability in acidic conditions. Hydroxyethylcellulose (HEC), a nonionic polymer, was modified with acrylamide (AAm) to improve the mechanical strength. In their work, diclofenac sodium as a drug was encapsulated into the IPN microspheres, and its release profile from the microspheres was investigated at pH 1.2 and 7.4. The results showed that the swellability of the microspheres was higher at pH 1.2 than at pH 7.4 due to the protonation of amine groups in chitosan chains, leading to structure relaxation and dissociation. The higher amounts of AAm-g-HEC induced higher swelling due to the hydrophilicity of the AAm-g-HEC matrix, leading to higher water uptake.

Chitosan-Based Devices for Wound Healing

Chitosan-based biomaterials have been used in the area of wound healing due to its ability to enhance the healing process, decrease treatment time, and protect wound surface areas without pain [14, 37, 71, 95]. Biodegradability and biocompatibility of chitosan are excellent characteristics for wound healing materials to activate host defenses, prevent infections, and accelerate healing process [14, 71, 100]. Chitosan is degraded by enzymatic hydrolytic processes, especially by lysozyme, resulting in the release of glucosamine, *N*-acetylglucosamine monomers, and oligomers. Its degraded products influence macrophage activation, cytokine production, anti-inflammatory reactions, angiogenesis, granulation, and scar formation [37, 71, 95]. Chitosan oligomers promote the synthesis of hyaluronan, which is an anionic glycosaminoglycan spread in epithelial, connective, and neural tissues [71]. The hyaluronan promotes cell adhesion, movement, and proliferation. It is involved in such processes as morphogenesis, inflammation, wound repair, and tissue reorganization. The released chitosan monomers after degradation are phosphorylated and incorporated into hyaluronan, keratan sulfate, chondroitin sulfate, and others [71].

Wound healing includes a variety of biochemical process regulated by humoral factors and anti-inflammatory mediators [71]. First, inflammatory cells from surrounding cells move into a wound area and fibroblasts appear to form collagen and connective fibers. Subsequently, many capillaries form to supply oxygen and nutrients, after which epithelial cells begin to grow under the scab, resulting in the formation of new epithelium. Chitosan-based materials have been shown to

facilitate fast wound healing and smooth scar formation because it enhances vascularization and continuously releases chito-oligomers to the wound area [37, 71]. Chitosan induces migration and proliferation of fibroblasts and vascular endothelial cells by stimulating fibroblasts to release interleukin-8, an important mediator of the immune reaction [71, 74, 101]. Therefore, chitosan promotes the formation of granulation tissue with angiogenesis and organization. As a result, using chitosan to treat wounds induces excellent deposition and orientation of collagen fibrils as well as its incorporation into extracellular matrix (ECM) components [37, 74].

In conventional therapies, irradiation and administration of drugs are commonly performed to treat wound areas. There are several types of chitosan-based biomaterials used in wound healing applications, including powders, filaments, granules, hydrogels, composite non-woven fabrics, and sponges [20, 24, 43, 52, 55, 75]. For example, Ono et al. investigated the feasibility of photocrosslinkable chitosan (Az-CH-LA) to induce an insoluble and flexible hydrogel using UV irradiation [43, 75]. The results demonstrated that the photocrosslinkable chitosan hydrogel completely stopped bleeding from a cut mouse tail after UV irradiation. The chitosan hydrogel significantly affected wound contraction and accelerated wound healing. The chitosan hydrogel-treated wounds exhibited the formation of granulation tissue and epithelialization. In addition, it was found that the binding strength of the chitosan hydrogel was higher than that of fibrin glue. Therefore, this study suggested that the photocrosslinkable chitosan (Az-CH-LA) hydrogel could be used as an excellent wound healing biomaterial in hemostasis conditions [43]. In another study, Kojima et al. evaluated tissue reactions in rats after implantation of a polyester non-woven fabric impregnated with chitin or chitosan [55]. This study investigated that the effect of the dose of chitin or chitosan on inflammatory reactions resulted in the formation of granulation tissue in vivo. The results indicated that excessive amounts of chitin and chitosan induce excessive formation of granulation tissue and inflammatory reactions. However, with suitable doses of chitin and chitosan, the synthesis of collagen was enhanced without scar formation around non-woven fabric, indicating an accelerated healing process [55, 74].

In an attempt to improve the water solubility of the healing agents, Cho et al. investigated the effect of water soluble chitin (WSC) on wound healing in rats by comparing it with chitin and chitosan [20]. In practical applications, it is required to improve interactions between the wounded sites and the healing agents. In their work, WSC was prepared by adjusting the DDA and molecular weight of chitin using alkaline and ultrasonic treatment. They found that the WSC was more efficient than chitin or chitosan as a wound healing accelerator. In addition, the WSC-treated wounds were completely reepithelialized and formed granulation tissues. Similarly, water soluble carboxymethyl (CM)-chitosans were investigated regarding their activities on the wound healing acceleration. Chen et al. found that CM-chitosan promoted the proliferation of normal skin fibroblasts significantly but inhibited the proliferation of keloid fibroblasts [16]. The results also proved that the water soluble chitosans play an important role in wound healing.

In another study, chitosan was combined with sodium alginate to form a complex sponge, which was evaluated as a potential wound healing material in rats [24]. In this study curcumin, a therapeutic agent, was loaded into the chitosan-alginate sponge to prevent wound infection. The results indicated that the sponge-treated wounds exhibited better formation of the granulation tissue and collagen alignment compared with cotton gauze-treated wounds. In addition, the sponge loaded with curcumin enhanced the therapeutic healing effect.

Summary

A major challenge in the drug delivery system is to control drug release in an appropriate dosage and sequence over an appropriate time period. Extensive study on controlled drug delivery has been executed for successful tissue regeneration and chemotherapy. Recently, a variety of new techniques and strategies have utilized the beneficial properties of chitosan, but few have shown its feasibility for long-term clinical applications. However, many studies are still continuing on new delivery systems based on chitosan polymers due to its excellent physicochemical and biological properties. It is also capable of accelerating wound healing and tissue regeneration. These properties of chitosan are significantly affected by its molecular weight and DDA. In addition, its functional groups such as amino and hydroxyl groups offer opportunities for chemical or physical modification via various crosslinking methods.

Chitosan can form covalently crosslinked networks via Schiff base formation reactions and Michael-type reactions using small molecule, functionalized polymer chains, photosensitive moieties, natural tissue enzymes, and UV irradiation. In contrast, non-covalent polymer networks can be formed with ionic molecules, polyelectrolyte polymers, and neutral polymers via several interactions, including electrostatic, hydrophobic, and hydrogen bonding between polymer chains. The physically bonded networks are formed under mild conditions without the addition of toxic chemicals such as crosslinkers, photo-initiators, and organic solvents. Hence, they are biocompatible, but may be disrupted or reversed by environmental factors such as pH, temperature, and others. The physically bonded polymers are suitable for short-term drug delivery. On the other hand, chemically crosslinked networks enhance mechanical strength and increase stability, but may be non-biocompatible. There are numerous approaches to controlling drug release and improving therapeutic efficacy at specific target regions. As discussed, drug release from the chitosan-based delivery system is triggered by several different mechanisms including diffusion, swelling, degradation, pH, temperature, and others. Therefore, the unique properties of the chitosan polymer should be applied to develop controlled drug release systems by modulating the release mechanisms. As such, a new approach combining both advantages of chemical and physical crosslinking strategies should be considered for tissue engineering and drug delivery.

Acknowledgments We would like to acknowledge the supports from March of Dimes Birth Defect Foundation, Wallace H. Coulter Foundation, Airlift Research Foundation, DOD OR090562 and NIH R01AR057837.

References

1. AL-Kahtani Ahmed, A., Bhojya Naik, H.S., Sherigara, B.S.: Synthesis and characterization of chitosan-based pH-sensitive semi-interpenetrating network microspheres for controlled release of diclofenac sodium. Carbohydr. Polym. **344**, 699–706 (2009)
2. Amidi, M., Mastrobattista, E., Jiskoot, W., Hennink, W.E.: Chitosan-based delivery systems for protein therapeutics and antigens. Adv. Drug Deliv. Rev. **62**, 59–82 (2010)
3. Back, J.F., Oakenfull, D., Smith, M.B.: Increased thermal stability of proteins in the presence of sugars and polyols. Biochemistry **18**(23), 5191–5196 (1979)
4. Bae, J.W., Go, D.H., Park, K.D.: Thermosensitive chitosan as an injectable carrier for local drug delivery. Macromol. Res. **14**(4), 461–465 (2006)
5. Berger, J., Reist, M., Mayer, J.M., Felt, O., Peppas, N.A., Gurny, R.: Structure and interactions in covalently and ionically crosslinked chitosan hydrogels for biomedical applications. Eur. J. Pharm. Biopharm. **57**, 19–34 (2004)
6. Berger, J., Reist, M., Mayer, J.M., Felt, O., Gurny, R.: Structure and interactions in chitosan hydrogels formed by complexation or aggregation for biomedical applications. Eur. J. Pharm. Biopharm. **57**, 35–52 (2004)
7. Bernkop-Schnurch, A.: Chitosan and its derivatives: potential excipients for peroral peptide delivery systems. Int. J. Pharm. **194**, 1–13 (2000)
8. Berrada, M., Serreqi, A., Dabbarh, F., Owusu, A., Gupta, A., Lehnert, S.: A novel non-toxic camptothecin formulation for cancer chemotherapy. Biomaterials **26**, 2115–2120 (2005)
9. Bhattarai, N., Gunn, J., Zhang, M.: Chitosan-based hydrogels for controlled, localized drug delivery. Adv. Drug Deliv. Rev. **31**(62, No.1), 83–99 (2010)
10. Bhattarai, N., Ramay, H.R., Gunn, J., Matsen, F.A., Zhang, M.Q.: PEG-grafted chitosan as an injectable thermosensitive hydrogel for sustained protein release. J. Control. Release **103**, 609–624 (2005)
11. Boddohi, S., Moore, S., Johnson, P.A., Kipper, M.J.: Polysaccharide-based polyelectrolyte complex nanoparticles from chitosan, heparin, and hyaluronan. Biomacromolecules **10**, 1402–1409 (2009)
12. Capitani, D., De Angelis, A.A., Crescenzi, V., Masci, G., Segre, A.L.: NMR study of a novel chitosan-based hydrogel. Carbohydr. Polym. **45**, 245–252 (2001)
13. Carreno-Gomez, B., Duncan, A.: Evaluation of the biological properties of soluble chitosan and chitosan microspheres. Int. J. Pharm. **148**, 231–240 (1997)
14. Chatelet, C., Damour, O., Domard, A.: Influence of the degree of acetylation on some biological properties of chitosan films. Biomaterials **22**, 261–268 (2001)
15. Chen, T., Embree, H.D., Brown, E.M., Taylor, M.M., Payne, G.F.: Enzyme-catalyzed gel formation of gelatin and chitosan: potential for in situ applications. Biomaterials **24**, 2831–2841 (2003)
16. Chen, X., Wang, Z., Liu, W., Park, H.: The effect of carboxymethyl-chitosan on proliferation and collagen secretion of normal and keloid skin fibroblasts. Biomaterials **23**, 4609–4614 (2002)
17. Chen, J.P., Cheng, T.H.: Thermo-responsive chitosan-graft-poly(N-isopropylacrylamide) injectable hydrogel for cultivation of chondrocytes and meniscus cells. Macromol. Biosci. **6**, 1026–1039 (2006)

18. Chenite, A., Chaput, C., Wang, D., Combes, C., Buschmann, M.D., Hoemann, D.D., et al.: Novel injectable neutral solutions of chitosan form biodegradable gels in situ. Biomaterials **21**, 2155–2161 (2000)
19. Chenite, A., Buschmann, M., Wang, D., Chaput, C., Kandani, N.: Rheological characterization of thermogelling chitosan/glycerolphosphate solutions. Carbohydr. Polym. **46**, 39–47 (2001)
20. Cho, Y., Cho, Y., Chung, S., Yoo, G., Ko, S.: Water-soluble chitin as a wound healing accelerator. Biomaterials **20**, 2139–2145 (1999)
21. Cho, J., Heuzey, M.C., Begin, A., Carreau, P.J.: Physical gelation of chitosan in the Presence of β-glycerophosphate: The effect of temperature. Biomacromolecules **6**, 3267–3275 (2005)
22. Cho, J., Heuzey, M.C., Begin, A., Carreau, P.J.: Chitosan and glycerophosphate concentration dependence of solution behaviour and gel point using small amplitude oscillatory rheometry. Food Hydrocolloids **20**, 936–945 (2006)
23. Crompton, K.E., Goud, J.D., Bellamkond, R.V., Gengenbach, T.R., Finkelstein, D.I., Forsythe, J.S., et al.: Polylysine-functionalised thermoresponsive chitosan hydrogel for neural tissue engineering. Biomaterials **28**, 441–449 (2007)
24. Dai, M., Zheng, X., Xu, X., Kong, X., Li, X., Guo, G., et al.: Chitosan-alginate sponge: preparation and application in curcumin delivery for dermal wound healing in rat. J. Biomed. Biotechnol. **2009**, 1–8 (2009)
25. Dai, Y., Li, P., Zhang, J., Wang, A., Wei, Q.: A novel pH sensitive *N*-succinyl chitosan/alginate hydrogel bead for nifedipine delivery. Biopharm. Drug Dispos. **29**, 173–184 (2008)
26. Dash, A.K., Cudworth, G.C.: Therapeutic applications of implantable drug delivery systems. J. Pharmacol. Toxicol. Methods **40**, 1–12 (1998)
27. Francis Suh, J.K., Matthew, H.W.T.: Application of chitosan-based polysaccharide biomaterials in cartilage tissue engineering: a review. Biomaterials **21**, 2589–2598 (2000)
28. Freier, T., Koh, H.S., Kazazian, K., Shoichet, M.S.: Controlling cell adhesion and degradation of chitosan films by N-acetylation. Biomaterials **26**, 5872–5878 (2005)
29. Gerentes, P., Vachoud, L., Doury, J., Domard, A.: Study of a chitin-based gel as injectable material in periodontal surgery. Biomaterials **23**, 1295–1302 (2002)
30. Gorochovceva, N., Makusuka, R.: Synthesis and study of water-soluble chitosan-O-poly (ethylene glycol) graft copolymers. Eur. Polym. J. **40**, 685–691 (2004)
31. Gunatillake, P.A., Adhikari, R.: Biodegradable synthetic polymers for tissue engineering. Eur. Cell. Mater. **5**, 1–16 (2003)
32. Guo, B., Gao, Q.: Preparation and properties of a pH/temperature-responsive carboxymethyl chitosan/poly(*N*-isopropylacrylamide)semi-IPN hydrogel for oral delivery of drugs. Carbohydr. Res. **342**, 2416–2422 (2007)
33. Gutowska, A., Jeong, B., Jasionowski, M.: Injectable gels for tissue engineering. Anat. Rec. **263**, 342–349 (2001)
34. Hamidi, M., Azadi, A., Rafiei, P.: Hydrogel nanoparticles in drug delivery. Adv. Drug Deliv. Rev. **60**, 1638–1649 (2008)
35. Hasegawa, M., Yagi, K., Iwakawa, S., Hirai, M.: Chitosan induces apoptosis via caspase-3 activation in bladder tumour cells. Jpn. J. Cancer Res. **4**, 459–466 (2001)
36. Hennink, W.E., van Nostrum, C.F.: Novel crosslinking methods to design hydrogels. Adv. Drug Deliv. Rev. **54**, 13–36 (2002)
37. Hiroshi Ueno, H., Fumio Nakamura, F., Murakami, M., Okumura, M., Kadosawa, T., Fujinaga, T.: Evaluation effects of chitosan for the extracellular matrix production by fibroblasts and the growth factors production by macrophages. Biomaterials **22**, 2125–2130 (2001)
38. Hoare, T.R., Kohane, D.S.: Hydrogels in drug delivery: Progress and challenges. Polymer **49**, 1993–2007 (2008)
39. Hoekstra, A., Struszczyk, H., Kivekas, O.: Percutaneous microcrystalline chitosan application for sealing arterial puncture sites. Biomaterials **19**(16), 1467–1471 (1998)

40. Hoemann, C.D., Chenite, A., Sun, J., Hurtig, M., Serreqi, A., Buschmann, M.D., et al.: Cytocompatible gel formation of chitosan-glycerol phosphate solutions supplemented with hydroxyl ethyl cellulose is due to the presence of glyoxal. J. Biomed. Mater. Res. A **56**(2), 521–529 (2007)
41. Holland, T.A., Tessmar, J.K.V., Tabata, Y., Mikos, A.G.: Transforming growth factor-b1 release from oligo(poly(ethylene glycol) fumarate) hydrogels in conditions that model the cartilage wound healing environment. J. Control. Release **94**, 101–114 (2004)
42. Hong, Y., Song, H., Gong, Y., Mao, Z., Gao, C., Shen, J.: Covalently crosslinked chitosan hydrogel: Properties of in vitro degradation and chondrocyte encapsulation. Acta Biomater. **3**, 23–31 (2007)
43. Ishihara, M., Nakanishi, K., Ono, K., Sato, M., Kikuchi, M., Saito, Y., et al.: Photocrosslinkable chitosan as a dressing for wound occlusion and accelerator in healing process. Biomaterials **23**, 833–840 (2002)
44. Ishihara, M., Obara, K., Ishizuka, T., Fujita, M., Sato, M., Masuoka, K.: Controlled release of fibroblast growth factors and heparin from photocrosslinked chitosan hydrogels and subsequent effect on in vivo vascularization. J. Biomed. Mater. Res. A **64A**, 551–559 (2003)
45. Jain, R.A.: The manufacturing techniques of various drug loaded biodegradable poly(lactide-co-glycolide) (PLGA) devices. Biomaterials **21**, 2475–2490 (2000)
46. Jameela, S.R., Jayakrishnan, A.: Glutaraldehyde cross-linked chitosan microspheres as a long acting biodegradable drug delivery vehicle: studies on the in vitro release of mitoxantrone and in vivo degradation of microspheres in rat muscle. Biomaterials **16**, 769–775 (1995)
47. Jarry, C., Leroux, J.C., Haeck, J., Chaput, C.: Irradiating or autoclaving chitosan/polyol solutions: Effect on thermogelling chitosan-b-glycerophosphate systems. Chem. Pharm. Bull. **50**(10), 1335–1340 (2002)
48. Jayakumar, R., Prabaharan, M., Reis, R.L., Mano, J.F.: Graft copolymerized chitosan-present status and applications. Carbohydr. Polym. **62**, 142–158 (2005)
49. Jin, R., Hiemstra, C., Zhong, Z., Feijen, J.: Enzyme-mediated fast in situ formation of hydrogels from dextran–tyramine conjugates. Biomaterials **28**, 2791–2800 (2007)
50. Jin, R., Moreira Teixeira, L.S., Dijkstra, P.J., Karperien, M., van Blitterswijk, C.A., Zhong, Z. Y., et al.: Injectable chitosan-based hydrogels for cartilage tissue engineering. Biomaterials **30**, 2544–2551 (2009)
51. Khan, T.A., Peh, K.K., Ching, H.S.: Reporting degree of deacetylation values of chitosan: the influence of analytical methods. J. Pharm. Pharmaceut. Sci. **5**(3), 205–212 (2002)
52. Khor, E., Lim, L.: Implantable applications of chitin and chitosan. Biomaterials **24**, 2339–2349 (2003)
53. Kim, M., Choi, Y., Noh, I., Tae, G.: Synthesis and characterization of in situ chitosan-based hydrogel via grafting of carboxyethyl acrylate. J. Biomed. Mater. Res. A **83**, 674–682 (2007)
54. Kim, S., Nishimoto, S.K., Bumgardner, J.D., Haggard, W.O., Gaber, M.W., Yang, Y.: A chitosan/β-glycerophosphate thermo-sensitive gel for the delivery of ellagic acid for the treatment of brain cancer. Biomaterials **31**, 4157–4166 (2010)
55. Kojima, K., Okamoto, Y., Miyatake, K., Tamai, Y., Shigemasa, Y., Minami, S.: Optimum dose of chitin and chitosan for organization of non-woven fabric in the subcutaneous tissue. Carbohydr. Polym. **46**, 2235–2239 (2001)
56. Kokufuta, E.: Polyelectrolyte gel transitions: experimental aspects of charge inhomogeneity in the swelling and segmental attractions in the shrinking. Langmuir **21**(22), 10004–10015 (2005)
57. Kumar, M.N.: A review of chitin and chitosan applications. React. Funct. Polym. **46**, 1–27 (2000)
58. Leach, J.B., Schmidt, C.E.: Characterization of protein release from photocrosslinkable hyaluronic acid-polyethylene glycol hydrogel tissue engineering scaffolds. Biomaterials **26**, 125–135 (2005)

59. Lee, J., Kim, K., Kwon, I., Ahn, H., Lee, S., Cho, H.: Effects of the controlled-released TGF-b1 from chitosan microspheres on chondrocytes cultured in a collagen/chitosan/glycosaminoglycan scaffold. Biomaterials **25**, 4163–4173 (2004)
60. Lee, J., Kim, S., Kwon, I., Ahn, H., Cho, H., Lee, S., et al.: Effects of a chitosan scaffold containing TGF-b1 encapsulated chitosan microspheres on in vitro chondrocyte culture, Artif. Organs **28**(9), 829–839 (2004)
61. Li, J., Du, Y., Liang, H.: Influence of molecular parameters on the degradation of chitosan by a commercial enzyme. Polym. Degrad. Stab. **92**, 515–524 (2007)
62. Lin, C., Metters, A.T.: Hydrogels in controlled release formulations: network design and mathematical modeling. Adv. Drug Deliv. Rev. **58**, 1379–1408 (2006)
63. Liu, Z., Jiao, Y., Wang, Y., Zhou, C., Zhang, Z.: Polysaccharides-based nanoparticles as drug delivery systems. Adv. Drug Deliv. Rev. **60**, 1650–1662 (2008)
64. Mao, S., Sun, W., Kissel, T.: Chitosan-based formulations for delivery of DNA and siRNA. Adv. Drug Deliv. Rev. **62**, 12–27 (2010)
65. Martino, A.D., Sittinger, M., Risbud, M.V.: Chitosan: A versatile biopolymer for orthopaedic tissue-engineering. Biomaterials **26**, 5983–5990 (2005)
66. Metters, A., Hubbell, J.: Network formation and degradation behavior of hydrogels formed by Michael-type addition reactions. Biomacromolecules **6**, 290–301 (2005)
67. Molinaro, G., Leroux, J.C., Damas, J., Adam, A.: Biocompatibility of thermo-sensitive chitosan-based hydrogels: an in vivo experimental approach to injectable biomaterials. Biomaterials **23**, 2717–2722 (2002)
68. Moses, M.A., Brem, H., Langer, R.: Advancing the field of drug delivery: Taking aim at cancer. Cancer Cell **4**, 337–341 (2003)
69. Murata, J., Saiki, I., Makabe, T., Tsuta, Y., Tokura, S., Azuma, I.: Inhibition of tumor-induced angiogenesis by sulfated chitin derivative. Cancer Res. **51**, 22–26 (1991)
70. Muzzarelli, R.: Human enzymatic activities related to the therapeutic administration of chitin derivatives. Cell. Mol. Life Sci. **53**, 131–140 (1997)
71. Muzzarelli, R.A.A., Mattioli-Belmonte, M., Pugnaloni, A., Biagini, G.: Biochemistry, histology and clinical uses of chitins and chitosans in wound healing. EXS **87**, 251–264 (1999)
72. Obara, K., Ishihara, M., Ozeki, Y., Ishizuka, T., Hayashi, T., Nakamura, S.: Controlled release of paclitaxel from photocrosslinked chitosan hydrogels and its subsequent effect on subcutaneous tumor growth in mice. J. Control. Release **110**, 79–89 (2005)
73. Obara, K., Ishihara, M., Ishizuka, T., Fujita, M., Ozeki, Y., Maehara, T., et al.: Photocrosslinkable chitosan hydrogel containing fibroblast growth factor-2 stimulates wound healing in healing-impaired *db*/*db* mice. Biomaterials **24**, 3437–3444 (2003)
74. Okamoto, Y., Watanabe, M., Miyatake, K., Morimoto, M., Shigemasa, Y., Minami, S.: Effects of chitin/chitosan and their oligomers/monomers on migrations of fibroblasts and vascular endothelium. Biomaterials **23**, 1975–1979 (2002)
75. Ono, K., Saito, Y., Yura, H., Ishikawa, K., Kurita, A., Akaike, T., et al.: Photocrosslinkable chitosan as a biological adhesive. J. Biomed. Mater. Res. A **49**, 289–295 (2000)
76. Pangburn, S.H., Trescony, P.V., Heller, J.: Lysozyme degradation of partially deacetylated chitin, its films and hydrogels. Biomaterials **3**, 105–108 (1982)
77. Park, J., Saravanakumar, G., Kim, K., Kwon, I.: Targeted delivery of low molecular drugs using chitosan and its derivatives. Adv. Drug Deliv. Rev. **62**(1), 28–41 (2010)
78. Philippova, O.E., Volkov, E.V., Sitnikova, N.L., Khokhlov, A.R., Desbrieres, J., Rinaudo, M.: Two types of hydrophobic aggregates in aqueous solutions of chitosan and its hydrophobic derivative. Biomacromolecules **2**, 483–490 (2001)
79. Pillai, C.K.S., Paul, W., Sharma, C.P.: Chitin and chitosan polymers: Chemistry, solubility and fiber formation. Prog. Polym. Sci. **34**, 641–678 (2009)
80. Ravi Kumar, M.N., Hudson, S.M.: Chitosan. Encyclopedia of Biomaterials and Biomedical Engineering (EBBE), New York: Marcel Dekker, Inc., pp. 310–323 (2006).

81. Ren, D., Yi, H., Wang, W., Ma, X.: The enzymatic degradation and swelling properties of chitosan matrices with different degrees of N-acetylation. Carbohydr. Res. **340**, 2403–2410 (2005)
82. Roughley, P., Hoemann, C., DesRosiers, E., Mwale, F., Antoniou, J., Alini, M.: The potential of chitosan-based gels containing intervertebral disc cells for nucleus pulposus supplementation. Biomaterials **27**, 388–396 (2006)
83. Ruel-Gariépy, E., Chenite, A., Chaput, C., Guirguis, S., Leroux, J.C.: Characterization of thermosensitive chitosan gels for the sustained delivery of drugs. Int. J. Pharm. **203**, 89–98 (2000)
84. Ruel-Gariepy, E., Shive, M., Bichara, A., Berrada, M., Garrec, D.L., Chenite, A., et al.: A thermo-sensitive chitosan-based hydrogel for the local delivery of paclitaxel. Eur. J. Pharmaceut. Biopharmaceut. **57**, 53–63 (2004)
85. Sakai, S., Yamada, Y., Zenke, T., Kawakami, K.: Novel chitosan derivative soluble at neutral pH and in-situ gellable via peroxidase-catalyzed enzymatic reaction. J. Mater. Chem. **19**, 230–235 (2009)
86. Sakai, S., Kawakami, K.: Synthesis and characterization of both ionically and enzymatically cross-linkable alginate. Acta Biomater. **3**(4), 3495–3501 (2007)
87. Sanborn, T.J., Messersmith, P.B., Barron, A.E.: In situ crosslinking of a biomimetic peptide-PEGhydrogel via thermally triggered activation of factor XIII. Biomaterials **23**, 2703–2710 (2002)
88. Sashiwa, H., Aiba, S.: Chemically modified chitin and chitosan as biomaterials. Prog. Polym. Sci. **29**, 887–908 (2004)
89. Shu, X.Z., Zhu, K.J., Song, W.: Novel pH-sensitive citrate cross-linked chitosan film for drug controlled release. Int. J. Pharm. **212**, 19–28 (2001)
90. Siepmann, J., Peppas, N.A.: Modeling of drug release from delivery systems based on hydroxypropyl methylcellulose (HPMC). Adv. Drug Deliv. Rev. **48**, 139–157 (2001)
91. Sokker, H.H., Abdel Ghaffar, A.M., Gad, Y.H., Aly, A.S.: Synthesis and characterization of hydrogels based on grafted chitosan for the controlled drug release. Carbohydr. Polym. **75**, 222–229 (2009)
92. Sokolsky-Papkov, M., Agashi, K., Olaye, A., Shakesheff, K., Domb, A.J.: Polymer carriers for drug delivery in tissue engineering. Adv. Drug Deliv. Rev. **59**, 187–206 (2007)
93. Sperinde, J.J., Griffith, L.G.: Synthesis and characterization of enzymatically-cross-linked poly(ethylene glycol) hydrogels. Macromolecules **30**, 5255–5264 (1997)
94. Stokke, B., Varum, K.M., Holme, H.K., Hjerde, R., Smidsrod, O.: Sequence specificities for lysozyme depolymerization of partially *N*-acetylated chitosans. Can. J. Chem. **73**, 1972–1981 (1995)
95. Suzuki, Y., Okamoto, Y., Morimoto, M., Sashiwa, H., Saimoto, H., Tanioka, S., et al.: Influence of physico-chemical properties of chitin and chitosan on complement activation. Carbohydr. Polym. **42**, 307–310 (2000)
96. Ta, H.T., Dass, C.R., Dunstan, D.E.: Injectable chitosan hydrogels for localised cancer therapy. J. Control. Release **126**, 205–216 (2008)
97. Ta, H.T., Han, H., Larson, I., Dass, C.R., Dunstan, D.E.: Chitosan-dibasic orthophosphate hydrogel: A potential drug delivery system. Int. J. Pharm. **371**, 134–141 (2009)
98. Tan, H., Chu, C.R., Payne, K.A., Marra, K.G.: Injectable in situ forming biodegradable chitosan–hyaluronic acid based hydrogels for cartilage tissue engineering. Biomaterials **30**, 2499–2506 (2009)
99. Tien, C.L., Lacroix, M., Ispas-Szabo, P., Mateescu, M.A.: *N*-acylated chitosan: hydrophobic matrices for controlled drug release. J. Control. Release **93**, 1–13 (2003)
100. Tomihata, K., Ikada, Y.: In vitro and in vivo degradation of films of chitin and its deacetylated derivatives. Biomaterials **16**, 567–575 (1997)
101. Ueno, H., Yamada, H., Tanaka, I., Kaba, N., Matsuura, M., Okumura, M., et al.: Accelerating effects of chitosan for healing at early phase of experimental open wound in dogs. Biomaterials **20**, 1407–1414 (1999)

102. Wang, M., Fang, Y., Hu, D.: Preparation and properties of chitosan-poly(N-isopropylacrylamide) full-IPN hydrogels. React. Funct. Polym. **48**, 215–221 (2001)
103. Wang, Q.Z., Chen, X.Z., Liu, N., Wang, S.X., Liu, C.S., Meng, X.H., et al.: Protonation constants of chitosan with different molecular weight and degree of deacetylation. Carbohydr. Polym. **65**, 194–201 (2006)
104. Wang, W., Xu, D.: Viscosity and flow properties of concentrated solutions of chitosan with different degrees of deacetylation. Int. J. Biol. Macromol. **16**, 149–152 (1994)
105. Weng, L., Chen, X., Chen, W.: Rheological characterization of in situ crosslinkable hydrogels formulated from oxidized dextran and N-carboxyethyl chitosan. Biomacromolecules **8**, 1109–1115 (2007)
106. Wu, J., Su, Z.G., Ma, G.H.: A thermo- and pH-sensitive hydrogel composed of quaternized chitosan/glycerophosphate. Int. J. Pharm. **315**, 1–11 (2006)
107. Wu, J., Wei, W., Wang, L.Y., Su, Z.G., Ma, G.H.: A thermosensitive hydrogel based on quaternized chitosan and poly(ethylene glycol) for nasal drug delivery system. Biomaterials **28**, 2220–2232 (2007)
108. Yeo, Y., Geng, W., Ito, T., Kohane, D.S., Burdick, J.A., Radisic, M.: Photocrosslinkable hydrogel for myocyte cell culture and injection. J. Biomed. Mater. Res. B Appl. Biomater. **81B**, 312–322 (2007)
109. Yoshifuji, A., Noishiki, Y., Wada, M., Heux, L., Kuga, S.: Esterification of β-chitin via intercalation by carboxylic anhydrides. Biomacromolecules **7**, 2878–2881 (2006)
110. Yoo, H.S.: Photo-cross-linkable and thermo-responsive hydrogels containing chitosan and Pluronic for sustained release of human growth hormone (hGH). J. Biomater. Sci. Polymer Edn **18**(11), 1429–1441 (2007)

Chapter 13
Conclusion: Translating Tissue Engineering into Successful Therapies

Sujata K. Bhatia

Abstract This volume has highlighted major advances in the design of biomaterials for regenerative medicine. Increasingly, tissue engineering is being recognized as a beneficial strategy for alleviating the global burden of disease. While significant progress has been made in the field of tissue regeneration, a number of scientific and engineering issues must be addressed before tissue-engineered scaffolds can be translated into clinical usage.

Going forward, biomaterials scientists must:

(1) Rigorously evaluate the short-term and long-term biocompatibility of engineered scaffolds;
(2) Determine the biological fates of both scaffolds and exogenous cells following implantation of engineered constructs;
(3) Track the function of native cells, and confirm that functional tissue is being generated;
(4) Find the best combinations of growth factors to promote the growth, differentiation, and proliferation of desirable cells;
(5) Discover the biochemical and biophysical stimuli that enable tissue engraftment;
(6) Thoughtfully address the bioethical issues arising from tissue regeneration;
(7) Weigh the risks versus benefits of implantable biomaterials for regenerative medicine;
(8) Cooperate with process engineers to ensure cost-effective scale-up and production of engineered scaffolds;
(9) Understand the shelf life of engineered matrices, and its impact on cost and safety;

S.K. Bhatia (✉)
Harvard University, Cambridge, MA, USA
e-mail: sbhatia@seas.harvard.edu

S.K. Bhatia (ed.), *Engineering Biomaterials for Regenerative Medicine: Novel Technologies for Clinical Applications*, DOI 10.1007/978-1-4614-1080-5_13,

(10) Join with mechanical engineers to create convenient delivery systems for biomaterials;
(11) Collaborate with clinicians to develop systems that are optimal for physician and patient use;
(12) Ensure that engineered biomaterials can be consistently and reliably produced to satisfy regulatory requirements;
(13) Convincingly demonstrate the value of tissue-engineered scaffolds in clinical trials.

Translation of regenerative medicine into widespread clinical use will not only require the concerted efforts of biomaterials scientists and physicians but also chemical engineers, mechanical engineers, bioethicists, and regulatory authorities. The technological developments described in this book reveal the potential of regenerative medicine as well as future research priorities. Continued progress in biomaterials science, along with the early involvement of physicians, surgeons, and patients, will allow the possibilities of regenerative medicine to become realities.

Index

S.K. Bhatia (ed.), *Engineering Biomaterials for Regenerative Medicine: Novel Technologies for Clinical Applications*, DOI 10.1007/978-1-4614-1080-5,